doi:10.7289/V5/TM-NOS-NCCOS-214

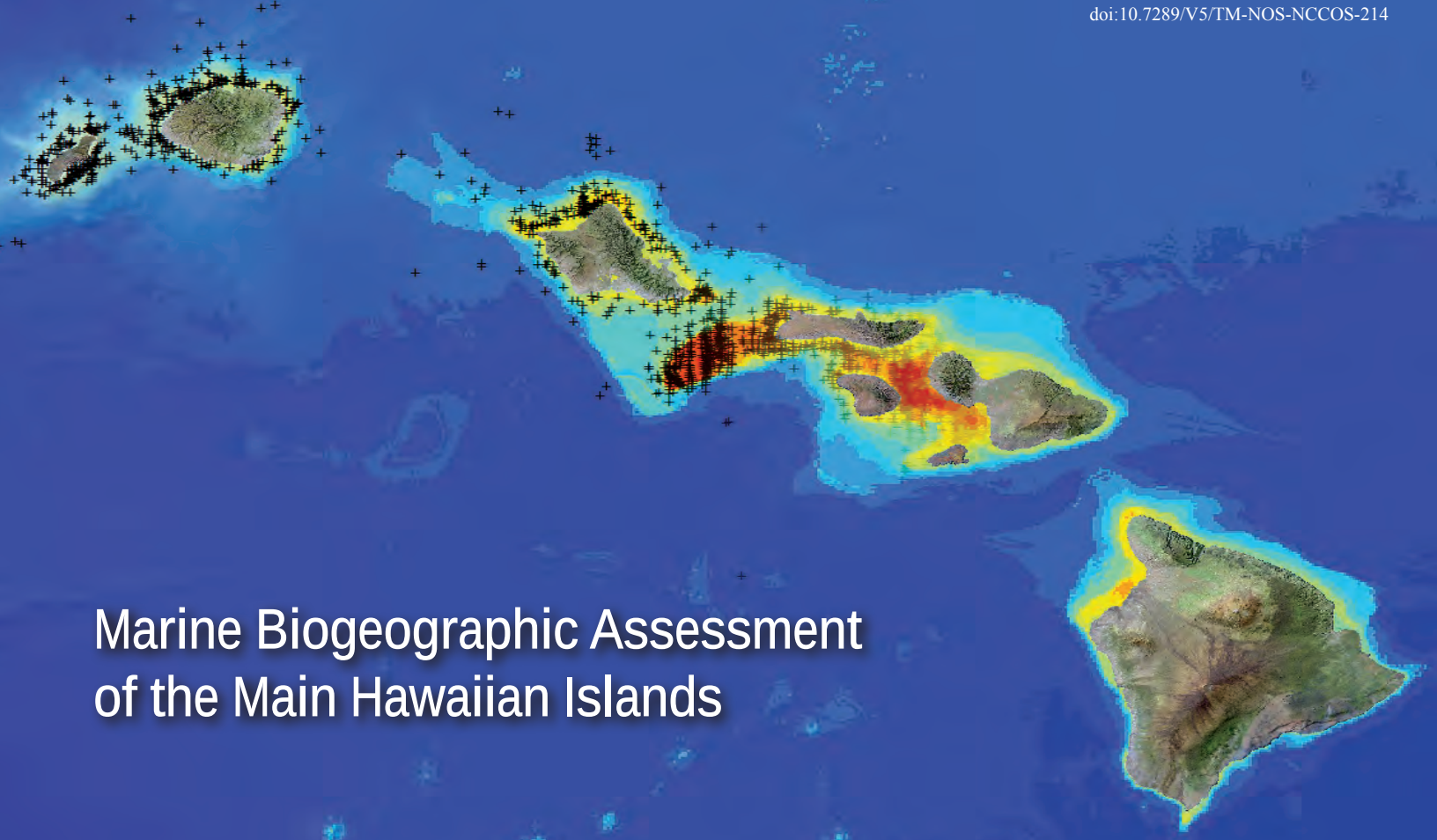

Marine Biogeographic Assessment of the Main Hawaiian Islands

NOAA National Centers for Coastal Ocean Science
Center for Coastal Monitoring and Assessment

Editors
Bryan M. Costa
Matthew S. Kendall

July 2016

OCS Study BOEM 2016-035
NOAA Technical Memorandum NOS NCCOS 214

BOEM
Bureau of Ocean Energy Management

NOAA National Centers for Coastal Ocean Science

Citations

Full report citation:
Costa, B.M. and M.S. Kendall (eds.). 2016. Marine Biogeographic Assessment of the Main Hawaiian Islands. Bureau of Ocean Energy Management and National Oceanic and Atmospheric Administration. OCS Study BOEM 2016-035 and NOAA Technical Memorandum NOS NCCOS 214. 359 pp. doi:10.7289/V5/TM-NOS-NCCOS-214

Chapter citation: example for Chapter 2
Costa, B.M., M. Poti, A.J. Winship, P.I. Miller, and J. Gove. 2016. Chapter 2: Environmental Setting. pp. 13-56. In: B.M. Costa and M.S. Kendall (eds.), Marine Biogeographic Assessment of the Main Hawaiian Islands. Bureau of Ocean Energy Management and National Oceanic and Atmospheric Administration. OCS Study BOEM 2016-035 and NOAA Technical Memorandum NOS NCCOS 214. 359 pp.

Acknowledgments

This study was funded by the U.S. Department of the Interior, Bureau of Ocean Energy Management (BOEM), Environmental Studies Program, Washington, D.C., through Interagency Agreement Number M13PG00021 with the National Oceanic and Atmospheric Administration (NOAA). This report has been technically reviewed by BOEM and it has been approved for publication. The views and conclusions contained in this document are those of the authors and should not be interpreted as representing the opinions or policies of the U.S. Government, nor does mention of trade names or commercial products constitute endorsement or recommendation for use.

Chris Caldow led the initial development of this project. BOEM Pacific OCS Region subject matter experts reviewed and provided feedback on the scope and desired outcomes at several points during the project. The covers for this document were designed and created by Gini Kennedy. The design, layout and formatting were completed by Jamie Higgins and Sarah D. Hile. Editorial content was improved by Kevin McMahon. CSS-Dynamac employees were supported under NOAA Contract No. EA133C-14-NC-1384.

This assessment would not have been possible without the cooperation and participation of many federal, state, academic and non-governmental partners (see Chapter 1, Table 1). Four of the major partners and data providers included: (1) NOAA's Pacific Island Fisheries Science Center, (2) NOAA's Southwest Fisheries Science Center, (3) University of Hawai'i at Mānoa, and (4) the State of Hawai'i. Many individuals at these institutions provided crucial contributions during every step of the project. They identified information that was relevant to the project's scope, contributed their time and expertise during analysis and review, and connected us to the local network of managers, scientists, and experts active in marine research throughout the State of Hawai'i.

Each chapter concludes with its own specific acknowledgments section to recognize unique contributions. It should be emphasized that (at its core) this assessment is a synthesis of many dozens of prior studies and research programs. Each contributing study and program has its own set of acknowledgements that should be recognized but cannot be duplicated here. This synthesis was possible because of the hard work over many years and millions of dollars invested by other organizations to support ocean and coastal management decisions in Hawai'i.

We dedicate this report to the memory of our friend and colleague John Rooney.

doi:10.7289/V5/TM-NOS-NCCOS-214

Marine Biogeographic Assessment of the Main Hawaiian Islands

A collaborative investigation by

National Oceanic and Atmospheric Administration's National Centers for Coastal Ocean Science and Bureau of Ocean Energy Management's Pacific Outer Continental Shelf Region

July 2016

BOEM Report OCS Study BOEM 2016-035

and

NOAA Technical Memorandum NOS NCCOS 214

EDITORS

Bryan M. Costa

Matthew S. Kendall

BOEM
Bureau of Ocean Energy Management

Report Availability

This report can be downloaded from the Bureau of Ocean Energy Management, Environmental Studies Program Information System (ESPIS) website by referencing OCS Study BOEM 2016-035. For more information about BOEM's Environmental Studies Program, please visit: http://www.boem.gov/Studies/

For more information on NOAA's National Centers of Coastal Ocean Science, please visit: https://coastalscience.noaa.gov/

For more information on this project, please visit: https://coastalscience.noaa.gov/projects/detail?key=163 or direct questions and comments to:

NOAA/NOS/National Centers for Coastal Ocean Science
Center for Coastal Monitoring and Assessment
Biogeography Branch

Bryan M. Costa
240-533-0364
bryan.costa@noaa.gov

or

Matthew S. Kendall, Ph.D.
240-533-0314
matt.kendall@noaa.gov

Table of Contents

Table of Contents

Table of Contents

Contributing Author's Affiliations

[1] NOAA National Centers for Coastal Ocean Science, Biogeography Branch, Silver Spring, MD, U.S.A.
[2] BOEM Pacific Outer Continental Shelf Region, Camarillo, CA, U.S.A.
[3] CSS-Dynamac, Fairfax, VA, U.S.A.
[4] Plymouth Marine Laboratory, Remote Sensing Group, Plymouth, United Kingdom
[5] NOAA Pacific Islands Fisheries Science Center, Ecosystem Sciences Division, Honolulu, HI, U.S.A.
[6] NOAA Office of National Marine Sanctuaries, Pahānaumokuākea Marine National Monument, Honolulu, HI, U.S.A.
[7] NOAA Pacific Islands Fisheries Science Center, Protected Species Division, Honolulu, HI, U.S.A.
[8] University of Hawai'i at Mānoa, Fisheries Ecology Research Lab, Hawai'i, U.S.A.
[9] State of Hawai'i, Department of Land and Natural Resources, Division of Aquatic Resources, Hawai'i, U.S.A.
[10] University of Hawai'i at Mānoa, Deep-Sea Fish Ecology Lab, Hawai'i, U.S.A.
[11] University of Hawai'i at Mānoa, Department of Natural Resources and Environmental Management, Hawai'i, U.S.A.
[12] NOAA Pacific Islands Fisheries Science Center, Protected Species Division, Marine Turtle Biology and Assessment Program, Honolulu, HI, U.S.A.
[13] Plymouth University, Centre for Marine and Coastal Policy Research, United Kingdom
[14] Cascadia Research Collective, WA, U.S.A.
[15] NOAA Southwest Fisheries Science Center, Marine Mammal and Turtle Division, CA, U.S.A.
[16] University of Hawai'i at Mānoa, Joint Institute for Marine and Atmospheric Research, HI, U.S.A.
[17] University of Hawai'i at Mānoa, HI, U.S.A.
[18] NOAA Pacific Islands Fisheries Science Center, Protected Species Division, Cetacean Research Program, Honolulu, HI, U.S.A.
[19] Nicholas School of the Environment, Duke University, NC, U.S.A.
[20] NOAA Alaskan Fisheries Science Center, National Marine Mammal Laboratory, WA, U.S.A.
[21] NOAA Pacific Islands Fisheries Science Center, Protected Species Division, Hawaiian Monk Seal Research Program, Honolulu, HI, U.S.A.
[22] Scripps Institution of Oceanography, U.C. San Diego, CA, U.S.A.

List of Tables and Figures

Chapter 1

Chapter 2

Chapter 3

List of Tables and Figures

List of Tables and Figures

Chapter 4

List of Tables and Figures

Chapter 5

Chapter 6

List of Tables and Figures

Chapter 7

List of Tables and Figures

Appendices

Acronyms

Aviso	Archiving, Validation and Interpretation of Satellite Oceanographic data
BOEM	Bureau of Ocean Energy Management
BRFA	Bottom Fish Restricted Area
BSEE	Bureau of Safety and Environmental Enforcement
C	Celsius
CAWCR	Centre for Australian Climate and Weather Research
CCMA	Center for Coastal Monitoring and Assessment
Cnes	Centre National d'Etudes Spatiales
CORTAD	Coral Reef Temperature Anomaly Database
CPC	Climatic Prediction Center
CRCP	Coral Reef Conservation Program
CREP	Coral Reef Ecosystem Program
CRM	U.S. Coastal Relief Model
CSCOR	Center for Sponsored Coastal and Ocean Research
CSIRO	Commonwealth Scientific and Industrial Research Organization
CZMP	Coastal Zone Management Program
DBEDT	Department of Business, Economic Development and Tourism
DEM	Digital Elevation Model
DOC	Department of Commerce
DOD	Department of Defense
DOE	Department of Energy
Duacs	Data Unification and Altimeter Combination System
EEZ	Exclusive Economic Zone
EMC	Environmental Modeling Center
ENSO	El Niño Southern Oscillation
EOD	Ecosystems and Oceanography Division
ESRI	Environmental Systems Research Institute
ESRL	Earth Systems Research Laboratory
FRMD	Fisheries Research and Monitoring Division
GEBCO	General Bathymetric Chart of the Oceans
GHRSST	Group for High Resolution Sea Surface Temperature
GIS	Geographic Information Systems
HCD	Habitat Conservation Division
HIHWNMS	Hawaiian Islands Humpback Whale National Marine Sanctuary
HIMB	Hawai'i Institute of Marine Biology
HLC	Hawaiian Lee Current
HLCC	Hawaiian Lee Counter Current
HMRG	Hawaii Mapping Research Group
HURL	Hawai'i Undersea Research Laboratory
HYCOM	HYbrid Coordinate Ocean Model
JPL	Jet Propulsion Laboratory
km	kilometer
LiDAR	Light Detection and Ranging
m	Meter
m/s	Meters per second
m^2	Square meter
MADT	Maps of Absolute Dynamic Topography
MAE	Mean Absolute Error
mg Carbon/m^2/day	Milligrams of Carbon per square meter per day
mg/m^3	Milligrams per meter cubed
MGET	Marine Geospatial Ecology Tools
MHI	Main Hawaiian Islands
MLCD	Marine Life Conservation District
MLD	Mixed layer depth
MODIS	Moderate Resolution Imaging Spectroradiometer
MPA	Marine Protected Area
MUR	Multi-scale Ultra-high Resolution
N/A	Not applicable
NASA	National Aeronautics and Space Administration
NAVFAC	Naval Facilities Engineering Command

Acronyms

NCCOS	National Centers for Coastal Ocean Science
NCEI	National Centers for Environmental Information
NCEP	National Centers for Environmental Prediction
NCODA	Navy Coupled Ocean Data Assimilation system
NEC	North Equatorial Current
NEPA	National Environmental Policy Act
NESDIS	National Environmental Satellite, Data and Information Service
NHRC	North Hawaiian Ridge Current
NMFS	National Marine Fisheries Service
NOAA	National Oceanic and Atmospheric Administration
NODC	National Oceanographic Data Center
NOS	National Ocean Service
NPP	Net Primary Productivity
NPS	National Park Service
NPSG	North Pacific Subtropical Gyre
NREL	National Renewable Energy Research Laboratory
NWHI	Northwestern Hawaiian Islands
OCM	Office of Coastal Management
OCS	Outer Continental Shelf
ONMS	Office of National Marine Sanctuaries
ORE	Ocean and Resources Engineering
PacIOOS	Pacific Integrated Ocean Observing System
PDO	Pacific Decadal Oscillation
PEACC	Pacific ENSO Applications Climate Center
PIBHMC	Pacific Islands Benthic Habitat Mapping Center
PIFSC	Pacific Islands Fisheries Science Center
PIRO	Pacific Islands Regional Office
PRD	Protected Resources Division
PSD	Protected Species Division
QuikSCAT	Quik Scatterometer
RMSE	Root Mean Squared Error
s	Seconds
SD	Standard Deviation
SMI	Standard Mapped Image
SOEST	School of Ocean and Earth Science and Technology
SoNAR	Sound Navigation and Ranging
Ssalto	Segment Sol multimissions d'ALTimétrie, d'Orbitographie et de localisation précise
SSH	Sea Surface Height
SST	Sea Surface Temperature
SSTA	Sea Surface Temperature Anomalies
SWFSC	Southwest Fisheries Science Center
TSA	Thermal Stress Anomalies
U.S.	United States
UH CGG	University of Hawai'i Coastal Geology Group
USFWS	U.S. Fish and Wildlife Service
USGS	U.S. Geological Survey
UTM	Universal Transverse Mercator

Executive Summary

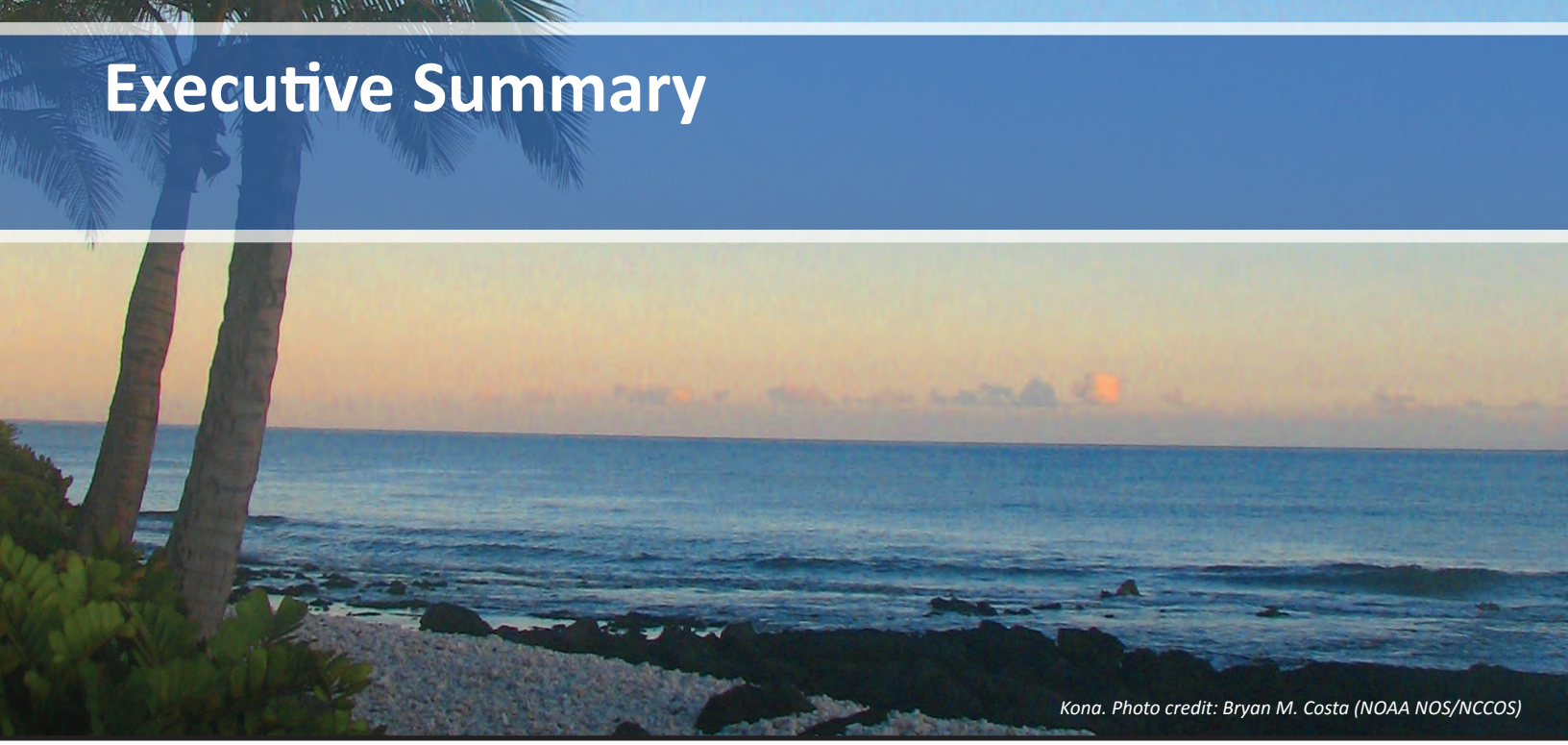

Kona. Photo credit: Bryan M. Costa (NOAA NOS/NCCOS)

The state of Hawai'i is working to develop local renewable energy sources to reduce its dependence on fossil fuels. Most of the State's potential renewable energy resources (notably, wind) are located in federal waters from 3 to 200 nm offshore. The Bureau of Ocean Energy Management (BOEM) regulates the leasing, construction and operation of most renewable energy projects in federal waters, and is required to evaluate potential human, coastal and marine impacts from these projects. BOEM partnered with the National Oceanic and Atmospheric Administration's (NOAA) National Centers for Coastal Ocean Science (NCCOS) to gather biogeographic information in support of this evaluation around the Main Hawaiian Islands (MHI). The complexity of products from this assessment range from simple animal distribution maps to mathematical models depicting the predicted distributions of animals. Biogeographic analyses and data products were specifically tailored to meet BOEM's needs, and designed to fit within BOEM's framework of offshore lease blocks.

This biogeographic assessment addresses three main questions: (1) how are select species or taxonomic groups distributed spatially and temporally around the MHI?; (2) what environmental conditions influence these distributions?; and (3) what significant gaps exist in our knowledge about the biogeography of the area? To answer these questions, existing, readily-available spatial information was compiled and synthesized, including information on the physical and biological environment, benthic habitats, fishes, sea turtles, marine mammals and seabirds. The assessment focused on federal waters and taxa that were: (1) more likely to interact with renewable energy infrastructure, (2) culturally significant, (3) legally protected, and/or (4) economically valuable. Collaborations with local managers, scientists, and experts from a variety of federal, state, academic and non-governmental organizations were crucial. These partners contributed their data, time and expertise, and many were contributing coauthors on this report.

The assessment includes two main components: (1) a technical report (this document) and (2) associated spatial datasets for use within Geographic Information System (GIS) software. Many of the spatial datasets presented here are publicly available from NOAA's National Centers for Coastal Ocean Science (https://coastalscience.noaa.gov/projects/detail?key=163) and from NOAA's National Centers for Environmental Information (NCEI Accession 0155189; http://data.nodc.noaa.gov/cgi-bin/iso?id=gov.noaa.nodc:0155189). These maps, databases, and analyses are one component of the larger BOEM and State processes to evaluate offshore renewable energy proposals around the MHI. They were not designed to replace any further analysis required by law. For more information about how these products may be used, please contact BOEM's Pacific OCS Region: http://www.boem.gov/Pacific-Region/. This report is organized thematically, and is comprised of seven chapters and supporting appendices. The main objective, basic approach, and important findings from each chapter are as follows:

Executive Summary

Chapter 1: Introduction

- The state of Hawai'i would like to develop local renewable energy sources (notably, wind). Much of the State's potential wind energy is located in federal waters. BOEM regulates most renewable energy projects in federal waters, and is required to assess the potential environmental impacts of these projects during the leasing process.
- To help inform this process, NOAA's NCCOS characterized the marine biogeography and identified key data gaps around the MHI. This project is a small piece of a much larger BOEM leasing process.

Chapter 2: Environmental Setting

- Atmospheric and oceanographic patterns were mapped using satellite imagery and oceanographic models. These maps were used to describe the regional environment, and to develop models predicting deep-coral, cetacean, and seabird distributions.
- Seasons around the MHI are driven by changes in the North Pacific Subtropical High and the Aleutian Low. Winter (November to April) is cooler, rainier, and dominated by the North Pacific swell. Summer (May to October) is warmer, less rainy, and dominated by the northeasterly trade winds and swell.
- Mountains and submerged topography change the direction and speed of winds and currents. These interactions cause the leeward sides of the island to be warmer and drier, and create frequent convergence, mixing, upwelling, fronts and eddies in the channels between the islands (e.g., the Kaiwi, Pailolo and 'Alenuihānā Channels), and on the leeward sides of the islands (e.g., Kona Coast, Hawai'i).

Chapter 3: Benthic Habitats and Corals

- Seafloor habitats were characterized within shallow (<30 m), mesophotic (30-150 m), and deep (>150 m) areas using existing maps, *in situ* survey data and spatial models.
- In shallow areas, rock/boulder habitats were less dominant, hard coral cover declined and algal cover increased moving from the southeast to the northwest. Hard coral cover was generally higher on leeward sides (e.g., Kona Coast, Hawai'i) and more sheltered areas (e.g., Kāne'ohe Bay, O'ahu) around the islands.
- In mesophotic areas, information was limited to the 'Au'au Channel. Predicted probabilities of occurrence were highest for three genera of hard corals along the western Maui coast.
- In deep areas, the distribution of observed deep-coral presences and predicted suitable habitats varied among 18 taxonomic groups, but were often concentrated nearby specific locations, such as Cross Seamount, Makapu'u Point, Makalawena Bank, Lō'ihi Seamount and the southern edge of Penguin Bank.

Chapter 4: Fishes

- The distribution of commercially important bottom fishes (i.e., the deep seven) was mapped using fisheries dependent and independent data. Predictive models were developed describing the spatial distribution of reef fishes (i.e., species richness and biomass, endemic species richness and biomass, and biomass of resource fishes).
- For bottom fishes, the fishery is most active in the winter months. Datasets identified Southern Penguin Bank, Maui Nui channels, west Hawai'i, southern Maui, and northern Moloka'i as important areas.
- For reef fishes, the highest biomass and richness values were in areas least accessible to humans such as the Hamakua and Puna districts on Hawai'i, northern Moloka'i, eastern Maui, and western and southeastern O'ahu. Conversely, areas more accessible to humans had overall lower richness and biomass values and included the Kona Coast, Hawai'i, west Maui and southern O'ahu.

Chapter 5: Sea Turtles

- Basking, nesting, and stranding locations were mapped (in the context of human populations, shoreline cliffs, and beaches) for the five species of sea turtles using *in situ* sightings data. All five species are protected under the Endangered Species Act (ESA).

Executive Summary

- Green turtles (*Chelonia mydas*), the most abundant species, were reported basking at 62 locations, with a majority of reports from northwest O'ahu and west Hawai'i.
- Most nesting reports are for green turtles with the majority occurring on Kaua'i and Maui. Hawksbill (*Eretmochelys imbricata*) have key nesting sites on southern Hawai'i.
- Stranding reports are mostly for green turtles, with many from O'ahu and parts of Maui. Fibropapillomatosis is the major cause along most coastlines. Other common causes include entanglement along northeast Kaua'i and southwest O'ahu, and illnesses, boat impacts and predation along the Kona Coast, Hawai'i.

Chapter 6: Marine Mammals

- The distributions of cetaceans (15 species) were mapped using *in situ* sightings data. Seasonal relative abundance predictions were created for seven of these species. Terrestrial and at-sea locations of the endangered Hawaiian monk seal (*Neomonachus schauinslandi*) were also mapped using *in situ* sightings and telemetry data.
- For cetaceans, species distributions were variable, although some species were sighted or predicted to be consistently closer to shore (e.g., Humpback whale, Spinner dolphin, Common bottlenose dolphin), while other species were generally located further offshore (e.g., Rough-toothed dolphin, Sperm whale). Several species were sighted along the Kona Coast, Hawai'i, including Cuvier's beaked whale, Dwarf sperm whale, Pygmy killer whale, Pantropical spotted dolphin, and Short-finned pilot whale.
- Critical habitat for Hawaiian monk seals includes 0-10 m above the seafloor from 200 m depths to the shoreline, then from the shoreline extending 5 m inland. Hawaiian monk seals were sighted around each of the MHI, although more haul-out sites were identified on the islands to the northwest. Ni'ihau, Kaua'i and O'ahu were also frequented by tagged seals, along with Penguin Bank, the east side of Lāna'i and Kahului Harbor, Maui.

Chapter 7: Seabirds

- The distributions of seabirds (24 species) were mapped using *in situ* data. Seasonal relative density predictions were created for 14 of these species, and maps of maximum potential foraging areas were created for seven species.
- Species distributions were variable, although several species were sighted or predicted to be offshore of the Kona Coast, Hawai'i (e.g., Sooty Tern, Wedge-tailed Shearwater, Juan Fernandez Petrel, Black-winged Petrel, and Bulwer's Petrel).
- Breeding species were generally located closer to land (e.g., Black Noddy, Brown Noddy, and Brown Booby) or occurred more evenly throughout the study area (e.g., Sooty Tern and Wedge-tailed Shearwater). Non-breeding/migratory species tended to be further offshore with some species being restricted to specific parts of the study area (e.g., Juan Fernandez Petrel and Mottled Petrel in the southeast).

The biogeography of the MHI is shaped by atmospheric and oceanographic conditions that operate at different temporal and spatial scales around the islands. Marine animals respond to these changing conditions in different ways. Some taxonomic groups and species use the same locations year round (e.g., on Penguin Bank or offshore of the Kona Coast, Hawai'i), while most taxa utilize different geographic areas at different times of the year. Understanding these spatial and temporal patterns is critical for marine spatial planning efforts, including offshore renewable energy development. For some taxa, this marine biogeographic assessment marks the first time that their space-use patterns were mapped or modeled in the MHI, and the associated data compilation made available online. It establishes a baseline for assessing potential impacts, a guide for monitoring change, a roadmap for prioritizing how to fill data gaps, and a framework for integrating ocean research and management efforts moving forward.

Chapter 1 Introduction

Bryan M. Costa[1], Matthew S. Kendall[1], and Greg Sanders[2]

Kualoa Point, O'ahu. Photo credit: Bryan M. Costa (NOAA NOS/NCCOS)

ABSTRACT

The state of Hawai'i is working to develop local renewable energy sources to reduce its dependence on fossil fuels. Most of the State's potential renewable energy resources (notably, wind) are located in federal waters from 3 to 200 nm offshore. The Bureau of Ocean Energy Management (BOEM) regulates the leasing, construction and operation of most renewable energy projects in federal waters. This regulatory responsibility requires BOEM to assess potential impacts of renewable energy development on the human, marine and coastal environments. BOEM funded the National Oceanic and Atmospheric Administration (NOAA) to characterize the marine biogeography around the Main Hawaiian Islands (MHI). This assessment describes the physical and biological environment and the spatial distributions of benthic communities, fishes, turtles, mammals and seabirds around the islands. The report and products generated during this assessment were designed to help BOEM evaluate future offshore renewable energy proposals. Chapter one sets the stage for this assessment by describing the reasons for conducting this work, introducing the biogeographic assessment process, describing its implementation in the MHI and outlining the contents of this report.

Citation for chapter
Costa, B.M, M.S. Kendall, and G. Sanders. 2016. Chapter 1: Introduction. pp. 1-12. In: B.M. Costa and M.S. Kendall (eds.), Marine Biogeographic Assessment of the Main Hawaiian Islands. Bureau of Ocean Energy Management and National Oceanic and Atmospheric Administration. OCS Study BOEM 2016-035 and NOAA Technical Memorandum NOS NCCOS 214. 359 pp.

[1] *NOAA National Centers for Coastal Ocean Science, Biogeography Branch, Silver Spring, MD, U.S.A.*
[2] *BOEM Pacific Outer Continental Shelf Region, Camarillo, CA, U.S.A.*

Introduction

1.1. BACKGROUND

The state of Hawai'i is comprised of several islands and atolls stretching approximately 2,400 km in the North Pacific Ocean. The State includes both the Northwestern Hawaiian Islands (NWHI) and the Main Hawaiian Islands (MHI; Figure 1.1a). The State's geographic location in the tropics makes it rich in potential renewable energy resources, including solar and wind (Schwartz et al., 2010; Lopez et al., 2012). At the same time, its geographic location and isolation makes importing and generating energy from fossil fuels costly (DOE, 2016). Given these issues, the state of Hawai'i is working to reduce its dependence on fossil fuels by developing local renewable energy sources and implementing new energy efficiency measures (Hawai'i Clean Energy Initiative, 2014).

Hawai'i's Department of Business, Economic Development and Tourism (DBEDT) regulates renewable energy development on land and in state waters from 0 to 3 nautical miles (nm) offshore (Figure 1.1b). Several dozen renewable energy projects already exist on land and nearshore in the state of Hawai'i (Hawai'i DBEDT, 2015). However, most of the State's potential renewable energy resources (notably wind) are located in federal waters (Schwartz et al., 2010; Lopez et al., 2012; Figure 1.1a). This uneven distribution of renewable energy potential makes consideration of future renewable energy development likely in waters from 3 to 200 nm offshore of the MHI.

Under the authority of the Energy Policy Act of 2005, the Bureau of Ocean Energy Management (BOEM) regulates the leasing, construction and operation of most renewable energy projects in federal waters. This legislation requires BOEM to obtain fair return for issued leases, coordinate with relevant federal, state and local agencies, and ensure that renewable energy development takes place in a safe and environmentally-responsible manner. This last mandate requires that BOEM assess potential impacts of renewable energy development on the human, marine, and coastal environments. BOEM funded the National Oceanic and Atmospheric Administration (NOAA) National Centers for Coastal Ocean Science (NCCOS) to characterize the biogeography around the MHI. This assessment describes the physical and biological environment, and the spatial distributions of benthic habitats, fishes, turtles, mammals and seabirds around the islands, including in marine managed areas (Figure 1.2). It was designed to help BOEM evaluate future offshore renewable energy proposals.

North East Maui on road to Hana. Photo credit: Bryan M. Costa (NOAA NOS/NCCOS)

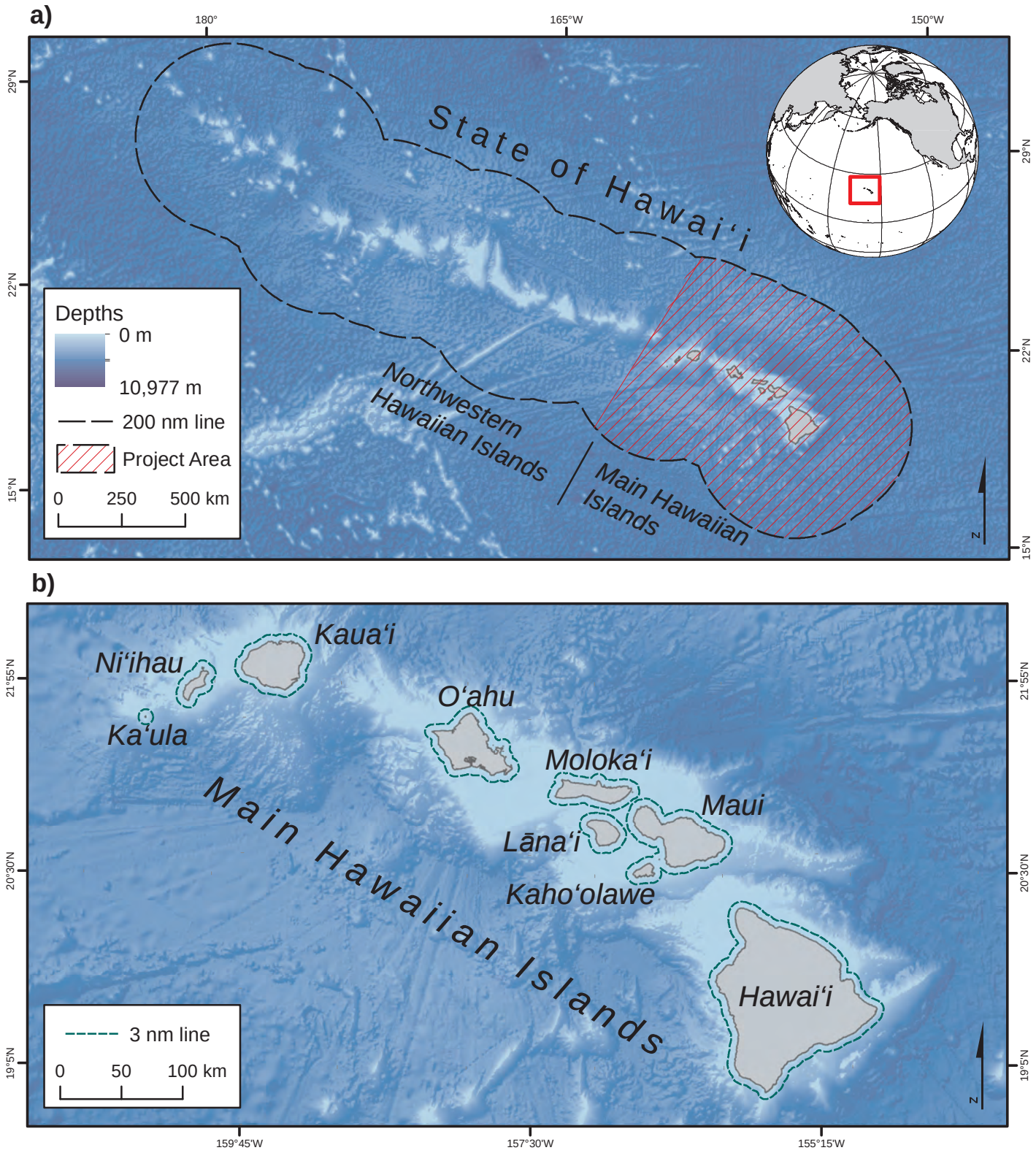

Figure 1.1. Overview of Hawaiian Archipelago a) shows the location of the Hawaiian Archipelago in the Pacific Ocean, the state of Hawai'i, and the boundary of the project area and of federal waters (i.e., 200 nm line); b) shows the Main Hawaiian Islands (MHI), including Ka'ula (Rock), Ni'ihau, Kaua'i, O'ahu, Moloka'i, Lāna'i, Maui, Kaho'olawe and Hawai'i. It also depicts the boundary of state waters (i.e., 3 nm line). Data sources: depth (GEBCO, 2008), MHI shoreline (Battista et al., 2007), federal water boundaries (NOAA MPA Center, 2014) and state water boundaries (Hawai'i Office of Planning, 2006)

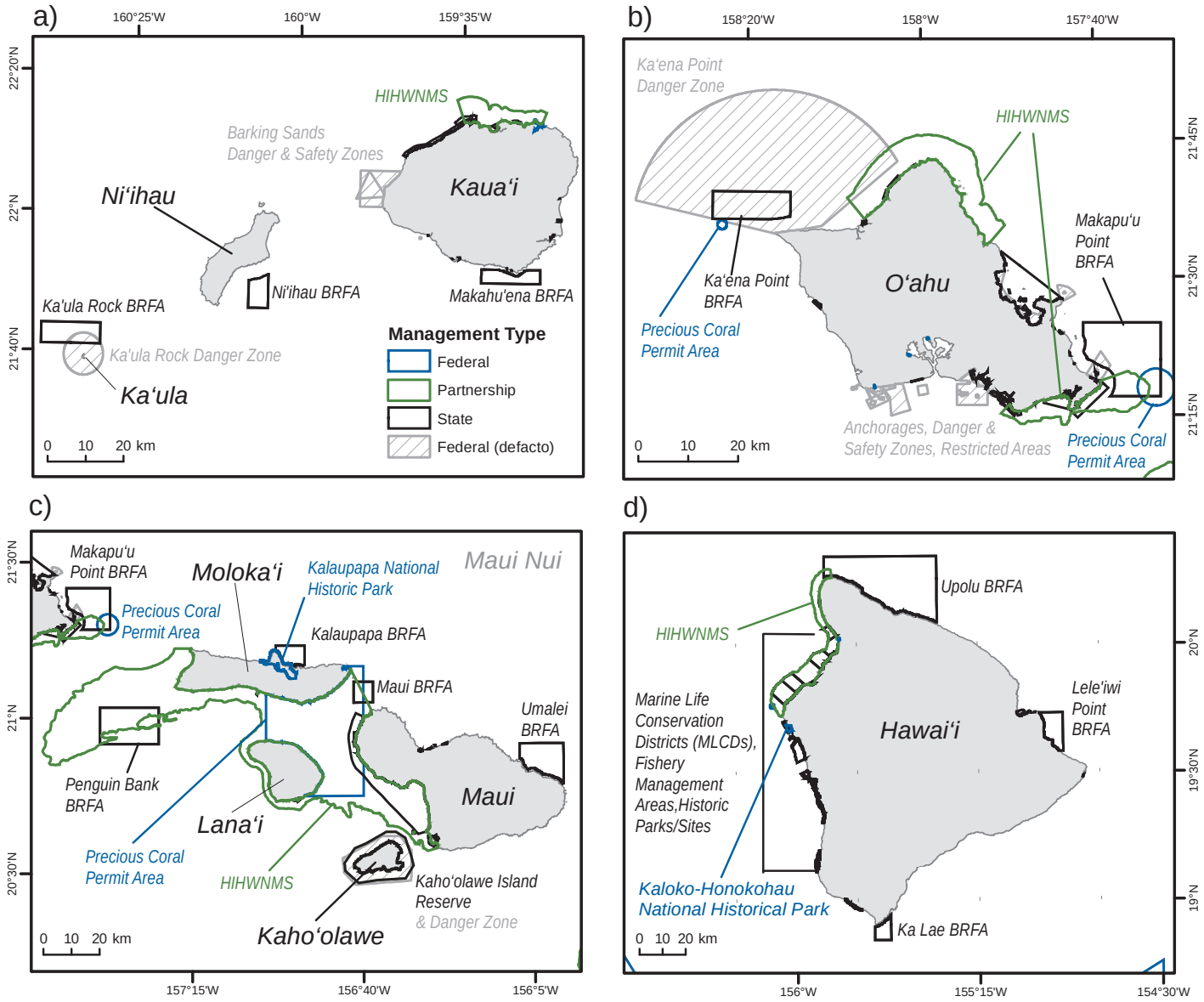

Figure 1.2. Marine managed areas (MMA) in the MHI. Maps showing the boundaries of several types of federal, state and partnership (i.e., jointly managed) marine areas around: a) Ka'ula, Ni'ihau and Kaua'i, b) O'ahu, c) Moloka'i, Lāna'i, Maui, Kaho'olawe, and d) Hawai'i. Federal (de facto) marine areas were established for reasons other than conservation, and may function like traditional marine managed areas. BRFA = Bottom Fish Restricted Area, and HIHWNMS = Hawaiian Islands Humpback Whale National Marine Sanctuary. Data sources: MHI shoreline (Battista et al., 2007) and MMAs (NOAA MPA Center, 2014; Anthropocene Institute, 2015)

1.2. THE BIOGEOGRAPHIC ASSESSMENT PROCESS

Biogeography is the study of spatial and temporal distributions of organisms, their associated habitats, and the historical and biological factors that influence species' distributions. The concept of a "biogeographic assessment" builds on these principles, and provides a process to compile and evaluate spatial and temporal data, characterize ecological patterns, fill data gaps, as well as measure and map spatial uncertainty in support of ecosystem-based management (Caldow et al., 2015). This process was developed by NCCOS through two decades of collaboration with scientists and resource managers. Geographic Information System (GIS), remote sensing and statistical software packages are used to conduct data synthesis and integration. By combining GIS, remote sensing and statistics, scientists are able to visualize spatial and temporal patterns in species' distributions, identify potential ecological drivers of these patterns, quantify their influence, and use these relationships to predict species' distributions and abundances (Battista and Monaco, 2004; Monaco et al., 2005). The products from biogeographic assessments range from simple species distribution maps (NOAA NCCOS, 2006; Friedlander et al., 2009) to complex Bayesian models depicting the predicted distributions of species' and the uncertainty associated with these predictions (Menza et al., 2012).

Biogeographic assessments (Caldow et al., 2015) typically have three steps (Figure 1.3). The first step (i.e., planning) is to understand the informational needs and priorities in a geographic area. This understanding helps place the project in the appropriate regional context and tailor the scope of work accordingly. This step requires engaging with resource managers and partners in person, and having in-depth discussions about potential datasets, products and management uses of the data. It also requires working with local partners and data administrators to acquire existing, readily-available data that is in the project area and relevant to the scope of work. These datasets may include information describing the physical and biological environment, benthic communities, fishes, mammals, sea turtles, seabirds and (in some cases) human uses within a project area. Since no new field data are usually collected during a biogeographic assessment, the availability, completeness and limitations associated with existing datasets has an enormous influence on the types of final products that can be produced.

An ancillary, but important outcome of a biogeographic assessment, is to identify and describe critical data and information gaps. This information can be used to prioritize future data collection efforts. The second step in a biogeographic assessment (i.e., ecosystem data analysis) is to develop methods to integrate these disparate datasets, and to characterize broad biogeographic patterns in the project area. The products that emerge from this integration can vary widely among projects, since each assessment is tailored to specific management needs and each product is developed within the limitations of the source data. Products produced during this step are reviewed by partners and local subject matter experts to ensure that they accurately portray biogeographic patterns to a wider audience. The third and final step in a biogeographic assessment (i.e., management applications) is to help managers and partners use these products to answer specific management questions and help identify and minimize potential conflicts among ocean users.

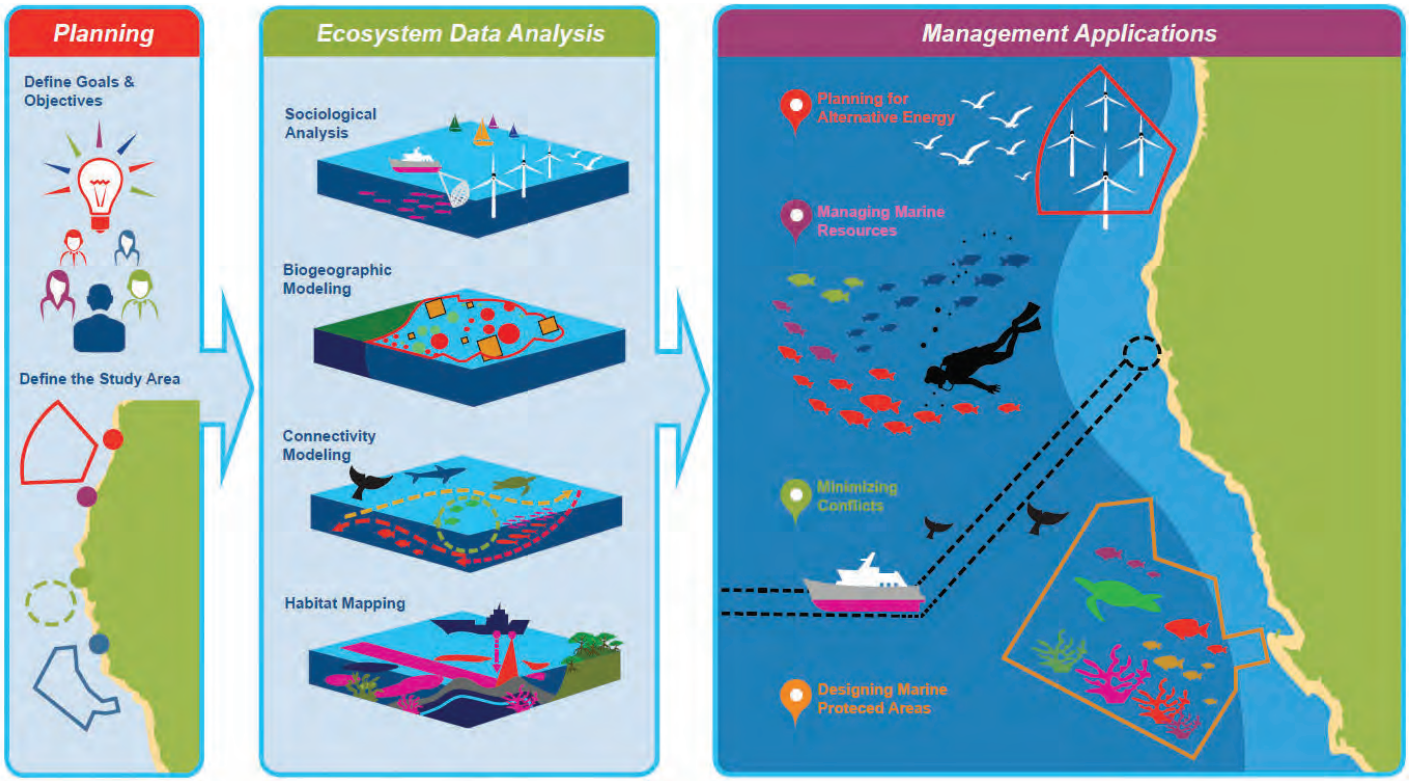

Figure 1.3. The Biogeographic Assessment Process. This diagram illustrates the three steps in the biogeographic assessment process. Step 1 (Planning): talking with managers to determine priorities, assess the data and identify data gaps; Step 2 (Ecosystem Data Analysis): characterizing the ecosystem patterns and processes across the area of interest; and Step 3 (Management Applications): working with managers to support specific management applications. Figure credit: Caldow et al., 2015

1.3. APPLYING THE BIOGEOGRAPHIC ASSESSMENT PROCESS IN THE MHI

The Hawaiian Archipelago can be geographically divided into the NWHI and the MHI. A biogeographic assessment of the NWHI was conducted in 2009 (Friedlander et al., 2009) to support Papahānaumokuākea Marine National Monument's scientific and management needs. In the MHI, we applied the biogeographic assessment process to help BOEM evaluate future offshore renewable energy proposals. Both state and federal waters are included in this assessment, although the focus is on federal waters. This assessment aims to address a number of key ecological questions, including but not limited to: (1) How are select species or taxonomic groups distributed spatially and temporally around the MHI?; (2) What physical and biological conditions may influence the spatial and temporal distribution of these species and taxonomic groups?; and (3) What significant gaps exist in our knowledge about the biogeography of the MHI?

To answer these questions, NOAA NCCOS compiled and synthesized existing, readily-available spatial information around the MHI, including information describing the physical and biological environment, benthic communities, fishes, turtles, whales, dolphins, seals, and seabirds. Species or groups that were: (1) more likely to interact with renewable energy infrastructure (e.g., wind turbines); (2) were culturally significant; (3) had state or federal protected status; and/or (4) were economically valuable were given special consideration. No new information was collected *in situ* during this assessment. Analyses, were specifically designed for compatibility with BOEM's regulatory framework of 1.2x1.2 kilometer (km) aliquots and 4.8x4.8 km lease blocks (Figure 1.4). Existing information came from a variety of federal, state, academic and non-governmental partners (Tables 1.1 and 1.2). These partners were crucial for identifying information relevant to the project's scope, and for connecting NOAA NCCOS with local managers, scientists and experts. Several partners (denoted by * in Tables 1.1 and 1.2) also shared their datasets, and provided technical expertise crucial for completing this assessment and are contributing coauthors. This assessment synthesizes their research over many years, and leverages millions of dollars invested by the management and research community in support of marine planning in the MHI.

Coral reef in the Main Hawaiian Islands. Photo credit: Lisa Wedding (Stanford University)

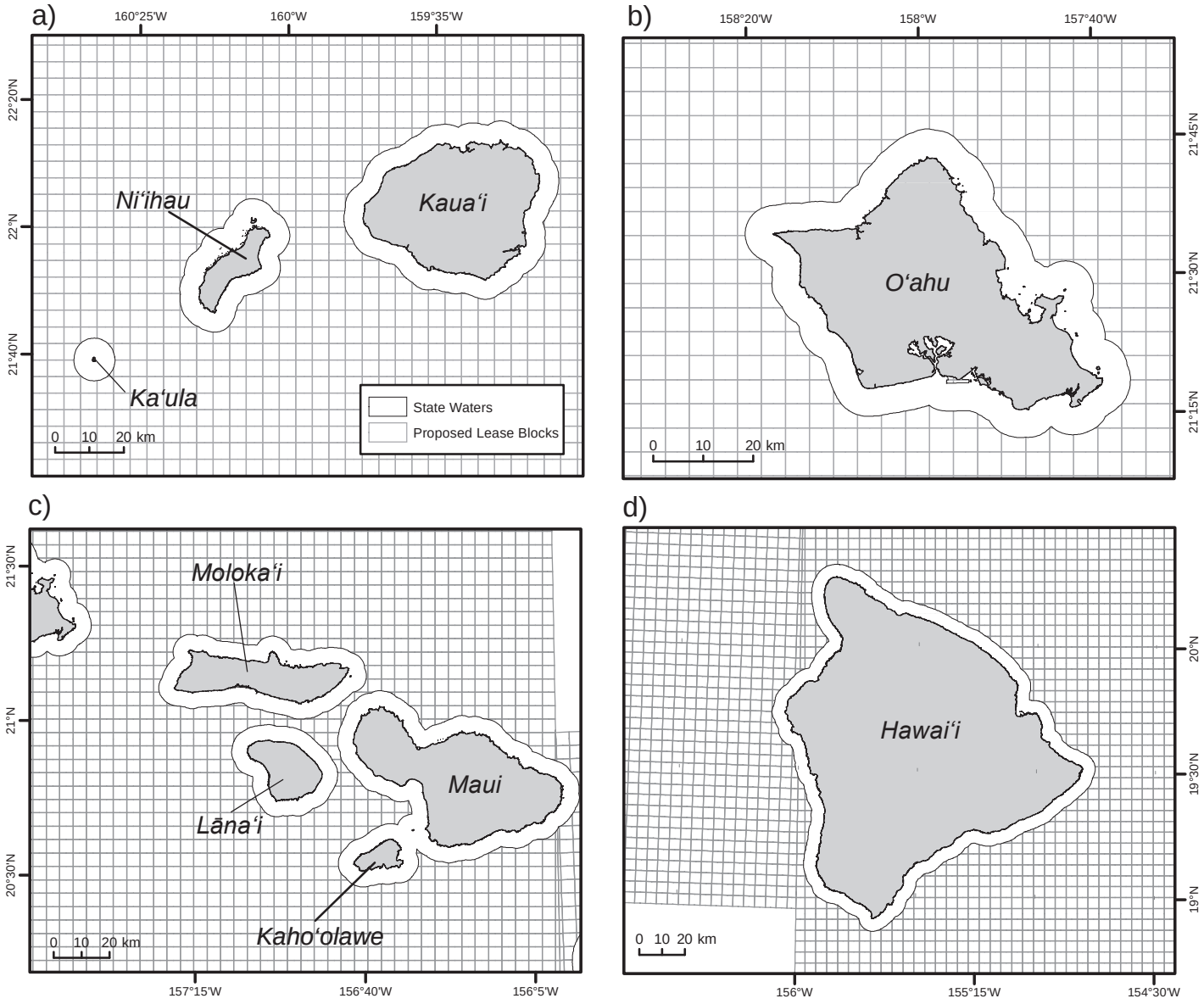

Figure 1.4. Proposed Lease Blocks in the MHI. Maps showing the boundaries of proposed 4.8x4.8 km lease blocks in the MHI. These GIS files are not an Official Record for BOEM offshore lease blocks and boundaries. Data sources: MHI shoreline (Battista et al., 2007), State water boundary (Hawai'i Office of Planning, 2006), and proposed lease blocks (BOEM, 2014)

Introduction

Table 1.1. Key partners in the Federal government. This table denotes the federal partners that were important to the biogeographic assessment process in the MHI. The funding agency is denoted by a "$." Key data partners are denoted by an asterisk (*). Many of these key partners were also contributing coauthors on this report.

Organization	Website
Federal Government	
Department of the Interior (DOI)	
Bureau of Ocean Energy Management (BOEM)	http://www.boem.gov
Pacific Outer Continental Shelf Office[$]	http://www.boem.gov/program-offices-pacific/
Bureau of Safety and Environmental Enforcement (BSEE)	http://www.bsee.gov
National Park Service (NPS)	http://www.nps.gov
Inventory and Monitoring Program*	http://science.nature.nps.gov/im/
U.S. Fish and Wildlife Service (USFWS)	http://www.fws.gov
U.S. Geological Survey (USGS)	http://www.usgs.gov
Pacific Islands Ecosystem Research Center	http://www.usgs.gov/ecosystems/pierc/
Pacific Coastal & Marine Science Center	http://walrus.wr.usgs.gov/
Department of Commerce (DOC)	
National Oceanic and Atmospheric Administration (NOAA)	http://www.noaa.gov/
National Marine Fisheries Service (NMFS)	http://www.nmfs.noaa.gov/
Pacific Islands Fisheries Science Center (PIFSC)	http://www.pifsc.noaa.gov/
Protected Species Division (PSD)*	http://www.pifsc.noaa.gov/psd/
Coral Reef Ecosystem Program (CREP)*	http://www.pifsc.noaa.gov/cred/
Ecosystems and Oceanography Division (EOD)	http://www.pifsc.noaa.gov/eod/
Fisheries Research and Monitoring Division (FRMD)	http://www.pifsc.noaa.gov/frmd/
Pacific Islands Regional Office (PIRO)	http://www.fpir.noaa.gov/
Habitat Conservation Division (HCD)	http://www.fpir.noaa.gov/HCD/hcd_index.html
Southwest Fisheries Science Center (SWFSC)	https://swfsc.noaa.gov/
Protected Resources Division (PRD)	
Marine Mammal and Turtle Division*	https://swfsc.noaa.gov/MMTD/
National Ocean Service (NOS)	http://oceanservice.noaa.gov/
Office of Coastal Management (OCM)	https://coast.noaa.gov/
Coastal Zone Management Program (CZMP)	http://coast.noaa.gov/czm/about/?redirect=301ocm
Coral Reef Conservation Program (CRCP)	http://coralreef.noaa.gov/
Office of National Marine Sanctuaries (ONMS)	
Papahānaumokuākea Marine National Monument	http://www.papahanaumokuakea.gov/
Hawaiian Islands Humpback Whale National Marine Sanctuary	http://hawaiihumpbackwhale.noaa.gov/
National Center for Coastal Ocean Science (NCCOS)	https://coastalscience.noaa.gov/
Center for Coastal Monitoring and Assessment (CCMA)	https://coastalscience.noaa.gov/about/centers/ccma
Center for Sponsored Coastal and Ocean Research (CSCOR)	https://coastalscience.noaa.gov/about/centers/cscor
Biogeography Branch*	https://coastalscience.noaa.gov/about/centers/ccma
National Environmental Satellite, Data and Information Service (NESDIS)	http://www.nesdis.noaa.gov/
National Centers for Environmental Information (NCEI)*	http://www.ngdc.noaa.gov/
Department of Defense (DOD)	
U.S. Army Corps of Engineers	http://www.usace.army.mil/
U.S. Navy	
Pacific Command	http://www.cpf.navy.mil/
Naval Facilities Engineering Command (NAVFAC)	http://www.navfac.navy.mil/navfac_worldwide/pacific.html
Living Marine Resources Program*	http://www.lmr.navy.mil/
National Aeronautics and Space Administration (NASA)	http://www.nasa.gov/
Ocean Biology Processing Group*	http://oceancolor.gsfc.nasa.gov/cms/

Table 1.2. Key state government, academic and non-governmental organization partners. This table denotes the state government, academic and non-governmental organization partners that were important to the biogeographic assessment process in the MHI. Key data partners are denoted by an asterisk (*). Many of these key partners were also contributing coauthors on this report.

Organization	Website
State Government	
Department of Business, Economic Development and Tourism	http://dbedt.hawaii.gov/
Office of Planning	http://planning.hawaii.gov/
Coastal Zone Management Program*	http://planning.hawaii.gov/czm/
State Energy Office	http://energy.hawaii.gov/
Department of Land and Natural Resources	**http://dlnr.hawaii.gov/**
Division of Aquatic Resources*	http://dlnr.hawaii.gov/dar/
Hawaiian Islands Humpback Whale National Marine Sanctuary	http://dlnr.hawaii.gov/sanctuary/
Academic	
University of Hawai'i (at Mānoa)	https://manoa.hawaii.edu/
Department of Biology	http://manoa.hawaii.edu/biology/
Fisheries Ecology Research Lab*	
School of Ocean and Earth Science and Technology (SOEST)	https://www.soest.hawaii.edu/
Deep Sea Fish Ecology Lab*	http://www.deepseafishecology.com/
Ocean and Resources Engineering (ORE)*	http://www.ore.hawaii.edu/
Hawai'i Institute of Marine Biology (HIMB)*	http://www.hawaii.edu/
Pacific Islands Benthic Habitat Mapping Center (PIBHMC)*	http://www.soest.hawaii.edu/pibhmc/pibhmc_mhi.htm
Hawai'i Undersea Research Laboratory (HURL)*	http://www.soest.hawaii.edu/HURL/
Pacific Integrated Ocean Observing System (PacIOOS)*	http://oos.soest.hawaii.edu/pacioos/index.php
Hawai'i Pacific University	http://www.hpu.edu/
Non-governmental Organization	
Cascadia Research Collective*	http://www.cascadiaresearch.org/
The Nature Conservancy	http://www.nature.org/
Hawai'i Marine Program*	http://www.nature.org/ourinitiatives/regions/northamerica/unitedstates/hawaii/index.htm?intc=nature.tnav.where.list
Pacific Rim Conservation	https://www.pacificrimconservation.org/
Plymouth Marine Laboratory	http://www.pml.ac.uk
Remote Sensing Group*	https://rsg.pml.ac.uk/

This report is divided into seven chapters with supporting appendices. Each chapter was written and reviewed in collaboration with subject matter specialists and local experts. Chapter 1 (Introduction) sets the stage for the subsequent chapters by describing the reasons for conducting this assessment, introducing the biogeographic assessment process and describing its implementation in the MHI. Chapter 2 (Environmental Setting) describes broad physical and biological conditions around the MHI, and provides regional environmental context for this assessment. It highlights environmental drivers that were more likely to affect the MHI's biogeography. These environmental drivers are also used to develop the deep coral, cetacean and seabird spatial predictions found in later chapters. The process used to develop spatial predictions is described in Figure 1.5. Chapter 3 (Benthic Habitats and Corals) is divided among seafloor habitats within three broad depth zones: shallow-water (<30 m), mesophotic (30 to 150 m), and deep-water (>150 m). Habitat maps and *in situ* information are mapped for shallow and mesophotic depths. Habitat suitability models are described for select species and taxonomic groups of mesophotic and deep corals. Chapter 4 (Fishes) models the distribution of reef fishes and maps the distribution of commercially important bottom fishes around the MHI. Chapter 5 (Sea Turtles) maps the locations of sea turtle terrestrial activities, including where sea turtles nest and bask and where sea

turtles have historically stranded. Causes for strandings are described spatially, illustrating differences among island geographies. Chapter 6 (Marine Mammals) maps at-sea observations and provides spatial predictions for select species of cetaceans within the project area. Maps of monk seal (*Monachus schauinslandi*) activity in the MHI, including recently updated critical habitat designations, are also provided. Chapter 7 (Seabirds) maps at-sea observations and provides spatial predictions for select species of seabirds in the MHI. Potential foraging areas are predicted for some species, based on known colony locations and descriptions in the literature. Digital copies of each chapter and their associated spatial datasets are available for download from NOAA's National Centers for Coastal Ocean Science(https://coastalscience.noaa.gov/projects/detail?key=163) and from NOAA's National Centers for Environmental Information (NCEI Accession 0155189; http://data.nodc.noaa.gov/cgi-bin/iso?id=gov.noaa.nodc:0155189).

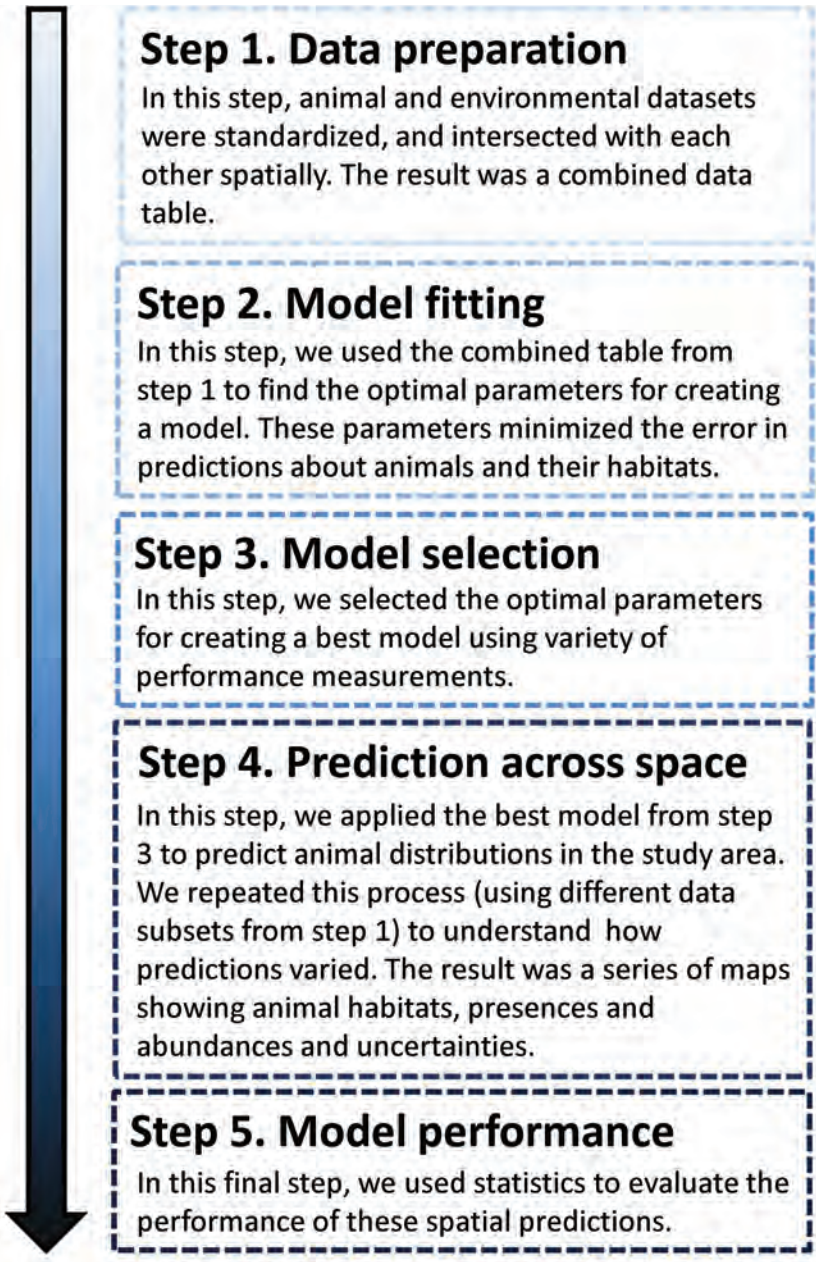

Figure 1.5. General modeling process applied in this assessment. This process was used to develop spatial predictions for deep coral, fishes, cetacean and seabirds. It had five steps, including data preparation, model fitting, model selection, prediction across space, and evaluation of model performance.

This assessment was designed specifically to inform renewable energy decisions by BOEM. Having the most up-to-date and comprehensive biogeographic information is an important part of BOEM's process to identify and fill critical data gaps, and to assess the potential direct and indirect impacts of renewable energy development on marine ecosystems. Products from this assessment may also support coastal and ocean management efforts by other local, state and federal agencies working in the MHI. These maps, products and analyses are one component of a much larger BOEM and State process to evaluate future offshore renewable energy proposals, including identifying topics for future study. These products were not designed to replace any further analysis required by law under the National Environmental Policy Act (NEPA) and other environmental statutes. For more information about how these products may be used, please contact BOEM's Pacific OCS Region: http://www.boem.gov/Pacific-Region/.

LITERATURE CITED

Anthropocene Institute. 2015. Marine Management Areas, Hawai'i Data. Anthropocene Institute. Data Downloaded 7 March 2016. Data Website: http://anthropoceneinstitute.com/node/39 (Site Accessed 8 June 2016).

Battista, T.A. and M.E. Monaco. 2004. Geographic information systems application in coastal marine fisheries. pp. 189-208. In: W.L. Fisher and R.J. Rahel (eds.), Geographic information systems in fisheries. American Fisheries Society, Bethesda, MD. 276 pp.

Battista, T.A., B.M. Costa, and S.M. Anderson. 2007. Benthic Habitats of the Main Hawaiian. NOAA Technical Memorandum NOS NCCOS CCMA 152. Silver Spring, MD. 48 pp. Data Downloaded 5 September 2014. Data Website: https://products.coastalscience.noaa.gov/collections/benthic/e97hawaii/data2007.aspx (Site Accessed 8 June 2016).

BOEM. 2014. Proposed lease blocks and aliquots in the MHI. Bureau of Ocean Energy Management, Pacific Outer Continental Shelf Region. Data Provided 23 April 2014. Provider Website: http://www.boem.gov/Pacific-Region/ (Site Accessed 8 June 2016).

Caldow, C., M.E. Monaco, S.J. Pittman, M.S. Kendall, T.L. Goedeke, C. Menza, B.P. Kinlan, and B. Costa. 2015. Biogeographic Assessments: A framework for information synthesis in marine spatial planning. Marine Policy 51: 423-432.

DOE. 2016. Energy Efficiency & Renewable Energy: State & Local Energy Data. Department of Energy. Data Downloaded 4 March 2016. Data Website: http://apps1.eere.energy.gov/sled/#/ (Site Accessed 8 June 2016).

Friedlander, A., K. Keller, L. Wedding, A. Clarke, and M. Monaco. 2009. A Marine Biogeographic Assessment of the Northwestern Hawaiian Islands. NOAA Technical Memorandum NOS NCCOS 84. Prepared by NCCOS's Biogeography Branch in cooperation with the Office of National Marine Sanctuaries Papahānaumokuākea Marine National Monument. Silver Spring, MD. 363 pp.

GEBCO. 2008. General Bathymetric Chart of the Oceans 08 Grid. GEBCO operates under the joint auspices of the International Hydrographic Organization and the Intergovernmental Oceanographic Commission of UNESCO. Data Downloaded 8 January 2014. Data Website: http://www.gebco.net/data_and_products/gridded_bathymetry_data/ (Site Accessed 8 June 2016).

Hawai'i Clean Energy Initiative. 2014. Hawai'i Clean Energy Initiative Objectives. State of Hawai'i. Online: http://www.hawaiicleanenergyinitiative.org/about-the-hawaii-clean-energy-initiative/goals-and-objectives/ (Site Accessed 8 June 2016).

Hawai'i DBEDT. 2015. Hawai'i State Energy Office Overview. Hawai'i State Energy Office, Department of Business, Economic Development and Tourism. Online: http://energy.hawaii.gov/renewable-energy/overview (Site Accessed 8 June 2016).

Hawai'i Office of Planning. 2006. Three Nautical Mile Boundaries. State of Hawai'i, Office of Planning. Data Downloaded 7 March 2016. Data Website: http://planning.hawaii.gov/gis/download-gis-data/ (Site Accessed 8 June 2016).

Lopez, A., B. Robers, D. Heimiller, N. Blair, and G. Porro. 2012. U.S. Renewable Energy Technical Potentials: A GIS-Based Analysis. Prepared under Task Nos. SA10.1012 and SA10.20A4, Technical Report NREL/TP-6A20-51946. U.S. Department of Energy, Office of Energy Efficiency and Renewable Energy, National Renewable Energy Laboratory. Golden, CO. 32 pp. Online: http://www.nrel.gov/docs/fy12osti/51946.pdf (Site Accessed 11 June 2016).

Menza, C., B.P. Kinlan, D.S. Dorfman, M. Poti, and C. Caldow. 2012. A biogeographic assessment of seabirds, deep sea corals and ocean habitats of the New York Bight: science to support offshore spatial planning. NOAA Technical Memorandum NOS NCCOS 141. Silver Spring, MD.

Monaco, M., M. Kendall, J. Higgins, C. Alexander, and M. Tartt. 2005. Biogeographic assessments of NOAA National Marine Sanctuaries: The integration of ecology and GIS to aid in marine management boundary delineation and assessment. pp. 1-10. In: D.J. Wright and A.J. Scholz. (eds.), Place Matters: Geospatial Tools for Marine Science, Conservation, and Management in the Pacific Northwest. Oregon State University Press. Corvallis, OR. 305 pp.

NOAA MPA Center. 2014. Data and Analysis: MPA Inventory and DeFacto MPAs. NOAA National Ocean Service, Marine Protected Areas Center. Data Downloaded 4 March 2016. Data Website: http://marineprotectedareas.noaa.gov/dataanalysis/ (Site Accessed 8 June 2016).

NOAA NCCOS. 2006. An Ecological Characterization of the Stellwagen Bank National Marine Sanctuary Region: Oceanographic, Biogeographic, and Contaminants Assessment. Prepared by NCCOS's Biogeography Team in cooperation with the National Marine Sanctuary Program. NOAA Technical Memorandum NOS NCCOS 45. Silver Spring, MD. 356 pp.

Schwartz, M., D. Heimiller, S. Haymes, and W. Musial. 2010. Assessment of Offshore Wind Energy Resources for the United States. Prepared under Task No. WE10.1211, Technical Report NREL/TP-500-45889. U.S. Department of Energy, Office of Energy Efficiency and Renewable Energy, National Renewable Energy Laboratory. Golden, CO. 96 pp. Online: http://www.nrel.gov/docs/fy10osti/45889.pdf (Site Accessed 11 June 2016).

Chapter 2 Environmental Setting

Bryan M. Costa[1], Matthew Poti[1,3], Arliss Winship[1,3], Peter Miller[4], and Jamison Gove[5]

Mokulua Islands, O'ahu. Photo credit: Bryan M. Costa (NOAA NOS/NCCOS)

ABSTRACT

The biogeography of the Main Hawaiian Islands (MHI) is shaped by physical, biological and chemical conditions and processes that operate on different spatial scales around the islands and throughout the Hawaiian Archipelago. Here, we map and describe many of the physical and biological conditions and processes (i.e., environmental drivers) critical for understanding and predicting biogeographic patterns. At a broad scale, the MHI's geographic location and isolation in the tropical Pacific Ocean keeps its climate relatively stable (compared to continental climates). Most climatic changes around the islands are driven by seasonal changes in the North Pacific Subtropical High and the Aleutian Low. Changes in these pressure systems create two seasons in the MHI: summer (May to October) and winter (November to April). The MHI's winter is cooler, wetter and is dominated by the North Pacific swell with infrequent occurrences of Kona Winds (from the southwest). The MHI's summer is warmer, drier and dominated by the northeasterly trade winds and trade wind swell. At finer scales, the MHI's topography influences almost every aspect of its weather and climate. The peaks, slopes and valleys interact with persistent trade winds, changing their direction and speed, and causing the leeward sides of the islands to be warmer and drier. It also creates frequent, localized convergence, mixing, upwelling, fronts and eddies in the channels between the islands (i.e., the Kaiwi, Pailolo and 'Alenuihānā Channels), and on the leeward sides of the islands (e.g., Kona Coast). These oceanographic patterns are also influenced by the interaction between currents and the MHI's seafloor topography. Its steep, narrow shelf, numerous seamounts (e.g., Hawaiian and West Hawaiian Seamounts) and prominent banks (e.g., Middle Bank and Penguin Bank) change the speed and direction of surface and subsurface currents as they flow in between and around the MHI islands. Combined, the temporal and spatial variability in the climate and ocean created by these physical and biological processes drives the distributions of marine organisms, and broadly influences the biogeography of the MHIs.

Citation for chapter

Costa, B.M., M. Poti, A. Winship, P. Miller, and J. Gove. 2016. Chapter 2: Environmental Setting. pp. 13-56. In: B.M. Costa and M.S. Kendall (eds.), Marine Biogeographic Assessment of the Main Hawaiian Islands. Bureau of Ocean Energy Management and National Oceanic and Atmospheric Administration. OCS Study BOEM 2016-035 and NOAA Technical Memorandum NOS NCCOS 214. 359 pp.

[1] *NOAA National Centers for Coastal Ocean Science, Biogeography Branch, Silver Spring, MD, U.S.A.*

[3] *CSS-Dynamac, Fairfax, VA, U.S.A.*

[4] *Plymouth Marine Laboratory, Remote Sensing Group, Plymouth, United Kingdom*

[5] *NOAA Pacific Islands Fisheries Science Center, Ecosystem Sciences Division, Honolulu, HI, U.S.A.*

Environmental Setting

2.1. INTRODUCTION

Distributions of marine organisms are influenced by the surrounding physical, biological and chemical conditions (e.g., depth, temperature, currents, light availability, chlorophyll-*a* concentrations, ocean pH, aragonite saturation, etc.), and ecological processes (e.g., food availability, competition, predation, reproduction and recruitment, etc.). The interplay of these conditions and processes drive the composition, configuration, and complexity of marine communities. The biogeography of the Hawaiian Archipelago (and the Main Hawaiian Islands [MHI] in particular) is no different. It has been shaped by its geographic location and isolation in the tropical Pacific (Figure 2.1). This isolation led to the evolution of more endemic species than any other island group in the insular tropical Pacific (Juvik and Juvik, 1998). The MHI's biogeography has also been shaped by environmental drivers that operate around the islands at local (i.e., intra- and inter-island) and global (i.e., world-wide) geographic scales (Juvik and Juvik, 1998; Department of the Navy, 2005). Combined, these drivers create variability in the MHI's climate and ocean that play a primary role in shaping the distribution of marine organisms. Mapping these environmental drivers is critical for understanding and predicting the distribution of animals around the MHI.

Trade winds blowing at Kualoa Point, O'ahu. Photo credit: Bryan M. Costa (NOAA NOS/ NCCOS)

This chapter's goal is to identify and describe broad temporal and spatial patterns in key environmental drivers around the MHI islands with a focus on federal waters. Its purpose is to provide environmental context for the remainder of the report, to help explain biogeographic patterns, and to help predict animal distributions in subsequent chapters. We highlight environmental drivers that are more likely to affect the distribution of specific species, and the MHI's biogeography as a whole. These drivers include depth, seafloor complexity, wind, waves, currents, temperature, turbidity, fronts, upwelling, eddy activity and biological productivity. We present maps of these drivers below and in Appendix A. These maps show seasonal (summer and winter), long-term (>10 year) means and standard deviations (SD). Maximum values were also calculated for waves and water temperature. Water chemical conditions and processes (e.g., ocean pH, calcite or aragonite saturation states) and potential changes due to climate change were beyond the scope of this project. Since the project area is large (approximately 860,250 km^2), the maps presented below are coarse, but the source datasets used to create these maps have more detail than seen here. This detail can be seen in the source Geographic Information System (GIS) layers, which are available online from National Oceanic and Atmospheric Administration's (NOAA) National Centers for Coastal Ocean Science (NCCOS; https://coastalscience.noaa.gov/projects/detail?key=163) and from NOAA's National Centers for Environmental Information (NCEI Accession 0155189; http://data.nodc.noaa.gov/cgi-bin/iso?id=gov.noaa.nodc:0155189). Many of these GIS layers were used in subsequent efforts to predict the distribution of certain species and taxonomic groups of deep corals (Chapter 3), reef fish (Chapter 4), cetaceans (including dolphins and whales; Chapter 6) and seabirds (Chapter 7). These datasets provide context to help better understand the physical and biological conditions that animals are responding to around the MHI.

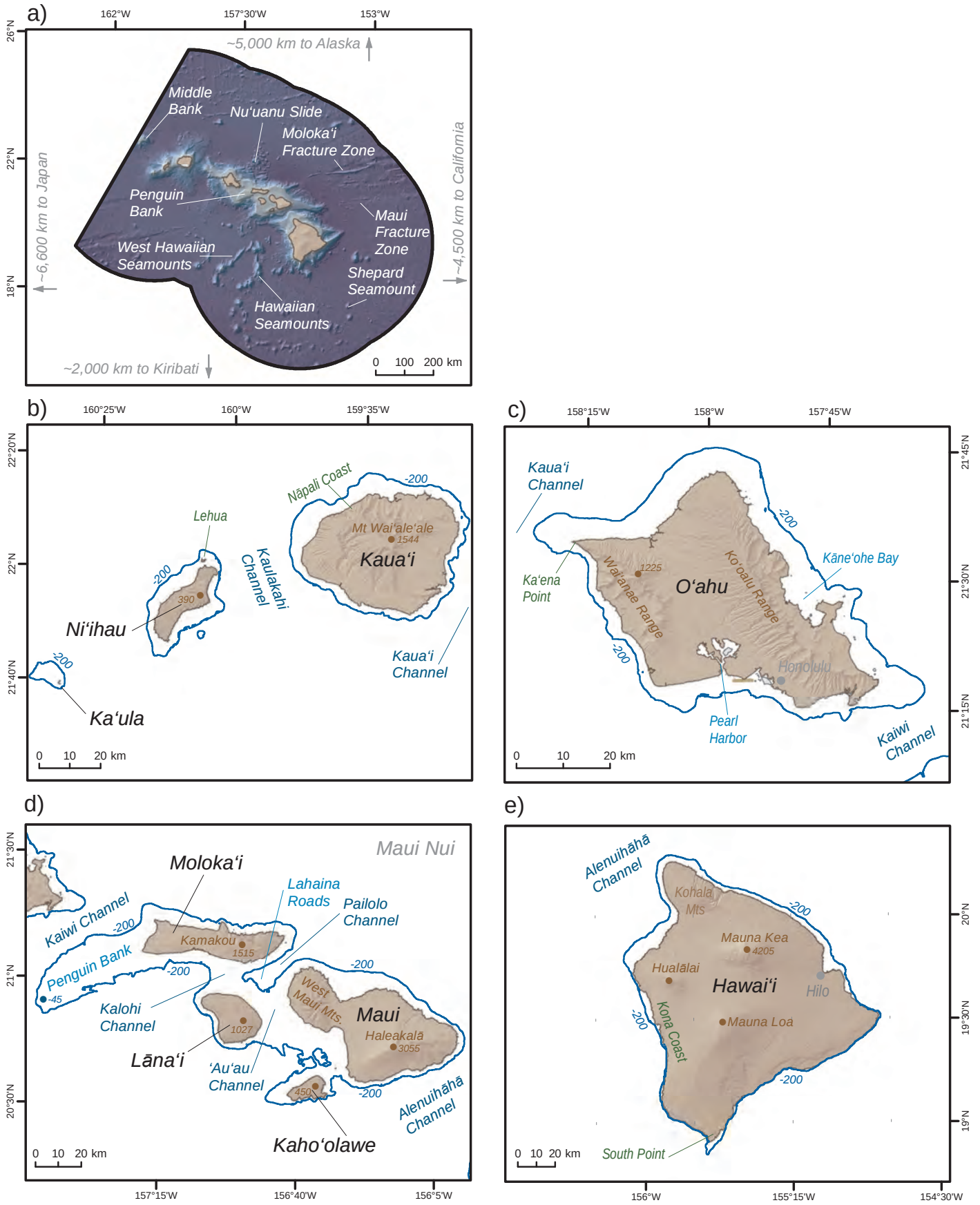

Figure 2.1. Key geographic features and place names around the Main Hawaiian Islands (MHI). These maps depict geographic features that are referenced in this chapter for: a) the project area; b) Ka'ula, Ni'ihau and Kaua'i; c) O'ahu; d) Maui Nui, which includes Moloka'i, Lāna'i, Maui and Kaho'olawe; and e) Hawai'i. All depths are in meters. Data sources: shoreline (Battista et al., 2007), elevation (USGS, 2015) and depths (NOAA NCEI, 2005; GEBCO, 2008)

2.2. METHODS AND DATA DESCRIPTION

We acquired and processed datasets describing climate (n=5), oceanography (n=32), distance (n=6), and seafloor topography (n=17) to describe key environmental drivers around the MHI. They were processed in ArcGIS (ESRI, 2014 or 2011), R and Matlab (Mathworks, 2014) software packages using different tools, and were acquired from a variety of sources, over several years and at multiple spatial resolutions. Tables 2.1-2.8 list these 60 datasets, including their definition, units, temporal resolutions, spatial resolutions, processing steps, source and download dates. These GIS datasets are available for download from NCEI (NCEI Accession 0155189; http://data.nodc.noaa.gov/cgi-bin/iso?id=gov.noaa.nodc:0155189). Datasets in Tables 2.1-2.6 and Table 2.8 are available for download 1.2x1.2 km spatial resolution. Table 2.7 datasets are at their native resolution. Preprocessing workflows were tailored to each dataset, depending on its type, source, and spatial resolution. For the atmospheric and oceanographic layers, datasets spanning 10 or more years were acquired, and binned temporally into seasonal climatologies. We binned these drivers into seasons to capture natural variability between summer (i.e., from May to October) and the winter (i.e., from November to April) in the MHI. There were also not enough animal sightings data to develop predictions at finer temporal resolutions (i.e., monthly or quarterly). Climatological means and standard deviations were calculated to capture broad temporal and spatial patterns in the seascape. Maximum values (e.g., above 95th percentile) were calculated for some environmental drivers (e.g., wave heights), and were inherent in other drivers (e.g., sea surface temperature anomalies and thermal stress anomalies). The distance, depth, and topographic datasets were not binned temporally, since broad-scale changes in these datasets would have occurred over much longer time scales (e.g., centuries) than studied here.

Table 2.1. Datasets describing the atmospheric conditions around the Main Hawaiian Islands (MHI) that influence its biogeography. These datasets were compiled to provide regional context for this assessment, and to be inputs for species distribution models. SD= Standard Deviation

	#	Dataset	Description	Units	Climatology & Statistic	Time Period	Source Dataset	Source Type	Native Spatial Resolution
Atmosphere	1	Wind Direction	Direction of wind at 10 m altitudes.	°	Circular Mean for Summer & Winter	7/1999 - 11/2009	Quik-SCAT (NASA, 2015a)	Sensor (Inactive as of 11/2009)	12.5x12.5 km
	2	Wind Divergence	Divergence (+) and convergence (-) of wind at 10 m altitudes.	m/s	Mean for Summer & Winter	7/1999 - 11/2009	Quik-SCAT (NASA, 2015a)	Sensor (Inactive as of 11/2009)	12.5x12.5 km
	3	Wind Speed	Speed of wind at 10 m altitudes.	m/s	Mean & SD for Summer & Winter	7/1999 - 11/2009	Quik-SCAT (NASA, 2015a)	Sensor (Inactive as of 11/2009)	12.5x12.5 km
	4	Wind Speed in the East-West Direction	Speed of wind in east-west direction at 10 m altitudes.	m/s	Mean & SD for Summer & Winter	7/1999 - 11/2009	Quik-SCAT (NASA, 2015a)	Sensor (Inactive as of 11/2009)	12.5x12.5 km
	5	Wind Speed in the North-South Direction	Speed of wind in north-south direction at 10 m altitudes.	m/s	Mean & SD for Summer & Winter	7/1999 - 11/2009	Quik-SCAT (NASA, 2015a)	Sensor (Inactive as of 11/2009)	12.5x12.5 km

	#	Processing Tools and Steps	Data Provider	Download Date
Atmosphere	1	Direction was calculated from wind speed in the easting (x-zonal) and northing y-(meridional) directions, binned, reprojected and resampled using custom R scripts.	NOAA NCCOS, 2016	May 2015
	2	Divergence was calculated from wind speed in the easting (x-zonal) and northing y-(meridional) directions, binned, reprojected and resampled using custom R scripts.	PacIOOS, 2015a	May 2015
	3	Speed was calculated from wind modulus, binned, reprojected and resampled using custom R scripts.	PacIOOS, 2015b	May 2015
	4	Speed was calculated in the east-west (x-zonal) direction, binned, reprojected and resampled using custom R scripts.	PacIOOS, 2015c	May 2015
	5	Speed was calculated in the north-south (y-meridional) direction, binned, reprojected and resampled using custom R scripts.	PacIOOS, 2015d	May 2015

Table 2.2. Datasets describing the biological oceanographic conditions around the MHI that influence its biogeography. These datasets were compiled to provide regional context for this assessment, and to be inputs for species distribution models. SD= Standard Deviation

	#	Dataset	Description	Units	Climatology & Statistic	Time Period	Source Dataset	Source Type	Native Spatial Resolution
Biological Oceanography	6	Chlorophyll-*a* Concentration	Chlorophyll-a concentrations at the sea surface.	mg/m³	Mean & SD for Summer & Winter	7/2002 - 10/2013	Aqua MODIS (NASA, 2016)	Sensor (Active as of 2/2016)	4x4 km
	7	Chlorophyll-*a* Front Frequency	The frequency of chlorophyll-*a* fronts. Frontal frequency is defined as the number of months for which a front was observed at a particular pixel, divided by the total number of months.	Number of occurrences	Mean for Summer & Winter	6/1/2002 - 12/1/2013	MUR (NASA, 2010)	Sensor composite (Ongoing as of 2/2016)	1x1 km
	8	Chlorophyll-*a* Front Persistence	The mean persistence of chlorophyll-*a* fronts. Frontal persistence is defined as the number of front observations divided by the number of cloud-free observations.	Number of occurrences	Mean for Summer & Winter	6/1/2002 - 12/1/2013	MUR (NASA, 2010)	Sensor composite (Ongoing as of 2/2016)	1x1 km
	9	Chlorophyll-*a* Front Strength	The mean strength of chlorophyll-*a* fronts. Frontal strength is the magnitude of change (log mg/m³) in surface chlorophyll-*a* concentrations within a moving window.	mg/m³ per pixel	Mean for Summer & Winter	6/1/2002 - 12/1/2013	MUR (NASA, 2010)	Sensor composite (Ongoing as of 2/2016)	1x1 km
	10	Net Primary Productivity (NPP)	Rate at which phytoplankton incorporate atmospheric carbon through photosynthesis.	mg Carbon/ m²/day	Mean for Summer & Winter	7/2002 - 10/2013	Aqua MODIS (NASA, 2016)	Sensor (Active as of 2/2016)	9x9 km

	#	Processing Tools and Steps	Data Provider	Download Date
Biological Oceanography	6	Datasets were downloaded and binned using MGET v0.8a56: Create Climatological Rasters for NASA OceanColor L3 SMI Product tool (Roberts et al., 2010) in ArcGIS (ESRI, 2011). Custom Python scripts were used to reproject and resample the datasets in ArcGIS (ESRI, 2011).	NASA, 2013a	October 2013
	7	A front was detected if there was a ≥0.06 log mg/m³ difference between two water masses within a moving window of 32x32 pixels. Daily front detections were then composited into monthly datasets (Scales et al., 2014, Miller et al., 2015b). Datasets were binned into seasons, reprojected and resampled using custom R scripts.	Miller, 2016	June 2015
	8	A front was detected if there was a ≥0.06 log mg/m³ difference between two water masses within a moving window of 32x32 pixels. The monthly mean of the front persistence was calculated, and spatially smoothed with a Gaussian filter of 5 pixels width. Datasets were binned into seasons, reprojected and resampled using custom R scripts.	Miller, 2016	June 2015
	9	A front was detected if there was a ≥0.06 log mg/m³ difference between two water masses within a moving window of 32x32 pixels. The monthly mean of the daily frontal gradient magnitude (i.e., strength) was calculated, and spatially smoothed with a Gaussian filter of 5 pixels width (Scales et al., 2014) Datasets were binned into seasons, reprojected and resampled using custom R scripts.	Miller, 2016	June 2015
	10	Datasets were downloaded, binned, reprojected and resampled using custom R scripts.	Oregon State University, 2013	December 2013

Table 2.3. Datasets describing key geographic features around the MHI that influence its biogeography. These datasets were compiled to provide regional context for this assessment, and to be inputs for species distribution models.

	#	Dataset	Description	Units	Climatology & Statistic	Time Period	Source Dataset	Source Type	Native Spatial Resolution
Distance	11	Shelf Edge	200 m isobath.	N/A	N/A	N/A	N/A	N/A	N/A
	12	Distance to Shelf Edge	Euclidean distance to/from the 200 m isobath.	m	N/A	N/A	N/A	N/A	N/A
	13	Shoreline	Shoreline of the MHI.	N/A	N/A	2007	N/A	N/A	N/A
	14	Distance to Shoreline	Euclidean distance to/from the shoreline.	m	N/A	N/A	N/A	N/A	N/A
	15	Seamounts	Seamount footprints at 50 m depth increments from 100 to 2,750 m depths, and 100 to 4,500 m depths.	N/A	N/A	N/A	N/A	N/A	N/A
	16	Distance to Seamounts	Average euclidean distance to/from seamount footprints 100-2,750 m deep and 100-4,500 m deep.	m	Mean	N/A	N/A	N/A	N/A

	#	Processing Tools and Steps	Data Provider	Download Date
Distance	11	The 200 m isobath was extracted from the 90x90 m modeled depth surface using ArcGIS Contour tool (ESRI, 2011).	NOAA NCCOS, 2016	N/A
	12	Distances were calculated in 1.2x1.2 km cells using ArcGIS's Euclidean Distance tool (ESRI, 2011).	NOAA NCCOS, 2016	N/A
	13	Shorelines were extracted from NOAA's 2007 Benthic Habitat Maps.	Battista et al., 2007	September 2014
	14	Distances were calculated in 1.2x1.2 km cells using ArcGIS's Euclidean Distance tool (ESRI, 2011).	NOAA NCCOS, 2016	N/A
	15	Footprints were extracted from the 90x90 m modeled depth surface at 50 m increments from 100 to 2,750 m depths, and 100 to 4,500 m depths using custom Python scripts. Middle Bank was included in these calculations because it like a seamount (i.e., it is isolated geographically and is much shallower than the surrounding seabed).	NOAA NCCOS, 2016	N/A
	16	Distance was measured to the edge of a seamount's footprint. Distances to these footprints were calculated in 1.2x1.2 km cells using ArcGIS's Euclidean Distance (ESRI, 2011), and averaged spatially using ArcGIS's Cell Statistics tool (ESRI, 2011) and custom Python scripts.	NOAA NCCOS, 2016	N/A

Environmental Setting

Table 2.4. Datasets describing the physical oceanographic conditions (Water Clarity, Water Height and Water Movement) around the MHI that influence its biogeography. These datasets were compiled to provide regional context for this assessment, and to be inputs for species distribution models. SD= Standard Deviation

	#	Dataset	Description	Units	Climatology & Statistic	Time Period	Source Dataset	Source Type	Native Spatial Resolution
Water Clarity	17	Euphotic Depth	Depth below which available light is insufficient to support significant photosynthesis.	m	Mean for Summer & Winter	7/2002 - 10/2013	Aqua MODIS (NASA, 2016)	Sensor (Active as of 2/2016)	4x4 km
	18	Turbidity	The amount of organic and inorganic suspended solids in the water at the sea surface.	Steridians^{-1}	Mean & SD for Summer & Winter	7/2002 - 3/2015	Aqua MODIS, 547 nanometers band (NASA, 2016)	Sensor (Active as of 2/2016)	4x4 km
Water Height	19	Sea Surface Height (SSH)	Sea surface heights above the geoid.	m	Mean & SD for Summer & Winter	10/1992 - 12/2012	MADT	Sensor composite (Ongoing as of 2/2016)	25x25 km
Water Movement	20	Bottom Current Direction	Direction of bottom currents at deepest point in the HYCOM oceanographic model.	m/s	Annual Circular Mean	10/1992 - 12/2012	HYCOM + NCODA Global 1/12° Reanalysis	Model (Updates planned as of 2/2016)	9x9 km
	21	Bottom Current Speed	Speed of currents at deepest point in HYCOM oceanographic model.	m/s	Annual Mean & SD	10/1992 - 12/2012	HYCOM + NCODA Global 1/12° Reanalysis	Model (Updates planned as of 2/2016)	9x9 km
	22	Bottom Current Speed in the East-West Direction	Speed of currents in the u (east-west direction) at deepest point in HYCOM oceanographic model.	m/s	Annual Mean	10/1992 - 12/2012	HYCOM + NCODA Global 1/12° Reanalysis	Model (Updates planned as of 2/2016)	9x9 km
	23	Bottom Current Speed in the North-South Direction	Speed of currents in the v (north-south direciton) at deepest point in HYCOM oceanographic model.	m/s	Annual Mean	10/1992 - 12/2012	HYCOM + NCODA Global 1/12° Reanalysis	Model (Updates planned as of 2/2016)	9x9 km
	24	Mixed Layer Depth (MLD)	Depth to which water is mixed because of various physical processes. Above this depth, the water column is fairly homogenous.	m	Mean for Summer & Winter	10/1992 - 12/2012	HYCOM + NCODA Global 1/12° Reanalysis	Model (Updates planned as of 2/2016)	9x9 km
	25	Probability of Anti-cyclonic Eddies	Probability that anti-cyclonic (clockwise) eddies will form.	%	Mean for Summer & Winter	1/1/1993 - 4/2014	MADT	Sensor composite (Ongoing as of 2/2016)	25x25 km

	#	Processing Tools and Steps	Data Provider	Download Date
Water Clarity	17	Datasets were downloaded and binned using MGET v0.8a56: Create Climatological Rasters for NASA OceanColor L3 SMI Product tool (Roberts et al., 2010) in ArcGIS (ESRI, 2011). Custom Python scripts were used to reproject and resample the datasets in ArcGIS (ESRI, 2011).	NASA, 2013b	October 2013
	18	Datasets were downloaded and binned using MGET v0.8a56: Create Climatological Rasters for NASA OceanColor L3 SMI Product tool (Roberts et al., 2010) in ArcGIS (ESRI, 2011). Custom Python scripts were used to reproject and resample the datasets in ArcGIS (ESRI, 2011).	NASA, 2015b	April 2015
Water Height	19	Maps of Absolute Dynamic Topography (MADT) were downloaded and binned using MGET v0.8a56: Create Climatological Rasters for Aviso SSH Product tool (Roberts et al., 2010) in ArcGIS (ESRI, 2011). Custom Python scripts were used to reproject and resample the datasets in ArcGIS (ESRI, 2011).	Aviso et al., 2014	December 2013
Water Movement	20	Direction was calculated from speed in the u (easting) and v (northing) directions, binned, reprojected and resampled using custom R scripts.	HYCOM consortium, 2014	September 2014
	21	Datasets were downloaded, binned, reprojected and resampled using custom R scripts.	HYCOM consortium, 2014	September 2014
	22	Datasets were downloaded, binned, reprojected and resampled using custom R scripts.	HYCOM consortium, 2014	September 2014
	23	Datasets were downloaded, binned, reprojected and resampled using custom R scripts.	HYCOM consortium, 2014	September 2014
	24	Datasets were downloaded using custom R scripts. MLD was calculated from HYCOM depth, water temperature and salinity values using custom Matlab scripts. Outputs were binned, reprojected and resampled using custom R scripts.	HYCOM consortium, 2014	September 2014
	25	Datasets were downloaded and binned using MGET v0.8a56: Find Okubo-Weiss Eddies in AVISO DUACS 2014 SSH Product tool (Roberts et al., 2010) in ArcGIS (ESRI, 2011). Custom Python scripts were used to reproject and resample the datasets in ArcGIS (ESRI, 2011).	Aviso et al., 2014	September 2014

Table 2.5. Datasets describing the physical oceanographic conditions (Water Movement continued) around the MHI that influence its biogeography. These datasets were compiled to provide regional context for this assessment, and to be inputs for species distribution models. SD= Standard Deviation

	#	Dataset	Description	Units	Climatology & Statistic	Time Period	Source Dataset	Source Type	Native Spatial Resolution
Water Movement Cont.	26	Probability of Cyclonic Eddies	Probability that cyclonic (counter-clockwise) eddies will form.	%	Mean for Summer & Winter	1/1/1993 - 4/2014	MADT	Sensor composite (Ongoing as of 2/2016)	25x25 km
	27	Probability of Eddy Rings	Probability that cyclonic or anticyclonic eddies will form.	%	Mean for Summer & Winter	1/1/1993 - 4/2014	MADT	Sensor composite (Ongoing as of 2/2016)	25x25 km
	28	Surface Current Direction	Direction of currents at sea surface.	°	Circular Mean for Summer & Winter	10/1992 - 12/2012	HYCOM + NCODA Global 1/12° Reanalysis	Model (Updates planned as of 2/2016)	9x9 km
	29	Surface Current Divergence	Divergence (+) and convergence (-) of currents at sea surface.	m/s	Mean for Summer & Winter	10/1992 - 12/2012	HYCOM + NCODA Global 1/12° Reanalysis	Model (Updates planned as of 2/2016)	9x9 km
	30	Surface Current Speed	Speed of currents at sea surface.	m/s	Mean & SD for Summer & Winter	10/1992 - 12/2012	HYCOM + NCODA Global 1/12° Reanalysis	Model (Updates planned as of 2/2016)	9x9 km
	31	Surface Current Speed in the East-West Direction	Speed of currents in the u (east-west direction) at sea surface.	m/s	Mean for Summer & Winter	10/1992 - 12/2012	HYCOM + NCODA Global 1/12° Reanalysis	Model (Updates planned as of 2/2016)	9x9 km
	32	Surface Current Speed in the North-South Direction	Speed of currents in the v (north-south direction) at sea surface.	m/s	Mean for Summer & Winter	10/1992 - 12/2012	HYCOM + NCODA Global 1/12° Reanalysis	Model (Updates planned as of 2/2016)	9x9 km
	33	Surface Current Vorticity	Clockwise (-) and counter-clockwise (+) rotation of currents at sea surface.	m/s	Mean for Summer & Winter	10/1992 - 12/2012	HYCOM + NCODA Global 1/12° Reanalysis	Model (Updates planned as of 2/2016)	9x9 km
	34	Upwelling	Upwelling (+) and downwelling (-) of surface waters due to surface winds and Ekman transport.	m/s	Mean for Summer & Winter	7/1999 - 11/2009	Quik-SCAT (NASA, 2015a)	Sensor (Inactive as of 11/2009)	12.5x12.5 km

	#	Processing Tools and Steps	Data Provider	Download Date
Water Movement Cont.	26	Datasets were downloaded and binned using MGET v0.8a56: Find Okubo-Weiss Eddies in AVISO DUACS 2014 SSH Product tool (Roberts et al., 2010) in ArcGIS (ESRI, 2011). Custom Python scripts were used to reproject and resample the datasets in ArcGIS (ESRI, 2011).	Aviso et al., 2014	September 2014
	27	Datasets were downloaded and binned using MGET v0.8a56: Find Okubo-Weiss Eddies in AVISO DUACS 2014 SSH Product tool (Roberts et al., 2010) in ArcGIS (ESRI, 2011). Custom Python scripts were used to reproject and resample the datasets in ArcGIS (ESRI, 2011).	Aviso et al., 2014	September 2014
	28	Direction was calculated from speed in the u (easting) and v (northing) directions, binned, reprojected and resampled using custom R scripts.	HYCOM consortium, 2014	September 2014
	29	Divergence was calculated from surface current speed in the u and v directions, binned, reprojected and resampled using custom R scripts.	HYCOM consortium, 2014	September 2014
	30	Datasets were downloaded, binned, reprojected and resampled using custom R scripts.	HYCOM consortium, 2014	September 2014
	31	Datasets were downloaded, binned, reprojected and resampled using custom R scripts.	HYCOM consortium, 2014	September 2014
	32	Datasets were downloaded, binned, reprojected and resampled using custom R scripts.	HYCOM consortium, 2014	September 2014
	33	Vorticity was calculated from surface current speed in the u and v directions, binned, reprojected and resampled using custom R scripts.	HYCOM consortium, 2014	September 2014
	34	Datasets were downloaded, binned, reprojected and resampled using custom R scripts.	PacIOOS, 2015e	May 2015

Environmental Setting

Table 2.6. Datasets describing the physical oceanographic conditions (Water Temperature and Waves) around the MHI that influence its biogeography. These datasets were compiled to provide regional context for this assessment, and to be inputs for species distribution models. SD= Standard Deviation

	#	Dataset	Description	Units	Climatology & Statistic	Time Period	Source Dataset	Source Type	Native Spatial Resolution
Water Temperature	35	Bottom Temperature	Temperature of water at deepest point in HYCOM oceanographic model.	°C	Annual Mean	10/1992 - 12/2012	HYCOM + NCODA Global 1/12° Reanalysis	Model (Updates planned as of 2/2016)	9x9 km
	36	Sea Surface Temperature (SST)	Temperature of water at sea surface.	°C	Mean & SD for Summer & Winter	7/2002 - 7/2014	MUR (NASA, 2010)	Sensor composite (Ongoing as of 2/2016)	1x1 km
	37	Sea Surface Temperature Anomaly (SSTA) Frequency	The number of times (over the previous 52 weeks) that SSTA were ≥1°C. SSTA is calculated as the weekly SST minus weekly climatological SST.	Number of occurrences	Mean for Summer & Winter	1/1982 - 12/2009	CORTAD v3	Sensor Derivative (Ongoing as of 2/2016)	4x4 km
	38	SST Front Frequency	The frequency of SST fronts. Frontal frequency is defined as the number of months for which a front was observed at a particular pixel, divided by the total number of months.	Number of occurrences	Mean for Summer & Winter	6/2002 - 12/2013	MUR (NASA, 2010)	Sensor composite (Ongoing as of 2/2016)	1x1 km
	39	SST Front Persistence	The mean persistence of SST fronts. Frontal persistence is defined as the number of front observations divided by the number of cloud-free observations.	Number of occurrences	Mean for Summer & Winter	6/2002 - 12/2013	MUR (NASA, 2010)	Sensor composite (Ongoing as of 2/2016)	1x1 km
	40	SST Front Strength	The mean strength of SST fronts. Frontal strength is defined as the magnitude of change (°C) in surface water temperatures within a moving window.	°C per pixel	Mean for Summer & Winter	6/2002 - 12/2013	MUR (NASA, 2010)	Sensor composite (Ongoing as of 2/2016)	1x1 km
	41	Thermal Stress Anomalies (TSA) Frequency	The number of times (over the previous 52 weeks) that TSA were ≥1°C. TSA is calculated as the weekly SST minus the maximum weekly climatological SST.	Number of occurrences	Mean for Summer & Winter	1/1982 - 12/2009	CORTAD v3	Sensor Derivative (Ongoing as of 2/2016)	4x4 km
Waves	42	Wave Peak Periods	Wave period with the highest energy.	s	Mean & SD for Summer & Winter	1/2000 - 12/2009	Wave Watch III (Tolman 2009; NOAA NCEP, 2015) Hindcast	Model (Updates planned as of 2/2016)	5x5 km
	43	Wave Significant Heights	Mean heights (from trough to crest) of the highest third of waves.	m	Mean & SD for Summer & Winter	1/2000 - 12/2009	Wave Watch III (Tolman 2009; NOAA NCEP, 2015) Hindcast	Model (Updates planned as of 2/2016)	5x5 km

	#	Processing Tools and Steps	Data Provider	Download Date
Water Temperature	35	Datasets were downloaded, binned, reprojected and resampled using custom R scripts.	HYCOM consortium, 2014	September 2014
	36	Datasets were downloaded and binned using MGET v0.8a56: Create Climatological Rasters for GHRSST L4 SST tool (Roberts et al., 2010) in ArcGIS (ESRI, 2011). Custom Python scripts were used to reproject and resample the datasets in ArcGIS (ESRI, 2011).	NASA, 2014	September 2014
	37	Datasets were downloaded and binned using MGET v0.8a56: Create Rasters for CoRTAD 3D Variable tool (Roberts et al., 2010) in ArcGIS (ESRI, 2011). Custom Python scripts were used to reproject and resample the datasets in ArcGIS (ESRI, 2011).	Casey, 2010	June 2014
	38	A front is defined as a ≥ 0.4 °C difference in SST between two water masses within a 32x32 pixel moving window. Daily front detections were then aggregated into monthly datasets (Scales et al., 2014; Miller and Christodoulou, 2014). Datasets were binned into seasons, reprojected and resampled using custom R scripts.	Miller, 2016	June 2015
	39	A front was detected if there was at least 0.4°C difference in SST between two water masses within a moving window of 32x32 pixels. The monthly mean of the front persistence was calculated, and spatially smoothed with a Gaussian filter of 5 pixels width. Datasets were binned into seasons, reprojected and resampled using custom R scripts.	Miller, 2016	June 2015
	40	A front was detected if there was at least 0.4°C difference in SST between two water masses within a moving window of 32x32 pixels. The monthly mean of the daily frontal gradient magnitude (i.e., strength) was calculated, and spatially smoothed with a Gaussian filter of 5 pixels width (Scales et al., 2014; Miller et al., 2015a). Datasets were binned into seasons, reprojected and resampled using custom R scripts.	Miller, 2016	June 2015
	41	Datasets were downloaded and binned using MGET v0.8a56: Create Rasters for CoRTAD 3D Variable tool (Roberts et al., 2010) in ArcGIS (ESRI, 2011). Custom Python scripts were used to reproject and resample the datasets in ArcGIS (ESRI, 2011).	Casey, 2010	June 2014
Waves	42	Wave periods were computed by the WAVEWATCH III (WW3) wave model (Tolman, 2009), forced by 10 years of wind observations over the Pacific Ocean (Stopa et al., 2013). Modeled datasets were binned, reprojected and resampled using custom Matlab and R scripts.	Cheung, 2016; Stopa et al., 2013	February 2014
	43	Wave heights were computed by the WAVEWATCH III (WW3) wave model (Tolman, 2009), forced by 10 years of wind observations over the Pacific Ocean (Stopa et al., 2013). Modeled datasets were binned, reprojected and resampled using custom Matlab and R scripts.	Cheung, 2016; Stopa et al., 2013	February 2014

Table 2.7. Datasets describing elevations and bathymetry (i.e., Seafloor Depth) around the MHI that influence its biogeography. These datasets were compiled to provide regional context for this assessment, to be inputs for species distribution models, to identify data gaps and to describe data precision. SD= Standard Deviation

	#	Dataset	Description	Units	Statistic	Time Period	Source Dataset	Native Spatial Resolution
	44	Elevation	Terrestrial elevations.	m	-, SD	2015	1/3 arc-second Digital Elevation Model	10x10 m
Seafloor Depth	45	Depth Source (<100 m)	Seafloor depths less than 100 m.	m	-	2005	3 arc-second CRM	90x90 m
	46	Depth Source (≥100 m)	Seafloor depths ≥100 m.	m	-	2008	30 arc-second GEBCO 08	1,094x1,094 m
	47	Depth Model ≥100 m	Modeled seafloor depths ≥100 m.	m	-	-	-	90x90 m
	48	Depth Model ≥100 m (Standard Error)	Standard error associated with the modeled depth surface for areas ≥100 m deep.	m	Mean	-	-	90x90 m
	49	Depth Model ≥100 m (Accuracy)	Accuracy of modeled depth surface for areas ≥100 m deep.	m	Mean	-	-	90x90 m
	50	Depth	Final depth surface for the entire project area created by blending datasets #45 and 47.	m	-	-	-	90x90 m
Seafloor Surveys	51	Digital Depth Data	The location of digital soundings data.	N/A	N/A	1900 -2009	Multiple. See NOAA NCEI, 2015b.	N/A
	52	Ship Tracklines (Multibeam SoNARs)	Ship tracklines for multibeam sound navigation and ranging (SoNAR) surveys.	N/A	N/A	1980-2014	Multiple. See NOAA NCEI, 2015b.	N/A
	53	Ship Tracklines (Singlebeam SoNARs)	Ship tracklines for singlebeam sound navigation and ranging (SoNAR) surveys.	N/A	N/A	1950-2009	Multiple. See NOAA NCEI, 2015b.	N/A

	#	Processing Tools and Steps	Data Provider	Download Date
	44	This 1/3 arc-second dataset was generated by the USGS. It was created by interpolating between contours in the USGS's 7.5' topographic maps. Standard deviations were calculated in 3x3 cell moving windows using ArcGIS's Focal Statistics tool (ESRI, 2011).	USGS, 2015	September 2015
Seafloor Depth	45	This 3 arc-seconds dataset is the U.S. Coastal Relief Model (CRM) for Hawai'i. It was created by NOAA's NCEI from multilple data sources.	NOAA NCEI, 2005	January 2014
	46	This 30 arc-seconds depth dataset was created by the GEBCO from multilple data sources.	GEBCO, 2008	January 2014
	47	This dataset was created using GEBCO data (≥100 m) and ordinary kriging. Please see the chapter text for a detailed description of the methods, and evaluation of the surface.	NOAA NCCOS, 2016	January 2014
	48	This dataset describes the precision associated with the modeled depth surface (#47). It was calculated during the kriging process using cross validation in ArcGIS's Geostatistical Analyst extension (ESRI, 2011).	NOAA NCCOS, 2016	January 2014
	49	This dataset describes the accuracy of the modeled depth surface (#47). It was calculated in R using an independent subset (50%) of depth points set aside at the beginning of the modelling process.	NOAA NCCOS, 2016	January 2014
	50	This dataset was created by blending NOAA's CRM (i.e., #45) with predicted depths generated using GEBCO data (≥100 m) and ordinary kriging (i.e., #47). Please see the chapter text for a detailed description of the methods, and evaluation of the surface.	NOAA NCCOS, 2016	January 2014
Seafloor Surveys	51	This dataset was downloaded from NOAA NCEI and clipped to the project area using ArcGIS's Clip tool (ESRI, 2011). These data are for visualization, and were used not used in the depth modeling process.	NOAA NCEI, 2015b	September 2015
	52	This dataset was downloaded from NOAA NCEI and clipped to the project area using ArcGIS's Clip tool (ESRI, 2011). These data are for visualization, and were used not used in the depth modeling process.	NOAA NCEI, 2015b	September 2015
	53	These datasets were downloaded from NOAA NCEI and clipped to the project area using ArcGIS's Clip tool (ESRI, 2011). These data are for visualization, and were used not used in the depth modeling process.	NOAA NCEI, 2015b	September 2015

Table 2.8. Datasets describing seafloor topography around the MHI that influence its biogeography. These datasets were compiled to provide regional context for this assessment, to be inputs for species distribution models, to identify data gaps and to describe data precision. SD= Standard Deviation

	#	Dataset	Description	Units	Statistic	Time Period	Source Dataset	Native Spatial Resolution
Seafloor Topography	54	Depth (Mean, SD)	Mean and standard deviation of modeled seafloor depths.	m	Mean, SD	-	Table 2.7, #50	90x90 m
	55	Total Curvature	Curvature of the seafloor. Seafloor can be convex (-), concave (+) or flat (0).	Radians per m^2	Mean	-	Table 2.7, #50	90x90 m
	56	Planform Curvature	Curvature of surface perpendicular to the direction of the maximum slope. Surface can be convex (-), concave (+) or flat (0).	Radians/m	Mean	-	Table 2.7, #50	90x90 m
	57	Profile Curvature	Curvature of surface parallel to the direction of the maximum slope. Surface can be convex (-), concave (+) or flat (0).	Radians/m	Mean	-	Table 2.7, #50	90x90 m
	58	Rugosity	Ratio of surface area to planar area. The higher the number, the bumpier the seafloor.	unit-less	Mean	-	Table 2.7, #50	90x90 m
	59	Slope	Maximum rate of change in depth.	°	Mean	-	Table 2.7, #50	90x90 m
	60	Slope Rate of Change	Maximum rate of change in slope.	°	Mean	-	Table 2.7, #50	90x90 m

	#	Processing Tools and Steps	Data Provider	Download Date
Seafloor Topography	54	This dataset was created from the final depth surface (#50), and was binned in in 1.2x1.2 km cells using ArcGIS's Zonal Statistics tool (ESRI, 2011).	NOAA NCCOS, 2016	-
	55	This dataset was created from the final depth surface (#50) using DEM Surface Tools Curvature tool (Jenness, 2013). It was binned in 1.2x1.2 km cells using ArcGIS's Zonal Statistics tool (ESRI, 2011).	NOAA NCCOS, 2016	-
	56	This dataset was created from the final depth surface (#50) using DEM Surface Tools Curvature tool (Jenness 2013). It was binned in 1.2x1.2 km cells using ArcGIS's Zonal Statistics tool (ESRI, 2011).	NOAA NCCOS, 2016	-
	57	This dataset was created from the final depth surface (#50) using DEM Surface Tools Curvature tool (Jenness, 2013). It was binned in 1.2x1.2 km cells using ArcGIS's Zonal Statistics tool (ESRI, 2011).	NOAA NCCOS, 2016	-
	58	This dataset was created from the final depth surface (#50) using DEM Surface Tools: Calculate Surface Ratio Raster tool (Jenness, 2013) in ArcGIS (ESRI, 2011). It was binned in 1.2x1.2 km cells using ArcGIS's Zonal Statistics tool (ESRI, 2011).	NOAA NCCOS, 2016	-
	59	This dataset was created from the final depth surface (#50) using ArcGIS's Slope tool (ESRI, 2011). It was binned in 1.2x1.2 km cells using ArcGIS's Zonal Statistics tool (ESRI, 2011).	NOAA NCCOS, 2016	-
	60	This dataset was created from the final depth surface (#50) using ArcGIS's Slope tool (ESRI, 2011). It was binned in 1.2x1.2 km cells using ArcGIS's Zonal Statistics tool (ESRI, 2011).	NOAA NCCOS, 2016	-

We created a 90x90 m depth surface for the entire project area. This surface was created by blending two modeled depth surfaces. We used NOAA's Coastal Relief Model (CRM) in areas less than 100 m deep (NOAA NCEI, 2005), and we created a geostatistical model using depths from the General Bathymetric Chart of the Oceans (GEBCO; GEBCO, 2008) for areas deeper than 100 m. Geostatistical modeling creates predictions by measuring spatial autocorrelation across a dataset, and uses those relationships to predict values at nearby locations. This workflow was completed in R and ArcGIS (ESRI, 2011). Depths greater than 100 m in the study area were extracted from GEBCO. Fifty percent of these GEBCO depths were randomly selected, and set aside for independent validation (i.e., to assess vertical error and bias). Ordinary kriging was used to develop a modeled depth surface for areas deeper than 100 m in ArcGIS (ESRI, 2011). The input parameters for the geostatistical model were as follows: transformation type = log, trend removal = second order local polynomial, kernel function = exponential, nugget = 5.3 e-7, range = 2,401, anisotropy = no, sector type = 4 with 45° offset. The spatial resolution of the kriged depth surface was 90x90 m. This resolution was chosen because it matched that of the CRM in the MHI (NOAA NCEI, 2005). The vertical error associated with this kriged depth surface was evaluated using cross validation and the dataset subset randomly extracted from GEBCO at the beginning. These different ways of measuring vertical error are described in Section 2.5. We blended the final kriged depth surface with the existing CRM using ArcGIS's Mosaic tool (ESRI, 2011) to create a seamless depth 90x90 m surface for the entire project area. Any remaining no data gaps were filled using a custom script in ArcGIS's raster calculator (ESRI, 2011).

Once the depth surface and preprocessing steps (listed in Tables 2.2-2.8) were complete, all datasets were reprojected to a common coordinate system (i.e., WGS 1984 Oblique Mercator) using reprojection tools in R and/or ArcGIS (ESRI, 2011). The properties of this customized coordinate system were as follows: linear unit = meter, angular unit = 0.017°, false easting = 0, false northing = 0, scale factor = 0.9996, azimuth = 60, longitude of center = -157.1895 and latitude of center = 20.5713. This coordinate system allowed us to use one common projection across the entire study area instead of using multiple Universal Transverse Mercator (UTM) zones. This projection is similar to a UTM zone, except it is angled to optimally align with the axis of the MHI. This orientation minimized the distortion of shapes and distances, and satisfied isotropy for spatial modelling within the project boundaries.

Maui coast. Photo: Bryan M. Costa (NOAA NOS/NCCOS)

After being reprojected, we aggregated each dataset into a common spatial framework consisting of 1.2x1.2 km square bins. The bin size and shape was chosen so that it matched BOEM's proposed lease aliquots in the MHI Exclusive Economic Zone (EEZ). Elevation was not spatially binned because there are no aliquots on land. Datasets that had native spatial resolutions finer than 1.2x1.2 km (e.g., depth) were binned into this spatial framework using the Zonal Statistics functions in R and or ArcGIS (ESRI, 2011). Datasets that had native, spatial resolutions coarser than 1.2x1.2 km (e.g., sea surface temperature) were resampled to this spatial resolution using cubic convolution resampling tools in R and ArcGIS (ESRI, 2011). Cubic convolution was used to better preserve the boundaries of spatial patterns in these datasets. Mean and/or standard deviations were calculated in each spatial bin. Nearshore data gaps were filled using the "inpaint" function in Matlab (D'Errico, 2014). We used the final datasets as inputs to predict spatial distributions of deep corals, reef fish, cetaceans and seabirds in the project area.

2.3. RESULTS AND DISCUSSION (ELEVATION, DEPTH AND TOPOGRAPHY)

The MHI are mountainous, oceanic islands. Their rugged topographies and complex shorelines (Figure 2.2; Figure 2.3a, b) were created by erupting volcanoes and sculpted by geologic forces over millions of years (Juvik and Juvik, 1998; Fletcher et al., 2008). The archipelago was formed as the Pacific Plate moved northwest across the Hawai'i hotspot, where molten rock and gases were pushed to the surface (Juvik and Juvik, 1998; Fletcher et al., 2008). This hotspot is currently under or nearby the island of Hawai'i (Fletcher et al., 2008), which has three of the MHI's five active volcanoes (USGS, 2016). These volcanoes include Mauna Loa (4,169 m), Hualālai (2,521 m) and Kīlauea (1,219 m). The MHI's other active volcanoes include Halealakā (3,055 m) on Maui, and the Lō'ihi Seamount located about 30 km southeast of the island of Hawai'i. The rest of the volcanoes in the MHI are dormant or extinct. These volcanoes include: Mauna Kea (4,205 m) and the Kohala Mountains (1,603 m) on Hawai'i, the west Maui Mountains (1,764 m) on Maui, Kamakou (1,515 m) on Moloka'i, the Wai'anae Range (1,225 m) and Ko'olau Range (960 m) on O'ahu, and Mauna Wai'ale'ale (1,544 m) on Kaua'i. Lāna'i (1,027 m), Kaho'olawe (450 m) and Ni'ihau (390 m) also have mountainous, volcanic landscapes, but their topographies are less rugged than the other islands. Although the size of volcanoes varies among islands, their elevations and topographies influence almost every aspect of the MHI's weather and climate as a whole (Juvik and Juvik, 1998). These impacts are discussed in detail in Section 2.4.4.

The seascape of the MHI was shaped by many of the same processes that formed its terrestrial landscape. Shifting tectonic plates, erupting volcanoes, changing sea levels and erosional processes shaped the topography of the seafloor over millions of years (Fletcher et al., 2008). These physical processes created a narrow shelf around

the MHI, which is often only a few kilometers wide (Figure 2.3c, d; Figures A.1 and A.2). This narrow shelf drops off quickly from 200 m depths to an abyssal plain at over 4,800 m. Such dramatic changes in depth occur over distances as short as 15 km (e.g., near South Point, Hawai'i). Consequently, the slopes along these drop-offs can be upwards of 35° in some steeper locations. Numerous seamounts protrude from the abyssal plains with heights up to 4,000 m. Some seamounts are located southeast of Hawai'i (e.g., Lō'ihi), but the majority are located south of O'ahu and Maui within the MHI EEZ (Figure 2.1a; Figure 2.3e, f). Collectively, these seamounts are known as the West Hawai'i and Hawaiian Seamounts (also called the Navigator or Geologist Seamounts). These seamounts include Cross, Bishop, Swordfish, Pensacola, McCall, Jaggar, Indianapolis and Day among others. Middle Bank and Penguin Bank (while not seamounts) are two other prominent underwater features within the MHI EEZ (Figure 2.1a). Middle Bank is an isolated bathymetric feature located about 130 km northwest of Ni'ihau. It has a flat top that plateaus around 35 m deep. Penguin Bank is slightly deeper than Middle Bank (i.e., its shallowest point is around 45 m), and extends southwest from Moloka'i's western shoreline. It is connected geologically to Maui Nui, which is made up of the islands of Maui, Moloka'i, Lāna'i and Kaho'olawe. Like with the MHI's mountains, these seamounts and banks interact with currents to influence local patterns in the MHI's oceanography (Boehlert and Genin, 1987). These impacts are discussed in more detail in Section 2.4.5.

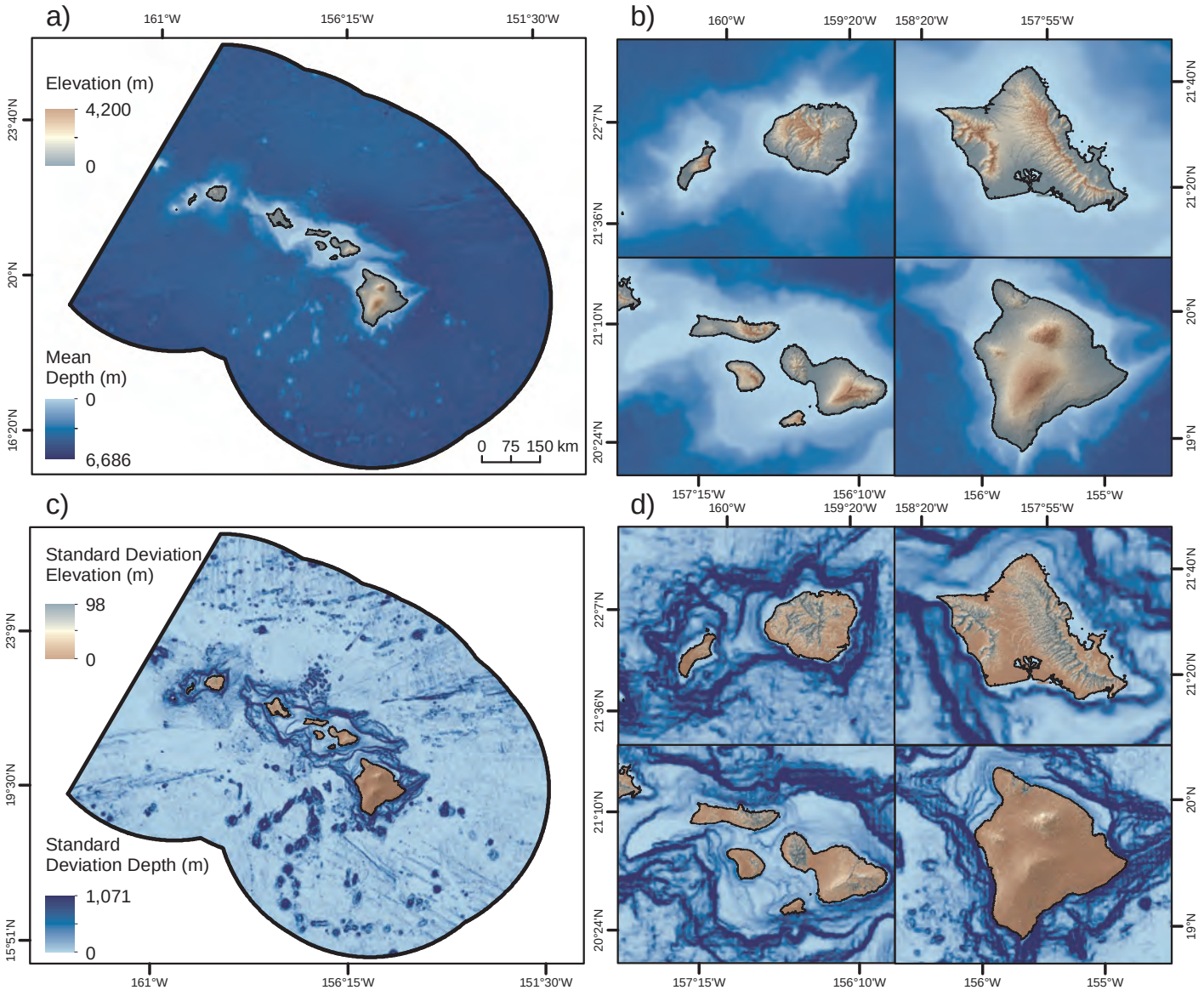

Figure 2.2. Elevations, depths and variation in both around the MHI. These maps depict the: (a, b) elevations (m) and mean seafloor depths (m), and (c, d) the standard deviation (SD) of elevations (m) and seafloor depths (m) within the study area. Mean depths were calculated within 1.2x1.2 km square spatial bins. SD of elevation and depth were calculated within 30x30 m and 1.2x1.2 km square spatial bins, respectively. Dates: N/A. Data sources: Table 2.7. #44 and Table 2.8. #54

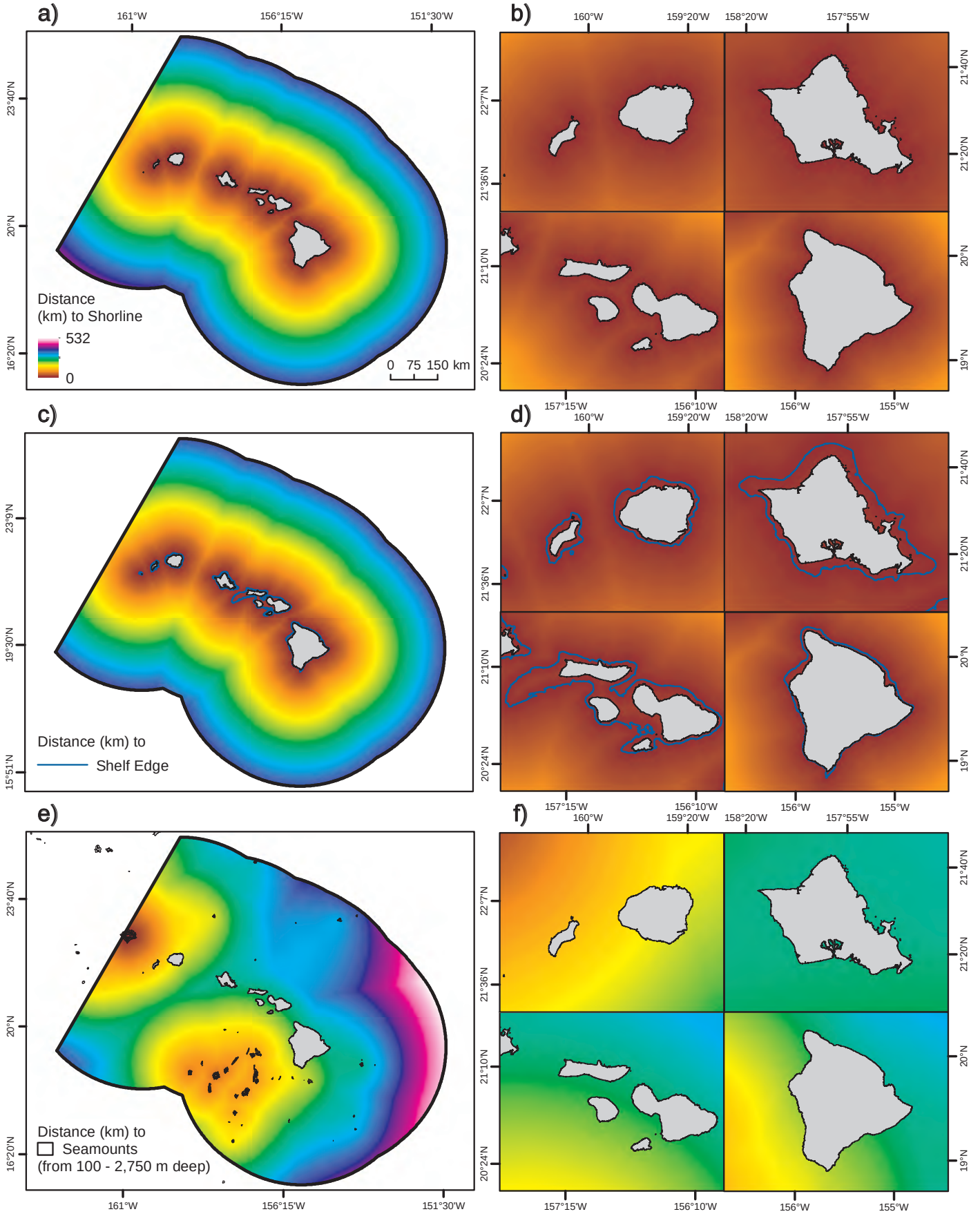

Figure 2.3. Distance from key geographic features around the MHI. These maps depict the distance (km) from: a) the shoreline, b) the shelf edge (i.e., 200 m isobath), and c) key seamounts (100 to 2,750 m deep) within the study area. The same color ramp was used for maps a) to (f). Dates: N/A. Data source: Table 2.3. #11-16

2.4. RESULTS AND DISCUSSION (THE COUPLED CLIMATE AND OCEAN)

Compared to continental climates, the maritime (i.e., ocean-influenced) climate of the MHI is relatively stable over time with little day-to-day and month-to-month variability in the weather at sea-level. The MHI's climate is relatively stable because of its location in the tropical latitudes (between 19° and 22° north) and its isolation in the middle of the Pacific Ocean. Its tropical latitude affects its climate because the amount of sunlight received by the MHI varies by only 2.5 hours over the year. This low variability keeps its average sea-level air temperatures (27 ± 5°C) and average sea surface temperatures (SST; 25 ± 1.9 °C) from varying widely seasonally (Juvik and Juvik, 1998; Fletcher et al., 2008; Department of the Navy, 2005). SSTs are slightly warmer south and west of the MHI, closer to the equator and in the lee of the islands (Figure 2.4). They vary by less than 1.9 °C when comparing seasonal means (Figure 2.5), but can vary more when comparing among specific months or years. Lower, seasonal amounts of variability make SST and thermal stress anomalies infrequent around the islands (Figures A.3 and A.4). The Pacific Ocean also helps stabilize the MHI's climate by acting like a thermal flywheel, dampening wide variations in diurnal air temperatures (and humidity levels) at sea-level (Juvik and Juvik, 1998). This dampening effect is due to water's unique ability to store, mix and dissipate heat. Much of this heat is transported across space and within the water column by currents, wind-driven mixing and other physical oceanographic processes.

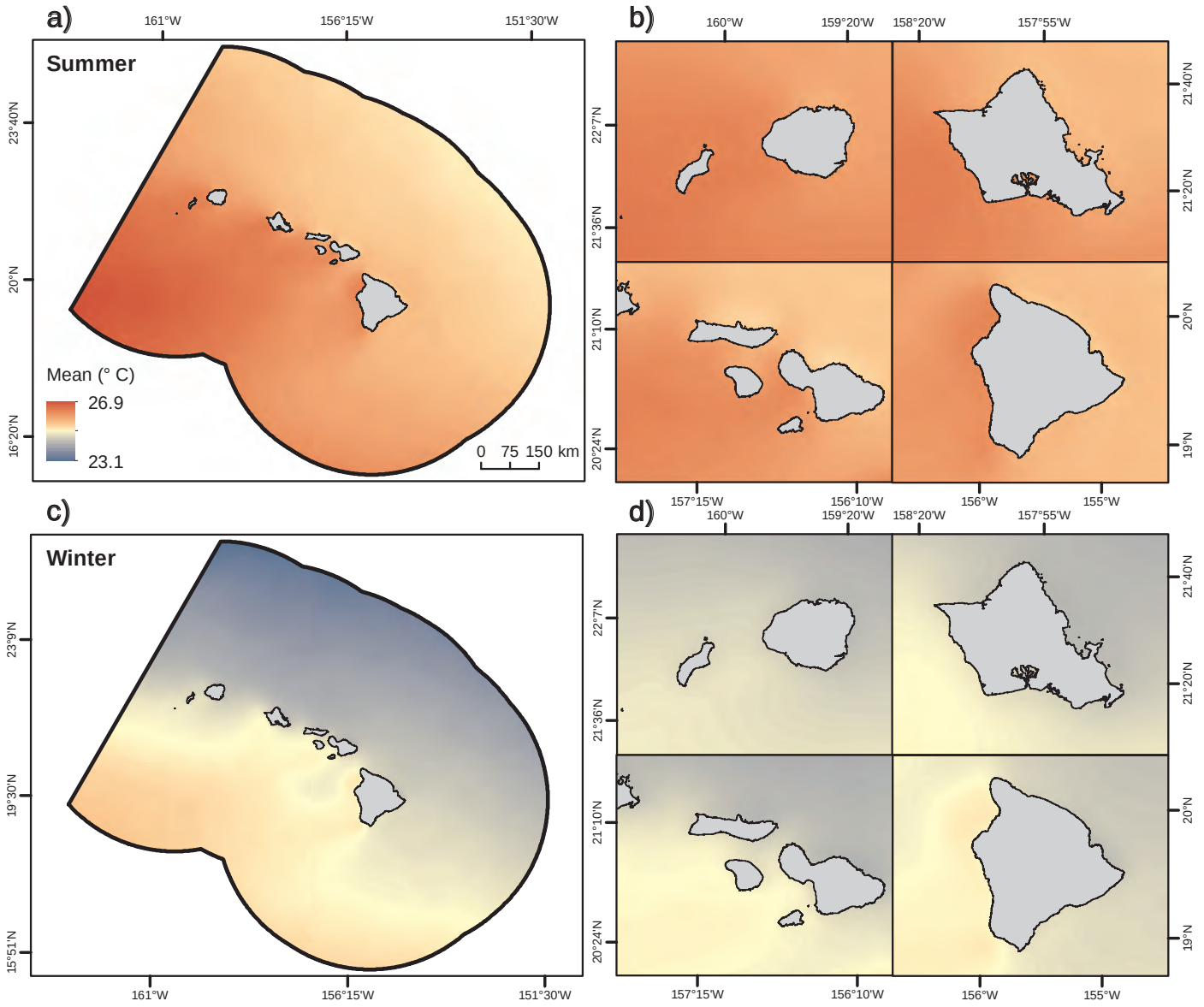

Figure 2.4. Sea surface water temperature (SST) around the MHI. These maps depict the average temperature (°C) of surface waters in the summer (a, b) and winter (c, d) within the study area. Dates: July 2002-July 2014. Data source: Table 2.6. #36

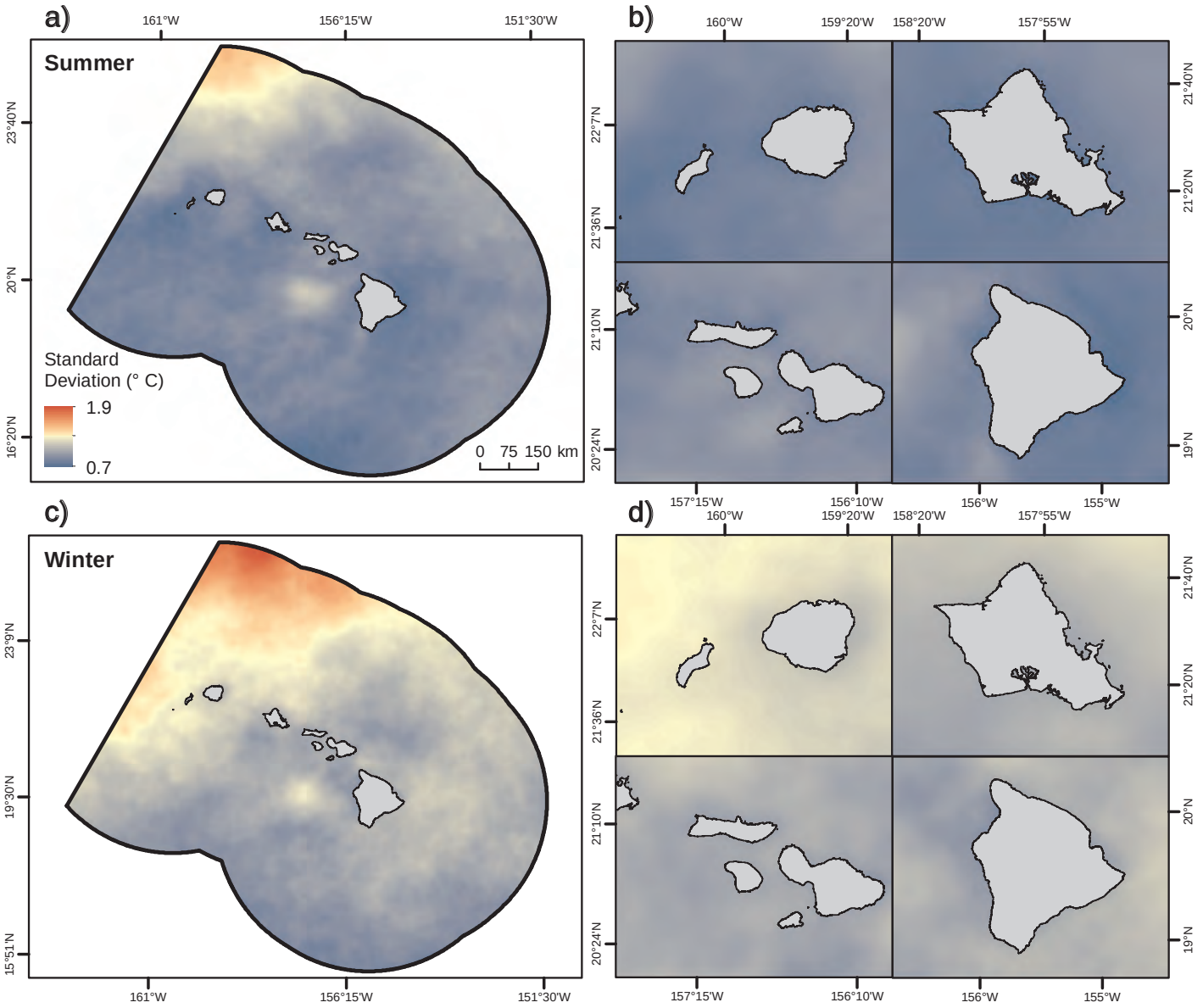

Figure 2.5. Variation in SST around the MHI. These maps depict the variation (standard deviation) in temperature (°C) of surface waters in the summer (a, b) and winter (c, d) within the study area. Dates: July 2002-July 2014. Data source: Table 2.6. #36

2.4.1. Atmospheric and Oceanographic Circulation

The MHI's location in the tropical latitudes also explains the long-term atmospheric and oceanographic circulation patterns around the islands. Trade winds from the northeast (i.e., azimuth of 40° to 90°) dominate the surface winds in the MHIs, occurring about 70-80 percent of the year (Juvik and Juvik, 1998; Vitousek et al., 2009). They have an average speed of approximately 7 ± 4.1 m/s (Juvik and Juvik, 1998; Vitousek et al., 2009), and are strongest and least variable during the summer (from May to October), and slacken during the winter (from November to April; Figures 2.6 and 2.7). They also interact with the MHI's mountainous terrain, causing wide variability in weather conditions within and among islands. The largest obstructions to the atmospheric flow are on the islands of Maui and Hawai'i, whose peaks (Halaelakā, Mauna Kea and Mauna Loa) penetrate the trade-wind inversion layer extending from 1,700 to 5,000 m (Smith and Grubisic, 1993). This interaction changes wind and rainfall patterns around the MHI islands, influencing its biogeography (Juvik and Juvik, 1998). The impacts of these changing wind patterns on the MHI's weather, climate and oceanography are discussed in detail in Section 2.4.4.

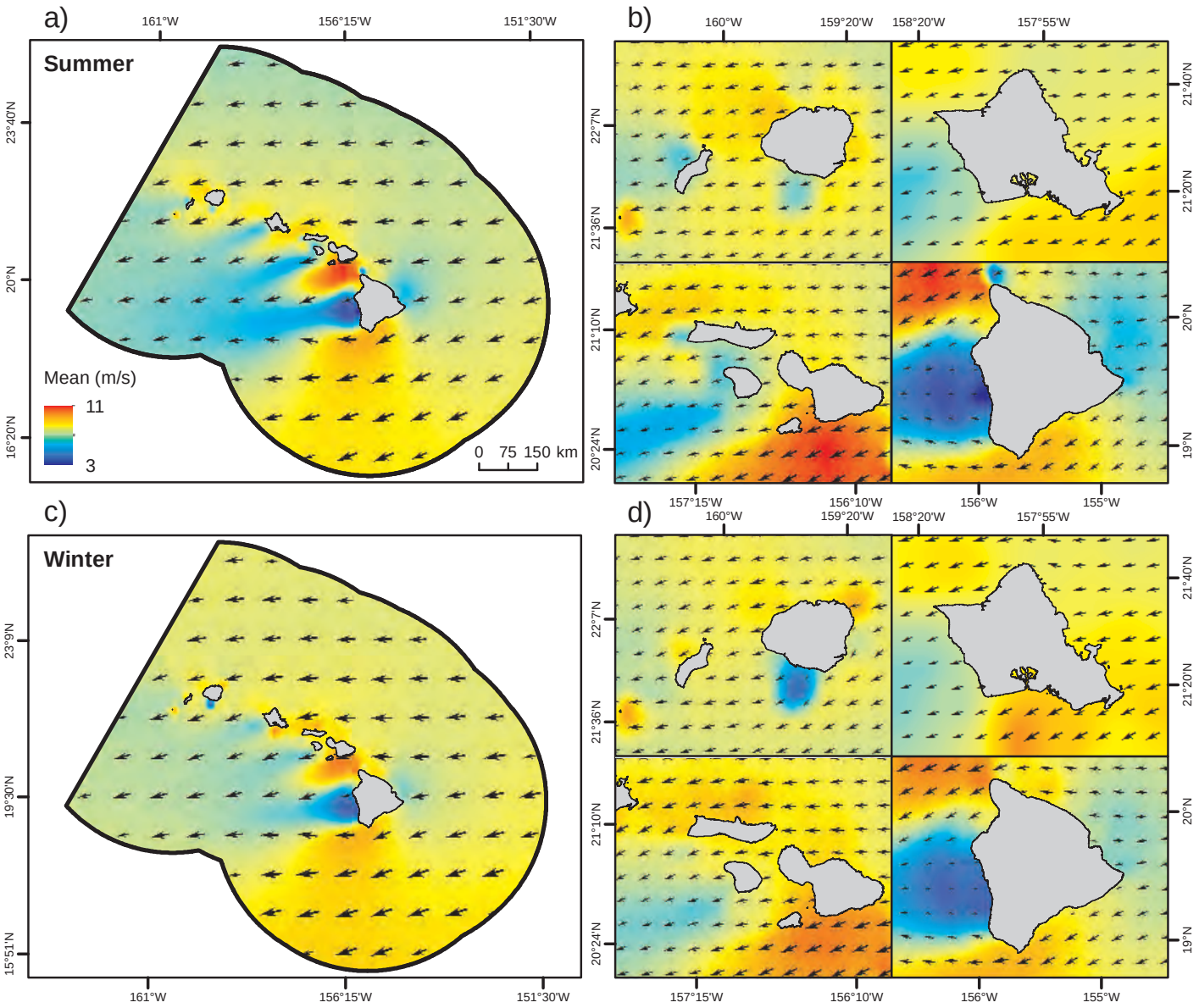

Figure 2.6. Speed and direction of wind around the MHI. These maps depict the average speed (m/s) and direction (° denoted by arrows) of winds in the summer (a, b) and winter (c, d) within the study area. Wind speeds were measured at an altitude of 30 m. Circular statistics were used to calculate the directional averages. The Hawaiian Lee Counter Current (HLCC) is not visible in these maps because of the coarse scale of the directional arrows. Dates: July 1999-November 2009. Data source: Table 2.1. #1 and #3

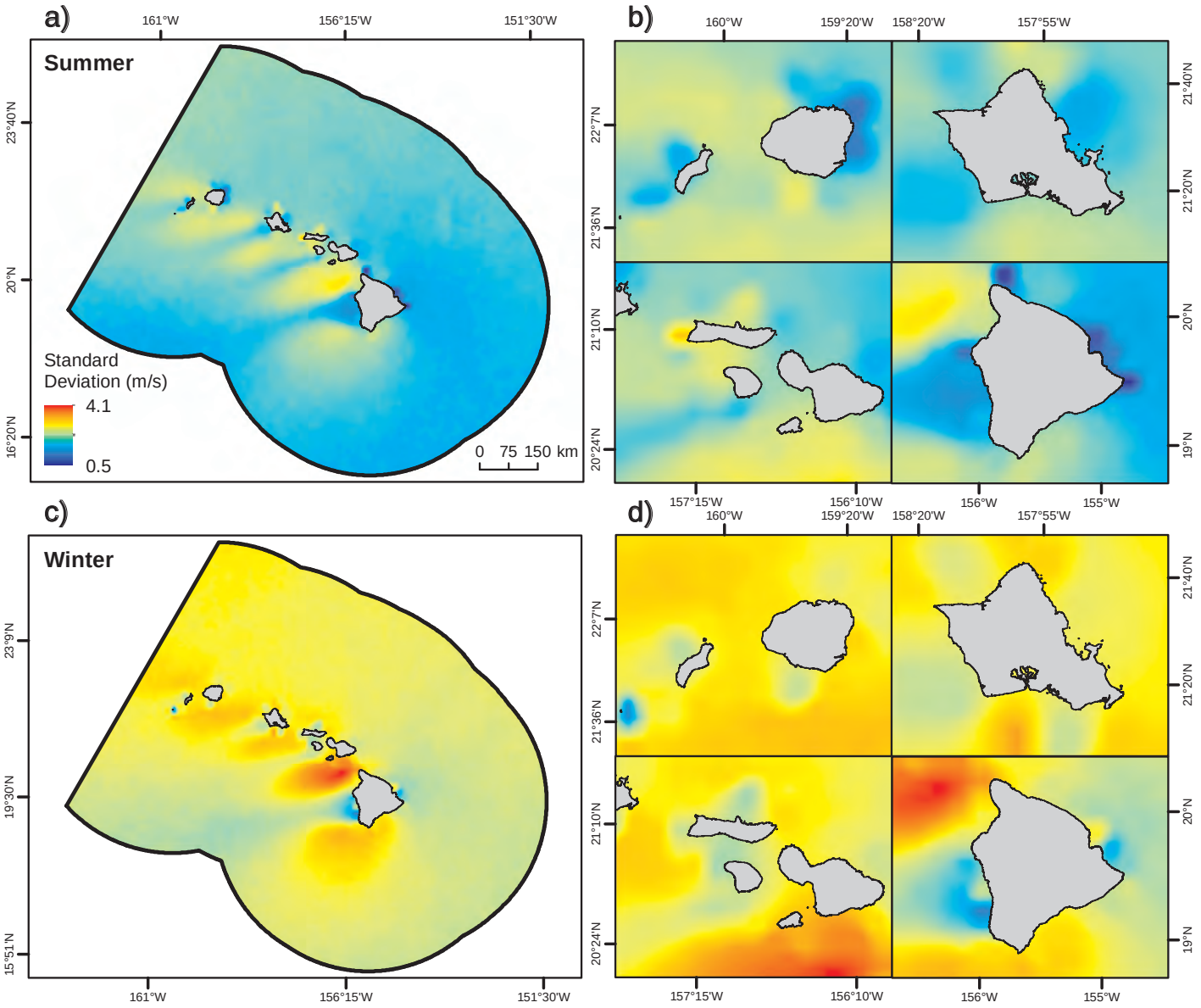

Figure 2.7. Variation in the speed of wind around the MHI. These maps depict the standard deviation of wind speeds (m/s) in the summer (a, b) and winter (c, d) within the study area. Wind speeds were measured at an altitude of 30 m. Dates: July 1999-November 2009. Data source: Table 2.1. #3

The trade winds are the main drivers of surface currents and broad-scale ocean circulation patterns in the north Pacific and around the MHIs (Juvik and Juvik, 1998; Department of the Navy, 2005). In the Northern Hemisphere, this surface water circulation is called the North Pacific Subtropical Gyre (NPSG). The MHI sits on the edge of this gyre within the North Equatorial Current (NEC; Figure 2.8). The NEC generally moves from east to west, although its speed and direction is strongly impacted by the MHI. Where the NEC meets the island of Hawai'i, it splits into a northern and southern branch (Juvik and Juvik, 1998; Department of the Navy, 2005). The southern branch continues westward and rejoins the NEC west of Ni'ihau. The northern branch, called the North Hawaiian Ridge Current (NHRC), travels along the MHI (at an average of 25 cm/s) towards the Northwestern Hawaiian Islands. Two other currents, called the Hawaiian Lee Current (HLC) and Hawaiian Lee Counter Current (HLCC), form on the leeward side of the MHI. The HLC flows from east to west parallel to the NHRC along the coastline. The HLCC flows in the opposite direction (i.e., from west to east) back towards the island of Hawai'i. These broad-scale currents also interact with wind patterns, causing local variability within and among islands (Figures 2.9 and 2.10). The area west of the 'Alenuihānā Channel is particularly variable across seasons. The interaction between surface currents and wind also influence other finer-scale oceanographic processes around the MHI, including water divergence, convergence, fronts, upwelling, downwelling and the formation of eddies. Fine-scale patterns in upwelling and eddy formation increase local primary productivity in the MHI (Seki et al., 2001), and are likely to influence the distribution of animals around the islands (Seki et al., 2002; Department of the Navy, 2005). These impacts and patterns are discussed in more detail in Section 2.4.5.

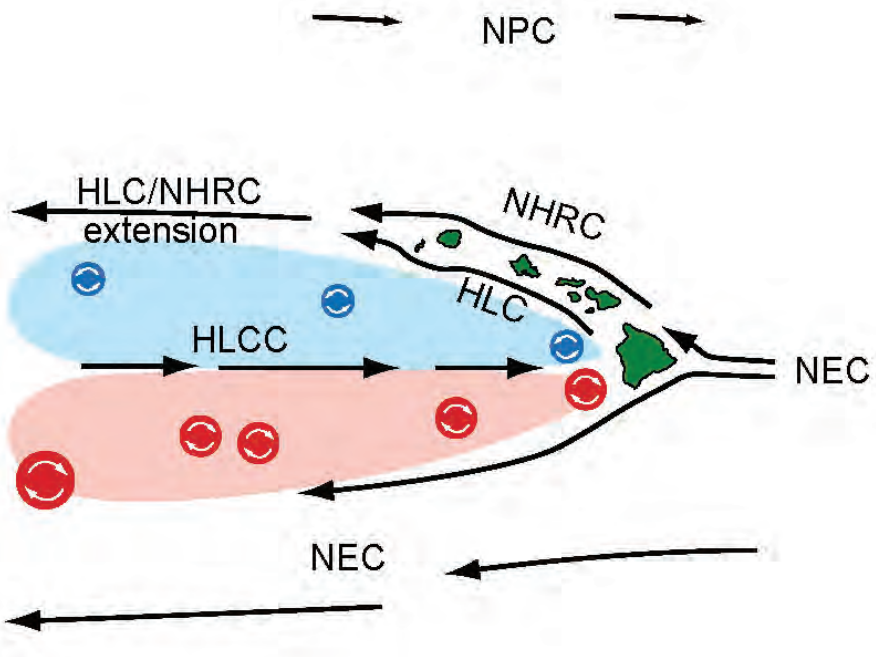

Figure 2.8. Ocean Circulation around the MHI. The MHI are located on the edge of the NEC within the NPSG. The NEC interacts with the MHI islands, splitting off into the Hawaiian Lee Current (HLC) and Hawaiian Lee Counter Current (HLCC). Cyclonic eddies (blue) frequently form north of the HLCC, and anti-cyclonic eddies (red) form to the south. Figure adapted from Lumpkin (1998) with permission from R. Lumpkin.

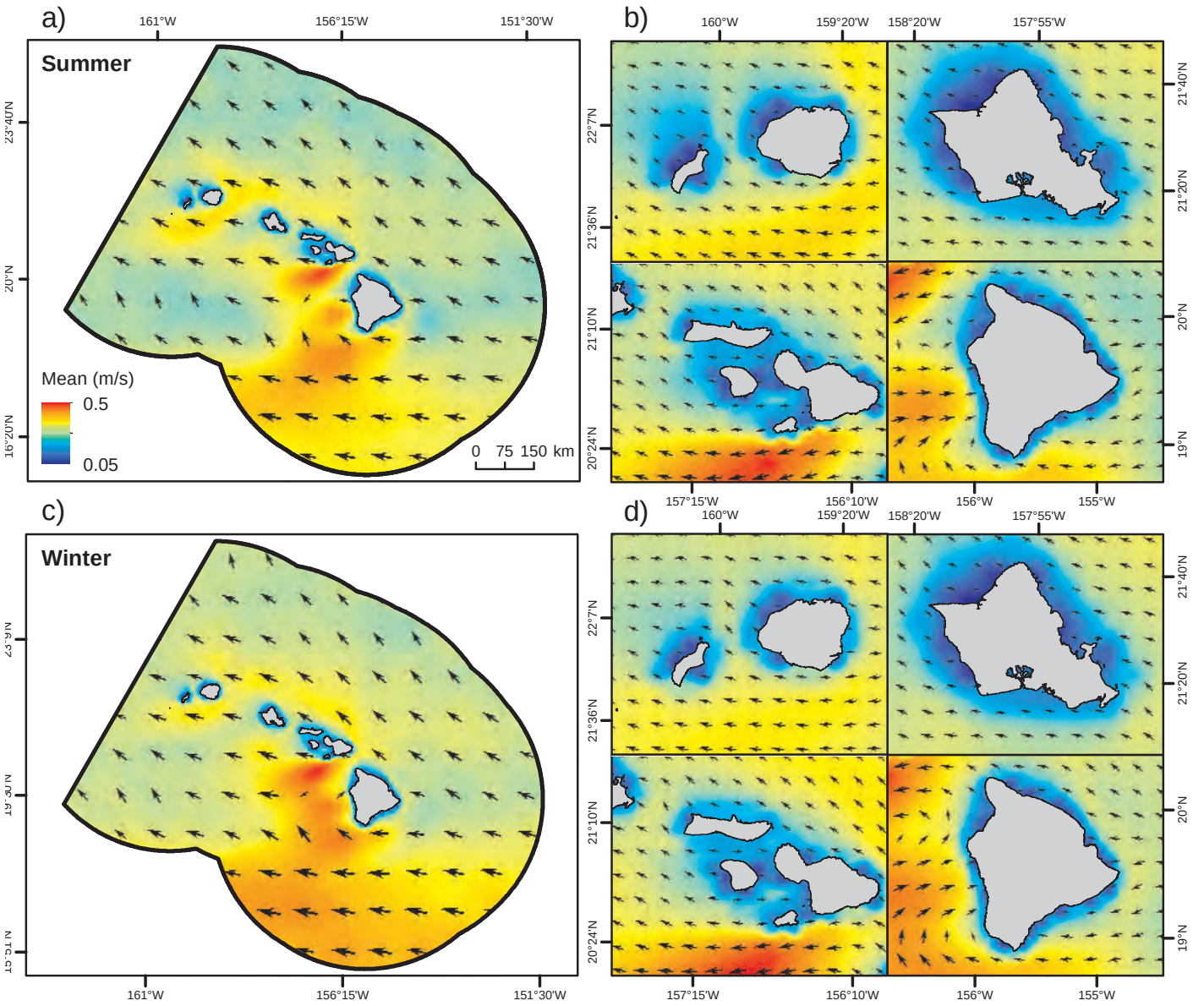

Figure 2.9. Speed and direction of surface currents around the MHI. These maps depict the average speed (m/s) and direction (° denoted by arrows) of surface currents in the summer (a, b) and winter (c, d) within the study area. Circular statistics were used to calculate the directional averages. Dates: 1992-2005. Data source: Table 2.5. #28 and 30

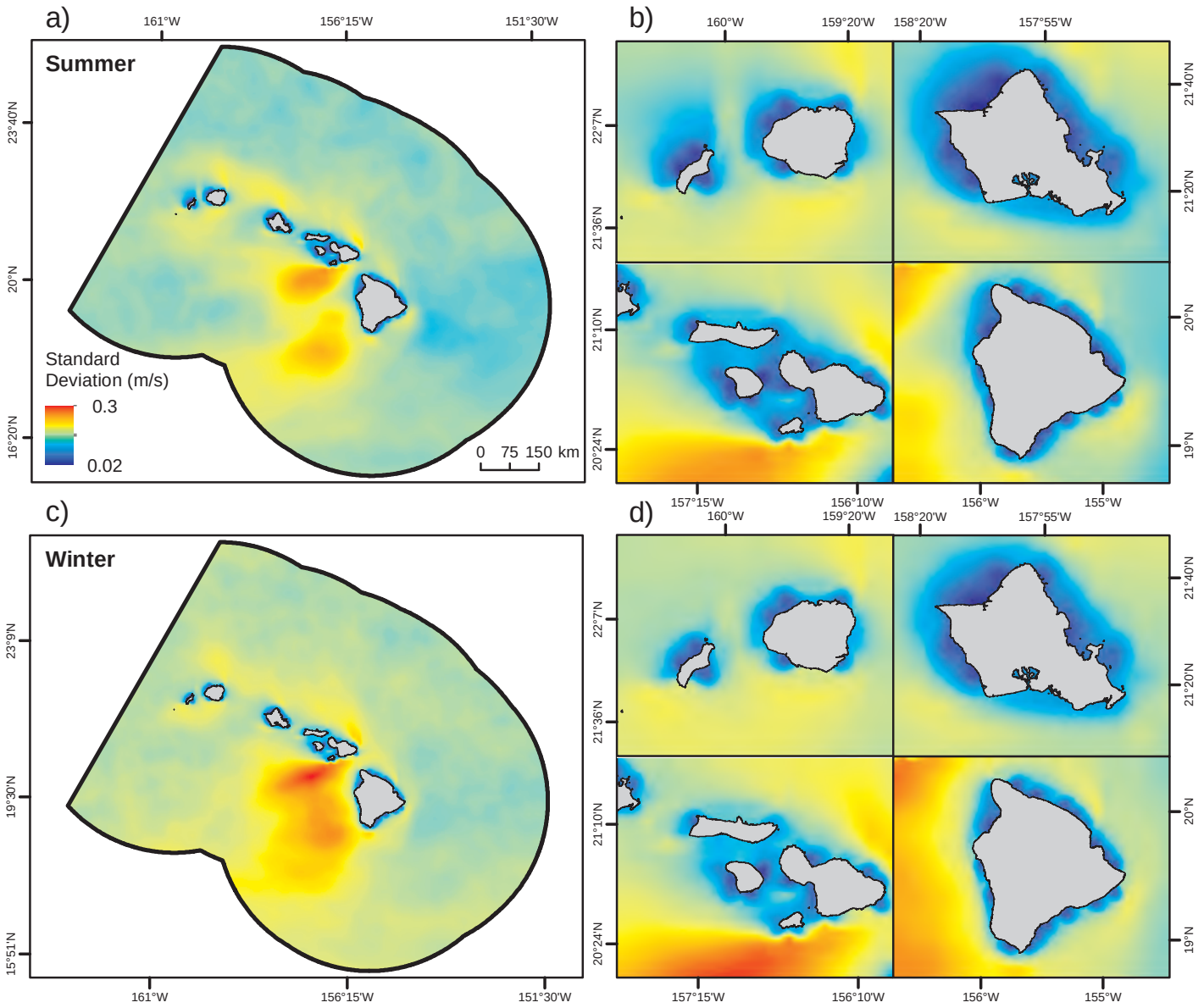

Figure 2.10. Variation in the speed of surface currents around the MHI. These maps depict the standard deviation of surface current speeds (m/s) in the summer (a, b) and winter (c, d) within the study area. Dates: 1992-2005. Data source: Table 2.5 #30

2.4.2. Ocean-Atmosphere Oscillations

The MHIs are impacted by two climate oscillations: (1) the Pacific Decadal Oscillation (PDO; Figure 2.11) and (2) the El Niño Southern Oscillation (ENSO; Figure 2.12). These oscillations affect the climate and ocean around the world on inter-decadal (for PDO) and inter-annual (for ENSO) time scales (NOAA NCEI, 2015a). While their exact causes are not fully understood (Mantua and Hare, 2002; NOAA NCEI, 2016), both the PDO and ENSO have positive (warm) and negative (cool) phases. PDO phases last between 20 to 30 years (Mantua et al., 1997; Minobe, 1997), while ENSO phases shift every 3 to 7 years, and persist for only 6 to 18 months (NASA, 2008). Around the MHI, the effect of these oscillations is not as pronounced as in other parts of the world (e.g., in the north Pacific for PDO and in the equatorial Pacific for ENSO). Neither oscillation is thought to have a strong effect on sea surface temperatures around the MHI (Karl et al., 1995; Fletcher et al., 2002). However, they are likely to affect wind speeds and rainfall amounts around the islands (Ropelewski and Halpert, 1989; Halpert and Ropelewski, 1992; Mantua and Hare, 2002).

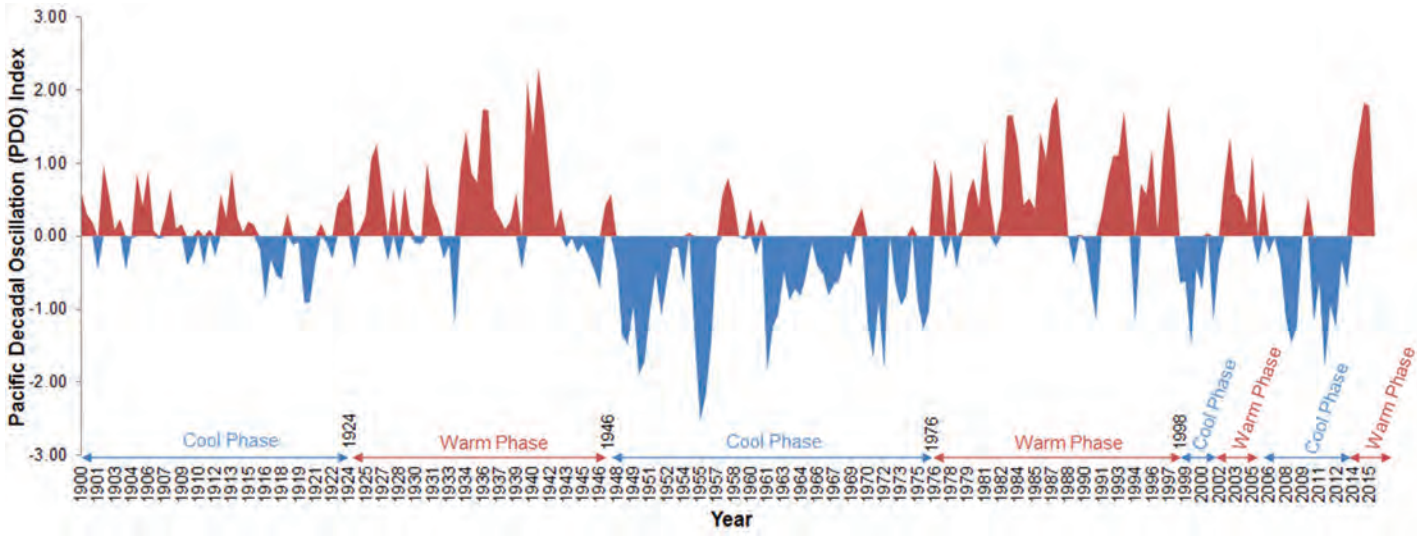

Figure 2.11. Pacific Decadal Oscillation (PDO) Events. Oscillations between warm and cool PDO phases from 1900 to September 2015 (binned into 6 month averages). Recent trends suggest that the PDO is switching to a warm phase. Data source: Mantua, 2015

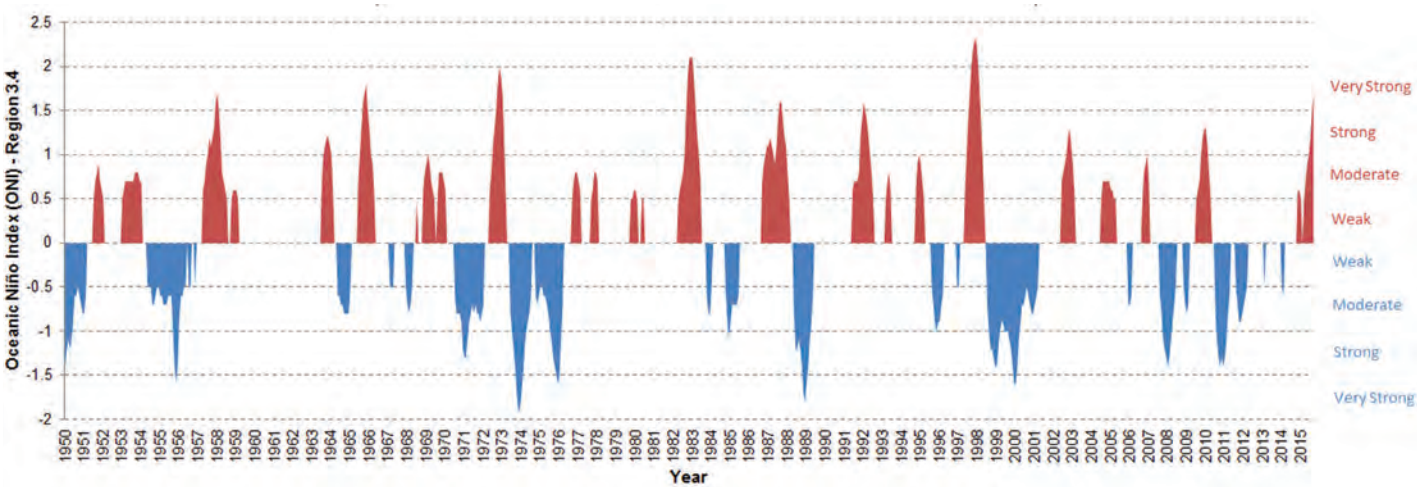

Figure 2.12. El Niño Southern Oscillation (ENSO) Events. Oscillations between warm (El Niño) and cool (La Niña) ENSO phases in Region 3.4 from 1950 to September 2015. One of the strongest El Niño events on record began in 2015. Data sources: NOAA CPC, 2015; NOAA ESRL, 2015

The MHI receives more rainfall when PDO is positive (i.e., in its warm phase), and less rainfall when it is negative (i.e., in its cool phase; Department of the Navy, 2005). ENSO is thought to have the opposite effect on the MHI during its positive and negative phases. When ENSO is positive (i.e., in its El Niño warm phase), the windward sides of the MHI may experience decreased rainfall and weaker trade winds (Department of the Navy, 2005; NOAA PEACC, 2016). Weakened trade winds (and warmer SSTs near the equator) can help tropical depressions and hurricanes form east of the MHI (Fletcher et al., 2002). These patterns reverse around the MHI when the ENSO phase is neutral or negative (i.e., in its La Niña cool phase), causing the windward sides of the MHI to experience stronger trade winds and increased amounts of precipitation (Ropelewski and Halpert, 1989; Halpert and Ropelewski, 1992). It is unclear how climate change will impact the frequency and/or magnitude of the PDO and ENSO (Department of the Navy, 2005; UH CGG, 2012), and consequently the regional climate around the MHI.

2.4.3. Seasonal Changes in the Climate and Ocean

The MHI has two main seasons: summer and winter. Summer includes the months of May to October, and winter includes November to April. Seasonal changes in the MHI's climate and ocean conditions are mainly driven by changes in (and interactions between) areas of atmospheric pressure called the North Pacific Subtropical High and the Aleutian Low. The Aleutian Low is an area of low pressure located over the Gulf of Alaska and the Bering Sea. It is strong in the winter, and nearly non-existent in the summer. The North Pacific Subtropical High is located off the west coast of North America, and is persistent nearly year round. It is stronger and closer to the North Pole during the summer (when the Aleutian Low is nearly absent), and weaker and closer to the equator during the winter (Juvik and Juvik, 1998). The weakening, strengthening and movements of the North Pacific Subtropical High and Aleutian Low bring about seasonal changes in the atmospheric and oceanographic conditions around the MHI.

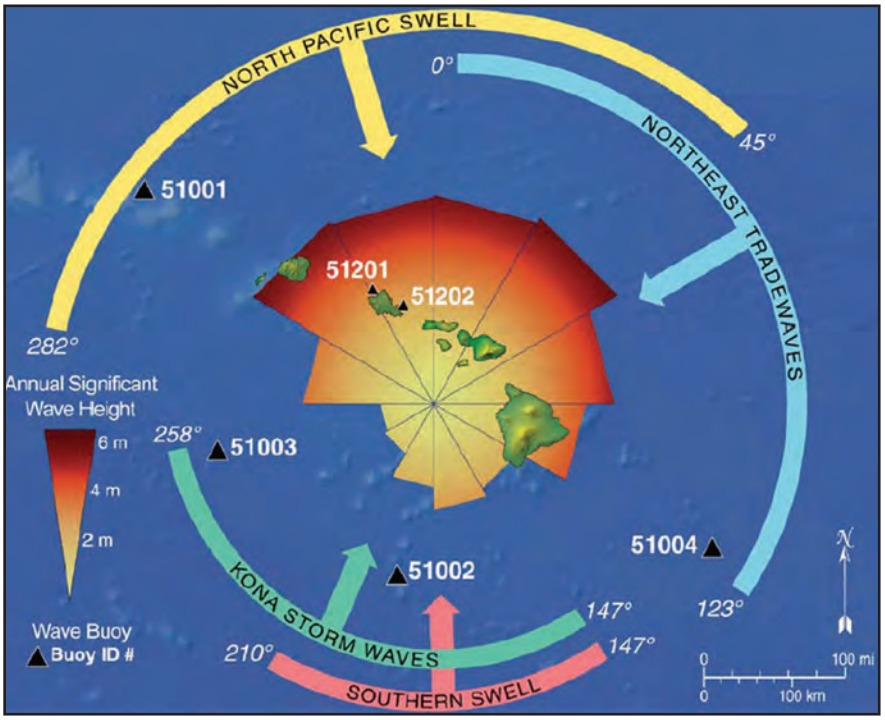

Figure 2.13. Seasonal wave patterns in the MHI. The North Pacific Swell is dominant in the winter, and swell from the north-east (i.e., trade wind swell) is prevalent in the summer. The maximum annual significant wave heights (symbolized as orange to brown colors) denote the maximum wave heights averaged over several years. Figure credit: Moberly and Chamberlain, 1964; Vitousek and Fletcher, 2008. Reprinted with permission from University of Hawai'i at Mānoa.

Summer in the MHI is warmer, drier and dominated by the northeasterly trade winds and trade-wind generated swell (Figure 2.13; Moberly and Chamberlain, 1964; Juvik and Juvik, 1998; Department of the Navy, 2005; Vitousek and Fletcher, 2008). Air temperatures typically range between 22° and 32° C, and the islands receive approximately 20 percent of their annual rainfall. Since there is less rain, nearshore waters tend to be less turbid during the summer, particularly in Kāne'ohe Bay and Pearl Harbor (Figures A.5 and A.6). The summer is warmer and drier because the North Pacific Subtropical High strengthens and moves north, pushing mid-latitude rain storms away from the islands. With fewer storms, the trade winds are less likely to be interrupted by atmospheric changes, making them more persistent. Persistent trade winds create swell with average, nearshore wave heights of 2 ±0.5 m and peak periods of 9 ±2.5 seconds (Vitousek et al., 2009). However, maximum annually recurring wave heights can be up to 6 m (Figure 2.13). Swell from the south (called the Southern swell) also can occur during the summer, although it is infrequent (Flament et al., 1996). The Southern swell is typically 2.5 to 3 m in height, and has periods of 14 to 22 seconds (Figures 2.14 and 2.15; Vitousek and Fletcher, 2008; Vitousek et al., 2009). This swell is generated by winter storms in the southern hemisphere, as far south as Australia, New Zealand and the Southern Ocean. They propagate northward (Snodgrass et al., 1966) until they reach the MHI's southern shores.

Winter in the MHI is cooler, wetter and dominated by the trade winds (which are weaker) and waves originating from north-northwest (called the North Pacific Swell; Figure 2.13; Moberly and Chamberlain, 1964; Juvik and Juvik, 1998; Department of the Navy, 2005; Vitousek and Fletcher, 2008). Air temperatures typically range between 22° and 26° C, and the islands receive nearly 80 percent of their annual rainfall (Department of the Navy, 2005). Fifty percent of this winter rainfall occurs between December and February alone. Nearshore levels of turbidity tend to rise in the winter, as the increased rainfall carries sediment into the ocean (Figures

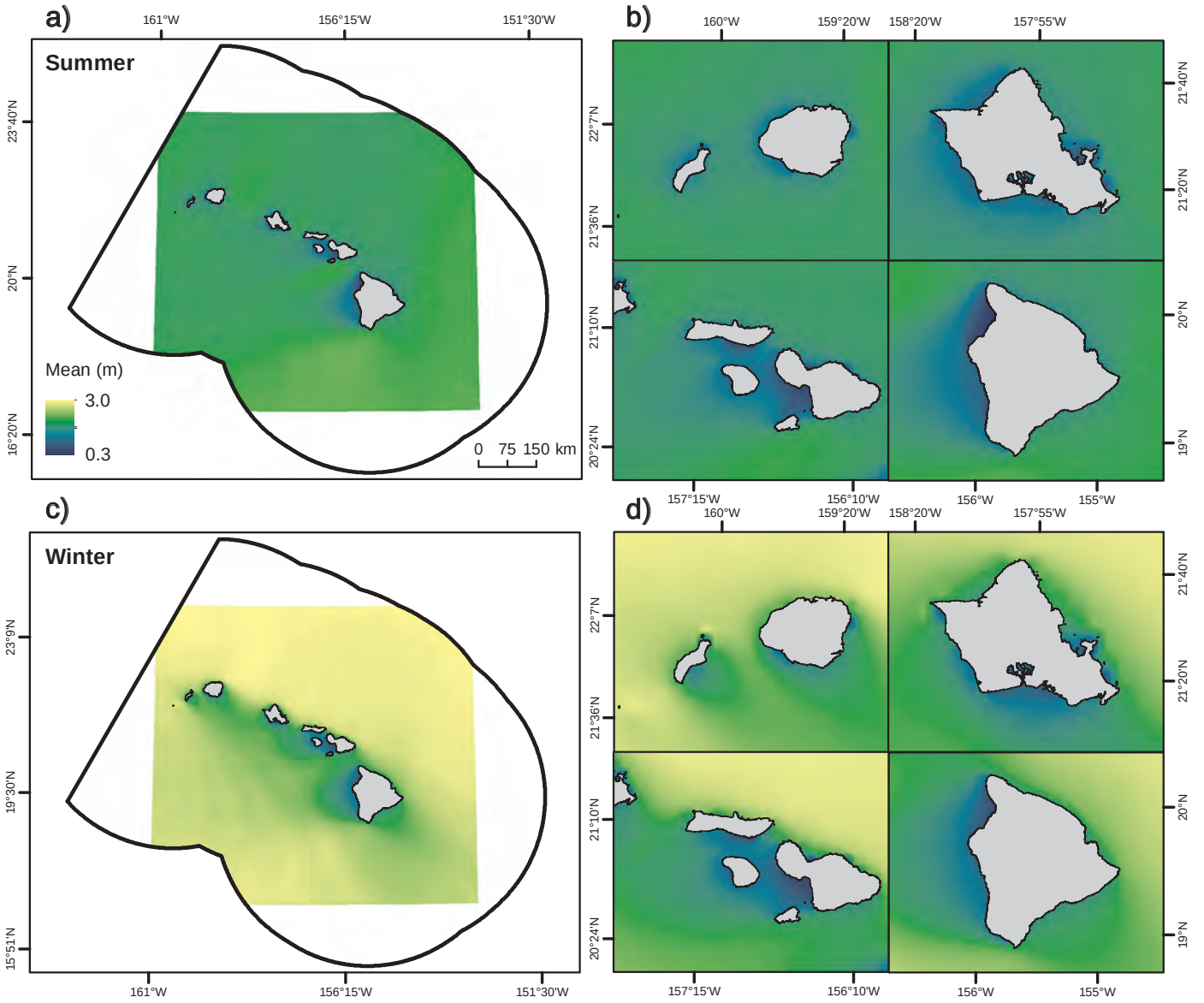

Figure 2.14. Wave heights around the MHI. These maps depict the average significant wave heights (m) in the summer (a,b) and winter (c,d) within the study area. Wave data is missing for portions of the project area (a,c). Dates: January 2000-December 2009. Data source: Table 2.6. #43

A.5 and A.6; Juvik and Juvik, 1998). It also causes local increases in chlorophyll-*a* concentrations and primary productivity, particularly along the Nāpali Coast in Kaua'i, offshore of Hilo in Hawai'i, in Kāne'ohe Bay and east of Ka'ena Point in O'ahu (Figures A.7, A.8, and A.9). The winter is cooler and wetter because the North Pacific Subtropical High weakens and moves south, allowing mid-latitude rain storms to move closer to the islands.

Occasionally, Kona winds (from the south) can bring strong storms and waves to the islands in the winter. These winds blow infrequently during the winter (i.e., for about 15 to 30 percent of the time) from the azimuths of 160° to 240°. They form because of low pressure systems less than 800 km northwest of the MHI (Department of the Navy, 2005). Kona winds and waves can be destructive to the MHIs southern and western coasts, causing localized wind damage and flooding. Kona storm waves are usually 3 to 4 m in height and have 8 to 11 second periods (Rooney and Fletcher, 2005; Vitousek et al., 2009). The intensity of these Kona storms is influenced partly by the PDO and ENSO events (Rooney and Fletcher, 2005). Positive (warm) PDO and El Niño phases tend to mitigate the intensity of Kona storms, although they can fuel the formation of hurricanes east of the MHIs (Fletcher et al., 2002). Negative (cold) PDO and La Niña events cause these storms to intensify, often leading to destruction along the west and south facing shorelines of the MHI.

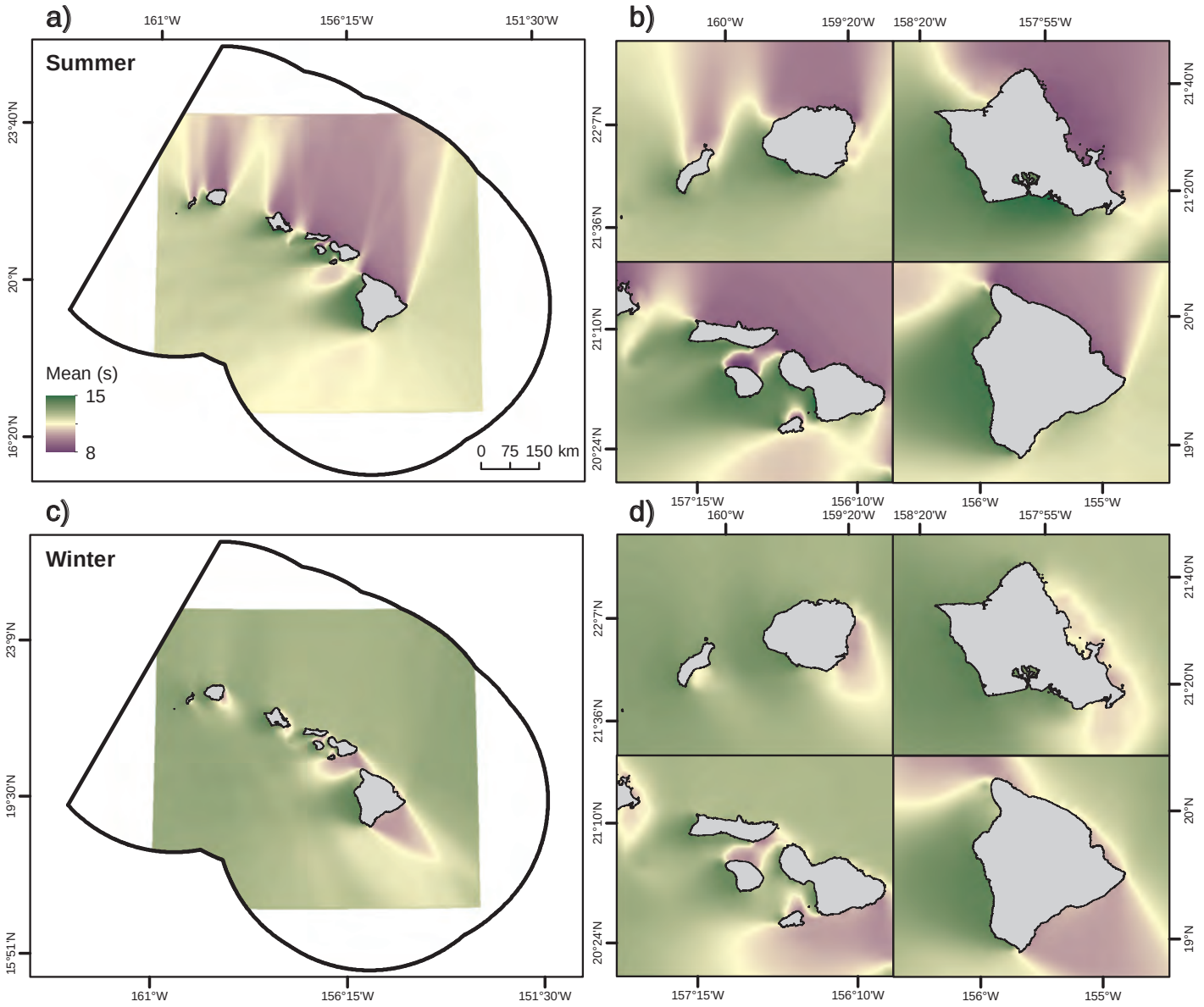

Figure 2.15. Wave periods around the MHI. These maps depict the average wave periods (s) in the summer (a,b) and winter (c,d) within the study area. Wave data is missing for portions of the project area (a, c). Dates: January 2000-December 2009. Data source: Table 2.6 #42

The North Pacific Swell can be similarly destructive on the MHI's northern and western coasts during the winter. It is generated by violent, winter storms in the North Pacific Ocean. Storm intensity and frequency increase when the Aleutian Low strengthens, and the North Pacific Subtropical High moves southward. The combination of high wind speeds, long duration winds events and long fetch lengths produce optimum conditions to generate large, long-period swell in the open ocean (Aucan, 2006; Rooney et al., 2008; Vitousek and Fletcher, 2008; Vitousek et al., 2009; Hoeke et al., 2011). Those swells reach the MHI unobstructed, resulting in maximum annually recurring wave heights of 6 m (Figure 2.13; Vitousek and Fletcher, 2008), with peak periods of 14 to 18 seconds (Vitousek et al., 2009). While maximum winter wave heights and periods can be large, average winter wave heights (0.3 to 3 m) and periods (8 to 15 seconds) are generally much smaller in the MHI, especially in the lee of the islands (Figures 2.14, 2.15, A.10, and A.11). Average wave heights are usually smaller because winter wave heights and the number of winter swell events are highly variable among years (Caldwell, 2005). This variation is largely due to the frequency and length of storms that develop in the North Pacific Ocean and Bering Sea. Longer, more frequent storms will produce larger, more frequent wave events.

2.4.4. Influence of Topography on Climate and Oceans

The MHI's mountainous landscape influences almost every aspect of its weather, climate and the surrounding ocean (Juvik and Juvik, 1998). The peaks, slopes and valleys change the direction and speed of the wind, causing it to slow in some locations and speed up in others. Winds in the MHI tend to flow around mountains greater than 1,700 m (e.g., Haleakalā, Hualālai, Mauna Kea and Mauna Loa; Smith and Grubisic, 1993; Juvik and Juvik, 1998). At this altitude, air temperatures are inverted, and the air above 1,700 m is warmer than the air below. This inversion layer prevents cooler air from rising further, forcing it around the mountain (Figure 2.16a). In contrast, wind can flow over mountains in the MHI that are less than 1,700 m high because it is not blocked by the inversion layer. This flow causes warm, moist air from the ocean to rise and cool, leading to consistently higher amounts of precipitation on the windward (i.e., northeast) sides of the islands (Figure 2.16b). As this air passes over the mountains, it descends and warms, creating a rain shadow and causing the leeward (i.e., southwest) sides of the islands to be sunnier and drier. Both the rain shadow effect and the effect of the inversion layer are clearly visible on the island of Hawai'i (Figure 2.16c). The amount of rainfall in the MHI ranges from 25 to 1,130 cm per year (Juvik and Juvik, 1998). The highest average rainfalls are at the summits of the West Maui Mountains and Wai'ale'ale on Kaua'i. This large range is mainly due to the orographic effect of the mountainous terrain. At sea level, rainfall amounts range between 56 and 70 cm per year, and are mainly from passing ocean storms.

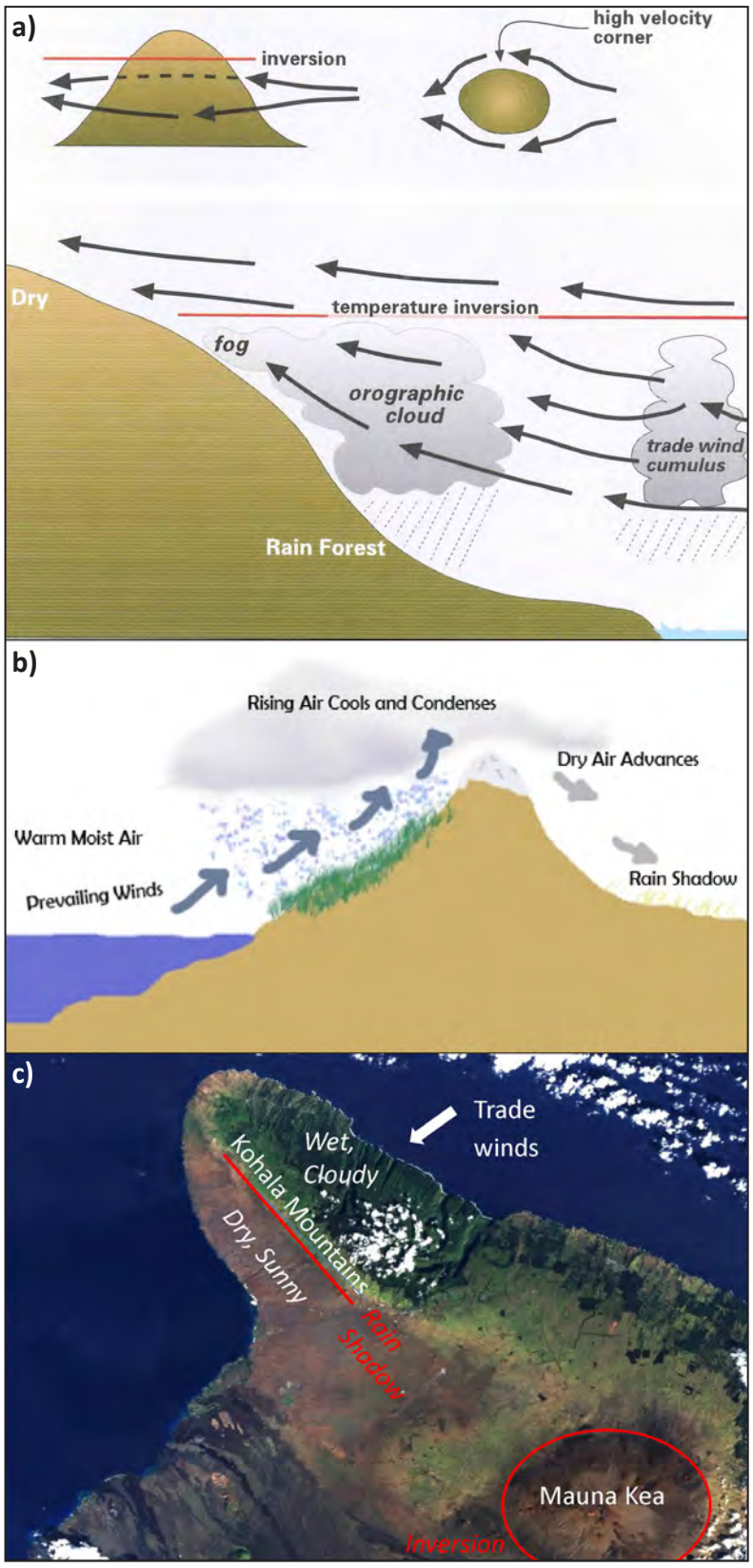

Figure 2.16. Orographic rainfall. a) Diagram illustrating how the temperature inversion layer can force wind to flow around mountains. Figure credit: Juvik and Juvik, 1998. Reprinted with permission from University of Hawai'i Press; b) Diagram illustrating how rain shadows are created when air rises and cools over mountains. Figure credit: Wikipedia, 2015; c) Natural color Landsat 7 image (taken January 2001) showing dry areas above the inversion layer around Mauna Kea, and the rain shadow created by the Kohala Mountains on the island of Hawai'i. Figure adapted from NOAA, 2015.

Environmental Setting

In addition to affecting precipitation and temperature, the interaction between MHI's mountains and persistent trade winds also influence the physical and biological oceanography in the region. Figure 2.17 illustrates how the interaction between topography and wind influences water temperatures, convergence, divergence, upwelling and downwelling patterns nearby. When wind is forced to flow around the mountainous islands, it creates wind shadows and localized surface warming on the leeward sides of the islands. Changing wind speeds and directions also cause convergence and divergence in the atmosphere and in the water column. Convergence zones cause the downwelling of surface waters, and depression in the local thermocline. Conversely, divergence zones cause the upwelling of deeper waters and the shoaling of the thermocline. When combined, these physical processes create oceanographic patterns that vary distinctly through time and across geographic space.

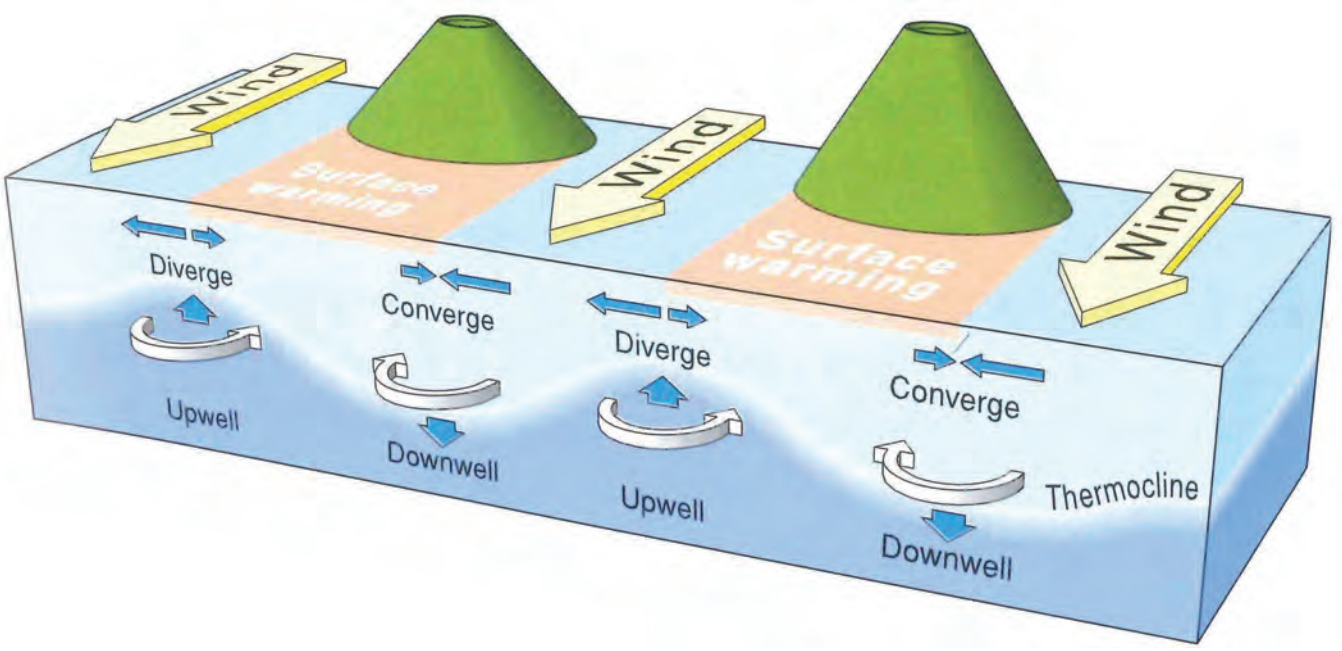

Figure 2.17. Effect of topography on wind and physical oceanography. The mountains in the MHI change the direction and speed of the trade winds, causing localized warming and the convergence, divergence, upwelling, and downwelling of surface waters. Figure credit: Juvik and Juvik, 1998. Reprinted with permission from University of Hawai'i Press.

In the MHI, this topographic effect explains many of the oceanographic patterns around the islands. The MHI's mountains block the persistent trade winds from the northeast, creating pockets of warmer, calmer water on the southwest side of the islands. Calmer waters are most noticeable and persistent in the lee of the some of the MHI's tallest mountains, including Mauna Kea, Mauna Loa and Hualālai on Hawai'i and Mauna Wai'ale'ale on Kaua'i (Figure 2.6). Winds are also accelerated in between the islands, particularly in the Kaua'i, Kaiwi, Pailolo and 'Alenuihānā Channels. In these locations, mountains constrict and speed up the trade winds, causing them to be 2.5 to 10.3 m/s faster than over the open ocean (Patzert, 1969; Department of Navy, 2005). Higher and more variable wind speeds cause ocean conditions to fluctuate more in these channels. For example, wave heights and periods in the 'Alenuihānā Channel often vary by up to 1 m and 5 seconds (respectively) during the summer when the trade winds are the strongest (Figures A.10 and A.11).

Additionally, the water column is often less stratified in these northeast/southwest oriented channels because the higher wind speeds cause more vertical and horizontal mixing of the ocean. Mixing can help bring nutrient rich waters to the surface (Seki et al., 2002). It can also force the mixed layer (i.e., the ocean layer of uniform or nearly uniform water density) deeper. Lahaina Roads (the deepest point in the Pailolo Channel) is one example

of where water column mixing occurs. There, the mixed layer can be up to 50 m deeper during the winter and summer than in the surrounding waters (Figure A.12). Thermal (SST) fronts (Miller and Christodoulou, 2014; Scales et al., 2014; Miller et al., 2015a; Miller, 2016) are also more frequent, stronger and more persistent in Lahaina Roads year round (Figures 2.18, A.13, and A.14). The same is true for SST fronts in the ʻAlenuihānā and Kaiwi Channels, as well as offshore of Kaʻena Point on Oʻahu, South Point on Hawaiʻi and the Nāpali Coast on Kauaʻi. Chlorophyll-*a* fronts (Scales et al., 2014; Miller et al., 2015b; Miller, 2016) follow similar patterns in the MHI. They are more frequent, persistent and stronger on the leeward sides of the islands, and in channels between the islands (Figures 2.19, A.15, and A.16). They also appear to persist longer in the winter, although there are longer-lived fronts offshore of the Kona Coast on Hawaiʻi, Lehua near Niʻihau, Kaʻena Point on Oʻahu, in the Au'au Channel and along Penguin Bank south of Oʻahu during the summer.

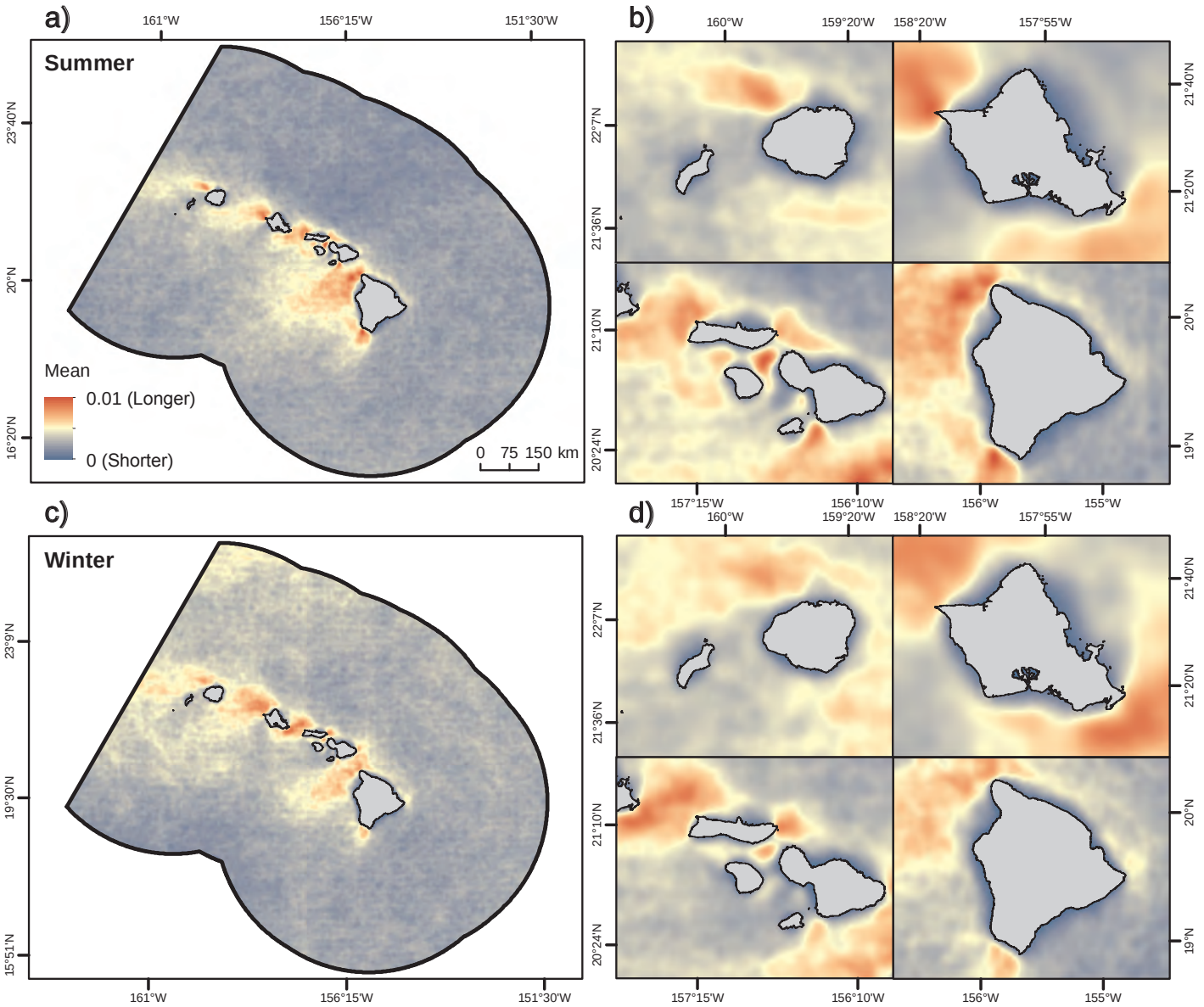

Figure 2.18. Persistence of SST fronts around the MHI. These maps denote the average persistence (#) of SST fronts in the summer (a,b) and winter (c,d) within the study area. Frontal persistence is defined as the number of front observations divided by the number of cloud-free observations. A front was detected if there was a ≥0.4 °C between two water masses within a 32x32 pixel moving window. Dates: June 2002-December 2013. Data source: Table 2.6. #39. Data provided courtesy of the Plymouth Marine Laboratory, Dr. Peter Miller.

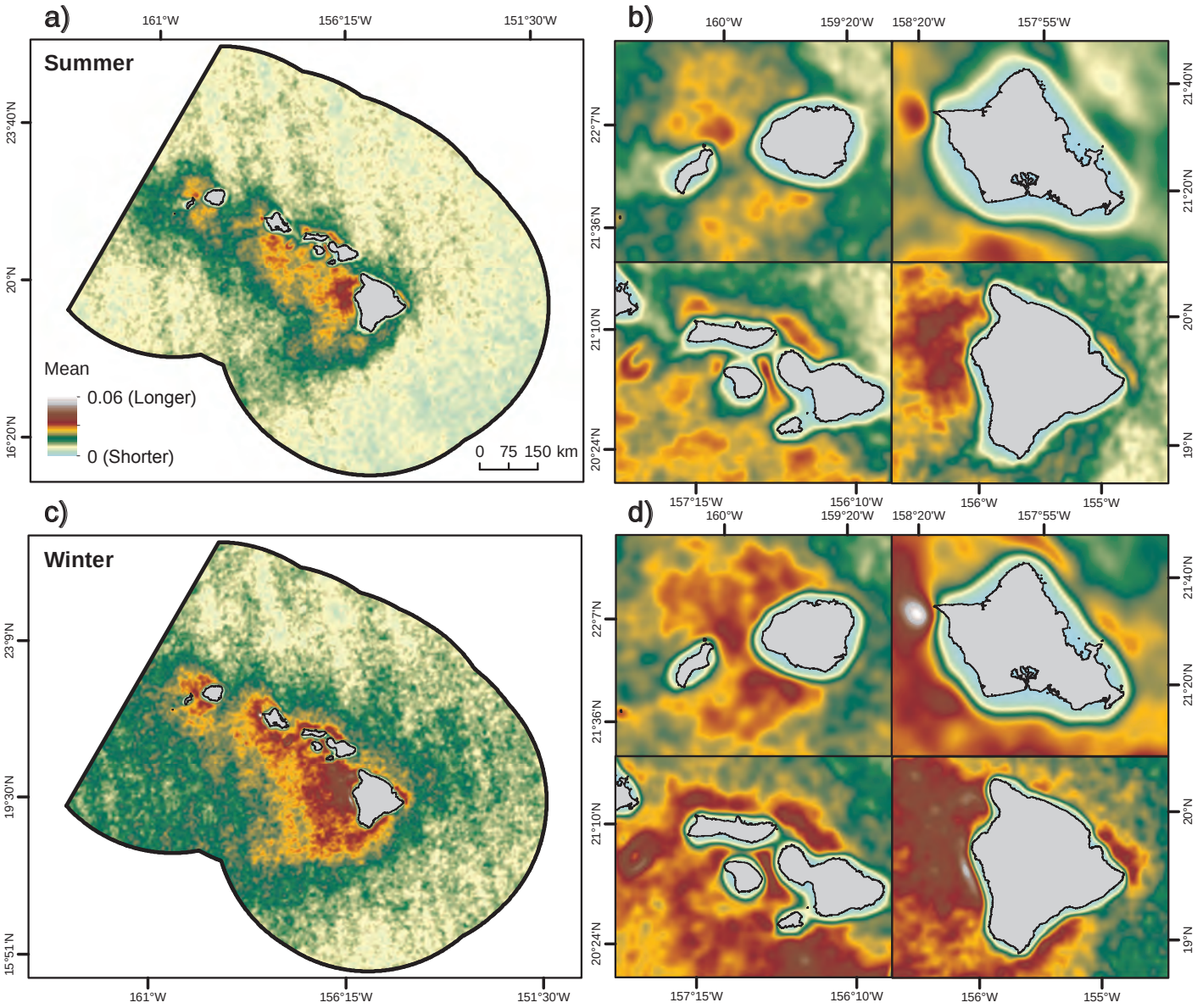

Figure 2.19. Persistence of surface chlorophyll-a fronts around the MHI. These maps denote the average persistence (#) of surface chlorophyll-a fronts in the summer (a,b) and winter (c,d) within the study area. Frontal persistence is defined as the number of front observations divided by the number of cloud-free observations. A front was detected if there was a ≥0.06 log mg/m³ between two water masses within a 32x32 pixel moving window. Dates: June 2002-December 2013. Data source: Table 2.2. #8. Data provided courtesy of the Plymouth Marine Laboratory, Dr. Peter Miller.

In addition to affecting waves, mixing and fronts, changes in wind speed and direction also cause the divergence and convergence of atmospheric winds. This convergence and divergence force atmospheric winds to circulate, creating atmospheric eddies on the leeward sides of the islands (Chavanne et al., 2002). Atmospheric eddies are most prevalent on the west side of Hawai'i during the summer when the trade winds are the strongest. Differences in atmospheric winds speeds can also cause the rotation of surface waters (Figure A.17), and for oceanographic eddies to form (Lumpkin, 1998; Chavanne et al., 2002; Calili et al., 2008). Oceanographic eddies can also spin-off from ocean currents, when they interact with the seafloor topography (Dong et al., 2009). In the MHI, eddies are most frequent offshore of the Kona Coast (Figure A.18). These eddies are generally shallow (i.e., in top 150 m of the water column), range from 5.7 to 150 km wide, and have rotating current speeds of up to 1 m/s. They typically last between 6 to 12 weeks, although some may persist longer (Falkowski et al., 1991; Seki et al., 2002; Department of the Navy, 2005).

There are two types of eddies: cyclonic (i.e., counter-clockwise rotating) and anticyclonic (i.e., clockwise rotating). The HLCC generally divides the formation and propagation of these two types of eddies (Figure 2.8). Eddies that form south of the HLCC are usually anti-cyclonic. They are more frequent during the summer than in the winter (Figure 2.20). These eddies are often regularly shaped, and move offshore of Hawai'i in a west-southwest direction (Calili et al., 2008). They are made up of warmer water (i.e., warm-core eddies), and have a slight convex or dome shape, making them visible in the variation of SST and variation in sea surface height (SSH) maps (Figures 2.5 and A.19). They are warm-core eddies because their anti-cyclonic rotation causes the downwelling of surface waters at their cores, and the upwelling of deeper waters around their periphery (Jia et al., 2011). This upwelling around the periphery is associated with increased biological productivity (Calil and Richards, 2010), and may be important for some species of cetaceans and seabirds (Department of the Navy, 2005).

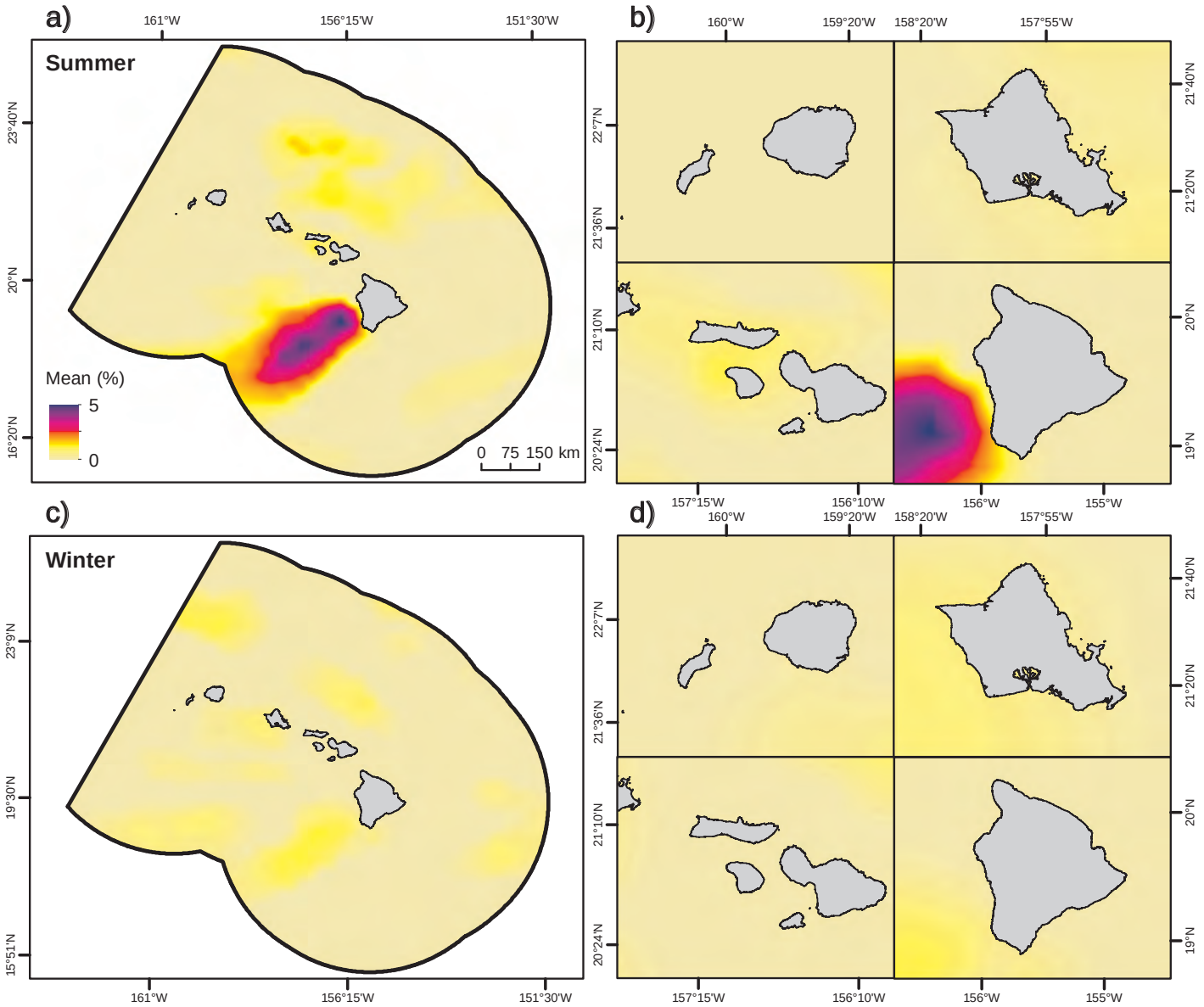

Figure 2.20. Probability of anti-cyclonic eddies around the MHI. These maps depict the average probability (%) that anti-cyclonic (clockwise rotating) eddies will form in the summer (a,b) and winter (c,d) within the study area. Dates: 1992-2014. Data source: Table 2.4. #25

Environmental Setting

Eddies that form north of the HLCC are cyclonic. These eddies are more frequent during the summer than in the winter (Figure 2.21). They are often irregularly shaped, and tend to stay close (<40 km) to the islands. They are made up of colder water (i.e., cold core eddies; Falkowski et al., 1991; Seki et al., 2002; Department of the Navy, 2005; Calil et al., 2008), and have a slight concave shape, making them visible in the SSH images during the winter (Figure A.20). They are cold-core eddies because their cyclonic rotation causes upwelling of deeper waters in their core, making them important for bringing nutrient-rich waters up to the surface. This nutrient-rich water can stimulate primary production by as much as 20 percent (Falkowski et al., 1991; Seki et al., 2002; Vaillancourt et al., 2003), and increase biological activity along the leeward sides of the MHI (McGillicuddy and Robinson, 1997; Seki et al., 2001).

In addition to upwelling and downwelling from oceanic eddies, the divergence and convergence of wind can force the upwelling and downwelling of surface waters on the leeward side of the islands (Figures 2.22, A.21, and A.22). Similar to eddies, these convergence and upwelling zones are biologically important, and utilized by a variety of species around the MHI, including fish, turtles and cetaceans (Department of the Navy, 2002).

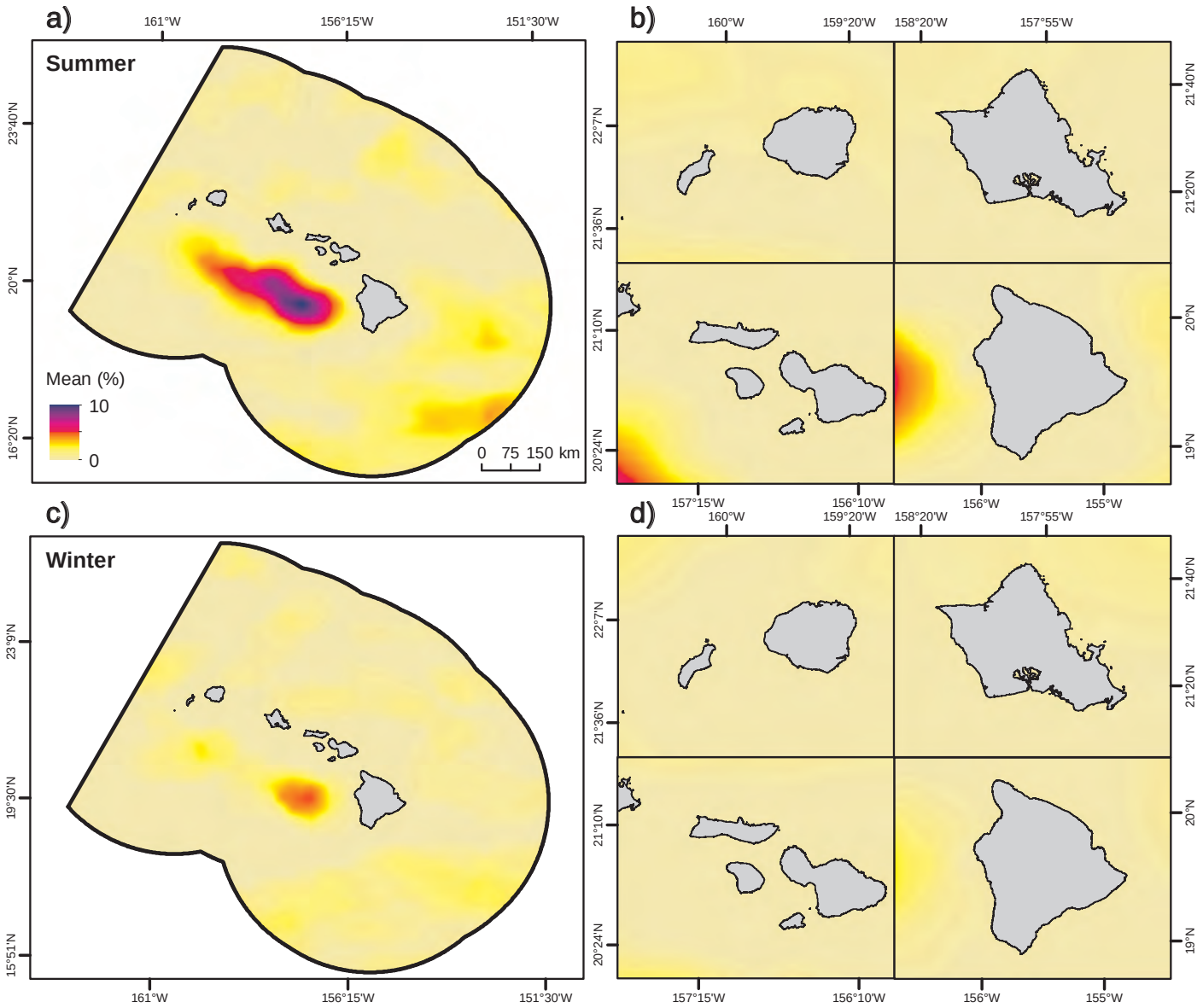

Figure 2.21. Probability of cyclonic eddies around the MHI. These maps depict the average probability (%) that cyclonic (counter-clockwise rotating) eddies will form in the summer (a,b) and winter (c,d) within the study area. Dates: 1992-2014. Data source: Table 2.5. #26

In the summer, upwelling zones are seen west of the Kohala Mountains on Hawai‘i, and west of the Kalohi Channel along Penguin Bank. Downwelling zones are persistent west of South Point in Hawai‘i and west of Kaho‘olawe. All of these upwelling and downwelling zones occur in the lee of the islands. In the winter, spatial patterns in upwelling and downwelling change. Downwelling continues west of South Point and west of Kaho‘olawe, although it weakens and contracts spatially. A weak downwelling zone appears northwest of Kaua‘i, which was not present during the summer. Weak upwelling zones also appear northwest of Kaua‘i and around Ka‘ula. These upwelling and downwelling zones are one of the few that occur on the windward sides of the MHI. Along Penguin Bank, upwelling weakens and becomes almost non-existent compared to the summertime conditions. The upwelling west of the Kohala Mountains remains strong in the winter, although its footprint changes shape and it moves closer inshore. Since the upwelling along Penguin Bank weakens, the area west of Kohala has the strongest upwelling across the islands, making it potentially attractive to many different types of species during the winter.

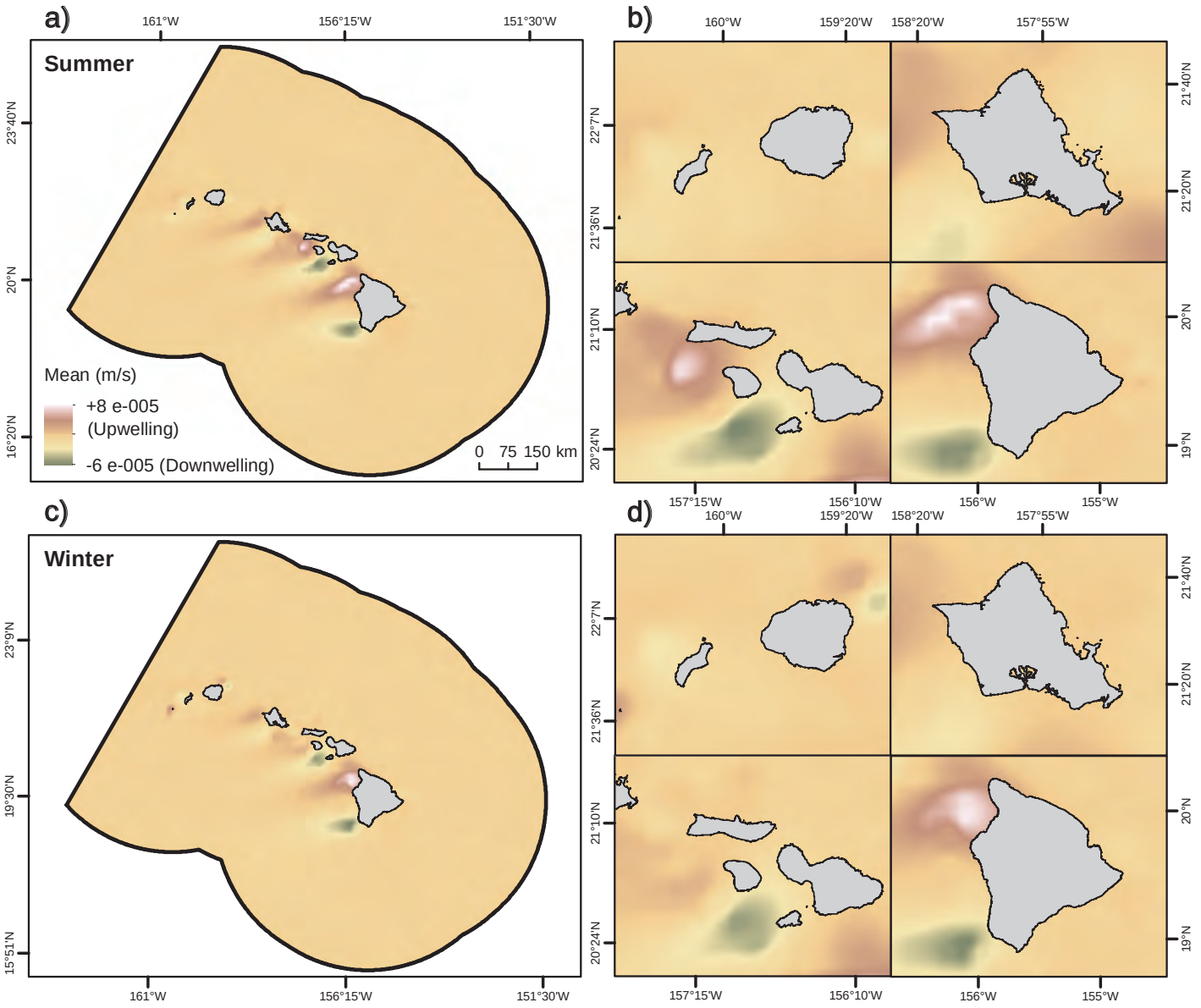

Figure 2.22. Upwelling and downwelling of surface waters around the MHI. These maps depict the average upwelling (+m/s) and downwelling (-m/s) of surface waters in the summer (a,b) and winter (c,d) within the study area. This water movement is driven by surface winds and Ekman transport. Dates: July 1999-November 2009. Data source: Table 2.5. #34

2.4.5. Influence of Bathymetry on Oceanography

The MHI's bathymetry and seafloor topography (e.g., underwater banks and seamounts) influence oceanographic conditions around the islands, similar to how the rugged mountains of the MHI influence its climate. These variable oceanographic conditions are known to affect the composition and distribution of organisms in the MHI (Department of the Navy, 2005; Clark et al., 2010). The exact mechanism by which the MHI's seafloor topography changes the local oceanographic conditions is complex and poorly understood (Rogers, 1993). However, underwater banks and seamounts are known to modify oceanographic currents at local and regional levels (Boehlert and Genin, 1987; Saenko and Merryfield, 2005). Far offshore of the MHI, the HYCOM oceanographic model suggests that the Hawaiian and West Hawaiian Seamounts cause bottom currents to speed up as they flow around their bases (Figure 2.23). These currents are often 0.05 m/s faster around these seamounts compared to the surrounding seascape. Areas north, west and south of Shepard Seamount also see faster and more variable current speeds. Rifts in the Moloka'i and Maui Fracture Zones and topographic changes in the Nu'uanu Slide also cause localized increases and variations in bottom currents northwest of the MHI. Middle Bank is another key seafloor feature that influences the oceanography around

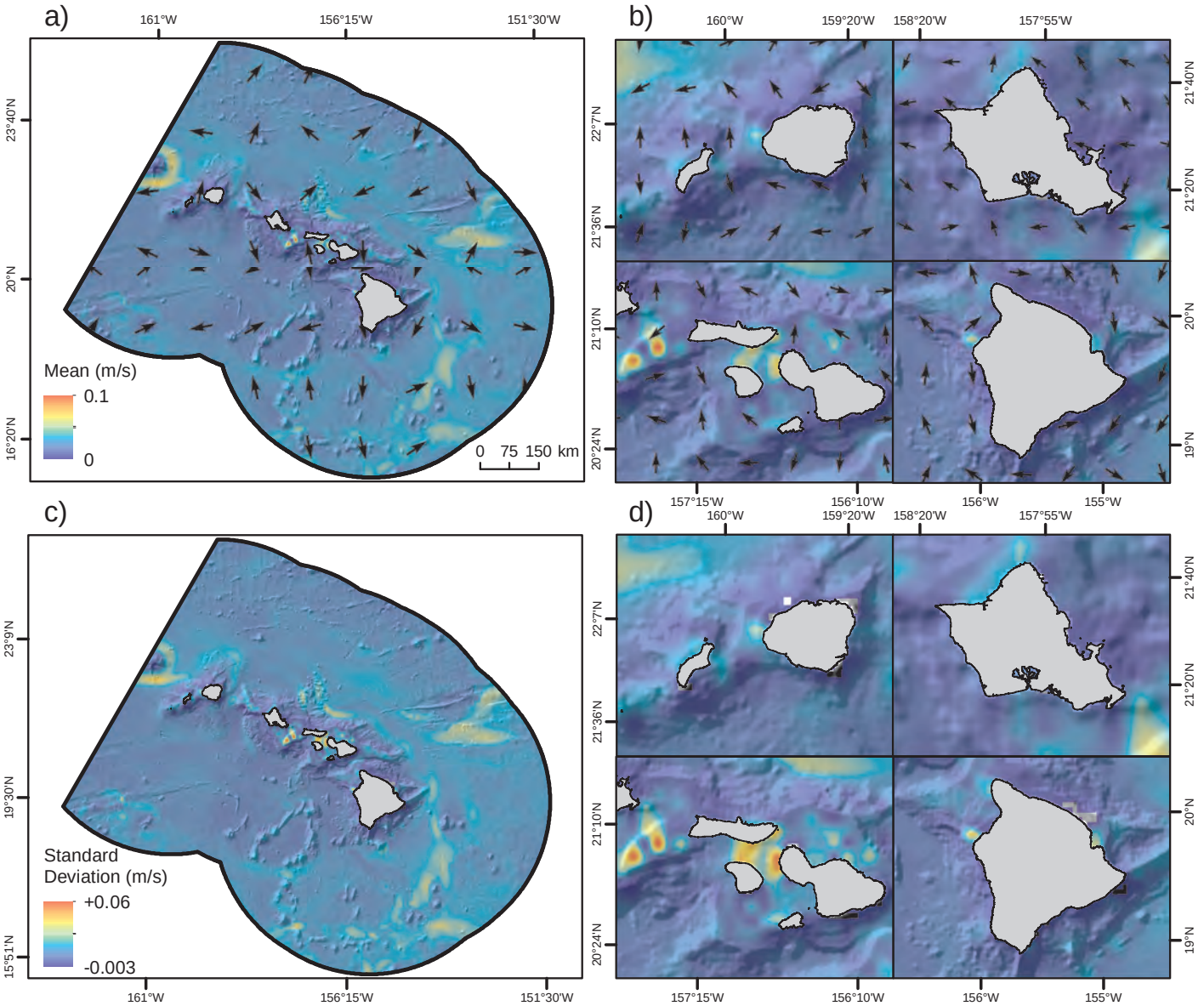

Figure 2.23. Direction, speed, variation in the speed of bottom currents around the MHI. These maps depict the: (a,b) average, annual speed (m/s) and direction (° denoted by arrows) of bottom currents, and (c,d) the standard deviation of annual bottom current speeds (m/s) within the study area. Circular statistics were used to calculate the directional averages. Dates: 1992-2005. Data source: Table 2.4. #20 and 21

the MHI. Middle Bank rises quickly (to 30 m) from the surrounding seafloor (from approximately 3,000 m deep). This abrupt feature disrupts bottom currents, causing them to speed up as they flow westward (Figure 2.23a, b). The speed of currents around Middle Bank are also more variable than in most other parts of the MHI, changing by up to 0.06 m/s over the course of the year (Figure 2.23c, d).

Closer to shore, Penguin Bank and the channels in Maui Nui are the main seafloor features that influence local currents and oceanographic patterns in the MHI. Penguin Bank (Figure 2.1d) is an extension of Maui Nui, which rises up quickly (to around 45 m) from the surrounding shelf (at 550 m). It is oriented in a northeast-southwest direction, paralleling the Kaiwi Channel between O'ahu and Moloka'i. This steep slope creates environmental conditions on the bank that are distinct from its surroundings. For example, bottom currents on top of Penguin Bank are almost twice as fast (0.1 m/s) as those off the Bank (approximately 0.05 m/s). Bottom currents on top of the Bank are also more variable than in many other places around the MHI, changing by up to 0.06 m/s annually. Also, since Penguin Bank is so shallow, the bottom temperature on top of the Bank is much higher (around 20 to 22° C annually) than bottom temperatures of the deep waters surrounding it (8 to 10° C year round; Figure 2.24).

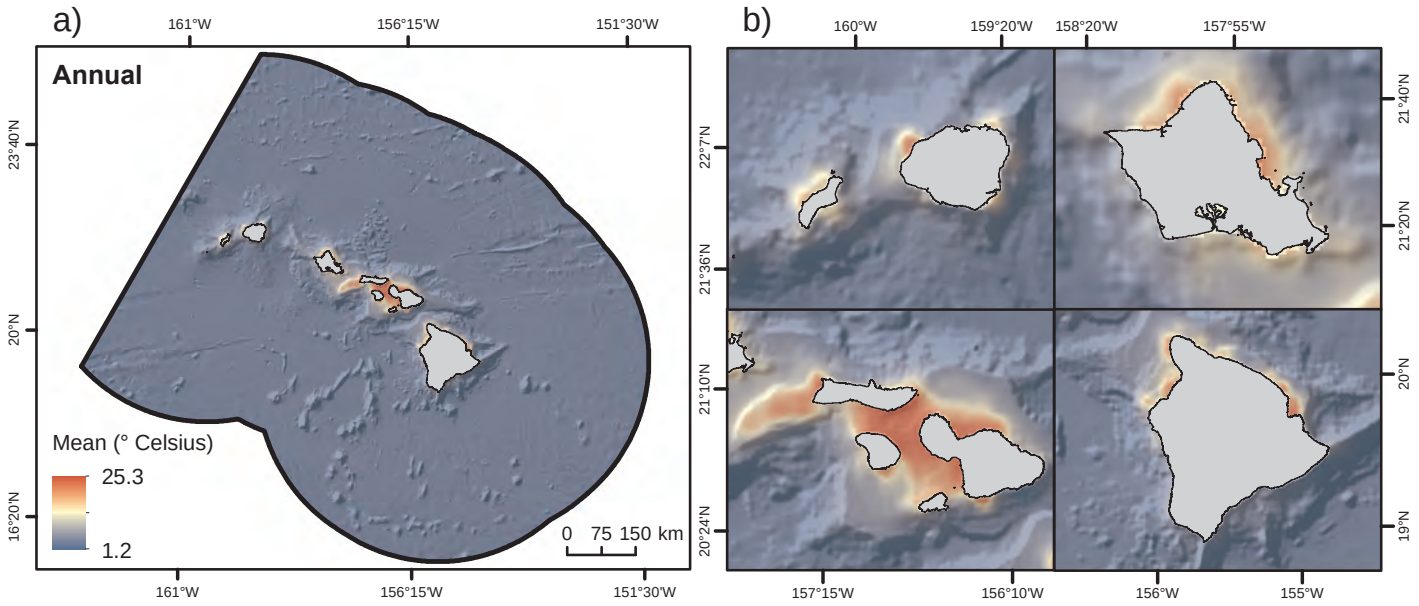

Figure 2.24. Bottom water temperature around the MHI. These maps (a,b) depict the average, annual temperature (°C) of water near the seafloor within the study area. Dates: 1992-2005. Data source: Table 2.6. #35

At the southern-most tip of Penguin Bank (where bottom current speeds increase), perturbations in chlorophyll-*a* concentrations, chlorophyll-*a* fronts, net primary productivity, turbidity and euphotic depth are visible in satellite imagery. Euphotic depth is approximately 20 m deeper during the summer, and as much as 40 m deeper during the winter (Figure 2.25). Light can penetrate deeper into the water column because turbidity is lower (although more variable) near the tip of Penguin Bank (Figures A.5 and A.6). Turbidity is most likely lower because there are fewer organic particles (e.g., plankton) in the water column, as seen in the chlorophyll-*a* concentrations and net primary productivity (NPP) satellite images (Figures A.7, A.8, and A.9). Chlorophyll-*a* fronts are also more frequent and persistent in this location, and are clearly visible following the tip of Penguin Bank (Figures 2.19 and A.15). Combined, these distinct oceanographic conditions and adjacent ecotones may help explain why Penguin Bank is utilized by many different animals in the MHI, most notably bottom fish and Hawaiian monk seals (*Neomonachus schauinslandi*).

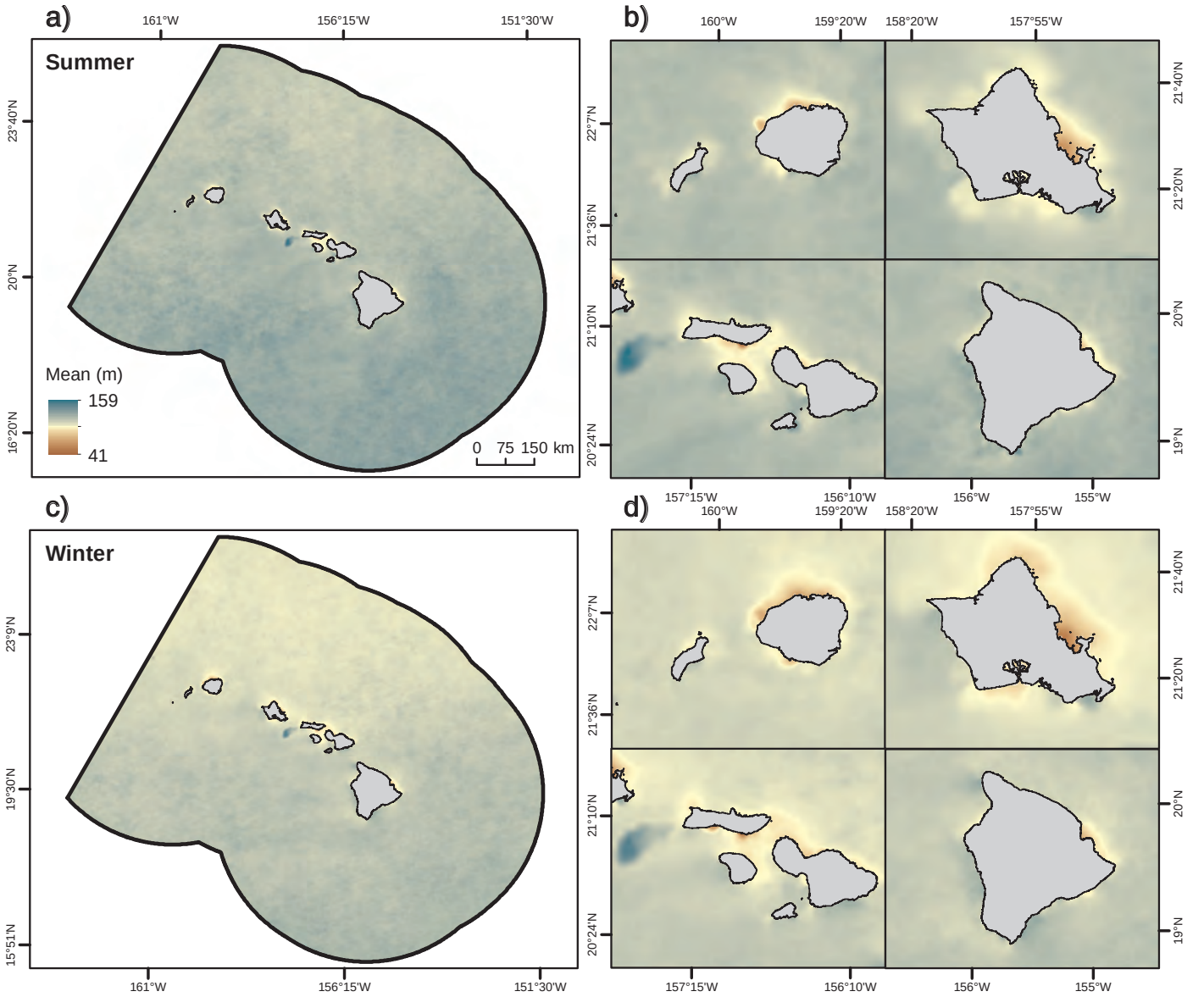

Figure 2.25. Euphotic depth around the MHI. These maps depict the average euphotic depth (m) in the summer (a,b) and winter (c,d) within the study area. Euphotic depth is defined the depth at which 99 percent of the sunlight (used for photosynthesis) is absorbed or reflected. Dates: July 2002-March 2015. Data source: Table 2.4. #17

2.5. DATA LIMITATIONS AND INFORMATION GAPS

2.5.1. Spatial Data Gaps

Mapping environmental drivers is critical for understanding the distribution of animals around the MHI. However, data describing environmental drivers have limitations associated with them, and it is important to understand these limitations before using the data. One of the more common limitations is spatial data gaps. Large (100s km^2) spatial gaps were present in a few of the environmental drivers presented here. These gaps prevented us from continuously mapping specific environmental patterns across the entire project area. For example, significant wave height and wave peak period data were missing from approximately 30 percent of the project area, most of it >100 km from shore (i.e., white areas in Figures 2.14, 2.15, A.10, and A.11). Seasonal wave patterns in these locations were consequently excluded from this assessment. Additional global wave hindcasts could be used to fill these gaps in the future, including NOAA's Wavewatch III Wave Hindcast model (NOAA NCEP, 2015) and the CAWCR Wave Hindcast model (CSIRO, 2016). Similar to the wave data, the depth information around the MHI also had large spatial data gaps (Figure 2.26). Many of these

gaps were either far from shore (>10 km) or very nearshore (<0.5 km). Spatial gaps were filled in the GEBCO surface using satellite altimetry, and by interpolating among depth soundings collected before 2008 (GEBCO, 2008). Depths measured from satellite altimetry are coarse, and could be vastly improved by conducting ship based hydrographic surveys in key geographic areas. Nearshore spatial gaps were filled in NOAA's CRM by extrapolating depths within a radius of 110 cells maximum (NOAA NCEI, 2005). These depth measurements could be improved by collecting LiDAR data in the nearshore. Nearshore data gaps also existed in the SST and chlorophyll-*a* front maps. Neighborhood statistics prevented the detection of fronts within several kilometers from the coast. This lack of detection resulted in erroneously low nearshore values for front persistence, strength and frequency.

2.5.2. Temporal Data Gaps

Most environmental drivers described in this chapter had temporal data gaps. For example, the wind climatologies did not include information after November 2009 because the QuikSCAT sensor stopped collecting information. These drivers may consequently describe environmental patterns that have since changed, or they may exclude new patterns in subsequent years (e.g., after November 2009 for wind drivers). We mitigated the potential impact from these temporal gaps by developing climatologies with >10 years of data, in an attempt to capture broad, long-term patterns in environmental drivers. The other potential impact of temporal data gaps has to do with evolving equipment and techniques for measuring these drivers. Newer equipment and techniques are often more accurate and precise. For the bathymetry surface, some depth measurements (i.e., soundings) date back to the early 1900s (Figure 2.26). These soundings were most likely collected using a lead weight attached to a line. Other soundings were collected using singlebeam Sound Navigation and Ranging (SoNAR) dating back to 1950. These SoNARs use a single beam of sound to measure seafloor depths. More advanced multibeam SoNARs were used to collect depth data around the MHI beginning in 1970. These SoNARs use multiple (>100) beams of sound to measure seafloor depths. The density and distribution of depth data from these different data sources and time periods vary widely across the project area. Depth data far offshore are probably less reliable because they are older, more sparse and measured by only a single sensor. Depth data closer to shore are probably more reliable because they were collected using several different technologies, many of which were more recent. All of these datasets, regardless of age or source, were included in the depth modeling process because they were the best available around the MHI.

2.5.3. Information Gaps

Satellite-mounted sensors and 3D ocean models (e.g., HYCOM) have made it possible to map many environmental drivers over broader spatial scales and longer time periods. However, satellite sensors and 3D ocean models cannot map every type of environmental driver. For example, many physical water chemistry metrics (e.g., ocean pH, calcite or aragonite saturation states) cannot be measured remotely, and require *in situ* field work to quantify their ranges temporally and spatially. Drivers related to competition, predation, reproduction and recruitment also cannot be mapped remotely, and require *in situ* research to identify specific ecological mechanisms. These types of environmental drivers are often too difficult or costly to measure over broad (100s km^2) geographic areas. For these reasons, we did not include chemical or community-level drivers in this study, and instead, relied upon surrogate variables (also known as proxies). Proxies are datasets that can be easily measured, and may be correlated with other environmental drivers that are challenging to measure. Distance to shoreline, shelf edge and seamounts are examples of proxies used in this study. While potentially useful, proxy datasets should be applied with caution because they are not directly linked to the underlying ecological mechanism(s) driving animal distributions.

In addition to missing environmental drivers, the resolution of data from satellites and from 3D ocean models is often coarse (i.e., 1x1 km to 25x25 km), and can limit linking seascape patterns with animal distributions. This limitation is particularly noticeable in the inshore (e.g., bays) and nearshore (i.e., littoral zone) where physical

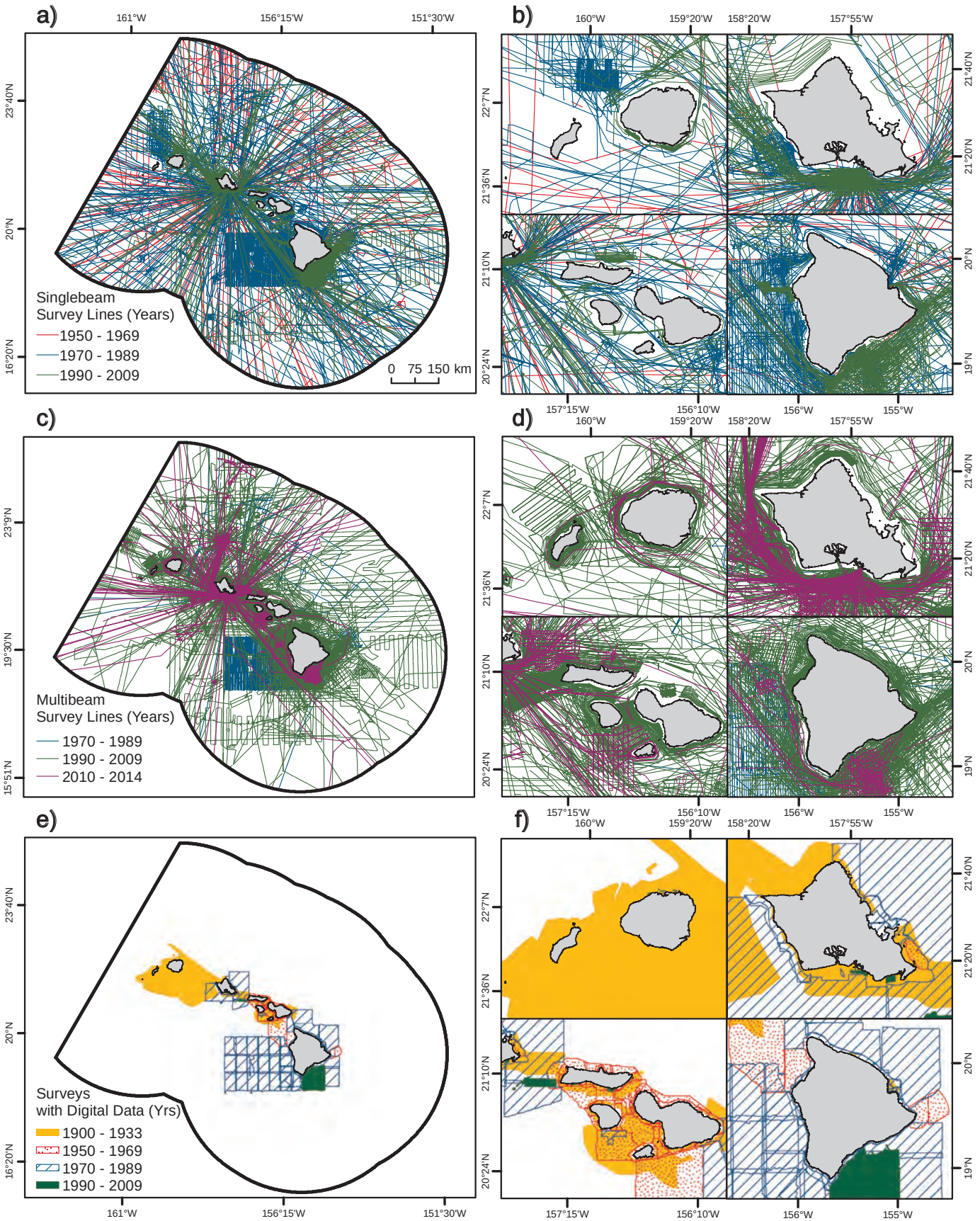

Figure 2.26. Depth surroundings around the MHI from 1900 to 2014. These maps depict the: (a,b) ship tracklines for singlebeam SoNAR surveys (Dates: 1950-2009); (c,d) ship tracklines for multibeam SoNAR surveys (Dates: 1970-2014); and (e,f) location of digital soundings data within the study area (Dates: 1900-2009). Soundings (seen here) collected before 2005 and 2008 were used in the development of NOAA's CRM and GEBCO's depth surfaces, respectively. For a complete list of the bathymetric sources, please see GEBCO, 2008 and NOAA NCEI, 2005. Data source: Table 2.7. #51, 52, 53

and biological conditions tend to be more spatially and temporally variable, and the range of environmental conditions tends to be much greater. The coarse resolution of these datasets is also limiting because their scales may not match the ecological scales (or range of scales) that animals respond to in their environment. This scale mismatch may cause potentially erroneous relationships and patterns to be detected across the seascape (Li and Wu, 2004). One option is to identify broad patterns using coarse datasets, and then target specific geographic areas for more detailed mapping, *in situ* sampling or other field research. Another option is to use modeling techniques (e.g., geostatistical modeling) to develop predictions at finer spatial scales. However, predictive models should be used with caution because they may over-simplify or incorrectly predict ecological patterns and processes.

2.5.4. Measurement Uncertainty

All ecological drivers have uncertainty associated with their values. Uncertainty describes the accuracy and precision associated with a dataset. Uncertainty is usually denoted in several ways, including standard error, mean error (or bias), mean absolute error (MAE) or root mean squared error (RMSE). Uncertainty is useful for making decisions about the quality of data in an area, and can help guide decisions about future data collection efforts. Only a handful of the ecological drivers that we used in this project were compared with *in situ* information, and therefore have published uncertainty values. These drivers include euphotic depth, chlorophyll-*a* concentrations, wind speed, wind direction and mixed layer depth. The RMSE for euphotic depth is 0.077 and mean error is ±13.8 percent (Lee et al., 2007). The RMSE for chlorophyll-*a* is 35.8 percent (within a range of 0.05 to 50 mg/m^3; Esaias et al., 1998). The RMSE differences for wind speed and direction are 1.01 m/s and 23°, respectively (Ebuchi et al., 2002). The RMSE for mixed layer depth is 39.7 m (Chassignet et al., 2006). It is important to note that these uncertainty values may change spatially and may not reflect the uncertainty associated in the MHI. For example, chlorophyll-*a* RMSE values tend to increase in the temperate latitudes, and may not reflect uncertainty in the tropics (Carder et al., 2004).

Uncertainty was also quantified in two ways for the predicted 90x90 m depth surface. First, uncertainty (i.e., standard error) was calculated using cross validation during the geostatistical modeling process to better understand the limitations of this prediction. The resulting standard error surface describes the variation and error associated with predicted depths, and not the error associated the sensors used to measure seafloor depths. The average standard error (calculated using cross validation) was 45 ±27 m across the entire surface (Figure A.23c, d). Error increased as depths increased, particularly deeper than 700 m isobath. Second, uncertainty (i.e., the difference between observed and predicted depths) was calculated using randomly chosen subset of GEBCO depths set aside at the beginning of the modeling process. The average difference between the observed and predicted depths was -0.4 ±27 m, suggesting that predicted depths were biased slightly deeper (Figure A.23e, f). The predicted depth surface's MAE was 12 ±27 m, and its RMSE was 30 m. In total, 99%, 95% and 88% of the errors were smaller than 100 m, 50 m and 25 m, respectively. These uncertainty surfaces and subsequent analyses can be used to help identify and prioritize areas that need to be resurveyed in the future. Areas that are shallower and/or that have higher amounts of error may be the highest priority.

ACKNOWLEDGEMENTS

CSS-Dynamac employees were supported under NOAA Contract No. EA133C-14-NC-1384 with CSS Dynamac, Inc. This chapter would not have been possible without the numerous people who shared their data, time and expertise throughout this process. In particular, we appreciate the support of Dr. Evan Howell from NOAA's Pacific Island Fisheries Science Center (PIFSC) and Dr. Rick Stumpf from NCCOS. A special thanks also to James Bowcott from the Plymouth Marine Laboratory for processing the oceanographic front products. This chapter was improved by the helpful reviews of Dr. Jeffrey Polovina from NOAA's PIFSC and Dr. Ron K. Hoeke from the Centre for Australian Climate and Weather Research. We dedicate this chapter to the memory of our friend and colleague John Rooney.

LITERATURE CITED

Aucan, J. 2006. Directional wave climatology for the Hawaiian Islands from buoy data and the influence of ENSO on extreme wave events from wave model hindcast. 9th International Workshop on Wave Hindasting and Forecasting. Victoria, BC, Canada. 20 pp. Online: ftp://ftp.wmo.int/Documents/PublicWeb/amp/mmop/documents/JCOMM-TR/J-TR-34-9th-waves-workshop/Papers/Aucan.pdf (Site Accessed 8 June 2016).

Aviso, Ssalto/Duacs, and Cnes. 2014. MADT - Maps of Absolute Dynamic Topography and Absolute Geostrophic Velocities. The altimeter products were produced by Ssalto/Duacs and distributed by Aviso, with support from Cnes. Data Downloaded 4 December 2013 and 12 September 2014. Data Website: http://www.aviso.altimetry.fr/en/data/data-access/aviso-opendap/opendap-adt-products.html (Site Accessed 8 June 2016).

Battista, T.A., B.M. Costa, and S.M. Anderson. 2007. Benthic Habitats of the Main Hawaiian. NOAA Technical Memorandum NOS NCCOS CCMA 152. Silver Spring, MD. 48 pp. Data Downloaded 5 September 2014. Data Website: https://products.coastalscience.noaa.gov/collections/benthic/e97hawaii/data2007.aspx (Site Accessed 8 June 2016).

Boehlert, G.W. and A. Genin. 1987. A review of the effects of seamounts on biological processes. Seamounts, islands and atolls 43: 319-334. Online: https://swfsc.noaa.gov/publications/CR/1987/8709.PDF (Site Accessed 8 June 2016).

Caldwell, P. 2005. Validity of North Shore, O'ahu, Hawaiian Islands Surf Observations. Journal of Coastal Research 21: 1127-1138.

Calil, P.H., K.J. Richards, Y. Jia, and R.R. Bidigare. 2008. Eddy activity in the lee of the Hawaiian Islands. Deep Sea Research Part II: Topical Studies in Oceanography 55(10): 1179-1194.

Calil, P.H.R. and K.J. Richards. 2010. Transient upwelling hot spots in the oligotrophic North Pacific. Journal of Geophysical Research: 115(C02003).

Carder, K.L., F.R. Chen, J.P. Cannizzaro, J.W. Campbell, and B.G. Mitchell. 2004. Performance of the MODIS semi-analytical ocean color algorithm for chlorophyll-*a*. Advances in Space Research 33: 1152-1159.

Casey, K. 2010. The Coral Reef Temperature Anomaly Database (CoRTAD) Version 3 - Global, 4 km Sea Surface Temperature and Related Thermal Stress Metrics for 1982-2009 (NODC Accession 0068999) Version 1.1. NOAA National Centers for Environmental Information. Dataset Downloaded 1 June 2014. Data Website: http://data.nodc.noaa.gov/cgi-bin/iso?id=gov.noaa.nodc:0068999 (Site Accessed 8 June 2016).

Chassignet, E.P., H.E. Hurlburt, O.M. Smedstad, G.R. Halliwell, P.J. Hogan, A.J. Wallcraft, and R. Bleck. 2006. Chapter 16: Ocean prediction with the hybrid coordinate ocean model (HYCOM). pp. 413-426. In: E.P. Chassignet and J. Verron (eds.), Ocean Weather Forecasting: An Integrated View of Oceanography. Springer Netherlands. 577 pp.

Chavanne, C., P. Flament, R. Lumpkin, B. Dousset, and A. Bentamy. 2002. Scatterometer observations of wind variations induced by oceanic islands: Implications for wind-driven ocean circulation. Canadian Journal of Remote Sensing 28(3): 466-474.

Cheung, K.F. 2016. Significant wave heights and peak periods around the Main Hawaiian Islands. University of Hawai'i at Mānoa, Department of Ocean Resources and Engineering. Data Provided 20 February 2014. Provider Website: http://www.ore.hawaii.edu/ (Site Accessed 8 June 2016).

Clark, M.R., A.A. Rowden, T. Schlacher, A. Williams, M. Consalvey, K.I. Stocks, A.D. Rogers, T.D. O'Hara, M. White, T.M. Shank, and J.M. Hall-Spencer. 2010. The ecology of seamounts: structure, function, and human impacts. Annual Review of Marine Science 2: 253-278.

CSIRO. 2016. CAWCR Wave Hindcast 1979-2010. Data Access Portal, Commonwealth Scientific and Industrial Research Organization. Online: https://data.csiro.au/dap/landingpage?pid=csiro%3A6616 (Site Accessed 8 June 2016).

D'Errico, J. 2014. inpaint_nans, MATLAB Central File Exchange (Software Downloaded April 2014). MathWorks, Inc. Natick, Massachusetts. Software Online: http://www.mathworks.com/matlabcentral/fileexchange/4551-inpaint-nans (Site Accessed 8 June 2016).

Department of the Navy. 2005. Marine Resources Assessment for the Hawaiian Islands Operating Area. Department of the Navy, Pacific Division, Naval Facilities Engineering Command. Pearl Harbor, Hawai'i. Contract #N62470-02-D-9997, CTO 0026. Prepared by Geo-Marine, Inc., Plano, Texas. Online: http://www.navfac.navy.mil/content/dam/navfac/Environmental/PDFs/MRA/HAWAII%20FINAL%20MRA%20-%20DECEMBER%202005.pdf (Site Accessed 8 June 2016).

Dong, C., T. Mavor, F. Nencioli, S. Jiang, Y. Uchiyama, J.C. McWilliams, T. Dickey, M. Ondrusek,H. Zhang, and D.K. Clark. 2009. An oceanic cyclonic eddy on the lee side of Lāna'i Island, Hawai'i. Journal of Geophysical Research: 114(C10008).

Ebuchi, N., H.C. Graber, and M.J. Caruso. 2002. Evaluation of wind vectors observed by QuikSCAT/SeaWinds using ocean buoy data. Journal of Atmospheric and Oceanic Technology 19(12): 2049-2062.

Esaias, W.E., M.R. Abbott, I. Barton, O.B. Brown, J.W. Campbell, K.L. Carder, D.K. Clark, R.H. Evans, F.E. Hoge, H.R. Gordon, W.M. Balch, R. Letelier, and P.J. Minnett. 1998. An overview of MODIS capabilities for ocean science observations. IEEE Transactions on Geoscience and Remote Sensing 36(4): 1250-1265.

ESRI. 2014. ArcGIS Desktop: Release 10.3. Environmental Systems Research Institute. Redlands, CA. Online: http://www.esri.com/ (Site Accessed 8 June 2016).

ESRI. 2011. ArcGIS Desktop: Release 10. Environmental Systems Research Institute. Redlands, CA. Online: http://www.esri.com/ (Site Accessed 8 June 2016).

Flament, P., S. Keenan, R. Lumpkin, M. Sawyer, and E.D. Stroup. 1996. The Ocean Atlas of Hawai'i. Pacific Islands Ocean Observing System (PacIOOS). School of Ocean and Earth Science and Technology, University of Hawai'i at Manoa. Online: http://oos.soest.hawaii.edu/pacioos/outreach/oceanatlas/index.php (Site Accessed 8 June 2016).

Fletcher, C.H., C. Bochicchio, C.L. Conger, M.S. Engels, E.J. Feirstein, N. Frazer, C.R. Glenn, R.W. Grigg, E.E. Grossman, J.N. Harney, E. Isoun, C.V. Murray-Wallace, J.J. Rooney, K.H. Rubin, C.E. Sherman, and S. Vitousek. 2008. Geology of Hawai'i reefs. pp. 435-487. In: B. Riegl and R.E. Dodge (eds.). Coral Reefs of the USA. Coral Reefs of the World, Volume 1. Springer Netherlands. 803 pp.

Fletcher, C.H., III, E.E. Grossman, B.M. Richmond, and A.E. Gibbs. 2002. Atlas of natural hazards in the Hawaiian Coastal Zone. U.S. Geological Survey, Geologic Investigations Series I-2761. Data Website: http://pubs.usgs.gov/imap/i2761/ (Site Accessed 8 June 2016).

Falkowski, P.G., D. Ziemann, Z. Kolber, and P.K. Bienfang. 1991. Role of eddy pumping in enhancing primary production in the ocean. Nature 352: 55-58.

GEBCO. 2008. General Bathymetric Chart of the Oceans 08 Grid. GEBCO operates under the joint auspices of the International Hydrographic Organization and the Intergovernmental Oceanographic Commission of UNESCO. Data Downloaded 8 January 2014. Data Website: http://www.gebco.net/data_and_products/gridded_bathymetry_data/ (Site Accessed 8 June 2016).

Halpert, M.S. and C.F. Ropelewski. 1992. Surface temperature patterns associated with the Southern Oscillation. Journal Climate 5(6): 577-593.

Hoeke, R., C. Storlazzi, and P. Ridd. 2011. Hydrodynamics of a bathymetrically complex fringing coral reef embayment: Wave climate, *in situ* observations, and wave prediction. Journal of Geophysical Research: 116(C04018).

HYCOM Consortium. 2014. HYCOM + NCODA Global 1/12 Reanalysis. Funding for the development of HYCOM has been provided by the National Ocean Partnership Program and the Office of Naval Research. Data assimilative products using HYCOM are funded by the U.S. Navy. Computer time was made available by the DoD High Performance Computing Modernization Program. Data Downloaded 1 September 2014. Data Website: https://hycom.org/dataserver/glb-reanalysis (Site Accessed 8 June 2016).

Jenness, J. 2013. DEM Surface Tools. Jenness Enterprises. Software Downloaded November 2015. Software Online: http://www.jennessent.com/arcgis/surface_area.htm (Site Accessed 8 June 2016).

Jia, Y., P.H.R. Calil, E.P. Chassignet, E.J. Metzger, J.T. Potemra, K.J. Richards, and A.J. Wallcraft. 2011. Generation of mesoscale eddies in the lee of the Hawaiian Islands. Journal of Geophysical Research: 116(C11009).

Juvik, J.O. and S.P. Juvik (Eds). 1998. Atlas of Hawai'i (3rd Ed.). University Of Hawai'i at Hilo Press. Honolulu, HI. 333 pp.

Karl D. M., Letelier R., Hebel D., Tupas L., Dore J., Christian J., and Winn C. 1995. Ecosystem changes in the North Pacific subtropical gyre attributed to the 1991–92 El Nino. Nature. 373:230-234.

Lee, Z., A. Weidemann, J. Kindle, R. Arnone, K.L. Carder, and C. Davis. 2007. Euphotic zone depth: Its derivation and implication to ocean-color remote sensing. Journal of Geophysical Research 112(C03009).

Li, H. and J. Wu. 2004. Use and misuse of landscape indices. Landscape ecology 19(4): 389-399.

Lumpkin, C.F. 1998. Eddies and currents in the Hawaiian Islands. Ph.D. Thesis. School of Ocean and Earth Science and Technology, University of Hawai'i at Mānoa. 282 pp.

Mantua, N.J., S.R. Hare, Y. Zhang, J.M. Wallace, and R.C. Francis. 1997. A Pacific decadal climate oscillation with impacts on salmon. Bulletin of the American Meteorological Society 78: 1069-1079.

Mantua, N.J. 2015. The Pacific Decadal Oscillation. Joint Institute for the Study of the Atmosphere and Ocean, University of Washington. Data Downloaded 30 December 2015. Data Website: http://research.jisao.washington.edu/pdo/PDO.latest (Site Accessed 8 June 2016).

Mantua, N.J. and S.R. Hare. 2002. The Pacific Decadal Oscillation. Journal of Oceanography 58: 35-44.

Mathworks. 2014. MATLAB and Statistics Toolbox Release 2014a. MathWorks, Inc. Natick, Massachusetts. Software Downloaded October 2014. Software Online: http://www.mathworks.com/products/matlab/index.html?s_tid=gn_loc_drop (Site Accessed 8 June 2016).

McGillicuddy, D. and A.R. Robinson. 1997. Eddy-induced nutrient supply and new production in the Sargasso Sea. Deep-Sea Research 44(8): 1427-1450.

Miller, P.I. and S. Christodoulou. 2014. Frequent locations of oceanic fronts as an indicator of pelagic diversity: application to marine protected areas and renewables. Marine Policy 45: 318-329.

Miller, P.I., K.L. Scales, S.N. Ingram, E.J. Southall, and D.W. Sims. 2015a. Basking sharks and oceanographic fronts: quantifying associations in the north-east Atlantic. Functional Ecology 29(8): 1099-1109.

Miller, P.I., W. Xu, and M. Carruthers. 2015b. Seasonal shelf-sea front mapping using satellite ocean colour and temperature to support development of a marine protected area network. Deep Sea Research Part II: Topical Studies in Oceanography 119: 3-19.

Miller, P.I. 2016. Oceanic Fronts in the Main Hawaiian Islands. Plymouth Marine Laboratory, Remote Sensing Group. Plymouth, United Kingdom. Data Provided 10 June 2015. Provider Website: https://rsg.pml.ac.uk/ (Site Accessed 8 June 2016).

Minobe, S. 1997. A 50-70 year climatic oscillation over the North Pacific and North America. Geophysical Research Letters 44: 683-686.

Moberly, R. and T. Chamberlain. 1964. Hawaiian beach systems. Hawai'i Institute of Geophysics Report 64-2. University of Hawai'i, Honolulu, HI. 95 pp.

NASA. 2008. La Niña and Pacific Decadal Oscillation Cool the Pacific. National Aeronautics and Space Administration, Earth Observatory. Online: http://earthobservatory.nasa.gov/IOTD/view.php?id=8703 (Site Accessed 8 June 2016).

NASA. 2010. GHRSST Level 4 MUR Global Foundation Sea Surface Temperature Analysis. Ver. 2. JPL MUR MEaSUREs Project. National Aeronautics and Space Administration, Jet Propulsion Laboratory. Online: http://mur.jpl.nasa.gov/ (Site Accessed 8 June 2016).

NASA. 2013a. Ocean Color Web - Standard, Aqua MODIS Chlorophyll Concentration, OCI Algorithm, Daily, 4 km. National Aeronautics and Space Administration, Goddard Space Flight Center, Ocean Biology Processing Group. Data Downloaded 7 October 2013. Data Website: http://oceancolor.gsfc.nasa.gov/cgi/l3 (Site Accessed 8 June 2016).

NASA. 2013b. Ocean Color Web – Evaluation, Aqua MODIS (Lee) Euphotic Depth, Monthly, 4 km. National Aeronautics and Space Administration, Goddard Space Flight Center, Ocean Biology Processing Group. Data Downloaded 7 October 2013. Data Website: http://oceancolor.gsfc.nasa.gov/cgi/l3 (Site Accessed 8 June 2016).

NASA. 2014. Multi-scale Ultra-high Resolution (MUR) Sea Surface Temperature. National Aeronautics and Space Administration, Jet Propulsion Laboratory. Data Downloaded 5 September 2014. Data Website: http://podaac-opendap.jpl.nasa.gov/opendap/allData/ghrsst/data/L4/GLOB/JPL/MUR/ (Site Accessed 8 June 2016).

NASA. 2015a. QuikSCAT (Quik Scatterometer). Winds: Measuring Ocean Winds from Space. National Aeronautics and Space Administration, Jet Propulsion Laboratory. Online: https://winds.jpl.nasa.gov/missions/quikscat/ (Site Accessed 8 June 2016).

NASA. 2015b. Ocean Color Web – Standard, Aqua MODIS Remote sensing reflectance at 547 nm, Monthly, 4 km. National Aeronautics and Space Administration, Goddard Space Flight Center, Ocean Biology Processing Group. Data Downloaded 22 April 2015. Data Website: http://oceancolor.gsfc.nasa.gov/cgi/l3 (Site Accessed 8 June 2016).

NASA. 2016. Aqua Earth-observing satellite mission. National Aeronautics and Space Administration, Aqua Project Science. Online: http://aqua.nasa.gov/ (Site Accessed 8 June 2016).

NOAA. 2015. Rain Shadows on the Summits of Hawai'i. National Oceanic and Atmospheric Administration, Climate.gov. Online: https://www.climate.gov/news-features/featured-images/rain-shadows-summits-hawaii (Site Accessed 8 June 2016).

NOAA CPC. 2015. Cold and Warm Episodes by Season. NOAA National Weather Service, National Centers for Environmental Prediction, Climatic Prediction Center. Data Downloaded 12 September 2015. Data Website: http://www.cpc.ncep.noaa.gov/products/analysis_monitoring/ensostuff/ensoyears.shtml (Site Accessed 8 June 2016).

NOAA ESRL. 2015. Climate Indices, Monthly Atmospheric and Ocean Time Series: ONI (Oceanic Niño Index). NOAA Earth Systems Research Laboratory, Physical Sciences Division. Data Downloaded 14 May 2015. Data Website: http://www.esrl.noaa.gov/psd/data/climateindices/list/ (Site Accessed 8 June 2016).

NOAA NCCOS. 2016. Biogeographic Assessment of the Main Hawaiian Islands. Projects Explorer. NOAA National Ocean Service, National Centers for Coastal Ocean Science. Online: http://coastalscience.noaa.gov/projects/detail?key=163 (Site Accessed 8 June 2016).

NOAA NCEI. 2005. U.S. Coastal Relief Model - Hawai'i. NOAA National Environmental Satellite, Data, and Information Service, National Centers for Environmental Information. Data Downloaded 8 January 2014. Data Website: https://www.ngdc.noaa.gov/mgg/coastal/grddas10/grddas10.htm (Site Accessed 8 June 2016).

NOAA NCEI. 2015a. Teleconnections: El Niño/Southern Oscillation (ENSO), Pacific Decadal Oscillation (PDO). NOAA National Environmental Satellite, Data, and Information Service, National Centers for Environmental Information. Online: http://www.ncdc.noaa.gov/teleconnections/ (Site Accessed 8 June 2016).

NOAA NCEI. 2015b. Bathymetric Data Viewer. NOAA National Environmental Satellite, Data, and Information Service, National Centers for Environmental Information. Data Provided 15 September 2015. Provider Website: https://maps.ngdc.noaa.gov/viewers/bathymetry/ (Site Accessed 8 June 2016).

NOAA NCEI. 2016. El Niño/Southern Oscillation (ENSO) Technical Discussion. NOAA National Environmental Satellite, Data, and Information Service, National Centers for Environmental Information. Online: https://www.ncdc.noaa.gov/teleconnections/enso/enso-tech.php (Site Accessed 8 June 2016).

NOAA NCEP. 2015. NOAA WAVEWATCH III® CFSR Reanalysis Hindcasts. NOAA National Weather Center, National Centers for Environmental Prediction, Environmental Modeling Center. Online: http://polar.ncep.noaa.gov/waves/CFSR_hindcast.shtml (Site Accessed 8 June 2016).

NOAA PEACC. 2016. El Niño and its impacts on Hawai'i. NOAA National Weather Service, Pacific ENSO Applications Climate Center. Online: http://www.weather.gov/media/peac/one_pagers/El%20Nino%20Impacts%20on%20Hawaii.pdf (Site Accessed 8 June 2016).

Oregon State University. 2013. Net Primary Productivity, Online Data: Standard VGPM. Ocean Productivity. College of Science, Oregon State University. Data Downloaded 1 December 2013. Data Website: http://orca.science.oregonstate.edu/1080.by.2160.monthly.hdf.vgpm.m.chl.m.sst.php (Site Accessed 8 June 2016).

PacIOOS. 2015a. Satellite Datasets Wind - Wind, QuikSCAT, Global, Science Quality, Divergence. Pacific Integrated Ocean Observing System. School of Ocean and Earth Science and Technology, University of Hawai'i at Manoa and National Oceanic and Atmospheric Administration. Data Downloaded 10 May 2015. Data Website: http://oos.soest.hawaii.edu/thredds/remoteCatalogService?catalog=http://oceanwatch.pfeg.noaa.gov/thredds/Satellite/aggregsatQS/divw/catalog.xml (Site Accessed 8 June 2016).

PacIOOS. 2015b. Satellite Datasets Wind - Wind, QuikSCAT, Global, Science Quality, Modulus. Pacific Integrated Ocean Observing System. School of Ocean and Earth Science and Technology, University of Hawai'i at Manoa and National Oceanic and Atmospheric Administration. Data Downloaded 10 May 2015. Data Website: http://oos.soest.hawaii.edu/thredds/remoteCatalogService?catalog=http://oceanwatch.pfeg.noaa.gov/thredds/Satellite/aggregsatQS/umod/catalog.xml (Site Accessed 8 June 2016).

PacIOOS. 2015c. Satellite Datasets Wind - Wind, QuikSCAT, Global, Science Quality, Zonal. Pacific Integrated Ocean Observing System. School of Ocean and Earth Science and Technology, University of Hawai'i at Manoa and National Oceanic and Atmospheric Administration. Data Downloaded 10 May 2015. Data Website: http://oos.soest.hawaii.edu/thredds/remoteCatalogService?catalog=http://oceanwatch.pfeg.noaa.gov/thredds/Satellite/aggregsatQS/ux10/catalog.xml (Site Accessed 8 June 2016).

PacIOOS. 2015d. Satellite Datasets Wind - Wind, QuikSCAT, Global, Science Quality, Merid. Pacific Integrated Ocean Observing System. School of Ocean and Earth Science and Technology, University of Hawai'i at Manoa and National Oceanic and Atmospheric Administration. Data Downloaded 10 May 2015. Data Website: http://oos.soest.hawaii.edu/thredds/remoteCatalogService?catalog=http://oceanwatch.pfeg.noaa.gov/thredds/Satellite/aggregsatQS/uy10/catalog.xml (Site Accessed 8 June 2016).

PacIOOS. 2015e. Satellite Datasets Wind - Wind, Ekman Upwelling, QuikSCAT, Global, Science Quality. Pacific Integrated Ocean Observing System. School of Ocean and Earth Science and Technology, University of Hawai'i at Manoa and National Oceanic and Atmospheric Administration. Data Downloaded 10 May 2015. Data Website: http://oos.soest.hawaii.edu/thredds/remoteCatalogService?catalog=http://oceanwatch.pfeg.noaa.gov/thredds/Satellite/aggregsatQS/wekm/catalog.xml (Site Accessed 8 June 2016).

Patzert, W.C. 1969. Eddies in Hawaiian waters. HIG Series 69(8). Hawai'i Institute of Geophysics, University of Hawai'i. 51 pp.

R Core Team. 2016. R: A language and environment for statistical computing (Versions 3.1.1 to 3.1.3). R Foundation for Statistical Computing. Vienna, Austria. Software Online: http://www.r-project.org (Site Accessed 8 June 2016).

Roberts, J.J., B.D. Best, D.C. Dunn, E.A. Treml, and P.N. Halpin. 2010. Marine Geospatial Ecology Tools: An integrated framework for ecological geoprocessing with ArcGIS, Python, R, MATLAB, and C++. Environmental Modelling & Software 25(10): 1197-1207.

Rogers, A.D. 1993. The biology of seamounts. Advances in Marine Biology 30: 305-305.

Rooney, J. and C.H. Fletcher. 2005. Shoreline Change and Pacific Climatic Oscillations in Kihei, Maui, Hawai'i. Journal of Coastal Research 21(3): 535-547.

Rooney, J.J., P. Wessel, R. Hoeke, J. Weiss, J. Baker, F. Parrish C.H. Fletcher, J. Chojnacki, M. Garcia, R. Brainard, and P. Vroom. 2008. Chapter 13: Geology and Geomorphology of Coral Reefs in the Northwestern Hawaiian Islands. pp. 519-571. In: B. Riegl and R.E. Dodge (eds.). Coral Reefs of the USA. Coral Reefs of the World, Volume 1. Springer Netherlands. 803 pp.

Ropelewski, C.F. and M.S. Halpert. 1989. Precipitation patterns associated with the high phase of the Southern Oscillation. Journal of Climate 1: 172-182.

Saenko, O.A. and W.J. Merryfield. 2005. On the effect of topographically enhanced mixing on the global ocean circulation. Journal of Physical Oceanography 35(5): 826-834.

Seki, M.P., J.J. Polovina, R.E. Brainard, R.R. Bidigare, C.L. Leonard, and D.G. Foley. 2001. Biological enhancement at cyclonic eddies tracked with GOES thermal imagery in Hawaiian waters. Geophysical Research Letters 28(8): 1583-1586.

Seki, M.P., R. Lumpkin, and P. Flament. 2002. Hawai'i cyclonic eddies and blue marlin catches: the case study of the 1995 Hawaiian International Billfish Tournament. Journal of Oceanography 58(5): 739-745.

Scales, K.L., P.I. Miller, C.B. Embling, S.N. Ingram, E. Pirotta, and S.C. Votier. 2014. Mesoscale fronts as foraging habitats: composite front mapping reveals oceanographic drivers of habitat use for a pelagic seabird. Journal of the Royal Society Interface 11(100): 1-9.

Snodgrass, F.E., G.W. Groves, K.F. Hasselmann, G.R. Miller, W.H. Munk, and W.H. Powers. 1966. Propagation of Ocean Swell across the Pacific. Philosophical Transactions of the Royal Society of London. Series A, Mathematical and Physical Sciences 259(1103): 431-497.

Smith, R.B. and V. Grubisic. 1993. Aerial observations of the Hawai'i's wake. Journal of Atmospheric Sciences 50: 3728-3750.

Stopa, J.E., J.F. Filipot, N. Li, K.F. Cheung, Y.L. Chen, and L. Vega. 2013. Wave energy resources along the Hawaiian Island chain. Renewable energy 55: 305-321.

Tolman, H.L. 2009. User manual and system documentation of WAVEWATCH III version 3.14. NOAA National Weather Service, National Centers for Environmental Prediction. 194 pp. Online: http://polar.ncep.noaa.gov/mmab/papers/tn276/MMAB_276.pdf (Site Accessed 8 June 2016).

UH CGG. 2012. Sea Level Rise Hawai'i: Hawai'i's Changing Climate. Coastal Geology Group, University of Hawai'i. Online: http://www.soest.hawaii.edu/coasts/sealevel/ (Site Accessed 8 June 2016).

USGS. 2015. The 3DEP National Map (1/3 arc-second DEMs for Hawai'i). The National Map. U.S. Geological Survey. Data Downloaded 15 September 2015. Data Website: http://viewer.nationalmap.gov/basic/?basemap=b1&category=ned,nedsrc&title=3DEP%20View#startUp (Site Accessed 8 June 2016).

USGS. 2016. Hawaiian Volcano Observatory. U.S. Geological Survey. Online: http://hvo.wr.usgs.gov/ (Site Accessed 8 June 2016).

Vaillancourt, R.D., J. Marra, M.P. Seki, M.L. Parsons, and R.R. Bidigare. 2003. Impact of a cyclonic eddy on phytoplankton community structure and photosynthetic competency in the subtropical North Pacific Ocean. Deep Sea Research Part I: Oceanographic Research Papers 50(7): 829-847.

Vitousek, S. and C.H. Fletcher. 2008. Maximum annually recurring wave heights in Hawai'i. Pacific Science 62(4): 541-553.

Vitousek, S., M.M. Barbee, C.H. Fletcher, B.M. Richmond, and A.S. Genz. 2009. Pu'ukoholā Heiau National Historic Site and Kaloko-Honokōhau Historical Park, Big Island of Hawai'i: Coastal Hazard Analysis Report. Natural Resource Technical Report NPS/NRPC/GRD/NRTR-2010/387. 105 pp. Online: http://www.soest.hawaii.edu/coasts/nps/ (Site Accessed 8 June 2016).

Wikipedia. 2015. Rainshadow. Data Website: https://commons.wikimedia.org/wiki/File:Rainshadow_copy.jpg (Site Accessed 8 June 2016).

Chapter 3 Benthic Habitats and Corals

Laurie Bauer[1,3], Matthew Poti[1,3], Bryan Costa[1], Daniel Wagner[6], Frank Parrish[7], Mary Donovan[8], and Brian Kinlan[1]

Photo credit: Kurt Kawamoto (NOAA NMFS/PIFSC)

ABSTRACT

An understanding of the distribution of marine benthic habitats and associated biota in the Main Hawaiian Islands (MHI) is necessary in order to assess potential direct and indirect effects of renewable energy development. Benthic habitats in the MHI can be divided into three broad categories based on their depth: shallow (<30 m), mesophotic (30-150 m) and deep (>150 m). Shallow-coral reefs provide numerous natural and economic benefits to the state's economy and are much better studied than mesophotic and deep-water coral reefs. Approximately 75 percent of the shallow-water (<30 m) area around the MHI has been characterized using satellite imagery, although the percentage varies by island, with less area mapped around Hawai'i and the windward sides of Maui and Kaho'olawe. Seventeen datasets from shallow reef monitoring programs were compiled into a standardized database of benthic cover. A qualitative assessment of the data indicates that percent cover of major benthic taxonomic groups (e.g., live coral, macroalgae) varies at both the island and local scales, with coral cover generally lower around the most northwestern islands. Recently published spatial predictive models of mesophotic hard coral distributions in the 'Au'au Channel provided maps of probability of occurrence for Leptoseris *spp*., Montipora *spp*. *and* Porites *spp*. *These models were created using presence and absence records for these genera and a suite of environmental predictor variables. Probability of occurrence for mesophotic hard corals was highest in the warmer, clearer, and calmer waters off the western coast of Maui between Hanakao'o Point and Papawai Point. Although less data is available in deeper habitats, a variety of deep-sea corals (DSC) have been documented in the Hawaiian Archipelago. Using presence-only data and a suite of environmental predictor variables, spatial predictive models were created for eighteen DSC groups to identify areas most likely to contain deep-sea coral habitat around the MHI. The distributions of DSC presence records varied among groups; however, records were often concentrated in particular locations, such as Cross Seamount, Makapu'u Point, Makalawena Bank, Lō'ihi Seamount, and the southern edge of Penguin Bank. Areas predicted to contain highly suitable DSC habitat broadly aligned with the locations of DSC presence records. The environmental variables of depth, distance to shore and slope were consistently the most important predictors across all models. For both mesophotic corals and DSC, model results can be used to guide future exploration and research, particularly in areas where few records exist.*

Citation for chapter
Bauer, L., M. Poti, B.M. Costa, D. Wagner, F. Parrish, M. Donovan, and B. Kinlan. 2016. Chapter 3: Benthic Habitats and Corals. pp. 57-136. In: B.M. Costa and M.S. Kendall (eds.), Marine Biogeographic Assessment of the Main Hawaiian Islands. Bureau of Ocean Energy Management and National Oceanic and Atmospheric Administration. OCS Study BOEM 2016-035 and NOAA Technical Memorandum NOS NCCOS 214. 359 pp.

[1] *NOAA National Centers for Coastal Ocean Science, Biogeography Branch, Silver Spring, MD, U.S.A.*
[3] *CSS-Dynamac, Fairfax, VA, U.S.A.*
[6] *NOAA Office of National Marine Sanctuaries, Pahānaumokuākea Marine National Monument, Honolulu, HI, U.S.A.*
[7] *NOAA Pacific Islands Fisheries Science Center, Protected Species Division, Honolulu, HI, U.S.A.*
[8] *University of Hawai'i at Mānoa, Fisheries Ecology Research Lab, Hawai'i, U.S.A.*

Benthic Habitats and Corals

3.1. INTRODUCTION

The Main Hawaiian Islands (MHI) consist of eight volcanic islands and comprise the southern portion of the Hawaiian Archipelago. The volcanic chain originated over a hot spot in Earth's mantle that currently lies just to the south of the island of Hawai'i and extends northwestward approximately 3,500 miles to the beginning of the Emperor Seamount Chain (Moore, 1987). The Pacific Plate is drifting to the northwest of this hot spot at a rate of about 10 cm/yr (Moore, 1987) such that the islands in the northwest are older than those in the southern part of the archipelago. For example, Kure Atoll is approximately 30 million years old, whereas the island of Hawai'i is less than one million years old (Clague, 1996). The eight main islands in the state comprise approximately 99 percent of the land area of the archipelago, with the remainder made up of small islets around the MHI and in the Northwestern Hawaiian Islands (NWHI;Fletcher et al., 2008). There are five active volcanoes in the MHI (USGS, 2016). Three of them are on the island of Hawai'i, including Mauna Loa (4,169 m), Hualālai (2,521 m) and Kīlauea (1,219 m). The MHI's other active volcanoes include Halealakā (3,055 m) on Maui, and the Lō'ihi Seamount located about 30 km southeast of the island of Hawai'i. As once active volcanoes erode and subside, fringing reefs develop atop the flanks and eventually form atolls as the volcanic features further submerge beneath the surface of the water (Fletcher et al., 2008). Over time, these drowned atolls become submerged seamounts, pinnacles and platforms as the features continue to subside. Numerous underwater seamounts are located throughout the archipelago, including the West Hawaiian Seamounts south of O'ahu and the Hawaiian Seamounts south of Maui (Figure 3.1).

The MHI are subjected to large ocean swells and strong trade winds (see Chapter 2) contributing to the development of distinctive reef communities that are sculpted by these dynamic natural processes. Climatological and oceanographic processes, such as circulation, windward and leeward exposure, and seasonal fluctuation in ocean swell have shaped the structure and distribution of benthic marine habitats (Fletcher et al., 2008). Benthic communities are highly structured by depth across the MHI and can be generally described by three broad categories: shallow-water (<30 m), mesophotic (30-150 m) and deep-water (>150 m), which all differ in their structure and species composition (Roberts et al., 2009; Hinderstein et al., 2010).

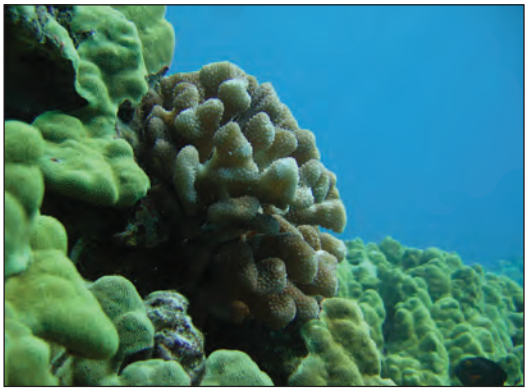

Coral on shallow-water coral reef ecosystem. Photo credit: Lisa Wedding (Stanford University)

Shallow-water coral reef ecosystems provide a range of natural and economic services to the coastal populations of Hawai'i, including tourism, fishing and shoreline protection, with a total estimated economic value of $360 million per year (Cesar and Beukering, 2004). The composition of reef communities are influenced by factors, such as wave exposure, depth, rugosity and island age, with coral species and morphology varying between environments such as reef flats, crests, fore reefs and vertical walls (Jokiel et al., 2004; Fletcher et al., 2008; Fletcher and Fiersten, 2010). Although over 50 species of scleractinian (hard) corals are present in the MHI (Maragos, 1995), the most common genera include massive and finger (*Porites* spp.), rice (*Montipora* spp.), cauliflower (*Pocillopora* spp.) and false brain (*Pavona* spp.) corals (Fenner, 2005). Other prominent components of shallow reef communities include crustose coralline algae and macroalgae. Calcareous macroalgae such as *Halimeda* spp. contain a calcium carbonate skeleton that breaks down upon death, and along with coralline algae and coral skeleton fragments, contributes to sand production, Gorgonian (soft) corals are largely absent on shallow-water reefs of Hawai'i.

Corallium *species in deep-sea coral and sponge community. Photo credit: NOAA Office of Ocean Exploration and Research, 2015 Hohonu Moana*

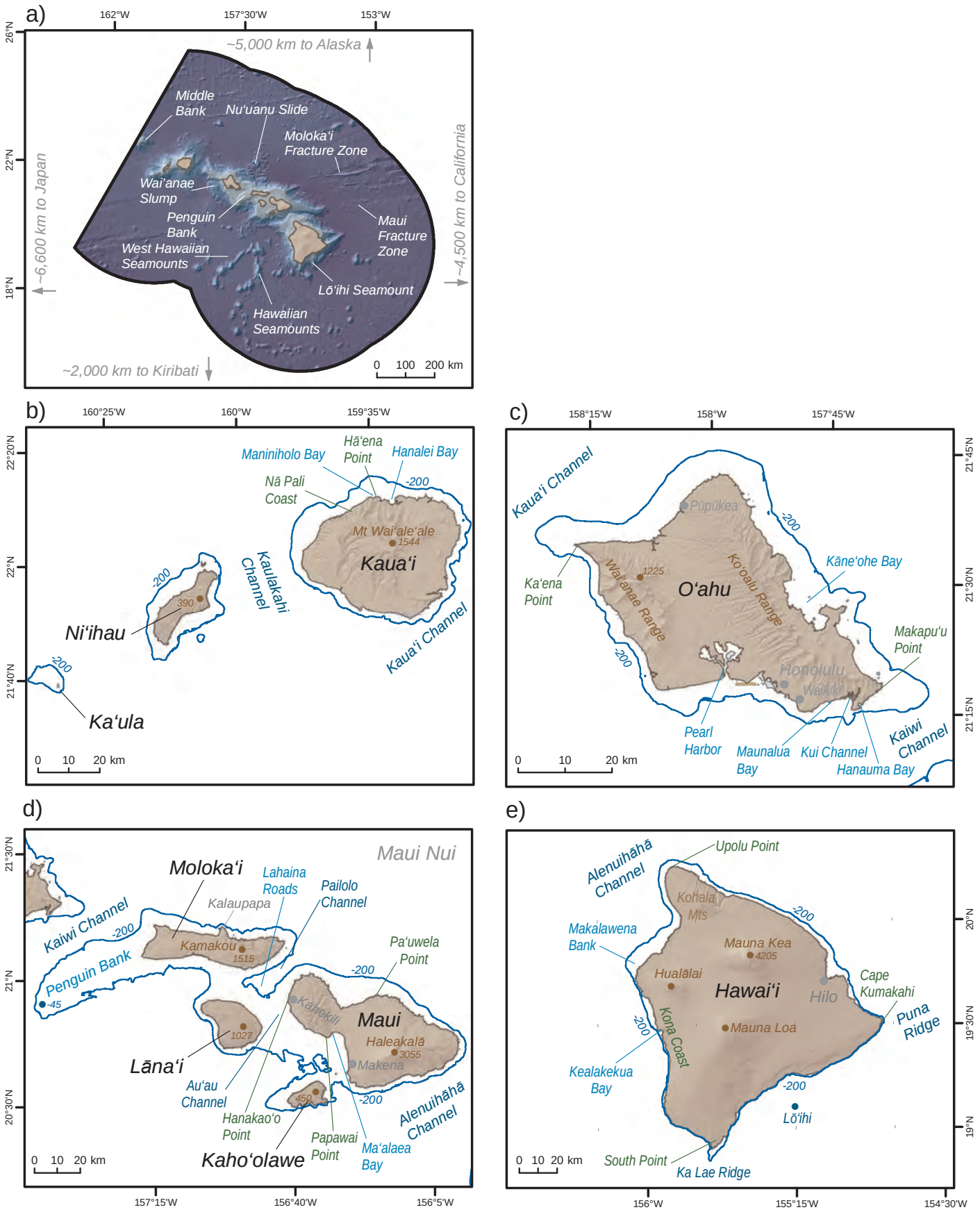

Figure 3.1. Key geographic features around the Main Hawaiian Islands (MHI). These maps depict geographic features that are referenced in this chapter for a) the project area, b) Ka'ula, Ni'ihau, and Kaua'i, c) O'ahu, d) Maui Nui, which includes Moloka'i, Lāna'i, Maui and Kaho'olawe, and e) Hawai'i. All depths and elevations are in meters. Elevations on the maps denoted the highest point on each island. Dates: N/A. Data sources: shoreline (Battista et al., 2007), elevation (USGS, 2015) and depths (NOAA NCEI, 2005; GEBCO, 2008)

Benthic Habitats and Corals

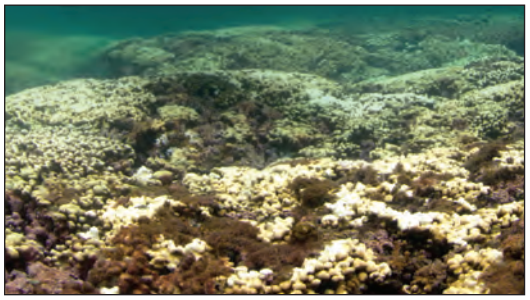

Bleached coral around Hawai'i. Photo credit: Catlin Seaview Survey

While no scleractinian coral species in the MHI are currently listed under the Endangered Species Act (ESA), all scleractinian corals are protected by Hawai'i State Law prohibiting the taking, breaking, or damaging of any stony corals from State waters (out to 3 nm from shore) unless permitted. Corals are subject to numerous stresses, including land-based sources of pollution, coastal development, tropical storms and climate change. Prior to 2014, few large-scale coral bleaching events had been documented in the Hawaiian Archipelago. In 1996 a bleaching event occurred in O'ahu, mainly restricted to Kāne'ohe Bay, following a period of prolonged elevated ocean temperatures (Jokiel and Brown, 2004; Friedlander et al., 2008), and bleaching was also documented in the NWHI in that same year (Aeby et al., 2003; Kenyon and Brainard, 2006). In 2014, a bleaching event spread across the North Pacific Ocean, including the MHI and NWHI, with over 80 percent of colonies showing signs of bleaching at some monitoring locations in O'ahu and Kaua'i (Neilson, 2014). The strong El Niño continued into 2015 (http://coralreefwatch.noaa.gov/satellite/index.php) and the MHI and NWHI again experienced widespread bleaching.

Mesophotic corals can show a range of adaptations that allow them to live in low-light environments, including flattened morphologies, pigment specialization, increased heterotrophy and lower metabolic demands (Kahng et al., 2010). In the Hawaiian Archipelago, Kahng and Kelley (2007) and Rooney et al. (2010) found that different types of mesophotic coral ecosystems (MCEs) dominated specific depth ranges. In 30-50 m of water, upper MCEs were dominated by a low diversity of hard corals with massive morphologies, while corals with branching and plate-like morphologies were characteristic of deeper depths (50-80 m). At 80-130 m depths, MCEs were dominated by *Leptoseris hawaiiensis*, which has a plate-like morphology. High habitat suitability for mesophotic corals was predicted for the 'Au'au Channel region (Costa et al., 2015), which is a unique area of relatively warm, clear, and protected water between Lāna'i, Maui, Kaho'olawe, and Moloka'i (Figure 3.1). In addition, a diversity of macroalgae proliferate the mesophotic zone, with species such as *Halimeda kanaloana* forming expansive meadows (Spalding, 2012).

Leptoseris *species interspersed with* Halimeda *algae. Photo credit: John Rooney (NOAA NMFS/PIFSC)*

Deep-sea corals (DSC) are generally long-lived, slow-growing organisms that often produce significant biological structure above the seafloor (including calcified structures). DSC are typically thought to be azooxanthelate and obtain their nutrition from a variety of non-photosynthetic sources including dissolved organic matter, particulate organic matter and zooplankton. However, Wagner et al. (2011) found that many black corals (Antipatharia) do in fact contain low densities of symbiotic algae. Currents and their interactions with local geomorphology can drive DSC distribution through a variety of mechanisms operating at multiple scales (e.g., Friewald et al., 2004; Mortensen and Buhl-Mortensen, 2004; Roberts et al., 2006; Lumsden et al., 2007; Long and Baco, 2014).

DSC observed in the Hawaiian Archipelago include stony corals (Order Scleractinia), black corals (Order Antipatharia), gorgonians (Order Alcyonacea), pen corals (Order Pennatulacea) and zoanthids (Order Zooantharia; Parrish and Baco, 2007). In general, DSC in the Hawaiian Islands do not form extensive reef structures as in the Atlantic and South Pacific; rather, they grow attached to existing hard substrates (Parrish and Baco, 2007). However, high densities of various DSC species are often present at features such as seamounts and ridges, forming coral gardens.

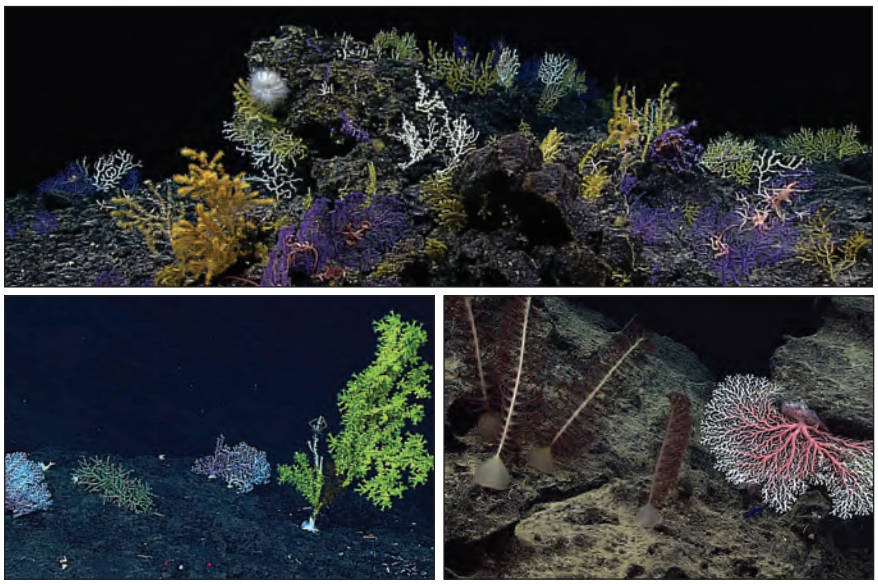

*Deep sea coral community (top); and pink (family Corallidae) and gold coral (*Kulamanamana haumeae*; bottom left); and rock pens and pink coral (*Pleurocorallium secundum*; bottom right). Photo credit: NOAA Office of Ocean Exploration and Research, 2015 Hohonu Moana*

DSC research has expanded in the Hawaiian Archipelago in the last few decades as discovery and harvest of precious coral beds has increased (Parrish and Baco, 2007). Precious corals, which include species of black corals (*Antipathes griggi, Antipathes grandis* and *Myriopathes cf. ulex*), red and pink corals (*Corallium* spp.), and gold corals (*Kulamanamana haumeaae*), have historically been harvested commercially for use in jewelry in Hawai'i (Grigg, 2010). Currently, there is only an active fishery for black coral in Hawai'i; most of the harvest is from an established bed in the 'Au'au Channel but harvesting also occurs offshore of Hawai'i and Kaua'i (reviewed by Wagner et al., 2015). Harvest of *Corallium* has historically occurred in the MHI, specifically off of Makapu'u Point, O'ahu (Grigg, 1993), but currently there is not an active fishery at that location as it is not economically profitable. There is currently a five-year moratorium on harvest of the Hawaiian gold coral that will be reviewed in 2018 (Federal Register 50 CFR Part 665; Federal Register, 2013).

In order to plan effectively for renewable energy development, an understanding of the distribution of benthic habitats and associated biota is necessary to assess potential direct and indirect effects of development on marine ecosystems. The amount and type of survey and monitoring data differs among shallow, mesophotic, and deep-sea benthic habitats. A number of routine monitoring programs exist for shallow-water reefs (e.g., Brown et al., 2004; Jokiel et al., 2004; Coles and Brown, 2007; Friedlander et al., 2008; Heenan et al., 2013; Walsh et al., 2013), as well as additional focused research projects. In contrast, data are more difficult to collect and sparser for mesophotic and deep-sea regions, where submersibles and remotely operated vehicles (ROVs) are required (Parrish and Baco, 2007; Kahng et al., 2014). The objectives of this chapter are to describe the available data, data gaps and limitations for shallow-water, mesophotic, and DSC benthic communities. For shallow-water benthic habitats, we provide a summary of mapped habitats as well as a new compilation of benthic cover monitoring datasets. For mesophotic habitats, predictive modeling was recently completed (Costa et al., 2015) and is summarized here. New habitat suitability models are presented for several DSC taxa in the MHI.

3.2. SHALLOW BENTHIC HABITATS

3.2.1. Methods and Data Description

Benthic habitat maps

A shallow-water (<30 m) benthic habitat map of the MHI was completed by NOAA in 2003 (Coyne et al., 2003) and updated in 2007 with a more refined classification scheme (Battista et al., 2007). The most recent effort (Batista, 2007) utilized commercial multispectral satellite imagery, collected from 2004-2007, to digitize benthic habitat features in ArcGIS (ESRI, 2011) at a minimum mapping unit of 1 acre (4,050 m^2). A hierarchical classification scheme, similar to what has been used to map shallow-water habitats in the U.S. Caribbean and Pacific Territories, was created to define and delineate shallow-water benthic habitats (Battista et al., 2007). The habitat classification scheme defines benthic habitats based on three attributes: 1) broad geographic zone; 2) geomorphological structure type; and 3) biological cover. Every feature in the map is assigned a designation from each level of the scheme. Ground validation was conducted at locations that were difficult to distinguish and warranted further field investigation. Following completion of the map, an independent accuracy assessment was conducted to quantify the thematic accuracy of the map. For further details on map creation, please see Battista et al. (2007).

The hierarchical classification scheme was developed to allow users to expand or collapse the thematic detail of the map (Battista et al., 2007). Thirteen mutually exclusive zones, which describe the geographic location of the feature, were identified from land to open water (Table 3.1). Geomorphological structure types indicate the predominant physical composition of the feature. Biological cover types included nine major classes combined with a density modifier representing the percentage of the predominant cover type. A coral-centric approach was used for the scheme such that if a polygon had greater than 10 percent scleractinian coral cover, it was mapped as live coral even if another cover type comprised a higher percentage of the polygon (Battista et al., 2007). If coral cover was less thank 10 percent, the dominant cover type was mapped. Areas of the imagery that could not be classified due to reasons such as depth, cloud cover, and turbidity were classified as "unknown."

Table 3.1. Classification scheme for the 2007 the Main Hawaiian Islands (MHI) benthic habitat map (Battista et al., 2007).

Classification		
Geographic Zone	**Geomorphological Structure**	**Biological Cover**
Back Reef	Coral Reef and Hardbottom	Major Cover
Bank/Shelf	*Aggregate Reef*	*Coral*
Bank/Shelf Escarpment	*Aggregated Patch Reef*	*Coralline Algae*
Channel	*Individual Patch Reef*	*Emergent Vegetation*
Dredged	*Pavement*	*Macroalgae*
Fore Reef	*Pavement w/ Sand Channels*	*Seagrass*
Lagoon	*Rock/Boulder*	*Turf*
Land	*Rubble*	*Uncolonized*
Reef Crest	*Scattered Coral/Rock*	*Unclassified*
Reef Flat	*Spur and Groove*	*Unknown*
Reef Hole	Unconsolidated Sediment	Percent Major Cover
Shoreline Intertidal	*Sand*	*10%-<50% (Sparse)*
Unclassified	*Mud*	*50%-<90% (Patchy)*
Unknown		*90%-100% (Continuous)*
	Artificial	*Unknown*
	Land	*Unclassified*

The U.S. Coastal and Marine Ecological Classification Standard (CMECS) provides a comprehensive national framework for organizing information about coasts and oceans and their living systems (CMECS, 2015). The MHI classification scheme (Battista et al., 2007) was translated to the CMECS to make it easier for users to compare the MHI habitat map with habitat data produced by other groups and from other regions (Tables 3.2 and 3.3).

Table 3.2. Crosswalk between the NOAA 2007 MHI benthic habitat map classification scheme (Battista et al., 2007) and the U.S. Coastal and Marine Ecological Classification (CMECS) for Geographic Zone, Major Structure and Geomorphological Structure.

GEOGRAPHIC ZONE	CMECS	CMECS Code	Relationship
Back Reef	Back Reef - Coral Reef Zone (Modifier)	(CRZ01)	Equal
Bank/Shelf	Bank/Shelf - Coral Reef Zone (Modifier)	(CRZ02)	Equal
Bank/Shelf Escarpment	Bank/Shelf Escarpment - Coral Reef Zone (Modifier)	(CRZ03)	Equal
Channel	Pass/Lagoon Channel - Level 2 Geoform Type (GC)	Gg1.9.1	Equal
Dredged	Dredged - Anthropogenic Impact (Modifier)	(AI04)	Equal
Fore Reef	Fore Reef - Coral Reef Zone (Modifier)	(CRZ04)	Equal
Lagoon	Lagoon - Coral Reef Zone (Modifier)	(CRZ05)	Equal
Land	No Equivalent		No Equivalent
Reef Crest	Reef Crest - Coral Reef Zone (Modifier)	(CRZ06)	Equal
Reef Flat	Reef Flat - Coral Reef Zone (Modifier)	(CRZ07)	Equal
Reef Hole	Hole/Pit - Level 1 Geoform (GC)	Gg1.25	Equal
Shoreline Intertidal	Shore Complex - Level 1 Geoform (GC)	Gp7	Nearly Equal
Unknown	Unknown	0	
Unclassified	N/A		
MAJOR STRUCTURE	**CMECS**	**CMECS Code**	**Relationship**
Coral Reef and Hardbottom	Rock Substrate- Substrate Class (SC) AND Coral Reef Substrate-Substrate Subclass (SC)	Gg2.5, Gg1.50	Greater Than
Unconsolidated Sediments	Unconsolidated Mineral Substrate - Substrate Class (SC)	S1.2	Greater Than
Other Delineations			No Equivalent
Unknown	Unknown (Mapping Convention)	0	
GEOMORPHOLOGICAL STRUCTURE	**CMECS**	**CMECS Code**	**Relationship**
Aggregate Reef	Aggregate Coral Reef- Level 1 and Level 2 Geoform Type (GC)	Gg2.5.1	Equal
Aggregated Patch Reefs	Patch Coral Reef - Level 1 and Level 2 Geoform Type (GC) Patchiness (Modifier)	Gg2.5.9(PC##)	Equal
Artificial	Anthropogenic - Geoform Origin (GC)	Gg3	Equal
Individual Patch Reef	Patch Coral Reef - Level 1 and Level 2 Geoform Type (GC)	Gg2.5.9	Equal
Land	No Equivalent	NULL	No Equivalent
Mud	Mud - Substrate Group AND Carbonate - Substrate Descriptor (Modifier)	S1.2.2.5	Equal
Pavement	Pavement Area-Level 1 and 2 Geoform (GC) AND Carbonate-Substrate Descriptor (Modifier)	Gg1.44(SD01)	Equal
Pavement with Sand Channels	Pavement Area- Level 1 and 2 Geoform (GC) AND Carbonate-Substrate Descriptor (Modifier) WITH Co-Occurring Element Sand Channel - Level 2 Geoform (GC)	Gg1.44(SD01), Gg1.9.2	Equal
Reef Rubble	Rubble Area- Level 1 Geoform (GC) AND Coral Rubble- Substrate Subclass (SC)	S2.2.2	Equal
Rock/Boulder	Rock Outcrop - Level 1 Geoform (GC)	Gg1.7	Greater Than
Sand	Sand - Substrate Group (SC)	S1.2.2.2	Nearly Equal
Scattered Coral/Rock	Sand - Substrate Group (SC) WITH Co-Occurring Element Coral Head - Level 2 Geoform Type (GC) AND/OR Co-Occurring Element Boulder - Subgroup (SC)	S1.2.2.2, S2.2.2, S1.1	Equivalent
Spur and Groove	Spur and Groove Coral Reef- Level 1 and Level 2 Geoform Type (GC)	Gg2.5.11	Equal
Unknown	Unknown (Mapping Convention)	0	

Table 3.3. Crosswalk between the NOAA 2007 MHI benthic habitat map classification scheme (Battista et al., 2007) and CMECS for Biological Cover and Percent Biological Cover.

BIOLOGICAL COVER	CMECS	CMECS Code	Relationship
Coral	Shallow/Mesophotic Coral Reef Biota - Biotic Subclass (BC)	B2.1.2	Supplemental
Coralline Algae	Coralline/Crustose Algal Bed - Biotic Group (BC)	B2.5.1.3	Equal
Emergent Vegetation	Tidal Mangrove Shrubland- Biotic Group (BC) OR Tidal Mangrove Forest - Biotic Group (BC)	B2.7.1.4, B2.8.1.4	Supplemental
Macroalgae	Benthic Macroalgae - Biotic Subclass (BC)	B2.5.1	Equal
Seagrass	Seagrass Bed- Biotic Group (BC)	B2.5.2.1	Supplemental
Turf Algae	Turf Algal Bed - Biotic Group (BC)	B2.5.1.8	Equal
Uncolonized	No Cover	NULL	Equal
Unclassified	N/A		
Unknown	Unknown (Mapping Convention)	0	
PERCENT BIOLOGICAL COVER	**CMECS**	**CMECS Code**	**Relationship**
10% - <50% (Sparse)	Patchy 1 (10% - <50%) - Percent Cover (Modifier)	(PC02-PC06)	Equivalent
50% - <90% (Patchy)	Patchy 2 (50% - <90%) - Percent Cover (Modifier)	(PC07-PC10)	Equivalent
90% - 100% (Continuous)	Continuous (90% - 100%) - Percent Cover (Modifier)	(PC11)	Equal
Unclassified	N/A		
Unknown	Unknown (Mapping Convention)	0	

The area and percentage of habitat classes surrounding each island (or island group in the case of Kaʻula and Niʻihau) in the MHI was calculated from Battista et al. (2007). In addition, the total area mapped within shallow waters (<30 m depth) was calculated by clipping the habitat polygons to grid cells <30 m depth in a 90x90 m bathymetry surface (Chapter 2, Table 2.7). Although a finer resolution (5x5 m) synthesis of multibeam sonar and Light Detection And Ranging (LiDAR) bathymetry exists for the MHI (HMRG, 2015), it was not used here because there are substantial gaps in its geographic coverage that may have led to an underrepresentation of the percentage of shallow area that has been mapped.

Benthic cover surveys

Shallow-water benthic cover survey data were compiled by the University of Hawaiʻi at Mānoa Fisheries Ecology Research Lab (UH FERL; UH FERL, 2015a) from multiple sources into a standardized database for analysis (Table 3.4). Datasets include broad-scale monitoring programs (National Oceanic and Atmospheric Administration (NOAA) National Marine Fisheries Service [NMFS] Pacific Islands Fisheries Science Center [PIFSC], Coral Reef Ecosystem Program [CREP]; State of Hawaiʻi Division of Aquatic Resources [DAR]; University of Hawaiʻi at Mānoa Coral Reef Assessment and Monitoring Program [UH CRAMP]), monitoring at specific sites (The Nature Conservancy Hawaiʻi Marine Program; UH FERL; National Park Service), and one-time assessments by individual researchers. As of December 2014, the database consists of 5,149 surveys from 4,318 sites with data on coral reef benthic assemblages within the MHI from 1993-2014.

The years of data collection, geographic coverage, survey methodology, and level at which data were collected varied across datasets (Table 3.4). For some monitoring programs, data were collected at the lowest taxonomic resolution possible for all taxa, while for others, some or all taxonomic groups were identified only to the functional group level. The individual datasets were combined and summarized by the following functional groups to provide consistency across all datasets: live scleractinian coral, macroalgae, turf algae, coralline algae and bare substrate. Where replicate surveys were conducted at a site, the mean percent cover was calculated to obtain site-based percent cover values. For surveys where species level information was consistently available for corals, species richness (i.e., the number of coral species) was calculated. Similar to percent cover, a mean richness value was calculated per site when replicates were present. Caution should be used when comparing coral richness values from different sub-datasets due to variations in survey methodology.

For permanent sites with more than one survey over the time period, means were taken across years for map display. Map symbologies were defined by classifying the survey data into quantiles using ArcGIS 10.3 (ESRI, 2011).

Table 3.4. List of data sources in the compiled benthic cover database for the shallow (<30 m) waters of the MHI.

Program	Geographic Coverage	Coral ID Level	Site Type	Sample Design	Method Type	Transect Length
UH FERL	Kāneʻohe Bay, Oʻahu	Genus/species	Permanent	Random Stratified	quadrat	25
UH FERL	Pūpūkea, Oʻahu	Functional group	Random	Random Stratified	photo-quad	25
UH FERL	Lānaʻi	Genus/species	Random	Random Stratified	quadrat	25
UH FERL	Kaʻūpūlehu-Kiholo, Hawaiʻi	Functional group	Random	Random Stratified	photo-quad	25
NPS I&M	Hanalei, Kauaʻi	Genus/species	Permanent	Selective	video (1999), photo-quad (all other years)	25
NOAA FHUS	Oʻahu, Lānaʻi, Maui, Hawaiʻi	Genus/species	Random	Random Stratified	quadrat	25
NOAA CREP (photo-quad)	MHI	Genus or morphological group	Random	Random	photo-quad	25
NOAA CREP (LPI)	MHI	Genus/species	Permanent	Selective	LPI**	25
DAR (Hawaiʻi)	Hawaiʻi	Genus/species	Permanent	Selective	photo-quad	25
DAR (Maui)	Maui	Genus/species	Permanent	Selective	photo-quad	10
UH CRAMP	MHI	Genus/species	Permanent	Selective	video (1999-2002), photo-quad (2003-2012)	25 (video), 10 (photo-quad)
NPS I&M	Kalaupapa, Molokaʻi	Genus/species	Permanent, Selective	Selective	photo-quad	25
TNC	Oʻahu, Maui, Hawaiʻi	Genus/species	Random	Random Stratified	photo-quad	30
UH FERL	Lāʻau, Molokaʻi	Genus/species	NA	Unknown	Unknown	Unknown
UH FERL	Kahoʻolawe	Genus/species	Random	Random	quadrat	25
UH FERL	Hā'ena, Kauaʻi	Genus/species	Random	Random Stratified	quadrat	25
NOAA CREP and DAR (Kahekili)	Kahekili, Maui	Genus/species	Random	Random	photo-quad	25

DAR = Division of Aquatic Resources, State of Hawaiʻi (DAR, 2015)
NPS I&M = Inventory and Monitoring, National Park Service (NPS I&M, 2015)
NOAA CREP = Coral Reef Ecosystem Program, NOAA Pacific Islands Fisheries Science Center (NOAA CREP, 2015)
NOAA FHUS = Fish Habitat Utilization Study, NOAA National Centers for Coastal Ocean Science, Biogeography Branch (NOAA FHUS, 2015)
TNC = The Nature Conservancy Hawaiʻi Marine Program (TNC, 2015)
UH CRAMP = Coral Reef Assessment and Monitoring Program, University of Hawaiʻi (UH CRAMP, 2015)
UH FERL= Fisheries Ecology Research Lab, University of Hawaiʻi at Mānoa (UH FERL, 2015b)

*Some corals identified to species but most classified as "Unknown."
**Prior to 2008, CREP Line Point-Intercept (LPI) measurements were taken at 50 cm intervals; from 2008-2010 they were taken at 20 cm intervals.

3.2.2. Results and Discussion

Benthic habitat maps

Within the 30 m isobath surrounding the MHI, approximately 75 percent of the benthic habitats have been mapped (Table 3.5). The percentage of mapped area varies among and within islands (Table 3.5 and Figure 3.2). The percent classified is largely consistent among attributes (geographic zone, detailed geomorphological structure and biological cover), although for a few islands a slightly higher percentage has been classified for geographic zone. The islands with the largest percentage of classified habitats are O'ahu, Kaua'i and Ka'ula/Ni'ihau. The more exposed windward portions of Maui, Kaho'olawe and Hawai'i are largely unmapped, as is the northeastern portion of Moloka'i.

Table 3.5. Percent of marine area within 30 m depth around the MHI that was classified in NOAA's 2007 shallow water benthic habitat map (Battista et al., 2007). The areas were calculated by clipping the benthic habitat map polygons to a 90x90 m bathymetry grid (Chapter 2).

Island	Total area <30 m depth (sq. km)	Geographic Zone (% mapped)	Detailed Structure (% mapped)	Biological Cover (% mapped)
Hawai'i	205	43	43	43
Kaho'olawe	24	46	46	46
Maui	201	74	73	73
Lāna'i	55	62	61	61
Moloka'i	191	70	69	68
O'ahu	408	90	88	88
Kaua'i	257	83	80	80
Ka'ula/ Ni'ihau	108	88	87	87
Total MHI	**1449**	**75**	**74**	**74**

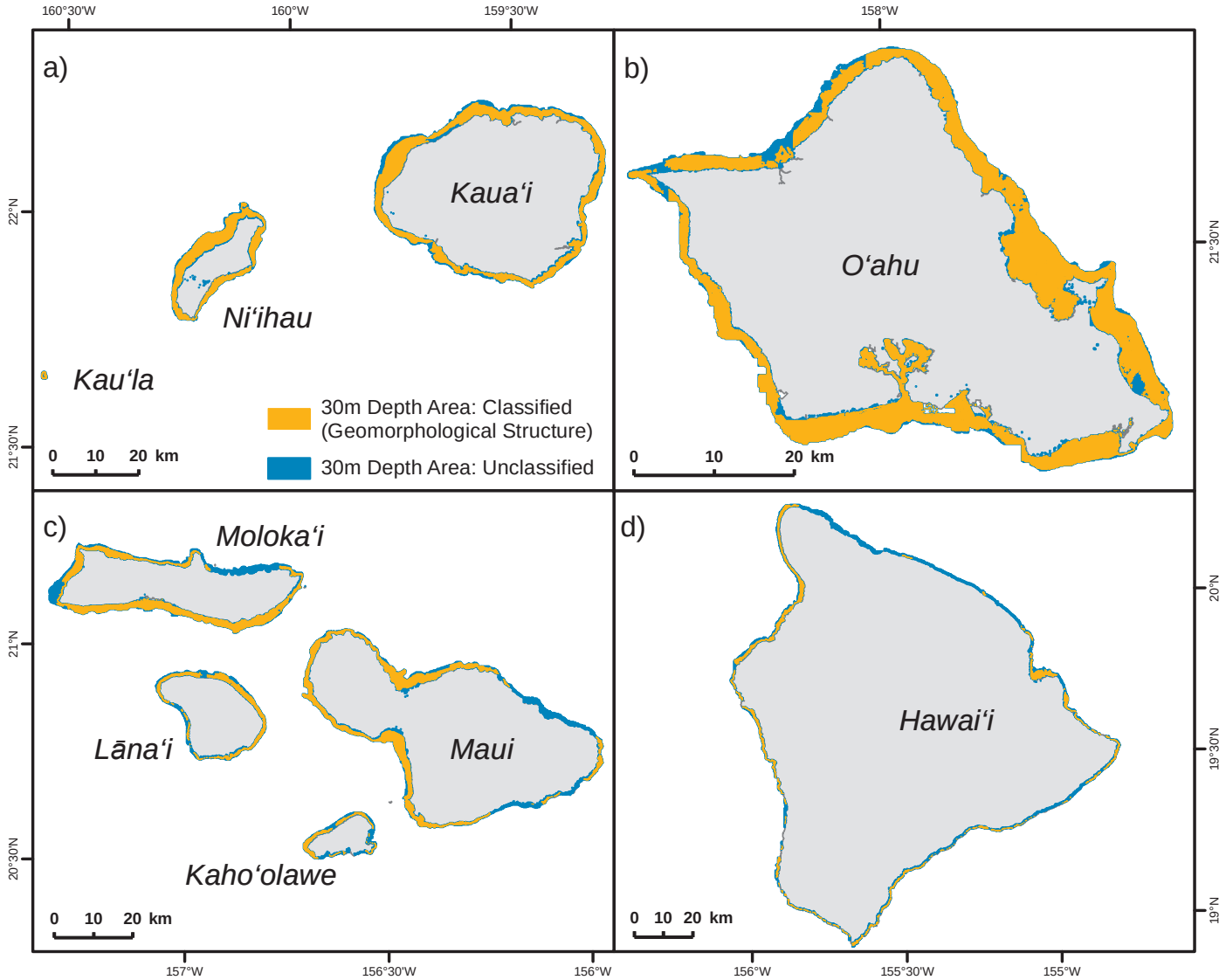

Figure 3.2. Area classified in NOAA's 2007 shallow-water benthic habitat map around the MHI relative to the 30 m depth of the 90x90 m bathymetry grid. Data source: Battista et al., 2007

An example of the distribution of benthic habitats (geographic zone, geomorphological structure and biological cover) are shown for a subsection of O'ahu (Figures 3.3 and 3.4). The spatial distribution of habitats varies across the island chain (Figures 3.5-3.7). Some islands have a complex mix of multiple zone types (including lagoons and reef flats; Figure 3.4), while other areas, such as Ka'ula, contain a simpler bank/shelf zone type (Figure 3.5). The portion of the Maui Nui complex adjacent to the 'Au'au Channel, for instance, is characterized by a relatively large swath (67.6 km^2) of shallow reef flat with sloping fore reef, particularly on the south shore of Moloka'i and eastern shore of Lāna'i. The majority of dredged features are located around the more densely populated island of O'ahu, with smaller amounts around Hawai'i.

Geomorphological structure varies across the island chain with rock/boulder being most prominent on the "newer" islands (e.g., Hawai'i) and steadily decreasing in proportion moving westward along the island chain, with the exception of Ka'ula/Ni'ihau (Figure 3.6). In contrast, other hardbottom types comprised a greater percentage of the mapped habitat around the older islands, with pavement being the dominant structure around O'ahu and Kaua'i. Sand accounted for approximately half of the mapped structure around Maui.

In general, there were also shifts in the mapped dominant biological cover moving northwestward from Hawai'i (Figure 3.7). Within the total area that was classified, over 50 percent of Hawai'i and Kaho'olawe were mapped as live coral, although the majority was at the 10-50 percent cover level. The percent of area mapped as coral ranged from approximately 25-35 percent around Maui, Lāna'i and Kaua'i, with lesser amounts around Moloka'i, O'ahu and Ka'ula/Ni'ihau. Around O'ahu and the islands to its west, virtually all of the area mapped as coral was at the lower percentage levels (10-50%). Macroalgae comprised a larger percentage of the mapped area from Maui and westward. Together, turf algae and uncolonized substrate ranged from 30-60 percent across the island chain, with the exception of Ka'ula/Ni'ihau, where over 90 percent of the substrate was mapped as turf algae. Emergent vegetation (mangroves), an invasive species, was mapped in small amounts around Moloka'i, O'ahu and Kaua'i, with the majority occurring along the south shore of Moloka'i and lining the northern shore of Pearl Harbor, O'ahu. Mangroves also exist along Kāne'ohe Bay, O'ahu, but they were not digitized in NOAA's 2007 map.

The benthic habitat maps for the MHI have supported a range of applications for regional science and management communities (Friedlander et al., 2007a, 2007b, 2009; Wedding et al., 2008). For example, they were used to evaluate the efficacy of existing marine protected areas using a spatially explicit stratified random sampling design (Friedlander et al., 2007a, 2007b, 2009). The maps also guide *in situ* studies of fish assemblages and benthic habitats, the results of which have been used to evaluate fish habitat utilization patterns. Although the extent of the shallow-water maps is entirely within state waters, the maps will support the Bureau of Ocean Energy Management's renewable energy citing process as cables will connect offshore projects to the islands. For example, knowledge of the distribution and location of benthic habitats will allow decision-makers to identify sensitive and highly complex habitats such as coral reefs.

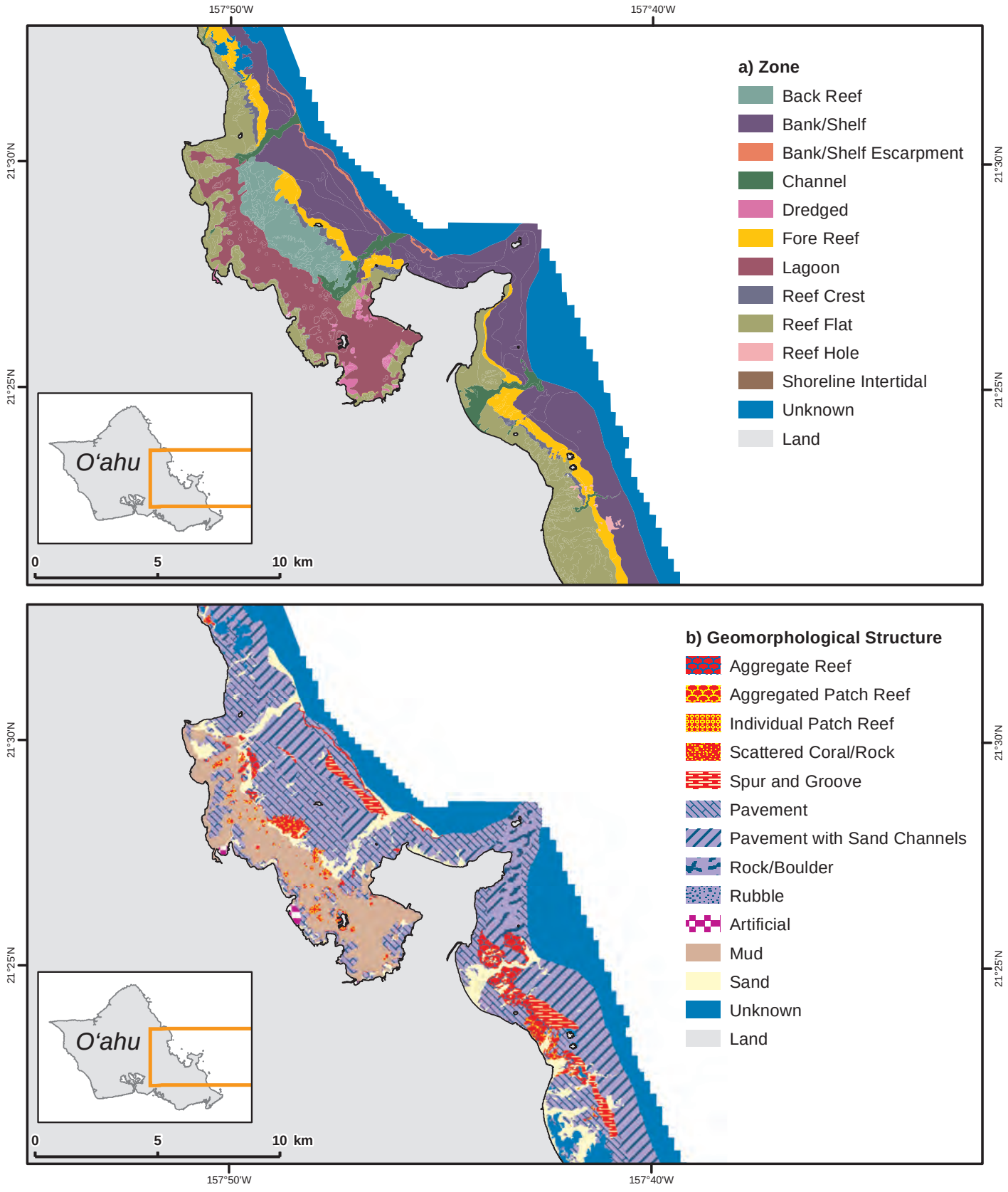

Figure 3.3. Distribution of mapped benthic habitat: geographic zones (top) and geomorphological structure types (bottom) in the Kāneohe Bay and Kailua area of O'ahu. Data source: Battista et al., 2007

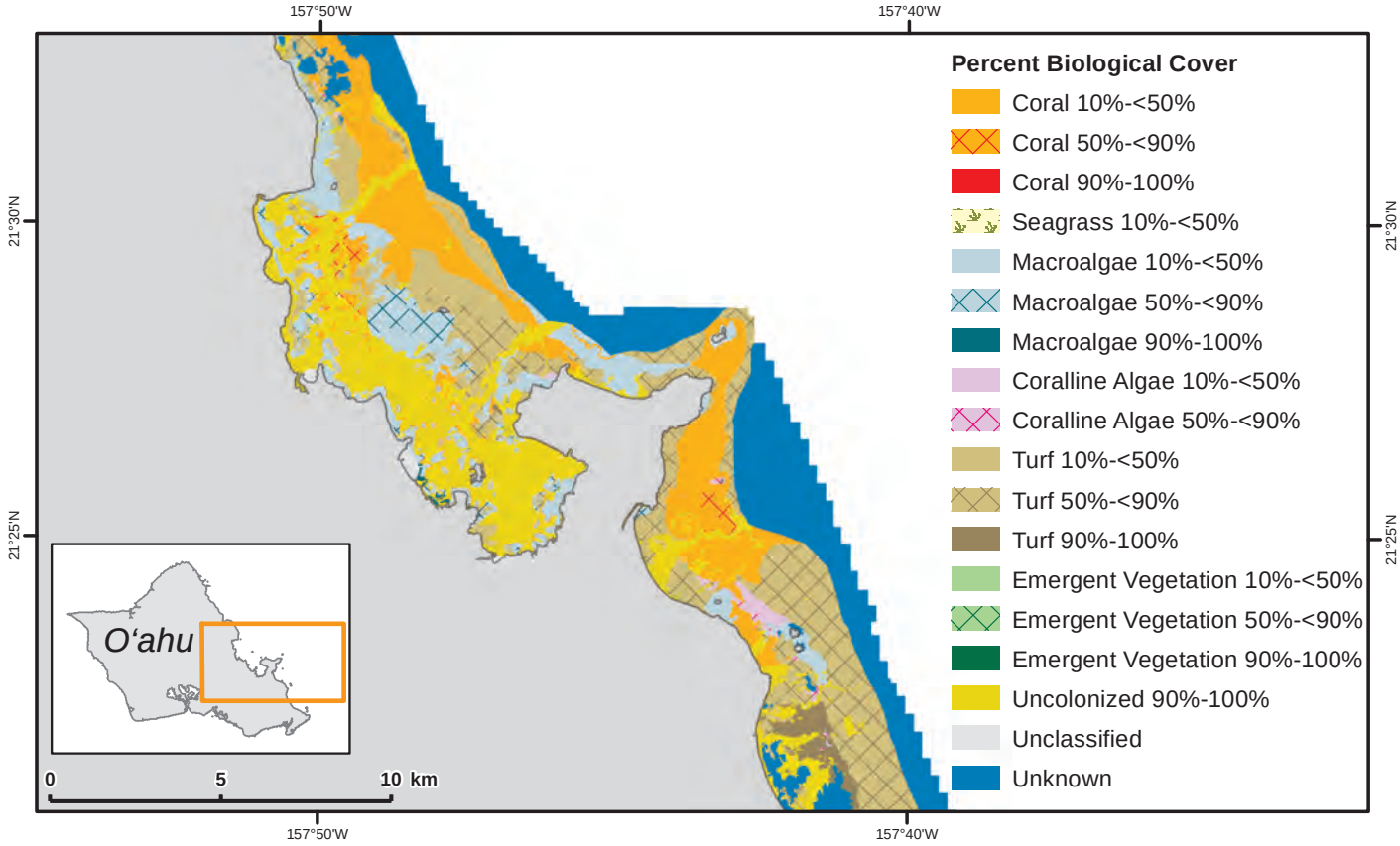

Figure 3.4. Distribution of mapped benthic habitat biological cover types in the Kāneohe Bay and Kailua area of O'ahu. Data source: Battista et al., 2007

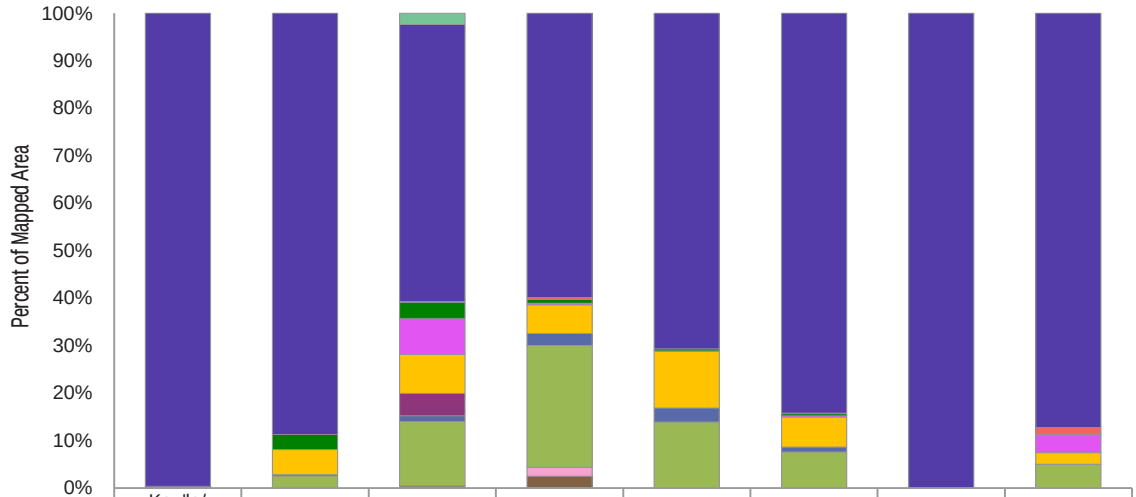

Zone	Kau'la/ Ni'ihau	Kaua'i	O'ahu	Moloka'i	Lāna'i	Maui	Kaho'olawe	Hawai'i
Back Reef	0	0	9.6	0	0	0	0	0
Bank/Shelf	114.8	206.2	238.6	107.5	29.3	171.1	21.2	116.1
Bank/Shelf Escarpment	0	0	0.7	0.7	0	0	0	2.0
Channel	0	7.3	13.9	1.5	0.2	0.9	0	0
Dredged	0	0.1	31.2	0.6	0	0.7	0	5.1
Fore Reef	0.2	12.2	33.5	10.9	5.0	12.8	0	3.2
Lagoon	0	0	19.1	0	0	0	0	0
Reef Crest	0	0.6	4.9	4.5	1.2	2.1	0	0.1
Reef Flat	0.2	5.7	55.3	46.0	5.8	15.4	0	6.6
Reef Hole	0	0	0.3	3.4	0	0.1	0	0
Shoreline Intertidal	0	0.3	1.8	4.5	0	0	0	0
	Area (km^2)							

Figure 3.5. Summary statistics describing the percent and amount of mapped area (km^2) by geographic zone for each island or island group in the MHI. Data source: Battista et al., 2007

Benthic Habitats and Corals

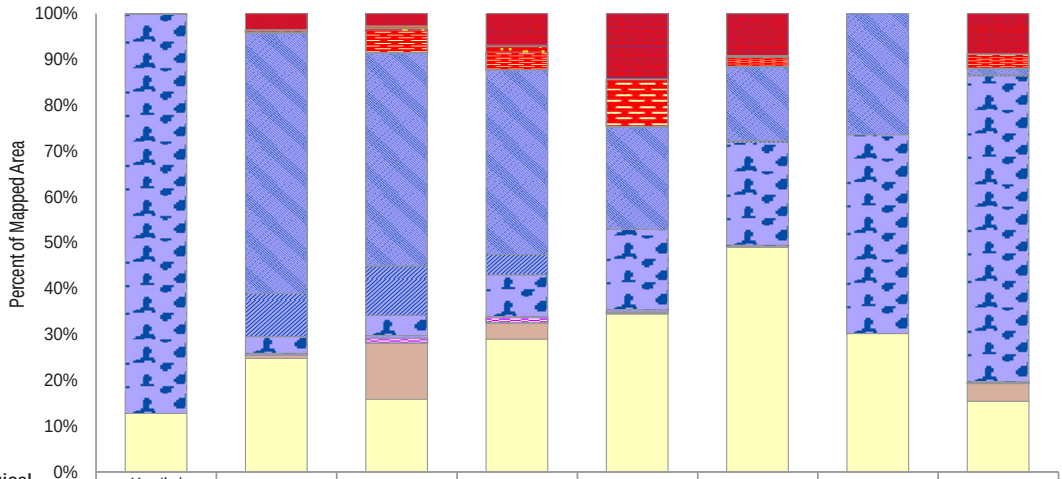

Geomorphological Structure	Kau'la/ Ni'ihau	Kaua'i	O'ahu	Moloka'i	Lāna'i	Maui	Kaho'olawe	Hawai'i
Aggregate Reef	0	7.8	10.7	12.1	5.8	18.4	0	11.4
Aggregated Patch Reef	0	0.0	0.6	0.6	0.0	0.5	0	0
Individual Patch Reef	0	0	1.8	0.0	0	0.1	0	0
Scattered Coral/Rock	0	0.5	1.3	2.1	0.0	0.1	0	0.1
Spur and Groove	0	1.1	20.0	6.9	4.2	4.2	0	4.1
Pavement	0.1	127.9	187.9	70.9	9.1	32.5	5.6	1.6
Pavement w/ Sand Channels	0	21.3	43.4	7.8	0	0.6	0	0.5
Rock/Boulder	98.6	8.1	17.9	16.0	7.1	45.3	9.2	86.8
Rubble	0	0.5	2.1	0.2	0.2	0.1	0	0.2
Artificial	0	0.4	4.7	2.2	0.1	0.2	0	0.3
Mud	0	1.6	49.4	6.2	0.1	0.7	0	5.1
Sand	14.4	55.7	64.0	51.0	14.1	98.8	6.4	20.1

Figure 3.6. Summary statistics describing the percent and amount of mapped area (km²) by detailed geomorphological structure type for each island or island group in the MHI. Data source: Battista et al., 2007

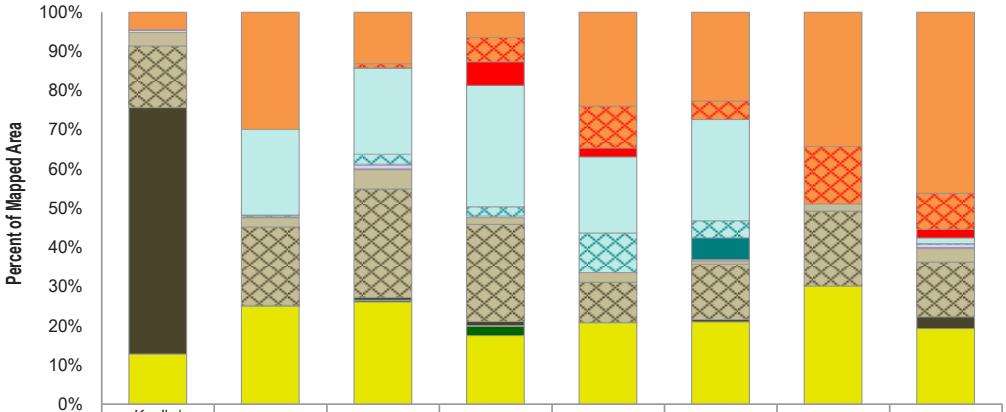

Detailed Biological Cover	Kau'la/ Ni'ihau	Kaua'i	O'ahu	Moloka'i	Lāna'i	Maui	Kaho'olawe	Hawai'i
Coral 10%-<50%	5.1	67.1	52.5	11.2	9.7	45.5	7.3	59.9
Coral 50%-<90%	0	0	4.3	10.8	4.3	9.6	3.1	11.9
Coral 90%-100%	0	0	0	10.4	0.9	0	0	2.9
Seagrass 10%-<50%	0	0	0	0	0	0	0	0
Macroalgae 10%-<50%	0.2	49.1	87.8	53.9	8	52.0	0	1.9
Macroalgae 50%-<90%	0	0.6	10.2	4.1	4.1	8.8	0	0.1
Macroalgae 90%-100%	0	0	0.8	0	0	11.1	0	0
Coralline Algae 10%-<50%	0.6	0.4	4.0	0.7	0	0.7	0	1.1
Coralline Algae 50%-<90%	0	0.5	0.8	0	0	0	0	0.4
Turf 10%-<50%	3.9	5.3	19.7	2.9	1.0	1.8	0.4	4.4
Turf 50%-<90%	17.8	44.8	110.3	43.1	4.2	28.4	4.1	18.1
Turf 90%-100%	71.1	0.2	2.8	1.8	0	1.1	0	3.9
Emergent Vegetation 10%-<50%	0	0	0.1	0.3	0	0	0	0
Emergent Vegetation 50%-<90%	0	0	0	0.1	0	0	0	0
Emergent Vegetation 90%-100%	0	0.3	1.7	4.1	0	0	0	0
Uncolonized 90%-100%	14.5	56.3	104.3	30.5	8.5	42.3	6.4	25.1
	Area (km²)							

Figure 3.7. Summary statistics describing the percent and amount of mapped area (km²) by biological cover type for each island or island group in the MHI. Data source: Battista et al., 2007

Benthic cover surveys

Data from the *in situ* surveys further demonstrates spatial differences in biological cover across the MHI (Figures 3.8-3.20). Mean coral cover was highest around Kahoʻolawe, although variability (i.e., standard error) was also high, followed by Maui, Hawaiʻi and Lānaʻi (Figure 3.8). Mean coral cover was lowest around the more northern and western islands of the chain, whereas turf algae and macroalgae often comprised a larger component of the benthic community. Differences between observed benthic cover in the *in situ* surveys versus what was mapped in the benthic habitat maps may be attributed to several factors. First, data were collected at different scales. Percent cover in the benthic habitat maps are an estimate of the average cover within an entire polygon, which were ≥1 acre (approximately 4,050 m^2), whereas the *in situ* surveys were conducted at a much finer scale (e.g., a 25 m transect). Second, the *in-situ* surveys are a mix of random, permanent and selectively sampled stations, with some areas sampled more heavily than others, so it is likely that this dataset is not a true spatial representation of the map in general. In addition, the imagery and ground-truthing data for the benthic habitat maps were collected over a limited time period (3 years), whereas the *in situ* data have been collected over a longer time range (almost 20 years).

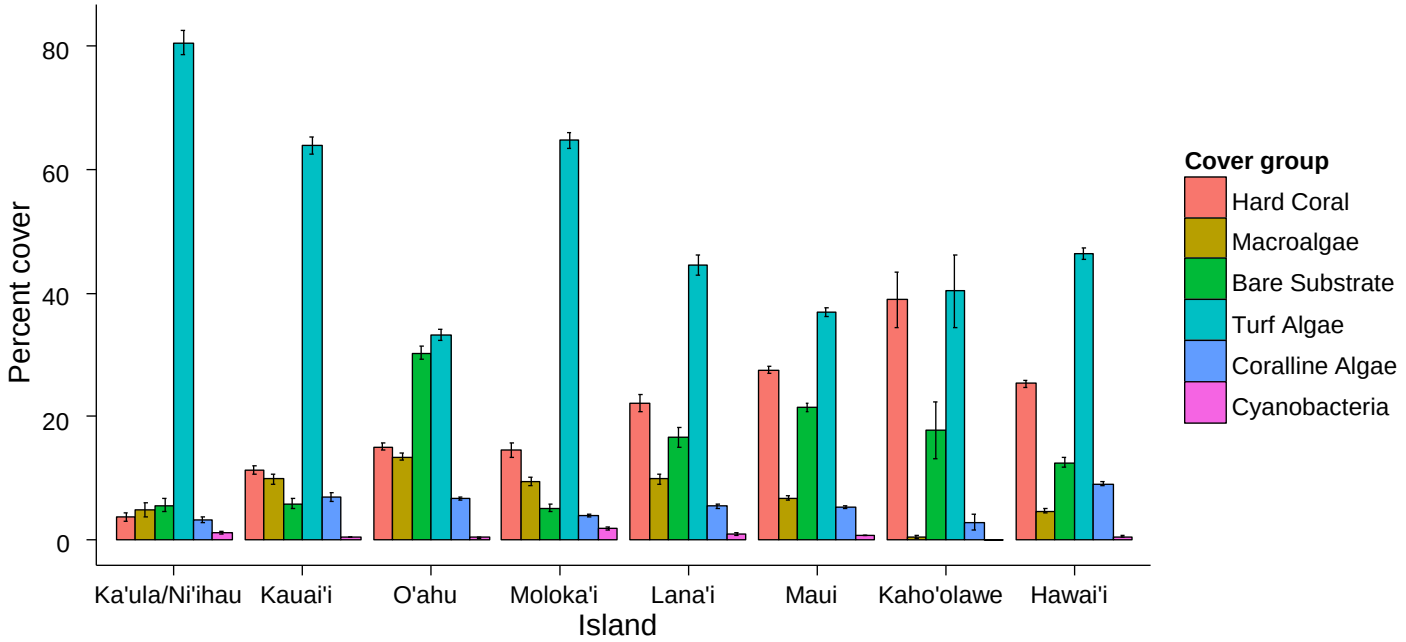

Figure 3.8. Mean (±SE) percent cover of major biological cover types in sampled areas <30 m for each island or island group in the MHI, as measured by scuba divers and compiled by University of Hawaiʻi Fisheries Ecology Research Lab (UH FERL) for 1993-2014. Data source: UH FERL, 2015a

Benthic cover values for the taxonomic groups varied across geographic locations within islands as well (Figures 3.9-3.20). On Hawaiʻi, the majority of sample sites were located on the western leeward side of the island. Lower coral cover values tended to be observed by Upolu Point, whereas higher values were observed along the western portion of the island, including along the Kona Coast (Figure 3.9a). Coral species richness was relatively low along much of the western portion of the island, with moderately higher values occurring in some embayments (e.g., Kealakekua Bay) and a few higher values scattered along the eastern and southern portions of the island (Figure 3.9b). Similarly, observed coralline algae values tended to be higher on the leeward side of the island (Figure 3.10a), and cover did not exceed 40 percent at any site on the eastern side. Macroalgal cover was variable, with the highest observed values occurring west of Kiholo Bay (Figure 3.10b). Turf algae cover was relatively higher around Upolu Point and along the Kona Coast (Figure 3.11a). Higher values of bare substrate tended to occur in embayments on the western side of the island (e.g., Kealakekua Bay; Figure 3.11b).

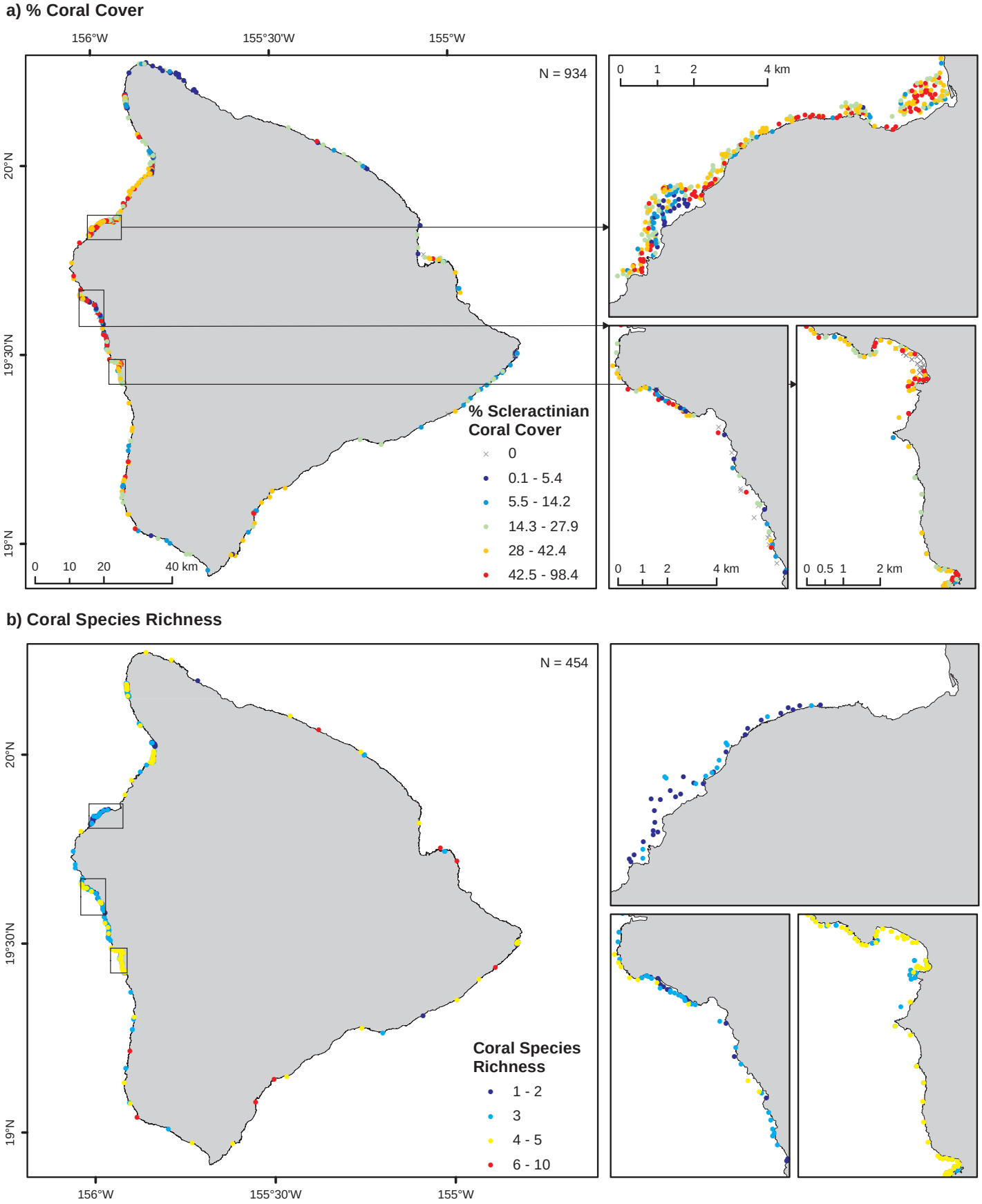

Figure 3.9. a) Percent cover of live scleractinian coral and b) coral species richness around the island of Hawai'i, as measured by scuba divers and compiled by UH FERL for 1999-2014. Data source: UH FERL, 2015a

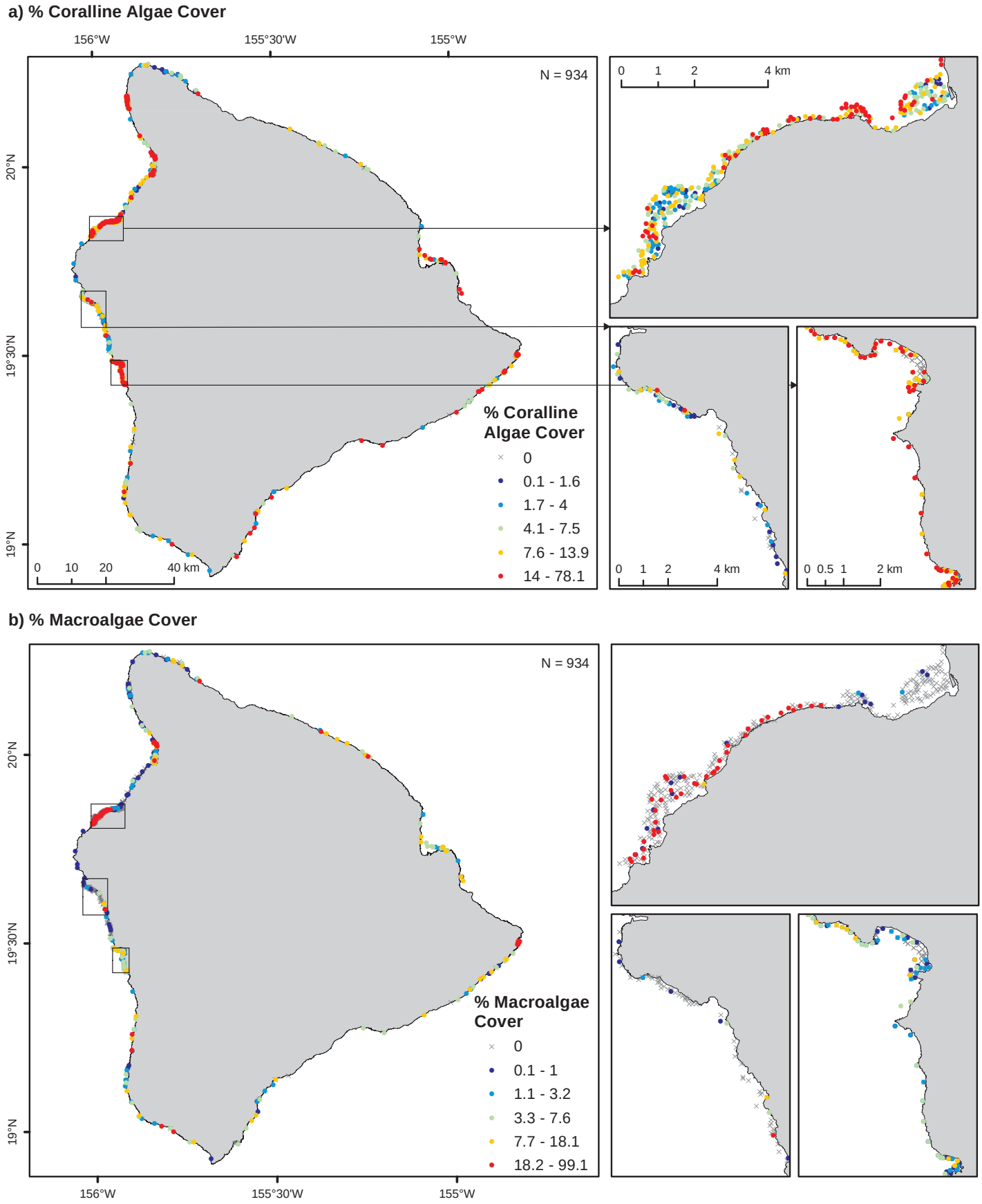

Figure 3.10. a) Percent cover of coralline algae and b) macroalgae around the island of Hawai'i, as measured by scuba divers and compiled by UH FERL for 1999-2014. Data source: UH FERL, 2015a

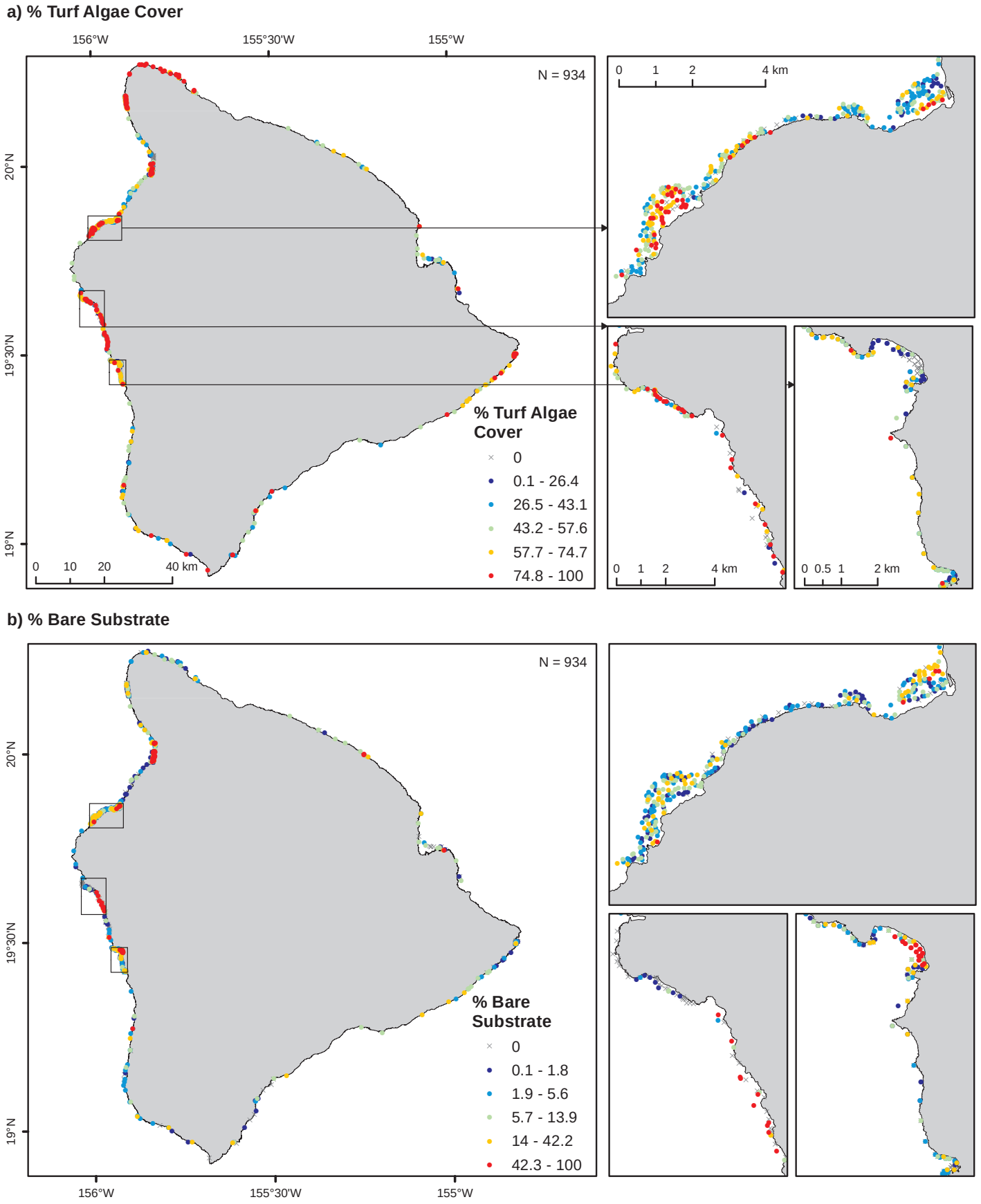

Figure 3.11. a) Percent cover of turf algae and b) bare substrate around the island of Hawai'i, as measured by scuba divers and compiled by UH FERL for 1999-2014. Data source: UH FERL, 2015a

Within the Maui Nui complex, relatively higher coral cover values were observed along the south shore of Molokaʻi, the western shore of Maui near Makena and Kahekili, the north shore of Kahoʻolawe, and the eastern coast of Lānaʻi (Figure 3.12a). Patterns in coral species richness tended to be similar, however, relatively higher richness values were observed around Kalaupapa and Molokaʻi, where relatively lower coral cover was observed (Figure 3.12b). Relatively higher values of coralline algae were observed on the western side of Maui (Figure 3.13a). Relatively lower values of macroalgae occurred southwest of Molokaʻi and coincided with the Kahekili Herbivore Fisheries Management Area (Figure 3.13b). Turf algae cover was relatively high around much of the Maui Nui complex, with a few locations of considerably lower cover on the eastern coast of Lānaʻi and the north shore of Kahoʻolawe (Figure 3.14a). Bare substrate cover varied across the Maui Nui complex, with notable areas of relatively higher bare substrate cover on the western coast of Maui and the eastern and southern coasts of Lānaʻi (Figure 3.14b).

Around the island of Oʻahu, relatively higher coral cover values were observed in Kāneʻohe Bay and Hanauma Bay (Figure 3.15a), although it should be noted that there was also more effort in these locations. Surveys in Kāneʻohe Bay were largely dominated by the species *Porites compressa* and *Montipora capitata*, leading to relatively lower coral species richness values (Figure 3.15b). Relatively higher values of coralline algae were also observed in Kāneʻohe Bay and Hanauma Bay, as well as the Pupukea Marine Life Conservation District MLCD; Figure 3.16a). Macroalgae was present around most of Oʻahu at lower densities (i.e., 10-50%) with higher densities (>50%) located in Maunalua and Kāneʻohe Bays (Figure 3.16b). Turf algae cover was relatively high around much of Oʻahu, with relatively low cover on the east coast, particularly in Kāneʻohe Bay (Figure 3.17a). Bare substrate cover was relatively low around much of Oʻahu, except around Waimea Bay on the North Shore, Kāneʻohe Bay on the east coast, and around Waikiki Beach, Kui Channel and Hanauma Bay on the south coast (Figure 3.17b).

Observed percent coral cover was generally lower around Kauaʻi and Niʻihau compared to the more eastern and southern islands in the MHI. Relatively higher values of coral cover (but still <25%) were found around Hāʻena Point and parts of Hanalei Bay (Figure 3.18a). Relatively higher coral species richness values were restricted to Hanalei Bay (Figure 3.18b). Similarly, relatively higher coralline algae cover was observed around the eastern part of Hanalei Bay and to the west of Hanalei Bay around Maniniholo Bay and Hāʻena Point (Figure 3.19a). Macroalgae cover was also relatively higher on the northern coast of Kauaʻi around Maniniholo Bay and Hāʻena Point, as well as along the Nā Pali Coast (Figure 3.19b). Turf algae cover was relatively high compared to the other islands and exceeded 80 percent at over half of the sites around Niʻihau (Figure 3.20a). Bare substrate cover was relatively low around Kauaʻi and Niʻihau, with only a few scattered locations with relatively higher values, such as along the Nā Pali Coast (Figure 3.20b).

The shallow-water benthic cover database compiled for this report could be utilized for a number of scientific and management purposes. These data can be used to: 1) identify gaps where additional monitoring effort is needed; 2) make a qualitative assessment of broad patterns in percent cover of coral and other taxonomic groups; and 3) to generate spatial predictive models (e.g., boosted regression trees) of coral cover and/or species richness. For renewable energy siting purposes, the *in situ* data could be used in conjunction with the benthic habitat maps to identify and potentially avoid activity in areas of high coral cover. Predictive modeling of the primary benthic cover groups could provide a more detailed, comprehensive overview of spatial patterns rather than point data alone, as well as provide information on what topographic and oceanographic factors are driving spatial patterns in benthic cover. For example, Franklin et al. (2013) used a similar data compilation to model distributions of key coral species using boosted regression trees, and found that mean and maximum significant wave height were the most important variables to explain the percent cover of all studied species. However, as noted in Chapter 4, gaps in the extent of fine-scale nearshore bathymetry would limit the current area for which predictions can be generated.

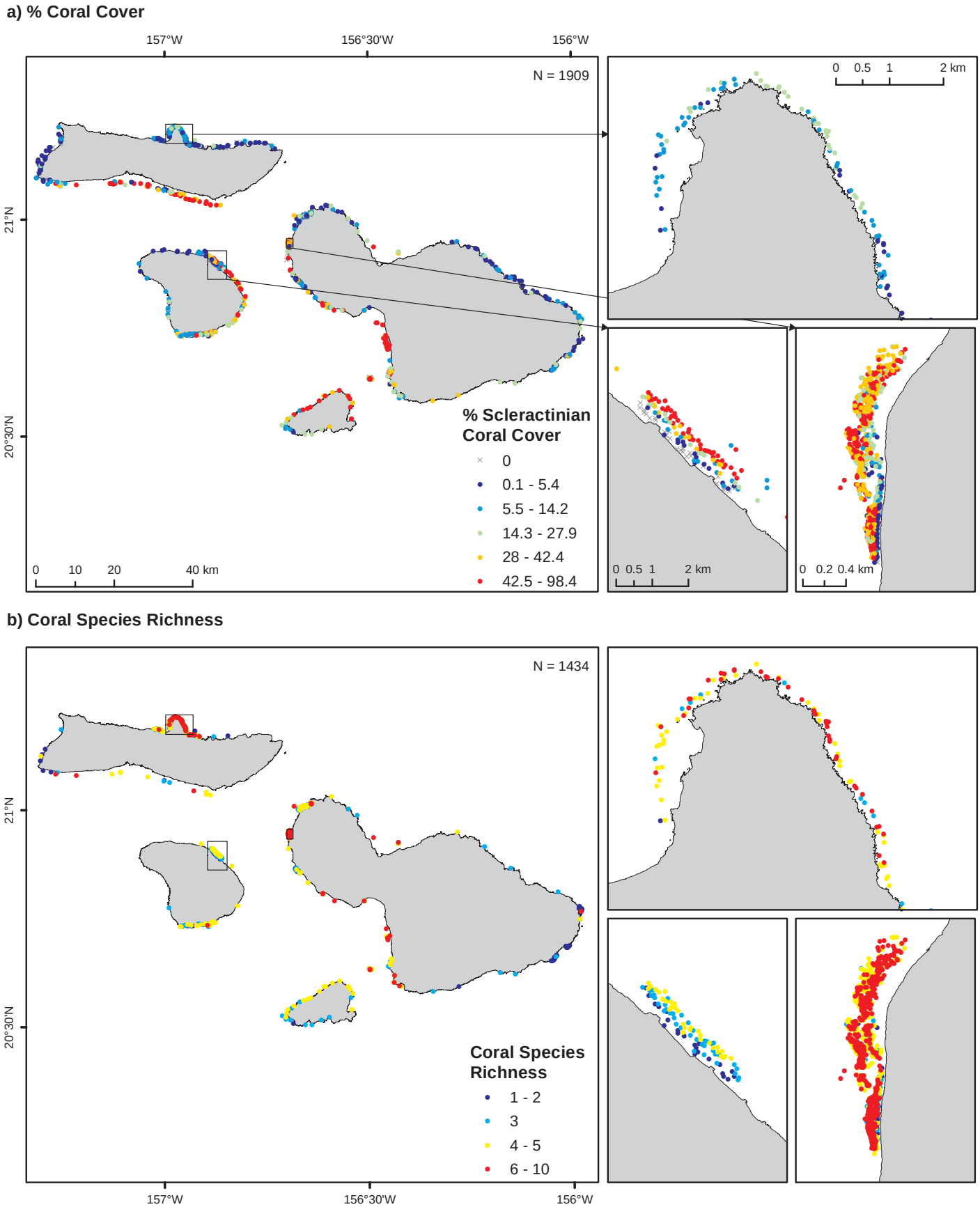

Figure 3.12. a) Percent cover of live scleractinian coral and b) coral species richness around the islands of Moloka'i, Lāna'i, Maui and Kaho'olawe as measured by scuba divers and compiled by UH FERL for 1999-2014. Data source: UH FERL, 2015a

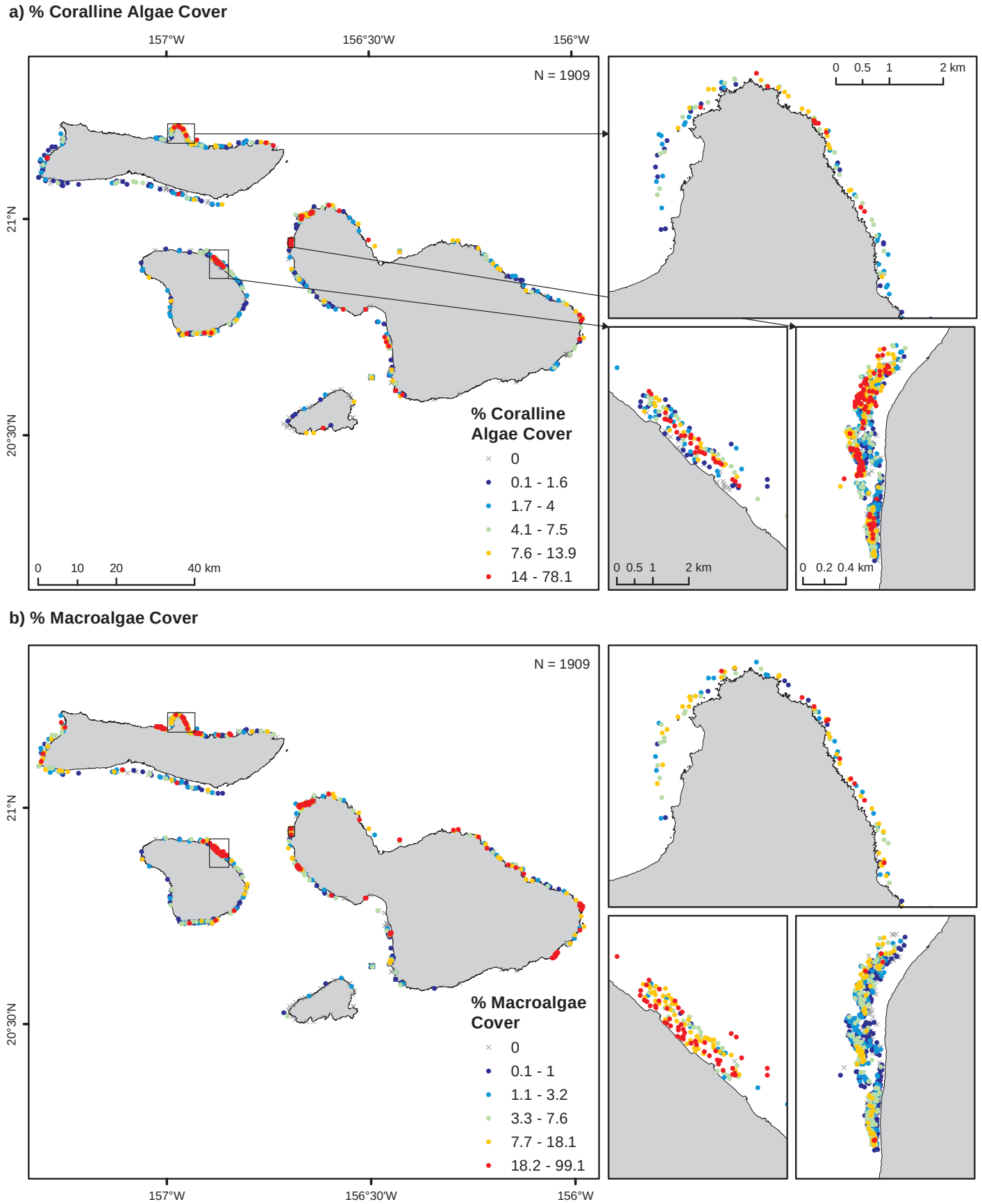

Figure 3.13. a) Percent cover of coralline algae and b) macroalgae around the islands of Moloka'i, Lāna'i, Maui and Kaho'olawe as measured by scuba divers and compiled by UH FERL for 1999-2014. Data source: UH FERL, 2015a

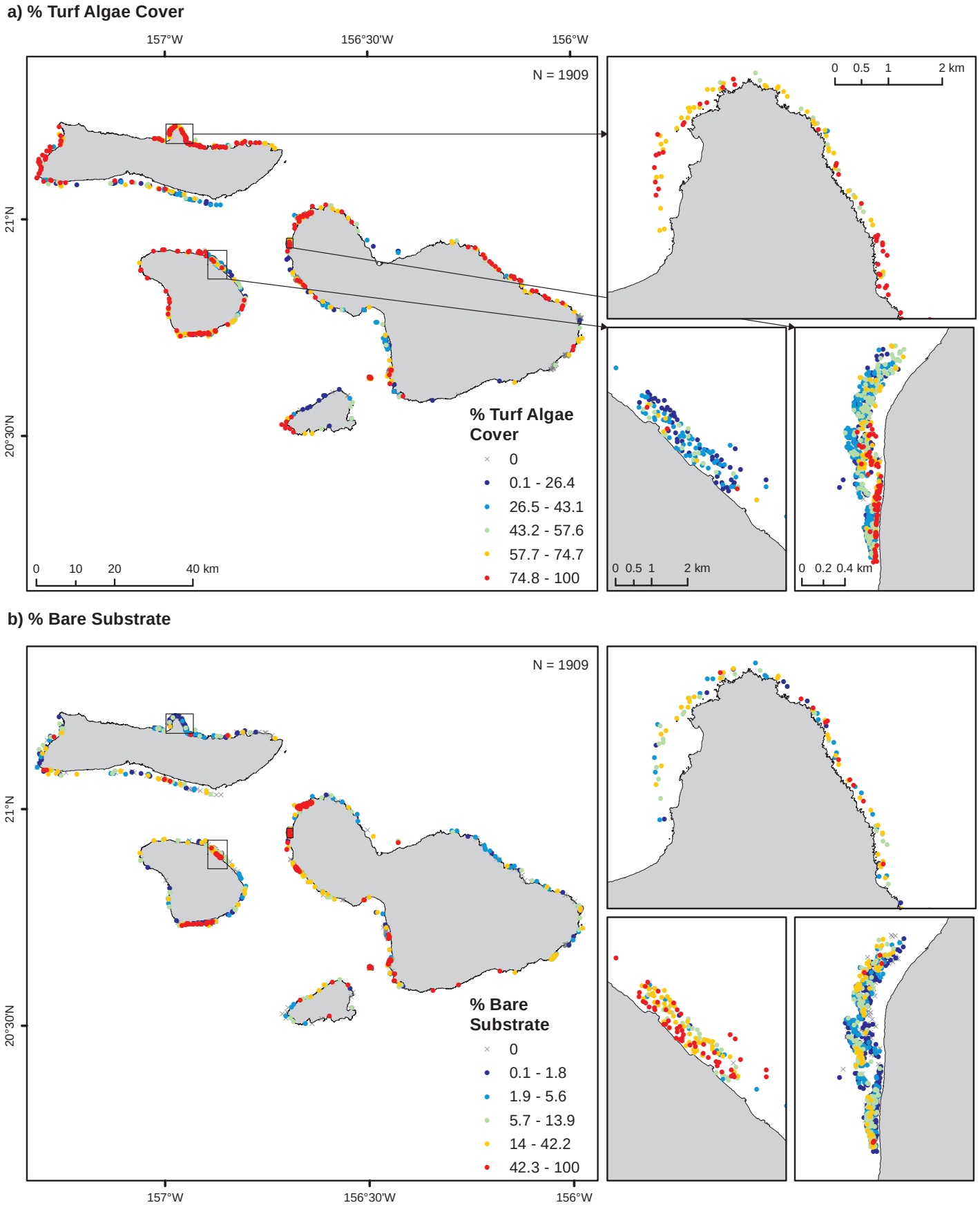

Figure 3.14. a) Percent cover of turf algae and b) bare substrate around the islands of Moloka'i, Lāna'i, Maui and Kaho'olawe as measured by scuba divers and compiled by UH FERL for 1999-2014. Data source: UH FERL, 2015a

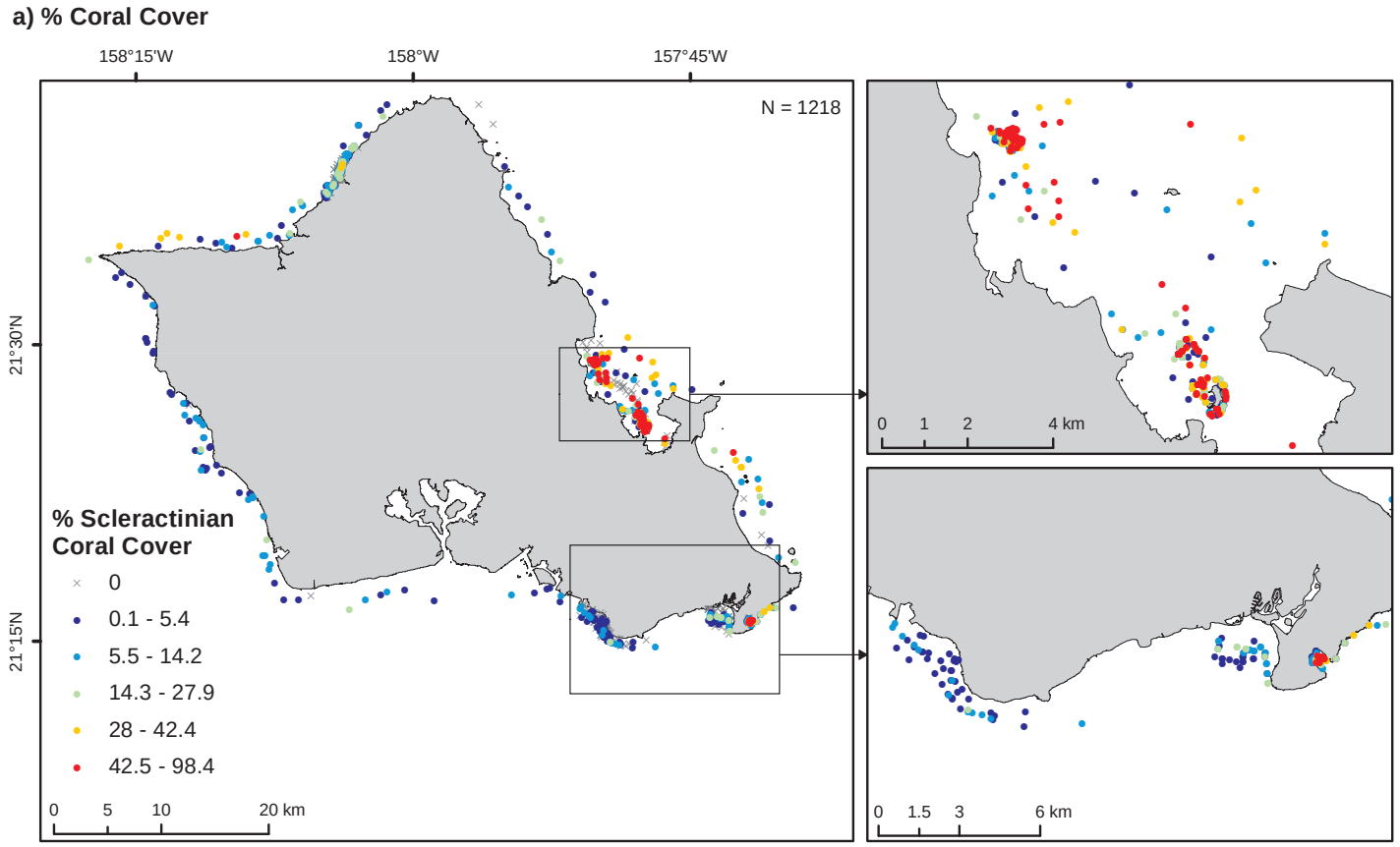

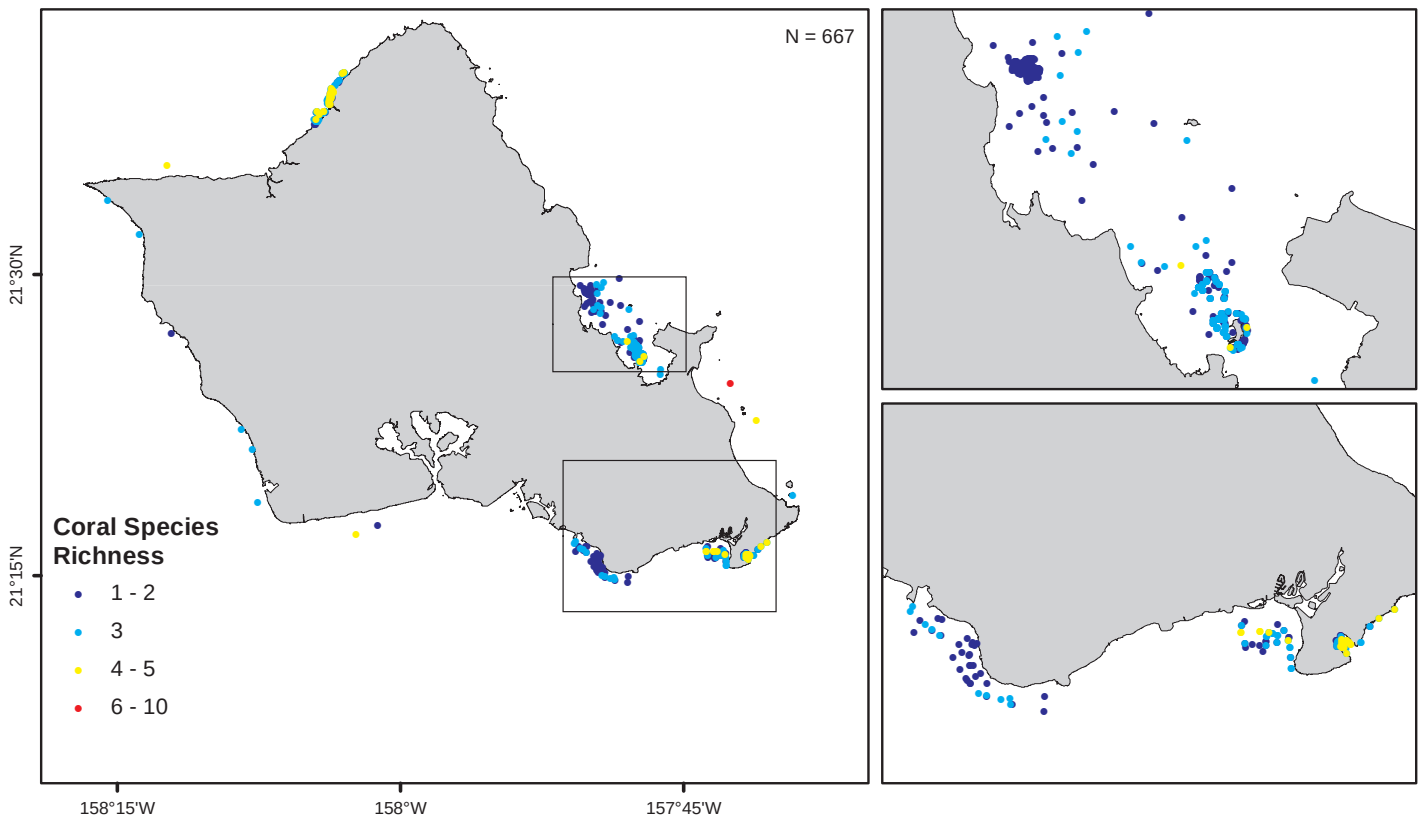

Figure 3.15. a) Percent cover of live scleractinian coral and b) coral species richness around the island of O'ahu, as measured by scuba divers and compiled by UH FERL for 1999-2014. Data sources: UH CRAMP, 2015; CREP, 2015; UH FERL, 2015a; TNC, 2015

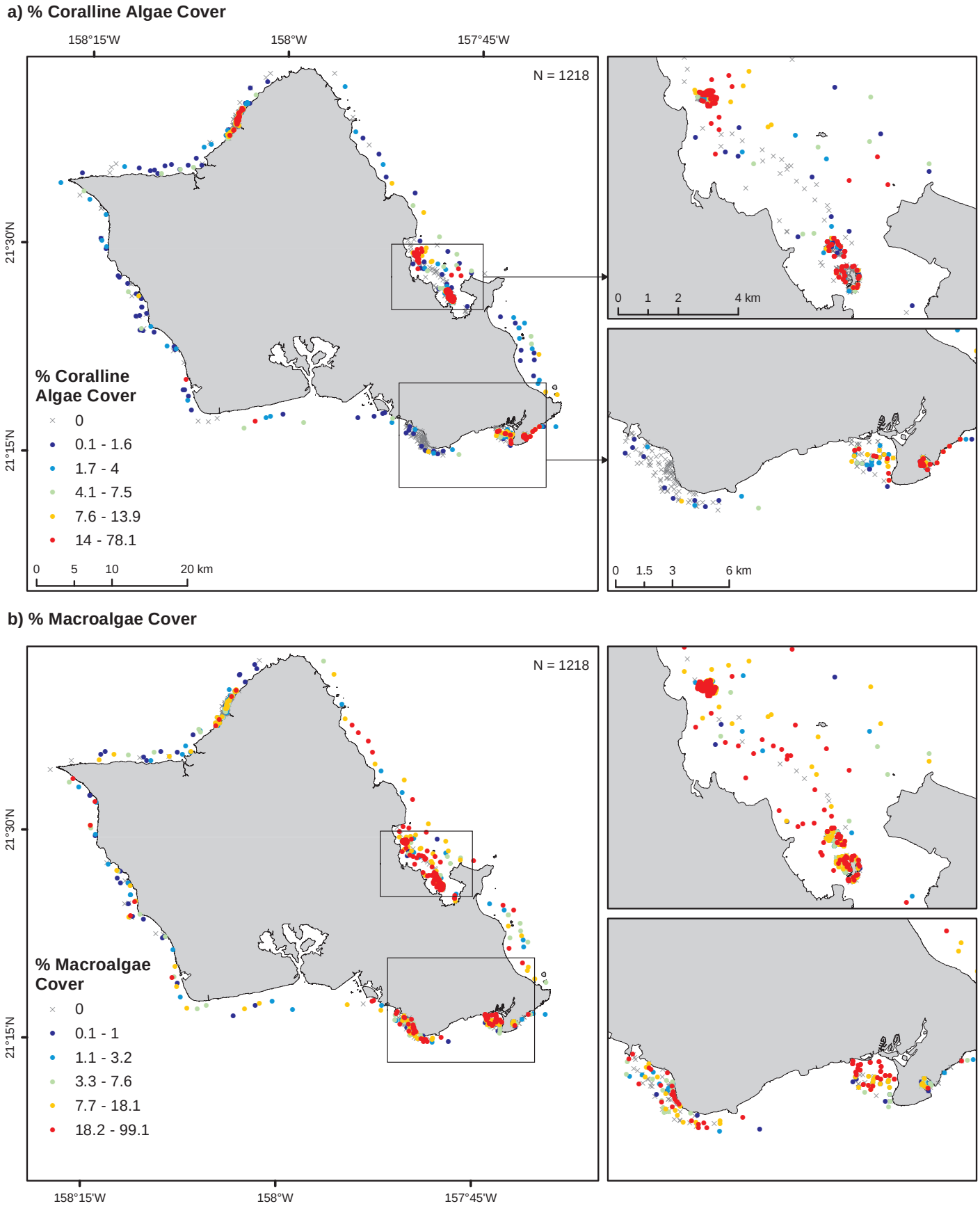

Figure 3.16. a) Percent cover of coralline algae and b) macroalgae around the island of O'ahu, as measured by scuba divers and compiled by UH FERL for 1999-2014. Data sources: UH CRAMP, 2015; CREP, 2015; UH FERL, 2015a; TNC, 2015

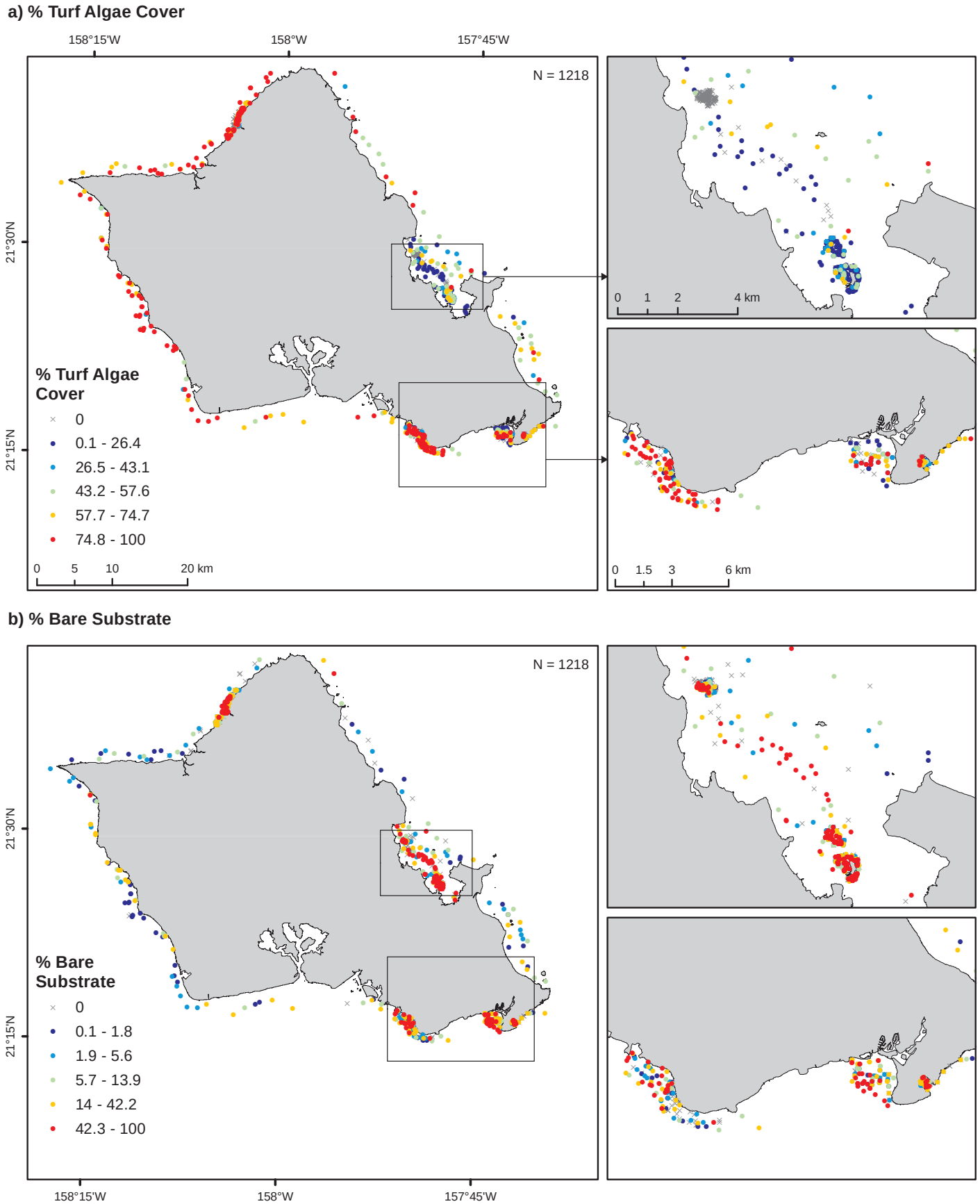

Figure 3.17. a) Percent cover of turf algae and b) bare substrate around the island of O'ahu, as measured by scuba divers and compiled by UH FERL for 1999-2014. Data sources: UH CRAMP, 2015; CREP, 2015; UH FERL, 2015a; TNC, 2015

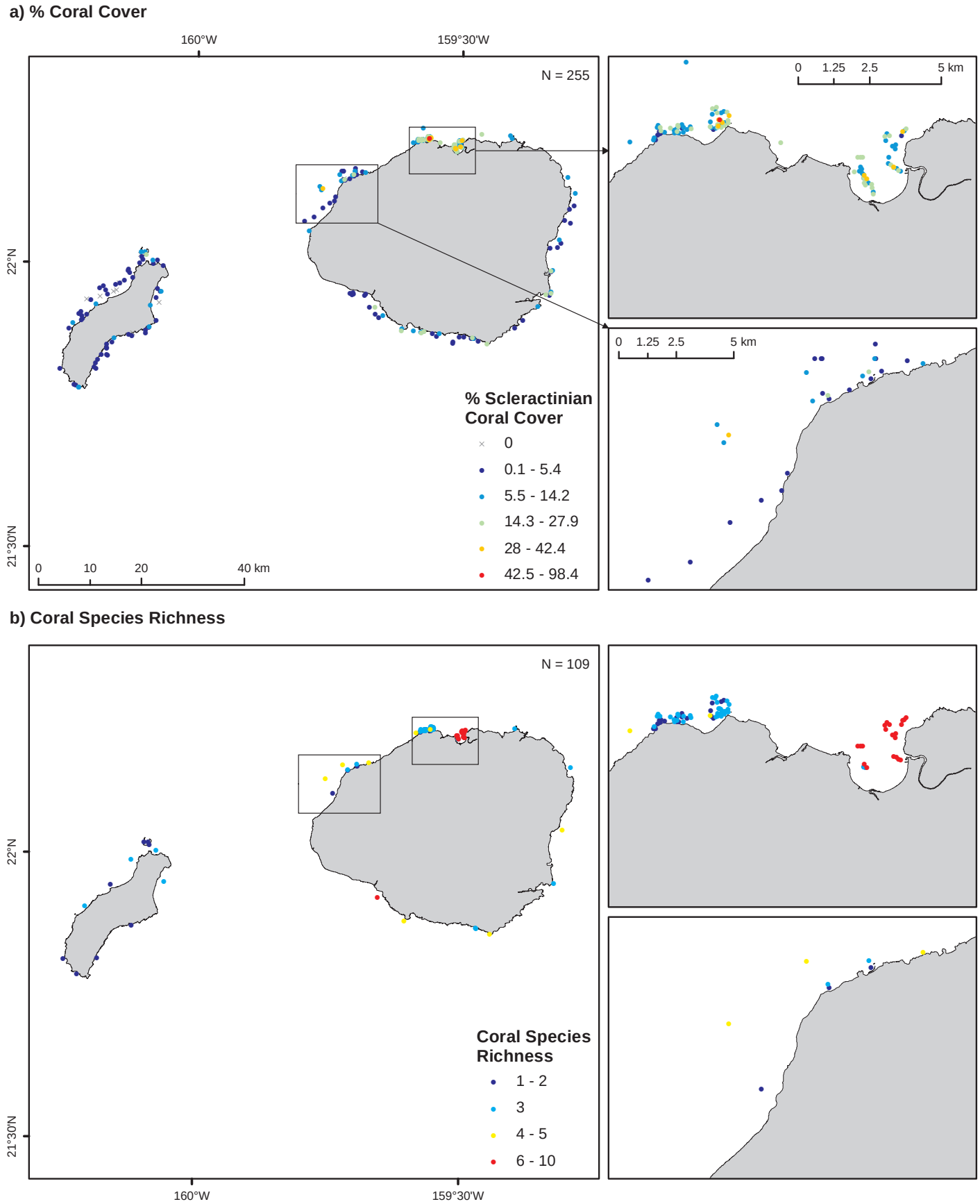

Figure 3.18. a) Percent cover of live scleractinian coral and b) coral species richness around the islands of Kaua'i and Ni'ihau, as measured by scuba divers and compiled by UH FERL for 1993-2013. Data sources: UH CRAMP, 2015; CREP, 2015; UH FERL, 2015a; NPS, 2015

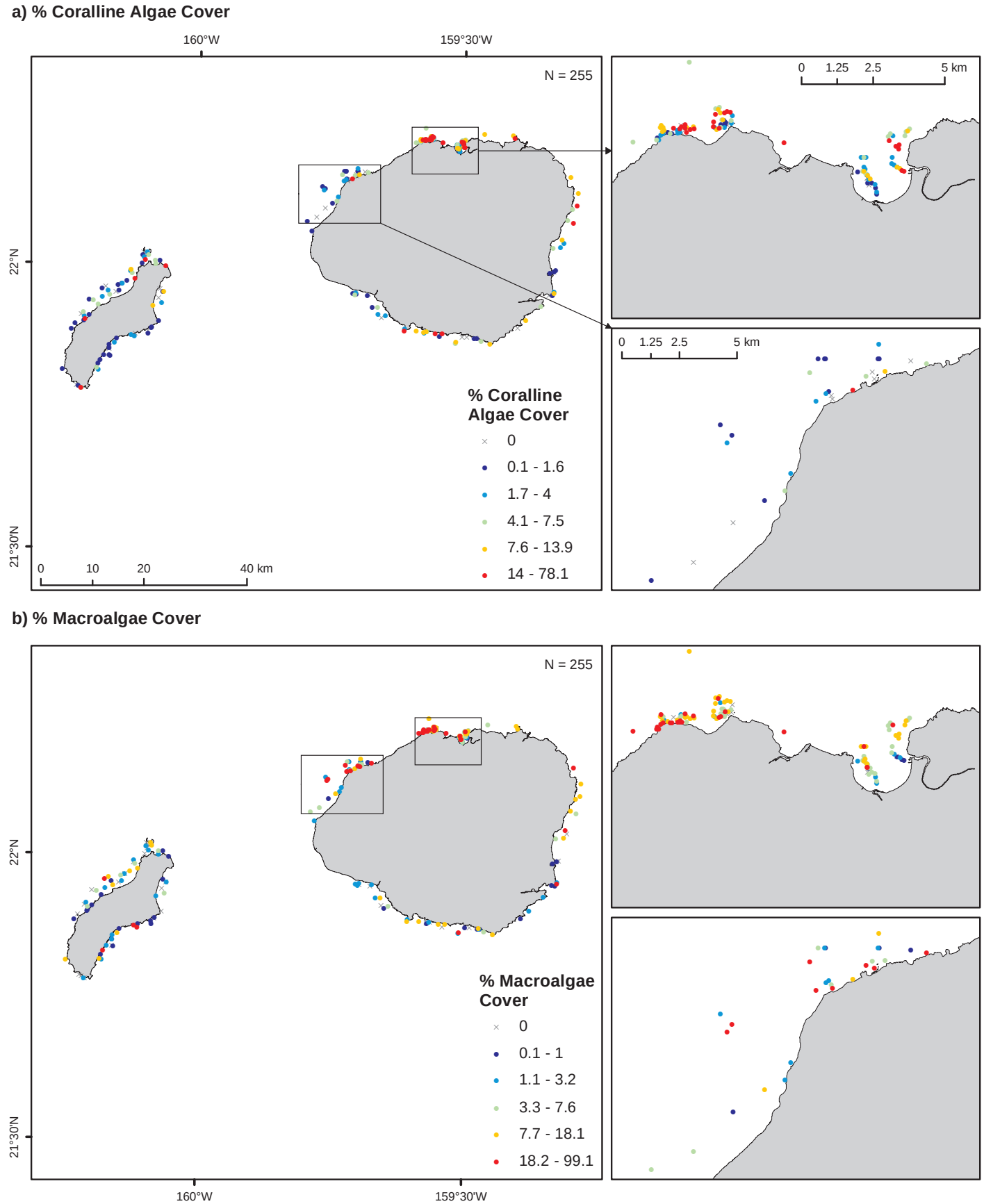

Figure 3.19. a) Percent cover of coralline algae and b) macroalgae around the islands of Kaua'i and Ni'ihau, as measured by scuba divers and compiled by UH FERL for 1993-2013. Data sources: UH CRAMP, 2015; CREP, 2015; UH FERL, 2015a; NPS, 2015

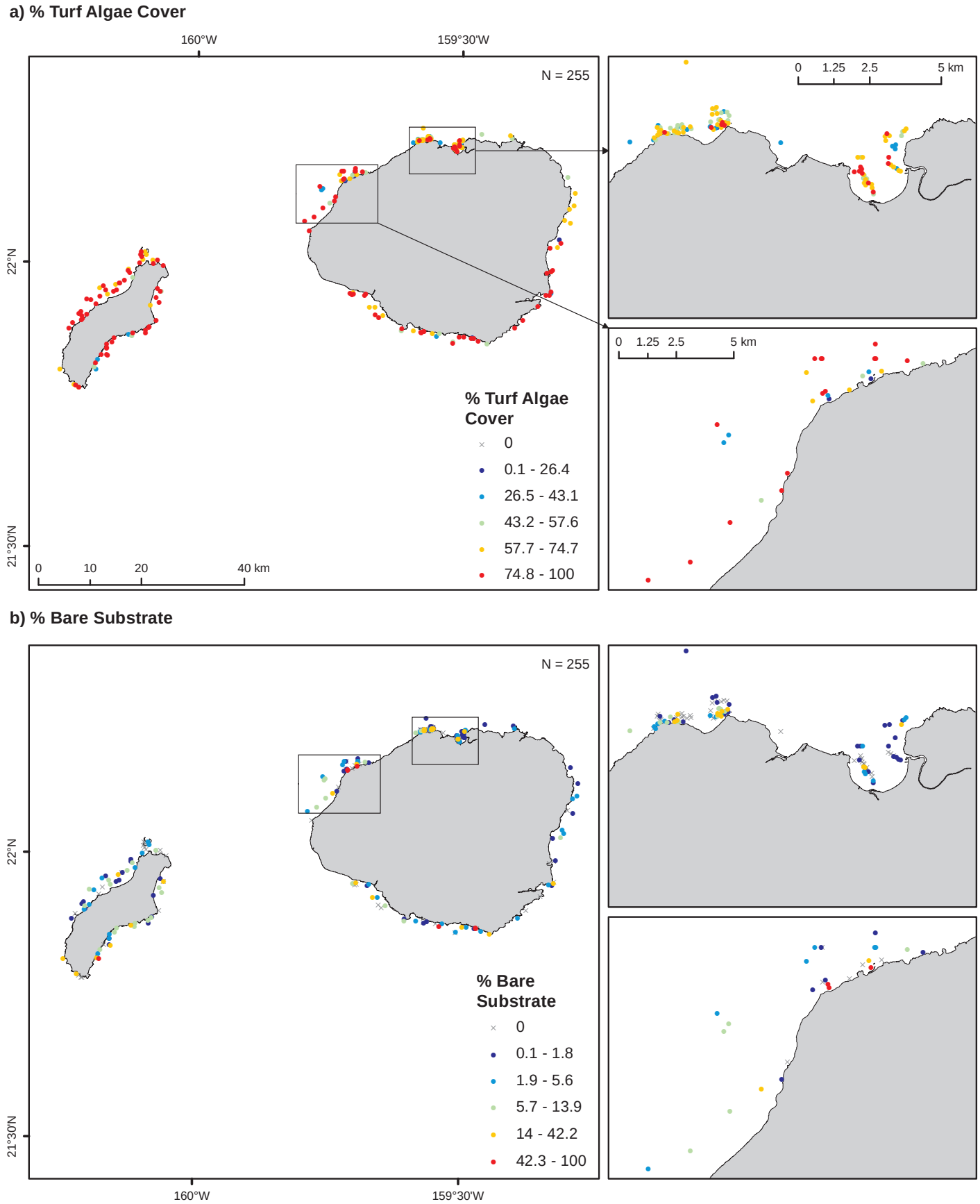

Figure 3.20. a) Percent cover of turf algae and b) bare substrate around the islands of Kaua'i and Ni'ihau, as measured by scuba divers and compiled by UH FERL for 1993-2013. Data sources: UH CRAMP, 2015; CREP, 2015; UH FERL, 2015a; NPS, 2015

3.2.3. Data and Information Gaps

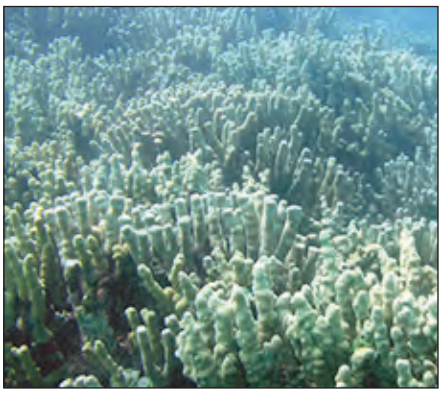

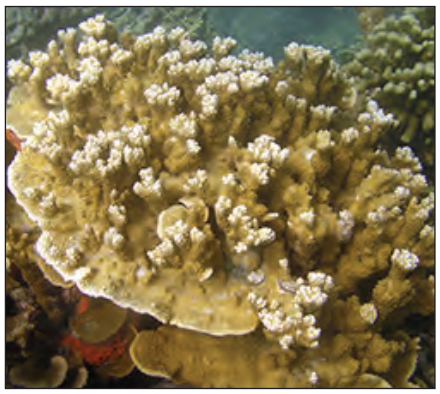

Porites compressa *(left; Photo credit: Bernardo Vargas-Ángel [NOAA NMFS/PIFSC/CREP])* *and* Montipora capitata *(right; Photo credit: Greta Aeby [Hawaii Institute of Marine Biology]).*

Benthic habitat maps created by visual interpretation are limited to shallow depths (<30 m), which represents a narrow band around the majority of the MHI (see Chapter 2). Although three-quarters of the shallow marine areas of the MHI have been classified, the percentage is much lower for particular islands. This is likely because it is difficult to obtain high quality multispectral imagery and to ground truth exposed windward areas such as the northeastern coast of Hawai'i. Other technologies, such as newly acquired LiDAR data, may aid in filling gaps. An additional limitation of the 2007 map is that the minimum mapping unit (MMU), which indicates the smallest sized feature in a map, is 1 acre. An MMU is determined based on management considerations, the effort needed to complete map production, and the ability to accurately interpret features in the imagery. More detailed maps of smaller, focused areas have been produced by U.S. Geological Survey (USGS) for the Pu'ukohola Heiau National Historic Site and the Pu'uhonua O Honaunau and Kaloko-Honokohau National Historical Parks on the Kona Coast (Gibbs et al., 2006, 2013). In addition, the mapped biological type was determined based on a coral-centric approach, which may lead to an underrepresentation of more prevalent cover types. Finally, it should be noted that imagery used in the most recent map was collected from 2004-2007. Periodic remapping should be conducted to assess changes in the benthic habitats around the MHI.

The *in situ* benthic cover database compiled here represents a compilation of multiple survey programs across the MHI. Data were collected using different sampling designs (permanent versus random sites), time periods, data collection methods (line point-intercept [LPI]; photo quadrat) and area surveyed/transect length. In addition, while some sampling programs are designed to monitor benthic cover across the archipelago (e.g., CREP), other studies were focused on particular geographic areas. This results in a high density of sites in specific areas such as Kāne'ohe Bay (O'ahu), Kahekili (Maui) and Ka'ūpūlehu-Kiholo (Hawai'i). Previous comparisons have demonstrated that species richness in particular may vary among survey methods (Jokiel et al., 2015); hence comparing richness values across the MHI should be done with caution. Macroalgae and turf algae cover can vary seasonally and inter-annually depending on nutrient availability and oceanographic conditions. Where permanent sites have been established, the data could be examined to assess temporal trends at those locations; however, due to the aforementioned differences in survey methods, objectives and spatial bias, further evaluation would be needed to determine whether the integrated dataset could be used to assess wider temporal trend patterns. For the UH CRAMP dataset, Rodgers et al. (2014) found that statewide coral cover and richness did not vary significantly since initiation of the surveys, although variation at some stations occurred due to acute disturbances (e.g., sedimentation events, crown-of-thorns outbreak). Although the long-term effects are not yet fully known, mortality from the 2014–2015 bleaching may result in decreased overall coral cover at many locations in the MHI.

Crown-of-thorns Seastar off O'ahu. Photo credit: Jean Kenyon (NOAA NMFS/PIFSC)

3.3. MESOPHOTIC CORALS

3.3.1. Existing Data/Research, Limitations, and Gaps

Mesophotic coral Leptoseris *species. Photo credit: Hawai'i Undersea Research Laboratory*

The majority of available survey data in mesophotic habitats of the MHI are from the ʻAuʻau Channel region, an area with unique geology and physical oceanography between the islands of Maui, Lānaʻi, Molokaʻi and Kahoʻolawe (Figure 3.21; Costa et al., 2015). Observations were compiled from underwater video and photos collected on research cruises from 2001-2011 conducted by the Bishop Museum, DAR, PIFSC, the University of Hawai'i and the Hawai'i Undersea Research Laboratory (HURL; UH PIBHMC, 2008; Rooney et al., 2010; Costa et al., 2015). Data were processed and provided by PIFSC CREP (PIFSC, 2014; Costa et al. 2015). Using Maximum Entropy (MaxEnt) modeling software, Costa et al. (2015) developed habitat suitability models from presence data for *Leptoseris* spp., *Montipora* spp. and *Porites* spp., and converted the model outputs to maps of probability of occurrence by calculating empirical prevalence from available presence and absence data (Figure 3.21). Several environmental variables were found to be important in predicting suitability for all hard corals, as well as the three individual coral genera, including depth, distance from shore, mean euphotic depth and variance of euphotic depth. For *Montipora* spp., predicted suitable conditions were the highest between Lahaina Roads Basin and Papawai Point. This area is characterized by relatively warmer (at the surface), moderately deep and less turbid waters than elsewhere in the study area, suggesting that *Montipora* spp. do better in moderately deep waters that remain optically clear and stable through time. For *Porites* spp., suitable conditions were highest between Hanakaoo Point and Hekili Point. This area is characterized by relatively warmer, slightly shallower and less turbid waters than found in other parts of the study area, suggesting that *Porites* spp. do well in shallower waters and can tolerate slightly more turbidity than *Montipora* spp. Lastly, for *Leptoseris* spp., suitable environmental conditions were highest offshore of Hekili Point, which has the deepest and most consistently warm and clear waters compared to any other part of the study area. This suggests that *Leptoseris* spp. does better in slightly deeper, substantially less turbid and less variable waters (in terms of turbidity) than *Montipora* spp. or *Porites* spp. Further information on data sources, modeling techniques and results can be found in Costa et al. (2015).

Additional records that were not included in the previous assessment (Costa et al., 2015) are located southwest of Molokaʻi on Penguin Bank and south of Maui. However, as the vast majority of the data was used in Costa et al.'s (2015) modeling effort, we chose not to replicate or develop additional models here. Further, the ʻAuʻau Channel is largely encompassed by the Hawaiian Islands Humpback Whale National Marine Sanctuary, where offshore energy development is unlikely.

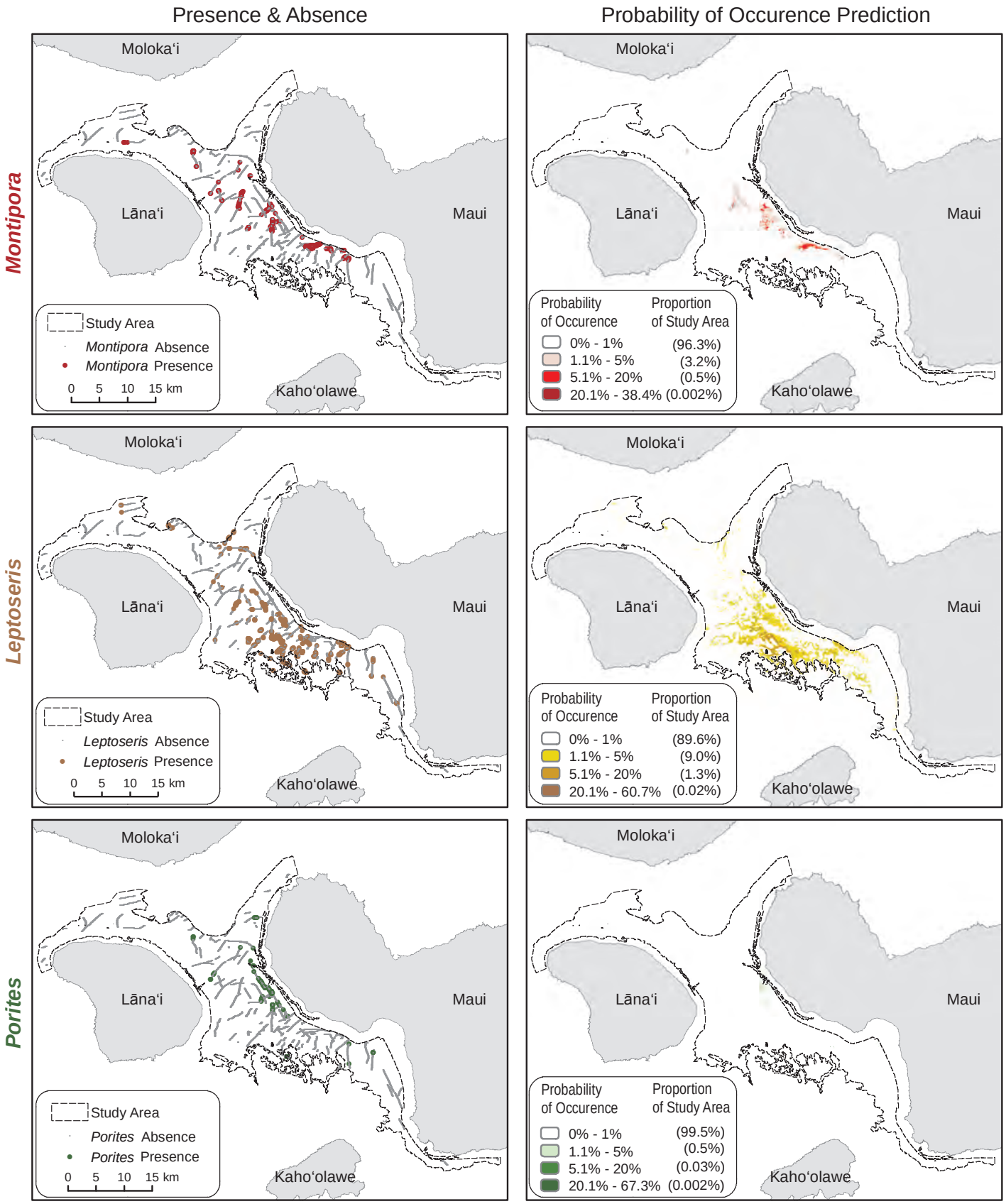

Figure 3.21. Location of presences and absences (left panel) and predicted distributions (right panel) of mesophotic coral genera Montipora *(top),* Leptoseris *(center) and* Porites *(bottom). Adapted from Costa et al. (2015). Data were collected by remotely operated vehicles (ROV) and a Towed Optical Assessment Device (TOAD) camera sled (UH PIBHMC, 2008; Rooney et al., 2010).*

3.4. DEEP-SEA CORALS

3.4.1. Methods and Data Description

Deep-sea coral presence data

Observational deep-sea coral (DSC) records were obtained from a database maintained by NOAA's Deep-Sea Coral Research and Technology Program (DSCRTP) and supplemented by additional records from HURL. The DSCRTP database was created to compile and disseminate the locations of existing biological observations of deep-sea corals and sponges, as well as serve as a repository for data from DSCRTP-funded projects (Hourigan et al., 2015). The database contains data from within NOAA and from other government/academic institutions and researchers, including museum collections. The database includes presence records and locations of Anthozoa and Hydrozoa cnidarians. These animals typically occur deeper than 50 m (although shallower records are included when they occur). Locations surveyed but lacking corals are not included. The geopositional accuracy of individual records varies depending on the source data; while some represent discrete locations, others represent multiple observations over a larger area (e.g., trawl) integrated into a single position value (Hourigan et al., 2015). In addition, methods of geographic positioning undoubtedly vary widely across records in this historical database. Earlier records were likely positioned by sextant, whereas later records may have been positioned by radio or modern global positioning system (GPS) . Within the MHI study area DSCRTP, the database contained 1,074 records from 1891–2009. Additional records (n=20080) obtained from HURL included deep-submergence rescue vehicle (DSR/V; *Pisces* IV and *Pisces V* DSR/V, *Makalii* DSR/V) and remotely operated vehicle (ROV) surveys carried out from 1981-2007.

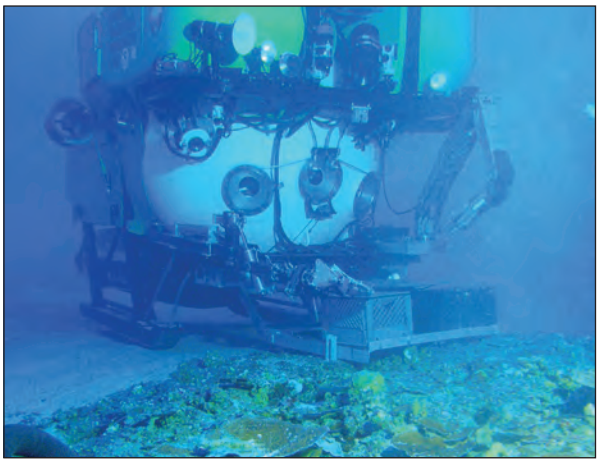

Pisces V, *NOAA/UH Hawai'i Undersea Research Laboratory (HURL) in the 'Au'au channel near Maui. Photo credit: NOAA Office of Ocean Exploration and Research*

The DSCRTP and HURL datasets were merged and duplicates (i.e., individual species records with the same latitude/longitude) were removed. Any points that fell on land were also removed. Each record was thoroughly checked for spelling errors, incomplete fields, and incorrect taxonomy. Incomplete taxonomic information was resolved, when possible, by cross checking with the World Register of Marine Species (WoRMS; WoRMS Editorial Board, 2014). In addition, expert opinion (C. Kelley, pers. comm.) was used to remove several species-specific depth outliers, to assign some previously unclassified Scleractinia records (Scleractinia "bramble") to the proper model group, and in one case to correct taxonomic information (*Cirrhipathes* sp. records over 100 m were changed to *Stichopathes* sp.). Following these revisions, the merged dataset contained 4,660 coral presence records within the study area.

For purposes of habitat suitability modeling, coral taxa were organized into groups based on ecological importance, management considerations, the number of presence records and recommendations from local DSC experts (Table 3.6). In addition, some model groups were included to enable comparisons to models developed for the U.S. Atlantic (NOAA NCCOS, 2015). Groups included three order-level groupings (Alcyonacea, Scleractinia, Pennatulacea) and nested groupings at the sub-order, family and genus level. For example, in addition to a model of all Alcyonacea, independent models were constructed for the Suborders Calcoxonia, Holaxonia and Scleraxonia, and for Family Isididae (Bamboo corals) within Calcoxonia. Within the Zoantharia order, only the Hawaiian gold coral *K. haumeaae* was considered. Black corals (Order Antipatharia) were separated into three groups based on common genera-specific depth ranges. Summary statistics and histogram/kernel density plots of observed depth distribution were examined for each genus to refine the groupings. Scleractinian (hard) corals were separated into two groups: 1) "framework" forming, or those that

colonize hard substrates and build structures, and 2) non-framework forming (e.g., solitary cup corals that can colonize both hard and soft substrates). The pen corals (Pennatulacea) were divided into two groups, as some genera are more likely to inhabit hard substrates while others inhabit soft substrates. Two additional groups, the presence of ≥4 and ≥7 DSC genera in a grid cell, respectively, were modeled to identify places that may support suitable habitat for a high diversity of corals.

For each model group (Table 3.6), the final step in processing the DSC presence records was to remove duplicate records within each model grid cell using ENMTools (Warren et al., 2010). While removing duplicate records decreases sample size, it can help reduce the effect of sampling bias in heavily sampled areas.

Table 3.6. Description of modeled deep-sea coral (DSC) groups, total number of presence records and number of records used in analysis after grid cell duplicates were removed. Data sources: DSCRTP, 2015; HURL, 2015

Group	Description	Total # Records	# Retained for Analysis
1	Gold corals (*Kulamanamana haumeaae*)	101	84
2	Framework-forming Scleractinia (includes *Enallopsammia rostrata*, *Madracis kauaiensis*, *Madrepora oculata*, Scleractinia "bramble")	104	93
3	Non-framework forming Scleractinia (includes all Scleractinia identified at the family level that are not in Group 2)	340	234
4	Antipatharia, shallow genera (30-100 m; includes *Antipathes*, *Cirrhipathes*)	168	109
5	Antipatharia, mid-depth genera (100-300 m; includes *Acanthopathes*, *Antipathella*, *Myriopathes*, *Stichopathes*)	217	196
6	Antipatharia, deep genera (>300 m; includes *Aphanipathes*, *Bathypathes*, *Chrysopathes*, *Dendropathes*, *Leiopathes*, *Parantipathes*, *Stauropathes*, *Trissopathes*, *Umbellapathes*)	447	204
7	Pennatulacea, hard substrate dwelling (includes *Anthoptilum* and *Calibelemnon*)	77	65
8	Pennatulacea, soft substrate dwelling (includes all Pennatulacea genera not in Group 7)	292	206
9	Non-gorgonian Alcyonacea (includes Suborders Alcyoniina, Stolonifera)	279	200
10	Gorgonian Alcyonacea (includes Suborders Calcaxonia, Holaxonia, Scleraxonia)	2,481	530
11	Alcyonacea, Suborder Calcaxonia	1,569	397
12	Alcyonacea, Suborder Calcaxonia, Family Isididae (Bamboo corals)	474	225
13	Alcyonacea, Suborder Holaxonia	355	186
14	Alcyonacea, Suborder Scleraxonia	557	274
15	Alcyonacea, Suborder Scleraxonia, Family Paragorgiidae (Bubblegum corals)	104	77
16	Alcyonacea, Suborder Scleraxonia, Family Corallidae, *Corallium* spp. (Red and pink corals)	405	234
17	4 or more genera/grid cell	317	317
18	7 or more genera/grid cell	169	169

Predictor datasets

An initial set of 65 environmental data layers were produced for potential use in predictive models of DSC habitat suitability around the MHI. Selection of the initial set of potential predictors was based on an extensive literature review and input from experts in Hawaiian DSC ecology. Predictor variables fell into one of three categories: topographic (Table 3.7), geographic (Table 3.8) and oceanographic (Table 3.9).

Topographic variables were included to account for variation in DSC habitat suitability arising from the direct and indirect effects of depth and seafloor geomorphology. Depth and a suite of seafloor complexity metrics were derived from a 90x90 m resolution bathymetry grid (see Chapter 2). The seafloor complexity metrics were also generated at multiple spatial scales (1,500 m, 5 km, 10 km, 20 km) by using a low-pass filter to smooth the 90 m resolution bathymetry dataset using neighborhoods at these sizes and then calculating the metrics on the smoothed bathymetry grids. Bathymetric position index (BPI), a measure of a location's depth relative to the surrounding area, was derived at the same spatial scales to identify ridges and valleys at these scales.

Table 3.7. Topographic variables considered as potential environmental predictors in models of DSC habitat suitability. Note that each of these variables was calculated at multiple spatial scales. SD = Standard Deviation

Dataset	Description	Unit	Statistic(s)	Data Source/ Provider	Native Resolution
Depth	Seafloor depth	m	mean, SD	Bathymetry Model (see Chapter 2)	90x90 m
Slope	Maximum rate of change in seafloor depth between each grid cell and its neighbors	Degree	mean	Bathymetry Model (see Chapter 2)	90x90 m
Slope of Slope	Maximum rate of change in seafloor slope between each grid cell and its neighbors	Degree	mean	Bathymetry Model (see Chapter 2)	90x90 m
Aspect	Downslope direction of maximum rate of change in seafloor depth between each grid cell and its neighbors	Unitless	sine and cosine circular mean	Bathymetry Model (see Chapter 2)	90x90 m
Rugosity	Ratio of seafloor surface area to planar area; value indicates topographic roughness; values can range from 1 (flat) to infinity	Unitless	mean	Bathymetry Model (see Chapter 2)	90x90 m
Total curvature	Surface curvature; value indicates surface ruggedness; values > 0, with 0 indicating surface is a plane	Radians/m^2	mean	Bathymetry Model (see Chapter 2)	90x90 m
Planar curvature	Seafloor curvature perpendicular to the line of maximum slope; value indicates whether flow will converge or diverge over a point; values can be - (concave), + (convex), or 0 (flat)	Radians /m	mean	Bathymetry Model (see Chapter 2)	90x90 m
Profile curvature	Seafloor curvature along the line of maximum slope; value indicates whether flow will accelerate or decelerate over the curve; values can be + (concave), - (convex), or 0 (flat)	Radians /m	mean	Bathymetry Model (see Chapter 2)	90x90 m
Bathymetric position index (BPI)	Difference in seafloor depth and the mean seafloor depth in an annular neighborhood of specified inner and outer radii; values indicate a location's position relative to the surrounding area; values can be + (ridges), - (valleys), or 0 (flat areas or areas of constant slope)	m	mean	Bathymetry Model (see Chapter 2)	90x90 m

Dataset	Processing Tools and Steps
Depth	Zonal mean and standard deviation of the 90 m resolution depth and the 90 m resolution depth smoothed in 1,500 m, 5 km, 10 km and 20 km neighborhoods were calculated in 360 m resolution model grid cells using the ArcGIS Zonal Statistics tool (ESRI, 2011)
Slope	Slope was calculated on the 90 m resolution depth and on the 90 m resolution depth smoothed in 1,500 m, 5 km, 10 km and 20 km neighborhoods using the ArcGIS Slope tool (ESRI, 2011); Zonal mean of each 90 m resolution slope dataset was calculated in 360 m resolution model grid cells using the ArcGIS Zonal Statistics tool (ESRI, 2011)
Slope of Slope	Slope of slope was calculated on the 90 m resolution slope and on the 90 m resolution slope derived from depth smoothed in 1,500 m, 5 km, 10 km and 20 km neighborhoods using the ArcGIS Slope tool (ESRI, 2011); Zonal mean of each 90 m resolution slope dataset was calculated in 360 m resolution model grid cells using the ArcGIS Zonal Statistics tool (ESRI, 2011)
Aspect	Aspect was calculated on the 90 m resolution depth and on the 90 m resolution depth smoothed in 1,500 m, 5 km, 10 km and 20 km neighborhoods using the ArcGIS Aspect tool (ESRI, 2011); Aggregate circular mean of each 90 m aspect dataset was calculated in 360 m resolution model grid cells using the R circular package (Agostinelli and Lund, 2013); Sine and cosine of the mean aspect were calculated in the R raster package (Hijmans, 2014)
Rugosity	Rugosity was calculated on the 90 m resolution depth and on the 90 m resolution depth smoothed in 1,500 m, 5 km, 10 km and 20 km neighborhoods using the DEM Surface Tools Surface Area tool (Jenness, 2013); Zonal mean of each 90 m resolution rugosity dataset was calculated in 360 m resolution model grid cells using the ArcGIS Zonal Statistics tool (ESRI, 2011)
Total curvature	Total curvature was calculated on the 90 m resolution depth and on the 90 m resolution depth smoothed in 1,500 m, 5 km, 10 km and 20 km neighborhoods using the DEM Surface Tools Curvature tool (Jenness, 2013); Zonal mean of each 90 m resolution total curvature dataset was calculated in 360 m resolution model grid cells using the ArcGIS Zonal Statistics tool (ESRI, 2011)
Planar curvature	Planar curvature was calculated on the 90 m resolution depth and on the 90 m resolution depth smoothed in 1,500 m, 5 km, 10 km and 20 km neighborhoods using the DEM Surface Tools Curvature tool (Jenness, 2013); Zonal mean of each 90 m resolution planar curvature dataset was calculated in 360 m resolution model grid cells using the ArcGIS Zonal Statistics tool (ESRI, 2011)
Profile curvature	Profile curvature was calculated on the 90 m resolution depth and on the 90 m resolution depth smoothed in 1,500 m, 5 km, 10 km and 20 km neighborhoods using the DEM Surface Tools Curvature tool (Jenness, 2013); Zonal mean of each 90 m resolution profile curvature dataset was calculated in 360 m resolution model grid cells using the ArcGIS Zonal Statistics tool (ESRI, 2011)
Bathymetric position index (BPI)	For 1,500 m, 5 km, 10 km and 20 km neighborhoods, BPI was calculated on the 90 m resolution depth using the Benthic Terrain Modeler tool (Wright et al., 2012); Zonal mean of each 90 m resolution BPI dataset was calculated in 360 m resolution model grid cells using the ArcGIS Zonal Statistics tool (ESRI, 2011)

Table 3.8. Geographic variables considered as potential environmental predictors in models of DSC habitat suitability.

Dataset	Description	Unit	Statistic(s)	Data Source/Provider	Native Resolution
Distance to shore	Straight line (Euclidean) distance to the shoreline	m	N/A	MHI benthic habitat maps (Battista et al., 2007)	N/A
Distance to seamounts	Average straight line (Euclidean) distance to seamount footprints	m	mean	Bathymetry Model (see Chapter 2)	90x90 m
Dataset	**Processing Tools and Steps**				
Distance to shore	Shorelines were extracted from MHI benthic habitat maps; Distance to shoreline was calculated in 360 m resolution grid cells using the ArcGIS Euclidean Distance tool (ESRI, 2011)				
Distance to seamounts	Seamount footprints were extracted from the 90 m resolution depth dataset at 50 m increments from 100–4500 m depths; Distances to these footprints were calculated in 360 m resolution grid cells using the ArcGIS Euclidean Distance tool (ESRI, 2011) and then averaged				

Table 3.9. Oceanographic variables considered as potential environmental predictors in models of DSC habitat suitability. SD = Standard Deviation

Dataset	Description	Unit	Statistic(s)	Data Source/Provider	Native Resolution
Bottom current speed	Ocean current speed at lowest HYCOM depth	m/s	annual mean, annual SD	HYCOM + NCODA Global 1/12° Reanalysis from HYCOM Consortium (2014)	9x9 km
Bottom current direction	Ocean current direction at lowest HYCOM depth	Unitless	sine and cosine of annual circular mean	HYCOM + NCODA Global 1/12° Reanalysis from HYCOM Consortium (2014)	9x9 km
Bottom salinity	Salinity at lowest HYCOM depth	PSU	annual mean	HYCOM + NCODA Global 1/12° Reanalysis from HYCOM Consortium (2014)	9x9 km
Bottom temperature	Temperature at lowest HYCOM depth	°C	annual mean	HYCOM + NCODA Global 1/12° Reanalysis from HYCOM Consortium (2014)	9x9 km
Surface chlorophyll-*a* concentration	Sea surface chlorophyll-*a* concentration	mg/m^3	annual mean	Monthly Aqua MODIS Chlorophyll Concentration Composites from NASA Ocean Biology Processing Group (2015)	4x4 km
Surface turbidity	Amount of organic and inorganic suspended solids in the water at the sea surface	sr^{-1}	annual mean	Monthly Aqua MODIS Remote Sensing Reflectance at 547 nm Composites from NASA Ocean Biology Processing Group (2015)	4x4 km
Mixed layer depth	Depth of the ocean mixed layer, within which salinity, temperature, and density are nearly uniform	m	annual mean	HYCOM + NCODA Global 1/12° Reanalysis from HYCOM Consortium (2014)	9x9 km
Dataset	**Processing Tools and Steps**				
Bottom current speed	HYCOM daily bottom current data from 1992-2012 were downloaded, speed was calculated from u and v component vectors, and annual mean and standard deviation of speed were calculated for each HYCOM grid cell using custom R scripts; The annual mean climatology was then projected and resampled to the 360 m resolution model grid using ArcGIS (ESRI, 2011)				
Bottom current direction	HYCOM daily bottom current data from 1992-2012 were downloaded, direction was calculated from u and v component vectors, and annual circular mean direction was calculated for each HYCOM grid cell using custom R scripts; The annual mean climatology was then projected and resampled to the 360 m resolution model grid using ArcGIS (ESRI, 2011). Sine and cosine of the annual circular mean direction were calculated in the R raster package (Hijmans, 2014)				
Bottom salinity	HYCOM daily salinity data from 1992-2012 were downloaded and annual mean salinity was calculated for each HYCOM grid cell using custom R scripts; The annual mean climatology was then projected and resampled to the 360 m resolution model grid using ArcGIS (ESRI, 2011)				
Bottom temperature	HYCOM daily temperature data from 1992-2012 were downloaded and annual mean temperature was calculated for each HYCOM grid cell using custom R scripts; The annual mean climatology was then projected and resampled to the 360 m resolution model grid using ArcGIS (ESRI, 2011)				
Surface chlorophyll-*a* concentration	Datasets were downloaded and binned using MGET Create Climatological Rasters for NASA Ocean Color L3 SMI tool (Roberts et al., 2010); The annual mean climatology was then projected and resampled to the 360 m resolution model grid using ArcGIS (ESRI, 2011)				
Surface turbidity	Datasets were downloaded and binned using MGET Create Climatological Rasters for NASA Ocean Color L3 SMI tool (Roberts et al., 2010); The annual mean climatology was then projected and resampled to the 360 m resolution model grid using ArcGIS (ESRI, 2011)				
Mixed layer depth	HYCOM daily salinity and temperature data from 1992-2012 were downloaded. Daily mixed layer depth for each HYCOM grid cell and the annual mean climatology were calculated using custom Matlab scripts; The annual mean climatology was then projected and resampled to the 360 m resolution model grid using ArcGIS (ESRI, 2011)				

Geographic variables were included to account for variation in DSC habitat suitability arising from spatial location. These included distance to shore and mean distance to seamounts at a range of depths (see Chapter 2).

Oceanographic variables were included to account for variation in DSC habitat suitability arising from the direct and indirect effects of the physical state and dynamics of the ocean or from the direct and indirect effects of ocean productivity. These datasets included annual climatologies derived from an ocean circulation model (HYCOM) or from remote sensing data (see Chapter 2).

All predictors were resampled to the 360 m resolution model grid with an oblique Mercator projected coordinate system. This resolution was chosen because of vertical and horizontal spatial uncertainty in the NOAA Coastal Relief Model depth values in deeper waters, positional uncertainty in the DSC presence data, and to avoid excessive downsampling of the coarser (1-9 km resolution) datasets representing the oceanographic variables. A pairwise correlation analysis was performed on the full set of potential environmental predictor datasets using the ENMTools software (Warren et al., 2010). Highly correlated pairs of environmental predictors (Spearman rank $R > 0.9$ or $R < -0.9$) were identified and the predictor that was highly correlated with the most other predictors was excluded. After this process, 39 environmental predictors were retained for use in the predictive models.

Statistical modeling framework

Overview

For DSC groups with a sufficient number (>50) of model grid cells containing presence records, spatial predictive modeling was conducted to identify areas around the MHI most likely to contain suitable DSC habitat. A Maximum Entropy (MaxEnt; Philips et al., 2004, 2006) modeling framework (Figure 3.22) was used to relate DSC presence data to a range of spatial environmental predictor datasets. The estimated relationships between DSC presence and the environmental predictors were then used to predict the relative likelihood of suitable DSC habitat across the entire study area (Phillips et al., 2004, 2006; Phillips and Dudik, 2008).

The objectives of this approach were to develop models with high predictive performance (i.e., in terms of model fit and stability) and to produce maps of predicted DSC habitat suitability likelihood with corresponding maps of prediction variability. Spatial predictions were generated at moderate resolution (360 m grid) because of the positional uncertainty associated with the presence records (±1 km or more) and the NOAA Coastal Relief Model (NOAA NCEI, 2005) and General Bathymetric Chart of the Oceans (GEBCO; GEBCO, 2008) bathymetry data used to generate the 90 m resolution depth dataset (see Chapter 2) that was used to derive many of the topographic variables. Therefore, maps depict moderate-scale information that can be used to identify areas more likely to contain suitable DSC habitat and to assess confidence in the predictions at these areas. The maps do not, however, indicate the abundance of DSC. Further, discussion on the limitations of the models can be found in the Data and Information Gaps section below.

MaxEnt is a machine learning algorithm first applied to species distribution modeling by Phillips et al. (2004, 2006). In simple terms, MaxEnt estimates functional relationships between habitat suitability and the environment predictor variables constrained by the mean value of the environmental predictors at observed presence locations. It then uses these relationships to estimate the relative likelihood of suitable habitat at each model grid cell.

Although modeling methods using presence-absence or abundance data, such as boosted regression trees (BRTs), would be preferred (and would allow predicted habitat suitability to be interpreted as a probability), DSC absence data was limited and potentially unreliable. Spatial predictive modeling of DSC habitat suitability

Step 1. Data preparation

DSC presence data

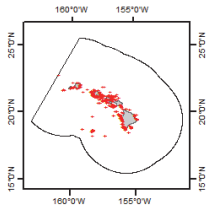

Match data by location

+

Environmental predictor grids

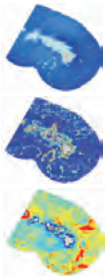

Depth

Slope of Slope

Bottom Current Speed

etc.

→ Combined data

Step 2. Model fitting

Combined data → Create 10 random subsets (70% training/30% test) → Model fitting → Multiple models

Step 3. Model selection

Multiple models → Calculate test AUC, AICc → Rank models by highest test AUC & lowest AICc → Best model (best overall rank)

Drop least important predictor, repeat model fitting

Step 4. Prediction across space

Best model functional relationships

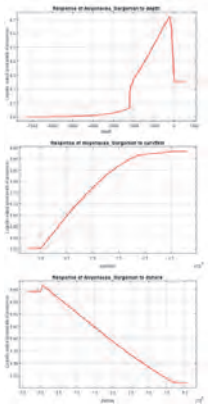

+

Environmental predictor grids

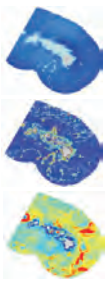

Depth

Slope of Slope

Bottom Current Speed

etc.

→ Prediction

Predicted likelihood of suitable habitat (logistic output)

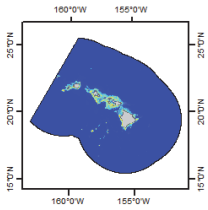

→ Classification applied

Predicted habitat suitability likelihood classes

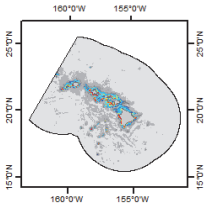

Predicted habitat suitability uncertainty

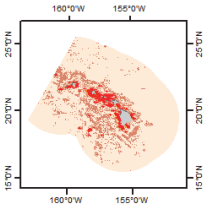

Step 5. Model performance

Predicted habitat suitability likelihood classes

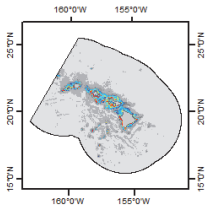

+

Prediction variability

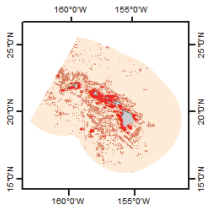

+

DSC presence data

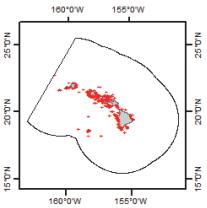

→ Performance metrics

Model performance badge

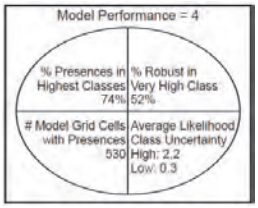

Figure 3.22. MaxEnt modeling approach used to create spatial predictions of DSC habitat suitability, including data preparation, model fitting, model selection, prediction across space and evaluation of model performance.

was therefore restricted to presence-only methods. Among these methods, MaxEnt has been shown to perform best for predicting habitat suitability, including for DSC (Tittensor et al., 2009; Davies and Guinotte, 2011; Yesson et al., 2012; Vierod et al., 2013; Guinotte and Davies, 2014).

Data preparation

Predictor data values at the DSC presence locations were extracted from the environmental predictor dataset grids. This was performed internally during model fitting by the MaxEnt Java software (version 3.3.3k, available at http://www.cs.princeton.edu/~schapire/maxent/; Phillips et al., 2004, 2006).

Model fitting

Models were fit independently for each of the selected coral groups (Table 3.6). In each model run, 10 fitting models were generated by randomly dividing the DSC presence records into 10 subsets of 70 percent of the data to use for model training and 30 percent of the data to use for model testing. Model training and testing were done in the MaxEnt Java software (Phillips et al., 2004, 2006). MaxEnt models were fit for each of the model training subsets. Model predictive performance was measured for each of the fitted models by testing predictions at the locations of the model testing subsets. One of the model performance metrics generated by MaxEnt, area under the receiver operating characteristic curve (AUC; Fielding and Bell, 1997), indicates how well a model predicts coral presences at the test locations compared to a random selection of locations (termed the background points in MaxEnt). The mean test AUC was calculated for the 10 fitted models (Phillips et al., 2006; Elith et al., 2011). Model predictive performance was also measured using Akaike's information criterion (AICc) corrected for small sample size (Akaike, 1974; Burnham and Andersion, 2002), which provides a measure of both how well a model fits the data and how complex the model is. AICc was calculated for the 10 fitted models using the ENMTools software (Warren et al., 2010).

Model selection

Since the ability of models to predict habitat suitability or to resolve the relationships between environmental predictors and habitat suitability can be reduced when models are overly complex or overly simple (Yost et al., 2008; Warren and Seifort, 2011), a stepwise model selection procedure (NOAA NCCOS, 2015) was used to choose a model that balanced model predictive performance with model complexity. First, an initial model run was generated using the full set of 39 environmental predictors as described above. At each iteration of the stepwise procedure, a single environmental predictor was removed from the set and a new model run was generated using the updated set of environmental predictors. The environmental predictor to be removed was identified as the most redundant environmental predictor remaining (i.e., the predictor whose omission from model fitting resulted in the smallest reduction in model performance [mean test AUC]). The stepwise procedure was repeated until the final model run, with a single remaining environmental predictor. The model runs were then ranked from best to worst by model performance (highest to lowest mean test AUC) and by model complexity (lowest to highest AICc). These two ranks were averaged, and the model run with the best average rank was selected as the best model.

Prediction across space

For each DSC group, a final MaxEnt model was fit using the entire set of coral presence records (rather than a 70/30 split) and the set of environmental predictors in the best model. Each final model generated spatially explicit predictions across the study area representing the relative likelihood a given model grid cell will contain suitable DSC habitat. These predictions are on a logistic scale that ranges from 0 to 1 (0 being relatively less suitable habitat and 1 being more). While the logistic output is related to the likelihood of habitat suitability, it is not a probability since the prevalence (i.e., presence/absence ratio) of a species or group is not known (Elith et al., 2011). In generating the logistic output, MaxEnt assumes that the global prevalence of the taxon being modeled is known *a priori* and is exactly equal to 0.5 (this is the default value in the software). Model

predictions on the MaxEnt logistic scale can be treated as probabilities and can be compared across multiple models for different taxa if this assumption holds (in practice, impossible) or if the empirical prevalence can be calculated from presence and absence data and used in place of the default value of 0.5.

To generate model predictions in a format that could be directly compared across groups, the logistic outputs were converted into classified habitat suitability likelihood classes, ranging from very low likelihood to very high likelihood. In this approach, breakpoints in the logistic output were identified independently for each DSC group using predictions made at the model test data locations and at the randomly selected background locations for each of the 10 fitted models in the best model run. For a given breakpoint, or threshold, in the logistic output scale, predictions can be classified as either suitable or unsuitable habitat. For a range of potential threshold values, predictions made at the model test locations were used to calculate the fraction of presences correctly classified as suitable habitat (i.e., sensitivity, or the true positive rate) and predictions made at the background locations were used to calculate the fraction of absences correctly classified as unsuitable habitat (i.e., specificity, where 1 - specificity is the false positive rate). It is important to note that since MaxEnt is a presence-only modeling approach, the background locations randomly selected from across the model domain were essentially used as pseudo-absences (Phillips et al., 2006). True positive rates were plotted against false positive rates to generate a receiver operating characteristic (ROC) curve (Fielding and Bell, 1997; Phillips et al., 2006). Choosing an optimal threshold in the MaxEnt logistic output that is appropriate for classifying suitable versus unsuitable habitat can be problematic because prevalence is typically unknown (Merow et al., 2013). Therefore, rather than selecting a single optimal threshold, a series of optimal threshold values were calculated from the ROC curve, each corresponding to a specific ratio of the cost for false positive errors versus the cost for false negative errors (e.g., for a 2:1 ratio, false positives are twice as costly as false negatives). By weighting false positive errors (i.e., predicting suitable habitat in locations that contain unsuitable habitat) as more costly, higher cost ratios result in thresholds that yield more conservative predictions of suitable habitat. The series of thresholds was generated for each of the 10 fitted models and average threshold values were calculated for each cost ratio. The average values were then used as breakpoints to reclassify the logistic output into habitat suitability likelihood classes. The 'ROCR' package in R was used to generate ROC curves and calculate optimal thresholds for the specified cost ratios (Sing et al., 2005). In addition, locations predicted to be in the very high habitat suitability likelihood class for all 10 fitted models from the best model run were classified as robust very high habitat suitability likelihood.

For each DSC group, map pages were generated to depict the coral presence data, the classified predicted habitat suitability likelihood, and the variability in predicted habitat suitability likelihood. Variability was calculated as the difference in predicted habitat suitability likelihood classes assigned to the upper limit and lower limit of the 95 percent confidence interval of the 10 fitted model predictions from the best model run. Within the map pages, inset panels depict individual islands or island groups. Note that due to the resolution of the model, fine-scale features may be difficult to discern even in the map insets; however, these features can be seen easily in the data products provided in the Geodatabase associated with this chapter.

Model performance

Model performance was evaluated using a set of performance metrics (Table 3.10). The "Percent Presences in Highest Classes" metric indicates the percentage of model grid cells containing presence locations that were predicted by the final model to be in the five highest habitat suitability likelihood classes. This metric provides a measure of model fit, as it reflects how well the model matches the data used to fit it. The "Percent Robust in Very High Class" metric indicates the percentage of model grid cells predicted by the final model to be in the very high habitat suitability likelihood class that were also classified in the very high habitat suitability likelihood class for each of the 10 fitted models comprising the best model run. This metric provides a measure of model stability and reflects how sensitive the model is to variation in the locations of the presence data (since each of

the 10 fitted models is generated with a subset of the presence data). For models with relatively higher values for this metric, there is greater confidence in areas predicted to have very high habitat suitability likelihood. The "# Model Grid Cells with Presences" metric indicates the number of model grid cells containing presence data. This is included because MaxEnt model performance generally degrades with decreasing number of observations. The "Average Likelihood Class Uncertainty" metric indicates variability in habitat suitability class predictions. It was calculated as the difference in predicted habitat suitability likelihood classes assigned to the upper limit and lower limit of 95 percent confidence interval of the 10 fitted model predictions from the best model run. Because a large percentage of the study area was generally predicted to have low to very low habitat suitability likelihood (unsurprisingly, as many DSC are rare), this metric was calculated separately for the 10 lowest likelihood classes and the 5 highest likelihood classes to distinguish between prediction variability in the large extent of the study area where DSCs are generally not found, and the more restricted areas where habitat suitability for DSCs are relatively higher.

Qualitative performance categories were defined for each performance metric (Table 3.10). The performance of the final model for each DSC group was assigned an overall model performance score equal to the average score across the four performance metrics. For the "Average Likelihood Class Uncertainty" metric, the metric score was defined as the average of the score for the lowest likelihood classes and the highest likelihood classes. Model performance is displayed on each map figure using a "badge." It is important to recognize that the model performance metrics and badge only reflect the statistical fit of the model to the data. They do not reflect the data quality or the quality of model predictions away from the coral presence records. These issues will be discussed further in the Data and Information Gaps section below.

In addition to the metrics used to quantify overall model performance, test AUC and test gain, which measures how well the model discriminates suitable habitat from background, were calculated for each final model. However, test AUC and test gain for different DSC groups are not directly comparable. These metrics are not included here to focus instead on model performance metrics that are comparable across DSC groups.

Table 3.10. Model performance metrics.

Name	Description	Stage	Quality Scores
Percent Presences in Highest Classes	Percentage of grid cells (with presence data) predicted to be in highest likelihood classes	Final model	5: >85% 4: 75–85% 3: 60–75% 2: 40–60% 1: <40%
Percent Robust in Very High Class	Percentage of grid cells predicted to be in the very highest likelihood class for all model runs	Model selection	5: > 55% 4: 45–55% 3: 35–45% 2: 25–35% 1: < 25%
# Model Grid Cells with Presences	Number of model grid cells containing presence data	Data preparation	5: >300 4: 150–300 3: 100–150 2: 50–100 1: <50
Average Likelihood Class Uncertainty	Average difference in likelihood classes (at 95% CI level) for all model runs	Model selection	5: <1 4: 1–1.5 3: 1.5–2 2: 2–3 1: >3

Variable importance

While the primary objective was not to determine the ecological drivers and mechanisms behind the spatial distributions of DSC habitat suitability, MaxEnt did provide multiple measures of the relative importance of the environmental predictor variables (Phillips et al., 2004, 2006). To measure permutation importance, for each environmental predictor variable the values at the model training data locations and background locations were randomly scrambled and model performance (in this case AUC on the training data) was re-evaluated. The resulting decline in model performance was used to identify the relative importance of the variable to the model. A higher permutation importance value indicated that the model depended more heavily on the variable. In the jackknife tests of variable importance, for each environmental predictor variable models were re-fit first using only the single variable and then omitting the variable while using all the other variables. For

both jackknife tests model performance was evaluated by calculating AUC on the test data and comparing the values to test AUC calculated for the final model. A relatively high test AUC value in the jackknife single variable test indicated that the information contained in the variable was important by itself for explaining DSC habitat suitability. A relatively low test AUC value in the jackknife omission test indicated that the variable contained information useful for explaining DSC habitat suitability that was not contained in the other environmental predictors (Phillips et al., 2004, 2006). The most consistently important environmental predictor variables were determined by identifying how often each variable occurred in the top three values for each variable importance test across the DSC groups.

The relative importance of the environmental predictor variables across the DSC groups was compared using bubble plots. In addition, response curves were generated to depict the individual effect of each predictor variable on habitat suitability for a given model (Phillips et al., 2004). However, these numerous plots were not included here due to space limitations and because they were beyond the primary objective of spatial prediction.

3.4.2. Results and Discussion

Spatial Distributions and Model Performance

The distributions of DSC presence records varied among groups, however, records were often concentrated in particular locations, such as Cross Seamount, Makapu'u Point (O'ahu), Makalawena Bank (Hawai'i), Lō'ihi Seamount (Hawai'i), and the southern edge of Penguin Bank (Maui Nui). Predicted spatial distributions of areas likely to contain suitable DSC habitat broadly aligned with the distributions of DSC presence records. However, in some cases areas outside the extent of the DSC presence records were predicted as highly likely to contain suitable habitat although they seem unlikely to support corals. This will be discussed further in the Data and Information Gaps section below.

Gold corals (*Kulamanamana haumeaae*)

Areas with robust predictions of highest likelihood of habitat suitability for gold corals included the Puna and Hilo Ridges east of Hawai'i, Makalawena Bank, Cross Seamount, and portions of the eastern and southern banks of Maui, O'ahu, and Kaua'i (Figure 3.23). Additional areas with robust predictions of highly likely suitable habitat were located around Ni'ihau, Ka'ula and Middle Bank, where no presence records of gold corals existed. Generally, areas of robust high likelihood of habitat suitability had correspondingly lower prediction variability.

*Gold coral (*Kulamanamana haumeaae*). Photo credit: NOAA Office of Ocean Exploration and Research, 2015 Hohonu Moana*

The percentage of gold coral presences occurring in model grid cells predicted to have the highest likelihood of habitat suitability was among the highest across all DSC models, indicating a relatively good model fit. In addition, the percentage of model grid cells predicted to have the highest likelihood of habitat suitability that were also considered robust was relatively high. However, since gold coral presence records were relatively rare, occurring in only 84 model grid cells, some caution should be exercised in using model predictions outside the extent of gold coral presence records.

Seventeen predictor variables were included in the final model for gold corals, with depth the most important predictor, followed by slope at 5 km scale and total curvature at 5 km scale (Figures 3.24–3.26). It is important to note that Hawaiian gold coral is a parasitic zooanthid that colonizes other coral fans, particularly bamboo corals (Sinniger et al., 2013; Parrish, 2015); hence, distributions of gold corals may be driven by distributions of bamboo corals rather than specific environmental variables.

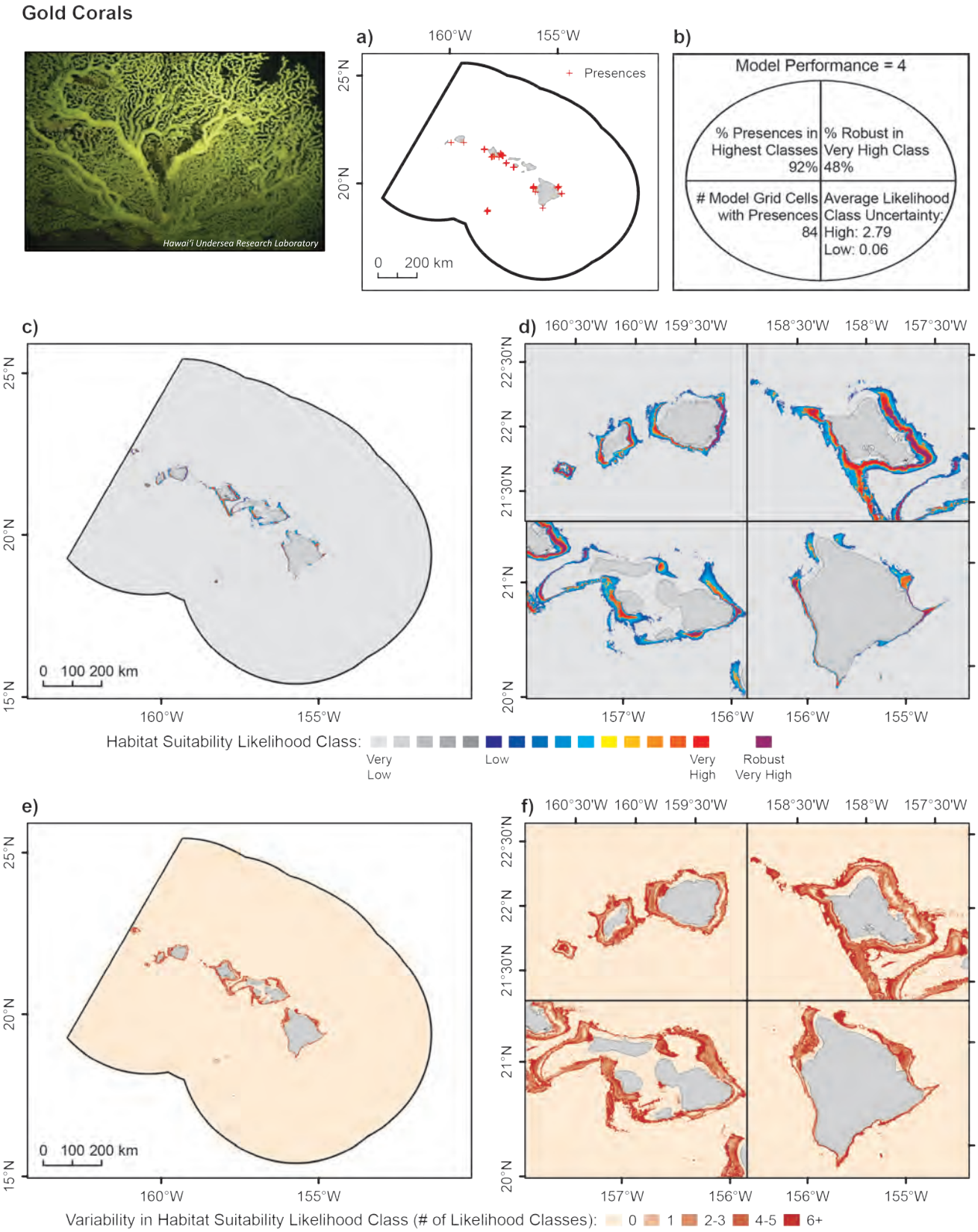

*Figure 3.23. Predicted likelihood of habitat suitability for gold corals (*Kulamanamana haumeaae*) in the MHI. Predictive modeling was applied to coral presence data from 1891-2009 provided by NOAA's Deep-Sea Coral Research and Technology Program (DSCRTP) and HURL. a) Locations of gold coral presences reported in the study area (N=101, depth range: 109-1,489 m). b) Model performance as determined as a function of four performance metrics. c,d) Habitat suitability likelihood classes derived from a categorical reclassification of the MaxEnt logistic output. Robust high likelihood areas represent locations that are always predicted to have the highest likelihood of habitat suitability for all bootstrap model runs with random sub-samples of the data. e,f) Variability in habitat suitability predictions, depicted as the difference in habitat suitability likelihood classes assigned to the bootstrap 95 percent confidence interval upper and lower limits. Photo credit: Hawai'i Undersea Research Laboratory*

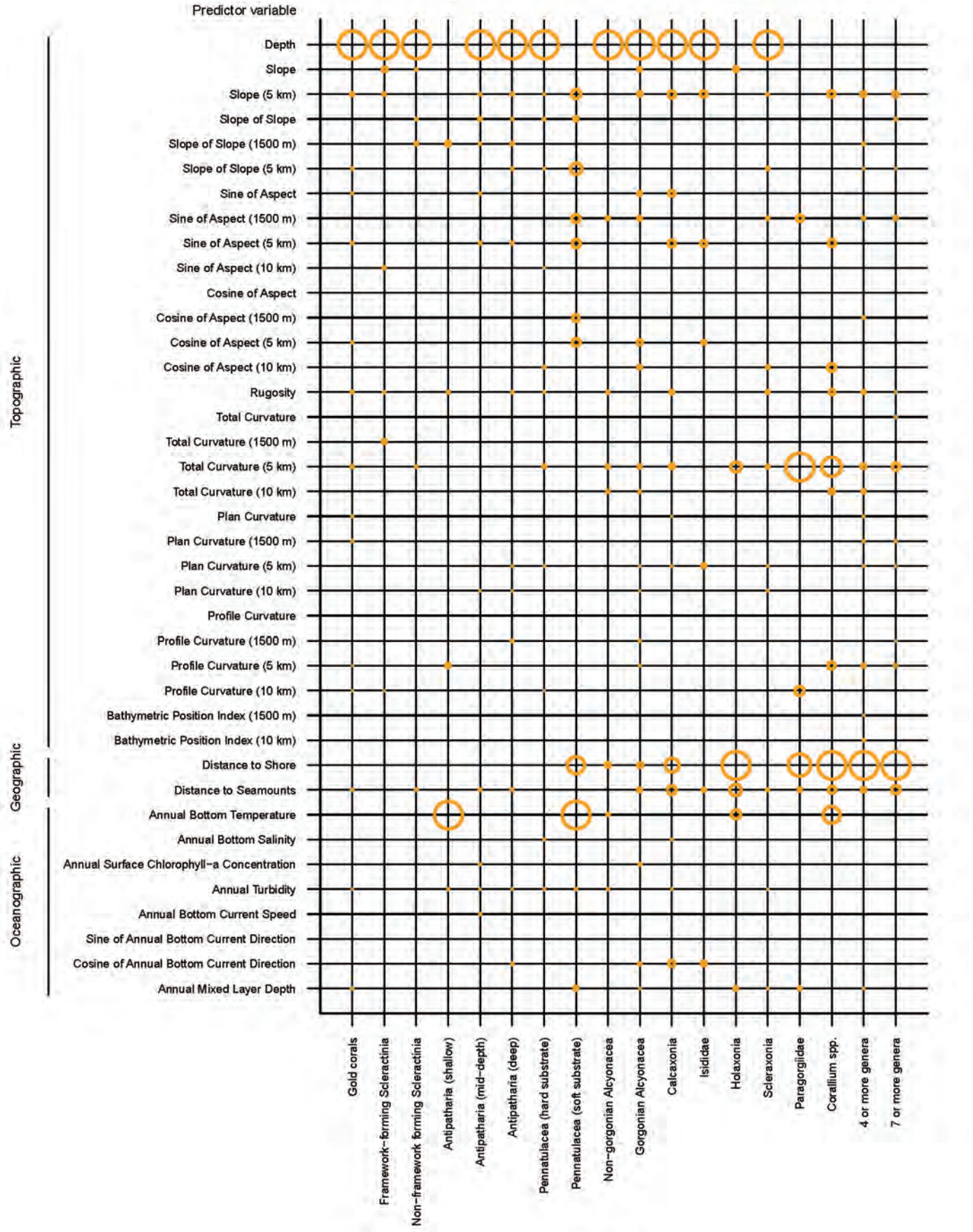

Figure 3.24. Predictor variable importance for each DSC model. The area of a circle is proportional to the permutation importance of the predictor variable in the final model. Larger circles indicate that the model depended more heavily on the variable. For example, the gold coral model depended more on depth than any other variable.

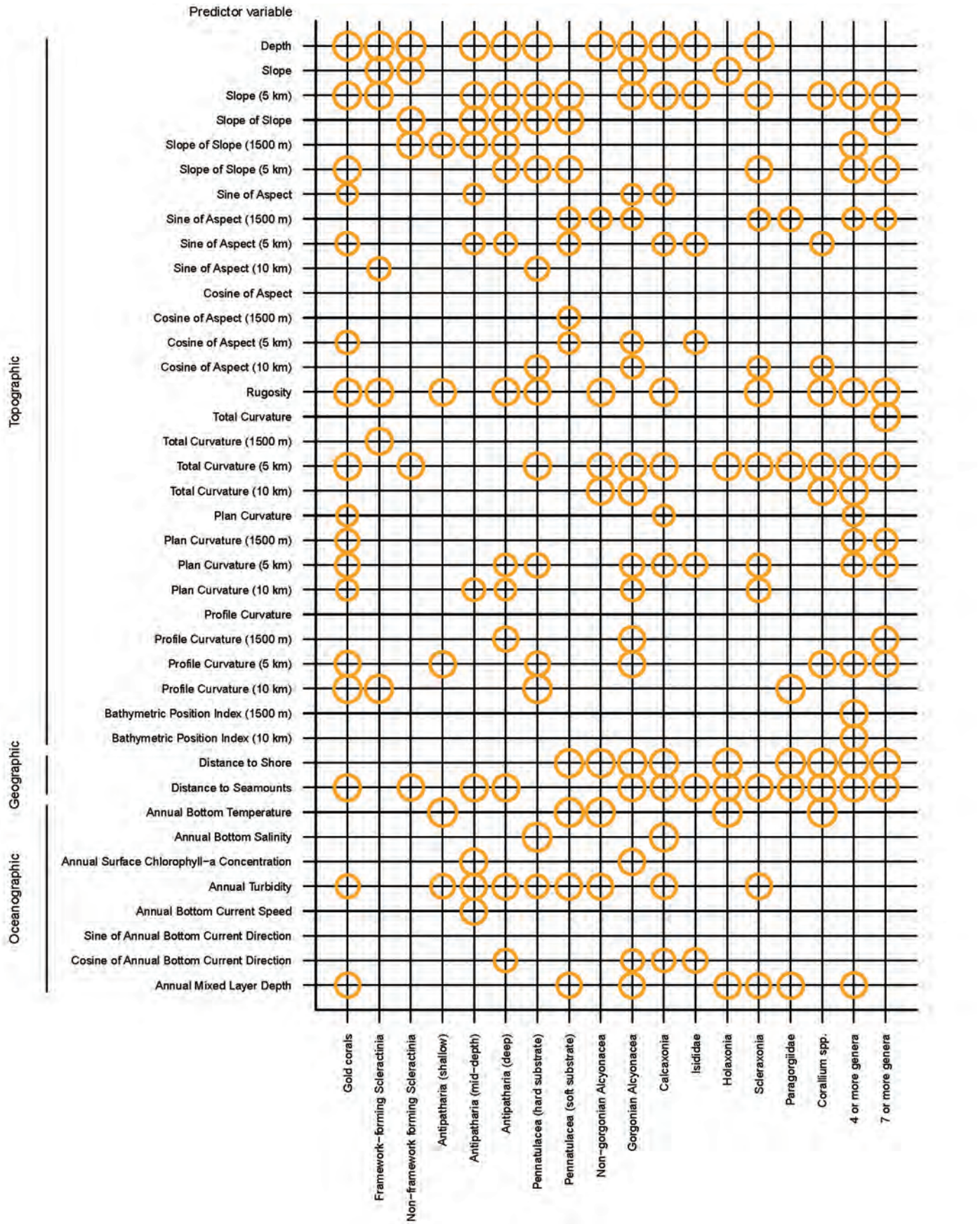

Figure 3.25. Predictor variable importance for each DSC model. The area of a circle is proportional to the test area under the receiver operator characteristic curve (AUC) for models built with only the predictor variable. Larger circles indicate that the variable by itself was more important for explaining habitat suitability. For example, depth alone was more important for explaining gold coral habitat suitability than the plan curvature variables.

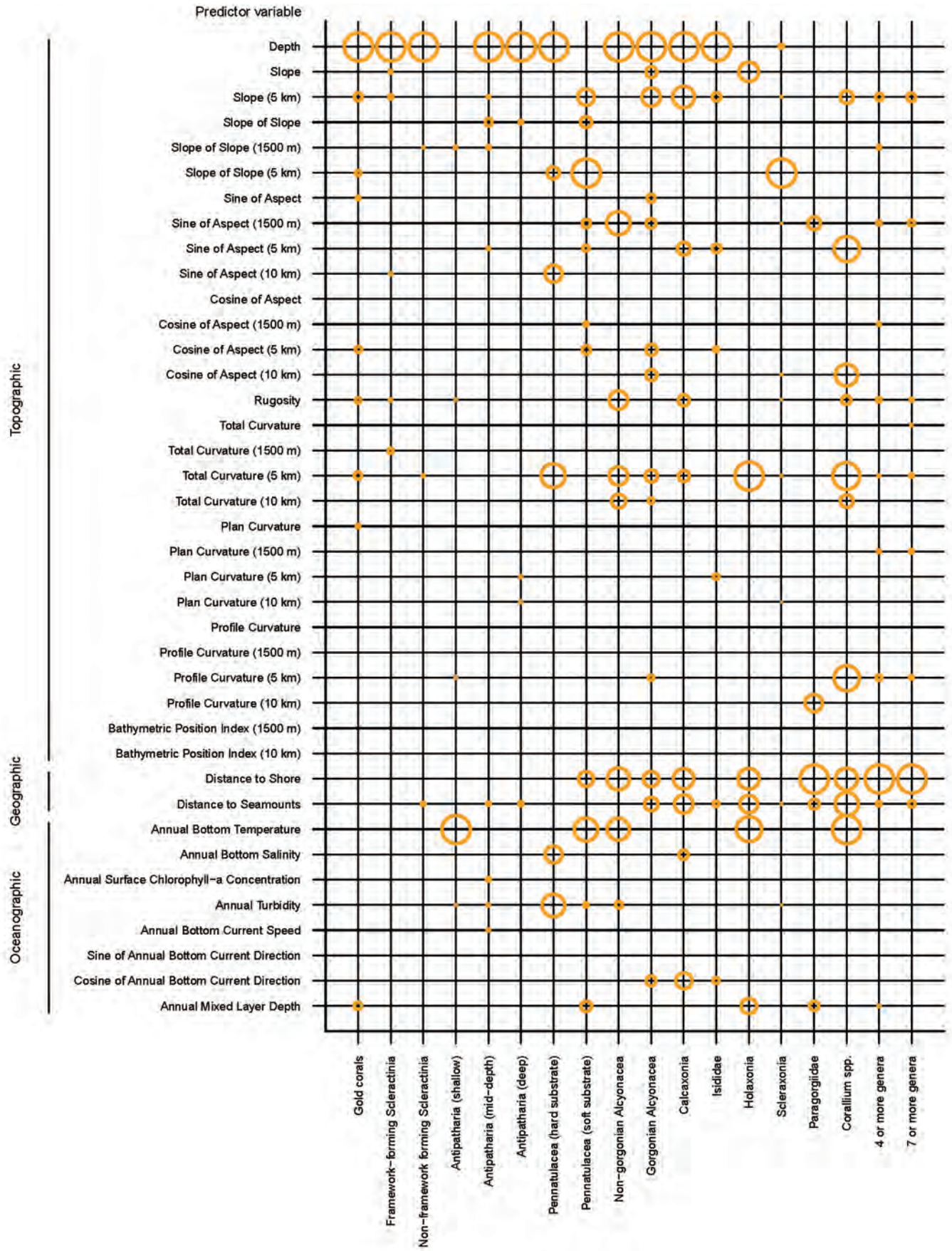

Figure 3.26. Predictor variable importance for each DSC model. The area of a circle is proportional to the reduction in test AUC for models built with all other predictor variables. Larger circles indicate that removing the variable will result in a greater reduction in model performance. For example, removing depth from the gold coral model would reduce model performance more than removing any other variable.

Benthic Habitats and Corals

Framework-forming Scleractinia

Areas with robust predictions of very high likelihood of habitat suitability for framework-forming scleractinians included a thin band around Ka‘ula, Ni‘ihau and all but the north shore of O‘ahu (Figure 3.27). Within the Maui Nui complex, areas with robust predictions of high likelihood of habitat suitability included north of Moloka‘i, south of Maui and Kaho‘olawe, and the edges of Penguin Bank. Around Hawai‘i, areas of high likelihood of habitat suitability included offshore of Kawaihae Bay, the Kona Coast and northern portion of the Ka Lae Ridge, with lower likelihood of habitat suitability on much of the eastern coast. Further offshore, Cross and McCall Seamounts also included areas of high likelihood of habitat suitability. Areas of highest prediction variability included portions of the ‘Au‘au Channel, south of O‘ahu and north of Maui.

Framework-forming Scleractinian Enallopsammia rostrata. *Photo credit: Hawai‘i Undersea Research Laboratory*

A relatively high percentage of framework-forming Scleractinia presences occurred in model grid cells predicted to have the highest likelihood of habitat suitability. In addition, the percentage of model grid cells predicted to have the highest likelihood of habitat suitability that were also considered robust was among the highest across all DSC models. However, some caution should be exercised in using model predictions outside the extent of framework-forming Scleractinia presence records because of the relatively low number of model grid cells with framework-forming Scleractinia presences.

Seven predictor variables were included in the final model for framework-forming Scleractinians, with depth, slope, and total curvature at 1,500 m scale the most important predictors (Figures 3.24–3.26).

Non-framework forming Scleractinia

Areas with robust predictions of very high likelihood of habitat suitability for non-framework-forming Scleractinians were present around all of the islands (Figure 3.28), including areas where a high concentration of presences were recorded (e.g., southern edge of Penguin Bank, offshore of Kona Coast) and where presence records were sparse or largely absent (e.g., southeast of Maui, north of Moloka‘i). Areas of higher prediction variability included the shallow, nearshore environment, and deeper depths seaward of the areas with the highest relative suitability.

The percentage of non-framework-forming Scleractinia presences occurring in model grid cells predicted to have the highest likelihood of habitat suitability was among the highest across all DSC models, indicating a relatively good model fit. In addition, the percentage of model grid cells predicted to have the highest likelihood of habitat suitability that were also considered robust was relatively high. Compared to many of the other DSC groups, there was a relatively high number of model grid cells with presence records, particularly offshore of the Kona Coast, the Maui Nui complex and around O‘ahu (Figure 3.28).

Non-framework forming Scleractinian Polymyces wellsi. *Photo credit: Hawai‘i Undersea Research Laboratory*

Six predictor variables were included in the final model for non-framework-forming Scleractinia. Depth, slope of slope at the 1,500 m scale, and distance to seamounts were the most important predictors (Figures 3.24–3.26).

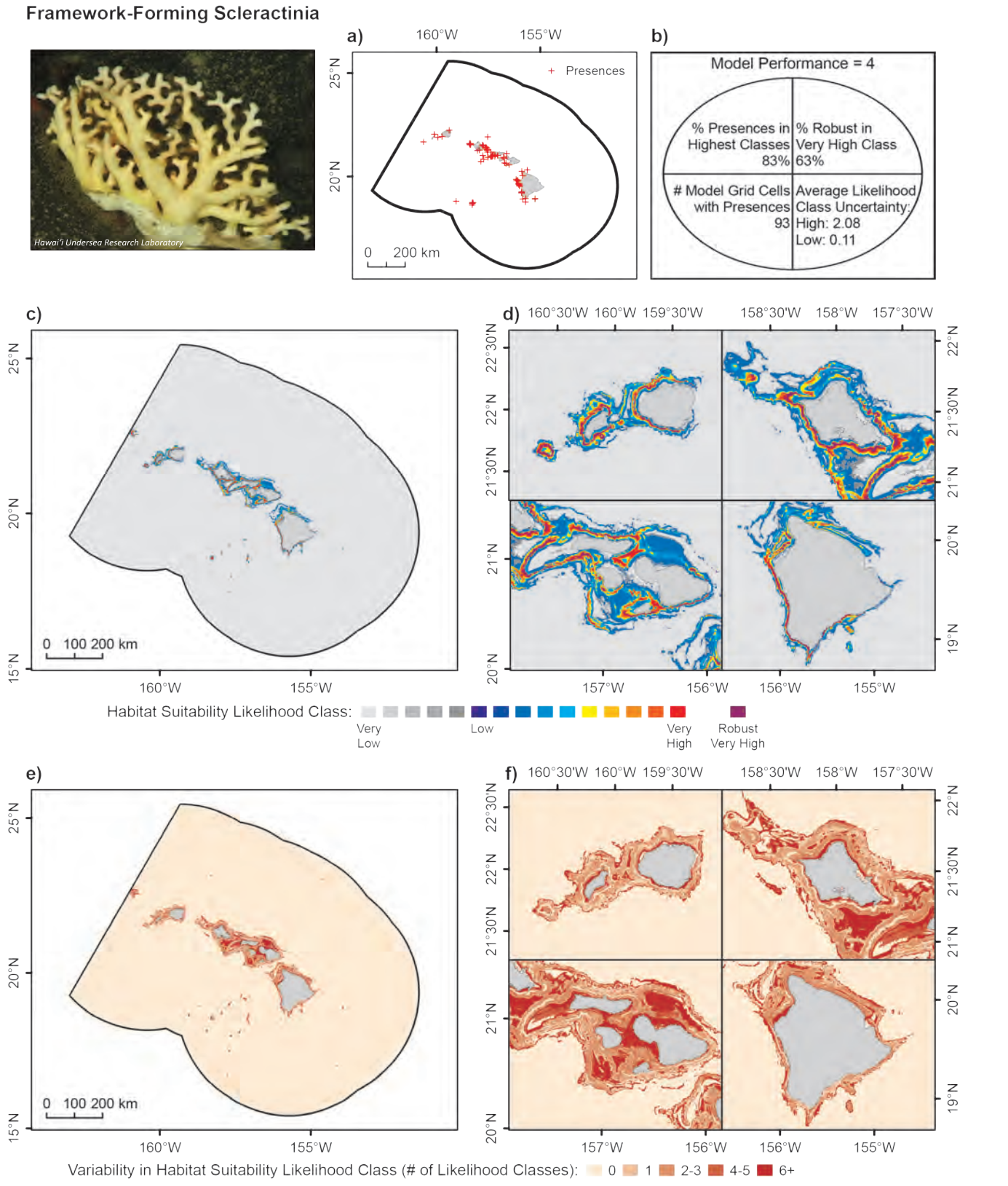

Figure 3.27. Predicted likelihood of habitat suitability for framework-forming Scleractinia (hard corals) in the MHI. Framework-forming Scleractinia includes Enallopsammia rostrata, Madracis kauaiensis, Madrepora oculata *and Scleractinia "bramble". Predictive modeling was applied to coral presence data from 1891-2009 provided by NOAA DSCRTP and HURL. a) Locations of framework-forming Scleractinia presences reported in the study area (N=104, depth range: 36-4,131 m). b) Model performance as determined as a function of four performance metrics. c,d) Habitat suitability likelihood classes derived from a categorical reclassification of the MaxEnt logistic output. Robust high likelihood areas represent locations that are always predicted to have the highest likelihood of habitat suitability for all bootstrap model runs with random sub-samples of the data. e,f) Variability in habitat suitability predictions, depicted as the difference in habitat suitability likelihood classes assigned to the bootstrap 95 percent confidence interval upper and lower limits. Photo credit: Hawai'i Undersea Research Laboratory*

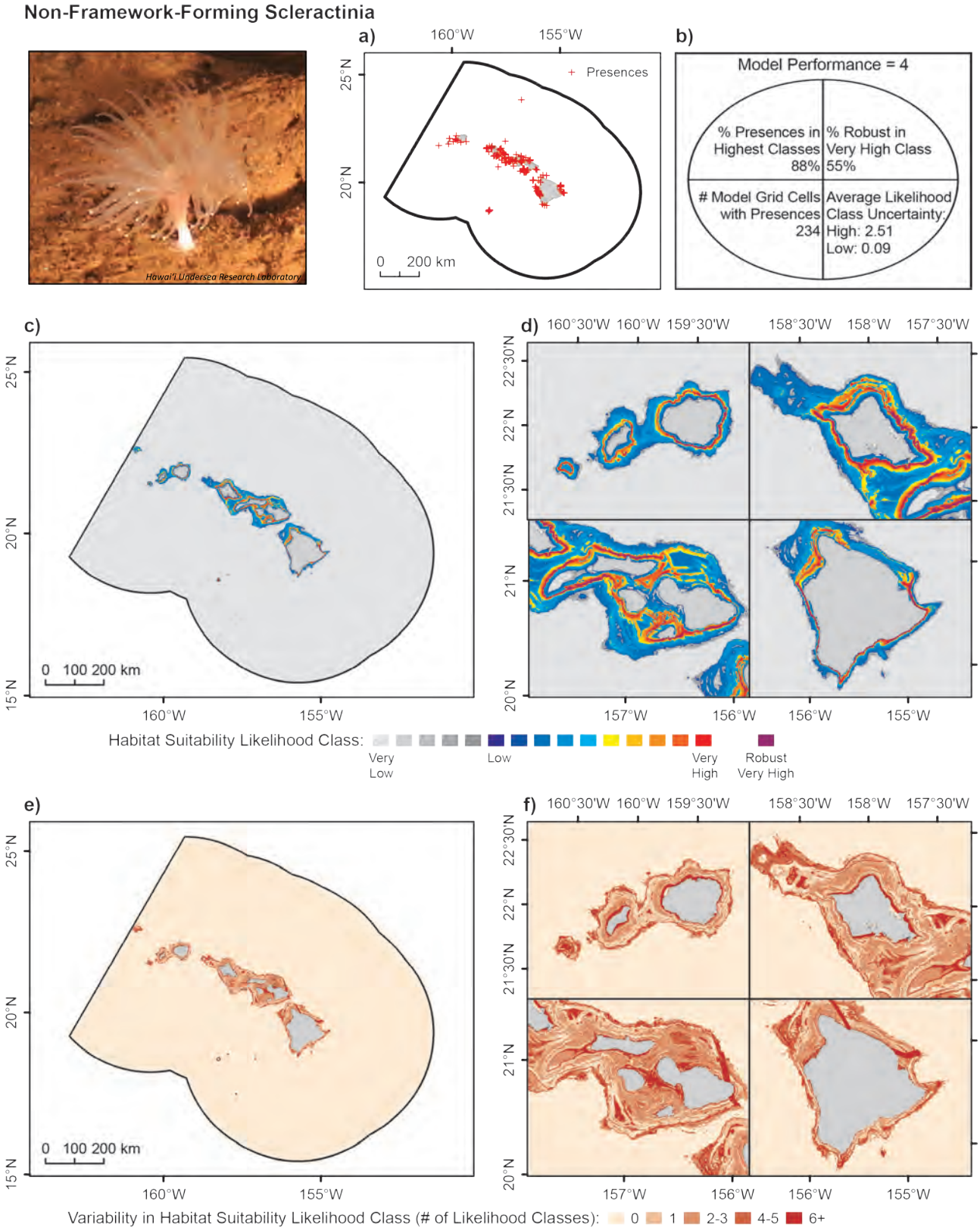

Figure 3.28. Predicted likelihood of habitat suitability for non-framework-forming Scleractinia (hard corals) in the MHI. Non-framework-forming Scleractinia includes all other genera not included in the framework-forming Scleractinia group. Predictive modeling was applied to coral presence data from 1891-2009 provided by NOAA DSCRTP and HURL. a) Locations of non-framework-forming Scleractinia presences reported in the study area (N=340, depth range: 22-4,375 m). b) Model performance as determined as a function of four performance metrics. c,d) Habitat suitability likelihood classes derived from a categorical reclassification of the MaxEnt logistic output. Robust high likelihood areas represent locations that are always predicted to have the highest likelihood of habitat suitability for all bootstrap model runs with random sub-samples of the data. e,f) Variability in habitat suitability predictions, depicted as the difference in habitat suitability likelihood classes assigned to the bootstrap 95 percent confidence interval upper and lower limits. Photo credit: Hawai'i Undersea Research Laboratory

Antipatharia, shallow depth genera (30–100 m)

The largest areas of robust predictions of very high likelihood of habitat suitability for shallow Antipatharians, which included *Antipathes* and *Cirrhipathes* species, were concentrated around the Maui Nui complex (Figure 3.29), including the ʻAuʻau Channel, where a large proportion of the presence records were located. In contrast, other areas of robust predictions of very high likelihood of habitat suitability included Maʻalaea Bay, north of Maui near Paʻuwela Point, and portions of the shelf adjacent to the east and west sides of Molokaʻi, and where there were no existing presence records.

Shallow Antipatharian species, Antipathes grandis. *Photo credit: Hawaiʻi Undersea Research Laboratory*

The percentage of shallow Antipatharia presences occurring in model grid cells predicted to have the highest likelihood of habitat suitability was relatively high, and the percentage of model grid cells predicted to have the highest likelihood of habitat suitability that were also considered robust was the highest across all DSC models. This indicates a model with a relatively good fit that is also stable to variability in the locations of presence records. While the number of model grid cells with presence records was relatively low compared to the other Antipatharia groups, this did not appear to hinder model performance.

Five predictor variables were included in the final model for shallow Antipatharians, with annual bottom temperature, profile curvature at 5 km scale, and slope of slope at 1,500 m scale the most important predictors (Figures 3.24–3.26). Although depth was not included in the final model, areas of high likelihood of habitat suitability generally occurred in shallow locations where bottom temperatures were warmest.

Antipatharia, mid-depth genera (100–300 m)

Areas of robust predictions of very high likelihood of habitat suitability for mid-depth Antipatharians, which included *Acanthopathes*, *Antipathella*, *Myriopathes* and *Stichopathes* species, often coincided with locations of known coral presence and included offshore of the Kona Coast and Cape Kumakahi near Hawaiʻi (Figure 3.30). Additional areas were found within the Maui Nui complex, such as south and east of Kahoʻolawe, Pailolo Channel between Maui and Molokaʻi, and the canyons to the north of Molokaʻi. Farther to the west, pockets of robust predictions of high likelihood of suitability included the edges of Penguin Bank and Makapuʻu Point/southeast Oʻahu.

Myriopathes ulex. *Photo credit: Hawaiʻi Undersea Research Laboratory*

Both the percentage of mid-depth Antipatharia presences occurring in model grid cells predicted to have the highest likelihood of habitat suitability and the percentage of model grid cells predicted to have the highest likelihood of habitat suitability that were also considered robust were relatively high. In addition, there were a relatively large number of model grid cells with presence records.

Eleven predictor variables were included in the final model for mid-depth Antipatharians. Depth, slope of slope, and slope at 5 km scale were the most important predictors (Figures 3.24–3.26).

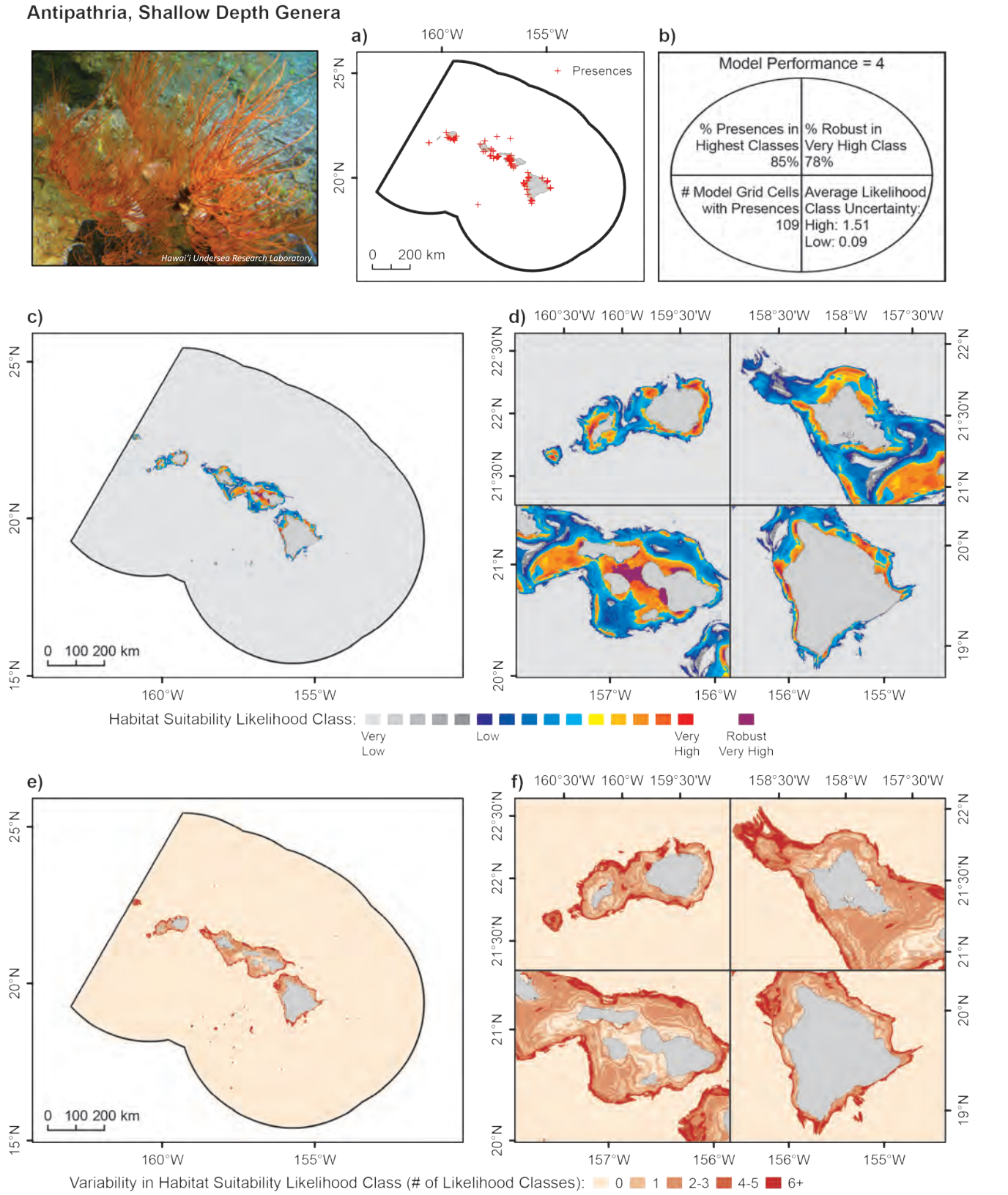

Figure 3.29. Predicted likelihood of habitat suitability for shallow Antipatharia (black coral) genera in the MHI. Shallow Antipatharia genera tend to occur in water depths of 30-100 m and include Antipathes *and* Cirrhipathes *species. Predictive modeling was applied to coral presence data from 1891-2009 provided by NOAA DSCRTP and HURL. a) Locations of shallow Antipatharia presences reported in the study area (N=168, depth range: 17-4,787 m). b) Model performance as determined as a function of four performance metrics. c,d) Habitat suitability likelihood classes derived from a categorical reclassification of the MaxEnt logistic output. Robust high likelihood areas represent locations that are always predicted to have the highest likelihood of habitat suitability for all bootstrap model runs with random sub-samples of the data. e,f) Variability in habitat suitability predictions, depicted as the difference in habitat suitability likelihood classes assigned to the bootstrap 95 percent confidence interval upper and lower limits. Photo credit: Hawai'i Undersea Research Laboratory*

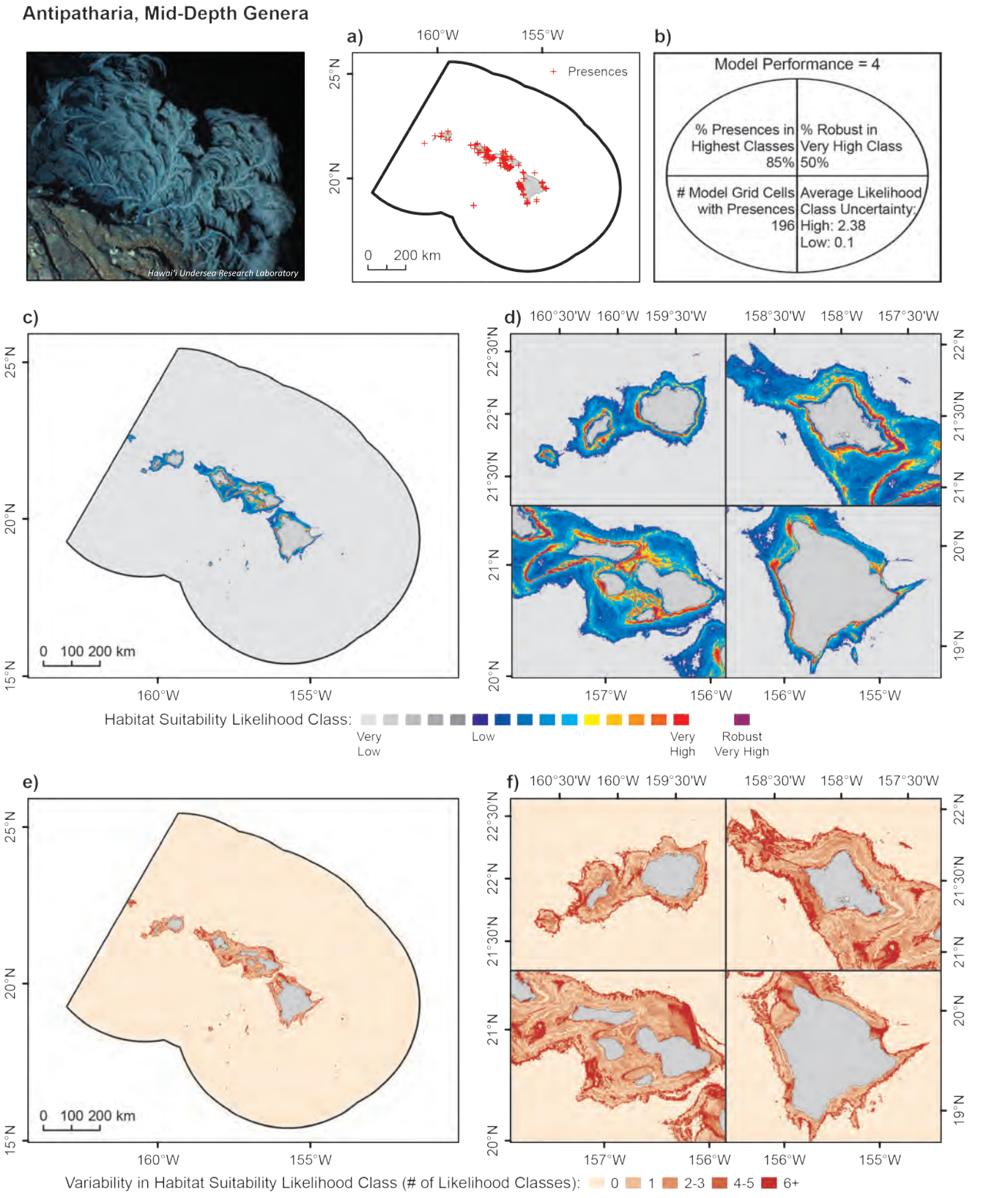

Figure 3.30. Predicted likelihood of habitat suitability for mid-depth Antipatharia (black coral) genera in the MHI. Mid-depth Antipatharia genera tend to occur in water depths of 100-300 m and include Acanthopathes, Antipathella, Myriopathes, *and* Stichopathes *species. Predictive modeling was applied to coral presence data from 1891-2009 provided by NOAA DSCRTP and HURL. a) Locations of mid-depth Antipatharia presences reported in the study area (N=217, depth range: 18-1,941 m). b) Model performance as determined as a function of four performance metrics. c,d) Habitat suitability likelihood classes derived from a categorical reclassification of the MaxEnt logistic output. Robust high likelihood areas represent locations that are always predicted to have the highest likelihood of habitat suitability for all bootstrap model runs with random sub-samples of the data. e,f) Variability in habitat suitability predictions, depicted as the difference in habitat suitability likelihood classes assigned to the bootstrap 95 percent confidence interval upper and lower limits. Photo credit: Hawai'i Undersea Research Laboratory*

Benthic Habitats and Corals

Antipatharia, deep genera (>300 m)

Areas of robust predictions of very high likelihood of habitat suitability for deep Antipatharians, which included species in the genera *Aphanipathes*, *Bathypathes*, *Chrysopathes*, *Dendropathes*, *Leiopathes*, *Parantipathes*, *Stauropathes*, *Trissopathes* and *Umbellapathes*, were often adjacent to, but slightly deeper than, corresponding areas of robust predictions of high likelihood of habitat suitability for the mid-depth Antipatharia genera (e.g., Makapu'u Point, edges of Penguin Bank; Figure 3.31). Additionally, Cross Seamount and Ka'ena Point were identified as highly likely to have suitable habitat for deep Antipatharians. Compared to mid-depth and shallow Antipatharians, the likelihood of suitable habitat around the Maui Nui complex was lower.

The percentage of deep Antipatharia presences occurring in model grid cells predicted to have the highest likelihood of habitat suitability was relatively high, although the percentage of model grid cells predicted to have the highest likelihood of habitat suitability that were also considered robust was somewhat lower than for the shallow and mid-depth Antipatharia models. Like the mid-depth Antipatharia, there were a relatively large number of model grid cells with presence records for deep Antipatharia.

Thirteen predictor variables were included in the final model for deep Antipatharians, with depth, slope of slope at 1,500 m scale, and slope at 5 km scale the most important predictors (Figures 3.24–3.26).

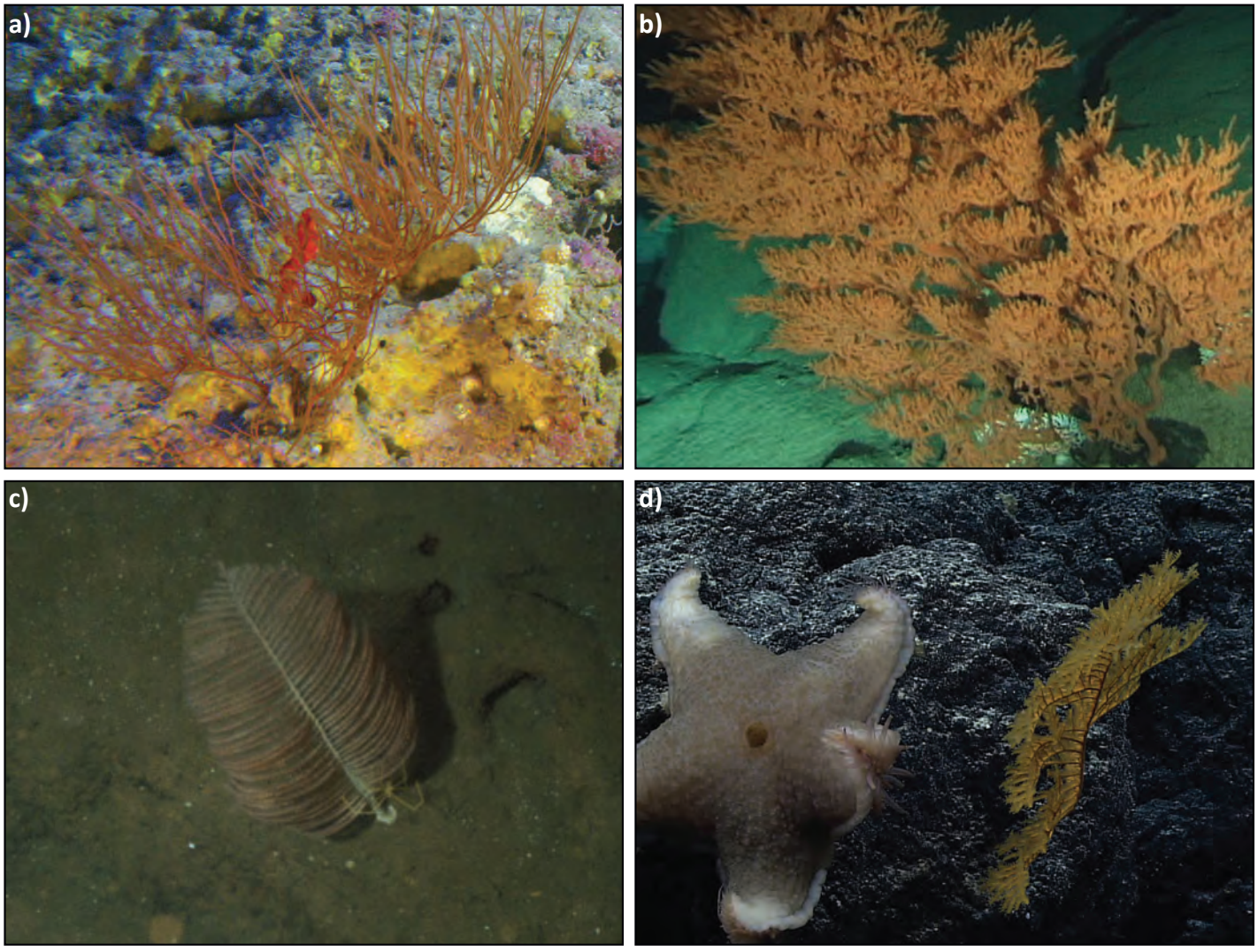

Deep antipatharians. a) Aphanipathes verticillata*, b)* Leiopathes annosa*, c)* Bathypathes conferta *cf and d)* Stauropathes staurocrada*. Photo credit: (a-c) Hawai'i Undersea Reseach Laboratory, and d) NOAA Office of Ocean Exploration and Research, 2015 Hohonu Moana*

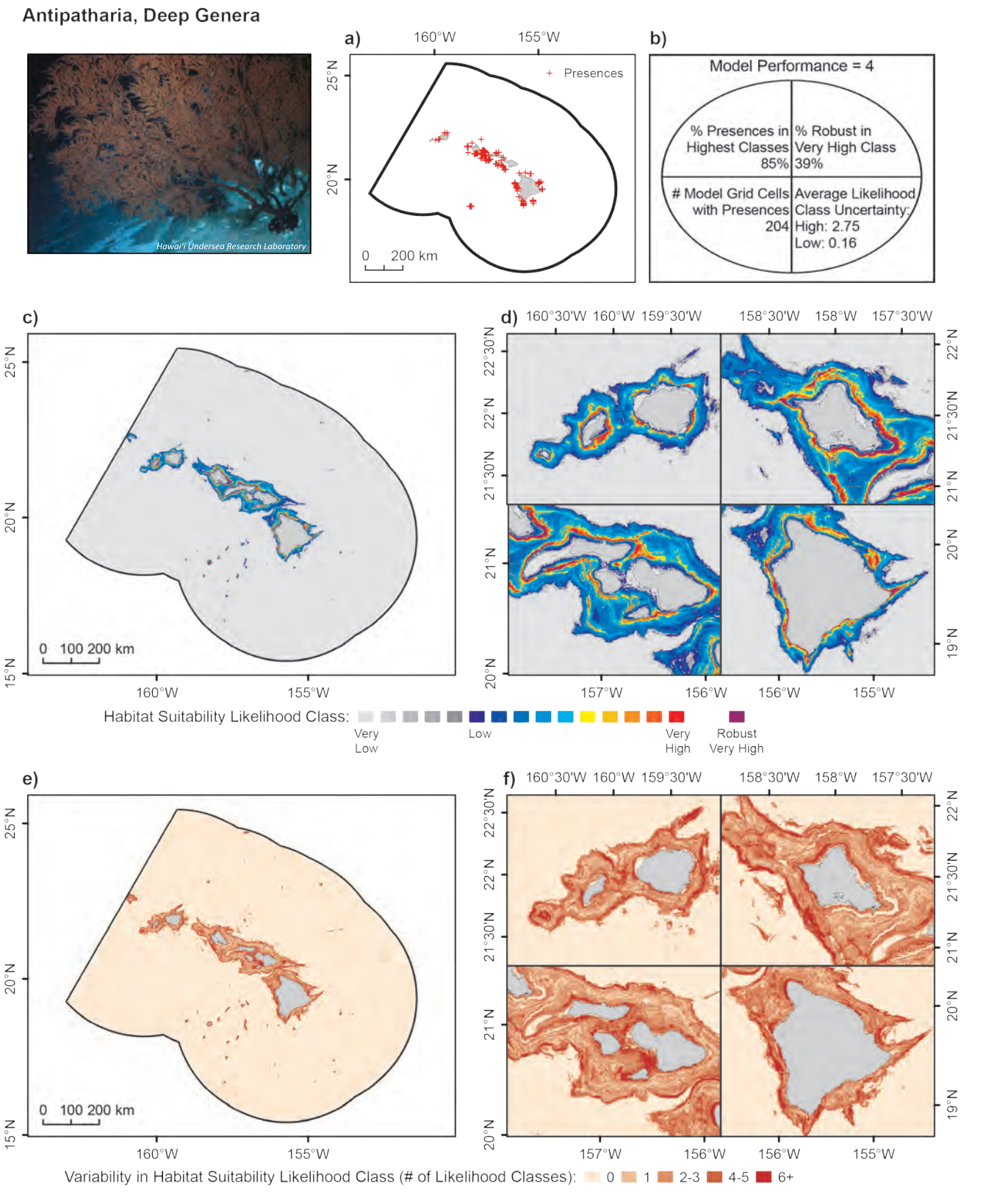

Figure 3.31. Predicted likelihood of habitat suitability for deep Antipatharia (black coral) genera in the MHI. Deep Antipatharia genera tend to occur in water depths >300 m and include Aphanipathes, Bathypathes, Chrysopathes, Dendropathes, Leiopathes, Parantipathes, Stauropathes, Trissopathes *and* Umbellapathes *species. Predictive modeling was applied to coral presence data from 1891-2009 provided by NOAA DSCRTP and HURL. a) Locations of deep Antipatharia presences reported in the study area (N=447, depth range: 119-4,038 m). b) Model performance as determined as a function of four performance metrics. c,d) Habitat suitability likelihood classes derived from a categorical reclassification of the MaxEnt logistic output. Robust high likelihood areas represent locations that are always predicted to have the highest likelihood of habitat suitability for all bootstrap model runs with random sub-samples of the data. e,f) Variability in habitat suitability predictions, depicted as the difference in habitat suitability likelihood classes assigned to the bootstrap 95 percent confidence interval upper and lower limits. Photo credit: Hawai'i Undersea Research Laboratory*

Pennatulacea, hard substrate

Areas of robust predictions of very high likelihood of habitat suitability for hard substrate dwelling Pennatulacea (sea pens) included Makapu‘u Point and Cross Seamount, where a large percentage of the presence records were also located (Figure 3.32). Additional small patches were located west and north of the Maui Nui complex and offshore of northwest Hawai‘i.

While the percentage of hard substrate dwelling sea pen presences occurring in model grid cells predicted to have the highest likelihood of habitat suitability was relatively high, the percentage of model grid cells predicted to have the highest likelihood of habitat suitability that were also considered robust was among the lowest across the DSC models. In addition, the prediction variability in areas predicted to have high likelihood of habitat suitability was among the highest across all the models. Therefore, some caution should be exercised in using model predictions outside the extent of these sea pen presence records. The reduced performance of the hard substrate dwelling sea pen model was likely a result of the fairly low number of model grid cells with coral presences.

Hard substrate dwelling sea pen, Anthoptilum grandiflorum. *Photo credit: Hawai‘i Undersea Research Laboratory*

Thirteen predictor variables were included in the final model for hard substrate dwelling sea pens. Depth, total curvature at 5 km scale, and cosine of aspect at 10 km scale were the most important predictors (Figures 3.24–3.26).

Pennatulacea, soft substrate

Areas of robust predictions of very high likelihood of habitat suitability for soft substrate dwelling Pennatulacea (sea pens) cover a broader area than for hard substrate dwelling sea pens. These included some areas where a high concentration of presence records were located (e.g., Cross Seamount, Makapu‘u and other portions of O‘ahu, Penguin Bank, Makalawena Bank) and those where presence records were largely absent (e.g., offshore of the Kohala Mountains, Hawai‘i, southeast of Maui, Ni‘ihau) (Figure 3.33).

Both the percentage of soft substrate dwelling sea pen presences occurring in model grid cells predicted to have the highest likelihood of habitat suitability and the percentage of model grid cells predicted to have the highest likelihood of habitat suitability that were also considered robust were relatively high. In addition, there were a relatively large number of model grid cells with presence records.

Eleven predictor variables were included in the final model, with annual bottom temperature, distance to shore, and slope of slope at 5 km scale the most important predictors (Figures 3.24–3.26).

Soft substrate dwelling sea pen, Pennatula inflata. *Photo credit: Hawai‘i Undersea Research Laboratory*

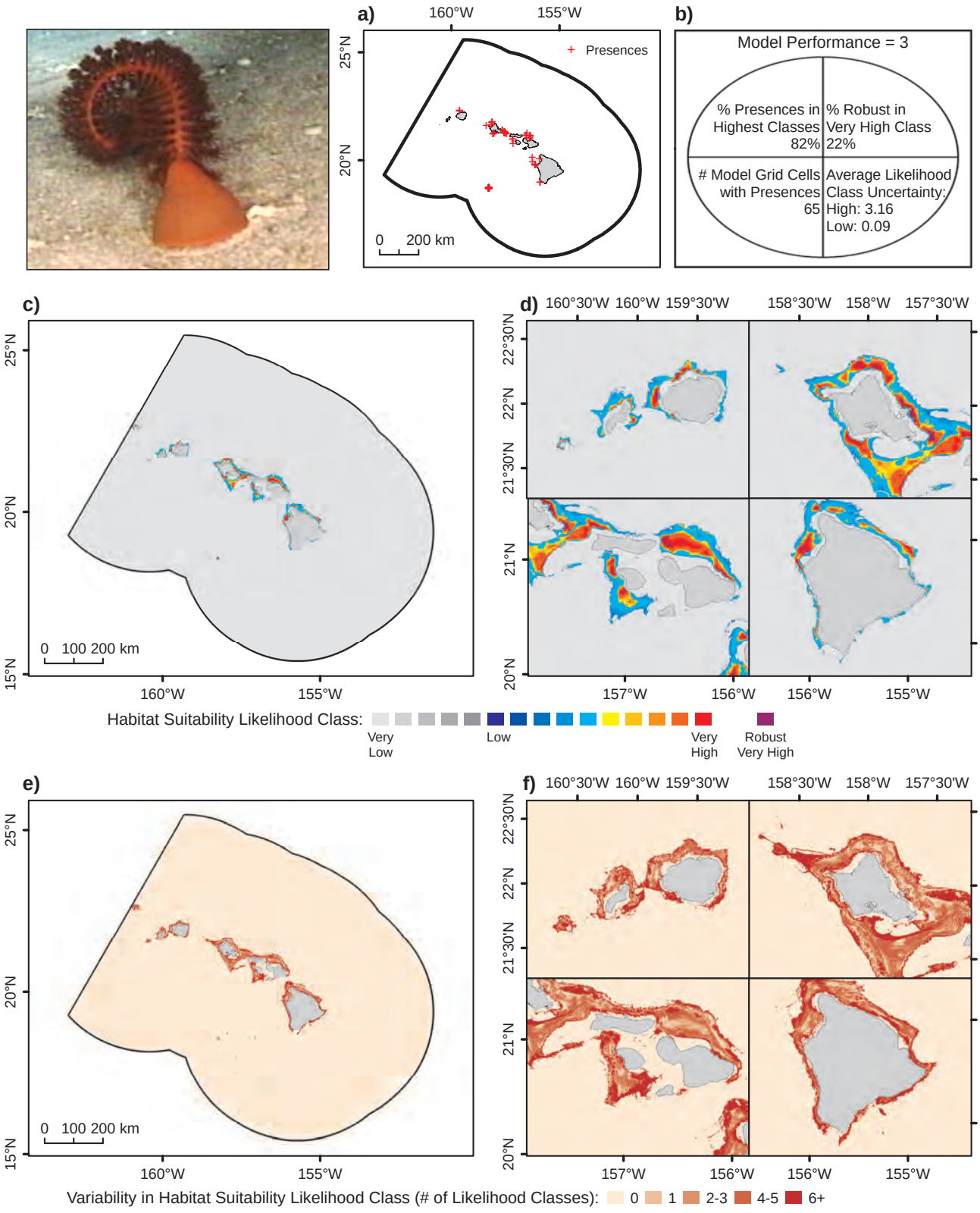

Figure 3.32. Predicted likelihood of habitat suitability for hard-substrate dwelling Pennatulacea (sea pens) in the MHI. Hard substrate dwelling Pennatulacea includes Anthoptilum *and* Calibelemnon spp. *Predictive modeling was applied to coral presence data from 1891-2009 provided by NOAA DSCRTP and HURL. a) Locations of hard-substrate dwelling Pennatulacea presences reported in the study area (N=77, depth range: 188-1,794 m). b) Model performance as determined as a function of four performance metrics. c,d) Habitat suitability likelihood classes derived from a categorical reclassification of the MaxEnt logistic output. Robust high likelihood areas represent locations that are always predicted to have the highest likelihood of habitat suitability for all bootstrap model runs with random sub-samples of the data. e,f) Variability in habitat suitability predictions, depicted as the difference in habitat suitability likelihood classes assigned to the bootstrap 95 percent confidence interval upper and lower limits. Photo credit: Hawai'i Undersea Research Laboratory*

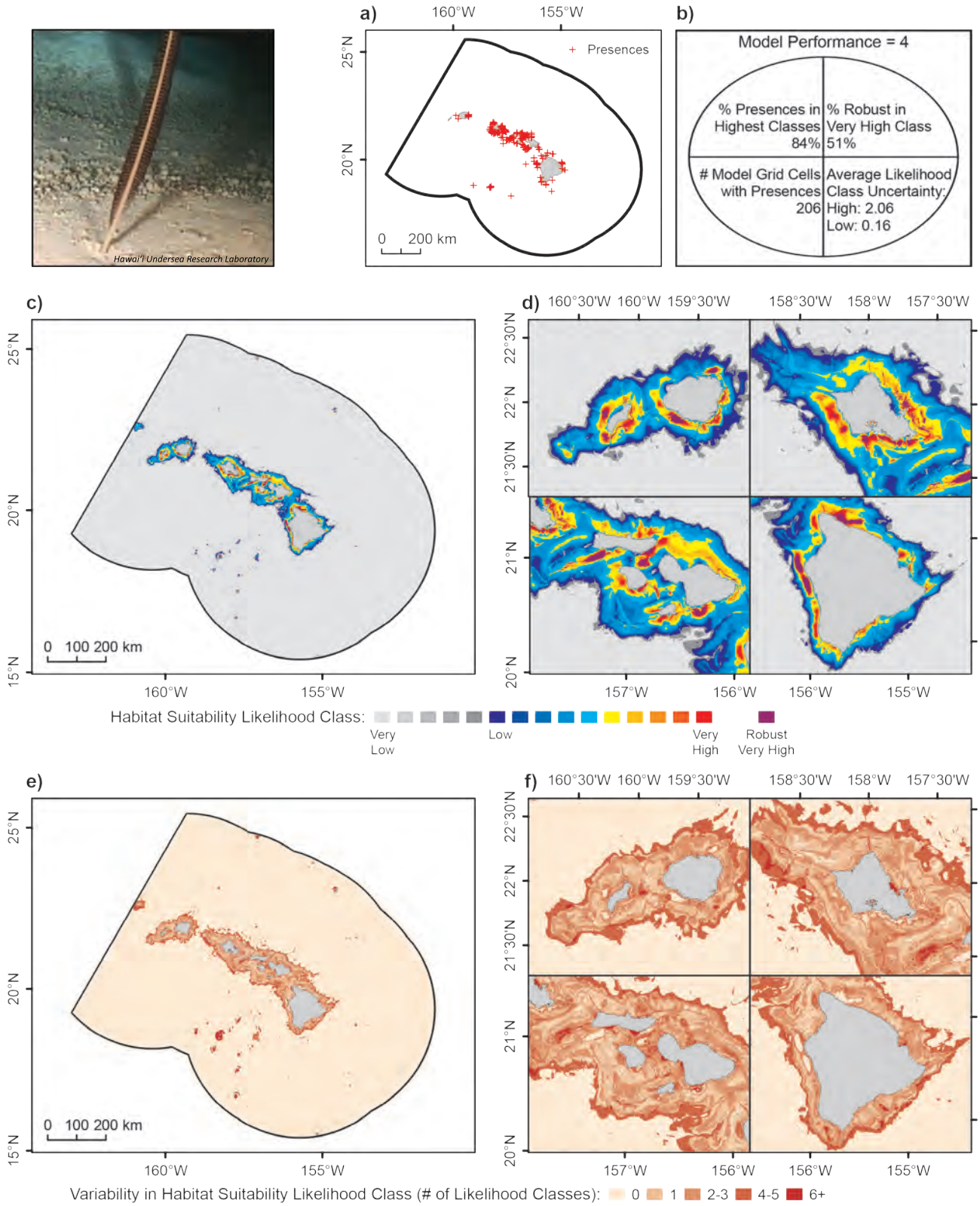

Figure 3.33. Predicted likelihood of habitat suitability for soft-substrate dwelling Pennatulacea (sea pens) in the MHI. Soft-substrate dwelling Pennatulacea includes all other genera not included in the hard-substrate dwelling Pennatulacea group (Figure X). Predictive modeling was applied to coral presence data from 1891-2009 provided by NOAA DSCRTP and HURL. a) Locations of soft-substrate dwelling Pennatulacea presences reported in the study area (N=292, depth range: 39-4,807 m). b) Model performance as determined as a function of four performance metrics. c,d) Habitat suitability likelihood classes derived from a categorical reclassification of the MaxEnt logistic output. Robust high likelihood areas represent locations that are always predicted to have the highest likelihood of habitat suitability for all bootstrap model runs with random sub-samples of the data. e,f) Variability in habitat suitability predictions, depicted as the difference in habitat suitability likelihood classes assigned to the bootstrap 95 percent confidence interval upper and lower limits. Photo credit: Hawai'i Undersea Research Laboratory

Non-gorgonian Alcyonacea (Suborders Alcyoniina, Stolonifera)

Areas of robust predictions of very high likelihood of habitat suitability for non-gorgonian Alcyonacea included portions of the ʻAuʻau and Pailolo Channels, the southern edge of Penguin Bank, portions of the Kona Coast and Makalawena Bank and Cross and Lō'ihi Seamounts (Figure 3.34). Additional areas of high likelihood of suitability included areas where no presence records currently exist, including McCall Seamount and east of Kauaʻi. Additional seamounts south of the MHI may also include areas of suitable habitat, although these areas had lower predicted likelihood of habitat suitability and higher prediction variability.

Non-gorgonian Alcyonacea species, Siphonogorgia alexandri. *Photo credit: Hawai'i Undersea Research Laboratory*

Both the percentage of non-gorgonian Alcyonacea presences occurring in model grid cells predicted to have the highest likelihood of habitat suitability and the percentage of model grid cells predicted to have the highest likelihood of habitat suitability that were also considered robust were relatively high. In addition, there were a relatively large number of model grid cells with presence records.

Eight predictor variables were included in the final model for non-gorgonian Alcyonacea. Depth, distance to shore, and total curvature at 5 km scale were the most important predictors (Figures 3.24–3.26).

Gorgonian Alcyonacea (Suborders Calcaxonia, Holaxonia, Scleraxonia)

Overall, the area predicted as likely to have suitable habitat for gorgonian Alcyonacea was geographically wider than for many other DSC groups, with robust predictions of very high likelihood of habitat suitability occurring near Cape Kumakahi and the western side of Hawaiʻi, portions of the Maui Nui complex including Pailolo Channel and around Kahoʻolawe, Makapuʻu and southern/western Oʻahu, southwestern Kauaʻi, and at Cross and Lō'ihi Seamounts (Figure 3.35). In addition, the western edge of Waiʻanae Slump was identified as having high likelihood of habitat suitability, even though presence records were largely absent from this area.

Although a relatively high number of gorgonian Alcyonacea presences were available in comparison to the other DSC groups, and the presences were generally more widely distributed across the MHI, the percentage of gorgonian Alcyonacea presences occurring in model grid cells predicted to have the highest likelihood of habitat suitability was relatively low compared to the DSC models. The percentage of model grid cells predicted to have the highest likelihood of habitat suitability that were also considered robust was still relatively high, though.

Gorgonian Alcyonacea species of the genus Rhodaniridogorgia. *Photo credit: Hawai'i Undersea Research Laboratory*

Eighteen predictor variables were used in the final model for gorgonian Alcyonacea, with depth, distance to shore, and total curvature at 5 km scale the most important predictors (Figures 3.24–3.26).

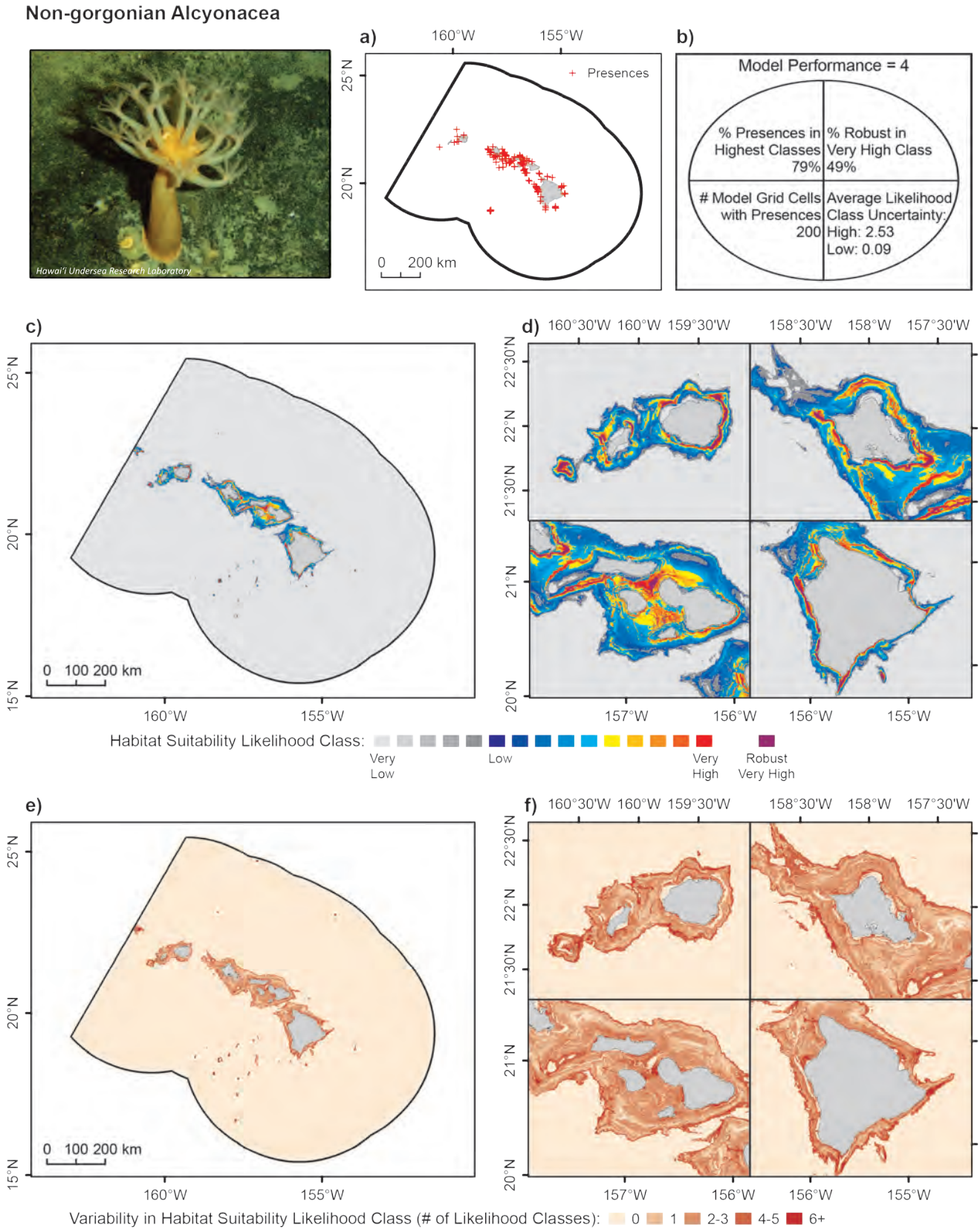

Figure 3.34. Predicted likelihood of habitat suitability for non-gorgonian Alcyonacea in the MHI. Predictive modeling was applied to coral presence data from 1891-2009 provided by NOAA DSCRTP and HURL. a) Locations of non-gorgonian Alcyonacea presences reported in the study area (N=279, depth range: 18-4,240 m). b) Model performance as determined as a function of four performance metrics. c,d) Habitat suitability likelihood classes derived from a categorical reclassification of the MaxEnt logistic output. Robust high likelihood areas represent locations that are always predicted to have the highest likelihood of habitat suitability for all bootstrap model runs with random sub-samples of the data. e,f) Variability in habitat suitability predictions, depicted as the difference in habitat suitability likelihood classes assigned to the bootstrap 95 percent confidence interval upper and lower limits. Photo credit: Hawai'i Undersea Research Laboratory

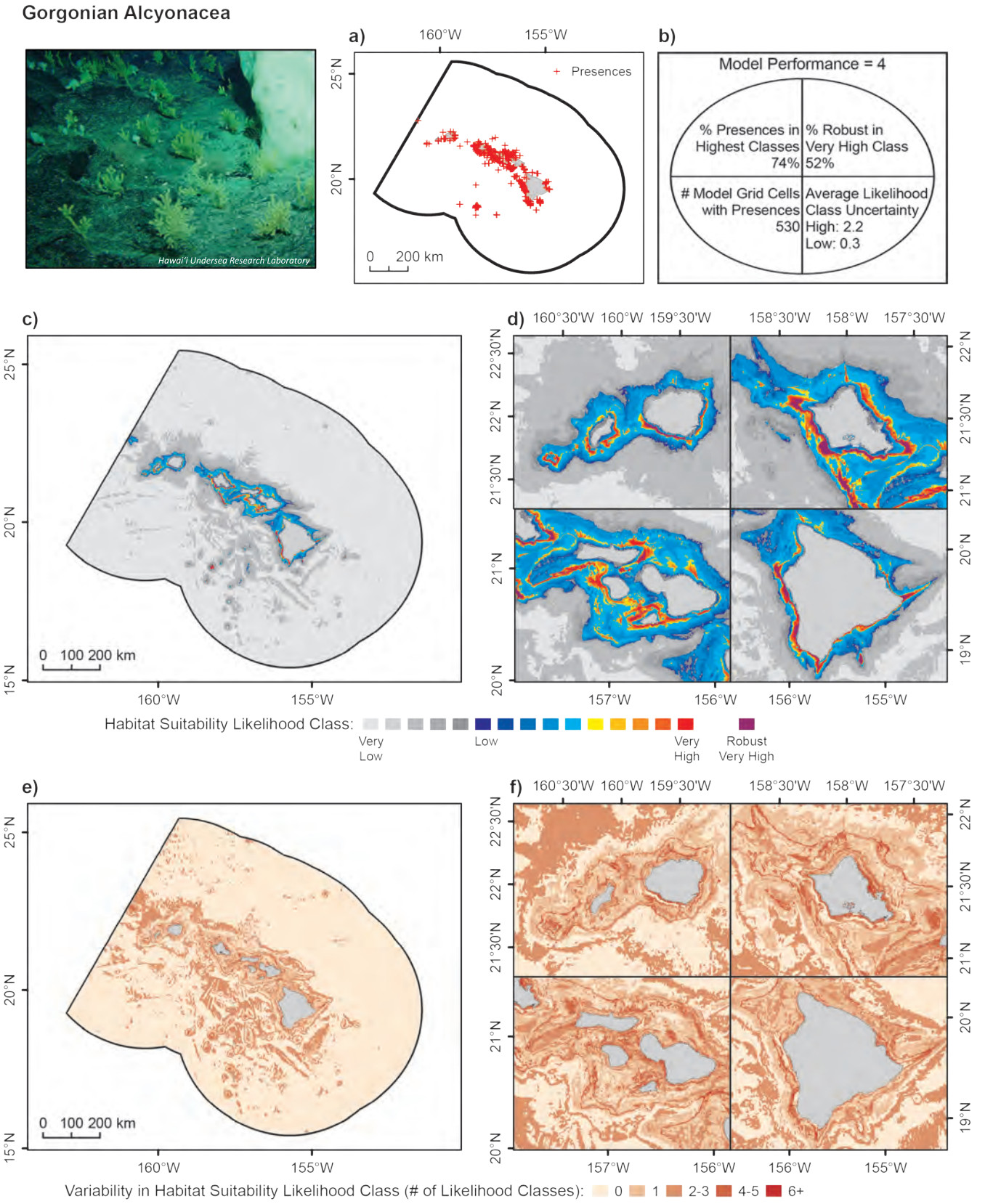

Figure 3.35. Predicted likelihood of habitat suitability for gorgonian Alcyonacea in the MHI. Predictive modeling was applied to coral presence data from 1891-2009 provided by NOAA DSCRTP and HURL. a) Locations of gorgonian Alcyonacea presences reported in the study area (N=2,481, depth range: 22-4,807 m). b) Model performance as determined as a function of four performance metrics. c,d) Habitat suitability likelihood classes derived from a categorical reclassification of the MaxEnt logistic output. Robust high likelihood areas represent locations that are always predicted to have the highest likelihood of habitat suitability for all bootstrap model runs with random sub-samples of the data. e,f) Variability in habitat suitability predictions, depicted as the difference in habitat suitability likelihood classes assigned to the bootstrap 95 percent confidence interval upper and lower limits. Photo credit: Hawai'i Undersea Research Laboratory

Alcyonacea, Suborder Calcaxonia

Areas with robust predictions of very high likelihood of habitat suitability for Calcaxonia occurred near Cross and Lō'ihi Seamounts, Cape Kumakahi and the western side of Hawai'i, and small pockets near O'ahu and Kaua'i (Figure 3.36). Despite the numerous presence locations within the Maui Nui complex, very little area was designated having robust predictions of suitable habitat, although areas of higher likelihood of habitat suitability were present, including east of Lāna'i and the canyons north of Moloka'i.

Both the percentage of Calcaxonia presences occurring in model grid cells predicted to have the highest likelihood of habitat suitability and the percentage of model grid cells predicted to have the highest likelihood of habitat suitability that were also considered robust were relatively high. In addition, there were a relatively large number of model grid cells presence records.

Thirteen predictor variables were included in the final model for Calcaxonia. Depth, distance to shore, and distance to seamounts were the most important predictors (Figures 3.24–3.26).

Calcaxonia species, Iridogorgia magnispiralis. *Photo credit: Hawai'i Undersea Research Laboratory*

Alcyonacea, Family Isididae (Bamboo corals)

Areas with robust predictions of very high likelihood of habitat suitability for Isididae (bamboo corals) were found across the MHI and on several offshore seamounts (Figure 3.37). In particular, this included a zone extending from Cape Kumakahi out onto Puna Ridge, and additional areas extending in a northwest-southeast line west of O'ahu and Kaiwi Channel. Additional areas with high likelihood of suitable habitat also occurred on several seamounts south of the MHI, often where no coral presence records occur.

A relatively high percentage of bamboo coral presences occurred in model grid cells predicted to have the highest likelihood of habitat suitability. In addition, the percentage of model grid cells predicted to have the highest likelihood of habitat suitability that were also considered robust was among the highest across all DSC models. There were a relatively large number of model grid cells with bamboo coral presences.

Seven predictor variables were used in the final model for bamboo corals, with depth, slope at 5 km scale, and sine of aspect at 5 km scale the most important predictors (Figures 3.24–3.26).

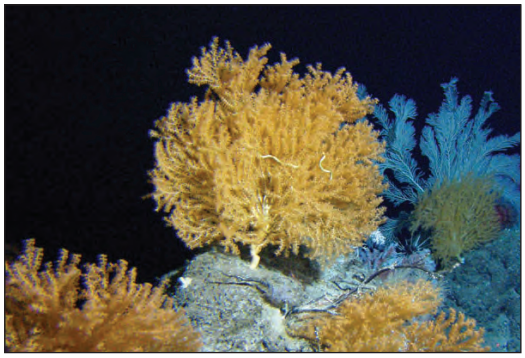

Bamboo coral, Acanella dispar. *Photo credit: Hawai'i Undersea Research Laboratory*

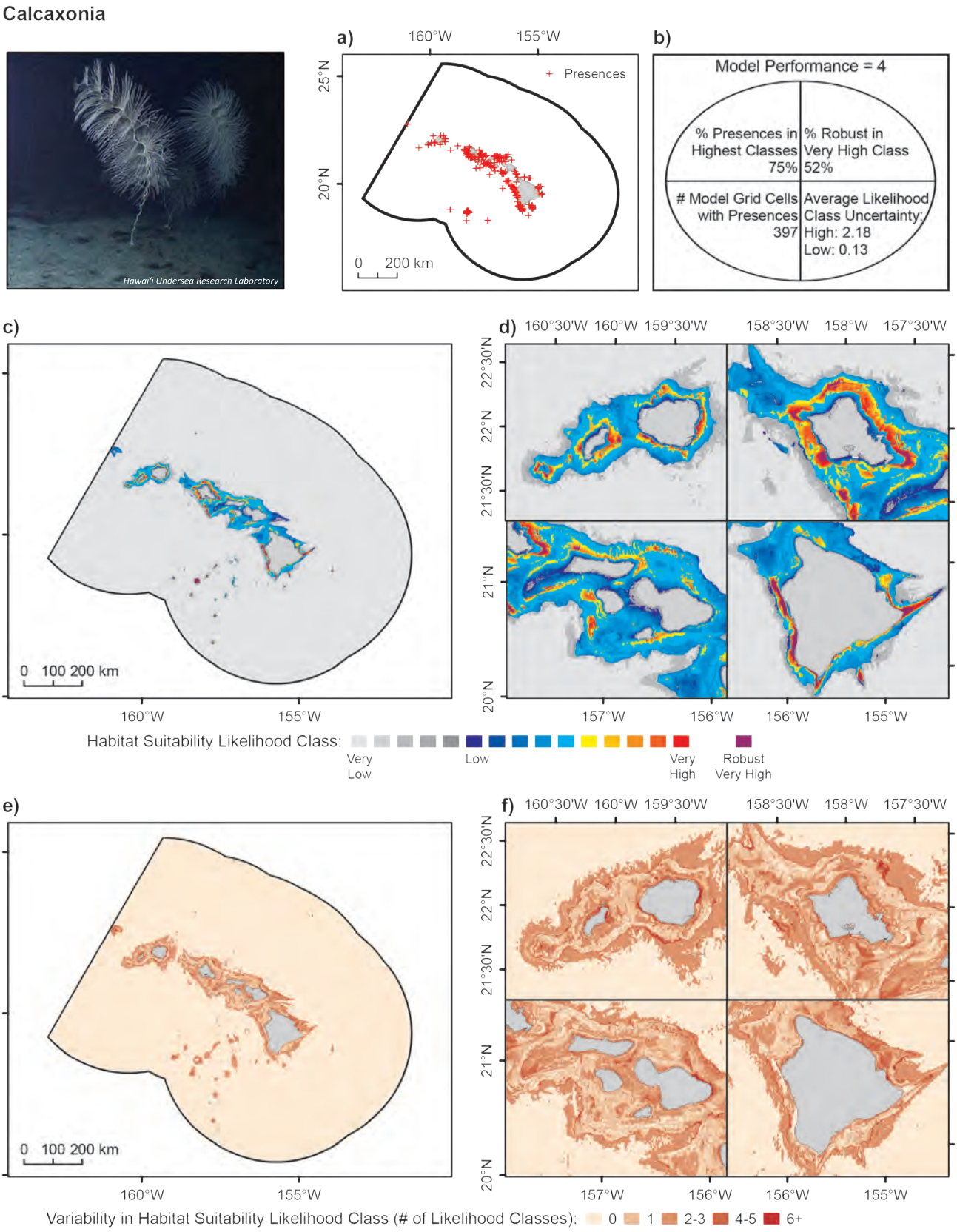

Figure 3.36. Predicted likelihood of habitat suitability for Calcaxonia in the MHI. Predictive modeling was applied to coral presence data from 1891-2009 provided by NOAA DSCRTP and HURL. a) Locations of Calcoxonia presences reported in the study area (N=1,569, depth range: 40-4,807 m). b) Model performance as determined as a function of four performance metrics. c,d) Habitat suitability likelihood classes derived from a categorical reclassification of the MaxEnt logistic output. Robust high likelihood areas represent locations that are always predicted to have the highest likelihood of habitat suitability for all bootstrap model runs with random sub-samples of the data. e,f) Variability in habitat suitability predictions, depicted as the difference in habitat suitability likelihood classes assigned to the bootstrap 95 percent confidence interval upper and lower limits. Photo credit: Hawai'i Undersea Research Laboratory

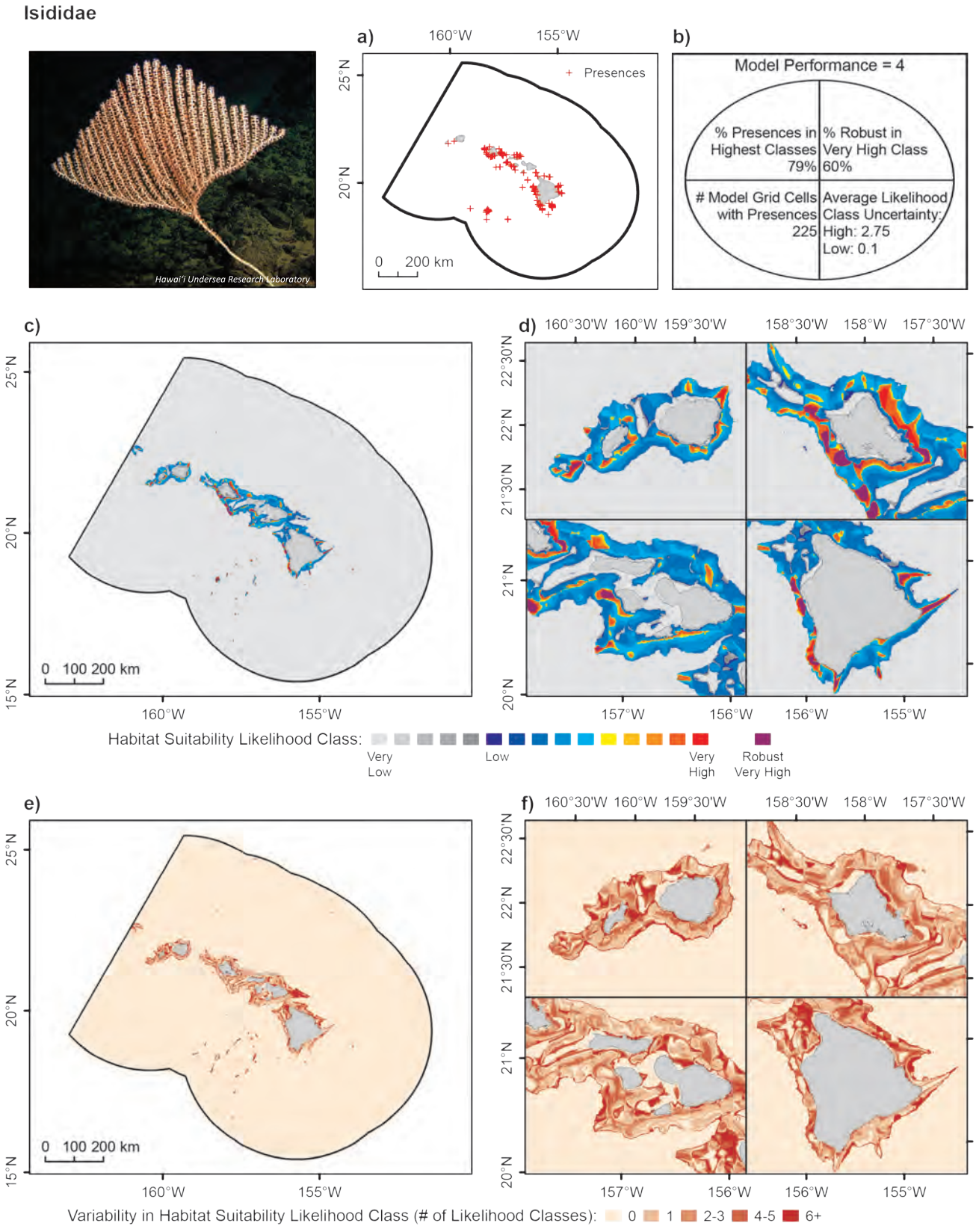

Figure 3.37. Predicted likelihood of habitat suitability for Family Isididae (bamboo corals) in the MHI. Predictive modeling was applied to coral presence data from 1891-2009 provided by NOAA DSCRTP and HURL. a) Locations of Isididae presences reported in the study area (N=474, depth range: 95-4,807 m). b) Model performance as determined as a function of four performance metrics. c,d) Habitat suitability likelihood classes derived from a categorical reclassification of the MaxEnt logistic output. Robust high likelihood areas represent locations that are always predicted to have the highest likelihood of habitat suitability for all bootstrap model runs with random sub-samples of the data. e,f) Variability in habitat suitability predictions, depicted as the difference in habitat suitability likelihood classes assigned to the bootstrap 95 percent confidence interval upper and lower limits. Photo credit: Hawai'i Undersea Research Laboratory

Alcyonacea, Suborder Holaxonia

Areas with robust predictions of very high likelihood of habitat suitability for Holaxonia included Puna Ridge and Makalawena Bank on Hawai‘i, Pailolo Channel, the southern edge of Penguin Bank and Makapu‘u (Figure 3.38). Areas highly likely to contain suitable habitat also occurred south of Maui and Kaua‘i, where few coral presence records were located. Areas of relatively higher prediction variability included the top of Penguin Bank, ‘Au‘au Channel and west of O‘ahu.

Both the percentage of Holaxonia presences occurring in model grid cells predicted to have the highest likelihood of habitat suitability and the percentage of model grid cells predicted to have the highest likelihood of habitat suitability that were also considered robust were relatively high. In addition, there were a relatively large number of model grid cells with presence records.

Six predictor variables were included in the final model for Holaxonia. Distance to shore, distance to seamounts, and total curvature at 5 km scale were the most important predictors (Figures 3.24–3.26).

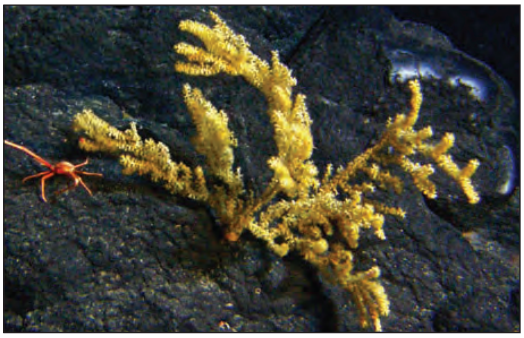

Acanthogorgia *species in Suborder Holaxonia. Photo credit: Hawai‘i Undersea Research Laboratory*

Alcyonacea, Suborder Scleraxonia

Areas with robust predictions of very high likelihood of habitat suitability for Scleraxonia included Puna and Ka Lae Ridges, as well as a thin strip along the western side of Hawai‘i extending north to Makalawena Bank (Figure 3.39). Additional areas with robust predictions of high likelihood of habitat suitability occurred on Cross Seamount, in the Maui Nui complex south of Maui/Kaho‘olawe and the southern edge of Penguin Bank, around O‘ahu, and south of Kaua‘i/Ni‘ihau and Ka‘ula.

Both the percentage of Scleraxonia presences occurring in model grid cells predicted to have the highest likelihood of habitat suitability and the percentage of model grid cells predicted to have the highest likelihood of habitat suitability that were also considered robust were relatively high. In addition, there were a relatively large number of model grid cells presence records.

Twelve predictor variables were used in the final model for Scleraxonia, with depth, rugosity, and total curvature at 5 km scale the most important predictors (Figures 3.24–3.26).

Corallium laauense *in Suborder Scleraxonia. Photo credit: Hawai‘i Undersea Research Laboratory*

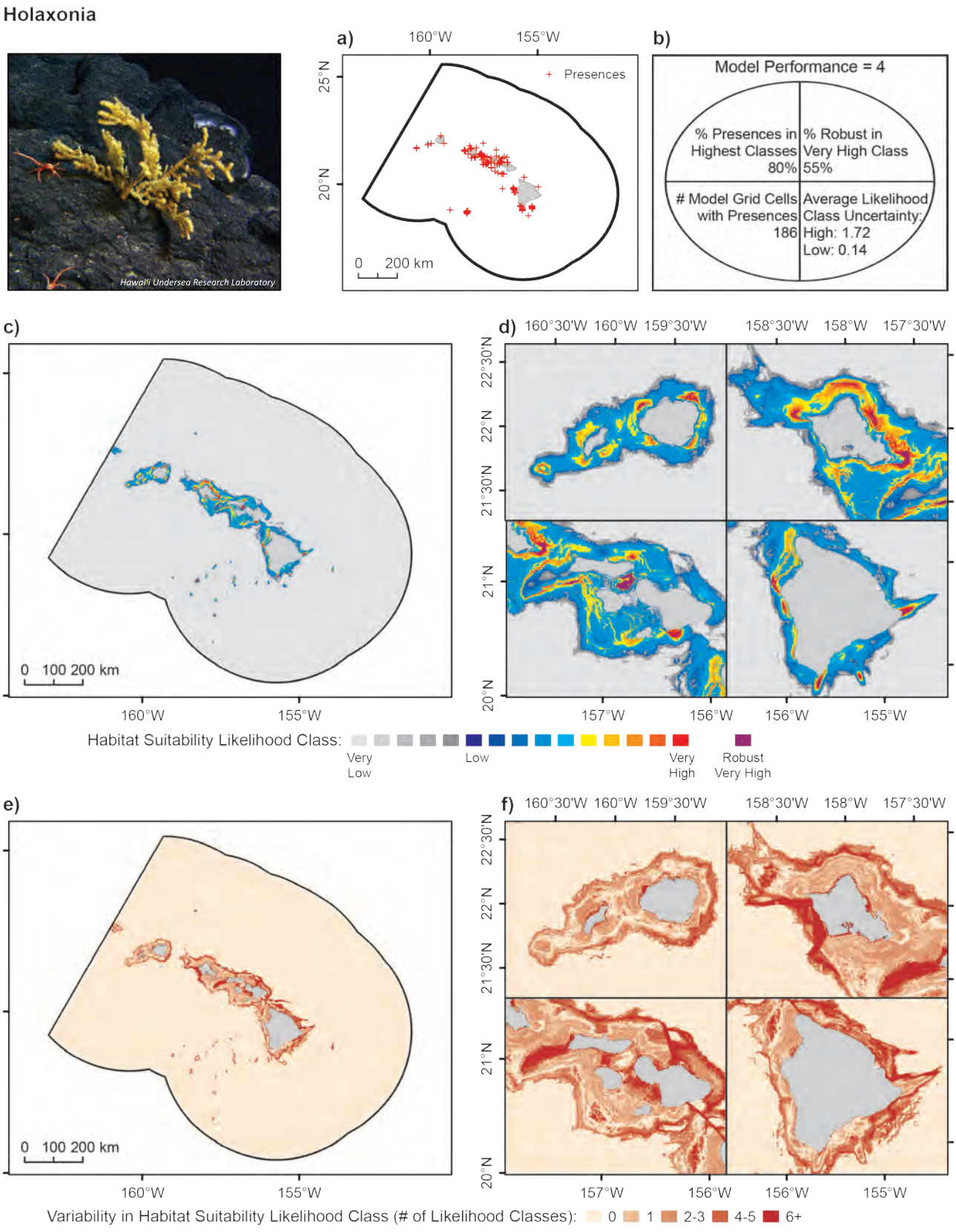

Figure 3.38. Predicted likelihood of habitat suitability for Holaxonia in the MHI. Predictive modeling was applied to coral presence data from 1891-2009 provided by NOAA DSCRTP and HURL. a) Locations of Holaxonia presences reported in the study area (N=355, depth range: 102-4,807 m). b) Model performance as determined as a function of four performance metrics. c,d) Habitat suitability likelihood classes derived from a categorical reclassification of the MaxEnt logistic output. Robust high likelihood areas represent locations that are always predicted to have the highest likelihood of habitat suitability for all bootstrap model runs with random sub-samples of the data. e,f) Variability in habitat suitability predictions, depicted as the difference in habitat suitability likelihood classes assigned to the bootstrap 95 percent confidence interval upper and lower limits. Photo credit: Hawai'i Undersea Research Laboratory

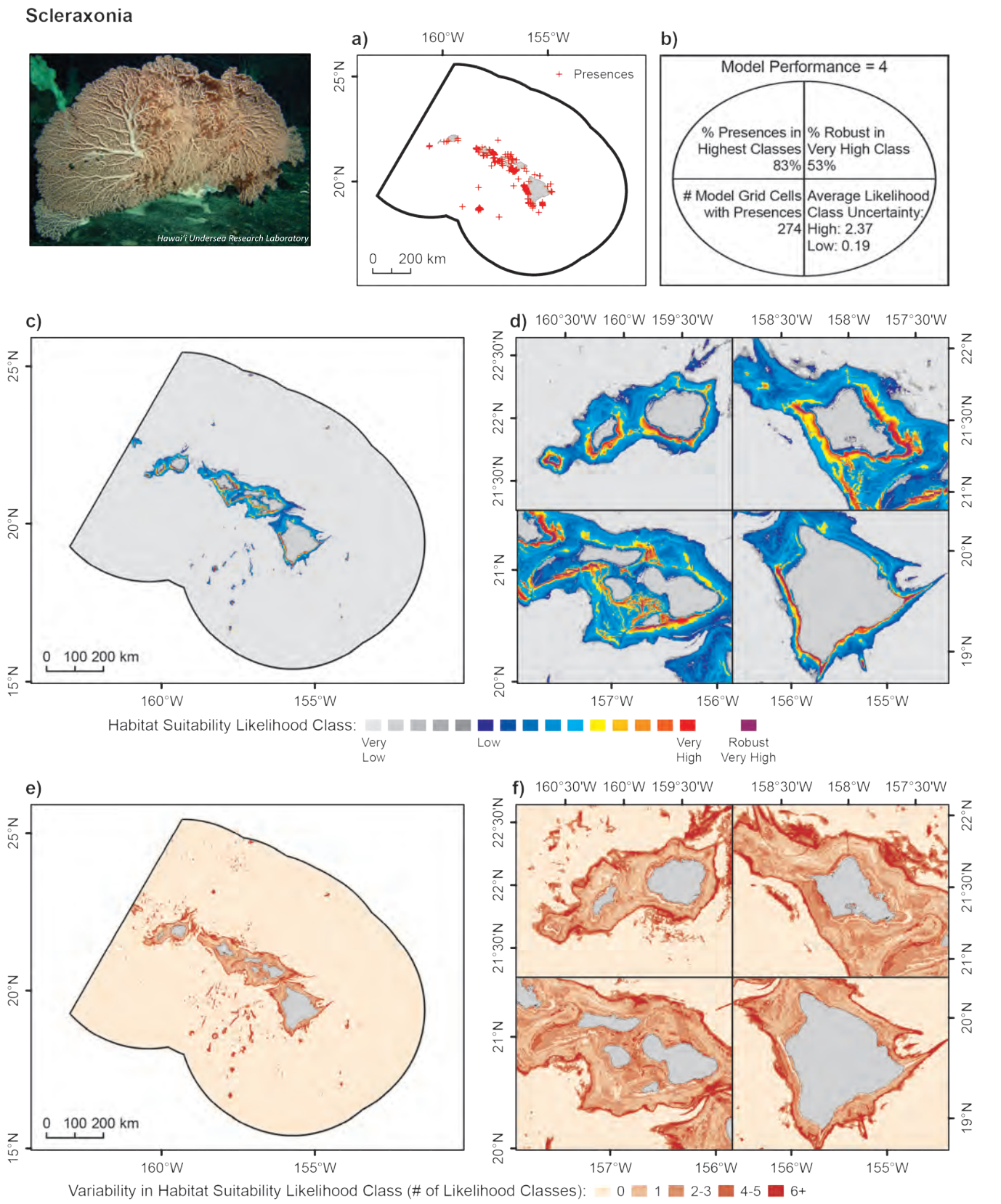

Figure 3.39. Predicted likelihood of habitat suitability for Scleraxonia in the MHI. Predictive modeling was applied to coral presence data from 1891-2009 provided by NOAA DSCRTP and HURL. a) Locations of Scleraxonia presences reported in the study area (N=557, depth range: 22-4,807 m). b) Model performance as determined as a function of four performance metrics. c,d) Habitat suitability likelihood classes derived from a categorical reclassification of the MaxEnt logistic output. Robust high likelihood areas represent locations that are always predicted to have the highest likelihood of habitat suitability for all bootstrap model runs with random sub-samples of the data. e,f) Variability in habitat suitability predictions, depicted as the difference in habitat suitability likelihood classes assigned to the bootstrap 95 percent confidence interval upper and lower limits. Photo credit: Hawai'i Undersea Research Laboratory

Corallium spp. (Red and pink corals)

Areas with robust predictions of very high likelihood of habitat suitability for *Corallium* were generally similar to that of all Scleraxonia, with slightly less area on the southwestern and southeastern sides of Hawai'i but broader areas in other regions, such as south of Maui, O'ahu and Penguin Bank (Figure 3.40). Additional areas likely to contain suitable habitat, but also that had higher prediction variability, were found at some of the offshore seamounts such as Wini Seamount to the east of Hawai'i.

The percentage of *Corallium* presences occurring in model grid cells predicted to have the highest likelihood of habitat suitability was among the highest across all DSC models, indicating a relatively good model fit. In addition, the percentage of model grid cells predicted to have the highest likelihood of habitat suitability that were also considered robust was relatively high and there were a relatively large number of model grid cells with presence records.

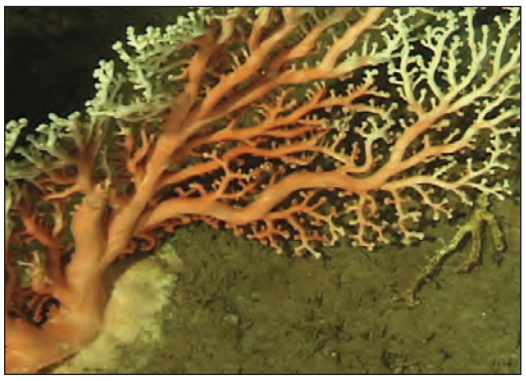

Corallium secundum. *Photo credit: Hawai'i Undersea Research Laboratory*

Ten predictor variables were included in the final model for *Corallium*. Distance to shore, total curvature at 5 km scale, and annual bottom temperature were the most important predictors (Figures 3.24–3.26).

Family Paragorgiidae (Bubblegum corals)

There was little area with robust predictions of very high likelihood of habitat suitability for Paragorgiidae (bubblegum corals) around the MHI (Figure 3.41). These few areas included several seamounts (e.g., Cross, Lō'ihi, McCall), Puna Ridge, Makapu'u and Ka'ula additional offshore seamounts contained areas with predicted high likelihood for habitat suitability, but these predictions were not considered robust.

The percentage of bubblegum coral presences occurring in model grid cells predicted to have the highest likelihood of habitat suitability was the lowest of all DSC models and indicated a relatively poor model fit. In addition, the percentage of model grid cells predicted to have the highest likelihood of habitat suitability that were also considered robust was relatively low, as well the number of model grid cells with bubblegum coral presences. Therefore, considerable caution should be exercised in using model predictions outside the extent of the bubblegum coral presence records.

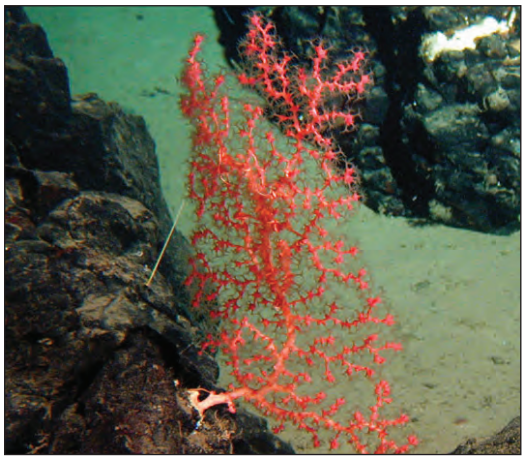

Bubblegum coral, Paragorgia *sp. Photo credit: Hawai'i Undersea Research Laboratory*

Six predictor variables were included in the final model for bubblegum corals, with total curvature at 5 km scale, distance to shore, and profile curvature at 10 km scale the most important predictors (Figures 3.24–3.26).

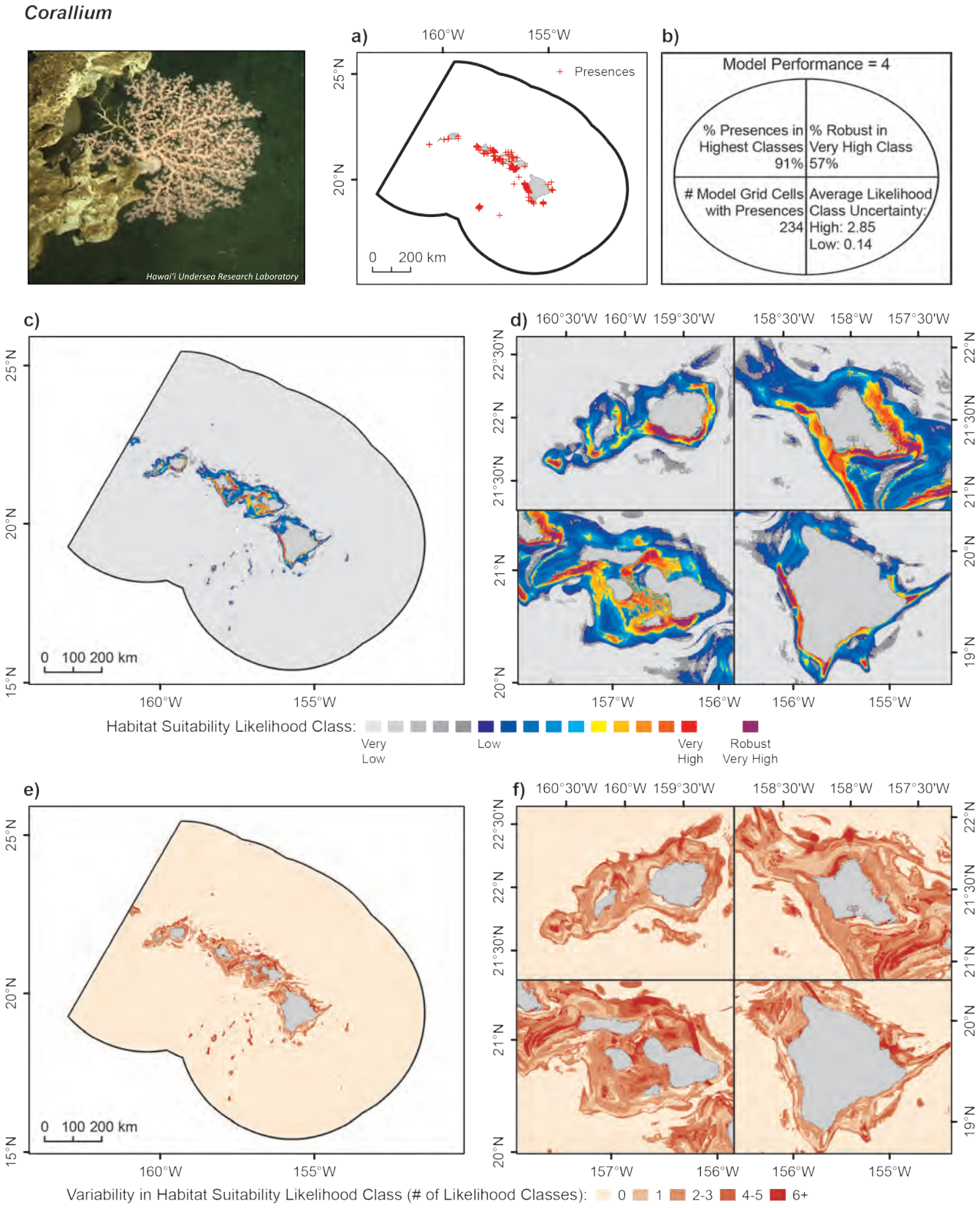

Figure 3.40. Predicted likelihood of habitat suitability for Corallium *spp. (red and pink corals) in the MHI. Predictive modeling was applied to coral presence data from 1891-2009 provided by NOAA DSCRTP and HURL. a) Locations of* Corallium *spp. presences reported in the study area (N=405, depth range: 22-4,807 m). b) Model performance as determined as a function of four performance metrics. c,d) Habitat suitability likelihood classes derived from a categorical reclassification of the MaxEnt logistic output. Robust high likelihood areas represent locations that are always predicted to have the highest likelihood of habitat suitability for all bootstrap model runs with random sub-samples of the data. e,f) Variability in habitat suitability predictions, depicted as the difference in habitat suitability likelihood classes assigned to the bootstrap 95 percent confidence interval upper and lower limits. Photo credit: Hawai'i Undersea Research Laboratory*

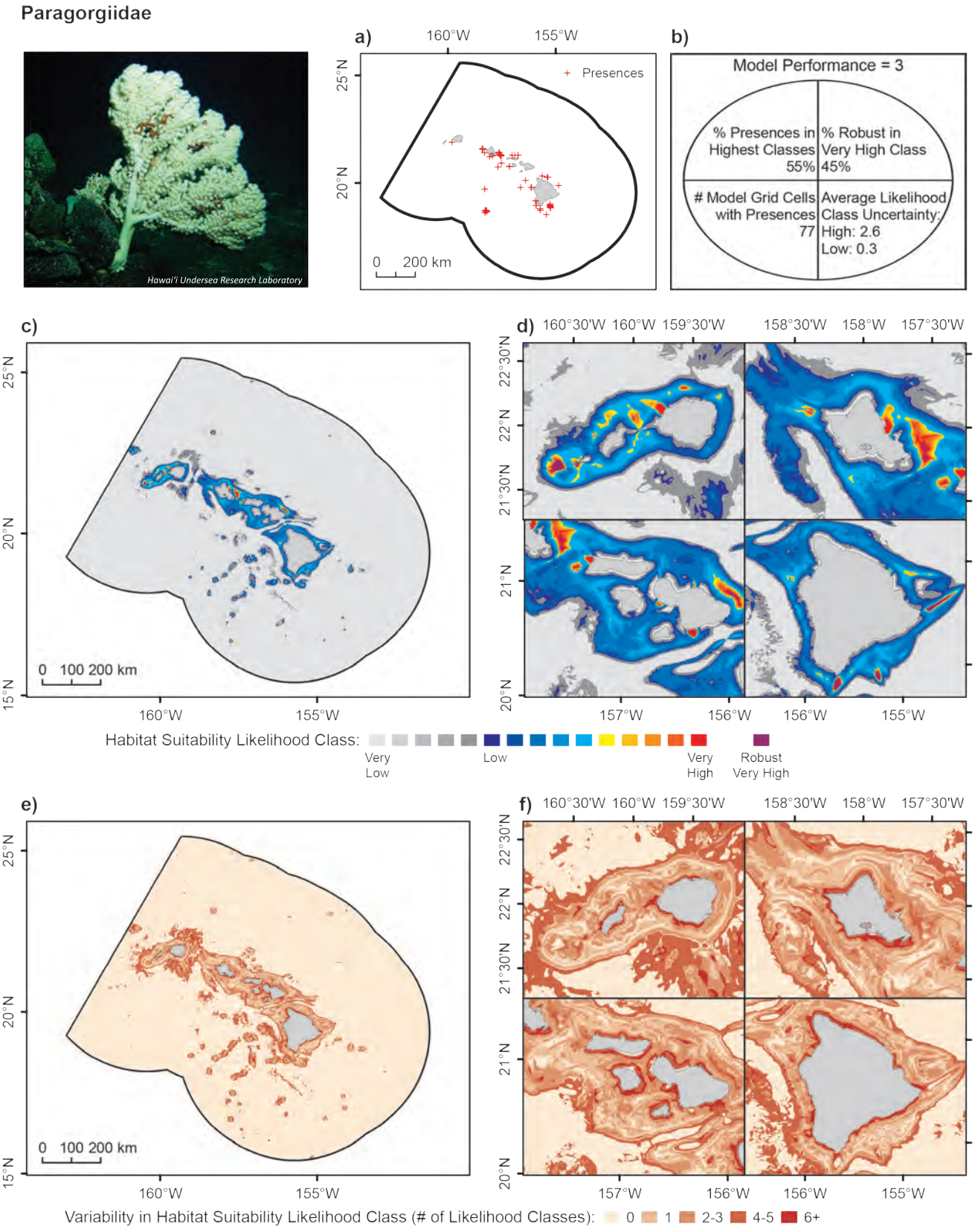

Figure 3.41. Predicted likelihood of habitat suitability for Paragorgiidae (bubblegum corals) in the MHI. Predictive modeling was applied to coral presence data from 1891-2009 provided by NOAA DSCRTP and HURL. a) Locations of Paragorgiidae presences reported in the study area (N=104, depth range:2035-4,807 m). b) Model performance as determined as a function of four performance metrics. c,d) Habitat suitability likelihood classes derived from a categorical reclassification of the MaxEnt logistic output. Robust high likelihood areas represent locations that are always predicted to have the highest likelihood of habitat suitability for all bootstrap model runs with random sub-samples of the data. e,f) Variability in habitat suitability predictions, depicted as the difference in habitat suitability likelihood classes assigned to the bootstrap 95 percent confidence interval upper and lower limits. Photo credit: Hawai'i Undersea Research Laboratory

4 or more genera/grid cell

Areas with robust predictions of very high likelihood of having ≥4 DSC genera occurred in small pockets across the MHI, including Puna and Ka Lae Ridges off Hawai'i, portions of 'Au'au, Pailolo and Kalohi Channels in the Maui-Bui complex, southern O'ahu including offshore of Ka'ena and Makapu'u Points, and Ka'ula (Figure 3.42).

The percentage of model grid cells with ≥4 DSC genera that were also predicted to have the highest likelihood of habitat suitability was relatively high. In addition, the percentage of model grid cells predicted to have the highest likelihood of having ≥4 DSC genera that were also considered robust was relatively high and there were a relatively large number of model grid cells with ≥4 DSC genera.

Seventeen predictor variables were in the final model for ≥4 DSC genera, with distance to shore, slope at 5 km scale, and total curvature at 5 km scale the most important predictors (Figures 3.24–3.26).

7 or more genera/grid cell

Areas with robust predictions of very high likelihood of having ≥7 DSC genera often overlapped with those for ≥4 genera, but in general areas likely to contain suitable habitat for ≥7 genera were more restricted (Figure 3.43). An area with robust predictions of high likelihood of habitat suitability unique to ≥7 genera occurred offshore of Cape Halawa, Moloka'i.

Although the percentage of model grid cells with ≥7 DSC genera that were also predicted to have the highest likelihood of habitat suitability was relatively high, the percentage of model grid cells predicted to have the highest likelihood of having ≥7 DSC genera that were also considered robust was relatively low. In addition, the prediction variability in areas predicted to have high likelihood of suitability was the highest across all the DSC models. Therefore, some caution should be exercised in using model predictions outside the extent of model grid cells with ≥7 DSC genera.

Thirteen predictor variables were used in the final model for ≥7 DSC genera. Distance to shore, distance to seamounts, and total curvature at 5 km scale were the most important predictors (Figures 3.24–3.26).

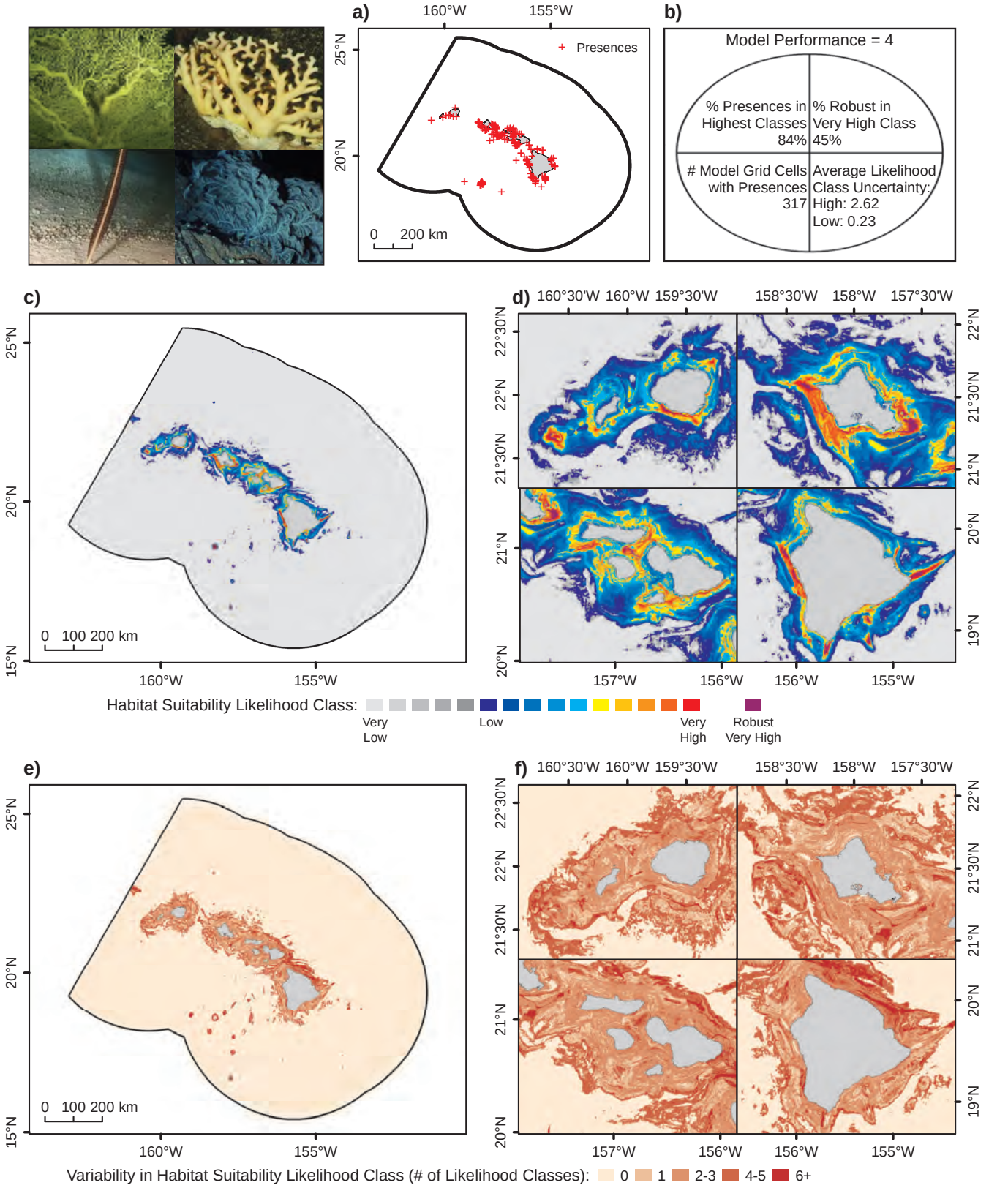

Figure 3.42. Predicted likelihood of habitat suitability for ≥4 genera/grid cell in the MHI. Predictive modeling was applied to coral presence data from 1891-2009 provided by NOAA DSCRTP and HURL. a) Locations of four or more genera presences reported in the study area (N=317, depth range: 30-4,807 m). b) Model performance as determined as a function of four performance metrics. c,d) Habitat suitability likelihood classes derived from a categorical reclassification of the MaxEnt logistic output. Robust high likelihood areas represent locations that are always predicted to have the highest likelihood of habitat suitability for all bootstrap model runs with random sub-samples of the data. e,f) Variability in habitat suitability predictions, depicted as the difference in habitat suitability likelihood classes assigned to the bootstrap 95 percent confidence interval upper and lower limits. Photo credit: Hawai'i Undersea Research Laboratory

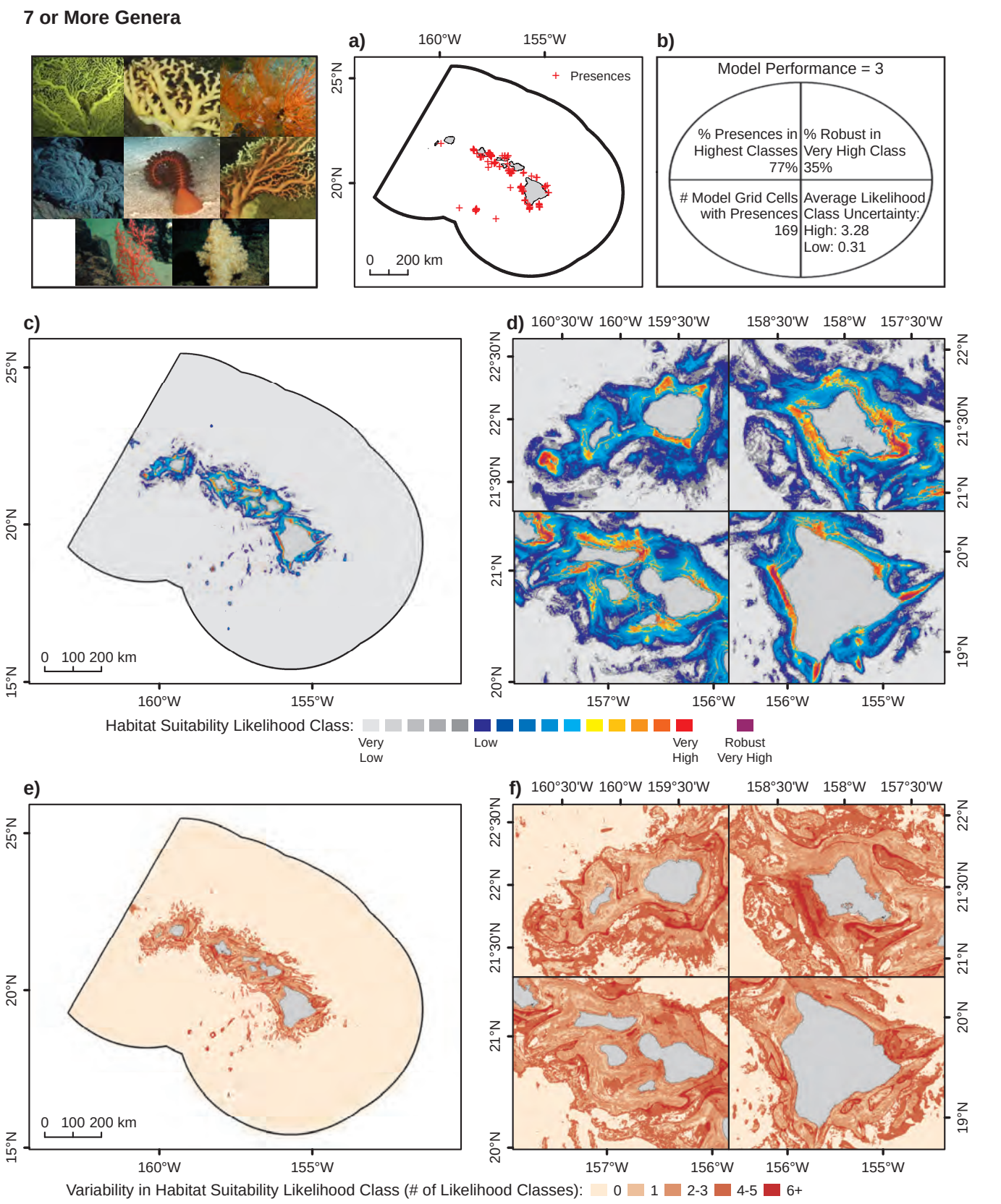

Figure 3.43. Predicted likelihood of habitat suitability for ≥7 genera/grid cell in the MHI. Predictive modeling was applied to coral presence data from 1891-2009 provided by NOAA DSCRTP and HURL. a) Locations of seven or more genera presences reported in the study area (N=169, depth range: 118-4,807 m). b) Model performance as determined as a function of four performance metrics. c,d) Habitat suitability likelihood classes derived from a categorical reclassification of the MaxEnt logistic output. Robust high likelihood areas represent locations that are always predicted to have the highest likelihood of habitat suitability for all bootstrap model runs with random sub-samples of the data. e,f) Variability in habitat suitability predictions, depicted as the difference in habitat suitability likelihood classes assigned to the bootstrap 95% confidence interval upper and lower limits. Photo credit: Hawai'i Undersea Research Laboratory

Potentially important ecological predictors

The number of predictor variables included in the final selected models ranged from five (shallow Antipatharia) to 18 (Gorgonian Alcyonacea), with a median of 11 variables. Distance to seamounts was the most frequently selected predictor, occurring in 14 of 18 final models, followed by slope at 5 km scale, total curvature at 5 km scale, depth and rugosity (Figure 3.44). Three predictors did not occur in any final models: cosine of aspect, sine of annual mean bottom current direction and profile curvature.

The relative importance of each environmental predictor variable, as measured by the permutation and jackknife tests, was assessed for each DSC group. The following five variables were most consistently important, in decreasing order of the average frequency at which they were identified: depth, distance to shore, slope at 5 km scale, total curvature at 5 km scale and annual bottom temperature.

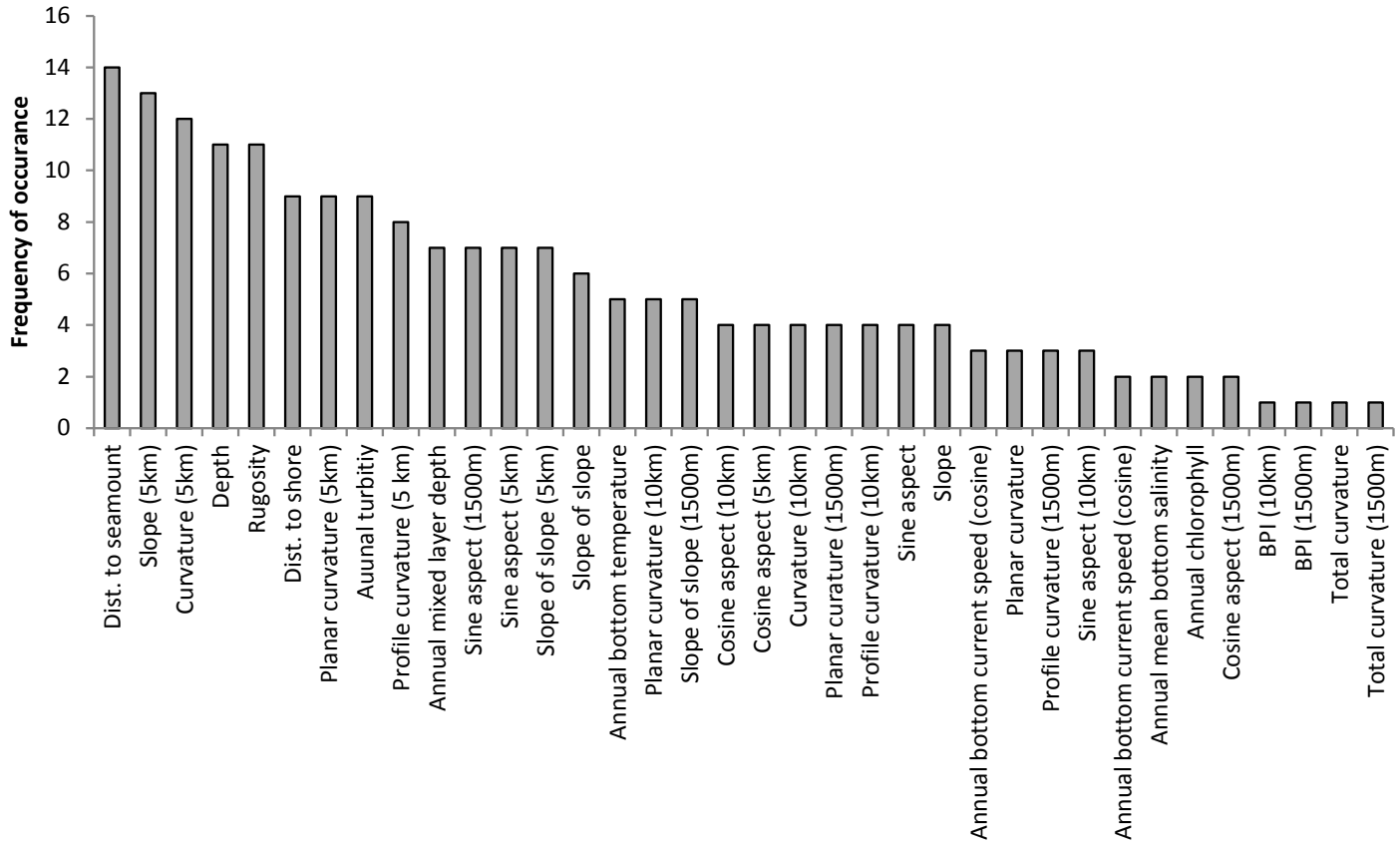

Figure 3.44. Frequency of occurrence of predictors in final DSC habitat suitability models in the MHI.

Data and Information Gaps

While predicted spatial distributions of areas likely to contain suitable DSC habitat broadly aligned with the distributions of DSC presence records, in some cases areas outside the extent of the DSC presence records were predicted as highly likely to contain suitable habitat although they seem unlikely to support corals. For example, the area extending southeast from Oʻahu that was predicted as highly likely to contain suitable habitat for many of the DSC groups probably represents an area of overprediction of suitable habitat for gold corals and red/pink corals. Red/pink coral habitat suitability is also likely overpredicted in a swath south of Lānaʻi. For bubblegum corals, there is likely not highly suitable habitat in the north end of Kāneʻohe Bay on Oʻahu as predicted by the model. In these cases, overprediction of the likelihood of suitable habitat could result from the relatively low numbers of model grid cells with coral presences, particularly for gold corals and bubblegum corals. For the shallow Antipatharia, areas south of Lānaʻi and north of Oʻahu predicted as highly likely to contain suitable habitat are likely too deep. Although care was taken to divide the Antipatharia records into

shallow, mid-depth, and deep groups by genera, it is possible that some records may have been misclassified. Finally, for Antipatharia there was a zone with robust predictions of high likelihood of suitable habitat between Molokini and Mā'alaea Bay where no coral presence existed. While it is possible that environmental conditions in this area could provide suitable habitat for Antipatharia that have been fished out, it is suspected that this area has predominantly soft substrate that would not be suitable for Antipatharia (F. Parrish, pers. comm.).

Although the habitat suitability models for DSC represent a foundation for further exploration and assessment, several improvements could be made in the future with improved data. The current availability of presence-only records restricted the modeling techniques that could be used to model the distribution of DSC. In addition, there is large (±1 km or more) positional uncertainty associated with the coral presence data (C. Kelley, pers. comm. and unpublished data). Currently, there is one GPS record available per transect, which may span several km in length. Thus, all taxa observed along a transect are attributed to that location, which may be over 1 km away from the true location. Were presence-absence data and more accurate geopositional information available, additional modeling avenues could be explored, such as BRT. In addition, for many of the DSC groups there were considerably fewer presence records on the windward sides of islands. Because absence data were not available, it is unclear if this was due to lack of effort or if there is not suitable DSC habitat on the windward sides of the islands. Additional surveys in these areas are needed.

Additional predictor variables and improved coverage and resolution of existing variables may further improve the models. For this effort, we used a bathymetry synthesis at a 90 m grid resolution (see Chapter 2) as this was the best available dataset encompassing the entire study area. However, the distribution of deep-sea corals may be influenced by finer scale features that are not captured at this resolution. A 5 m grid resolution multibeam/LiDAR synthesis layer (see Chapter 4; HMRG, 2015) is available for the nearshore areas of the MHI and could potentially be used in finer-scale models for localized areas of interest. However, as previously mentioned the positional uncertainty in the coral presence data makes using finer scale data difficult because coral presence records may be in the wrong pixel or even many pixels away from their true location, and associated with the wrong features and environmental characteristics. In addition, the resolution of other predictors (e.g., oceanographic variables, currents) is much coarser, ranging from 1x1 km to 9x9 km. Downsampling these predictors to the 360x360 m scale involves significant assumptions, but downsampling even further is unsupportable. Hence, finer-scale versions of the other predictors would be needed to reduce model resolution further.

A comprehensive sediment grain size dataset, which can be used to create a layer depicting surficial sediment grain size and composition, is not available for the MHI, but this has proven to be an important predictor in other regions (NOAA NCCOS, 2015). A backscatter synthesis is currently available at the same resolution and extent as the 5 m resolution bathymetry synthesis; however, this was not utilized for similar reasons (e.g., limited spatial coverage and depth extent) and due to numerous radiometric and geometric artifacts that would propagate through the modeling process. An updated backscatter synthesis out to the 500 m depth contour is currently in development (C. Kelley, pers. comm.), which may prove more useful for future modeling efforts. The usSEABED database (http://walrus.wr.usgs.gov/usseabed/index.html), which is a compilation of information on surficial and subbottom sediment grain size and composition, does not currently include data for MHI, although the area is slated for inclusion in a future publication.

The habitat suitability model results presented here can be used in several ways. For several groups, areas of very high likelihood of habitat suitability occurred in areas with no existing coral presence records. These areas often share characteristics with regions with existing presence records and could be targeted for future exploration. For example, model predictions could be overlaid with finer resolution backscatter, bathymetry, and depth derivatives such as slope to identify target hardbottom areas to select for submersible deployment.

ACKNOWLEDGEMENTS

Many thanks to Chris Kelley at the Hawai'i Undersea Research Lab for sharing his data, time, and expertise. Data providers for the shallow-water benthic cover dataset include Alan Friedlander (University of Hawai'i at Mānoa), Ku'ulei Rodgers (University of Hawai'i at Mānoa), Bernardo Vargas-Ángel (NOAA PIFSC CREP), William Walsh (Hawai'i DAR), Steve Cotton (Hawai'i DAR), Eric Brown (NPS), Eric Conklin (TNC), Dwayne Minton (TNC), Russell Sparks (Hawai'i DAR), and Ivor Williams (NOAA PIFSC CREP). Bernardo Vargas-Ángel provided useful comments and editorial assistance. Chris Kelley and Michael Parke (NOAA PIFSC) evaluated model outputs and provided useful comments.

LITERATURE CITED

Aeby, G.S., J.C. Kenyon, J.E. Maragos, and D.C. Potts. 2003. First record of mass coral bleaching in the Northwestern Hawaiian Islands. Coral Reefs 22(3): 256.

Agostinelli, C. and U. Lund. 2013. R package, circular: Circular statistics. R-Forge. Software Downloaded January 2014. Software Online: https://r-forge.r-project.org/projects/circular (Site Accessed 8 June 2016).

Akaike, H. 1974. A new look at the statistical model identification. IEEE Transactions on Automatic Control 19(6): 716-723. doi: 10.1109/TAC.1974.1100705.

Battista, T.A., B.M. Costa, and S.M. Anderson. 2007. Benthic Habitats of the Main Hawaiian. NOAA Technical Memorandum NOS NCCOS CCMA 152. Silver Spring, MD. 48 pp. Data Downloaded 5 September 2014. Data Website: https://products.coastalscience.noaa.gov/collections/benthic/e97hawaii/data2007.aspx (Site Accessed 8 June 2016).

Brown, E.K., E. Cox, P.L. Jokiel, S.K. Rodgers, W.R. Smith, B.N. Tissot, S.L. Coles, and J. Hultquist. 2004. Development of benthic sampling methods for the Coral Reef Assessment and Monitoring Program (CRAMP) in Hawai'i. Pacific Science 58(2): 145-158.

Burnham, K.P. and D.R. Anderson. 2002. Model selection and multimodel inference: a practical information-theoretic approach. Springer-Verlag, New York. 488 pp.

Cesar, H.S.J. and P.J.H. van Beukering. 2004. Economic valuation of coral reefs of Hawai'i. Pacific Science 58(2): 231-242.

Clague, D.A. 1996. The growth and subsidence of the Hawaiian-Emperor volcanic chain. pp. 35-50. In: A. Keast and S.E. Miller (eds.), The origin and Evolution of Pacific Island Biotas, New Guinea to Eastern Polynesia: Patterns and Processes. SPB Academic Publishing, Amsterdam, The Netherlands. 537 pp.

CMECS. 2015. Coastal and Marine Ecological Classification Standard. Online: https://cmecscatalog.org/ (Site Accessed 8 June 2016).

Coles, S.L. and E.K. Brown. 2007. Twenty-five years of change in coral coverage on a hurricane impacted reef in Hawai'i: the importance of recruitment. Coral Reefs 26: 705-717.

Costa, B., M.S. Kendall, F.A. Parrish, J. Rooney, R.C. Boland, M. Chow, J. Lecky, A. Montgomery, and H. Spalding. 2015. Identifying Suitable Locations for Mesophotic Hard Corals Offshore of Maui, Hawai'i. PLoS ONE 10(7): e0130285. doi:10.1371/journal.pone.0130285.

Coyne, M.S., T.A. Battista, M. Anderson, J. Waddell, W. Smith, P. Jokiel, M.S. Kendall, and M.E. Monaco. 2003. Benthic Habitats of the Main Hawaiian Islands – Interim Product. NOAA Technical Memorandum NOS NCCOS CCMA 152. Silver Spring, MD. 48 pp.

DAR. 2015. Coral Reefs: Monitoring. State of Hawai'i, Department of Land and Natural Resources, Division of Aquatic Resources. Honolulu, HI. Online: http://dlnr.hawaii.gov/coralreefs/monitoring/ (Site Accessed 8 June 2016).

Davies, A.J. and J.M. Guinotte. 2011. Global habitat suitability for framework-forming cold-water corals. PLos ONE 6(4): e18483.

DSCRTP. 2015. NOAA Deep-Sea Coral Data Portal. NOAA National Marine Fisheries Service, Office of Habitat Conservation, NOAA Deep-Sea Coral Research and Technology Program. Data Downloaded 16 September 2014. Data Website: https://deepseacoraldata.noaa.gov/ (Site Accessed 8 June 2016).

Elith, J., S.J. Phillips, T. Hastie, M. Dudík, Y.E. Chee, and C.J. Yates. 2011. A statistical explanation for MaxEnt for ecologists. Diversity and Distributions 17: 43-57.

ESRI. 2011. ArcGIS Desktop: Release 10. Environmental Systems Research Institute. Redlands, CA. Online: http://www.esri.com/ (Site Accessed 8 June 2016).

Federal Register. 2013. Fisheries in the Western Pacific; 5-Year Extension of Moratorium on Harvest of Gold Corals. 78 Fed. Reg. 18302 (March 26, 2013)(to be codified at 50 CFR 665). NOAA National Marine Fisheries Service.

Fenner, D. 2005. Corals of Hawai'i: a field guide to the hard, black and soft corals of Hawai'i and the Northwest Hawaiian Islands, including Midway. Mutual Publishing, Honolulu, HI. 192 pp.

Fielding, A.H. and J.F. Bell. 1997. A review of methods for the assessment of prediction errors in conservation presence/absence models. Environmental Conservation 24: 38-49.

Fletcher, C.H., C. Bochicchio, C.L. Conger, M.S. Engels, E.J. Feirstein, N. Frazer, C.R. Glenn, R.W. Grigg, E.E. Grossman, J.N. Harney, E. Isoun, C.V. Murray-Wallace, J.J. Rooney, K.H. Rubin, C.E. Sherman, and S. Vitousek. 2008. Geology of Hawai'i reefs. pp. 435-487. In: B. Riegl and R.E. Dodge (eds.). Coral Reefs of the USA. Coral Reefs of the World, Volume 1. Springer Netherlands. 803 pp.

Fletcher, C.H. and E.J. Fiersten. 2010. Chapter 1.16 - Hawai'i. pp. 125-132. In: E.C.F. Bird (ed.), Encyclopedia of the World's Coastal Landforms. Springer Netherlands. 1,516 pp.

Franklin, E.C., P.L. Jokiel, and M.J. Donohue. 2013. Predictive modeling of coral distribution and abundance in the Hawaiian Islands. Marine Ecology Progress Series 481: 121-132.

Friedlander, A.M., E.K. Brown, and M.E. Monaco. 2007a. Coupling ecology and GIS to evaluate efficacy of marine protected areas in Hawaii. Ecological Applications 17: 715-730.

Friedlander, A.M., E.K. Brown, and M.E. Monaco. 2007b. Defining reef fish habitat utilization patterns in Hawai'i: comparisons between MPAs and areas open to fishing. Marine Ecology Progress Series 351: 221-233.

Friedlander, A., G. Aeby, E. Brown, A. Clark, S. Coles, S. Dollar, C. Hunter, P. Jokiel, J. Smith, B. Walsh, I. Williams, and W. Wiltse. 2008. The State of Coral Reef Ecosystems of the Main Hawaiian Islands. pp. 222-269. In: J.E. Waddell and A.M. Clarke (eds.), The State of Coral Reef Ecosystems of the United States and Pacific Freely Associated States: 2008. NOAA Technical Memorandum NOS NCCOS 73. Silver Spring, MD. 569 pp.

Friedlander, A., K. Keller, L. Wedding, A. Clarke, and M. Monaco. 2009. A Marine Biogeographic Assessment of the Northwestern Hawaiian Islands. NOAA Technical Memorandum NOS NCCOS 84. Prepared by NCCOS's Biogeography Branch in cooperation with the Office of National Marine Sanctuaries Papahānaumokuākea Marine National Monument. Silver Spring, MD. 363 pp.

Freiwald A., J.H. Fossa, A. Grehan, T. Koslow, and J.M. Roberts. 2004. Cold-water coral reefs. UNEP-WCMC, Cambridge, UK. 84 pp.

GEBCO. 2008. General Bathymetric Chart of the Oceans 08 Grid. GEBCO operates under the joint auspices of the International Hydrographic Organization and the Intergovernmental Oceanographic Commission of UNESCO. Data Downloaded 8 January 2014. Data Website: http://www.gebco.net/data_and_products/gridded_bathymetry_data/ (Site Accessed 8 June 2016).

Gibbs, A.E, S.A Cochran, J.B. Logan, and E.E. Grossman. 2007. Benthic Habitats and Offshore Geological Resources of Kaloko-Honokōhau National Historical Park, Hawai'i. U.S. Geological Survey Scientific Investigations Report 2006-5256. 62 pp.

Gibbs, A.E., S.A. Cochran, and P.W. Tierney. 2013. Seafloor video footage and still-frame grabs from U.S. Geological Survey cruises in Hawaiian nearshore waters: U.S. Geological Survey Data Series 735. 11 pp.

Grigg, R.W. 1993. Precious coral fisheries in Hawai'i and the U.S. Pacific Islands. Marine Fisheries Review 55(2): 50-60.

Grigg, R.W. 2010. The precious corals fishery management plan of the Western Pacific Regional Fishery Management Council. Pacific Islands Fishery Monographs 1: 1-9.

Guinotte, J.M. and A.J. Davies. 2014. Predicted deep-sea coral habitat suitability for the U.S. West Coast. PLoS ONE 9(4): e93918. doi: 10.1371/journal.pone.0093918.

Heenan, A., P. Ayotte, A. Gray, K. Lino, K. McCoy, J. Zamzow, and I. Williams. 2014. Pacific Reef Assessment and Monitoring Program Data Report: Ecological monitoring 2012-2013—reef fishes and benthic habitats of the main Hawaiian Islands, American Samoa, and Pacific Remote Island Areas. NOAA National Marine Fisheries Service, Pacific Islands Fisheries Science Center. PIFSC Data Report DR-14-003. 112 pp.

Hijmans, R.J. 2014. R package, Raster: Geographic data analysis and modeling. Software Downloaded October 2014. Software Website: http://CRAN.R-project.org/package=raster (Site Accessed 8 June 2016).

Hinderstein, L.M., J.C.A. Marr, F.A. Martinez, M.J. Dowgiallo, K.A. Puglise, R.L. Pyle, D.G. Zawada, and R. Appeldoorn. 2010. Theme section on "mesophotic coral ecosystems: Characterization, ecology, and management". Coral Reefs 29(2): 247-251.

HMRG. 2015. Hawai'i Mapping Research Group. Hawai'i Mapping Research Group, School of Ocean and Earth Science and Technology, University of Hawai'i at Manoa. Online: http://www.soest.hawaii.edu/HMRG/cms/ (Site Accessed 8 June 2016).

Hourigan, T.F., P.J. Etnoyer, R.P. McGuinn, C. Whitmire, D.S. Dorfman, M. Dornback, S. Cross, and D. Sallis. 2015. An Introduction to NOAA's National Database for Deep-Sea Corals and Sponges. NOAA Technical Memorandum NOS NCCOS 191. Silver Spring, MD. 27 pp.

HURL. 2015. Hawai'i Undersea Research Laboratory. Hawai'i Undersea Research Laboratory, School of Ocean and Earth Science and Technology, University of Hawai'i at Manoa and National Oceanic and Atmospheric Administration. Data Provided 28 May 2015. Provider Website: http://www.soest.hawaii.edu/HURL/index.html (Site Accessed 8 June 2016).

HYCOM Consortium. 2014. HYCOM + NCODA Global 1/12 Reanalysis. Funding for the development of HYCOM has been provided by the National Ocean Partnership Program and the Office of Naval Research. Data assimilative products using HYCOM are funded by the U.S. Navy. Computer time was made available by the DoD High Performance Computing Modernization Program. Data Downloaded 1 September 2014. Data Website: https://hycom.org/dataserver/glb-reanalysis (Site Accessed 8 June 2016).

Jenness, J. 2013. DEM Surface Tools. Jenness Enterprises. Software Downloaded November 2015. Software Online: http://www.jennessent.com/arcgis/surface_area.htm (Site Accessed 8 June 2016).

Jokiel, P.L. and E.K. Brown. 2004. Global warming, regional trends and inshore environmental conditions influence coral bleaching in Hawai'i. Global Change Biology 10: 1627-1641.

Jokiel, P.L., E.K. Brown, A. Friedlander, S. K. Rodgers, and W. R. Smith. 2004. Hawai'i Coral Reef Assessment and Monitoring Program: Spatial Patterns and Temporal Dynamics in Reef Coral Communities. Pacific Science 58(2): 159-174.

Jokiel, P.L., K.S. Rodgers, E.K. Brown, J.C. Kenyon, G. Aeby, W.R. Smith, and F. Farrell. 2015. Comparison of methods used to estimate coral cover in the Hawaiian Islands. PeerJ 3: e954.

Kahng, S.E., J.M. Copus, and D. Wagner. 2014. Recent advances in the ecology of mesophotic coral ecosystems (MCEs). Current Opinion in Environmental Sustainability 7: 72-81.

Kahng, S.E., J.R. Garcia-Sais, H.L. Spalding, E. Brokovich, D. Wagner, E. Weil, L. Hinderstein, and R.J. Toonen. 2010. Community ecology of mesophotic coral reef ecosystems. Coral Reefs 29: 255-275.

Kahng, S.E. and C.D. Kelley. 2007. Vertical zonation of megabenthic taxa on a deep photosynthetic reef (50-140 m) in the Au'au Channel, Hawai'i. Coral Reefs 26(3): 679-687.

Kelley, C. Hawai'i Undersea Research Laboratory (HURL), School of Ocean and Earth Science and Technology, University of Hawai'i at Manoa. Honolulu, HI. Personal Communication.

Kenyon, J.C. and R.E. Brainard. 2006. Second recorded episode of mass coral bleaching in the Northwestern Hawaiian Islands. Atoll Research Bulletin 543: 505-523.

Long, D.J. and A.R. Baco. 2014. Rapid change with depth in megabenthic structure-forming communities of the Makapu'u deep-sea coral bed. Deep-Sea Research II 99: 158-168.

Lumsden, S.E., T.F. Hourigan, A.W. Bruckner, and G. Dorr (eds.). 2007. The State of Deep Coral Ecosystems of the United States. NOAA Technical Memorandum CRCP-3. Silver Spring, MD. 365 pp.

Maragos, J.E. 1995. Revised checklist of extant shallow-water stony coral species from Hawaii (Cnidara: Anthozoa: Scleractinia). Bishop Museum Occasional Papers 42: 54-55.

Merow, C., M.J. Smith, and J.A. Silander, Jr. 2013. A practical guide to MaxEnt for modeling species' distributions: what it does, and why inputs and settings matter. Ecography 36: 1058-1069.

Moore, J.G. 1987. Subsidence of the Hawai'i Ridge. pp. 85-100. In: R.W. Decker, T.L. Wright, and P.H. Stauffer (eds.), Volcanism in Hawai'i. U.S. Geological Survey Professional Paper 1350. 1,667 pp.

Mortensen, P.B. and L. Buhl-Mortensen. 2004. Distribution of deep-water gorgonian corals in relation to benthic habitat features in the Northeast Channel (Atlantic Canada). Marine Biology 144: 1223-1238.

NASA. 2013. Ocean Color Web - Standard, Aqua MODIS Chlorophyll Concentration, OCI Algorithm, Daily, 4 km. National Aeronautics and Space Administration, Goddard Space Flight Center, Ocean Biology Processing Group. Data Downloaded 7 October 2013. Data Website: http://oceancolor.gsfc.nasa.gov/cgi/l3 (Site Accessed 8 June 2016).

Neilson, B. 2014. Coral Bleaching Rapid Response Surveys September-October 2014. State of Hawai'i, Department of Land and Natural Resources, Division of Aquatic Resources. Online: http://dlnr.hawaii.gov/reefresponse/files/2014/10/DARCoralBleachingSrvy_Results_10.28.2014.pdf (Site Accessed 8 June 2016)

NOAA CREP. 2015. Coral Reef Ecosystem Program. NOAA National Marine Fisheries Service, Pacific Islands Fisheries Science Center. Honolulu, HI. Online: http://www.pifsc.noaa.gov/cred/ (Site Accessed 8 June 2016).

NOAA FHUS. 2015. Comparing Reef Fish Habitat Use Patterns In and Out of Hawaiian Marine Protected Areas. Fish Habitat Utilization Study, Projects Explorer. NOAA National Ocean Service, National Centers for Coastal Ocean Science. Online: http://coastalscience.noaa.gov/projects/detail?key=31 (Site Accessed 8 June 2016).

NOAA NCCOS. 2015. Deep coral predictive habitat modeling in the U.S. Atlantic and Gulf of Mexico: focusing on uncharted deep-sea corals. Projects Explorer. NOAA National Ocean Service, National Centers for Coastal Ocean Science. Online: https://coastalscience.noaa.gov/projects/detail?key=35 (Site Accessed 8 June 2016).

NOAA NCEI. 2005. U.S. Coastal Relief Model - Hawaii. National Oceanic and Atmospheric Administration, National Environmental Satellite, Data, and Information Service, National Centers for Environmental Information. Data Downloaded 8 January 2014. Data Website: https://www.ngdc.noaa.gov/mgg/coastal/grddas10/grddas10.htm (Site Accessed 8 June 2016).

NPS I&M. 2015. National Park Service, Inventory and Monitoring. Online: http://science.nature.nps.gov/im/ (Site Accessed 8 June 2016).

Parrish, F.A. NOAA National Marine Fisheries Service, Pacific Islands Fisheries Science Center, Protected Species Division. Honolulu, HI. Personal Communication.

Parrish, F.A. and A.R. Baco. 2007. State of Deep Coral Ecosystems in the U.S. Pacific Islands Region: Hawaii and the U.S. Pacific Territories. pp. 155-194. In: S.E. Lumsden, T.F. Hourigan, A.W. Bruckner, and G. Dorr (eds.), The State of Deep Coral Ecosystems of the United States. NOAA Technical Memorandum CRCP-3. Silver Spring, MD. 365 pp.

Parrish, F.A. 2015. Settlement, colonization, and succession patterns of gold coral *Kulamanamana haumeaae* in Hawaiian deep coral assemblages. Marine Ecology Progress Series 533: 135-147.

Phillips, S.J., M. Dudik, and R.E. Schapire. 2004. A maximum entropy approach to species distribution modeling. pp. 655-662. In: R. Greiner and D. Schuurmans (eds.), Proceedings of the 21st International Conference on Machine Learning. Banff, Canada. ACM Press.

Phillips, S.J., R.P. Anderson, and R.E. Schapire. 2006. Maximum entropy modeling of species geographic distributions. Ecological Modeling. 190: 231-259.

Phillips, S.J. and M. Dudík. 2008. Modeling of species distributions with MaxEnt: new extensions and comprehensive evaluation. Ecography 31: 161-175.

PIFSC. 2014. Optical Analysis Overview. NOAA National Marine Fisheries Service, Pacific Islands Fisheries Science Center. Data Provided 29 February 2012. Provider Website: https://pifsc-www.irc.noaa.gov/cred/ (Site Accessed 8 June 2016)

Roberts, J.M., A.J. Wheeler, and A. Freiwald. 2006. Reefs of the deep: the biology and geology of cold-water coral ecosystems. Science 312: 543-547.

Roberts, J.M., A.J. Wheeler, A. Freiwald, and S. Cairns. 2009. Cold-water corals: the biology and geology of deep-sea coral habitats. Cambridge University Press, New York, NY. 334 pp.

Roberts J.J., B.D. Best, D.C. Dunn, E.A. Treml, and P.N. Halpin. 2010. Marine Geospatial Ecology Tools: An integrated framework for ecological geoprocessing with ArcGIS, Python, R, MATLAB, and C++. Environmental Modelling & Software 25(10): 1197-1207.

Rodgers, K.S., P.L. Jokiel, E.K. Brown, S. Hau, and R. Sparks. 2014. Over a Decade of Change in Spatial and Temporal Dynamics of Hawaiian Coral Reef Communities. Pacific Science 69(1): 1-13.

Rooney, J., E. Donham, A. Montgomery, H. Spalding, F. Parrish, R. Boland, D. Fenner, J. Gove, and O. Vetter. 2010. Mesophotic coral ecosystems in the Hawaiian Archipelago. Coral Reefs 29:361-367.

Sing, T., O. Sander, N. Beerenwinkel, and T. Lengauer. 2005. ROCR: visualizing classifier performance in R. Bioinformatics 21(20): 7881.

Sinniger, F., O.V. Ocaña, and A.R. Baco. 2013. Diversity of zoanthids (Anthozoa: Hexacorallia) on Hawaiian seamounts: description of the Hawaiian gold coral and additional zoanthids. PLoS ONE 8: e52607.

Spalding, H.L. 2012. Ecology of mesophotic macroalgae and *Halimeda kanaloana* meadows in the Main Hawaiian Islands. PhD Dissertation, University of Hawai'i. 199 pp.

Tittensor, D.P., A.R. Baco, P.E. Brewin, M.R. Clark, M. Consalvey, J. Hall-Spencer, A.A. Rowden, T. Schlacher, K.I. Stocks, and A.D. Rogers. 2009. Predicting global habitat suitability for stony corals on seamounts. Journal of Biogeography 36:1111-1128.

TNC. 2015. The Nature Conservancy Hawai'i Marine Program. Online: http://www.nature.org/ourinitiatives/regions/northamerica/unitedstates/hawaii/index.htm (Site Accessed 8 June 2016).

UH CRAMP. 2015. Coral Reef Assessment and Monitoring Program. Hawai'i Institute of Marine Biology, School of Ocean and Earth Science and Technology, University of Hawai'i at Manoa. Online: http://cramp.wcc.hawaii.edu/CRAMP_Information/overview.htm (Site Accessed 8 June 2016).

UH FERL. 2015a. Compilation of reef fish data. Fisheries Ecology Research Lab, College of Natural Sciences, University of Hawai'i at Manoa. Data Provided 11 December 2015. Provider Website: https://fisheriesecologyresearchlab.wordpress.com (Site Accessed 8 June 2016).

UH FERL. 2015b. University of Hawai'i Fisheries Ecology Research Lab. College of Natural Sciences, University of Hawai'i at Manoa. Data Provided 11 December 2015. Provider Website: https://fisheriesecologyresearchlab.wordpress.com (Site Accessed 8 June 2016).

UH PIBHMC. 2008. Main Hawaiian Islands: Maui, Optical Validation. Pacific Islands Benthic Habitat Mapping Center, School of Ocean and Earth Science and Technology, University of Hawai'i at Mānoa. Online: http://www.soest.hawaii.edu/pibhmc/pibhmc_mhi_mai_optical.htm (Site Accessed 8 June 2016).

USGS. 2015. The 3DEP National Map (1/3 arc-second DEMs for Hawai'i). The National Map. U.S. Geological Survey. Data Downloaded 15 September 2015. Data Website: http://viewer.nationalmap.gov/basic/?basemap=b1&category=ned,nedsrc&title=3DEP%20View#startUp (Site Accessed 8 June 2016).

USGS. 2016. Hawaiian Volcano Observatory. U.S. Geological Survey. Online: http://hvo.wr.usgs.gov/ (Site Accessed 8 June 2016).

Vierod, A.D.T., J.M. Guinotte, and A.J. Davies. 2013. Predicting the distribution of vulnerable marine ecosystems in the deep sea using presence-background models. Deep-Sea Research II 99:6-18.

Wagner, D., D.M. Opresko, A.D. Montgomery, and F.A. Parrish. 2015. Chapter 6: Spotlight: An Update on Recent Research and Management of Hawaiian Black Corals. pp. 6.1-6.15. In: Hourigan, T.F., P.J. Etnoyer, S.D. Cairns, and C.F. Tsao (eds.). The State of Deep-Sea Coral and Sponge Ecosystems of the United States: 2015. NOAA Technical Memorandum. Silver Spring, MD.

Wagner, D., X. Pochon, L. Irwin, R.J. Toonen, and R.D. Gates. 2011. Azooxanthellate? Most Hawaiian black corals contain Symbiodinium. Proceedings of the Royal Society B 278: 1,323-1,328.

Walsh, W., S. Cotton, C. Barnett, C. Couch, L. Preskitt, B. Tissot, and K. Osada-D'Avella. 2013. Long-Term Monitoring of Coral Reefs of the Main Hawaiian Islands. Final Report, 2009 NOAA Coral Reef Conservation Program: Hawai'i Island Monitoring Report. State of Hawai'i, Department of Land and Natural Resources, Division of Aquatic Resources. 97 pp.

Warren, D.L., R.E. Glor, and M. Turelli. 2010. ENMTools: a toolbox for comparative studies of environmental niche models. Ecography 33: 607-611.

Warren, D.L. and S.N. Seifort. 2011. Ecological niche modeling in Maxent: the importance of model complexity and the performance of model selection criteria. Ecological Applications 21(2): 335-342.

Wedding, L., A. Friedlander, M. McGranaghan, R. Yost, and M.E. Monaco. 2008. Using bathymetric Lidar to define nearshore benthic habitat complexity: implications for management of reef fish assemblages in Hawaii. Remote Sensing of Environment 112: 4159-4165.

Wright, D.J., M. Pendleton, J. Boulware, S. Walbridge, B. Gerlt, D. Eslinger, D. Sampson, and E. Huntley. 2012. ArcGIS Benthic Terrain Modeler (BTM), v. 3.0. Environmental Systems Research Institute, NOAA Coastal Services Center, Massachusetts Office of Coastal Zone Management. Software Downloaded February 2014. Software Website: http://esriurl.com/5754 (Site Accessed 8 June 2016).

WoRMS Editorial Board. 2014. World Register of Marine Species. Online: http://marinespecies.org (Site Accessed 8 June 2016).

Yesson, C., M.L. Taylor, D.P. Tittensor, A.J. Davies, J. Guinotte, A. Baco, J. Black, J.M. Hall-Spencer, and A.D. Rogers. 2012. Global habitat suitability of cold-water octocorals. Journal of Biogeography 39: 1278-1292.

Yost, A.C., S.L. Peterson, M. Gregg, and R. Miller. 2008. Predictive modeling and mapping sage grouse (*Centrocercus rophasianus*) nesting habitat using Maximum Entropy and a long-term dataset from Southern Oregon. Ecological Informatics 3: 375-386.

Chapter 4 Fishes

BOTTOM FISH
Laughlin Siceloff[1,3], Matthew S. Kendall[1], Reginald Kokubun[9], Jeffrey Drazen[10], and Virginia Moriwake[10]

REEF FISH
Kostantinos A. Stamoulis[8], Matthew Poti[1,3], Jade M.S. Delevaux[11], Mary K. Donovan[8], Alan Friedlander[8], and Matthew S. Kendall[1]

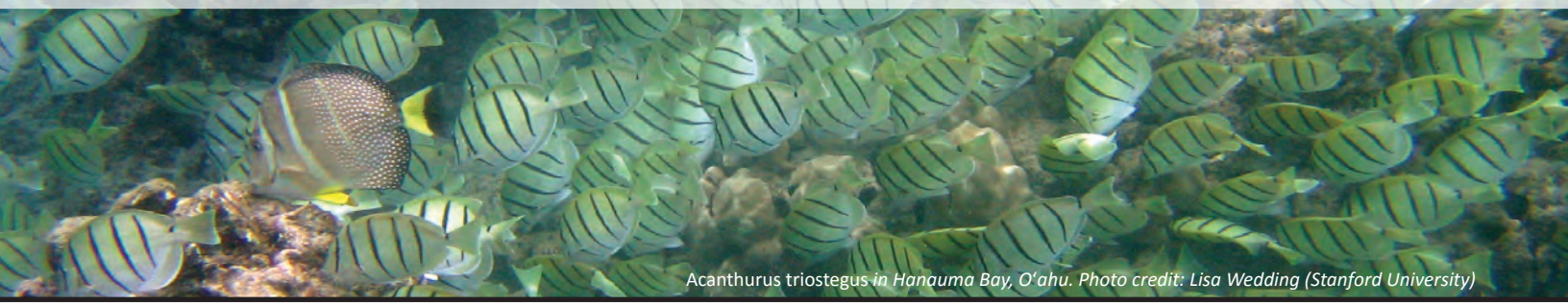

Acanthurus triostegus *in Hanauma Bay, O'ahu. Photo credit: Lisa Wedding (Stanford University)*

ABSTRACT

Understanding distributions of Hawaiian fish communities will be an important component of minimizing impacts from developing offshore wind power. Reef-, bottom-, and pelagic-fishes may each be affected by the construction and ongoing presence of mooring systems, floating platforms, and transmission cables. Pelagic fishes will likely utilize new offshore structures as they do the existing network of Fish Aggregating Devices. Bottom fish distributions were evaluated spatially using recent fisheries-dependent (Hawai'i's Division of Aquatic Resources catch reports) and fisheries-independent (bottom camera) data. Focused on the 'Deep 7' species of commercial importance, data were summarized around each island using the State's catch reporting framework and Bureau of Ocean Energy Management's (BOEM) lease-block system. The fisheries-dependent dataset indicates that the winter months and specific areas are most important to the fishery such as Penguin Bank, Maui Nui channels, west Hawai'i, southern Maui, and northern Moloka'i. The fishery-independent dataset also highlights the importance of Penguin Bank and Maui Nui, and offers an effective approach for site-specific assessments. Analysis of reef fish distributions was based on a compilation of visual survey datasets and was focused on total species richness and biomass, endemic species richness and biomass, and biomass of commercial fishes. Spatial predictions of these variables were generated for each island on a 60 m grid to help plan for the narrow right-of-way needed for power transmission cables. Predictions were created using boosted regression tree models relating the survey data to predictor variables representing seafloor topography, habitat, geography, and oceanography. Reef fish variables showed highest values in areas least accessible to humans, such as the Hamakua and Puna districts on the island of Hawai'i, northern Moloka'i, eastern Maui and northeastern O'ahu. Conversely, areas more accessible to humans had overall lower richness and biomass values and included Kailua Kona, west Maui and southern O'ahu. Findings were limited by data gaps in several areas including a lack of bottom fish catch data around Kaua'i and Ni'ihau, as well as less bottom-camera samples around Kaua'i, Ni'ihau, Moloka'i, western Hawai'i and Maui Nui apart from Penguin Bank and the channels. Data gaps that limited analyses for reef fish included a lack of samples in northwest and eastern Moloka'i, northern and southeast Maui, southwest O'ahu, northern exposures of the island of Hawai'i, Kaua'i and Lāna'i, and all of Ni'ihau and Kaho'olawe. In addition, a lack of high-resolution bathymetry prevented predictive modelling in several areas.

Citation for Bottom Fish section
Siceloff, L., M.S. Kendall, R. Kokubun, J. Drazen, and V. Moriwake. 2016. Chapter 4: Fishes - Bottom Fish. pp. 137-155. In: B.M. Costa and M.S. Kendall (eds.), Marine Biogeographic Assessment of the Main Hawaiian Islands. Bureau of Ocean Energy Management and National Oceanic and Atmospheric Administration. OCS Study BOEM 2016-035 and NOAA Technical Memorandum NOS NCCOS 214. 359 pp.

Citation for Reef Fish section
Stamoulis, K.A., M. Poti, J.M.S. Delevaux, M.K. Donovan, A. Friedlander, and M.S. Kendall. 2016. Chapter 4: Fishes - Reef Fish. pp. 156-196. In: B.M. Costa and M.S. Kendall (eds.), Marine Biogeographic Assessment of the Main Hawaiian Islands. Bureau of Ocean Energy Management and National Oceanic and Atmospheric Administration. OCS Study BOEM 2016-035 and NOAA Technical Memorandum NOS NCCOS 214. 359 pp.

[1] *NOAA National Centers for Coastal Ocean Science, Biogeography Branch, Silver Spring, MD, U.S.A.*
[3] *CSS-Dynamac, Fairfax, VA, U.S.A.*
[8] *University of Hawai'i at Mānoa, Fisheries Ecology Research Lab, Hawai'i, U.S.A.*
[9] *State of Hawai'i, Department of Land and Natural Resources, Division of Aquatic Resources, Hawai'i, U.S.A.*
[10] *University of Hawai'i at Mānoa, Deep-Sea Fish Ecology Lab, Hawai'i, U.S.A.*
[11] *University of Hawai'i at Mānoa, Department of Natural Resources and Environmental Management, Hawai'i, U.S.A.*

Fishes

4.1. INTRODUCTION

Fish communities in the state of Hawai'i can be divided into three broad categories based on their primary habitat. These are reef fishes, bottom fishes, and pelagic fishes. Reef fishes include a diverse assemblage of species that are strongly associated with structurally complex habitats such as coral reefs and other hard bottoms in the shallow (0-50 m) coastal fringes around the Hawaiian Islands. Nearly all reef fish habitat in the Main Hawaiian Islands (MHI) is in State waters within 3 nm of shore. Hawai'i's nearshore marine environment provides many ecosystem services, has cultural importance for the native Hawaiian community (Kikiloi and Graves, 2010), and is vital to the 11.4 billion dollar per year tourism industry (Friedlander et al., 2008). The economic value of Hawai'i's coral reefs was estimated at $10 billion, with direct economic benefits of $360 million per year in 2002 (Cesar and van Buekering, 2004). A portion of this is derived from nearshore fisheries, which are a combination of commercial, recreational, and subsistence catch (Friedlander et al., 2014). Despite their significance, reef fish populations have decreased dramatically around Hawai'i due to high fishing pressure, land-based pollution, habitat destruction, and other threats (Williams et al., 2008; Friedlander et al., 2014).

Reef fish communities may primarily be impacted by offshore wind development activities such as the construction of power transmission lines through the reef zone that connect offshore production facilities to the onshore electrical grid. Essential Fish Habitat (EFH) is defined collectively for the MHI Coral Reef Ecosystem by the Western Pacific Regional Fishery Management Council (WPRFMC), and includes the water column and all bottom habitat to a maximum depth of 50 fathoms within the Exclusive Economic Zone (EEZ; NOAA NMFS, 2016; Figure 4.1). In addition, a network of dozens of state and federal marine protected areas (MPA) have been established to assist with reef fish management (Figure 4.1).

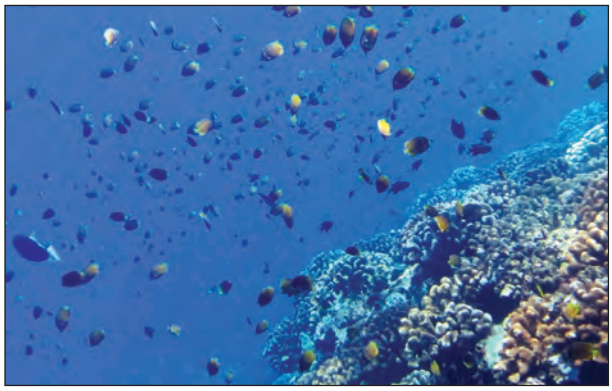

Reef fish assemblage. Photo credit: Kostantinos Stamoulis (University of Hawai'i)

Bottom fishes consist primarily of eteline snappers found in deeper water (100-400 m) and are targeted by a mixture of commercial, recreational, cultural, and subsistence fishermen (Hospital and Beavers, 2012). Annual catch reported by commercial fishermen reached 1.2 million pounds in 1988, but has ranged between 300 and 500 thousand pounds in recent years (DAR, 2012; Hospital and Beavers, 2012). Bottom fishes are often found at structurally complex habitats with hard bottom and/or high slope, but may also be found on other bottom types (Misa et al., 2013; Moore et al., 2013). In the MHI, approximately 50 percent of bottom fish habitat lies in State waters (Parke, 2007), with large areas in Federal waters on Penguin Bank and Middle Bank.

Bottom fish Hyporthodus quernus. *Photo credit: NOAA NMFS/ PIFSC*

Bottom fish communities may primarily be impacted by the construction and ongoing presence of mooring systems that secure wind turbines to the seafloor, as well as transmission lines that pass through these deeper habitats (Hammar et al., 2014). WPRFMC designated EFH for adult and juvenile bottom fishes as the water column and all bottom habitat extending from the shoreline to a depth of 400 m (WPRFMC, 2009; NOAA NMFS, 2016; Figure 4.1). The fishery is managed through a total-allowable-catch quota that once surpassed, results in closure of the fishery until the next fishing season. Also, a group of 12 Bottom Fish Restricted Fishing Areas (BRFA) have been established as MPAs as an additional management tool (Parke, 2007; Moore et al., 2013; Sackett et al., 2014; Figure 4.1).

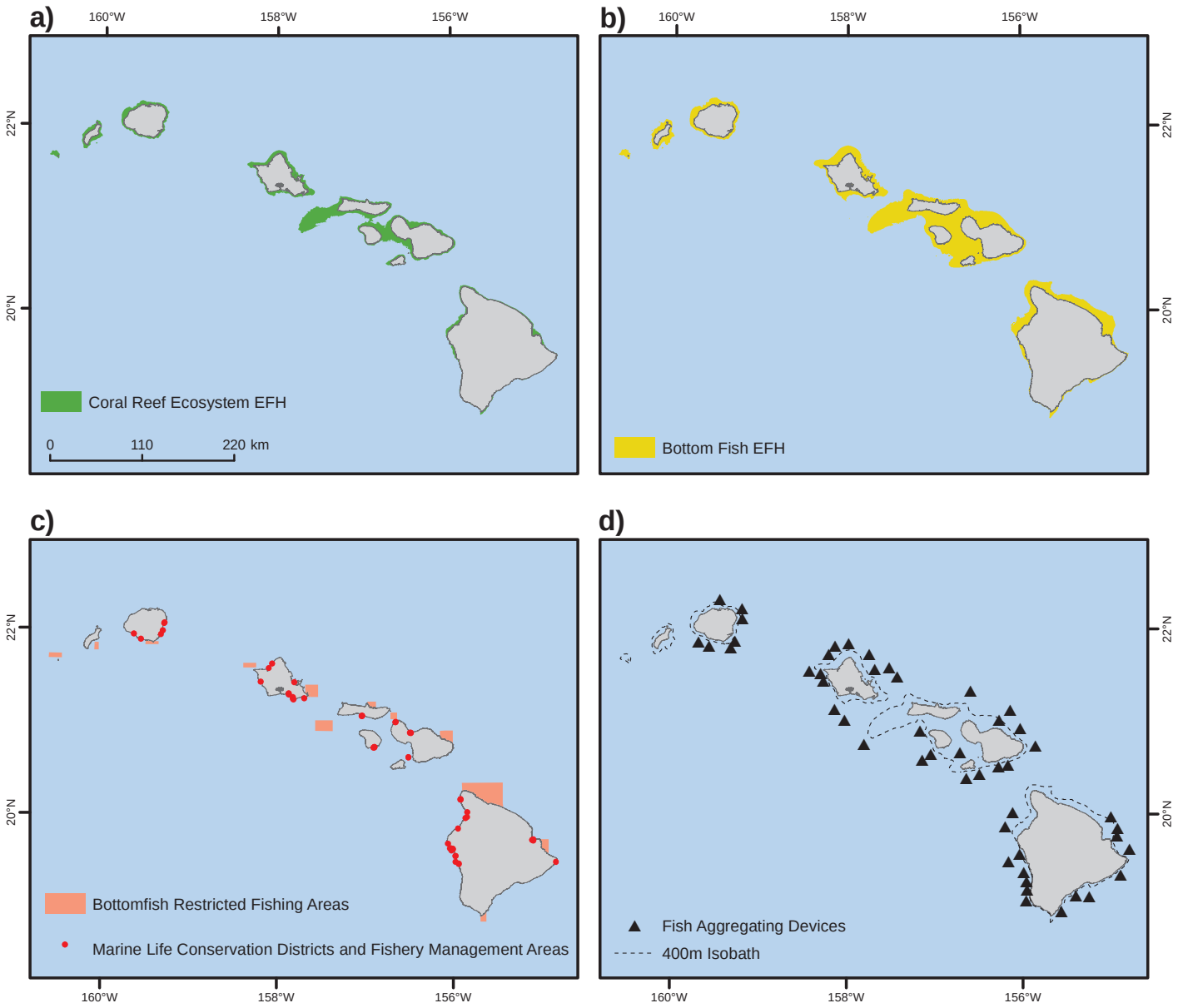

Figure 4.1. Management areas for reef, bottom, and pelagic fishes (various dates). Locations of a) Essential Fish Habitat (EFH) for coral reef ecosystems; b) bottom fish; c) Bottom Fish Restricted Fishing Areas (BRFAs) and marine protected areas for reef fish; and d) Fish Aggregation Devices (FADs). Data sources: a) NOAA NMFS, 2016; b) NOAA NMFS, 2016; c) NOAA MPA Center, 2014; d) State of Hawai'i, 2016 and HIMB, 2014.

Both reef fishes and bottom fishes are closely associated with particular habitats and have heterogeneous but predictable spatial distributions. Biogeographic characterization of reef and bottom fish communities will be an important part of predicting and minimizing impacts from construction and operation of offshore wind facilities, and is the focus of this chapter of the assessment. Geographic locations including bays, banks, points, and cities relevant to reef fish or bottom fish distributions are noted in a locator map (Figure 4.2).

The third category of fishes is pelagic, and includes tunas, billfish, sharks, and other species that inhabit the open ocean. Although the largest sector of Hawaiian fisheries (DAR, 2012) in both landings and value, previous studies of catch data and fish behavior indicate that these taxa have several characteristics that make them unsuitable for this assessment. Specifically, they: 1) can be found anywhere throughout the EEZ of the MHI during any season or year (He et al., 1997; Itano and Holland, 2000; Gilman et al., 2012); 2) can rapidly move from one distant location to another (Brill et al., 1999; Itano and Holland, 2000; Sibert et al., 2003); and 3) will be highly attracted to any physical structure placed anywhere offshore (Brill et al., 1999; Itano and Holland, 2000; Holland, 2011; Robert et al., 2012). Further analysis for spatial or temporal patterns would

Fishes

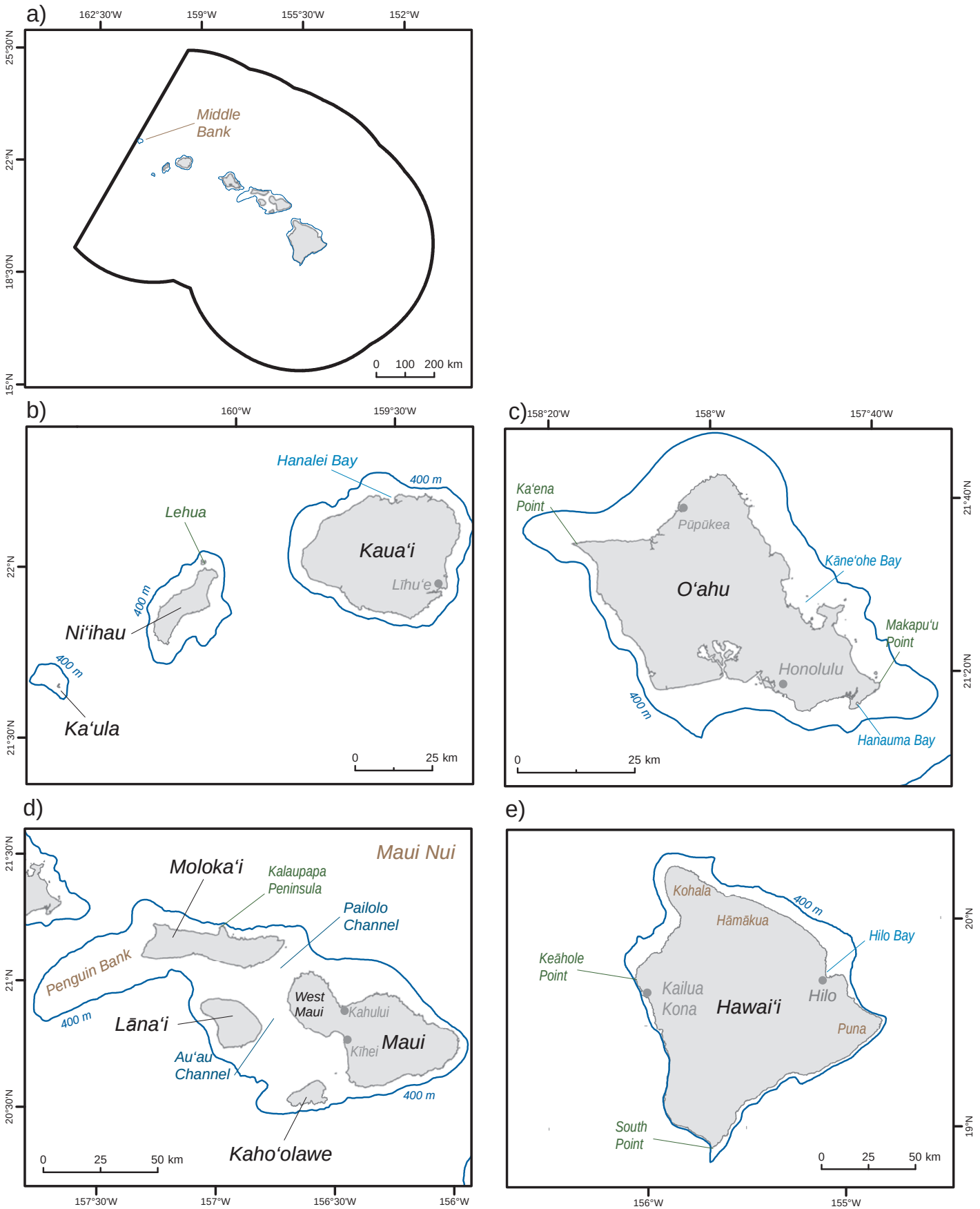

Figure 4.2. Key geographic features and place names around the Main Hawaiian Islands (MHI). These maps depict geographic features that are referenced in this chapter for: a) the project area; b) Ka'ula, Ni'ihau and Kaua'i; c) O'ahu; d) Maui Nui, which includes Moloka'i, Lāna'i, Maui and Kaho'olawe; and e) the island of Hawai'i. All depths are in meters. Data sources: shoreline (Battista et al., 2007), elevation (USGS, 2015) and depths (NOAA NCEI, 2005; GEBCO, 2008)

not yield useful products for planning development of offshore energy resources given the unpredictable distribution of these fishes and that new structures, such as a wind power generating platform, will alter present distributions. A network of Fish Aggregating Devices (FADs) around the MHI operated by the Hawai'i Institute of Marine Biology (HIMB), School of Ocean and Earth Science and Technology, University of Hawai'i at Mānoa, in cooperation with Hawai'i's Division of Aquatic Resources (DAR) offers insight into those species that may be associated with future platforms floating offshore (HIMB, 2014). A list of pelagic species most commonly caught at FADs in various seasons can be found at the HIMB website along with a list of coordinates for the FAD network that is updated periodically with information on which FADs may have recently broken free, been replaced, or discontinued. FAD locations are also included in the geodatabase associated with this project (Figure 4.1). Although certain to be affected by offshore wind development, pelagic fishes will not be included in this biogeographic analysis as a result of these issues.

4.2. BOTTOM FISHES

4.2.1. Methods and Data Description

Bottom fish data were obtained from two sources: 1) State of Hawai'i Commercial Marine Landings database from Department of Land and Natural Resources (DLNR)/DAR, and 2) Bottom Camera Bait Station data from University of Hawai'i at Mānoa's Deep Sea Fish Ecology Lab.

Fishery-Dependent Data

The goal of analyzing the DAR's commercial marine landing database was to examine the spatial distribution and seasonal patterns of fishing activity. Spatial patterns of catch and fishing effort could offer insight into patterns of bottom fish relative abundance and likely locations of significant bottom fish habitat. It is recognized that this fishery-dependent dataset tracks spatial patterns of human activity rather than bottom fish distribution per se. However, understanding spatial and seasonal patterns of fishing will be important for minimizing conflicts during construction and ongoing operation of offshore wind platforms. Interannual differences are available in DAR summary reports and were not the focus of this assessment (e.g., DAR, 2012).

Commercial fishermen are required to provide monthly reports to DAR specifying the species and number of bottom fish taken as well as the general location, method of harvest, and level of effort. Only the most recent decade of data available (2004-2013) was used in this analysis to best reflect present patterns of catch. Prior years of data were collected using a different format that is not readily comparable to current information. Also of note, although a change in enforcement of catch reporting was implemented in 2007 that resulted in greater reporting compliance, preliminary analysis revealed no difference in bottom fish catch patterns before or after this change. Therefore, all years were analyzed together. In their monthly reports, fishermen must specify the general area where the fishing activity took place using the "Commercial Fisheries Statistical Charts" provided by DAR. These charts divide Hawaiian waters into polygons of varying size and shape depending on distance from shore (DAR, 2015a; Figure 4.3). This is the most detailed level of catch location reported by fishermen. In this reporting framework, the perimeter of each island is separated into narrow segments from the shoreline to approximately 2 nm offshore that include the coast and most shallow reef habitats. Farther offshore there is a zone from approximately 2-20 nm around each island that includes much of the deep bottom fish habitat. Then from approximately 20-80 nm, reporting zones fall into a semi-regular grid (1/3°x1/3° latitude and longitude) that is further broadened (1°x1°) in the outer EEZ. This irregular set of polygons and grids are hereafter referred to as reporting areas. Due to historical precedence, there is unfortunately no division for State and Federal waters at 3 nm. Also of note, the Bureau of Ocean Energy Management (BOEM) lease blocks are based on a 4.8x4.8 km grid, which is much smaller than the reporting area divisions and do not easily overlay with the chart format until the regular grid begins far offshore. For example, the 0-2 nm coastal zone is approximately the same width as the lease blocks. The 2-20 nm zones are 6-7 lease blocks wide and each include dozens of blocks. Nearly all bottom fish are taken in a boat-based fishery using mechanical haulers from which individual

Fishes

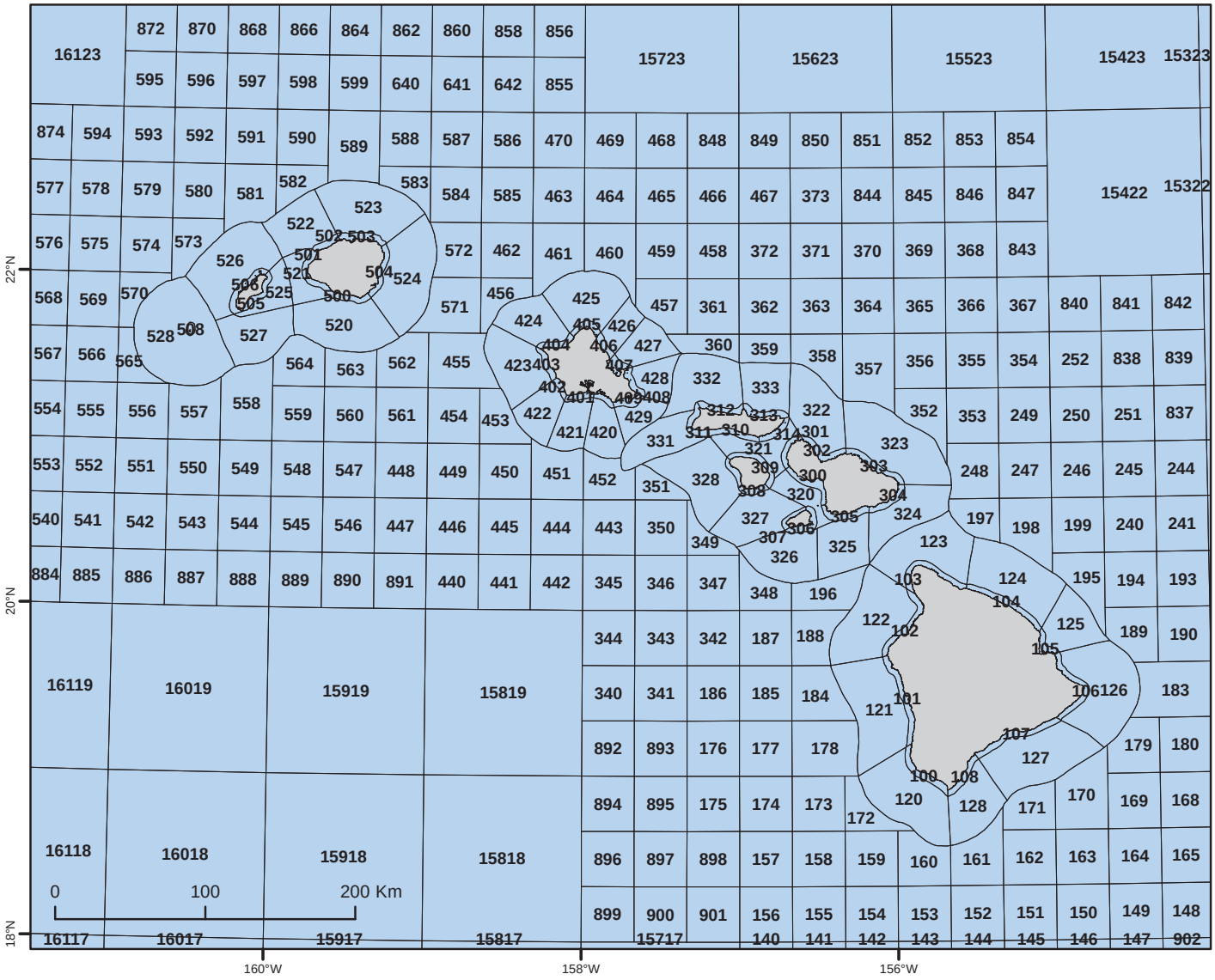

Figure 4.3. Commercial Fisheries Statistical Charts (2003). All commercial fishing effort and catch must be reported within this spatial framework. Data source: DAR, 2015a

"handlines" are deployed down to approximately 100-400 m depth. Typical terminal tackle on each line consists of a five pound bottom weight, 6-8 circle hooks baited with squid, and chum bags filled with chopped anchovy and squid to attract fish (WPRFMC, 2009). Most other gear types are prohibited (e.g., traps, trawls, gillnets) or ineffective for bottom fish. For this analysis, only DAR records reporting use of deep-sea handlines (DSHL) were considered.

There are 16 species of bottom fish that are commercially harvested, however, the "Deep 7" group of six snapper and one grouper species are considered the most valued and sought-after members of the bottom fish complex (Table 4.1). In this analysis, fishery catch was measured as "Catch in Pounds (Lbs)," fishing effort was measured as "Number of Trips," and catch-per-unit-effort (CPUE) was calculated as "Catch in Lbs/Number of Trips." These are the metrics used by DAR to report on the DSHL fishery, and by National Oceanic and Atmospheric Administration's (NOAA) National Marine Fisheries Service (NMFS) Pacific Islands Fisheries Science Center (PIFSC) for bottom fish stock assessment (DAR, 2012; Brodziak et al., 2014).

Table 4.1. Deep bottom fishes listed by Hawai'i's Division of Aquatic Resources (DAR, 2012), as commercially harvested.

Family	Species (Scientific Name)	Species (Hawaiian and Common Names)	Deep 7 (y/n)
Berycidae	*Beryx decadactylus*	Alfonsin, Alfonsino	n
Carangidae	*Seriola dumerili* or *S. rivoliana*	Kahala, Amberjack	n
Emmelichthyidae	*Erythrocles schlegelii, E. scintilii*	Golden Kale, Schlegel's Boga Fish, Japanese Rubyfish, Yanaginomai (per Myron Fuellas)	n
Lutjanidae	*Aphareus rutilans*	Lehi, Silverjaw Snapper, Ironjaw Snapper	y
Lutjanidae	*Aprion virescens*	Uku, Green Jobfish, Gray Snapper	n
Lutjanidae	*Etelis marshi* or *E. carbunculus (KL)*	Ula'ula, Ehu, Eahu, Red Snapper, Ruby Snapper	y
Lutjanidae	*Etelis coruscans*	Ula'ula Koa'e, Onaga, Ulu, Long-Tail Red Snapper	y
Lutjanidae	*Lutjanus kasmira*	Taape; Bluestripe Snapper	n
Lutjanidae	*Pristipomoides auricilla*	Yellowtail Kale, Purple Paka, Goldflag Jobfish	n
Lutjanidae	*Pristipomoides filamentosus*	'Ōpakapaka, Pink Snapper, Crimson Jobfish	y
Lutjanidae	*Pristipomoides sieboldii*	Kalekale, Kalikali, Siebold's Snapper	y
Lutjanidae	*Pristipomoides zonatus*	'Ūkīkiki, Gindai, Tai, Kindai, Kentai, Yellow-Barred Snapper, Oblique-Banded Snapper, Brigham's Snapper	y
Lutjanidae	*Randallichthys filamentosus*	Randall's Snapper; Bake-Akamutsu	n
Priacanthidae	*Cookeolus japonicus*	Aweoweo (Deepsea), Bulleye	n
Scorpaenidae	*Pontinus macrocephalus*	Hogo, Red Seabass, Largeheaded Scorpionfish, Oopu Kae Nohu	n
Serranidae	*Hyporthodus quernus*	Hāpu'upuu, Seabass, Shapon, Sapon	y

Two subsets of the DAR database were obtained for analysis: species-specific catch for the Deep 7, and total DSHL catch. First, species-level catch records were summed across all months and years to generate a single value of total catch for the Deep 7 within each reporting area. Preliminary evaluation revealed no spatial differences in catch patterns among months or years, and therefore we combined all seasons/years into a single analysis. Total catch, total effort and CPUE for Deep 7 were compared among reporting areas to identify locations of high fishing intensity and high catch. High catch and/or high CPUE were used to indicate presence of potentially important habitat areas. Those areas shallower than the 400 m isobath, the focus of the fishery, are highlighted in maps of catch and fishing effort. Due to confidentiality restrictions with the commercial fishery database, only 28.4 percent of records were available for this analysis.

The second data subset was the same in most respects but the separation by species was removed. This resulted in total catch values for the DSHL fishery grouped by area and month without any details of catch contents. This more general dataset had the benefit of less confidentiality restrictions, such that 79.1 percent of records were available and improved data coverage in areas with lower fishermen population or less participation in the reporting program (e.g., Kaua'i, parts of O'ahu; R. Kokobun, pers. comm.). This provided a better depiction of overall bottom fishing effort. In particular, this format provided more data for areas around Ni'ihau and Kaua'i that were poorly represented or absent altogether from the species-specific query. To examine seasonal differences in fishing intensity the DSHL dataset was examined separately by month. Fishing effort was grouped by month and summed across the 10 year time span, giving each reporting area multi-year sums of catch for each month. Preliminary analysis revealed that spatial patterns of relative effort were similar across all months, whereas the overall level of effort did vary seasonally. Therefore, we compared total values by month in bar graph format and compared spatial patterns in effort for December (highest effort) and July (lowest effort).

Fishes

Fishery-Independent Data

Fishery-independent assessment for bottom fish is based primarily on Bottom Camera Bait Station data (hereafter BotCam; Merritt et al., 2011; Misa et al., 2012; Moore et al., 2013). There are some bottom fish sightings from other sources, such as observations from submersibles (Kelley et al., 2006), but these are relatively infrequent, have limited spatial scope, are influenced by different biases (attraction or avoidance) than the BotCam data, and were therefore not used in this analysis. The goal of analyzing the BotCam data was to examine the spatial distribution, diversity and relative abundance of the Deep 7 bottom fish species.

BotCam is a stereo-video camera system developed by PIFSC specifically for fishery-independent sampling of deepwater bottom fish (Merritt et al., 2011). BotCam is deployed at depths of 100 to 300 m, is suspended approximately 3 m off the bottom, uses a bait similar to that used by bottom fishermen as an attractant, and typically records 30-45 minutes of video using ambient light. Fish are identified to the species level (not always possible for the *Pristipomoides* genus), and the video is used to calculate relative abundance at each deployment as the maximum number of a particular species observed in a single video frame, hereafter referred to as Nmax. Presence/absence, species richness and other measures of community structure can be derived from this data. Using available bathymetry and acoustic backscatter information, as well as video observations, BotCam sites are characterized as hard or soft bottom and high or low slope (Misa et al., 2013; Moore et al., 2013). This analysis is based on BotCam data collected from 2007-2014.

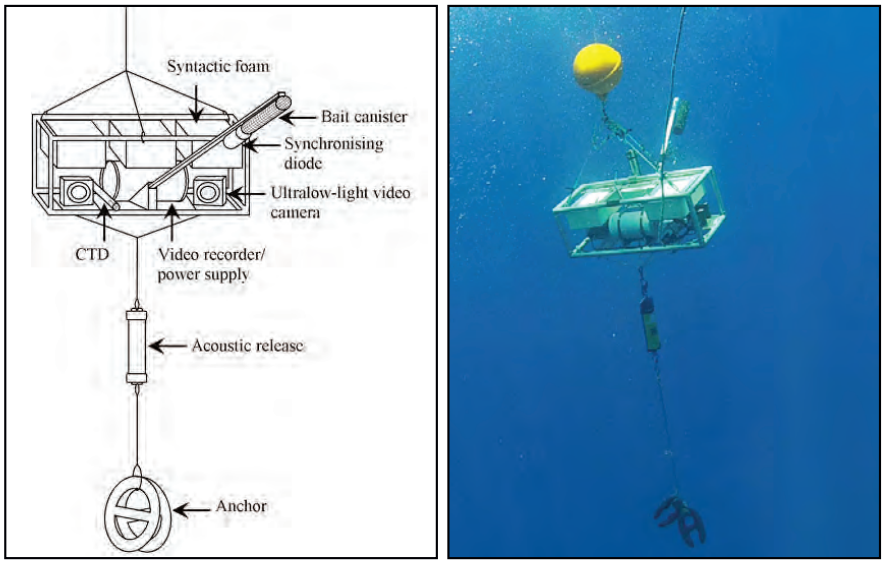

Schematic and photo of BotCam. Source/Credit: Jeff Drazen (University of Hawai'i)

The spatial distribution of BotCam sampling is uneven around the MHI (Figure 4.4). Some regions have been sampled extensively, such as those associated with monitoring of the BRFA (Moore et al., 2013; Sackett et al., 2014; Figure 4.1). Heavily sampled areas include southeastern Ni'ihau, O'ahu, Penguin Bank, West Maui and the eastern tip of the island of Hawai'i. Maps of BotCam samples are focused on each of these areas. Islands with less or no sampling include Kaua'i, Moloka'i and most of the island of the island of Hawai'i. Due to patchy distribution with dense concentration of sites in only some areas and low or no sampling in others, BotCam data were not readily amenable for interpolation or for creating spatially predictive models over the entire MHI as was done for reef fish and several other taxa in this report. Due to this patchiness, it was also difficult to visualize and interpret raw data points in map form at any scale. In order to account for the variable density of sites and analyze the data in a spatially standardized format, a simple grid was overlayed and used to calculate average values from multiple BotCam sites within each cell (Figure 4.4). This approach reduced the influence of any single data point, smoothed out unusual or extreme observations, conveyed the average patterns of relative abundance and diversity around each island, and highlighted the areas lacking data. BOEM's system of lease block aliquots (1.2x1.2 km) was an appropriate size relative to BotCam site density to serve as the spatial framework for this analysis. It should be noted that this scale is very broad relative to the habitat and depth ranges utilized by most species and the heterogeneity of bottom types in the region. Use of the aliquots also enables direct comparison of results to eventual permit applications for offshore energy development. For each Botcam site, the Nmax values for the Deep 7 were summed and species richness (0 to 7) was calculated.

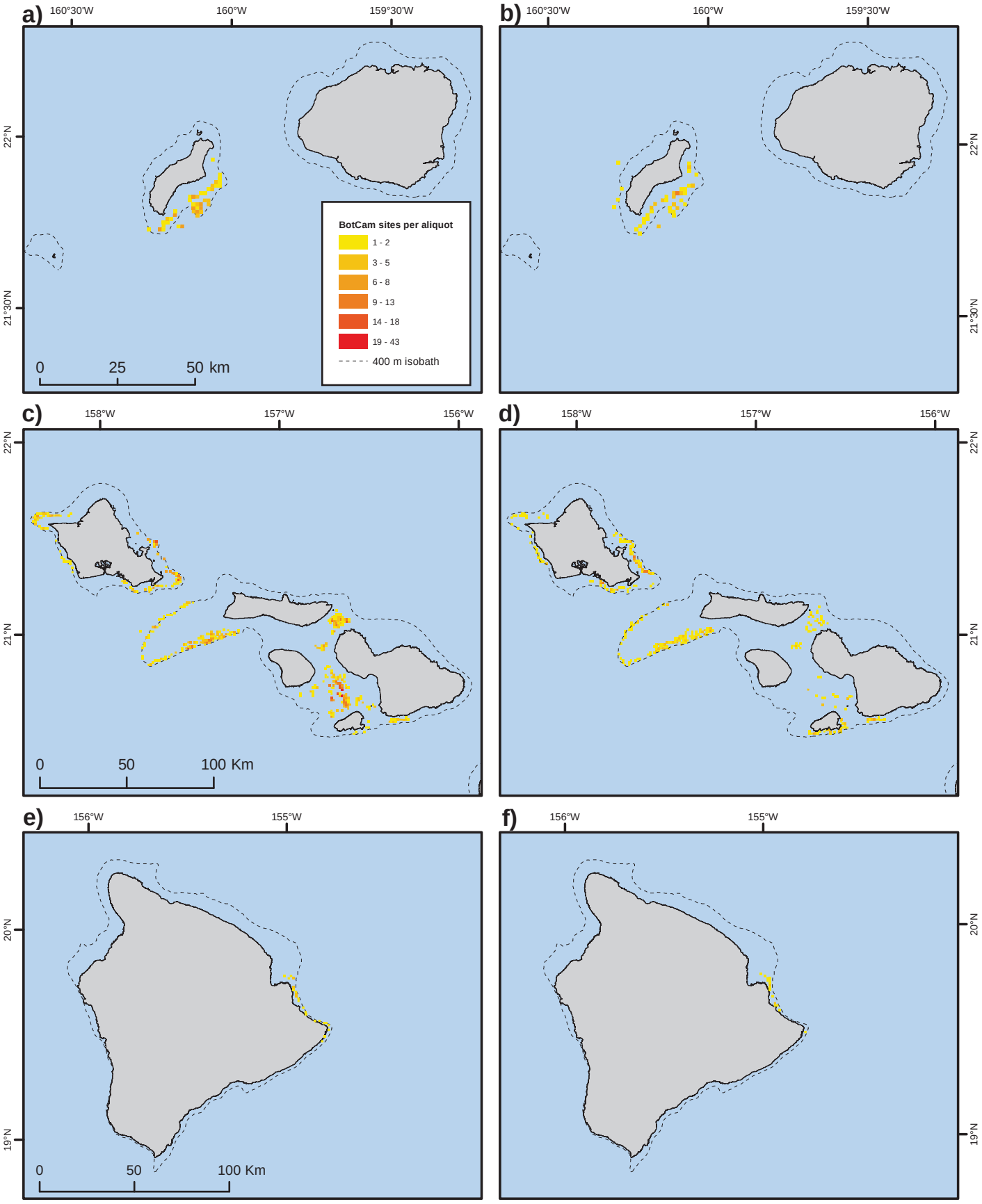

Figure 4.4. BotCam sampling effort (2007-2014). The number of sample sites within each BOEM lease block aliquot shown as: a) total hard substrate sites; b) total soft substrates sites per aliquot off Ni'ihau and Kaua'i; c) total hard substrate sites; d) total soft substrates sites per aliquot off O'ahu, Penguin Bank, and central Maui Nui; e) total hard substrate sites; and f) total soft substrates sites per aliquot off the island of Hawai'i. Data source: UH Deep-Sea Fish Ecology Lab, 2014

Fishes

Sites were separated by bottom type (hard versus soft) for all maps and analysis. This separation was necessary because bottom type is a significant factor determining bottom fish community structure (Misa et al., 2013; Moore et al., 2013) and because the proportion of hard and soft bottom sites varies among aliquots. It was therefore not appropriate to average observations made on these two bottom types. Using the values from each site, average Nmax, as well as average species richness, were calculated within each grid cell. This resulted in four maps for each area sampled; average Nmax and average species richness for hard and soft bottom respectively.

Only aliquots with a minimum of two sites on a given bottom type were included for analysis and mapped. Higher site-minimums were tested but resulted in substantial data loss. Average Nmax and average richness values for each grid cell were color coded using the natural breaks function in ArcGIS ESRI, 2011 and plotted around each island. The maximum depth of EFH designated for these species (400 m isobath) is highlighted for reference. In addition to the average Nmax and richness plots based on all Deep 7 species, individual plots for each species were produced. These were used to help determine which species were responsible for the geographic patterns in the data but are not included in this report.

4.2.2. Results: Spatial Distributions

Bottom fishes

Fishery-Dependent Data

The most popular and significant fishing areas for bottom fish are Penguin Bank (DAR reporting area 331) and the Maui Nui channels (areas 320, 321 and 327, between Maui, Lānaʻi, Molokaʻi and Kahoʻolawe; Figure 4.5). These areas show the highest catch and fishing effort for both Deep 7 and the DSHL fishery as a whole. Fishing occurs there year-round although it is reduced in summer months. Other areas of high catch and effort include the west side of the island of Hawaiʻi (121, 122), the south side of Maui (305) and north side of Molokaʻi (313). Penguin Bank, Maui Nui, and west Hawaiʻi are generally regarded as the best fishing grounds, with excellent bottom fish habitat and accessibility (R. Kokubun, pers. comm.). Some of these high-effort areas, such as those in Maui Nui, also show high CPUE as well. Other locales with high catch, such as Penguin Bank, have a counterintuitively lower CPUE. Despite being productive fishing grounds, such areas may experience high effort due to their proximity to major ports and population centers as well as their relatively sheltered weather conditions suitable for fishing. Low CPUE but high overall catch is observed at such locations.

Other high CPUE areas for either Deep 7 or the fishery as a whole include the Middle Bank (593), Niʻihau and Kauʻla (505, 506, 508, 525, 526, 528), Kauaʻi (522), north Molokaʻi (312, 313, 333), south island of Hawaiʻi (127, 128) and northeast island of Hawaiʻi (124; Figure 4.5). Many of these areas are distinguished by relatively low effort and low numbers of vessels potentially due to small local populations, long distance from ports, or weather conditions that offer few opportunities to access bottom fish habitats at those sites.

Example of bottom fish Pristipomoides zonatus *(at auction). Photo credit: Kurt Kawamoto (NOAA NMFS/PIFSC/FRMD)*

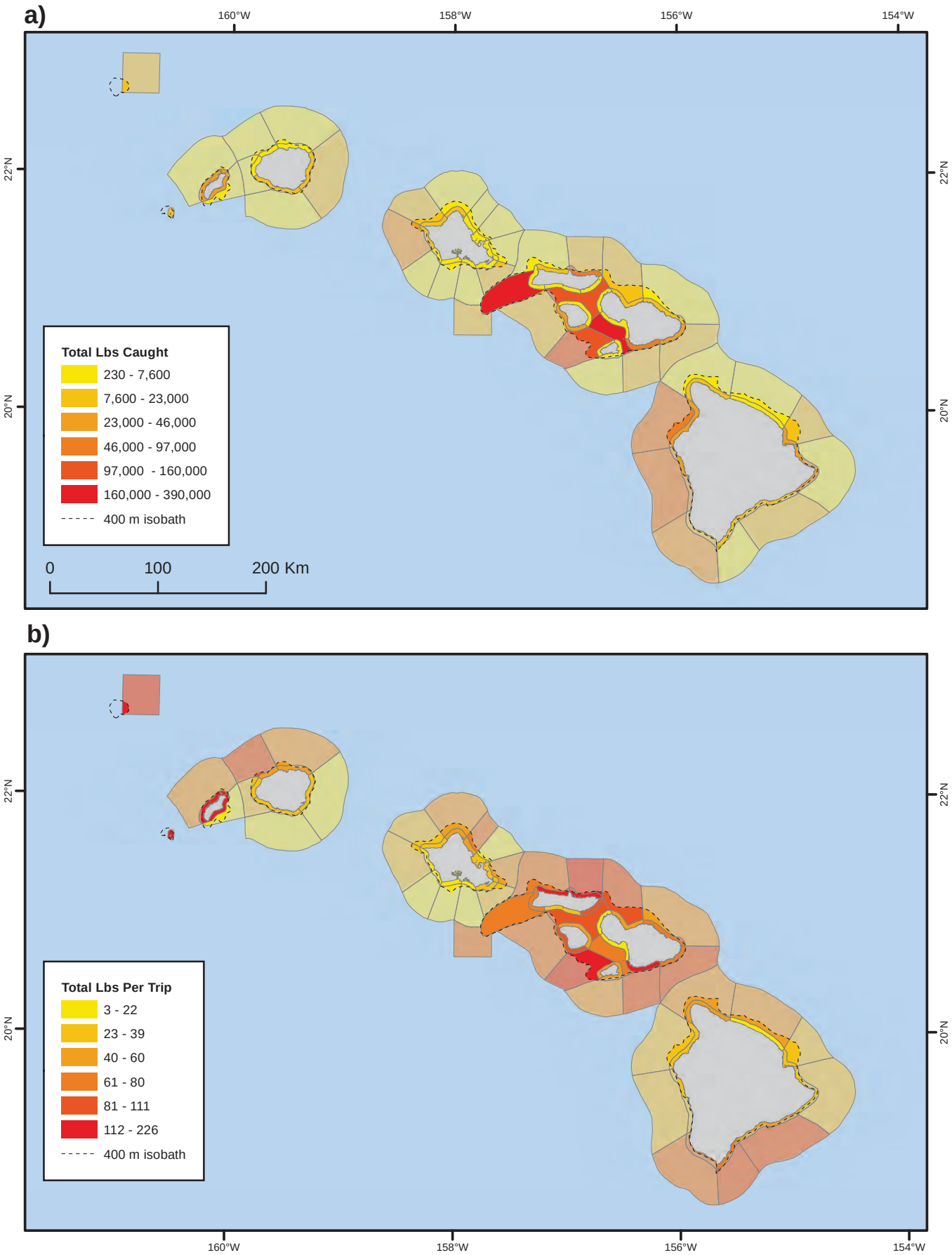

Figure 4.5. Commercial bottom fishing activity in the MHI (2004-2013): a) total catch of the Deep 7, and b) catch-per-unit-effort (CPUE) for Deep 7. Data source: DAR, 2014

Fishes

Most areas are not fished all months of the year. Comparison by month illustrates that the fishery peaks in winter months, both in terms of catch and effort, as well as number of areas fished (Figure 4.6). However, relative effort is consistently highest on Penguin Bank, Maui Nui and west Hawai'i regardless of month (Figure 4.7). There is no evidence from these data to suggest whether bottom fish spatial distribution or relative abundance changes seasonally.

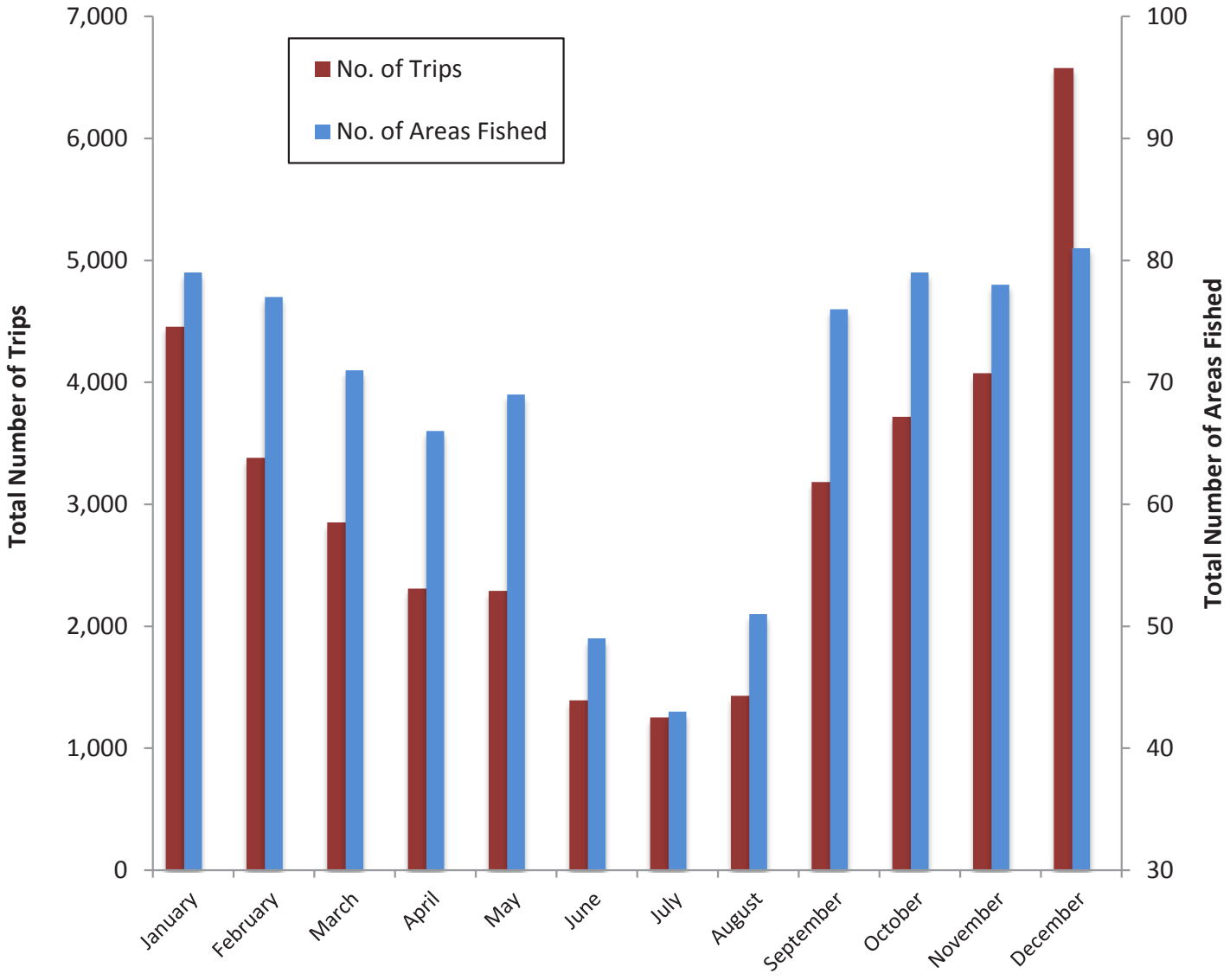

Figure 4.6. Monthly values for the deep-sea handline (DSHL) fishery (2004-2013). Total effort and number of reporting areas fished are summed by month. Data source: DAR, 2014

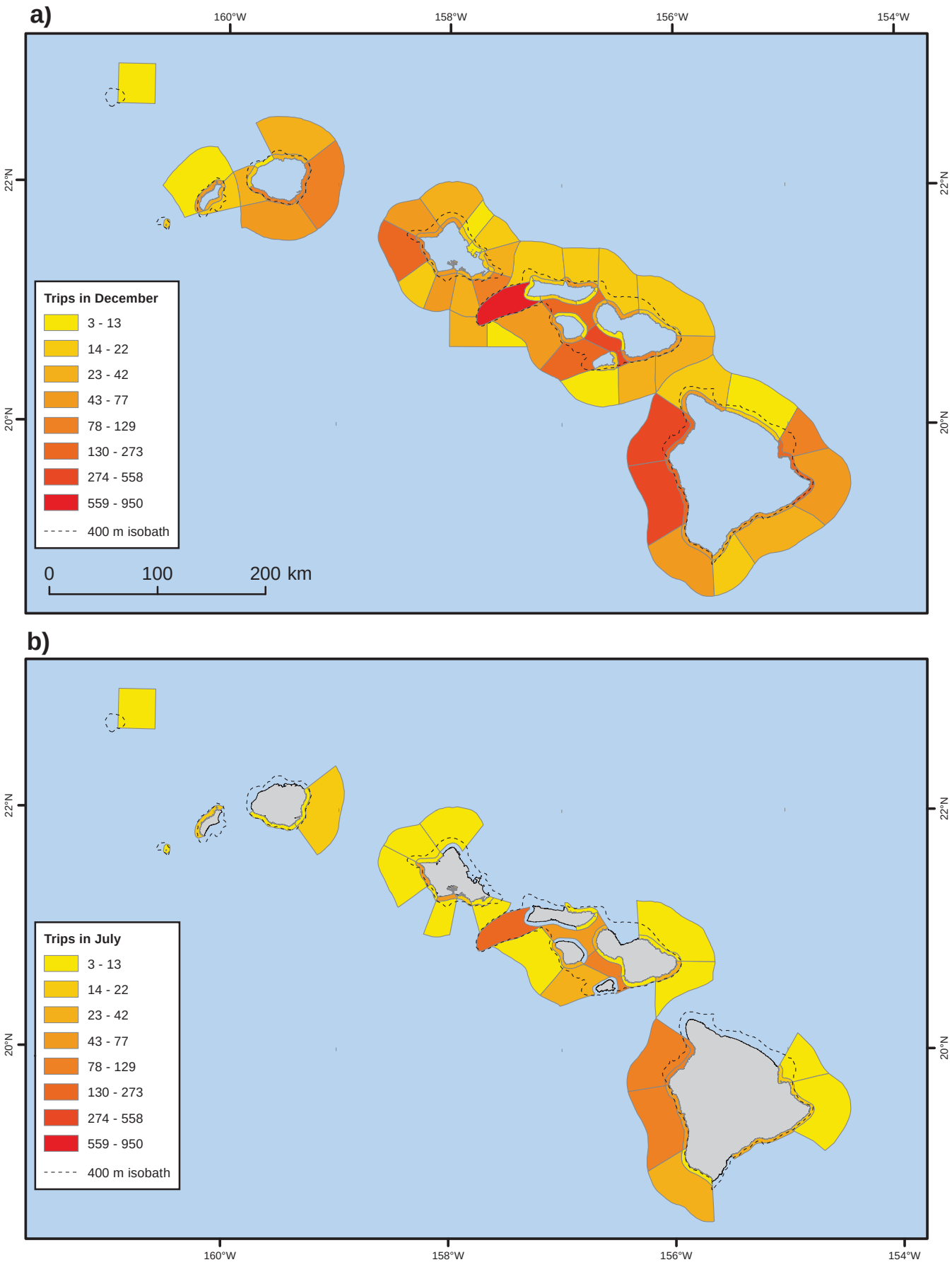

Figure 4.7. Seasonal comparison of DSHL fishery effort (2004-2013). Summed effort in a) December and b) July. Data source: DAR, 2014

Fishes

Fishery-Independent Data

In the BotCam data, three of the Deep 7 species were most frequently seen, occurred in highest abundance, and were responsible for most of the pattern in average abundance by aliquot. Specifically, *Etelis coruscans* occurred mostly in deeper cells (210-310 m) farthest from land, *Pristipomoides filamentosus* was found mostly in shallower cells (90-120 m), and *Pristipomoides seiboldii* at intermediate depths (180-270 m; Sackett et al., 2013). *Etelis carbunculus* were seen less frequently and two species, *Aphareus rutilans* and *Pristipomoides zonatus,* were detected quite infrequently, in very low abundance (Moore et al., 2013) and consequently were primarily influential only in the species richness analysis. In general, average abundance and richness values were higher for hard bottom than soft bottom.

Patterns of abundance and species dominance in the BotCam results varied among sampling areas. The east coast of the island of Hawai'i was sparsely sampled for both hard and soft bottom substrates. Average abundance on both bottom types along this coast was driven mainly by *P. filamentosus,* although it never occurred in high abundance compared to other regions (Figure 4.8). There were few observations of the

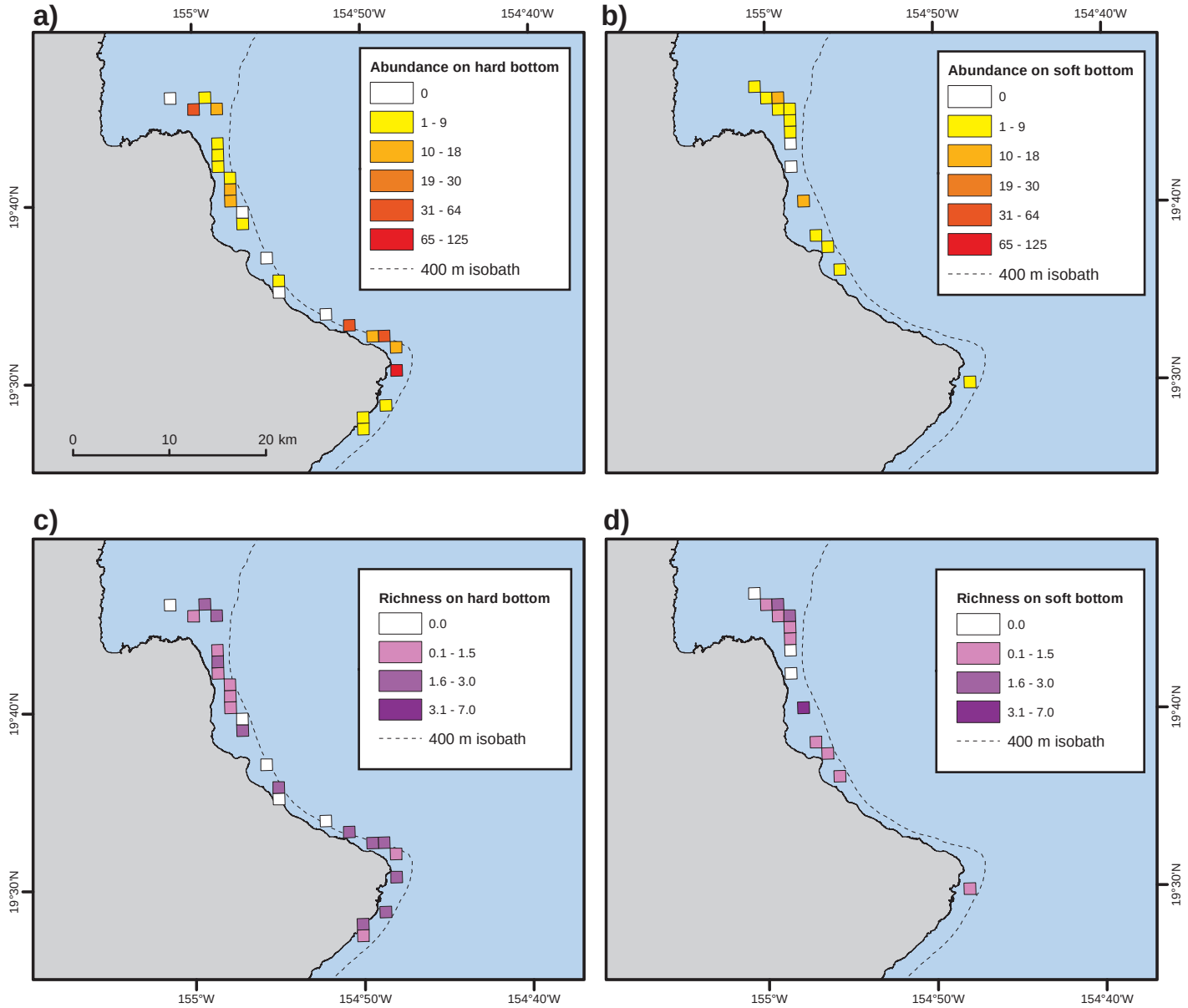

Figure 4.8. BotCam observations of the Deep 7 off eastern Hawai'i island (2007-2014): a) average abundance on hard bottom; b) average abundance on soft bottom; c) average species richness on hard bottom; and d) average species richness on soft bottom. Data source: UH Deep Sea Fish Ecology Lab, 2014

In situ *image from BotCam of* Etelis carbunculus. *Photo credit: Jeff Drazen (University of Hawai'i)*

other six species. In the channels of the Maui Nui area, soft bottom had very low bottom fish abundance in general and in many cases none were observed (Figure 4.9). The south side of Kaho'olawe had higher average abundance, mainly driven by *P. filamentosus* and *E. carbunculus,* with other species contributing only rarely to the species richness of this area. On hard bottom in the channels of Maui Nui, there were few *P. zonatus* and *Hyporthodus quernus*. Among the highest average abundances observed in the study occurred in the Pailolo Channel between west Maui and Moloka'i, as well as deeper areas northwest of Kaho'olawe, and were driven primarily by *E. carbunculus*, *P. seiboldii* and *E. coruscans* on hard bottom habitat. High average abundance in the shallower 'Au'au channel was due to *P. filamentosus*. The southern edge of Penguin Bank had some high average abundance values on both hard and soft bottom compared to the northern edge (Figure 4.10). Higher average abundance on soft substrate was due to bottom fish *E. carbunculus* in deeper waters, and *P. filamentosus* in shallower aliquots.

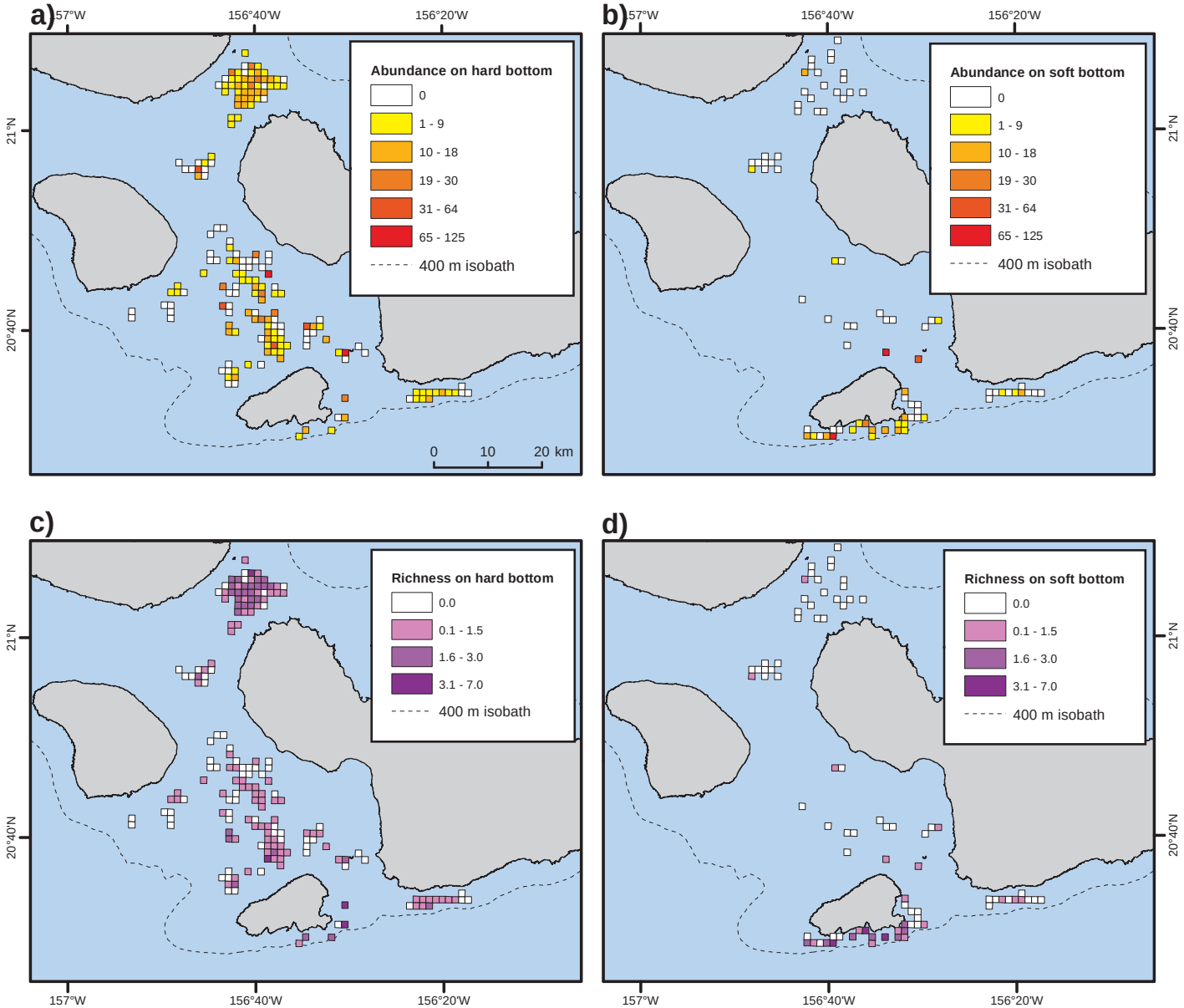

Figure 4.9. BotCam observations of the Deep 7 in central Maui Nui (2007-2014): a) average abundance on hard bottom; b) average abundance on soft bottom; c) average species richness on hard bottom; and d) average species richness on soft bottom. Data source: UH Deep Sea Fish Ecology Lab, 2014

Fishes

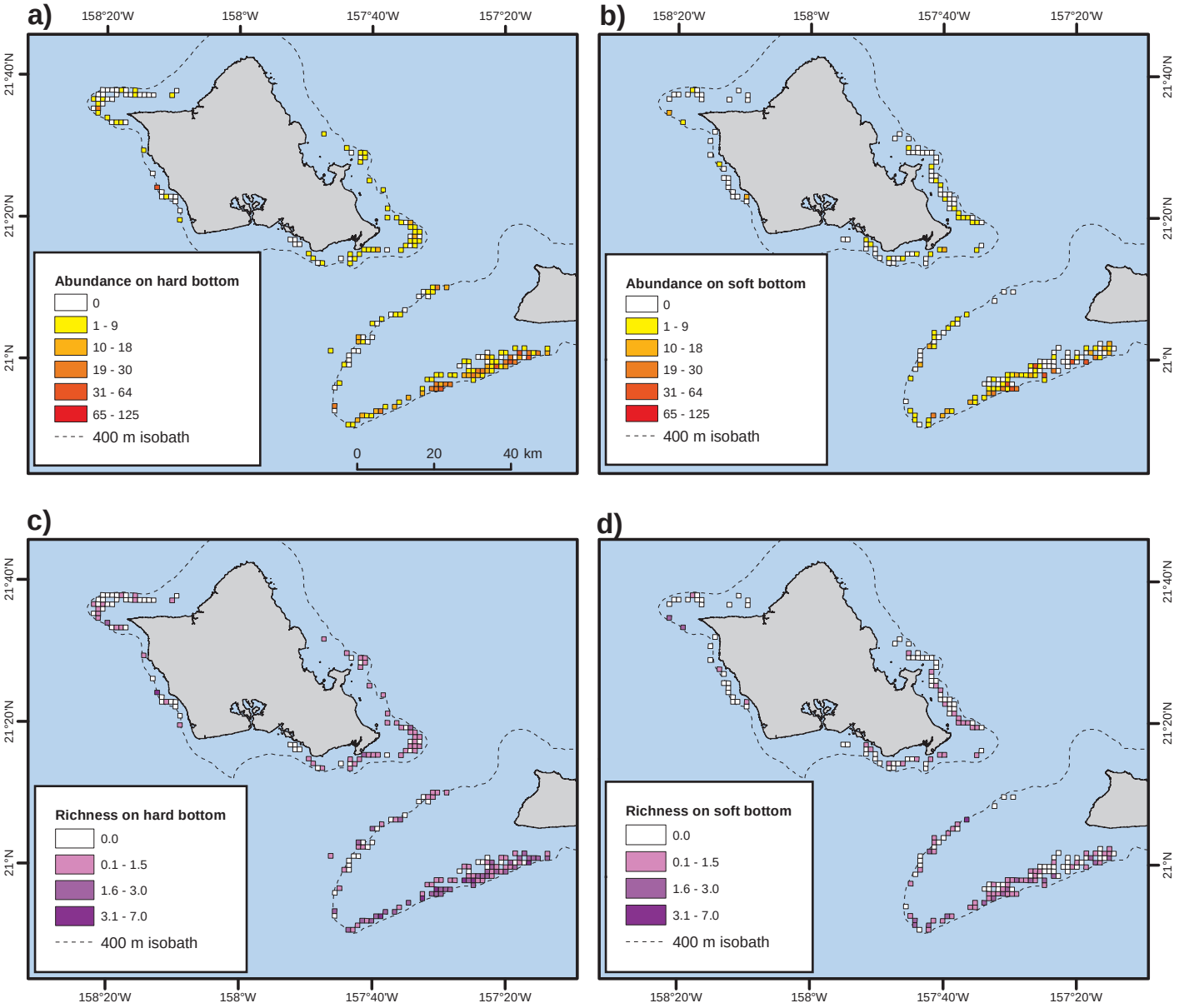

Figure 4.10. BotCam observations of the Deep 7 for Penguin Bank and O'ahu (2007-2014): a) average abundance on hard bottom; b) average abundance on soft bottom; c) average species richness on hard bottom; and d) average species richness on soft bottom. Data source: UH Deep Sea Fish Ecology Lab, 2014

Other species occurred less frequently and in low abundance but contributed to the higher species richness values on soft bottom along the southern edge of Penguin Bank. On hard substrate off the southern edge of Penguin Bank, higher average abundance was due to *E. coruscans* and *E. carbunculus* in deeper areas and *P. filamentosus* in shallower waters. The other species occurred less frequently and contributed mostly to the patterns in species richness. Around O'ahu, abundance and richness values were generally lower than in other regions when comparing the same bottom types. *P. filamentosus* was responsible for much of the pattern in higher abundance off of Ka'ena and Makapu'u Points. Off of southeastern Ni'ihau, on soft bottom, high average abundance was due mainly to *P. seiboldii*, *E. coruscans* and *E. carbunculus*, with only a few observations of *P. filamentosus* and *H. quernus* contributing to species richness (Figure 4.11). Off of southeastern Ni'ihau, on hard bottom, average abundance had high values relative to O'ahu and eastern Hawai'i island, and was driven mostly by *E. coruscans*, *E. carbunculus* and *P. seiboldii* with some *P. filamentosus* in shallower areas.

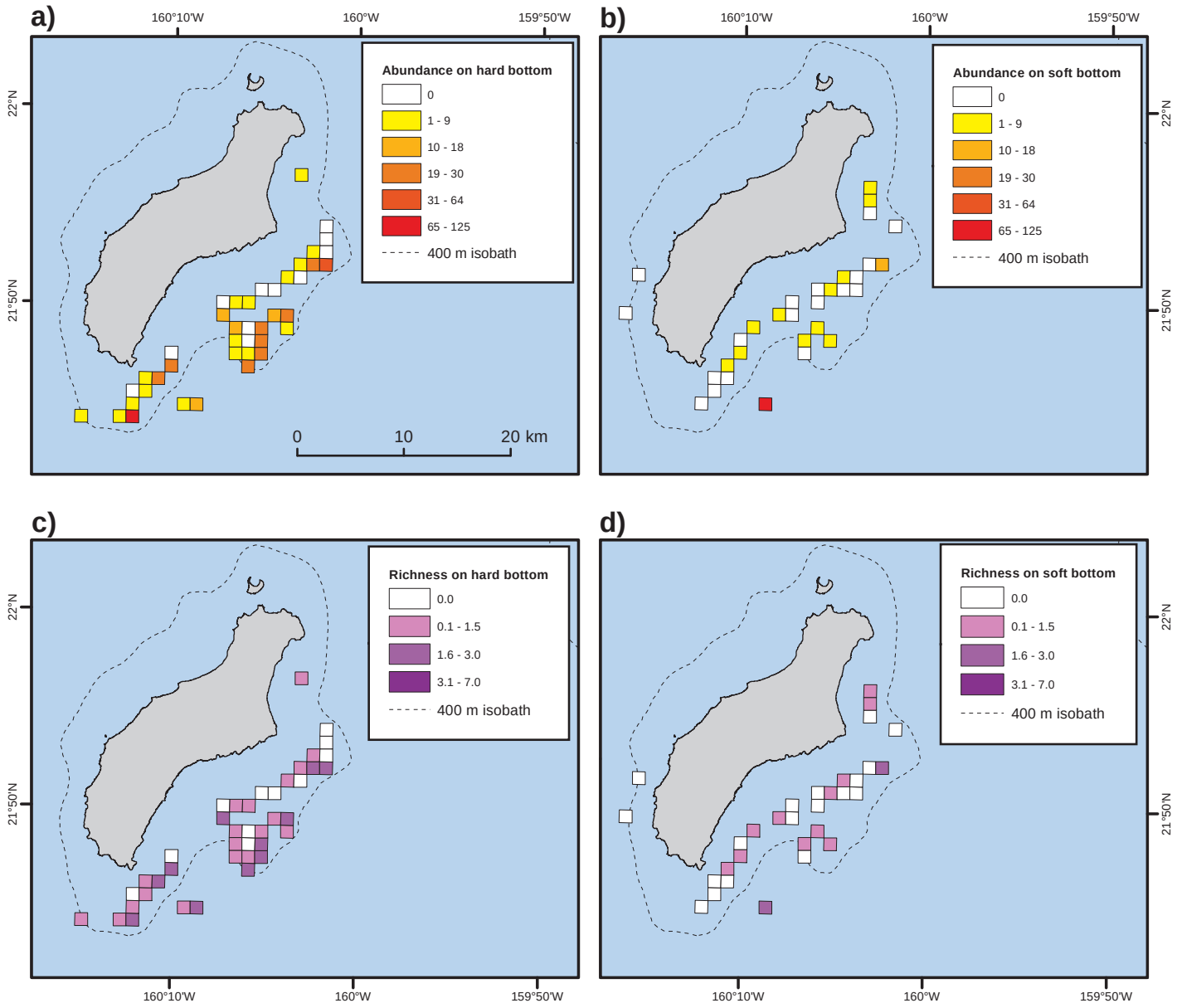

Figure 4.11. BotCam observations of the Deep 7 off southeastern Ni'ihau (2007-2014): a) average abundance on hard bottom; b) average abundance on soft bottom; c) average species richness on hard bottom; and d) average species richness on soft bottom. Data source: UH Deep-Sea Fish Ecology Lab, 2014

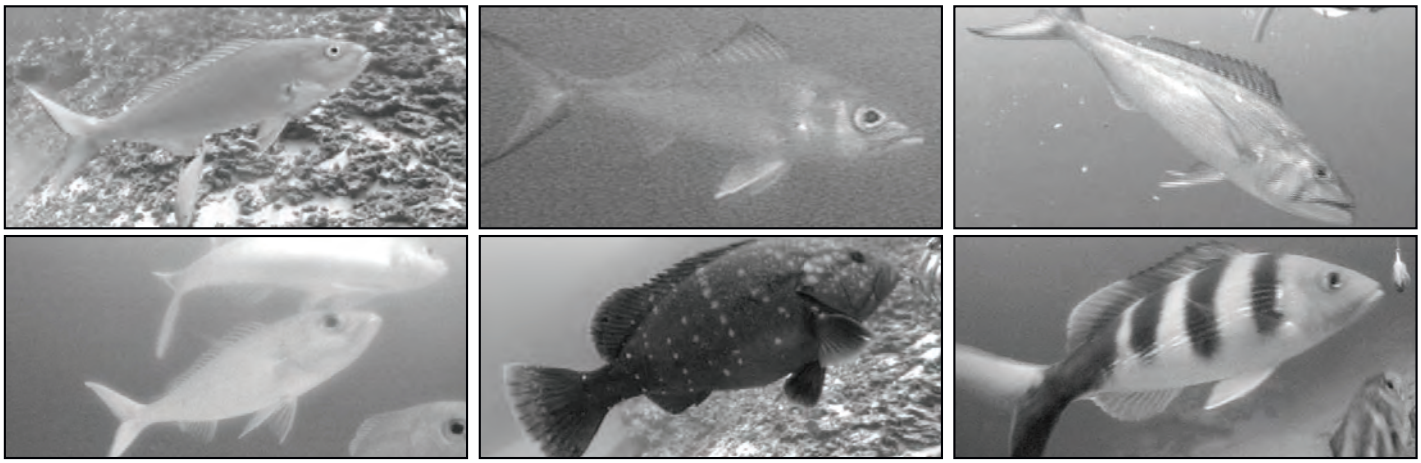

In situ *images from BotCam of bottom fish: (top L-R)* Pristipomoides filamentosus, Etelis coruscans *and* Aphareus rutilans*; (bottom L-R)* Pristipomoides sieboldii, Hyporthodus quernus *and* Pristipomoides zonatus*. Photo credit: Jeff Drazen (University of Hawai'i)*

Fishes

4.2.3. Discussion

This component of the study identified some important areas of bottom fish populations and fishing activity that can be considered during the development of offshore-wind energy. Areas with high values in these datasets are driven by a combination of habitat quality, distance from ports and population centers, and accessibility of fishing grounds. The DAR dataset offers insight into which general locations and seasons may result in conflicts with fishermen. The BotCam dataset provides a finer-scale snapshot of bottom fish communities and habitats and would be an effective approach for additional, site-specific assessments. Where DAR's fishery-dependent data overlaps with the fishery-independent data from BotCam, the two datasets are in general agreement, although quantitative comparison is not possible due to different spatial resolution, extent and biases. Despite this, consistent peaks in catch and abundance are discernible in regions such as Penguin Bank and Maui Nui.

Comparison by month illustrates that the fishery peaks in winter months, in terms of catch and effort, as well as number of areas fished. This can be due to several factors including: 1) fishery closure due to exceedance of the total-allowable-catch quota; 2) increased market demand for red-colored fish, including deep-water snappers, which are a symbol of prosperity and good luck served in association with the Japanese and Chinese New Year traditions; and 3) effort shifting to other fisheries during summer months (Schug, 2001; DAR, 2012; Hospital and Beavers, 2012).

Etelis coruscans *at auction. Photo credit: Kurt Kawamoto (NOAA NMFS/PIFSC/FRMD)*

In many locations, the typical bottom fish depth range (100-400 m) straddles the division between small nearshore DAR reporting areas (0-2 nm offshore) and the larger adjacent areas farther offshore (2-20 nm). This depth range forms a relatively narrow band of likely fish abundance and fishing activity compared to the size of many reporting areas. Although greatest catch and effort are typically reported from the larger offshore areas, this depth range suggests that only a small proportion of those areas is utilized by the fishery, with the majority of offshore areas deeper than 400 m and the majority of bottom-fishermen claiming that they fish only in state waters in a recent survey (Hospital and Beavers, 2012).

Where it is available, the BotCam data offers a finer-scale understanding of variability within the DAR reporting areas. For example, there are differences in bottom fish communities on the north and south sides of Penguin Bank, and on hard versus soft bottom within Maui Nui that are not discernable from the DAR reporting format.

4.2.4. Data and Information Gaps

There is less DAR fishery data from the northern islands (Kaua'i, Ni'ihau, Ka'ula) due to low fishing effort and participation in the reporting program, which is compounded by confidentiality restrictions. In these areas, CPUE may be the most useful indicator of important bottom fish habitat, and the DSHL summary dataset provides more thorough assessment.

Fishing area is self-reported by fishermen and may be accidently or intentionally misreported at times. The depth and location of typical bottom fish habitat often straddles the borders of many offshore and inshore reporting areas at approximately 2 nm from shore. This makes it difficult for fishermen to know which reporting

area they are in and increases the chance that fishing effort or catch can be reported for the wrong area. Fishing was reported in some areas in which the entirety of the reporting area is deeper than 400 m, but it is possible that the area was misreported and the fishing activity actually occurred in a shallower adjacent reporting area. Even when fishing area is accurately reported, the precise location of fishing within the area is still unknown. Given that large proportions of many fishery areas are outside of typical bottom fish depth ranges, it may be that only small sections of many reporting areas are significant for the DSHL fishery and bottom fish habitat.

BRFAs are not yet having a consistent effect on abundance and richness of Deep 7 fishes (Moore et al., 2013; Sackett et al., 2013). This is probably due to the slow growth rates of bottom fish, and the comparatively short time since most BRFAs were implemented. Fish size and maturity are showing more positive changes in response to older BRFAs (Sackett et al., 2013), but these variables were not the focus of this analysis.

Distribution of BotCam sampling is biased towards BRFAs, the Hawaiian Islands Humpback Whale National Marine Sanctuary and adjacent areas. The BRFAs have a significant positive effect on bottom fish size and maturity, variables not considered here, and in a few cases abundance in comparison to neighboring fished zones (Moore et al., 2013; Sackett et al., 2014). For example, at Penguin Bank and Makapu‘u, abundance declines with distance from the BRFAs for some species, suggesting a spillover effect (J. Drazen, pers. obs.). Therefore, some consideration should be given to regional variation in abundance created by the BRFAs.

Areas with less or no Botcam sampling include Kaua‘i, Moloka‘i, western Ni‘ihau, most of the island of Hawai‘i and most of Maui Nui apart from Penguin Bank and the channels between islands. Also of note, Botcam sampling is limited to depths shallower than 300 m due to reliance on ambient light. EFH and fishing occur down to 400 m however, and those deeper areas are not assessed by this technology. In addition, potential seasonal movements cannot be determined based on the present extent of Botcam sampling; funding and logistical constraints have prevented survey designs that test for those effects. Much higher density of sampling has occurred at Penguin Bank, allowing for more detailed habitat assessments presently under development. Ultimately, once a sufficient density and spatial distribution of BotCam samples become available around the rest of the MHI, spatial predictions could be modeled using the approaches for other taxa in this assessment (see Section 4.3 on reef fish).

Fishes

4.3. REEF FISHES

4.3.1. Methods and Data Description

Visual reef fish survey data

Reef fish survey data were compiled by University of Hawai'i's Fisheries Ecology Research Lab (UH FERL; UH FERL, 2015a) from multiple sources into a standardized database for analysis (Table 4.2). Datasets include broad-scale monitoring programs (PIFSC's Coral Reef Ecosystem Program [CREP], DAR's Coral Reef Assessment and Monitoring Program [CRAMP]), monitoring at specific sites (The Nature Conservancy Hawai'i Marine Program, UH FERL, National Park Service) and one-time assessments by individual researchers. As of December 2015, the database consists of 20,986 observations from 4,782 sites with data on fish assemblages within the MHI.

The overall goal of analyzing the database was to use environmental data to predict spatial patterns of reef fish distribution throughout the nearshore waters (0-30 m depth) of the MHI. Specific objectives were to develop models with the greatest predictive power, to produce maps of spatial predictions along with prediction variability, and to identify gaps in reef fish data and predictor datasets. Variables characterizing the overall reef fish community included in this analysis were: 1) total species richness, 2) biomass, 3) endemic

Table 4.2. List of compiled reef fish survey datasets, including source, years, number of sites, and basic methodology.

Program	Year Range	Geographic Coverage	# Transects	# Sites	Method Type	Survey Dimensions
UH FERL	2012-2013	Kāneʻohe Bay, Oʻahu	180	60	Transect	25x5 m
UH FERL	2010	Pūpūkea, Oʻahu	80	80	Transect	25x5 m
UH FERL	2012	Lānaʻi	74	74	Transect	25x5 m
UH FERL and TNC	2012	Kaʻūpūlehu-Kiholo, Hawaiʻi	299	299	Transect	25x5 m
UH FERL and NPS I&M	1992-2012	Hanalei, Kauaʻi	120	20	Transect	25x5 m
NOAA FHUS	2002-2008	Hanauma Bay, Pūpūkea, Honolua, Kealakekua	1,006	748	Transect	25x4 m
NOAA CREP	2000-2013	NWHI and MHI	1,748	882	Transect; Point Count	25x4 and 2 m; 15 m diameter
NOAA RAMP - NWHI	2005	NWHI	120	40	Transect	
DAR - Kona	1999-2012	West Hawaiʻi	8,138	49	Transect	25x4 m
DAR - Oʻahu	2007-2012	Oʻahu	462	16	Transect	25x4 m
DAR - Maui	2000-2012	Maui	1,640	601	Transect	25x5 m
UH CRAMP	1998-2012	Oʻahu, Maui, Kauaʻi	380	200	Transect	25x5 m
NPS I&M	2004-2012	Kalaupapa, Molokaʻi and Hawaiʻi	501	351	Transect	25x5 m
TNC	2008-2012	Maui, Hawaiʻi, Oʻahu	452	425	Transect	25x5 m
TNC	2009	Kahoʻolawe	42	42	Transect	25x5 m
UH FERL	2000	Moʻomomi, Molokaʻi	6	6	Transect	25x5 m
UH FERL	2005	Laʻau, Molokaʻi	18	6	Transect	25x5 m
UH FERL	2007	Lāwaʻi, Kauaʻi	17	17	Transect	25x5 m
UH FERL	2013-2014	Hāʻena, Kauaʻi	55	55	Transect	25x5 m
DAR - Maui and CREP	2008-2013	Kahekili, Maui	811	811	Transect	25x4 and 2 m
		Total	**20,986**	**4,782**		

DAR - Division of Aquatic Resources, State of Hawaiʻi (DAR, 2015b)
NPS I&M - Inventory and Monitoring, National Park Service (NPS I&M, 2015)
NOAA FHUS - Fish Habitat Utilization Study, NOAA NCCOS (NOAA FHUS, 2015)
NOAA CREP - Coral Reef Ecosystem Program, NOAA NMFS Pacific Islands Fishery Science Center (NOAA CREP, 2015)
NOAA RAMP - Pacific Reef Assessment and Monitoring Program, NOAA NMFS Pacific Islands Fisheries Science Center (NOAA RAMP, 2015)
TNC - The Nature Conservancy Hawaiʻi Marine Program (TNC, 2015)
UH CRAMP - Coral Reef Assessment and Monitoring Program, University of Hawaiʻi (UH CRAMP, 2015)
UH FERL - Fisheries Ecology Research Lab, University of Hawaiʻi (UH FERL, 2015b)

species richness, 4) biomass, and 5) resource-fish biomass. Resource species were defined as those having ≥450 kg (1,000 lbs) of annual commercial harvest, or recognized as important to the recreational, subsistence, or cultural fishing sectors. Biomass was estimated using the allometric length-weight conversion: $W = a \times TL^b$, where parameters *a* and *b* are species-specific fitting parameters, TL is total length (cm), and W is weight (g). Parameters were obtained from a comprehensive assessment of Hawai'i length-weight fitting parameters (M. Donovan, pers. comm.) and FishBase (Froese and Pauly, 2011). Because of the dimensions of many reef fish survey methods and the positional accuracy of global positioning system (GPS) used to navigate to them in the field, spatial predictions were generated on a 60 m resolution grid. This is also a more suitable scale for assisting with the planning of power-cable right-of-way corridors in the nearshore waters in contrast to the much larger BOEM lease blocks used offshore.

Prior to analysis, each dataset was checked for errors and completeness, transformed into a consistent format, and standardized to account for overall differences in survey dimensions and methods. Calibration factors standardizing data among methods were calculated using an automated software program that utilizes general linear models and Monte Carlo simulations (Nadon, 2014). To further account for variability of individual observers, extreme observations of density for schooling species were adjusted so that no observations fell above the 99 percent quantile for a given species. Where multiple surveys were conducted at a single site they were averaged to obtain single value for each location.

Predictor datasets

A set of 62 gridded environmental datasets at 60 m resolution was generated for each island group as potential predictor variables used to model the reef fish community metrics. Selection of the predictors was based on an extensive literature review and input from experts in Hawaiian reef ecology. Predictor variables fell into one of four categories: topographic, benthic habitat composition, geographic and oceanographic (Tables 4.3-4.6).

Seafloor topography variables were included to account for variation in reef fish communities arising from the direct and indirect effects of depth and seafloor geomorphology. A gridded synthesis of multibeam sonar and Light Detection And Ranging (LiDAR) bathymetry at 5 m resolution was used as the depth variable and also to derive a suite of seafloor complexity datasets (Table 4.3). In addition, several metrics were computed for multiple neighborhood sizes (60 m, 120 m and 240 m radii) to identify locations with high complexity within home range sizes broadly representative of reef fish taxa. Bathymetric position index (BPI), a measure of a location's depth relative to the surrounding area, was derived for each of these neighborhood sizes to identify ridges and valleys at these scales (Table 4.3). The neighborhood maximum within each neighborhood size was initially calculated for several of the seafloor complexity datasets, but following initial inspection of these datasets, only the neighborhood maximum in the 240 m neighborhood was included in the models and table (Table 4.3). Seafloor topography variables at 60 m resolution were created by calculating the aggregate mean or standard deviation of the 5 m resolution datasets within a 60x60 m grid.

Benthic habitat composition variables were included to account for variation in reef fish communities arising from the direct and indirect effects of the spatial configuration of benthic habitats. Benthic habitat maps of the MHI (Battista et al., 2007) were simplified into 5 benthic cover classes based on ecological relevance and adequate spatial coverage. These included crustose coralline algae (CCA), coral, macroalgae, turf algae, and soft bottom. Class-level metrics of seascape pattern were computed to depict the extent and distribution of patches of each class type. Landscape-level metrics incorporating all classes were computed to depict landscape diversity and heterogeneity (Table 4.4).

Fishes

Table 4.3. Datasets of seafloor topography variables considered as potential environmental predictors in models of reef fish assemblage metrics. SD= Standard Deviation; max= maximum in 240 m neighborhood.

Dataset	Description	Unit	Statistic(s)	Data Source/ Provider	Native Resolution
Depth	Seafloor depth	m	mean, SD	Bathymetry synthesis (HMRG, 2015)	5x5 m
Slope	Maximum rate of change in seafloor depth between each grid cell and its neighbors	Degree	mean, SD, max	Bathymetry synthesis (HMRG, 2015)	5x5 m
Slope of Slope	Maximum rate of change in seafloor slope between each grid cell and its neighbors	Degree	mean, SD, max	Bathymetry synthesis (HMRG, 2015)	5x5 m
Aspect	Downslope direction of maximum rate of change in seafloor depth between each grid cell and its neighbors	Unitless	sine circular mean, cosine circular mean, circular SD	Bathymetry synthesis (HMRG, 2015)	5x5 m
Rugosity	Ratio of seafloor surface area to planar area; value indicates topographic roughness; values can range from 1 (flat) to infinity	Unitless	mean, SD, max	Bathymetry synthesis (HMRG, 2015)	5x5 m
Total curvature	Seafloor curvature; value indicates surface ruggedness; values > 0, with 0 indicating surface is a plane	Radians/ m^2	mean, SD, max	Bathymetry synthesis (HMRG, 2015)	5x5 m
Plan curvature	Seafloor curvature perpendicular to the line of maximum slope; value indicates whether flow will converge or diverge over a point; values can be - (concave), + (convex), or 0 (flat)	Radians/ m	mean, SD	Bathymetry synthesis (HMRG, 2015)	5x5 m
Profile curvature	Seafloor curvature along the line of maximum slope; value indicates whether flow will accelerate or decelerate over the curve; values can be + (concave), - (convex), or 0 (flat)	Radians/ m	mean, SD	Bathymetry synthesis (HMRG, 2015)	5x5 m
Bathymetric position index (BPI)	Difference in seafloor depth and the mean seafloor depth in an annular neighborhood of specified inner and outer radii; values indicate a location's position relative to the surrounding area; values can be + (ridges), - (valleys), or 0 (flat areas or areas of constant slope)	m	mean	Bathymetry synthesis (HMRG, 2015)	5x5 m
Terrain ruggedness (VRM)	Variation in 3D orientation of grid cells within a neighborhood; value indicates topographic roughness; values can range from 0 (no variation) to 1 (complete variation)	Unitless	mean, SD, max	Bathymetry synthesis (HMRG, 2015)	5x5 m

Dataset	Processing Tools and Steps
Depth	Aggregate mean and standard deviation of 5 m grid resolution depth were calculated at 60 m grid resolution using the R raster package (Hijmans, 2014)
Slope	Slope was calculated on the 5 m grid resolution depth using the ArcGIS Slope tool (ESRI, 2011); Maximum slope in a 240 m radius neighborhood was calculated using the ArcGIS Focal Statistics tool (ESRI, 2011); Aggregate mean and standard deviation of slope and aggregate mean of max slope were calculated at 60 m grid resolution using the R raster package (Hijmans, 2014)
Slope of slope	Slope of slope was calculated on the 5 m grid resolution slope using the ArcGIS Slope tool (ESRI, 2011); Maximum slope of slope in a 240 m radius neighborhood was calculated using the ArcGIS Focal Statistics tool (ESRI, 2011); Aggregate mean and standard deviation of slope of slope and aggregate mean of max slope of slope were calculated at 60 m grid resolution using the R raster package (Hijmans, 2014)
Aspect	Aspect was calculated on the 5 m grid resolution depth using the ArcGIS Aspect tool (ESRI, 2011); Aggregate circular mean and circular standard deviation of aspect, and the sine and cosine of aggregate circular mean were calculated at 60 m grid resolution using the R circular package (Agostinelli and Lund, 2013) and raster package (Hijmans, 2014)
Rugosity	Rugosity was calculated on the 5 m grid resolution depth using the DEM Surface Tools Surface Area tool (Jenness, 2013); Maximum rugosity in a 240 m radius circular neighborhood was calculated using the ArcGIS Focal Statistics tool (ESRI, 2011); Aggregate mean and standard deviation of rugosity and aggregate mean of max rugosity were calculated at 60 m grid resolution using the R raster package (Hijmans, 2014)
Total curvature	Total curvature was calculated on the 5 m grid resolution depth using the DEM Surface Tools Curvature tool (Jenness, 2013); Maximum curvature in a 240 m radius circular neighborhood was calculated using the ArcGIS Focal Statistics tool (ESRI, 2011); Aggregate mean and standard deviation of curvature and aggregate mean of max curvature were calculated at 60 m grid resolution using the R raster package (Hijmans, 2014)
Plan curvature	Planar curvature was calculated on the 5 m grid resolution depth using the DEM Surface Tools Curvature tool (Jenness, 2013); Aggregate mean and standard deviation of planar curvature were calculated at 60 m grid resolution using the R raster package (Hijmans, 2014)
Profile curvature	Profile curvature was calculated on the 5 m grid resolution depth using the DEM Surface Tools Curvature tool (Jenness, 2013); Aggregate mean and standard deviation of profile curvature were calculated at 60 m grid resolution using the R raster package (Hijmans, 2014)
Bathymetric position index (BPI)	For each scale, BPI was calculated on the 5 m grid resolution depth using the Benthic Terrain Modeler tool (Wright et al., 2012); Aggregate mean of each BPI dataset was calculated at 60 m grid resolution using the R raster package (Hijmans, 2014)
Terrain ruggedness (VRM)	VRM was calculated on the 5 m grid resolution depth for a 3x3 grid cell neighborhood using the Benthic Terrain Modeler (Wright et al., 2012); Maximum VRM in a 240 m radius circular neighborhood was calculated using the ArcGIS Focal Statistics tool (ESRI, 2011); Aggregate mean and standard deviation of VRM and aggregate mean of max VRM were calculated at 60 m grid resolution using the R raster package (Hijmans, 2014)

Table 4.4. Datasets of benthic habitat composition variables considered as potential environmental predictors in models of reef fish assemblage metrics. SD= Standard Deviation.

Dataset	Description	Unit	Statistic(s)	Data Source/ Provider	Native Resolution
Percentage of landscape	The total area of patches of the specified cover class divided by the total area of the seascape and multiplied by 100; values indicate seascape composition	Percent	N/A	MHI benthic habitat maps (Battista et al., 2007)	N/A
Edge density	Total edge length of the specified cover class divided by total seascape area and multiplied by 10, 000; values indicate seascape configuration in terms of the amount of edge present	m/ hectare	N/A	MHI benthic habitat maps (Battista et al., 2007)	N/A
Patch shape index	Patch perimeter divided by square root of patch area and adjusted by a constant so values will not vary with patch size; values indicate patch shape complexity compared to a square standard; values can range from 1 (square, least complex) to infinity (more complex)	Unitless	N/A	MHI benthic habitat maps (Battista et al., 2007)	N/A
Contiguity index	Index related to the average contiguity value in a patch of the specified cover class, where contiguity is a function of the number and location of pixels of the specified cover class within a 3x3 pixel moving window; values indicate patch shape complexity in terms of the spatial connectedness of pixels in the patch, emphasizing patch compaction and/or elongation; values range from 0 (a one-pixel patch) to 1, where larger values correspond to large contiguous patches; statistical distribution of patch contiguity index values can be calculated for patches of specified cover class	Unitless	mean, SD	MHI benthic habitat maps (Battista et al., 2007)	N/A
Fractal dimension index	Patch perimeter, corrected for raster bias in perimeter, divided by the natural logarithm of patch area; values indicate patch shape complexity across a range of patch sizes; values range from 1 (shapes with simple perimeters) to 2 (shapes with highly convoluted perimeters); statistical distribution of patch fractal dimension index values can be calculated for patches of the specified cover class	Unitless	mean, SD	MHI benthic habitat maps (Battista et al., 2007)	N/A
Proximity index	For a focal patch of the specified cover class, the sum, over all patches of that class within a given distance, of patch area divided by the square of the distance between the patch and the focal patch; values indicate the spatial context of both the degree of patch isolation and degree of seascape fragmentation; a value of 0 indicates no neighbors of the same cover class within the search radius, and values increase as patches of the same class become more numerous, closer, and more contiguous; statistical distribution of patch proximity index values can be calculated for patches of specified cover class	Unitless	mean, SD	MHI benthic habitat maps (Battista et al., 2007)	N/A

Dataset	Processing Tools and Steps
Percentage of landscape	The simplified benthic habitat map was converted to a 5 m grid resolution raster. For each benthic cover class, percentage of landscape was calculated from the raster using a 60x60 m moving window in Fragstats v4.2 (McGarigal et al., 2012). Aggregate mean of Percentage of landscape was calculated at 60 m grid resolution using ArcGIS (ESRI, 2011)
Edge density	The simplified benthic habitat map was converted to a 5 m grid resolution raster. For each benthic cover class, edge density was calculated from the raster using a 60x60 m moving window in Fragstats v4.2 (McGarigal et al., 2012). Aggregate mean of edge density was calculated at 60 m grid resolution using ArcGIS (ESRI, 2011)
Patch shape index	The simplified benthic habitat map was converted to a 5 m grid resolution raster. For each benthic cover class, mean and standard deviation of patch shape index were calculated from the raster using a 60x60 m moving window in Fragstats v4.2 (McGarigal et al., 2012). Aggregate mean of the mean and standard deviation of patch shape index were calculated at 60 m grid resolution using ArcGIS (ESRI, 2011)
Contiguity index	The simplified benthic habitat map was converted to a 5 m grid resolution raster. For each benthic cover class, mean and standard deviation of patch contiguity index were calculated from the raster using a 60x60 m moving window in Fragstats v4.2 (McGarigal et al., 2012). Aggregate mean of the mean and standard deviation of patch contiguity index were calculated at 60 m grid resolution using ArcGIS (ESRI, 2011)
Fractal dimension index	The simplified benthic habitat map was converted to a 5 m grid resolution raster. For each benthic cover class, mean and standard deviation of patch fractal dimension were calculated from the raster using a 60x60 m moving window in Fragstats v4.2 (McGarigal et al., 2012). Aggregate mean of the mean and standard deviation of patch fractal dimension were calculated at 60 m grid resolution using ArcGIS (ESRI, 2011)
Proximity index	The simplified benthic habitat map was converted to a 5 m grid resolution raster. For each benthic cover class, mean and standard deviation of patch proximity index were calculated from the raster using a 60x60 m moving window in Fragstats v4.2 (McGarigal et al., 2012). Aggregate mean of the mean and standard deviation of patch proximity index were calculated at 60 m grid resolution using ArcGIS (ESRI, 2011)

Fishes

Table 4.4. continued. Datasets of benthic habitat composition variables considered as potential environmental predictors in models of reef fish assemblage metrics.

Dataset	Description	Unit	Statistic(s)	Data Source/ Provider	Native Resolution
Shannon's diversity index	Negative of the sum, over all cover classes, of the proportion of the seascape occupied by a class times the natural logarithm of that proportion; values indicate habitat diversity in terms of the number of different cover classes present (richness) and the proportional distribution of area among the different cover classes (evenness); a value of 0 indicates only 1 patch (no diversity) and values increase as either the number of different cover classes increases or area becomes more evenly distributed among classes	Unitless	N/A	MHI benthic habitat maps (Battista et al., 2007)	N/A
Shannon's evenness index	Shannon's diversity index divided by the natural logarithm of the number of cover classes present in the seascape; values indicate habitat diversity in terms of the proportional distribution of area among the different cover classes; values range from 0 to 1, with a value of 0 indicating only 1 patch is present (no diversity) and values increasing as area becomes more evenly distributed among classes until a value of 1 where area proportions are the same among all classes	Unitless	N/A	MHI benthic habitat maps (Battista et al., 2007)	N/A
Dataset	**Processing Tools and Steps**				
Shannon's diversity index	The simplified benthic habitat map was converted to a 5 m grid resolution raster. Shannon's diversity index was calculated from the raster using a 60x60 m moving window in Fragstats v4.2 (McGarigal et al., 2012). Aggregate mean of the Shannon's diversity index was calculated at 60 m grid resolution using ArcGIS (ESRI, 2011)				
Shannon's evenness index	The simplified benthic habitat map was converted to a 5 m grid resolution raster. Shannon's evenness index was calculated from the raster using a 60x60 m moving window in Fragstats v4.2 (McGarigal et al., 2012). Aggregate mean of the Shannon's evenness index was calculated at 60 m grid resolution using ArcGIS (ESRI, 2011)				

Geographic variables were included to account for variation in reef fish communities arising from spatial location. These included projected latitude and longitude, distance to shore, and proximity to human population (Table 4.5). Position relative to MPAs was considered as a predictor in early models but ultimately not included for two reasons. First, Marine Life Conservation District (MLCD) boundaries were chosen partly on the basis of good habitat with high rugosity, which resulted in strong correlation with the seafloor variables (see above). Second, MPA status has nuanced and variable influences on fish communities depending on MPA dimensions, regulations, enforcement, and duration since establishment, which are unique to each protected area.

Hanauma Bay Nature Preserve, both a Marine Life Conservation District and Nature Preserve. Photo credit: Lisa Wedding (Stanford University)

Oceanographic variables were included to account for variation in reef fish communities arising from the direct and indirect effects of the physical state and dynamics of the ocean. These consisted of datasets representing wave conditions around the islands derived from a 10 year (2000-2009) hindcast model at 500 m resolution (Stopa et al., 2013; Table 4.6).

For each island group, a pairwise correlation analysis was performed on the full set of predictors. Highly correlated pairs of predictors (Spearman rank $R > 0.9$ or $R < -0.9$) were identified, and the predictor that was highly correlated with the most other predictors was excluded. In general, predictors that were highly correlated with two or more others were removed, whereas ecologically important variables (based on expert opinion and scientific literature) and variables common among island groups were retained. After the correlation analyses, 29 predictors were identified for model development in Maui Nui, Kaua'i and O'ahu, and 35 were identified for the island of Hawai'i.

Table 4.5. Datasets of geographic variables considered as potential environmental predictors in models of reef fish assemblage metrics.

Dataset	Description	Unit	Statistic(s)	Data Source/ Provider	Native Resolution
Latitude	Latitude at each model grid cell centroid	Meters	N/A	N/A	N/A
Longitude	Longitude at each model grid cell centroid	Meters	N/A	N/A	N/A
Distance to shore	Straight line (Euclidean) distance to the shoreline	Meters	N/A	MHI benthic habitat maps (Battista et al., 2007)	N/A
Proximity to human population	Sum of human population in 15 km radius neighborhood	Number of people	N/A	2010 census block data from State of Hawai'i Office of Planning	N/A
Dataset	**Processing Tools and Steps**				
Latitude	The latitude raster was created at 60 m grid resolution using the Marine Geospatial Ecology Tools (MGET) Create Y Coordinate Raster tool (Roberts et al., 2010)				
Longitude	The longitude raster was created at 60 m grid resolution using the Marine Geospatial Ecology Tools (MGET) Create X Coordinate Raster tool (Roberts et al., 2010)				
Distance to shore	Shorelines were extracted from benthic habitat maps of the MHI; Distance to shore was calculated at 60 m grid resolution using the ArcGIS Euclidean Distance tool (ESRI, 2011)				
Proximity to human population	Following Williams et al. (2008), census block data from 2010 (State of Hawai'i, 2010) in shapefile format was converted to a 60 m grid resolution raster; Sum of human population in a 15 km radius circular neighborhood was calculated using the ArcGIS Focal Statistics tool (ESRI, 2011)				

Table 4.6. Datasets of oceanographic variables considered as potential environmental predictors in models of reef fish assemblage metrics. SD= Standard Deviation.

Dataset	Description	Unit	Statistic(s)	Data Source/ Provider	Native Resolution
Wave height	Significant wave height derived from a 10 year (2000-2009) hindcast wave model	Meters	mean, 90th percentile, 95th percentile, SD	Hindcast wave model (Stopa et al., 2013) from the Department of Ocean and Resources Engineering, University of Hawai'i at Mānoa	500x500 m
Wave power	Wave power (wave height x wave period) derived from a 10 year (2000-2009) hindcast wave model	Kilowatts per meter	mean, 90th percentile, 95th percentile, SD	Hindcast wave model (Stopa et al., 2013) from the Department of Ocean and Resources Engineering, University of Hawai'i at Mānoa	500x500 m
Dataset	**Processing Tools and Steps**				
Wave height	Wave data were created by modeling the shoreward propagation of deep-water waves using the Simulating Waves Nearshore (SWAN) wave model (Booij et al., 1999; Holthuijsen, 2010) on a 500 m resolution grid. Deep water wave characteristics were computed by the WAVEWATCH III (WW3) wave model (Tolman, 2009), forced by 10 years of wind observations over the Pacific Ocean (Stopa et al., 2013); Wave height datasets were resampled to 60 m grid resolution. Grid cells nearest to shore were removed because of artifacts. Missing nearshore values were then extrapolated from nearest neighbors using the Matlab inpaint_nans function (D'Errico, 2014)				
Wave power	Wave data were created by modeling the shoreward propagation of deep-water waves using the Simulating Waves Nearshore (SWAN) wave model (Booij et al., 1999; Holthuijsen, 2010) on a 500 m resolution grid. Deep water wave characteristics were computed by the WAVEWATCH III (WW3) wave model (Tolman, 2009), forced by 10 years of wind observations over the Pacific Ocean (Stopa et al., 2013); Wave power datasets were resampled to 60 m grid resolution. Grid cells nearest to shore were removed because of artifacts. Missing nearshore values were then extrapolated from nearest neighbors using the Matlab inpaint_nans function (D'Errico, 2014)				

Statistical modeling framework

Overview

A boosted regression tree (BRT) modeling framework (Figure 4.12) was used to estimate relationships between reef fish community metrics (total reef fish species richness and biomass, endemic reef fish species richness and biomass, resource fish species biomass) and the predictor datasets. The estimated relationships were then used to create spatial predictions of the reef fish metrics. Each reef fish metric was modeled independently at the island group scale. The objectives of this approach were to develop models with the greatest predictive power (i.e., models that explained the most variation in the response variables when fit to new data), and to produce maps of spatial predictions and prediction variability. Statistical modeling and spatial prediction were performed in R (R Core Team, 2014) using the dismo (Hijmans et al., 2014) and raster (Hijmans, 2014) packages.

Fishes

Step 1. Data preparation

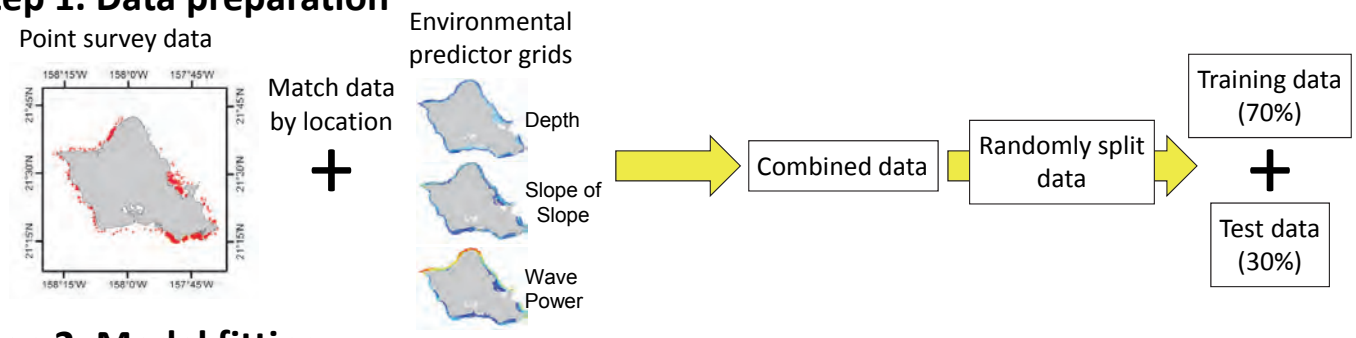

Step 2. Model fitting

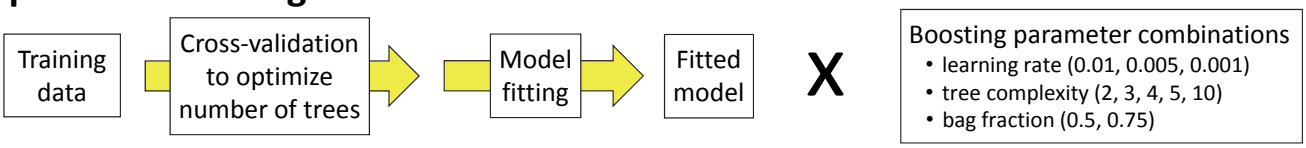

Step 3. Model selection

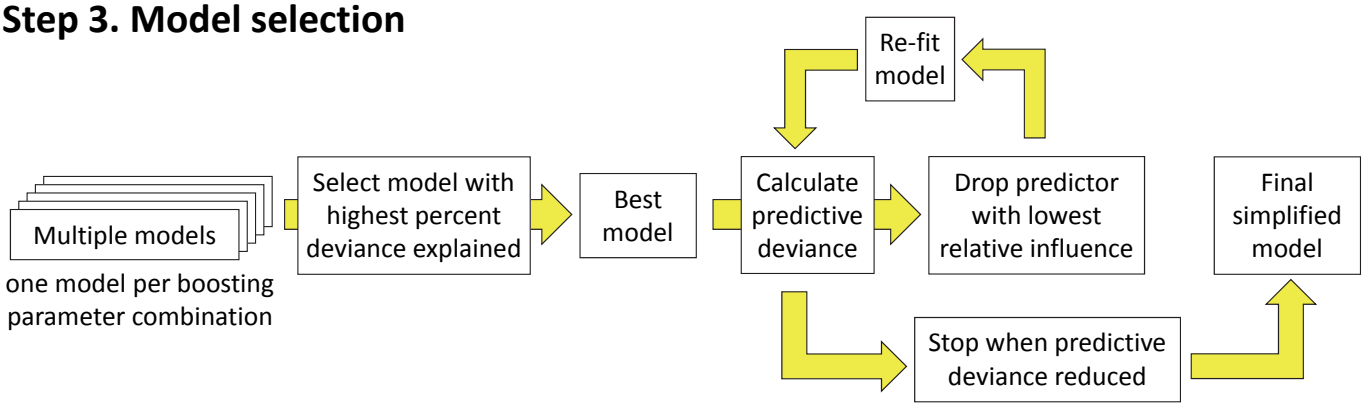

Step 4. Prediction across space

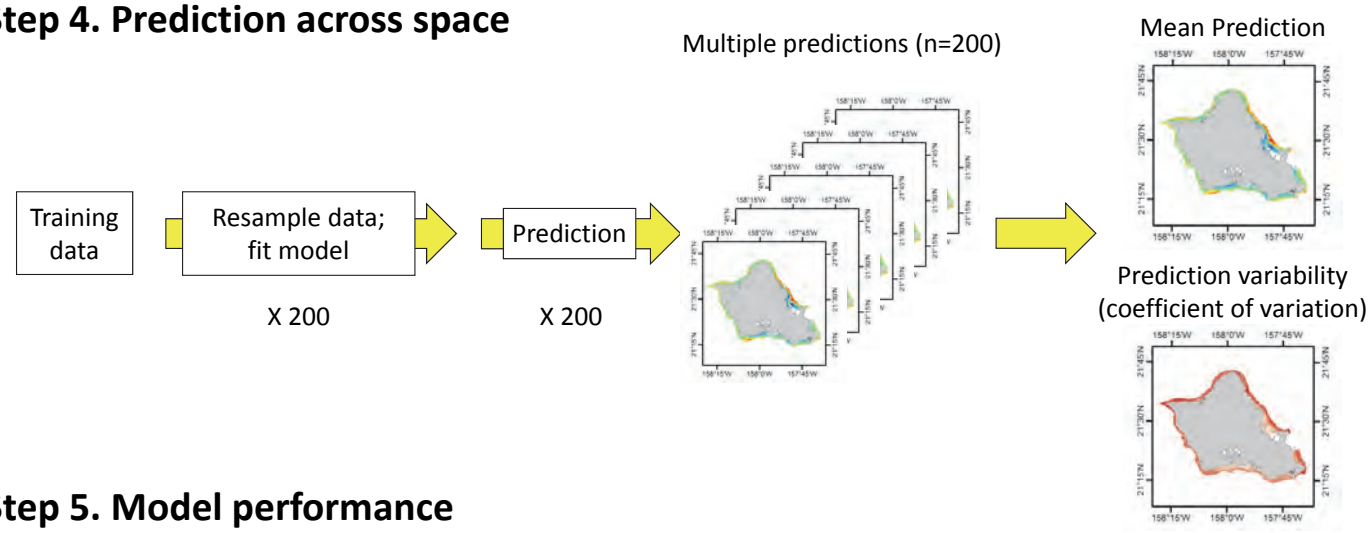

Step 5. Model performance

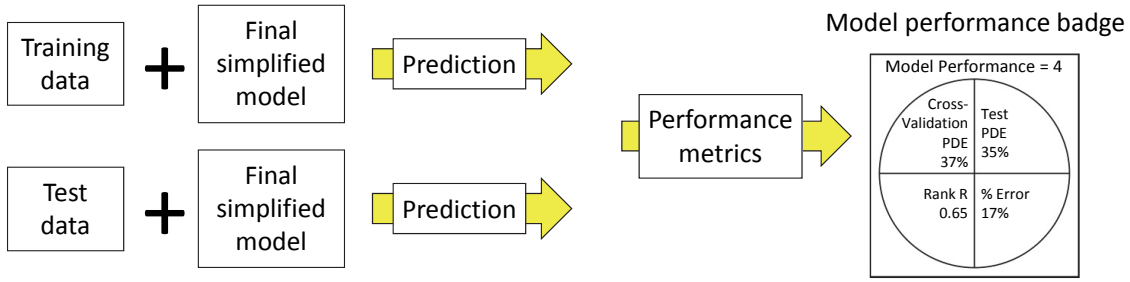

Figure 4.12. Boosted regression tree modeling framework, including data preparation, model fitting, model selection, prediction across space and evaluation of model performance.

Tree-based modeling approaches estimate relationships between response and predictor variables by using a series of binary splits on the predictor variables to partition the data into groups as homogeneous as possible in terms of the response variable (Breiman et al., 1984; De'ath and Fabricius, 2000). These approaches are particularly well suited for handling the non-linear relationships and high-order interactions of complex ecological data (De'ath and Fabricius, 2000), as well as incomplete predictor variable data (Breiman et al., 1984; Elith et al., 2008). However, constructing a single parsimonious tree-based model can result in overfitting of the data and a reduction in predictive power (Elith et al., 2008). To improve predictive performance relative to single tree models, BRT models employ a machine learning technique, boosting, in which a large number of regression trees are fit stagewise (i.e., after each tree is fit, the remaining variation in the data is used to fit the next tree), and then combined to generate a final, ensemble model (Friedman, 2002; De'ath, 2007; Elith et al., 2008). In stochastic gradient boosting, at each stage the tree is fit using a random subsample of the training data. This helps prevent overfitting and further improves model performance (Friedman, 2002; Elith et al., 2008).

Data preparation

BRTs can accommodate many types of response variables, including presence/absence, count, diversity, and abundance data (De'ath, 2007; Elith et al., 2008). Since the reef fish community metrics were all continuous variables, the response variables were all modeled using a Gaussian (normal) distribution, and appropriate data transformations (square root for fish richness, fourth root for fish biomass) were applied to improve the normality of the response variable distributions. Predictor data values at the locations of the reef fish surveys were extracted from the gridded predictor datasets. The reef fish community metric values and predictor values at these locations were combined in a single data table.

Prior to model fitting, reef fish survey data for each island were randomly divided into model training (70%) and test (30%) subsets of the data. The test dataset was withheld from model fitting and used only to evaluate model performance. Although boosting makes BRT models less prone to overfitting to the training data (Friedman, 2002; Elith et al., 2008), model performance was evaluated on the independent test data subset to measure how well the model generalized to new data.

Model fitting

Several model parameters can be used to control the model fitting process. These include the learning rate, tree complexity, and bag fraction (see Glossary for a description of each parameter). Models were fit for a range of parameter value combinations. For each parameter value combination, the optimal number of boosting iterations (trees) was determined using 10-fold cross-validation. In this process, the model training dataset was subset into 10 random samples of equal size. Ten training subsets were created from these samples, each containing a combination of nine samples to be used for model fitting and leaving out one sample for validation. Starting with a setting of 50 trees, BRT models were fit to each training subset. For each model the predictive deviance, which indicates the amount of variation in the response variable unexplained by the model, was calculated using predictions made at the data locations of the subset withheld from model fitting. Model fitting and validation were repeated for increasing numbers of trees, and the predictive deviance was calculated at each iteration. The number of trees that minimized predictive deviance was selected as the optimal number of trees for that combination of parameter values. A final BRT model was fit to the full training dataset using the optimal number of trees. Predictive performance of the final model was evaluated by making predictions at the data locations in each of the 10 cross-validation training subsets and calculating the predictive deviance. The mean predictive deviance across the 10 subsets was used to calculate a cross-validation estimate of the percent deviance explained (PDE). PDE is essentially the percentage of variation in the response variable explained by a simpler model without predictor variables. A final model and cross-validation estimate of PDE was generated for each combination of parameter values (Elith et al., 2008).

Fishes

Model selection

A final model and cross-validation estimate of PDE was generated for each combination of model parameter values as described above. The final model with the highest PDE was selected as the best model, and the model parameter values and optimal number of trees for this model were used in model simplification, to evaluate model performance, and to make spatial predictions.

Although uninformative predictor variables are generally ignored during BRT model fitting and, therefore, do not influence prediction (Elith et al., 2008), the potential to remove unimportant predictor variables (and thus create a simpler model) was assessed. Beginning with the selected best model and full set of predictor variables, the least contributing predictor was identified and dropped, the model was re-fit, and the change in predictive deviance was computed relative to the initial model. The number of predictors to remove was determined by evaluating how many predictors could be dropped without resulting in a reduction in predictive performance (see Appendix B in Elith et al., 2008 for a detailed description of the model simplification algorithm). Following model simplification, a final model was fit using the simplified set of predictor variables.

Prediction across space

Bootstrapping was used to calculate spatially explicit predictions and prediction uncertainties. The model training dataset was repeatedly sampled with replacement to create 200 bootstrap samples. Using the optimal parameter values and simplified predictor variable set, a BRT model was fit to each bootstrap sample and used to make a prediction to a spatially explicit gridded map using the values of the predictor variables at each grid cell. This resulted in a set of 200 spatial predictions, which were used to calculate the prediction mean and coefficient of variation (Leathwick et al., 2006). No model predictions were possible for the many large segments of coastline lacking bathymetry, and therefore a major set of predictor variables.

For each combination of island group and reef fish community metric, map pages were generated to depict the *in situ* survey data, the prediction mean, and the prediction coefficient of variation. Within these, inset panels depict areas of interest (e.g., areas with relatively high or low predictions, areas near population centers). Note that due to the 60 m resolution of the model, fine-scale features are difficult to discern even in the insets, but are easily seen in the Geodatabase associated with this chapter.

Map symbology for survey data and prediction means were defined by classifying the survey data into 10 equal groups (deciles). Coefficient of variation of predictions was also depicted using deciles. This resulted in many fine divisions at the low ends of scales because the survey data distributions were generally skewed toward lower values. Because the ranges of values for the reef community metrics often varied considerably among island groups, map symbologies were created independently for each island group to ensure that areas of relatively high values for each individual island group were discernible.

Model performance

Model performance was evaluated from a suite of four performance metrics (Table 4.7). The key performance metrics were the “Cross-validation PDE” and “Test PDE”. The “Cross-validation PDE” is the cross-validation estimate of the percent deviance explained for the best model (as described above). Similar to the “Cross-validation PDE”, the “Test PDE” was determined by calculating the percent deviance explained by the model when evaluated using the model test dataset. Both of these metrics indicate overall model fit, but the “Test PDE” metric also provides a measure of how well the model performs when predicting data that was independent of model fitting. Relatively higher values for these metrics suggest models can be used with greater confidence to make spatial predictions. However, models with relatively high “Cross-validation PDE” but considerably lower “Test PDE” are likely overfit to the model training dataset, and greater caution should be used in making spatial predictions.

Like the "Test PDE", the remaining metrics were generated using the independent model test dataset. These metrics were calculated using only the non-zero data, though, to emphasize model performance at locations where fishes were observed. The "Rank R" metric is the Gaussian rank correlation coefficient, calculated between the observed values at the model test dataset locations and predictions at these locations for non-zero values. This metric indicates how well a model predicts fish richness or biomass at locations where fish were observed. The "Percent Error" metric is the median absolute residual error for non-zero data as a percentage of the mean of the non-zero observed values. The median absolute residual error was calculated by taking the median of the absolute differences between observed values at the model test dataset locations and predictions at these locations for non-zero data. The median absolute residual error was converted to a percentage of the mean to normalize the values for comparison across models. Similar to the "Rank R" metric, the "Percent Error" metric also indicates how well a model predicts fish richness or biomass at locations where fish were observed. Relatively high values for "Rank R", and relatively low values for "Percent Error" suggest greater confidence in model predictions at locations where reef fish were observed.

Table 4.7. Metrics used to evaluate boosted regression tree (BRT) model performance.

Name	Description	Data	Stage	Quality categories
Cross-validation PDE	percent deviance explained	training	final fit	5: > 60% 4: 40-60% 3: 20-40% 2: 10-20% 1: < 10%
Test PDE	percent deviance explained	test	final fit	5: > 60% 4: 40-60% 3: 20-40% 2: 10-20% 1: < 10%
Rank R	Gaussian rank correlation coefficient	non-zero test	final fit	5: >0.6 4: 0.4-0.6 3: 0.2-0.4 2: 0.1-0.2 1: <0.1
Percent Error	median absolute residual error as percentage of data mean	non-zero test	final fit	5: <25% 4: 25-50% 3: 50-100% 2: 100-200% 1: >200%

Qualitative performance categories were defined for each performance metric (Table 4.7). The performance of the final model for each island-response variable combination was assigned an overall quality equal to the average quality across the four performance metrics. Model performance is displayed on each map figure using a "badge". It is important to recognize that the model performance metrics and badge only reflect the statistical fit of the model to the data. They do not reflect the data quality or the quality of model predictions away from the survey data. These issues will be discussed further in the *Data and information gaps* section below.

Variable importance

While the primary objective of modeling the reef fish community metrics was not to determine the ecological drivers and mechanisms behind the spatial distributions of these metrics, the BRT model outputs did provide a summary of the relative importance of the predictor variables used in model fitting, based on how often a variable is used for tree splitting (Elith et al., 2008). The relative importance of predictor variables across reef fish community metrics and island groups was compared using a bubble plot. In addition, partial dependence plots were generated for each predictor variable to interpret the individual effect of each predictor variable on the response variable (De'ath, 2007; Elith et al., 2008). However, these numerous plots were not included here due to space limitations and because they were beyond the primary objective of spatial prediction.

Fishes

4.3.2. Results: Spatial Distributions

Hawai'i

Highest predicted values of total species richness for reef fishes around the island of Hawai'i occurred in areas that were deep, inaccessible to humans or had low human populations nearby (Figure 4.13). These included southern portions of the island where there are few inhabitants, and the northeast (Hāmākua) coast where high sea cliffs prevent access to the ocean, as well as the relatively inaccessible coast of the Puna district south of Hilo. Protected bays along the west (Kona) coast showed low total fish richness, while the area around the westernmost point (Keāhole Point) had particularly high variability in predictions. The final model explained 35 percent of the deviance in the independent test data. Mean slope and depth were the most influential predictors in the model (Figure 4.14).

Total biomass of reef fishes showed similar spatial patterns, although the final model only explained 19 percent of the deviance in the test data (Figure 4.15). Spatial predictions generated with this model should be used with caution, particularly in areas outside of reef fish survey coverage. In this case, distance to humans and wave power were the most influential environmental predictors (Figure 4.14). Shallow areas close to human population along the Kona coast, such as Kawaihae and Kailua Kona, showed the lowest predicted biomass. Deeper areas along north Kohala and south of Kailua Kona had high variability in predictions.

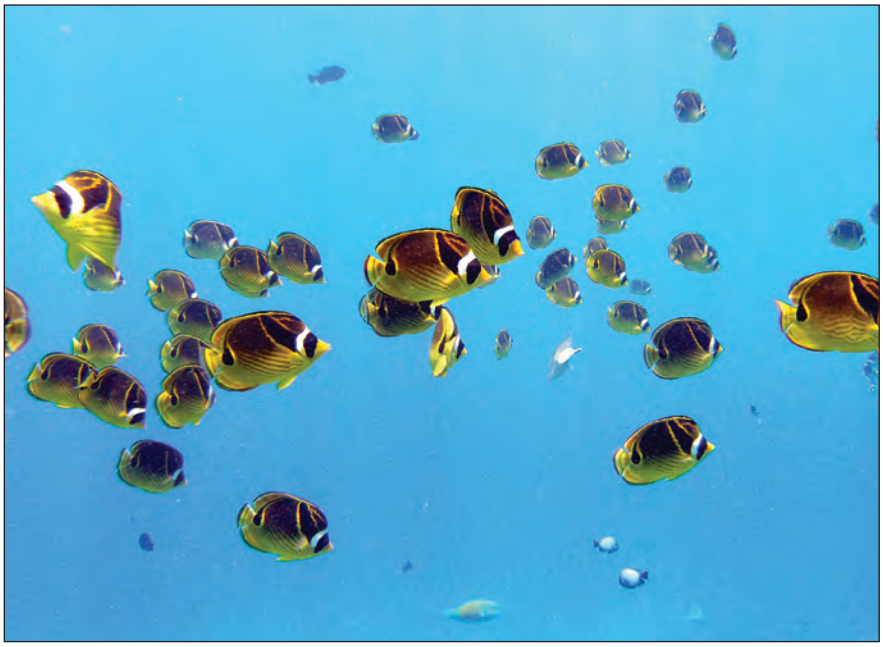

Chaetodon lunula *in Kona, Hawai'i. Photo credit: Kostantinos Stamoulis (University of Hawai'i)*

Highest predicted values of species richness for endemic reef fishes occurred in deeper areas, or those with high wave exposure such as the northeast (Hāmākua) and southeast coasts, and portions of the west (Kona) coast (Figure 4.16). The final model explained 36 percent of the deviance in the test data. Depth and wave power were the most influential predictors (Figure 4.14). High spatial variability in predictions seemed to be related to depth, with deeper areas showing higher variability. Biomass of endemics showed similar spatial patterns, though the final model only explained 18 percent of the deviance in the test data (Figure 4.17). Spatial predictions generated with this model should be used with caution, particularly in areas outside of reef fish survey coverage. Wave power, distance to shore, and depth were the most influential predictors (Figure 4.14). Areas with high variability in predictions included north Kohala and Keāhole Point.

Biomass of resource fishes, like overall biomass, had the highest values predicted in deep, inaccessible areas, and areas with low human populations (Figure 4.18). These included the northeast (Hāmākua) and southeast coasts. The north Kona coast generally had low biomass of resource fishes. The final model for resource fish biomass explained 22 percent of the deviance in the test data. High variability in predictions seemed related to depth, with deeper areas having higher variation. A large number of predictors were included in the final models with structural complexity (slope of slope) the most influential followed by distance to shore (Figure 4.14).

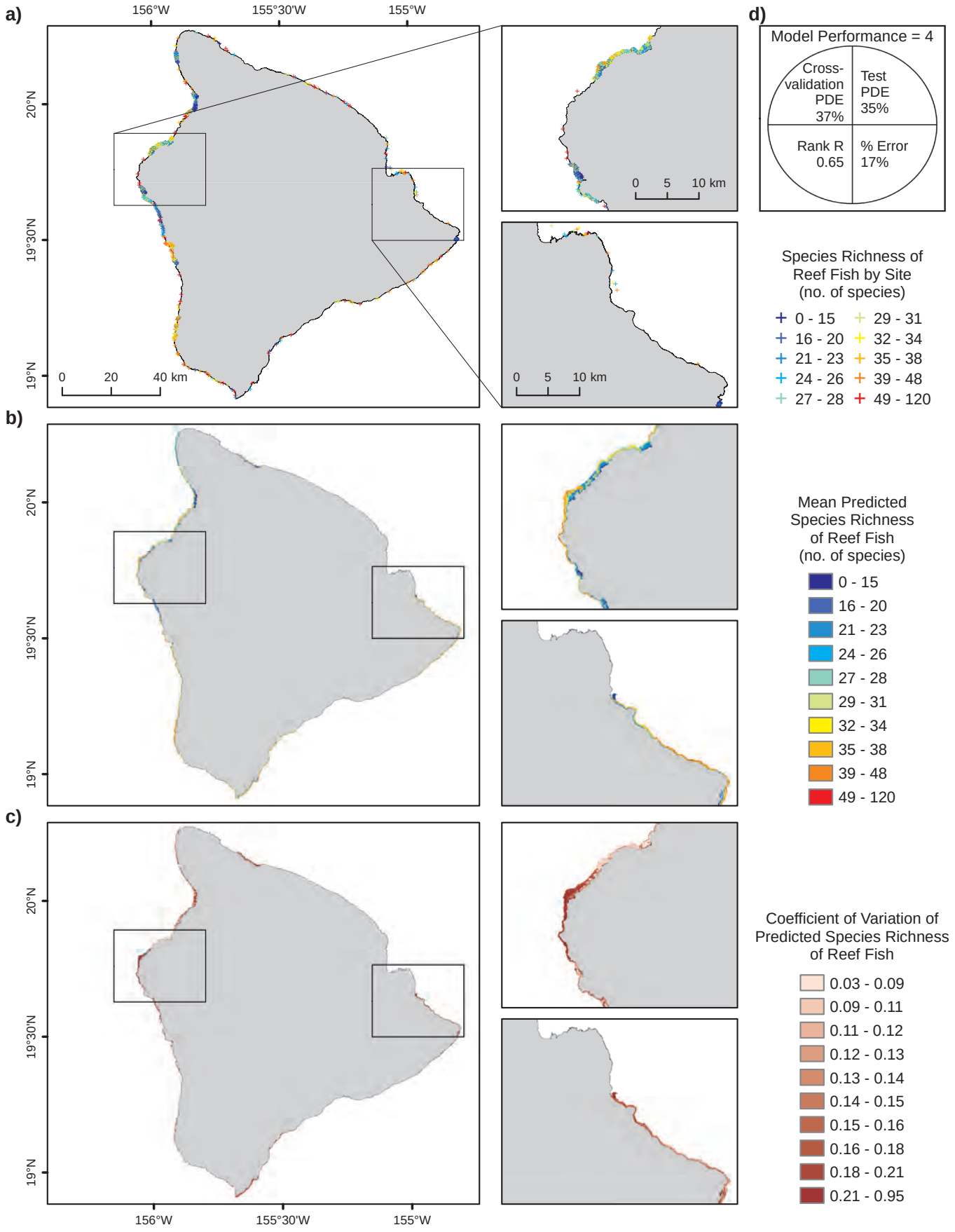

Figure 4.13. Predicted total species richness of reef fish for the island of Hawai'i. a) Total species richness by site summarized from in-situ *data (UH FERL, 2015a); b) mean; c) coefficient of variation of predicted total species richness of reef fish; and d) model quality derived from performance metrics (Table 4.7).*

Fishes

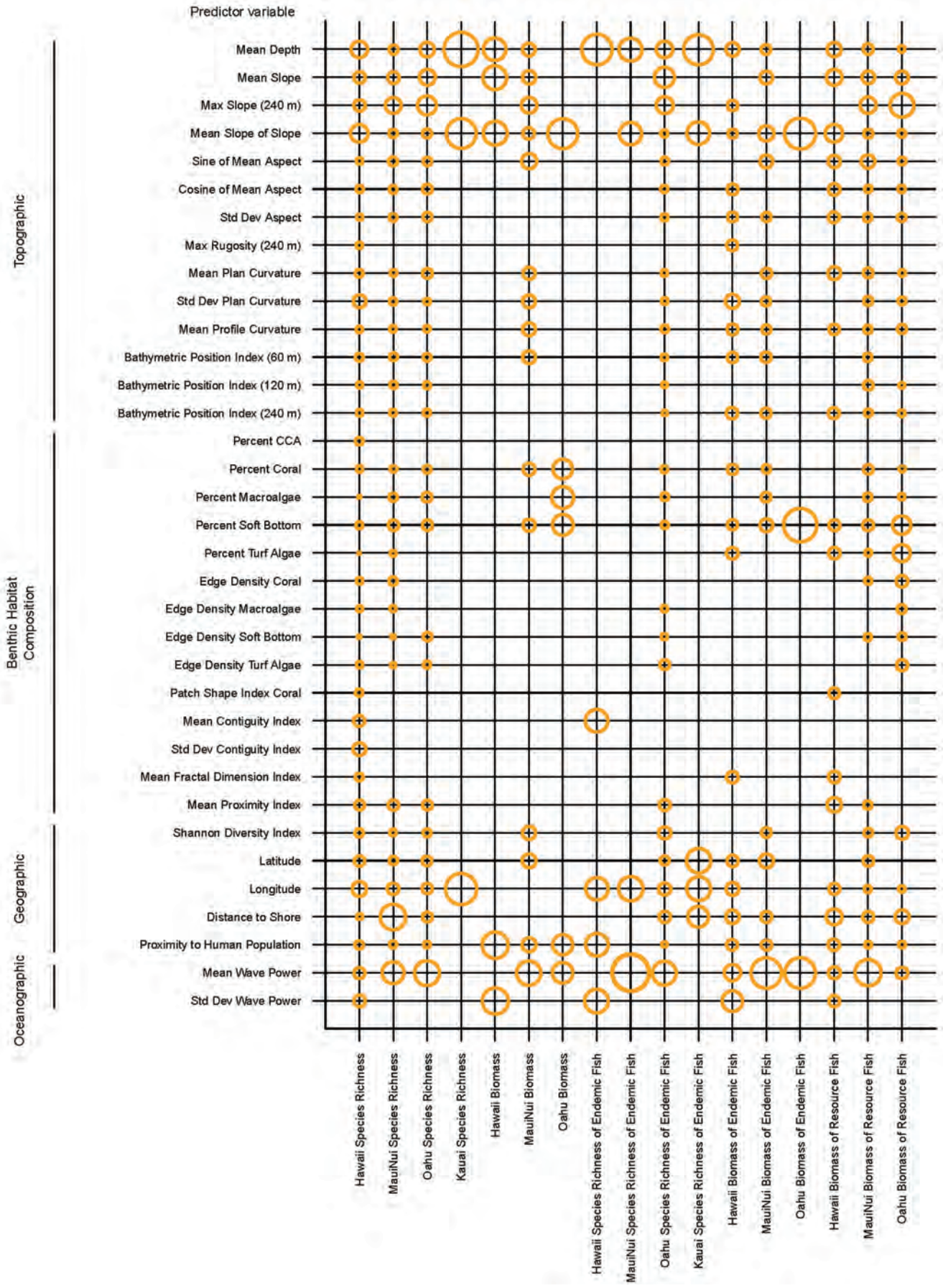

Figure 4.14. Predictor variable importance for each model. The area of a circle is proportional to the mean relative importance of the predictor variable across the bootstrap models.

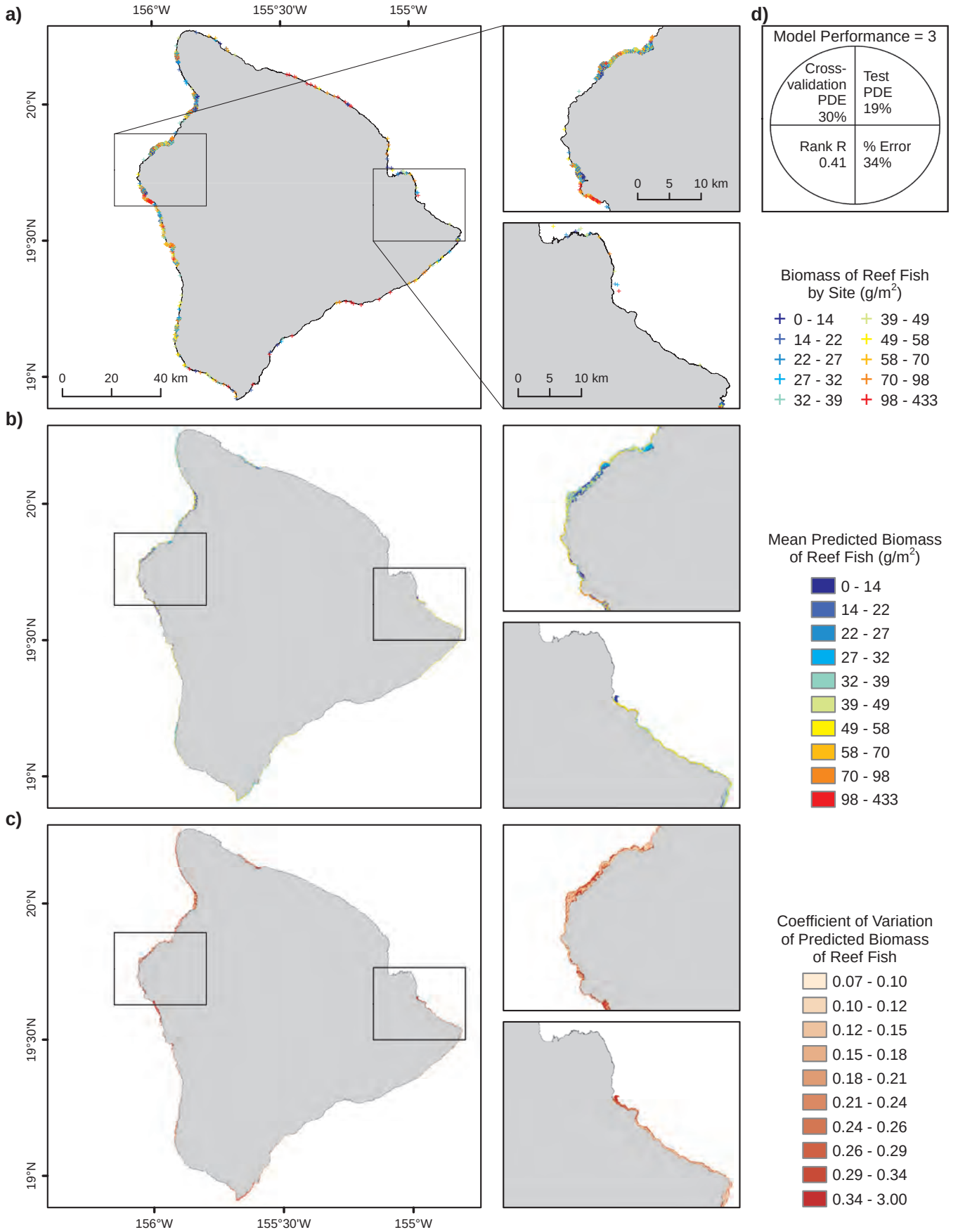

Figure 4.15. Predicted total biomass of reef fish for the island of Hawai'i. a) Total biomass of reef fish by site summarized from in-situ *data (UH FERL, 2015a); b) mean; c) coefficient of variation of predicted total biomass of reef fish; and d) model quality derived from performance metrics (Table 4.7).*

Fishes

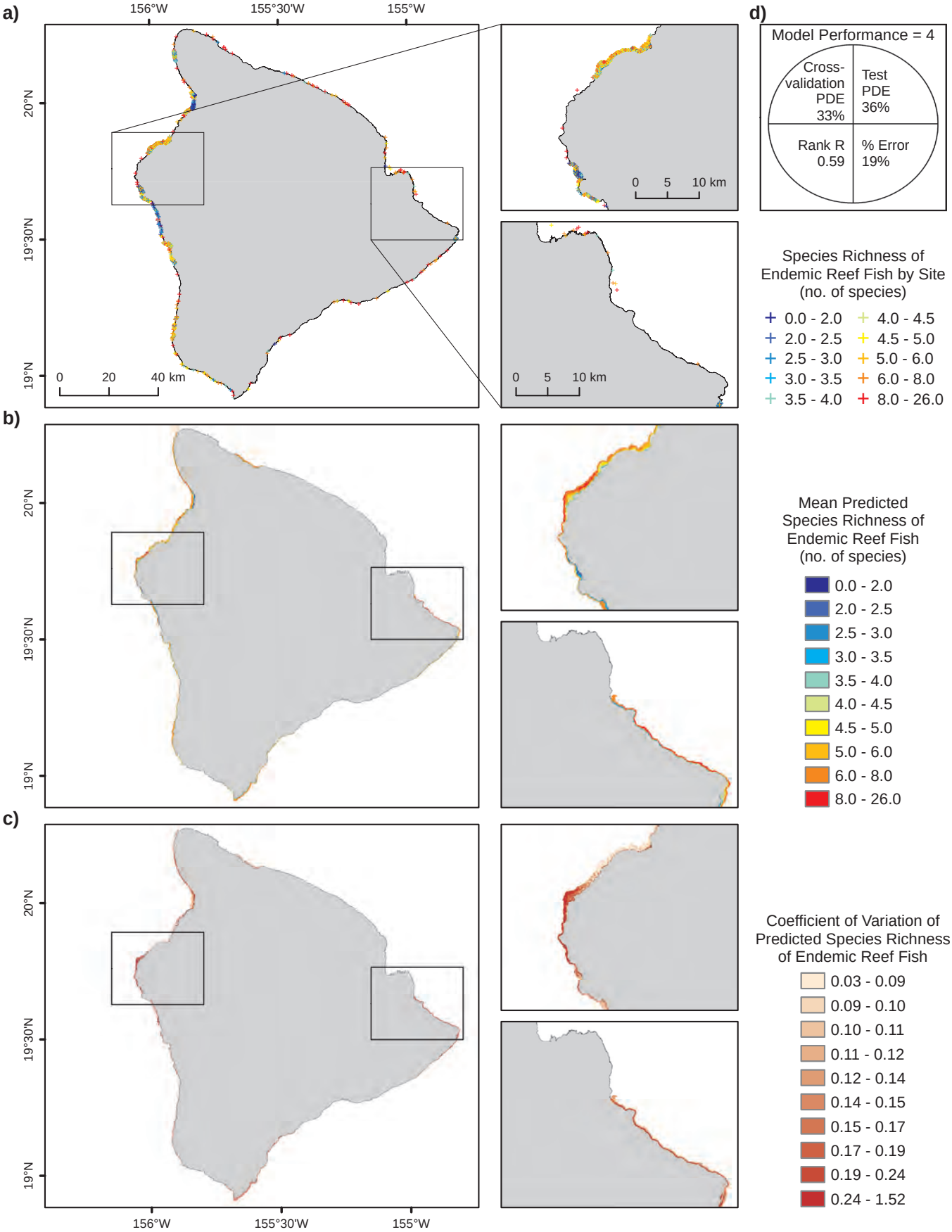

Figure 4.16. Predicted species richness of endemic reef fish for the island of Hawai'i. a) Species richness of endemic reef fish by site summarized from in-situ *data (UH FERL, 2015a); b) mean; c) coefficient of variation of predicted species richness of endemic reef fish; and d) model quality derived from performance metrics (Table 4.7).*

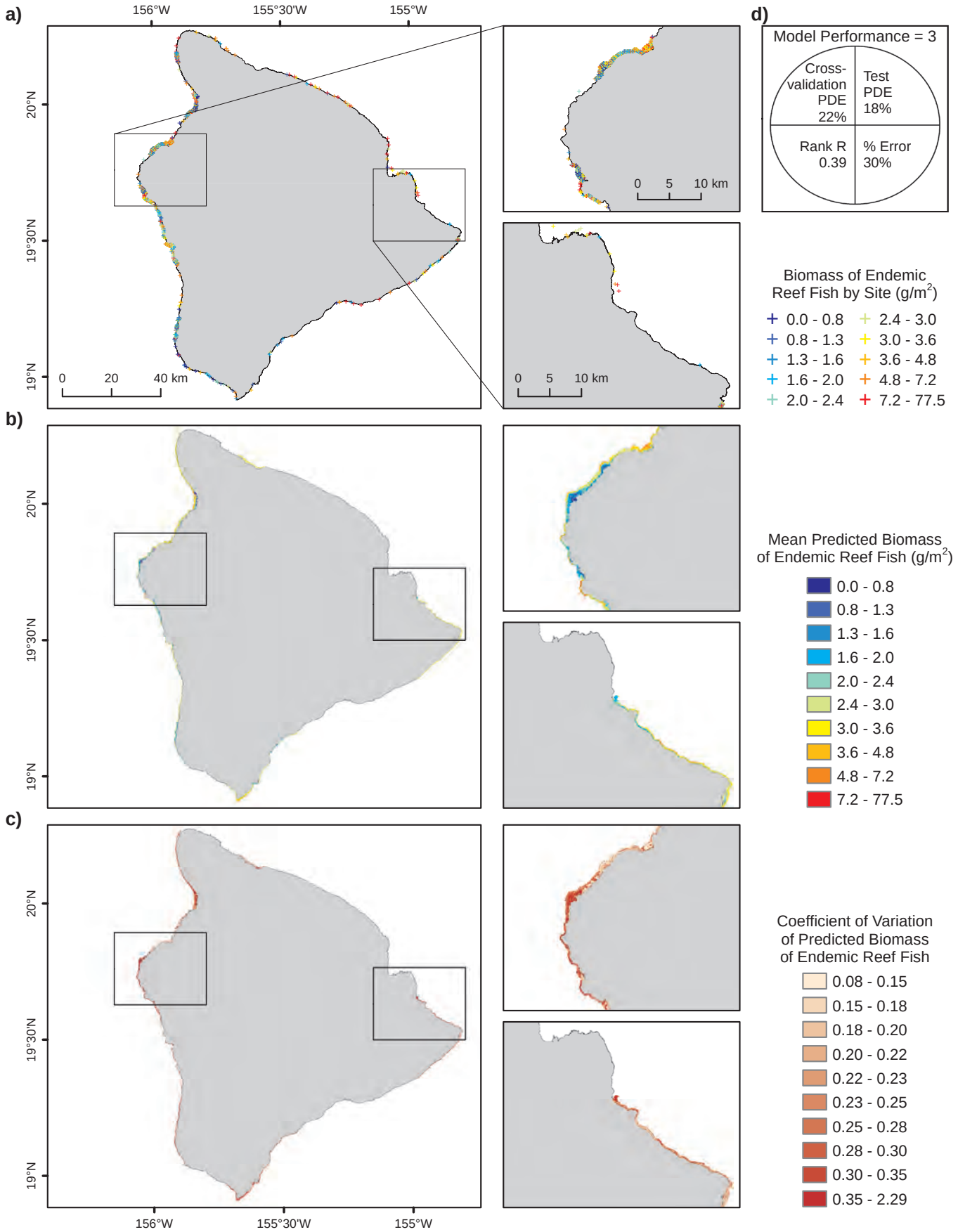

Figure 4.17. Predicted biomass of endemic reef fish for the island of Hawai'i. a) Biomass of endemic reef fish by site summarized from in-situ *data (UH FERL, 2015a); b) mean; c) coefficient of variation of predicted biomass of endemic reef fish; and d) model quality derived from performance metrics (Table 4.7).*

Fishes

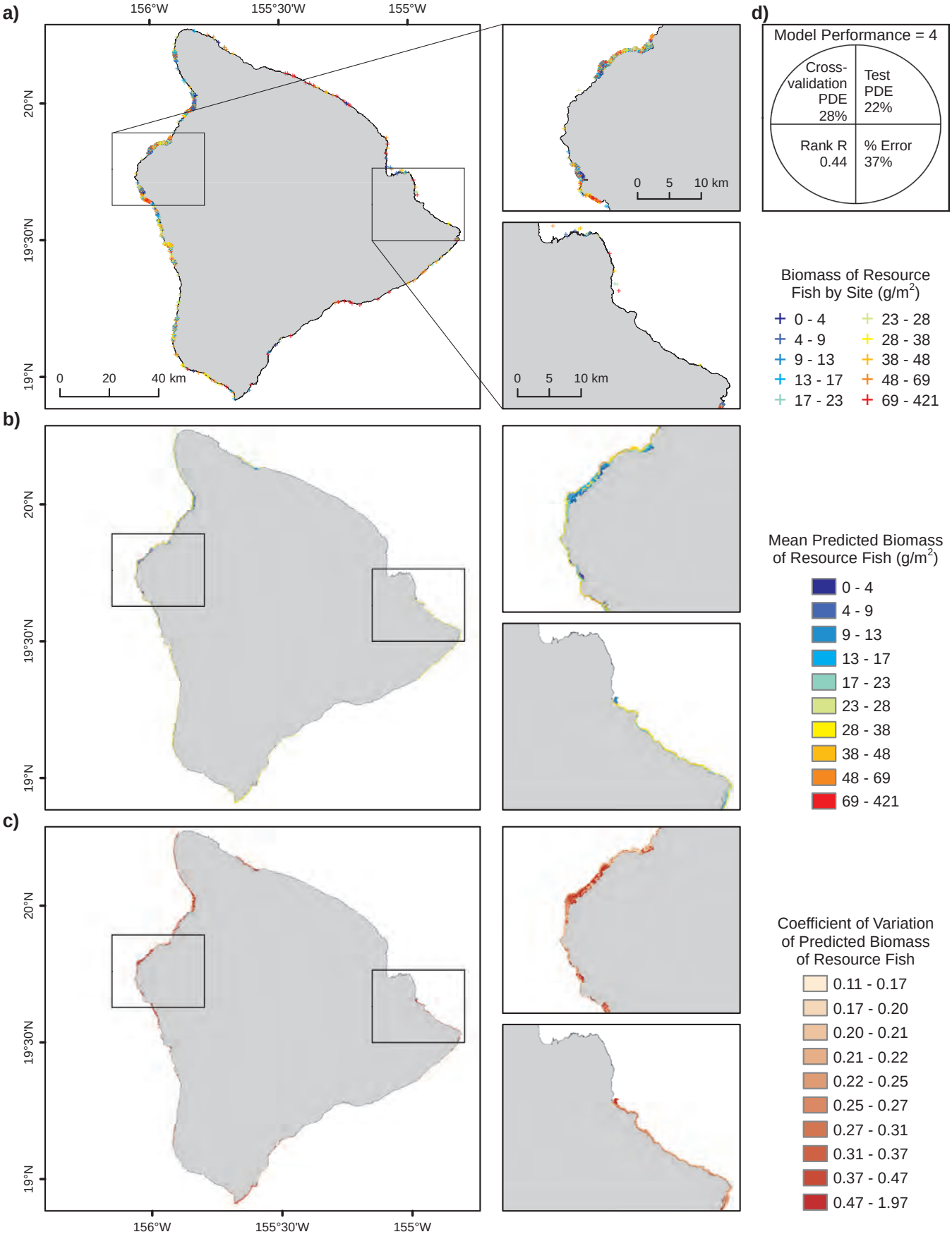

Figure 4.18. Predicted biomass of resource fish for the island of Hawai'i. a) Biomass of resource fish by site summarized from in-situ *data (UH FERL, 2015a); b) mean; c) coefficient of variation of predicted biomass of resource fish; and d) model quality derived from performance metrics (Table 4.7).*

Maui Nui

Highest predicted values of total species richness for reef fishes around Maui Nui were found primarily in areas of high wave exposure, as well as areas far from shore where wave exposure was low (Figure 4.19). These included the north shore of Molokaʻi and north and east/southeast shores of Maui, and to a lesser extent offshore areas of south Molokaʻi and east Maui. The Kalaupapa Peninsula on the north shore of Molokaʻi was a location with particularly high species richness, while the west shores of Maui had relatively low richness. The final model was among the top three models in overall performance and explained 51 percent of the deviance in the test data. High variability of predictions was found around west and southwest Maui, as well as around parts of south Molokaʻi. Most influential predictors included distance to shore, wave power and maximum slope in a 240 m neighborhood (Figure 4.14). Total fish biomass showed similar spatial patterns as species richness, but was more influenced by proximity to human population (Figure 4.20). The north shore of Molokaʻi, particularly the northeast side of Kalaupapa peninsula, and northeast Maui had notably high predicted biomass, whereas west facing shores of Maui generally had low values. High variability was shown along west shores of Molokaʻi and west and southwest Maui. The final model explained 31 percent of the deviance in the test data. Wave power was the most influential predictor, followed by maximum slope in a 240 m neighborhood (Figure 4.14).

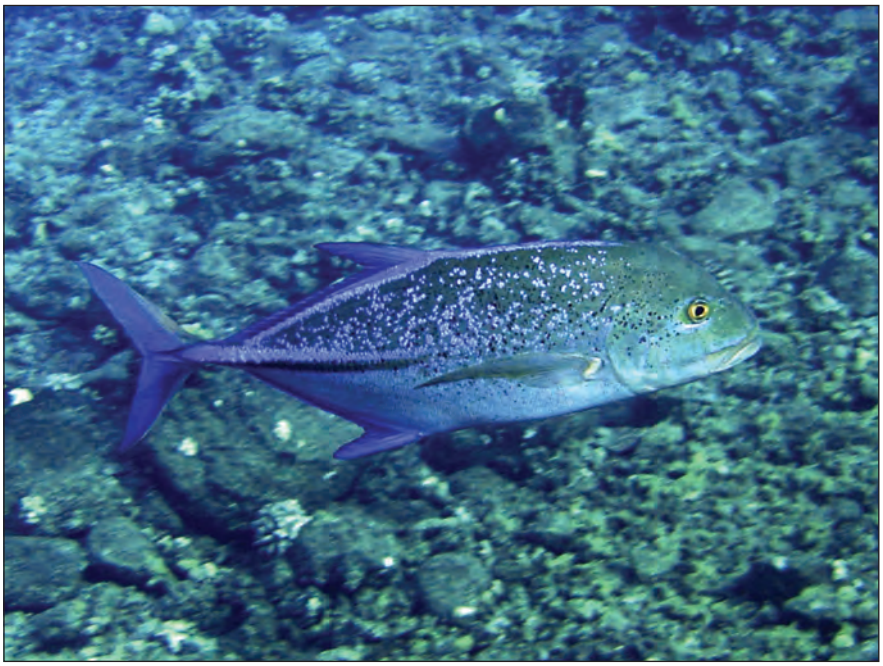

Resource fish Caranx melanpygus *in Molokini, Maui. Photo credit: Kostantinos Stamoulis (University of Hawaiʻi)*

Highest predicted values of species richness for endemic reef fishes were associated primarily with areas of high wave exposure, such as north and northeast shores of Maui and Molokaʻi (Figure 4.21). The west coast of West Maui and nearshore areas of south Molokaʻi had low predicted richness for endemics. Areas with high variability of predictions included west Maui and south Molokaʻi. The final model explained 44 percent of the deviance in the test data. Wave power was the most influential predictor (Figure 4.14). Biomass of endemic reef fishes showed similar patterns with high biomass predicted along north exposures of Maui and Molokaʻi, especially Kalaupapa Peninsula (Figure 4.22). Relatively low biomass of endemics was predicted in the west Maui and Kīhei areas. High variability in predictions coincided with low predicted endemic biomass. The final model explained 36 percent of the deviance in the test data. Wave power was the most influential predictor followed by structural complexity (slope of slope; Figure 4.14).

Biomass of resource fish was also influenced primarily by wave exposure, with north exposures of Molokaʻi and Maui exhibiting high predicted biomass of resource fishes and all other shores showing relatively low values (Figure 4.23). Again, Kalaupapa Peninsula, particularly the northeast shore, showed high predictions for biomass of resource fishes. High variability of predictions was coincident with low predicted resource fish biomass. The final model explained 29 percent of the deviance in the test data. Wave power was by far the most influential predictor, followed by maximum slope in a 240 m neighborhood (Figure 4.14).

Fishes

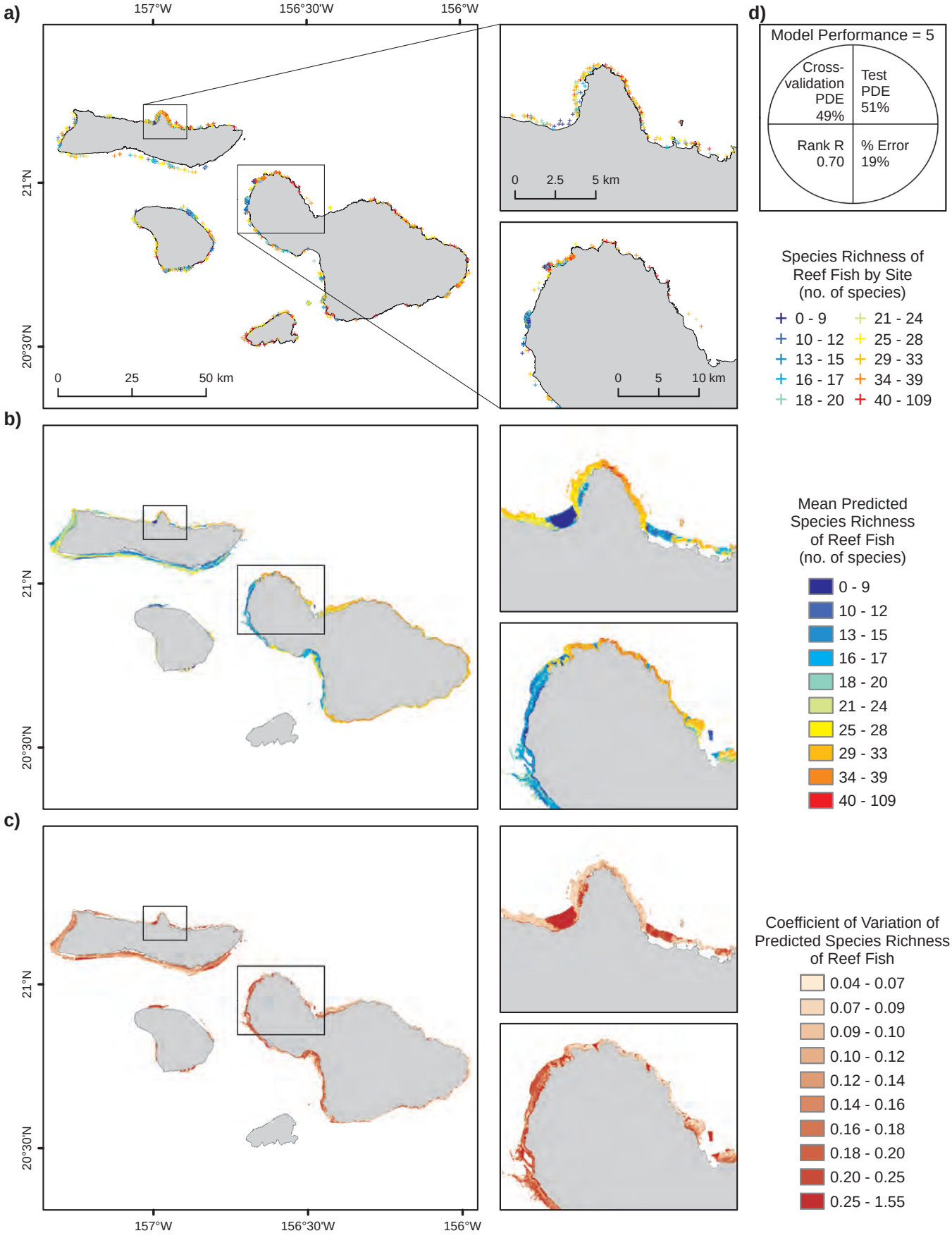

Figure 4.19. Predicted total species richness of reef fish for Maui Nui. a) Total species richness by site summarized from in-situ *data (UH FERL, 2015a); b) mean; c) coefficient of variation of predicted total species richness of reef fish; and d) model quality derived from performance metrics (Table 4.7).*

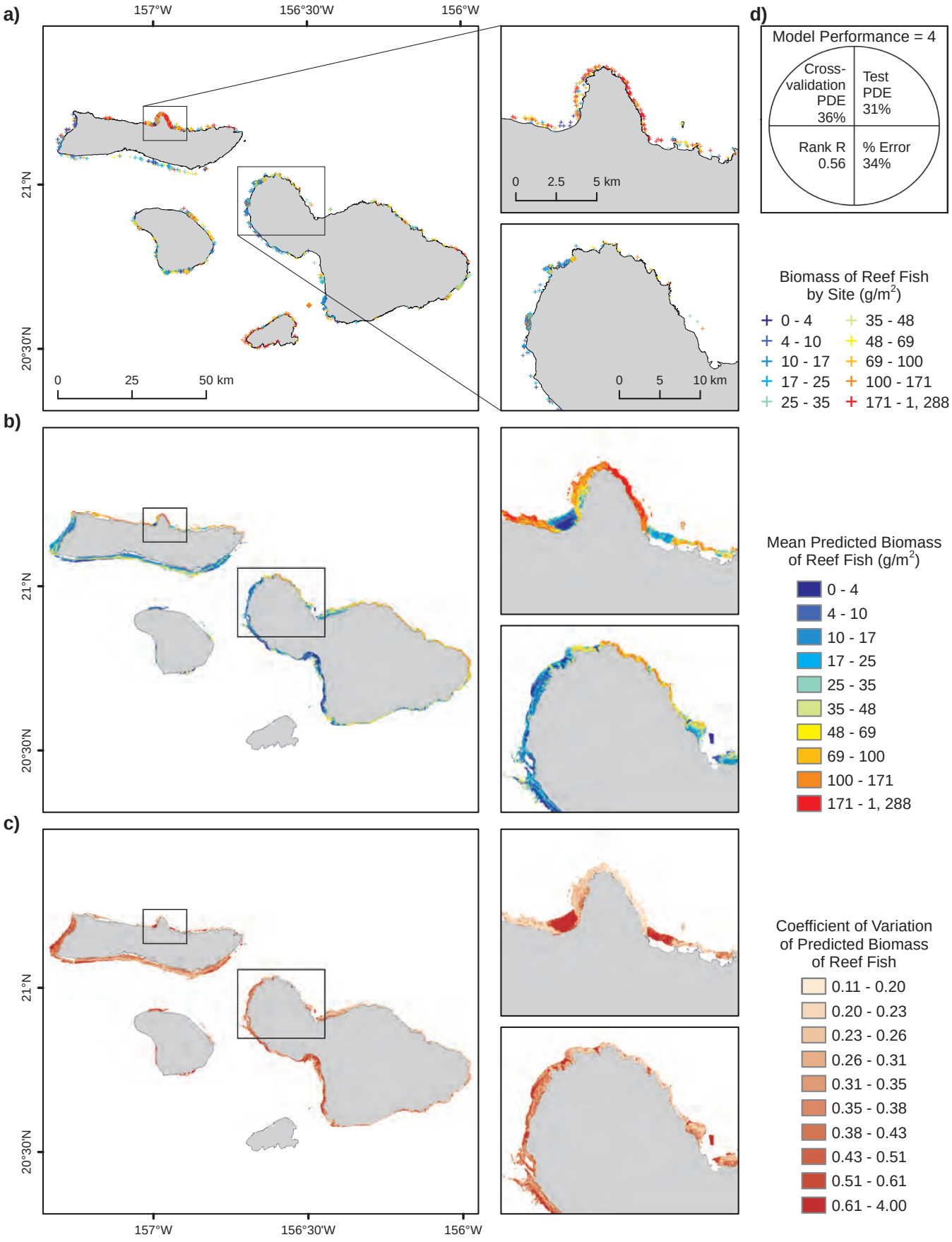

Figure 4.20. Predicted total biomass of reef fish for Maui Nui. a) Total biomass of reef fish by site summarized from in-situ *data (UH FERL, 2015a); b) mean; c) coefficient of variation of predicted total biomass of reef fish; and d) model quality derived from performance metrics (Table 4.7).*

Fishes

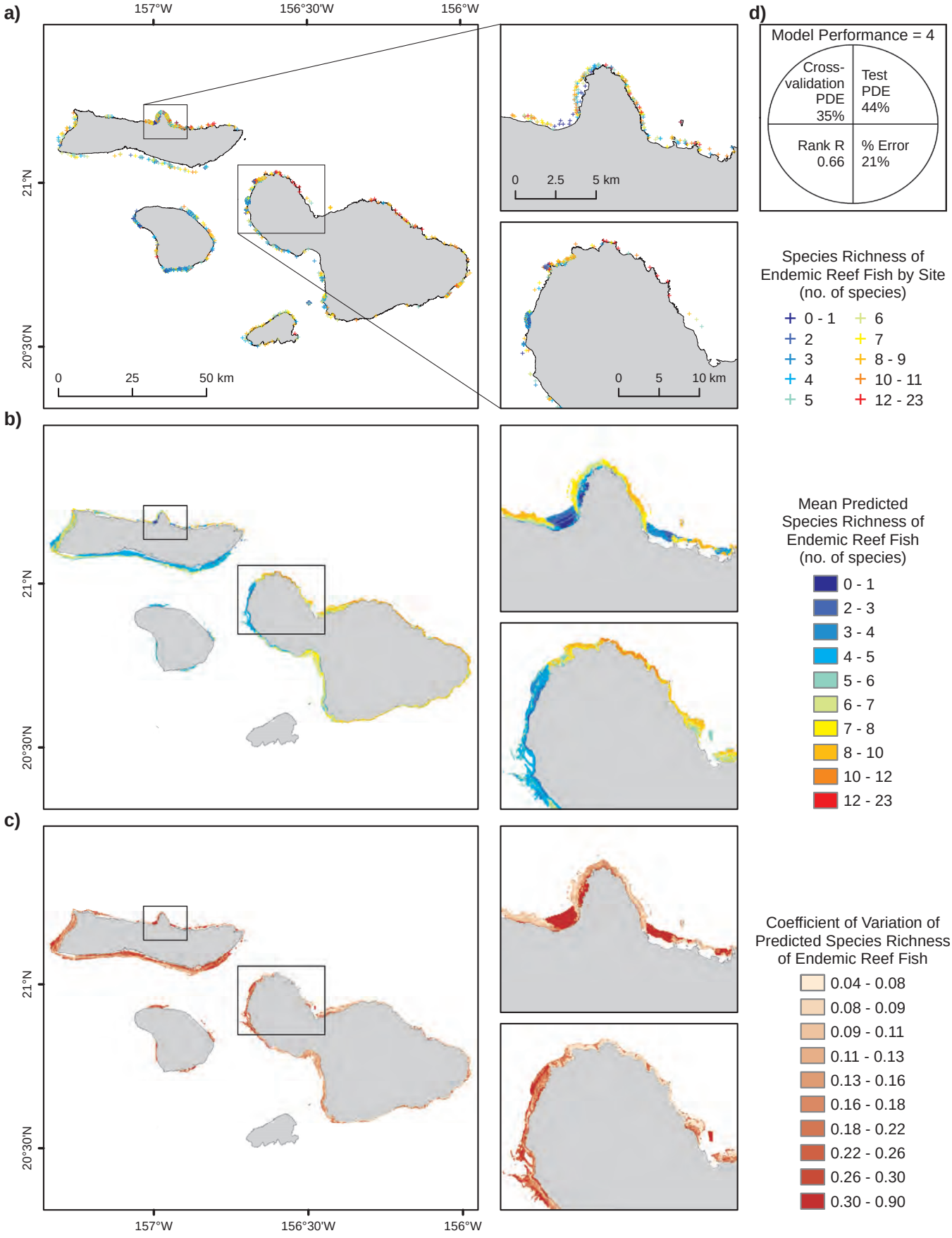

Figure 4.21. Predicted species richness of endemic reef fish for Maui Nui. a) Species richness of endemic reef fish by site summarized from in-situ *data (UH FERL, 2015a); b) mean; c) coefficient of variation of predicted species richness of endemic reef fish; and d) model quality derived from performance metrics (Table 4.7).*

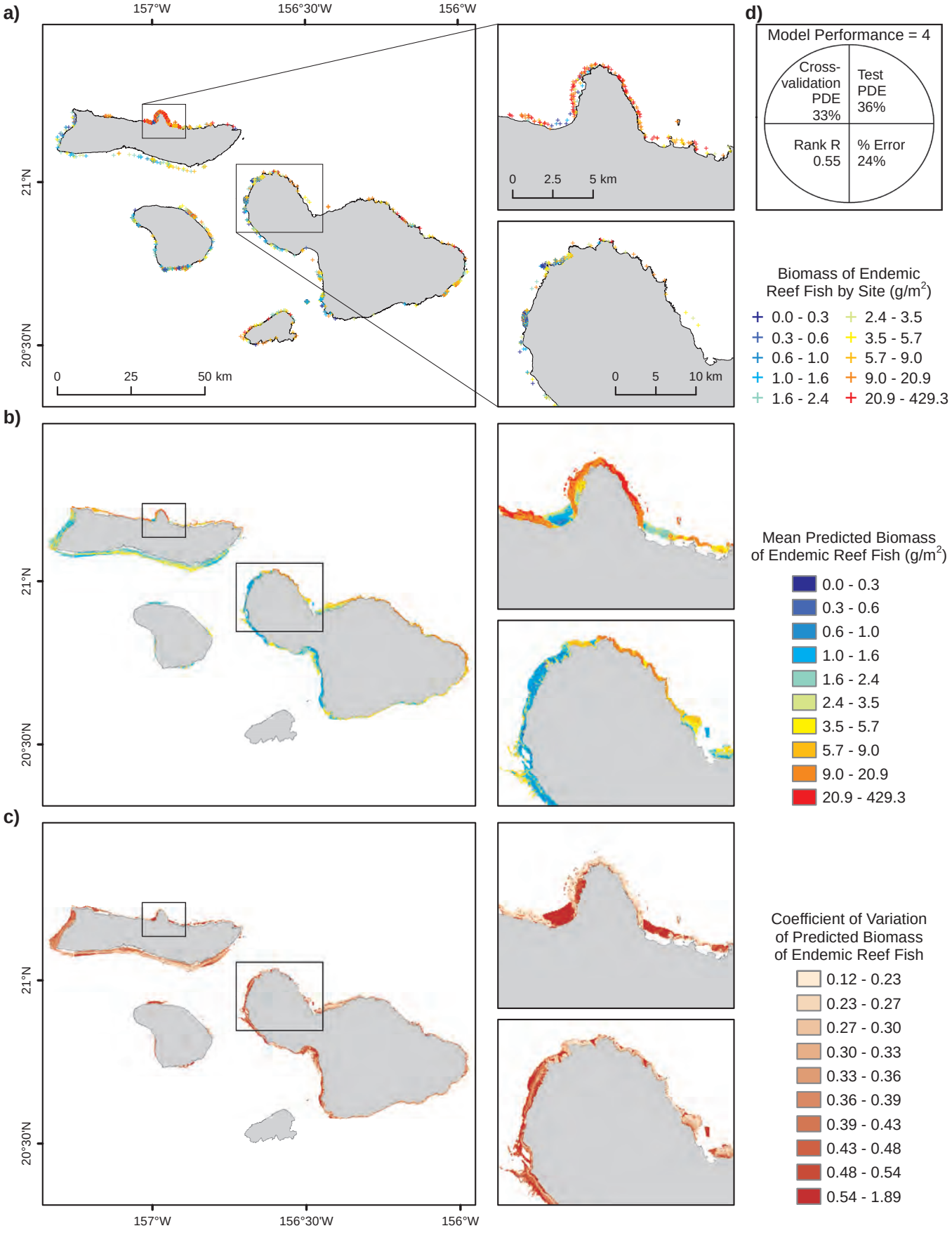

Figure 4.22. Predicted biomass of endemic reef fish for Maui Nui. a) Biomass of endemic reef fish by site summarized from in-situ *data (UH FERL, 2015a); b) mean; c) coefficient of variation of predicted biomass of endemic reef fish; and d) model quality derived from performance metrics (Table 4.7).*

Fishes

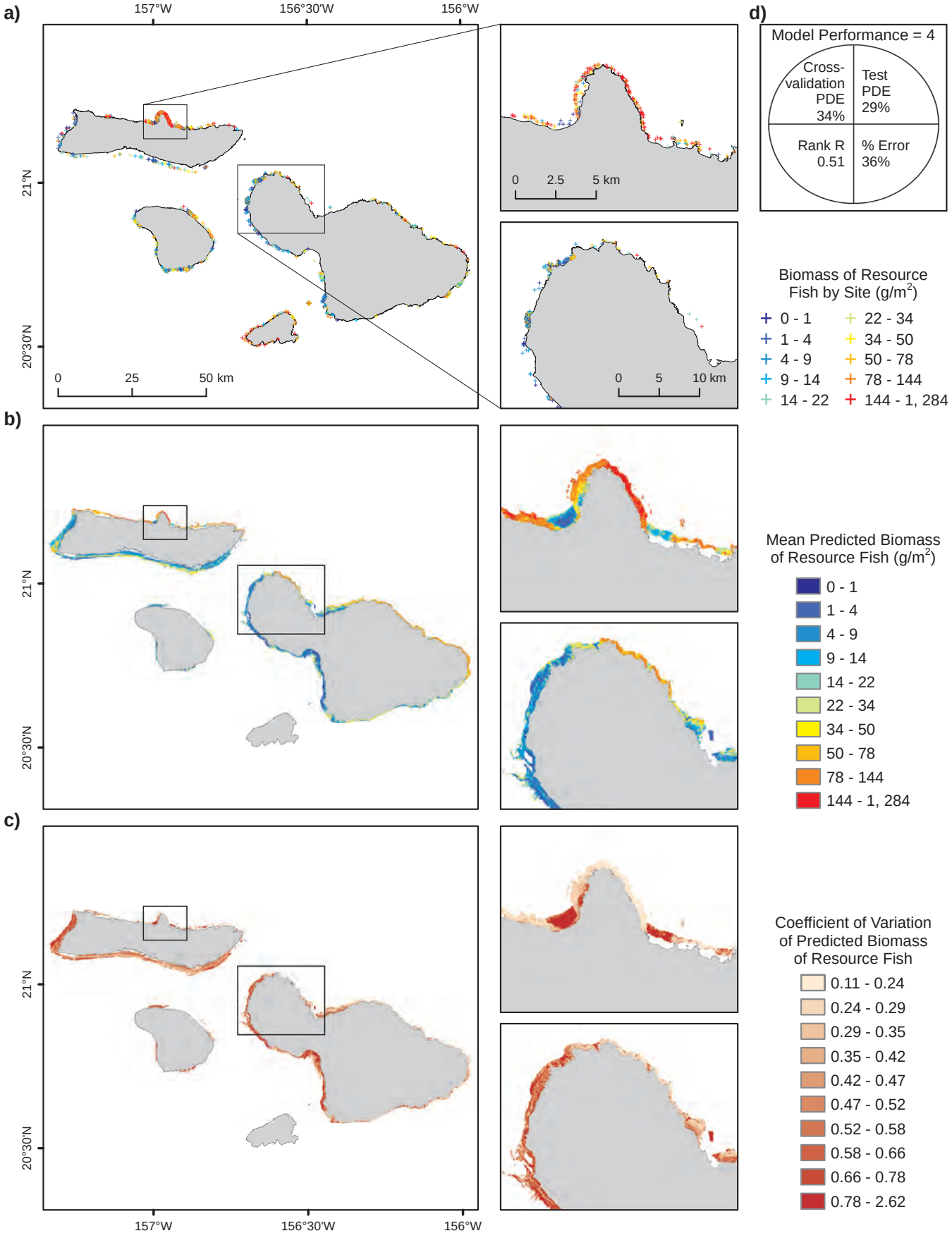

Figure 4.23. Predicted biomass of resource fish for Maui Nui. a) Biomass of resource fish by site summarized from in-situ *data (UH FERL, 2015a); b) mean; c) coefficient of variation of predicted biomass of resource fish; and d) model quality derived from performance metrics (Table 4.7).*

O'ahu

Highest predicted values of total species richness for reef fishes were located around the westernmost point of O'ahu (Ka'ena point), as well as around Makapu'u Point and deeper areas along the east shore, including outside of Kāne'ohe Bay (Figure 4.24). These areas generally correspond with high wave exposure. Areas with low values of species richness included the south shore and Kāne'ohe Bay. High spatial variability of predictions were shown along south shores and east shores around Kāne'ohe Bay. The final model was among the top three models in overall performance and explained 52 percent of the deviance in the test data. The most influential predictors were wave power and maximum slope in a 240 m neighborhood, followed by slope and depth (Figure 4.14). Overall biomass of reef fishes showed a generally similar pattern only more closely related to structural complexity, such that locations of high biomass were predicted along reef edges and channels (Figure 4.25). Hanauma Bay on the southeast point and Pūpūkea on the north shore are no-take marine reserves with high quality habitat, and are locations with particularly high predicted total biomass. South and west shores had low predicted biomass values. High variability in predictions generally coincided with low predicted values and were focused along south and east shores near Kāne'ohe Bay. The final model explained 45 percent of the deviance in the test data. Structural complexity (slope of slope) was the most influential predictor, followed by macroalgae cover and wave power (Figure 4.14).

Highest predicted values of species richness for endemic reef fishes were somewhat uniformly distributed along deeper areas of the north and east shores of O'ahu, corresponding with high wave exposure (Figure 4.26). Shallow areas along the south shore and Kāne'ohe Bay had low predicted species richness of endemics. The final model explained 49 percent of the deviance in the test data. The top predictor was wave power, followed by slope, mean slope in a 240 m neighborhood, and then depth (Figure 4.14). High variability in predicted values were focused primarily on south and east shores near Kāne'ohe Bay. Biomass of endemics was also predicted at high levels on north and east shores, although it was not as uniformly distributed as endemic richness (Figure 4.27). Patch reefs in Kāne'ohe Bay showed particularly high biomass of endemics. The south shore of O'ahu had low predicted biomass of endemics. Spatial variability in predictions was related to depth as well as low predicted values. The final model explained 33 percent of the deviance in the test data. The most influential predictor was proximity to soft bottom, followed by structural complexity (slope of slope) and wave power (Figure 4.14).

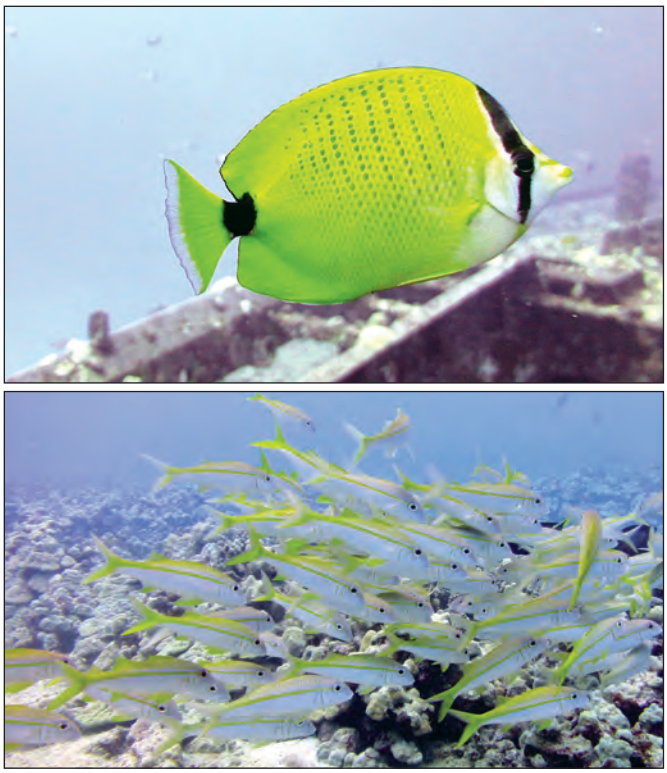

Endemic reef fish Chaetodon miliaris *in Waikiki, O'ahu (top), and resource reef fish* Mulloidichthys vanicolensis *in Kewalo, O'ahu (bottom). Photo credit: Kostantinos Stamoulis (University of Hawai'i)*

High biomass of resource fishes was predicted predominantly on the east shore of O'ahu, as well as the westernmost point (Kaena Point) and the southeast point of the island (Figure 4.28). Notable locations of high predicted biomass for resource fishes were no-take marine reserves located at Pūpūkea on the north shore and Hanauma Bay on the southeast shore. South and west shores had low predicted biomass of resource fishes. High variability in predictions corresponded with low predicted values. The final model explained 42 percent of the deviance in the test data. The most influential predictor was maximum slope in a 240 m neighborhood, followed by proximity to soft bottom and turf cover (Figure 4.14).

Fishes

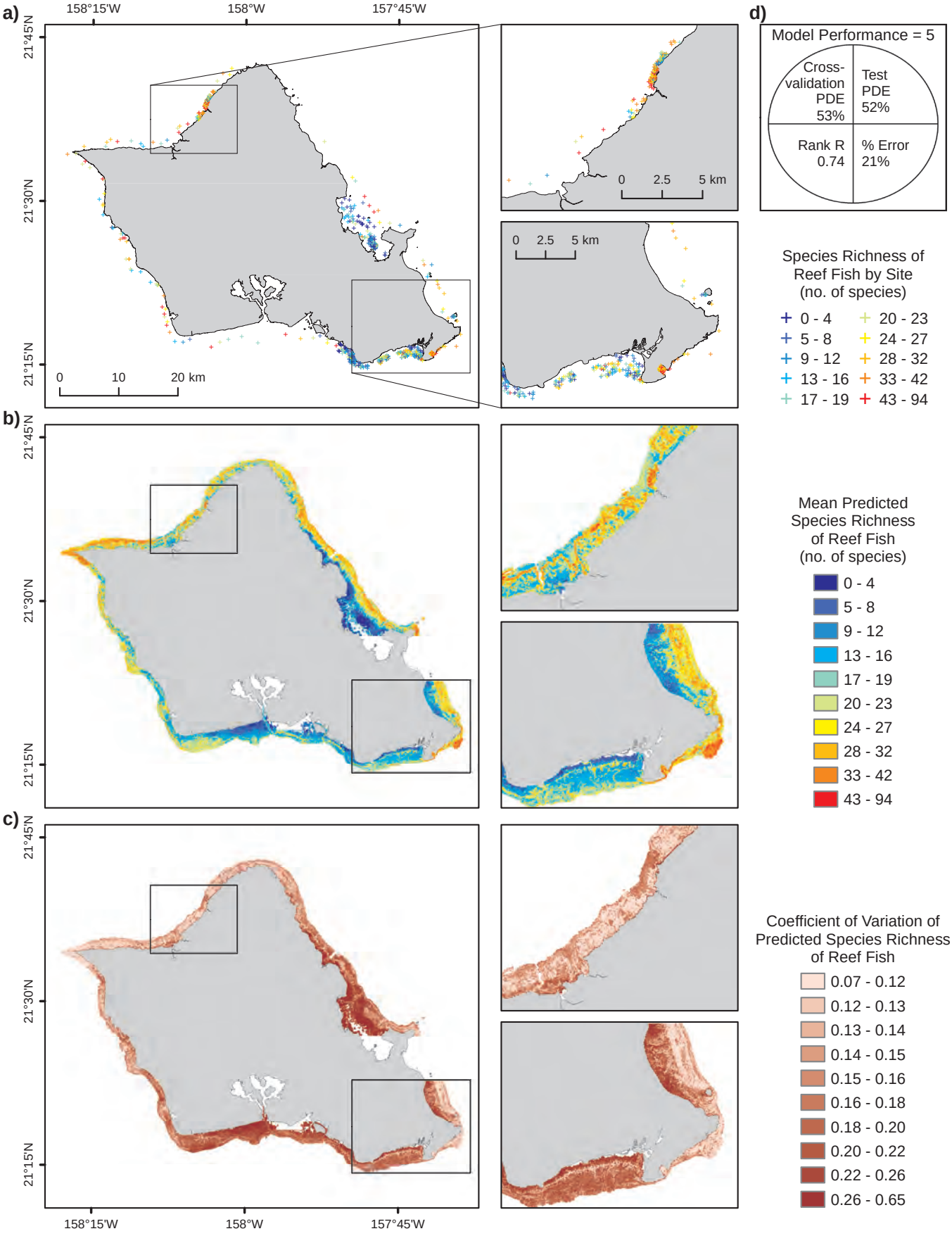

Figure 4.24. Predicted total species richness of reef fish for O'ahu. a) Total species richness by site summarized from in-situ *data (UH FERL, 2015a); b) mean; c) coefficient of variation of predicted total species richness of reef fish; and d) model quality derived from performance metrics (Table 4.7).*

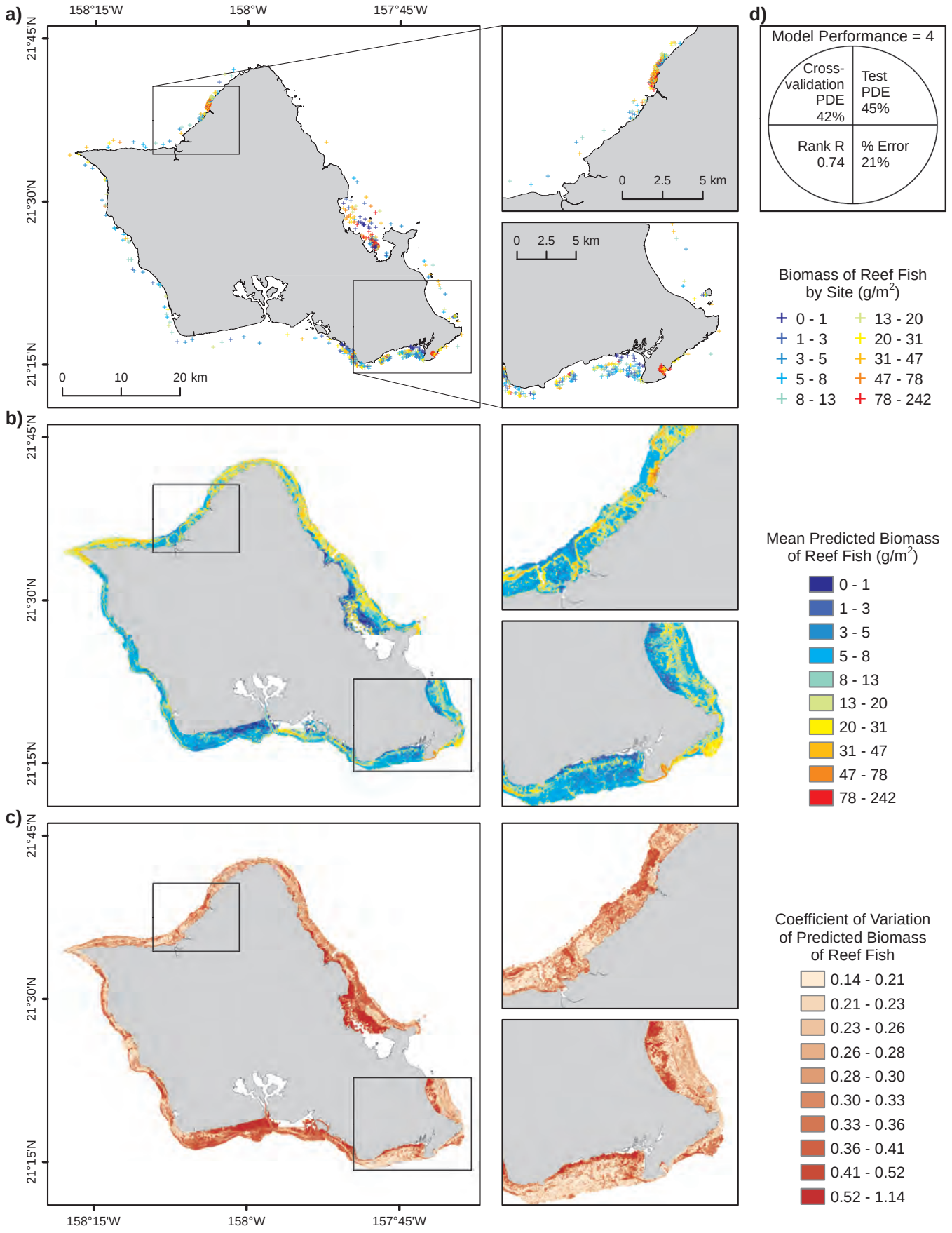

Figure 4.25. Predicted total biomass of reef fish for O'ahu. (a) Total biomass of reef fish by site summarized from in-situ *data (UH FERL, 2015a); b) mean; c) coefficient of variation of predicted total biomass of reef fish; and d) model quality derived from performance metrics (Table 4.7).*

Fishes

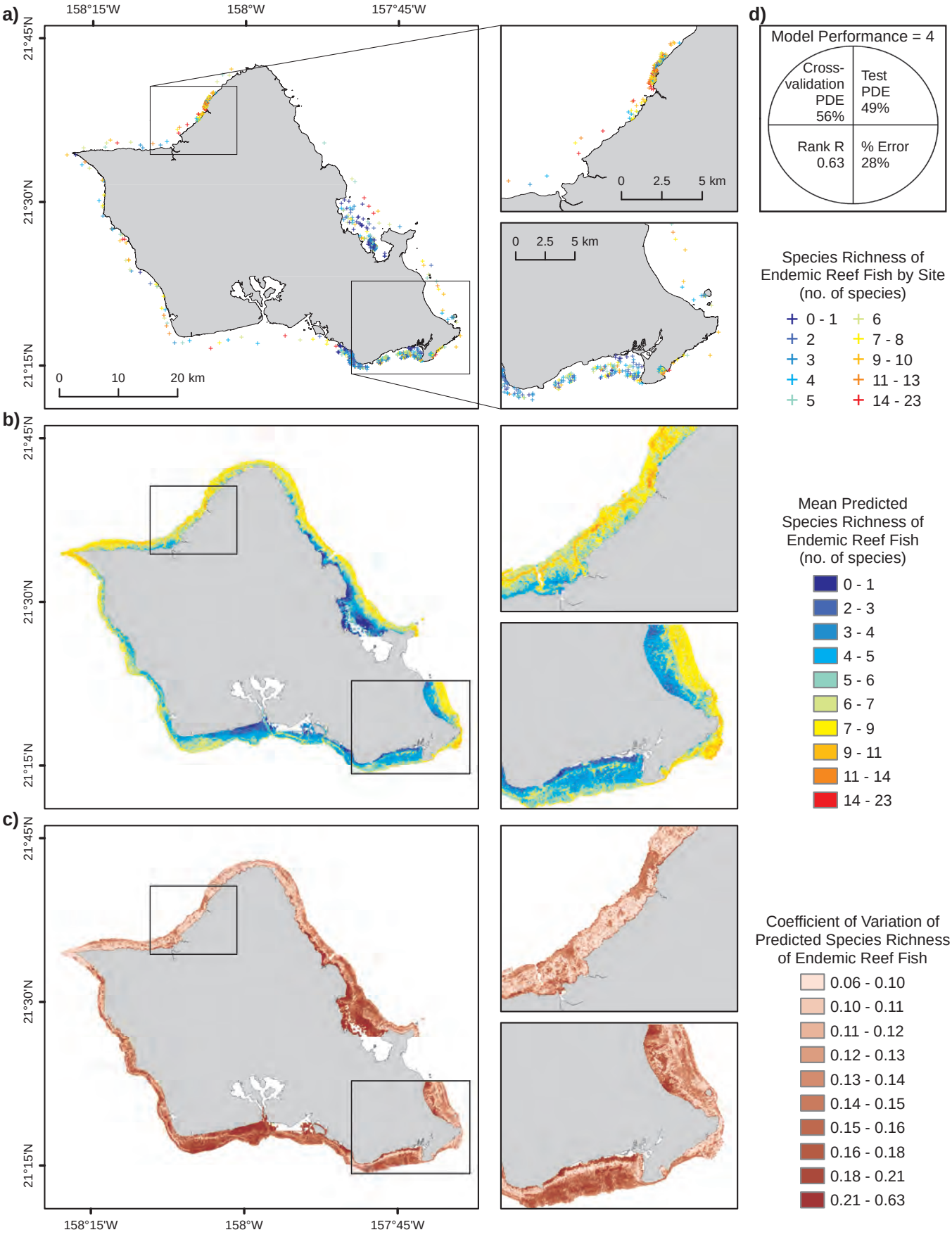

Figure 4.26. Predicted species richness of endemic reef fish for O'ahu. a) Species richness of endemic reef fish by site summarized from in-situ *data (UH FERL, 2015a); b) mean; c) coefficient of variation of predicted species richness of endemic reef fish; and d) model quality derived from performance metrics (Table 4.7).*

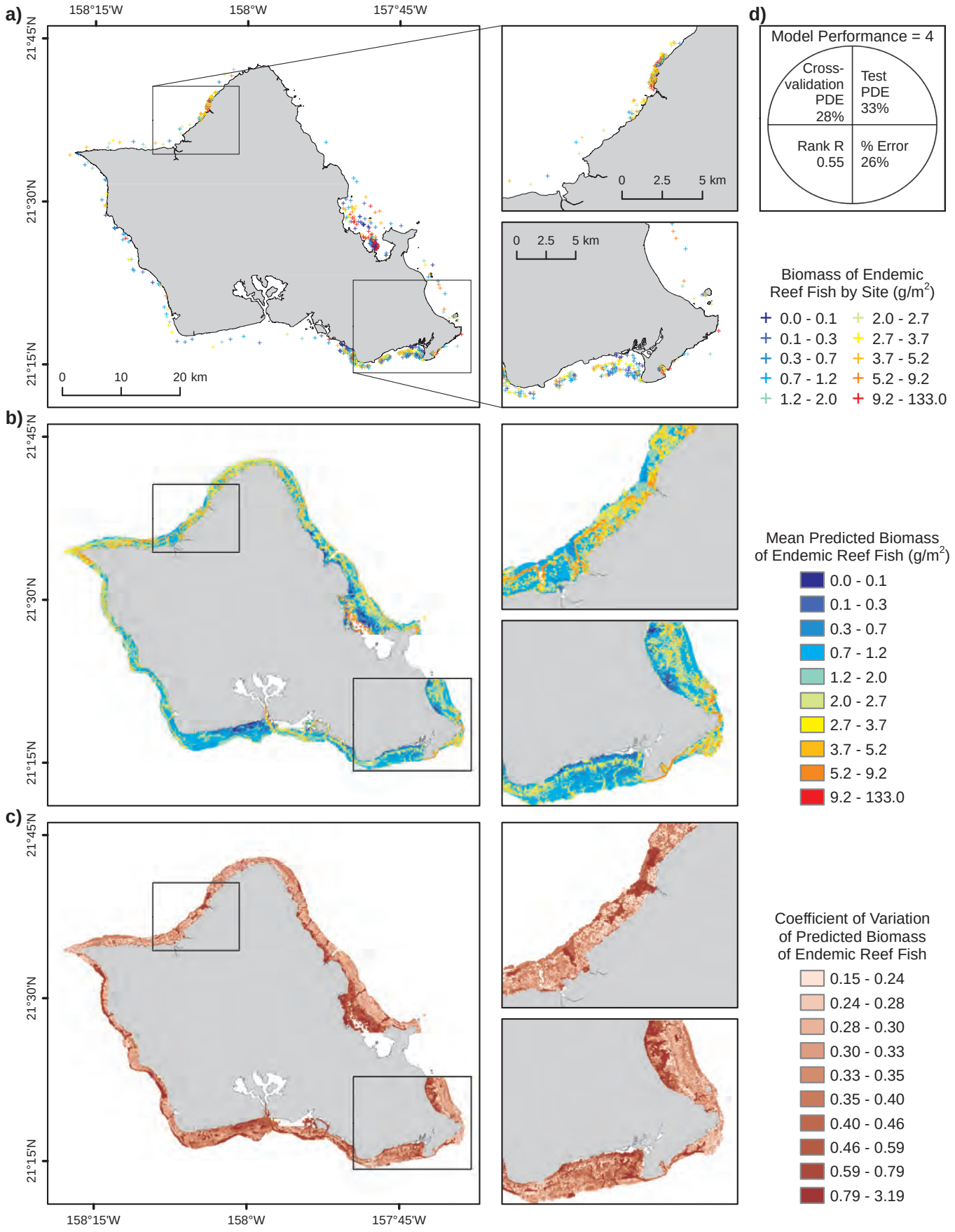

Figure 4.27. Predicted biomass of endemic reef fish for O'ahu. a) Biomass of endemic reef fish by site summarized from in-situ *data (UH FERL, 2015a); b) mean; c) coefficient of variation of predicted endemic reef fish biomass; and d) model quality derived from performance metrics (Table 4.7).*

Fishes

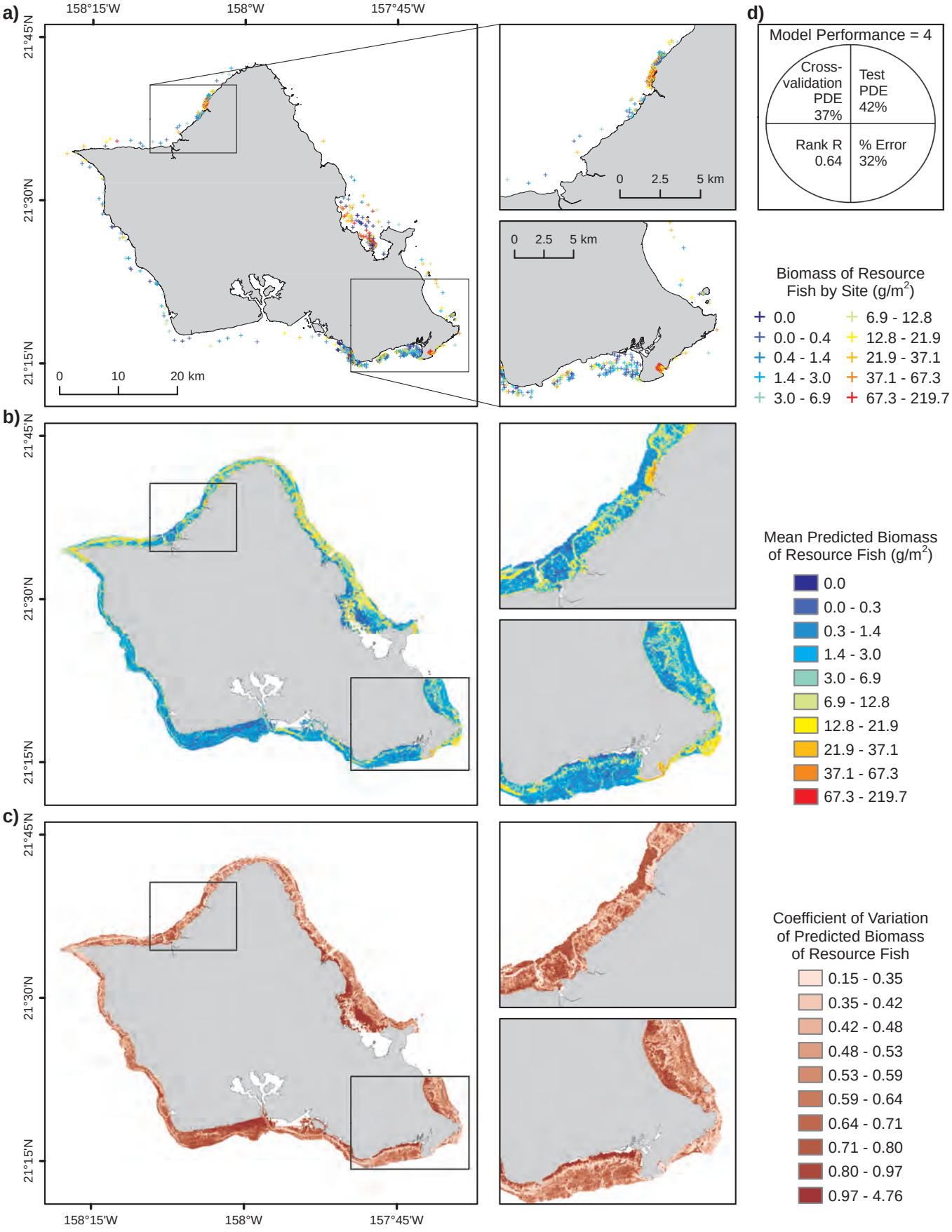

Figure 4.28. Predicted biomass of resource fish for O'ahu. a) Biomass of resource fish by site summarized from in-site data (UH FERL, 2015a); b) mean; c) coefficient of variation of predicted resource fish biomass; and d) model quality derived from performance metrics (Table 4.7).

Kaua'i

Highest predicted values of total species richness for reef fishes were found along the northeast and east shores of Kaua'i, primarily along reef edges (Figure 4.29). The north shore east of Hanalei Bay showed particularly high values. Shallow areas along the northwest, west and southwest shores had lower values. High spatial variability of predictions was found around the entire island, but especially the south and north coast, near Hanalei Bay. The final model was among the top three models in overall performance and explained 47 percent of the deviance in the test data. Models utilized only three predictors; depth, longitude, and structural complexity (Figure 4.14). Use of additional variables did not improve model performance.

Highest predicted values for species richness of endemic reef fishes was primarily focused on the northeast corner of the island and occurred in moderate to deeper areas, whereas shallow areas along west exposures had lower values of endemic richness (Figure 4.30). High variability of predictions was primarily on the north and southeast shore. The final model explained 36 percent of the deviance in the test data. The most influential predictor was depth (Figure 4.14).

Endemic reef fish Coris flavovittata*. Photo credit: Andrew Gray (NOAA NMFS/ PIFSC/CREP)*

Models for total biomass of reef fish, biomass of endemic reef fish, and biomass of resource reef fish explained only 0-9 percent of the deviance in the test data, indicating that these models performed poorly when confronted with data not used in model fitting. Maps are not shown for these models since they do not provide reliable predictions away from training data.

Fishes

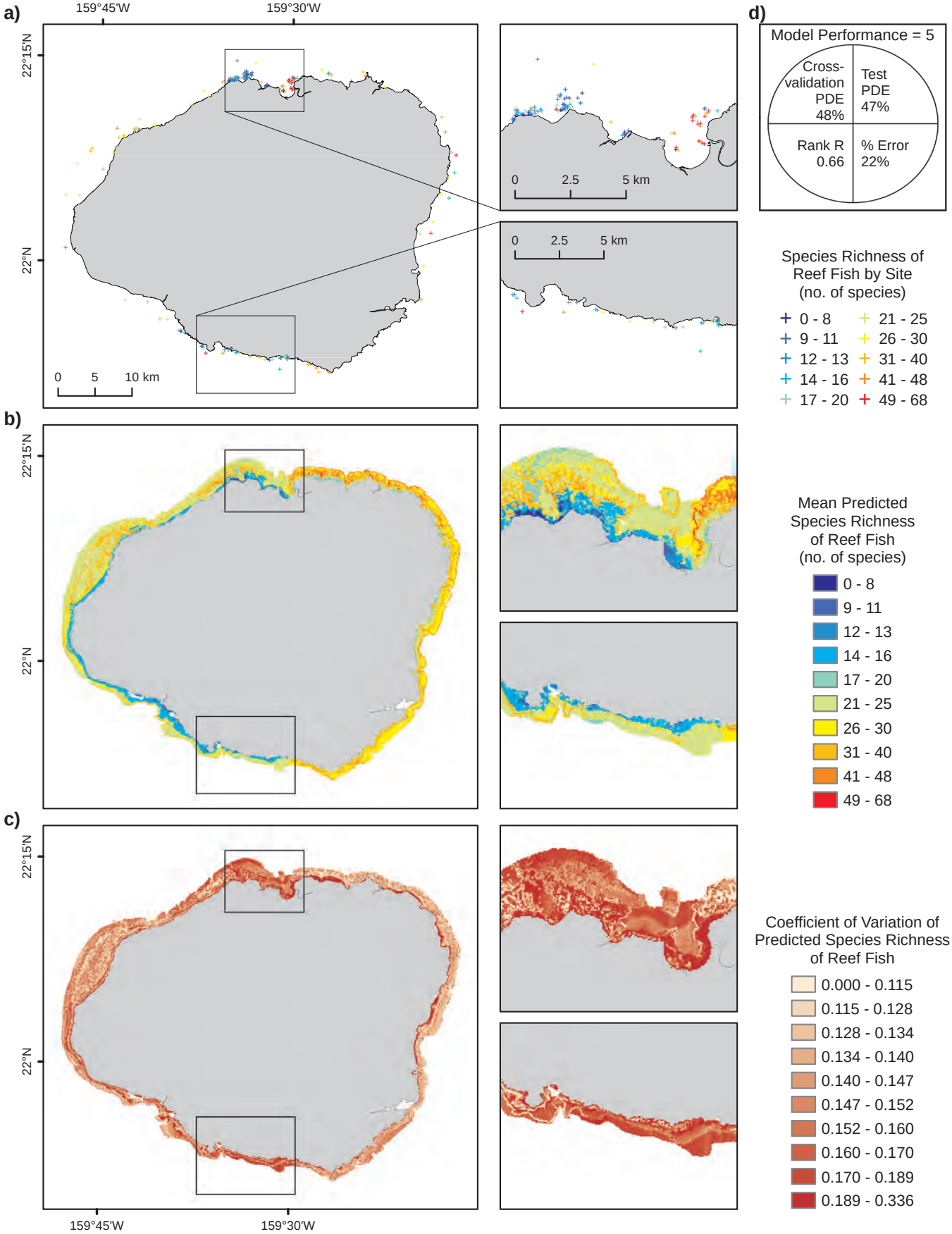

Figure 4.29. Predicted total species richness of reef fish for Kaua'i. a) Total species richness by site summarized from in-situ *data (UH FERL, 2015a); b) mean; c) coefficient of variation of predicted total species richness of reef fish; and d) model quality derived from performance metrics (Table 4.7).*

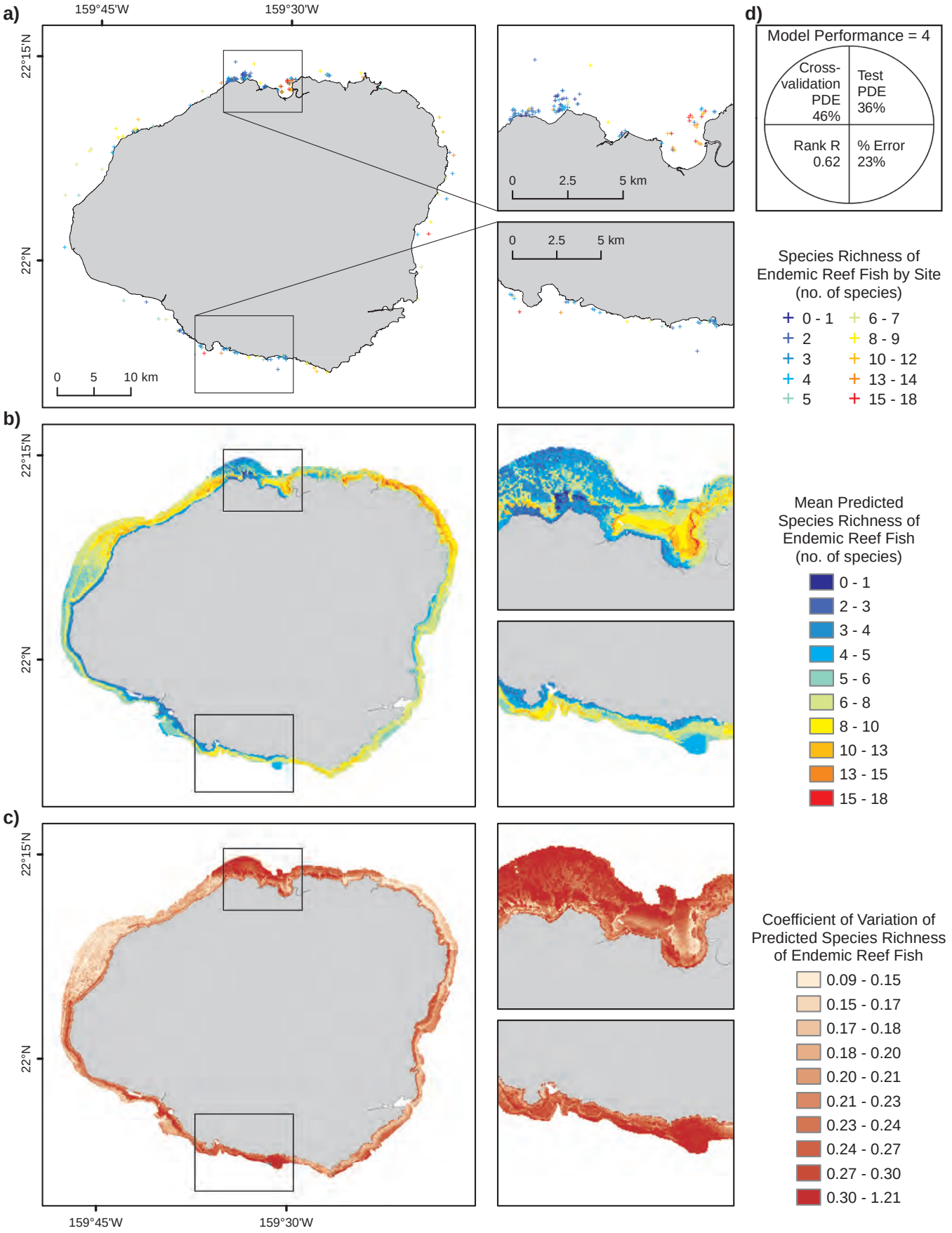

Figure 4.30. Predicted species richness of endemic reef fish for Kaua'i. a) Species richness of endemic reef fish by site summarized from in-situ *data (UH FERL, 2015a); b) mean; c) coefficient of variation of predicted species richness of endemic reef fish; and d) model quality derived from performance metrics (Table 4.7).*

Fishes

4.3.3. Discussion

Zebrasoma flavescens *in Kealakekua Bay on the Kona coast of the island of Hawai'i. Credit: Lisa Wedding (Standford University)*

A number of locations within the island groups had notably high or low predicted richness and biomass as reported in the results. High values generally corresponded with areas that were not easily accessible to humans due to remoteness, depth, distance to shore and/or high wave energy. These include the Hāmākua and Puna districts on the island of Hawai'i, the north shore of Moloka'i, the east shore of Maui, the west and southeast points as well as the northeast shore of O'ahu, and the northeast shore of Kaua'i. These areas are less susceptible to fishing and indirect human impacts and thus harbor more robust fish communities (Fabricius, 2005; Williams et al., 2008; Brewer et al., 2013). Conversely, areas more accessible to humans had low species richness and biomass values. These included shallow locations near human population centers, and areas with low wave energy. Locations with particularly low values included Kailua Kona on Hawai'i, the leeward shore of west Maui and the Kīhei area, the south shore of O'ahu, and the southeast shore of Kaua'i. On O'ahu, the long-term MPAs at Pūpūkea on the north shore and Hanauma Bay on the south shore had locally high predicted values of species richness and biomass. Although management status was not included as a predictor in the models, the beneficial effects of marine reserves on fish communities have been well documented in Hawai'i and elsewhere (Friedlander et al., 2007; Lester et al., 2009). Even before designation as MPAs, these areas contained high quality benthic habitats (structurally complex with a variety of habitat cover types) and healthy fish communities (DAR, 1992).

Model performance varied among island groups due to inherent differences in environmental factors, benthic habitats, and fish communities, as well as response variable sample sizes (number of fish surveys). Sample size likely had the greatest effect on overall model performance (i.e., PDE; Stockwell and Peterson, 2002), whereas environmental and ecological factors influenced the ranking of key predictors for each response variable. In general, models predicting species richness had higher explanatory power than those predicting biomass, in part due to higher variability in biomass values. Predictive models for O'ahu and Maui Nui performed the best, likely due to high sample sizes and spatial coverage of fish surveys. For Hawai'i, total reef fish richness, endemic reef fish richness, and resource fish biomass models performed fairly well in terms of the amount of deviance explained, although they did not perform as well as the corresponding models for O'ahu. Total fish biomass and endemic fish biomass did not perform as well for Hawai'i and were likely overfit to the training data. Though Hawai'i had a large number of fish surveys along the west (Kona) coast, other portions of this large island were not well sampled. These were mostly remote, wave-exposed areas that may harbor higher biomass and richness. In addition, some of the remote areas with high fish biomass where there were fish surveys, did not have high resolution bathymetry data. For Kaua'i, fish richness models performed well, but all three fish biomass models performed poorly. These models appeared to be over-fit to the training data and could not be used reliably to make spatial predictions. Kaua'i as a whole was under sampled, which contributed to poor predictive model performance for some response variables. Kaua'i also experiences higher oceanographic variability than other islands which may have hindered model performance, including higher wave power, coolest temperatures, and highest rainfall.

While the most influential predictors for each response variable differed within and among island groups, there were some consistencies. For Hawai'i and Kaua'i islands, depth was among the most influential predictors for both total and endemic species richness. On O'ahu and Maui Nui, wave power was among the most influential predictors for species richness variables. For biomass variables, seafloor topography variables representing structural complexity were among the most influential predictors for all island groups. The relationship between structural complexity and reef fish biomass is well documented in the literature, as structurally complex habitats provide shelter for fishes in Hawai'i (Friedlander and Parrish, 1998), and elsewhere (Pittman et al., 2009; Graham and Nash, 2013). Wave power and distance to humans were among the most influential predictors of biomass variables for all island groups, with the exception of Kaua'i. Fish biomass is often negatively related to fishing pressure which was represented in our models through these two proxy variables. Areas with high human population and/or low wave power typically experience higher fishing pressure (Williams et al., 2008). In addition, wave power can mitigate sedimentation and other land-based stressors because it promotes mixing and reduces the retention time of sediments and nutrients in the nearshore areas (Larcombe et al., 1995; Fabricius et al., 2005; De'ath and Fabricius, 2010). For biomass of resource fish specifically, maximum slope in a 240 m neighborhood was an influential predictor for all island groups, with the exception of the island of Hawai'i. This broad scale predictor variable may be important for resource species given that they tend to be highly mobile thus utilizing larger areas (Green et al., 2015). Slope at this broad scale may not be as important for resource fish biomass on the island of Hawai'i, however, due to its' unique geomorphology as the youngest island in the Hawaiian chain. Reefs on Hawai'i Island tend to be very narrow and give way quickly to deep water compared to the other islands, which could explain why slope measured at the 60 m scale was the top predictor. On Maui Nui and O'ahu, proximity to soft bottom was also a key predictor for resource fish biomass, perhaps reflecting the fact that reef predators, often targeted by fishermen, tend to utilize reef edges (Friedlander et al., 2007b).

4.3.4. Data and information gaps

Data gaps were encountered in both the response and predictor datasets. Broad areas were lacking data from the response dataset derived from underwater visual surveys, including northwest Moloka'i, east Moloka'i, north central Maui, southeast Maui and north Hawai'i. These areas are difficult for divers to access from either boats or shoreline due to their high wave energy and distance from boat harbors. Sample sizes of fish surveys also varied among areas. Sample sizes were particularly low for Ni'ihau, northeast Kaua'i, north Lāna'i, southwest O'ahu and Kaho'olawe. These areas are less sampled primarily due to their remoteness, lack of management priority, or limited resources available for monitoring. Poor performance of spatial predictive models of biomass for Kaua'i was likely a result of the relatively limited extent of reef fish survey data, as well as more dynamic oceanographic conditions around Kaua'i compared to the other islands.

Mo'omomi Preserve on northwest Moloka'i. Photo credit: Bryan M. Costa (NOAA NOS/NCCOS)

Beyond the spatial differences of sampling effort among islands, coastlines and bio-physical heterogeneity, visual surveys were also limited by the depth range of the surveys, which are determined by safe depths for open circuit SCUBA (max approximately 30 m). Likewise, fish surveys under-sample species that are especially wary of divers as well as cryptic or nocturnally active taxa. Lastly, visual survey data includes data from a range of years (Table 4.1), and time was not included in our analyses. However, the occurrence of data was

Fishes

spread relatively evenly across years, with the bulk of the replicates occurring from 1999-2011. Data were also collected with higher frequency in the summer (May-November), so there could be a bias associated with seasonality in the fish assemblages.

Complete predictor data were not available for the entire spatial extent of the study. For example, benthic habitat maps had incomplete spatial coverage. Due to cloud cover, turbidity, or other interference, 75 percent of the MHI coastal areas 0-30 m depth were not mapped (Battista et al., 2007). Most notably, high resolution bathymetric data (i.e., LiDAR) is unavailable for large areas, particularly for Niʻihau, Lānaʻi and Kahoʻolawe. Small areas of Lānaʻi have been surveyed, but a majority of the coastline is missing, and Kahoʻolawe has no nearshore high resolution bathymetric information. The island of Hawaiʻi has no high resolution bathymetry data for large portions of the northeast and southeast coastline. In addition, a notable area on Oʻahu along the coastline near Kailua is missing high resolution bathymetry data. These areas with no high resolution bathymetric data were the major limitation for the spatial extent of the predictions. Some of these data gaps were filled by the U.S. Army Corps of Engineers (USACE) in 2013. The USACE collected nearshore LiDAR around Oʻahu, Kauaʻi, Maui, Molokaʻi and Hawaiʻi. This data is still being processed (as of December 16, 2015), and is not yet available publicly. However, it will be made available through NOAA's Digital Coast Data Access Viewer when ready: https://www.coast.noaa.gov/dataviewer/#.

ACKNOWLEDGEMENTS

This work would not have been possible without the generous contribution of fish survey data from multiple groups as facilitated by Ivor Williams (NOAA CREP), Randy Kosaki (NOAA NMS), Bill Walsh (HI DAR), Paul Murakawa (HI DAR), Russell Sparks (HI DAR), Kuʻulei Rodgers (HIMB), Eric Brown (NPS), and Eric Conklin (TNC). Special thanks to Ivor Williams, Eric Conklin, Russell Sparks, and Eric Brown for reviewing portions of this document. Chris Kelley, Cordelia Moore, and Dana Sackett contributed to early discussions that focused on the bottom fish section. BOEM provided guidance and recommendations for improvement on multiple stages of this analysis. Lisa Wedding provided initial data sets and suggestions for further contacts. Kurt Kawamoto generously provided photographs of bottom fish.

LITERATURE CITED

Agostinelli, C., and U. Lund. 2013. R package, circular: Circular statistics. R-Forge. Software Downloaded January 2014. Software Online: https://r-forge.r-project.org/projects/circular (Site Accessed 8 June 2016).

Battista, T.A., B.M. Costa, and S.M. Anderson. 2007. Benthic Habitats of the Main Hawaiian. NOAA Technical Memorandum NOS NCCOS CCMA 152. Silver Spring, MD. 48 pp. Data Downloaded 5 September 2014. Data Website: https://products.coastalscience.noaa.gov/collections/benthic/e97hawaii/data2007.aspx (Site Accessed 8 June 2016).

Booij, N., R.C. Ris, and L.H. Holthuijsen. 1999. A third-generation wave model for coastal regions: 1. Model description and validation. Journal of Geophysical Research: Oceans 104: 7649-7666.

Breiman, L., J.H. Friedman, R.A. Olshen, and C.I. Stone. 1984. Classification and regression trees. Taylor & Francis, Belmont, CA. 368 pp.

Brewer, T.D., J.E. Cinner, A. Green, and R.L. Pressey. 2013. Effects of Human Population Density and Proximity to Markets on Coral Reef Fishes Vulnerable to Extinction by Fishing. Conservation Biology 27: 443-452.

Brill, R.W., B.A. Block, C.H. Boggs, K.A. Bigelow, E.V. Freund, and D.J. Marcinek. 1999. Horizontal movements and depth distribution of large adult yellowfin tuna (*Thunnus albacares*) near the Hawaiian Islands, recorded using ultrasonic telemetry: implications for the physiological ecology of pelagic fishes. Marine Biology 133: 395-408.

Brodziak, J., A. Yau, J. O'Malley, A. Andrews, R. Humphreys, M. DeMartini, M. Pan, M. Parke, and E. Fletcher. 2014. Stock Assessment Update for the Main Hawaiian Islands Deep 7 Bottomfish Complex Through 2013 With Projected Annual Catch Limits Through 2016. NOAA National Marine Fisheries Service, Pacific Island Fisheries Science Center. NOAA Technical Memorandum NMFS PIFSC 42. Honolulu, HI. 61 pp.

Cesar, H.S.J. and P. van Beukering. 2004. Economic Valuation of the Coral Reefs of Hawai'i. Pacific Science 58: 231–242.

DAR. 1992. Marine life conservation district plan. State of Hawai'i, Department of Land and Natural Resources, Division of Aquatic Resources. 18 pp.

DAR. 2012. Commercial marine landings summary trend report, Calendar Year 2012. State of Hawai'i, Department of Land and Natural Resources, Division of Aquatic Resources. 17 pp.

DAR. 2014. Fishery-Dependent Data. State of Hawai'i, Department of Land and Natural Resources, Division of Aquatic Resources. Data Provided 28 October 2015. Provider Website: http://dlnr.hawaii.gov/dar/ (Site Accessed 8 June 2016).

DAR. 2015a. State of Hawai'i Commercial Fish Catch Statistical Areas. State of Hawai'i, Department of Land and Natural Resources, Division of Aquatic Resources. Data Provided 28 October 2015. Provider Website: http://dlnr.hawaii.gov/dar/fishing/commercial-fishing/ (Site Accessed 8 June 2016).

DAR. 2015b. Coral Reefs: Monitoring. State of Hawai'i, Department of Land and Natural Resources, Division of Aquatic Resources. Online: http://dlnr.hawaii.gov/coralreefs/monitoring/ (Site Accessed 8 June 2016).

De'ath, G. 2007. Boosted trees for ecological modeling and prediction. Ecology 88: 243-251.

De'ath, G. and K.E. Fabricius. 2000. Classification and regression trees: a powerful yet simple technique for ecological data analysis. Ecology 81: 3178-3192.

De'ath, G. and K. Fabricius. 2010. Water quality as a regional driver of coral biodiversity and macroalgae on the Great Barrier Reef. Ecological Applications 20: 840-850.

Fishes

D'Errico, J. 2014. inpaint_nans, MATLAB Central File Exchange (Software Downloaded April 2014). MathWorks, Inc. Natick, Massachusetts. Software Online: http://www.mathworks.com/matlabcentral/fileexchange/4551-inpaint-nans (Site Accessed 8 June 2016).

Donovan, M. University of Hawai'i at Mānoa, Fisheries Ecology Research Lab. Honolulu, HI. Personal Communication.

Drazen, J. University of Hawai'i at Mānoa, Deep-Sea Fish Ecology Lab. Honolulu, HI. Personal Observation.

Elith, J., J.R. Leathwick, and T. Hastie. 2008. A working guide to boosted regression trees. Journal of Animal Ecology 77: 802-813.

ESRI. 2011. ArcGIS Desktop: Release 10. Environmental Systems Research Institute. Redlands, CA. Online: http://www.esri.com/ (Site Accessed 8 June 2016).

Fabricius, K.E. 2005. Effects of terrestrial runoff on the ecology of corals and coral reefs: review and synthesis. Marine Pollution Bulletin 50: 125-146.

Friedlander, A.M. and J.D. Parrish. 1998. Habitat characteristics affecting fish assemblages on a Hawaiian coral reef. Journal of Experimental Marine Biology and Ecology 224: 1-30.

Friedlander, A.M., E.K. Brown, and M.E. Monaco. 2007a. Coupling ecology and GIS to evaluate efficacy of marine protected areas in Hawaii. Ecological Applications 17: 715-730.

Friedlander, A.M., E.K. Brown, and M.E. Monaco. 2007b. Defining reef fish habitat utilization patterns in Hawaii: comparisons between MPAs and areas open to fishing. Marine Ecology Progress Series 351: 221-233.

Friedlander, A., G. Aeby, S. Balwani, B. Bowen, R. Brainard, A. Clark, J. Kenyon, J. Maragos, C. Meyer, P. Vroom, and J. Zamzow. 2008. The State of Coral Reef Ecosystems of the Northwestern Hawaiian Islands. pp. 263-306. In: J.E. Waddell and A.M. Clarke (eds.), The State of Coral Reef Ecosystems of the United States and Pacific Freely Associated States: 2008. NOAA Technical Memorandum NOS NCCOS 73. Silver Spring, MD. 569 pp.

Friedlander, A., K. Stamoulis, J. Kittinger, J. Drazen, and B. Tissot. 2014. Understanding the Scale of Marine Protection in Hawai'i: From Community-Based Management to the Remote Northwestern Hawaiian Islands Marine National Monument. Advances in Marine Biology 69: 153-203.

Friedman, J.H. 2002. Stochastic gradient boosting. Computational Statistics and Data Analysis 38: 367-378.

Froese, R. and D. Pauly. 2011. FishBase. Online: http://www.fishbase.org (Site Accessed 8 June 2016)

Gilman, E., M. Chaloupka, A. Read, P. Dalzell, J. Holetschek, and C. Curtice. 2012. Hawai'i longline tuna fishery temporal trends in standardized catch rates and length distributions and effects on pelagic and seamount ecosystems. Aquatic Conservation: Marine and Freshwater Ecosystems 22: 446-488.

Graham, N.A.J. and K.L. Nash. 2013. The importance of structural complexity in coral reef ecosystems. Coral Reefs 32: 315-326.

Green, A.L., A.P. Maypa, G.R. Almany, K.L. Rhodes, R. Weeks, R.A. Abesamis, M.G. Gleason, P.J. Mumby, and A.T. White. 2015. Larval dispersal and movement patterns of coral reef fishes, and implications for marine reserve network design. Biological Reviews 90: 1215-1247.

Hammar, L., A. Wikstrom, and S. Molander. 2014. Assessing ecological risks of offshore wind power on Kattegat cod. Renewable Energy 66: 414-424.

He, X., K.A. Bigelow, and C.H. Boggs. 1997. Cluster analysis of longline sets to determine fishing strategies within the Hawai'i-based fishery. Fisheries Research 31: 147-158.

Hijmans, R.J. 2014. R package, Raster: Geographic data analysis and modeling. Software Downloaded October 2014. Software Website: http://CRAN.R-project.org/package=raster (Site Accessed 8 June 2016).

Hijmans, R.J., S. Phillips, J. Leathwick, and J. Elith. 2014. R package, dismo: Species distribution modeling. Software Downloaded October 2014. Software website: http://CRAN.R-project.org/package=dismo (Site Accessed 8 June 2016).

HIMB. 2014. State of Hawaii's Fish Aggregation Device Program. Hawai'i Institute of Marine Biology, School of Ocean and Earth Science and Technology, University of Hawai'i at Manoa. Online: http://www.hawaii.edu/HIMB/FADS/ (Site Accessed 8 June 2016)

HMRG. 2015. Hawai'i Mapping Research Group. Hawai'i Mapping Research Group, School of Ocean and Earth Science and Technology, University of Hawai'i at Manoa. Online: http://www.soest.hawaii.edu/HMRG/cms/ (Site Accessed 8 June 2016).

Holland, K. 2011. Programmatic environmental assessment: Hawai'i fish aggregating device system. Prepared for State of Hawai'i Department of Land and Natural Resources, Division of Aquatic Resources. Hawai'i Institute of Marine Biology, School of Ocean and Earth Science and Technology, University of Hawai'i at Manoa. 35 pp.

Holthuijsen, L.H. 2010. Waves in oceanic and coastal waters. Cambridge University Press. New York, NY. 404 pp.

Hospital, J. and C. Beavers. 2012. Economic and social characteristics of bottomfish fishing in the Main Hawaiian Islands. NOAA National Marine Fisheries Service, Pacific Islands Fishery Science Center. Administrative Report H-12-01. Honolulu, HI. 44 pp.

Itano, D.G. and K.N. Holland. 2000. Movement and vulnerability of bigeye (*Thunnus obesus*) and yellowfin tuna (*Thunnus albacares*) in relation to FADs and natural aggregation points. Aquatic Living Resources 13: 213-223.

Jenness, J. 2013. DEM Surface Tools. Jenness Enterprises. Software Downloaded November 2015. Software Website: http://www.jennessent.com/arcgis/surface_area.htm (Site Accessed 8 June 2016).

Kelley, C.K., R. Moffit, and J.R. Smith. 2006. Mega- to micro-scale classification and description of bottomfish essential fish habitat on four banks in the northwestern Hawaiian Islands. Atoll Research Bulletin 543: 319-332.

Kikiloi, K. and M. Graves. 2010. Rebirth of an archipelago: sustaining a Hawaiian cultural identity for people and homeland. Hulili: Multidisciplinary Research on Hawaiian Well-Being 6: 73-114.

Kokubun, R. State of Hawai'i, Department of Land and Natural Resources, Division of Aquatic Resources. Honolulu, HI. Personal Communication.

Larcombe, P., P.V. Ridd, A. Prytz, and B. Wilson. 1995. Factors controlling suspended sediment on inner-shelf coral reefs, Townsville, Australia. Coral Reefs 14: 163-171.

Leathwick, J.R., J. Elith, M.P. Francis, T. Hastie, and P. Taylor. 2006. Variation in demersal fish species richness in the oceans surrounding New Zealand: an analysis using boosted regression trees. Marine Ecology Progress Series 321: 267-281.

Lester, S.E., B.S. Halpern, K. Grorud-Colvert, J. Lubchenco, B.I. Ruttenberg, S.D. Gaines, S. Airamé, and R.R. Warner. 2009. Biological effects within no-take marine reserves: a global synthesis. Marine Ecology Progress Series 384: 33-46.

Fishes

McGarigal, K., S.A. Cushman, and E. Ene. 2012. FRAGSTATS v4: Spatial Pattern Analysis Program for Categorical and Continuous Maps. Computer software program produced by the authors at the University of Massachusetts, Amherst. Software Downloaded December 2014. Software Website: http://www.umass.edu/landeco/research/fragstats/fragstats.html (Site Accessed 8 June 2016).

Merritt, D.W., M.K. Donovan, C. Kelley, L. Waterhouse, M. Parke, K. Wong, and J.C. Drazen. 2011. BotCam: a baited camera system for nonextractive monitoring of bottom fish species. Fishery Bulletin 109: 56-67.

Misa, W.F.X.E., J. Drazen, C. Kelley, and V.N. Moriwake. 2013. Establishing species-habitat associations for 4 eteline snappers with the use of a baited stereo-video camera system. Fishery Bulletin 111: 293-308.

Moore, C.H., J.C. Drazen, C.D. Kelley, and W.F.X.E. Misa. 2013. Deepwater marine protected areas of the main Hawaiian Islands: establishing baselines for commercially valuable bottom fish populations. Marine Ecology Progress Series 476: 167-183.

Nadon, M.O. 2014. Improving Stock Assessment Capabilities for the Coral Reef Fishes of Hawaii and the Pacific Region. Open Access Dissertations Paper 1314.

NOAA CREP. 2015. Coral Reef Ecosystem Program. NOAA National Marine Fisheries Service, Pacific Islands Fisheries Science Center. Honolulu, HI. Online: http://www.pifsc.noaa.gov/cred/ (Site Accessed 8 June 2016).

NOAA FHUS. 2015. Comparing Reef Fish Habitat Use Patterns In and Out of Hawaiian Marine Protected Areas. Fish Habitat Utilization Study, Projects Explorer. NOAA National Ocean Service, National Centers for Coastal Ocean Science. Online: http://coastalscience.noaa.gov/projects/detail?key=31 (Site Accessed 8 June 2016).

NOAA MPA Center. 2014. Data and Analysis: MPA Inventory and DeFacto MPAs. NOAA National Ocean Service, Marine Protected Areas Center. Data Downloaded 4 March 2016. Data Website: http://marineprotectedareas.noaa.gov/dataanalysis/ (Site Accessed 8 June 2016).

NOAA NMFS. 2016. Western Pacific, Information & GIS Data Download, Hawaii Bottomfish EFH 0-400 m. NOAA National Marine Fisheries Service, Office of Habitat Conservation. Data Downloaded 25 July 2014. Data Website: http://www.habitat.noaa.gov/protection/efh/newInv/index.html (Site Accessed 8 June 2016).

NOAA RAMP. 2015. Pacific Reef Assessment and Monitoring Program. NOAA National Marine Fisheries Service, Pacific Islands Fisheries Science Center. Online: https://pifsc-www.irc.noaa.gov/cred/pacific_ramp.php (Site Accessed 14 June 2016)

NPS I&M. 2015. National Park Service, Inventory and Monitoring. Online: http://science.nature.nps.gov/im/ (Site Accessed 8 June 2016).

Parke, M. 2007. Linking Hawaii fisherman reported commercial bottomfish catch data to potential bottomfish habitat and proposed restricted fishing areas using GIS and spatial analysis. NOAA Technical Memorandum NMFS-PIFSC-11. 37 pp.

Pittman, S.J., B.M. Costa, and T.A. Battista. 2009. Using Lidar Bathymetry and Boosted Regression Trees to Predict the Diversity and Abundance of Fish and Corals. Journal of Coastal Research 25: 27-38.

R Core Team. 2014. R: A language and environment for statistical computing (Versions 3.1.1 to 3.1.3). R Foundation for Statistical Computing, Vienna, Austria. Software Online: http://www.r-project.org (Site Accessed 8 June 2016).

Robert, M., L. Dagorn, J.L. Deneubourg, D. Itano, and K. Holland. 2012. Size-dependent behavior of tuna in an array of fish aggregating devices (FADs). Marine Biology 159: 907-914.

Roberts, J.J., B.D. Best, D.C. Dunn, E.A. Treml, and P.A. Halpin. 2010. Marine Geospatial Ecology Tools: An integrated framework for ecological geoprocessing with ArcGIS, Python, R, Matlab, and C++. Environmental Modelling & Software 25: 1197-1207.

Sackett, D.K., J.C. Drazen, V.N. Moriwake, C.D. Kelley, B.D. Schumacher, and M.F.X.E. Misa. 2014. Marine protected areas for deepwater fish populations: an evaluation of their effects in Hawai'i . Marine Biology 161: 411-425.

Schug, D.M. 2001. Hawai`i's commercial fishing industry: 1820-1945. The Hawaiian Journal of History 35: 15-34.

Sibert, J.R., M.K. Musyl, and R.W. Brill. 2003. Horizontal movements of bigeye tuna (*Thunnus obesus*) near Hawai'i determined by Kalman filter analysis of archival tagging data. Fisheries Oceanography 12: 141-151.

State of Hawai'i. 2010. 2010 Census Data, Census Blocks – 2010, Cultural and Demographic, GIS Data. Data from U.S. Census Bureau. State of Hawai'i, Office of Planning, Hawaii Statewide GIS Program. Data Downloaded September 2015. Data Website: http://planning.hawaii.gov/gis/download-gis-data-expanded/ (Site Accessed 8 June 2016).

State of Hawai'i. 2016. Fish Aggregating Devices, Oceans and Estuaries, GIS Data. State of Hawai'i, Office of Planning, Hawaii Statewide GIS Program. Data Downloaded 5 May 2015. Data Website: http://planning.hawaii.gov/gis/download-gis-data/ (Site Accessed 8 June 2016)

Stockwell, D.R.B. and A.T. Peterson. 2002. Effects of sample size on accuracy of species distribution models. Ecological Modelling 148: 1–13.

Stopa, J.E., J.F. Filipot, N. Li, K.F. Cheung, Y.L. Chen, and L. Vega. 2013. Wave energy resources along the Hawaiian Island chain. Renewable Energy 55: 305-321.

TNC. 2015. The Nature Conservancy Hawai'i Marine Program. Online: http://www.nature.org/ourinitiatives/regions/northamerica/unitedstates/hawaii/index.htm (Site Accessed 8 June 2016).

Tolman, H.L. 2009. User manual and system documentation of WAVEWATCH III version 3.14. NOAA National Weather Service, National Centers for Environmental Prediction. 194 pp. Online: http://polar.ncep.noaa.gov/mmab/papers/tn276/MMAB_276.pdf (Site Accessed 8 June 2016).

UH CRAMP. 2015. Coral Reef Assessment and Monitoring Program. Hawai'i Institute of Marine Biology, School of Ocean and Earth Science and Technology, University of Hawai'i at Manoa. Online: http://cramp.wcc.hawaii.edu/CRAMP_Information/overview.htm (Site Accessed 8 June 2016).

UH Deep-Sea Fish Ecology Lab. 2014. Bottom Camera Bait Station Data. Deep-Sea Fish Ecology Lab, Department of Oceanography, School of Ocean and Earth Science and Technology, University of Hawai'i at Manoa. Data Provided September 2015. Provider Website: http://www.deepseafishecology.com/home.html (Site Accessed 8 June 2016).

UH FERL. 2015a. Compilation of reef fish data. Fisheries Ecology Research Lab, College of Natural Sciences, University of Hawai'i at Manoa. Data Provided 11 December 2015. Provider Website: https://fisheriesecologyresearchlab.wordpress.com (Site Accessed 8 June 2016).

UH FERL. 2015b. University of Hawai'i Fisheries Ecology Research Lab. College of Natural Sciences, University of Hawai'i at Manoa. Data Provided 11 December 2015. Provider Website: https://fisheriesecologyresearchlab.wordpress.com (Site Accessed 8 June 2016).

USGS. 2015. The 3DEP National Map (1/3 arc-second DEMs for Hawai'i). The National Map. U.S. Geological Survey. Data Downloaded 15 September 2015. Data Website: http://viewer.nationalmap.gov/basic/?basemap=b1&category=ned,nedsrc&title=3DEP%20View#startUp (Site Accessed 8 June 2016).

Fishes

Williams, I.D., W.J. Walsh, R.E. Schroeder, A.M. Friedlander, B.L. Richards, and K.A. Stamoulis. 2008. Assessing the importance of fishing impacts on Hawaiian coral reef fish assemblages along regional-scale human population gradients. Environmental Conservation 35: 261-272.

WPRFMC. 2009. Fishery ecosystem plan for the Hawai'i Archipelago. Western Pacific Regional Fishery Management Council. Honolulu, HI. 266 pp.

Wright, D.J., M. Pendleton, J. Boulware, S. Walbridge, B. Gerlt, D. Eslinger, D. Sampson, and E. Huntley. 2012. ArcGIS Benthic Terrain Modeler (BTM), v. 3.0. Environmental Systems Research Institute, NOAA Coastal Services Center, Massachusetts Office of Coastal Zone Management. Software Downloaded February 2014. Software Website: http://esriurl.com/5754 (Site Accessed 8 June 2016).

Chapter 5 Sea Turtles

Kimberly Roberson[1], Matthew S. Kendall[1], Denise Parker[12], and Shawn Murakawa[12]

Green turtle. Photo credit: Mark Sullivan (NOAA NMFS/PIFSC/PRD)

ABSTRACT

*Five species of sea turtles occur in the Main Hawaiian Islands (MHI), all of which are protected under the Endangered Species Act (ESA). Of the five, green turtles (*Chelonia mydas*) are the most abundant and present year round. Hawksbill (*Eretmochelys imbricata*, also present year round), olive ridley (*Lepidochelys olivacea*), leatherback (*Dermochelys coriacea*) and loggerhead (*Caretta caretta*) are also found throughout the MHI, with varying types and degrees of activity. Basking, nesting, and stranding data were compiled by National Oceanic and Atmospheric Administration's (NOAA) Pacific Islands Fisheries Science Center (PIFSC) from a diversity of State and Federal agencies, as well as community organizations, volunteers and private citizens. These data were mapped in the context of shoreline cliffs and beaches to identify locations of turtle activity. Green turtles were reported basking at 62 locations around the MHI, with 34 percent of the reports from O'ahu and 31 percent from the island of Hawai'i. Nesting locations by green (n=47), hawksbill (n=27), olive ridley (n=4) and leatherback (n=1) turtles were reported throughout the MHI. Kaua'i had the highest number of nesting locations reported (19 of 47 or 40%). The majority of strandings are green turtles, with the largest proportions reported on O'ahu (77%) and Maui (11%). Stranding causes varied among and within islands. These data may be used to document current spatial patterns and for comparison to future patterns post-wind farm installation. However, it is important to note that the density and frequency of reported sea turtle activities are biased by unequal survey effort. Effort was not consistently quantified and is presumably higher close to population centers and nearby beaches that were easily accessible. Future data collection efforts would benefit from island-wide monitoring that is controlled for effort as well as identification of foraging and offshore distributions of sea turtles throughout the entire MHI.*

Citation for chapter
Roberson, K., M.S. Kendall, D. Parker, and S. Murakawa. pp. 197-226. In: B.M. Costa and M.S. Kendall (eds.), Marine Biogeographic Assessment of the Main Hawaiian Islands. Bureau of Ocean Energy Management and National Oceanic and Atmospheric Administration. OCS Study BOEM 2016-035 and NOAA Technical Memorandum NOS NCCOS 214. 359 pp.

[1] *NOAA National Centers for Coastal Ocean Science, Biogeography Branch, Silver Spring, MD, U.S.A.*
[12] *NOAA Pacific Islands Fisheries Science Center, Protected Species Division, Marine Turtle Biology and Assessment Program, Honolulu, HI, U.S.A.*

Sea Turtles

5.1. INTRODUCTION

Five species of sea turtles occur in the Main Hawaiian Islands (MHI). Green turtles (*Chelonia mydas*) are the most abundant and present year round. A small population of hawksbill turtles (*Eretmochelys imbricata*) nest and forage mostly around the island of Hawai'i and the Maui Nui area (Mangel et al., 2000; King et al., 2007; Parker et al., 2009; Seitz et al., 2012). Other species present, but rarely found, include olive ridley (*Lepidochelys olivacea*), leatherback (*Dermochelys coriacea*), and loggerhead (*Caretta caretta*). All sea turtles are long-lived, grow to large sizes, have specific diets, and spend the majority of their lives at sea (Table 5.1). With the notable exception of the basking behavior of green turtles on Hawaiian beaches (Balazs et al., 1980; Whittow and Balazs, 1982; Balazs et al., 2015), adult male sea turtles do not come ashore, and adult females come ashore only for nesting. Mature females nest seasonally (Table 5.1) every 2-3 years, laying several clutches of 50-200 eggs in sand cavities within a nesting season (Witzell, 1983; Dodd, 1988; Hirth, 1997; Balazs et al., 2015). After a 2-3 month incubation period wherein temperature determines sex, hatchlings emerge from nests, spend several years maturing in the ocean, and ultimately return to nest at natal beaches (Miller, 1996).

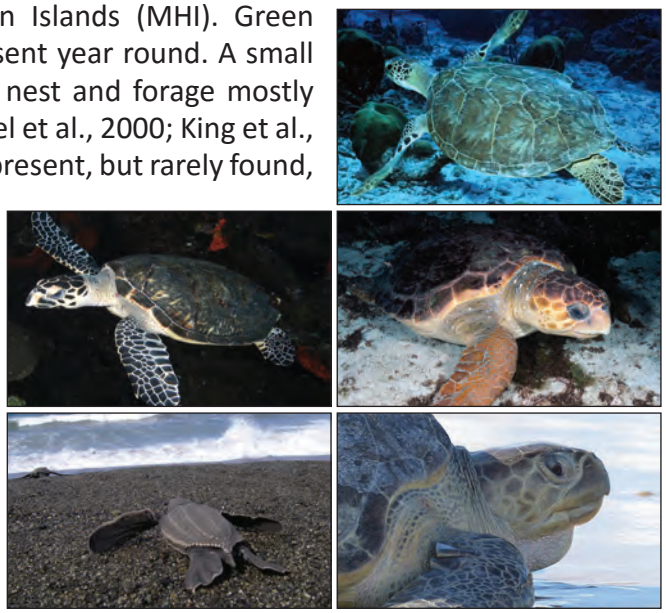

*Top: Green turtle (*Chelonia mydas*), Photo credit: Andy Bruckner (NOAA). Middle (L-R): Hawksbill (*Eretmochelys imbricata*) and loggerhead (*Caretta caretta*); Photo credit: G.P. Schmahl (NOAA NOS/ONMS/FGBNMS). Bottom (L-R): leatherback (*Dermochelys coriacea*), Photo credit: Scott Benson (NOAA); and olive ridley (*Lepidochelys olivacea*), Photo credit: NOAA*

Development of offshore renewable energy platforms may potentially impact Hawaiian sea turtles in several ways. Female turtles utilize undeveloped beaches for nesting and can be disrupted when they encounter developed or artificially lit beaches (Witherington and Bjorndal, 1991). Emerging hatchlings use the brightest point on the horizon to navigate to the ocean. They may become disoriented if artificial beachfront lighting is brighter than the natural seaward horizon (Witherington and Bjorndal, 1991). It is estimated that only one in 1,000 hatchlings will survive to reproductive maturity (Frazer, 1986), so nesting success is important for maintaining the viability of sea turtle populations. Similarly, disturbances to basking beaches may have detrimental effects to sea turtles. Basking can be an important behavior for turtles to thermoregulate, avoid predators, accelerate metabolism and egg development, and to dry epiphytic growth on carapaces. All these factors contribute to turtle health and fitness (Whittow and Balazs, 1982; Spotila et al., 1996).

Sea turtle interactions with offshore renewable energy structures may occur. However, it is noteworthy that during the past 25 years of operating an extensive network of offshore Fish Aggregating Devices (FADs)

Table 5.1. Sea turtles present in the Main Hawaiian Islands (MHI), their species-specific life history traits and Endangered Species Act (ESA) status. Data sources: USFWS, 2015; NOAA PIRO, 2016

Scientific Name	*Caretta caretta*	*Chelonia mydas*	*Dermochelys coriacea*	*Eretmochelys imbricata*	*Lepidochelys olivacea*
Species Common Name	Loggerhead	Green	Leatherback	Hawksbill	Olive Ridley
ESA Status, HI	Endangered	Threatened	Endangered	Endangered	Threatened
Adult Size (average)	3 ft	4 ft	4-8 ft	3 ft	2.5 ft
Age at Maturity (estimated)	32-35 yr	25-35 yr	16 yr	20+ yr	10-18 yr
Diet	crustaceans, mollusks	seagrasses, algae	jellyfish	sponges	crustaceans
Clutch Size	100-126	75-200	80-85	140-200	100-110
Hawaiian Nesting Season	N/A	May-September	Year round (Jan-Jun, Jul-Dec)	May-September	June-December

throughout the MHI, there have been no reports of deleterious interaction with sea turtles. Consultations with local experts suggest that development of offshore wind energy in the MHI may have impacts to sea turtles that are similar to those caused by FADs (NOAA PIRO, 2016). In addition, the mechanisms by which sea turtles navigate are not well understood, but could be a combination of olfaction, sight and electromagnetic senses (Lohmann et al., 2007; Lusci et al., 2007). Disturbances to these, by construction and ongoing presence of offshore platforms and power transmission lines, may deleteriously affect sea turtles' ability to navigate especially in open-water (Lohmann et al., 2007; Lusci et al., 2007). Ongoing programs that monitor stranding of injured or dead turtles provide important time-series datasets that can be monitored during the construction and operation of offshore renewable energy facilities.

Biogeographic characterization of sea turtle activities will be an important part of planning for potential impacts from construction of offshore renewable energy facilities. Given this informational need, the objectives of this chapter are to: 1) identify beaches used for nesting, 2) identify beaches used for basking, and 3) document present spatial patterns and causes of stranding. Place names mentioned in this chapter are depicted in Figure 5.1.

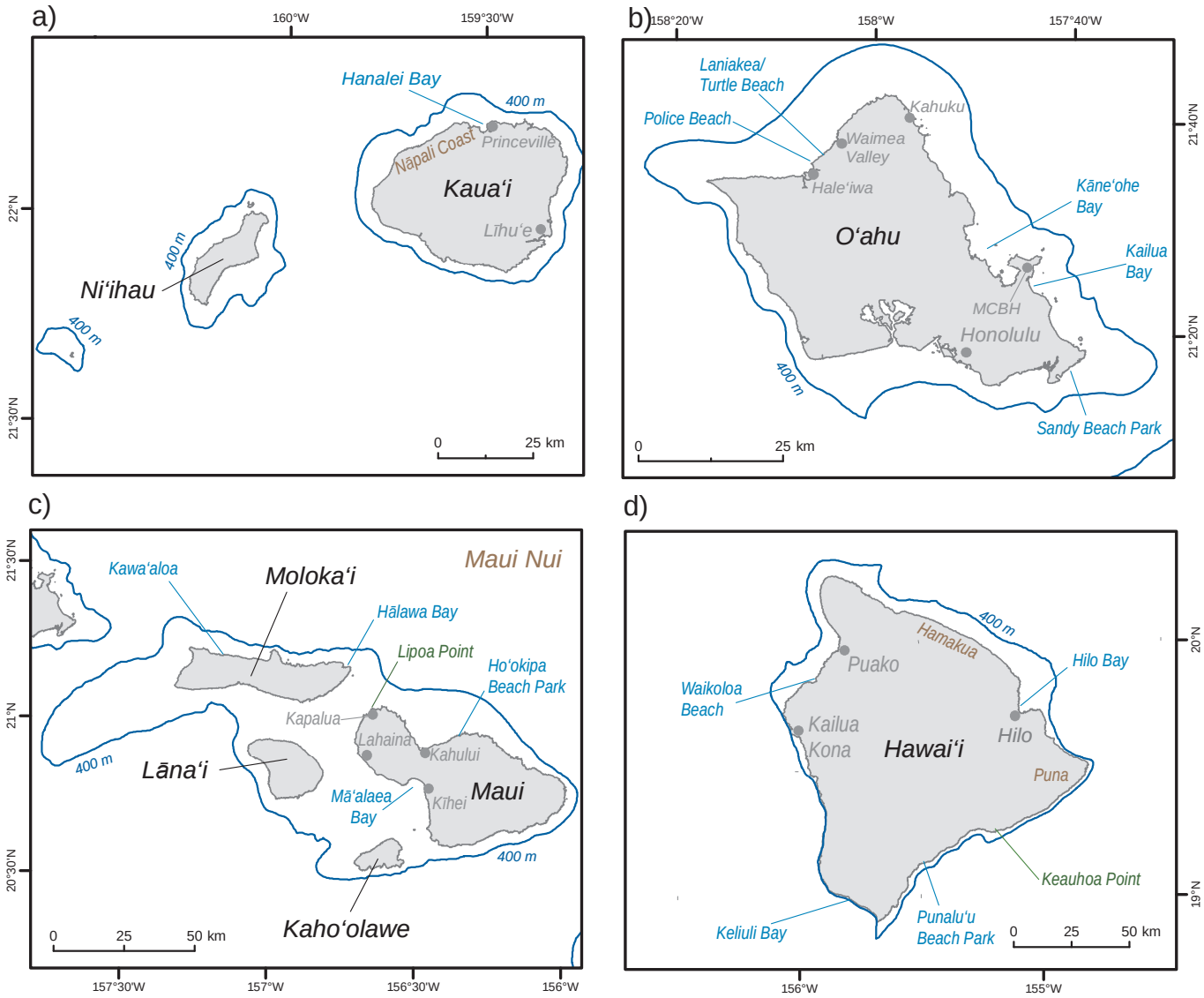

Figure 5.1. Key geographic features and place names around the Main Hawaiian Islands (MHI). These maps depict geographic features that are referenced in this chapter for: a) Ni'ihau and Kaua'i; b) O'ahu; c) Maui Nui, which includes Moloka'i, Lāna'i, Maui and Kaho'olawe; and d) Hawai'i. All depths are in meters. Data sources: shoreline (Battista et al., 2007), elevation (USGS, 2015), and depths (NOAA NCEI, 2005; GEBCO, 2008)

Sea Turtles

5.2. METHODS AND DATA DESCRIPTION

Sea turtle nesting, basking, and stranding data have been compiled by the National Oceanic and Atmospheric Administration's (NOAA) National Marine Fisheries Service (NMFS), Pacific Islands Fisheries Science Center (PIFSC) from a diversity of State and Federal agencies, as well as community organizations, volunteers, and private citizens that report sea turtle sightings (e.g., Parker et al., 2015). Due to the varying level of monitoring effort and quantitative rigor among these groups and across the diverse islands and shorelines of the MHI, a semi-quantitative approach is used to convey the frequency and magnitude of sea turtle activities. Frequency refers to how often an activity is reported at a particular location (Table 5.2), and magnitude refers to the maximum number of incidences or individuals involved or reported (Table 5.3). Descriptors of nesting, basking, and stranding values are explained in Table 5.2. Stranding data are reported as events for individual turtles with location, turtle demographics, and cause described to the degree possible given the circumstances of each occurrence.

Table 5.2. Descriptors of sea turtle nesting and basking frequencies.

Frequency scale	Nesting	Basking
Regular	Annually (every year)	Daily – regularly sighted
Intermittent	Less than annual – (Not yearly, maybe every other year or similar)	Not Daily – sighted once a week to once a month
Rare	Sporadic nesting with multiple year gaps between nesting	Sighted once a year or greater
Unknown	Nesting noted, but nesting cycle unknown	Basking noted, but frequency unknown

Table 5.3. Nesting and basking magnitudes (individuals per year).

Green turtle		Hawksbill turtle
Nesting Magnitudes	Basking Magnitudes	Nesting Magnitudes
<1	1-5	<1
1-2	6-10	1-3
3-4	11-20	3-5
	30-50	

Basking green turtles. Credit: Mark Sullivan (NOAA NMFS/ PIFSC/PRD).

Nesting, basking, and stranding data were mapped onto the MHI shoreline, and patterns of distribution and abundance were visually evaluated. Any coordinates more than one kilometer inland or offshore were removed. Although sea turtles utilize Hawaiian waters more than one kilometer offshore, the focus of this report is the nearshore activities of the turtles. For stranding events, NMFS is notified via widely advertised hotline numbers. Experts recover the specimens, record the stranding location, and, if possible, determine the cause of the stranding event. For simplicity, the 115 unique causes for strandings in the database were combined into eight general categories. These were: boat impact, entanglement, fibropapillomatosis (FP), human-caused mortality, ingestion, natural predation, other illnesses and trauma. Reasons for stranding were summarized along coastlines of each island using pie charts. Unknown (n=864, all islands), pending (n=6, O'ahu only), and hatchling mortality (n=19, O'ahu only) counts were removed from totals used for the pie charts because reasons for stranding were not available. Hatchling mortality (n=19) data were also not used in O'ahu stranding counts. Coastal segments varied in size depending on island shape, shoreline type, positions of coastal promontories, environmental exposure and stranding density. In cases where stranding records included multiple causes, only the primary cause was depicted in plots and used in summary figures.

While managing a community-based call-in "hotline" for people to report sea turtle activities is a major undertaking and has several benefits (education opportunities, community participation and support, conservation), it also means that geographic specificity and survey effort are highly variable, if recorded at all. The density and frequency of reported sea turtle activities are biased by different amounts of survey effort and

accessibility of locations surveyed. Therefore, to place the distribution of turtle records into context, human population density within census tracks, as well as shoreline types, including cliffs and beaches, were added to the maps. Human population density provides a proxy for monitoring effort. A higher density of people means greater potential to observe and report sea turtle activities. Human population density data were obtained from the State of Hawai'i (2010) and divided into five classes of individuals per square meter within each island. The 'natural breaks' function in ArcMap was used to identify break points that maximize differences between classes within each island. These data are displayed as relative human population data for each island to highlight the areas that were more populated on each island.

Shoreline type also influences the variety of sea turtle activities that can occur and be observed. Sand beaches are used for nesting, whereas basking and stranding can also occur in rocky areas. Beaches have easier access so reporting turtle activity by the public is easier in this area than in rocky areas or areas with steep cliffs. Shoreline attribute data were obtained from the Environmental Sensitivity Index, Hawai'i (NOAA ORR, 2001). Shore segments attributed as 'exposed rocky cliffs' (ESI Code 1A) and 'exposed wave-cut platforms in bedrock' (ESI Code 2A) were extracted to represent cliffs, and thus areas where stranded turtles most likely will not wash ashore. Beaches included shoreline segments attributed as 'fine- to medium-grained sand beaches' (ESI Code 3A), 'coarse-grained beaches' (ESI Code 4), and 'mixed sand and gravel beaches' (ESI Code 5), areas where nesting is most likely to occur, and may be where some basking occurs. Basking is also reported on flat, rocky shorelines (i.e., Kiholo and Kona Coast areas). Only those segments equal to or longer than 370 m are displayed on maps due to scale.

5.3. RESULTS AND DISCUSSION

5.3.1. Basking

There were basking activities reported for green turtles at 62 locations around MHI from 1990 to 2014. Of these 62 reports, 34 percent were from O'ahu, and 31 percent from the island of Hawai'i (Table 5.4). These two islands have relatively high human population densities and, therefore, a higher likelihood of humans observing and reporting basking activity. O'ahu reports were dominated by small numbers of turtles basking intermittently. In contrast, Hawai'i Island reports were dominated by larger numbers of turtles basking more regularly. Although Maui reported only 16 percent of total basking reports, Ho'okipa Beach is a regular basking beach with a magnitude of 30-50. Similarly, Kaua'i reported 13 percent of total basking reports, but has two northwest locations with regular basking and magnitudes of 30-50. Moloka'i and Lāna'i had the fewest reports of basking (two basking areas reported on each island). These two islands are sparsely populated, so more

*Table 5.4. Frequency, magnitude and number of basking activities by green turtles (*Chelonia mydas*) in MHI, 1990-2014. Frequency refers to how often an activity is reported at a particular location and magnitude refers to the number of incidences or individuals involved per year. Data source: Parker et al., 2015*

Frequency	Magnitude	Hawai'i	Kaua'i	Lāna'i	Maui	Moloka'i	O'ahu	Totals
Intermittent	1-5	4	3	1	8	2	12	30
	6-10	2	0	0	0	0	0	2
Regular	1-5	0	1	0	0	0	0	1
	6-10	4	1	0	0	0	4	9
	11-29	6	0	1	1	0	3	11
	30-50	3	2	0	1	0	0	6
Rare	1-5	0	0	0	0	0	2	2
Unknown	1-5	0	1	0	0	0	0	1
Totals		**19**	**8**	**2**	**10**	**2**	**21**	**62**
Percent of total		**31**	**13**	**3**	**16**	**3**	**34**	**100**

basking may occur on these islands than is reported. No basking has been reported on Niʻihau and Kahoʻolawe. Niʻihau is privately owned with limited contact to people outside the island, and few scientific surveys have been conducted there. Kahoʻolawe has no permanent human population, and access to the island is limited to cultural restoration and ordinance clearing. However, as access to both of these islands increases, reports of basking turtles may also increase.

O'ahu

On Oʻahu, most basking activity was reported along the northwest coast (Figure 5.2) between Haleʻiwa and Waimea Valley, where the aptly named Laniakea "Turtle" Beach is located. There was a secondary concentration of basking activities reported in the southeast, near Marine Corps Base Hawaiʻi (MCBH), in both Kāneʻohe and Kailua Bays. These locations offer a combination of good shoreline habitat and easy access for humans to observe and report basking.

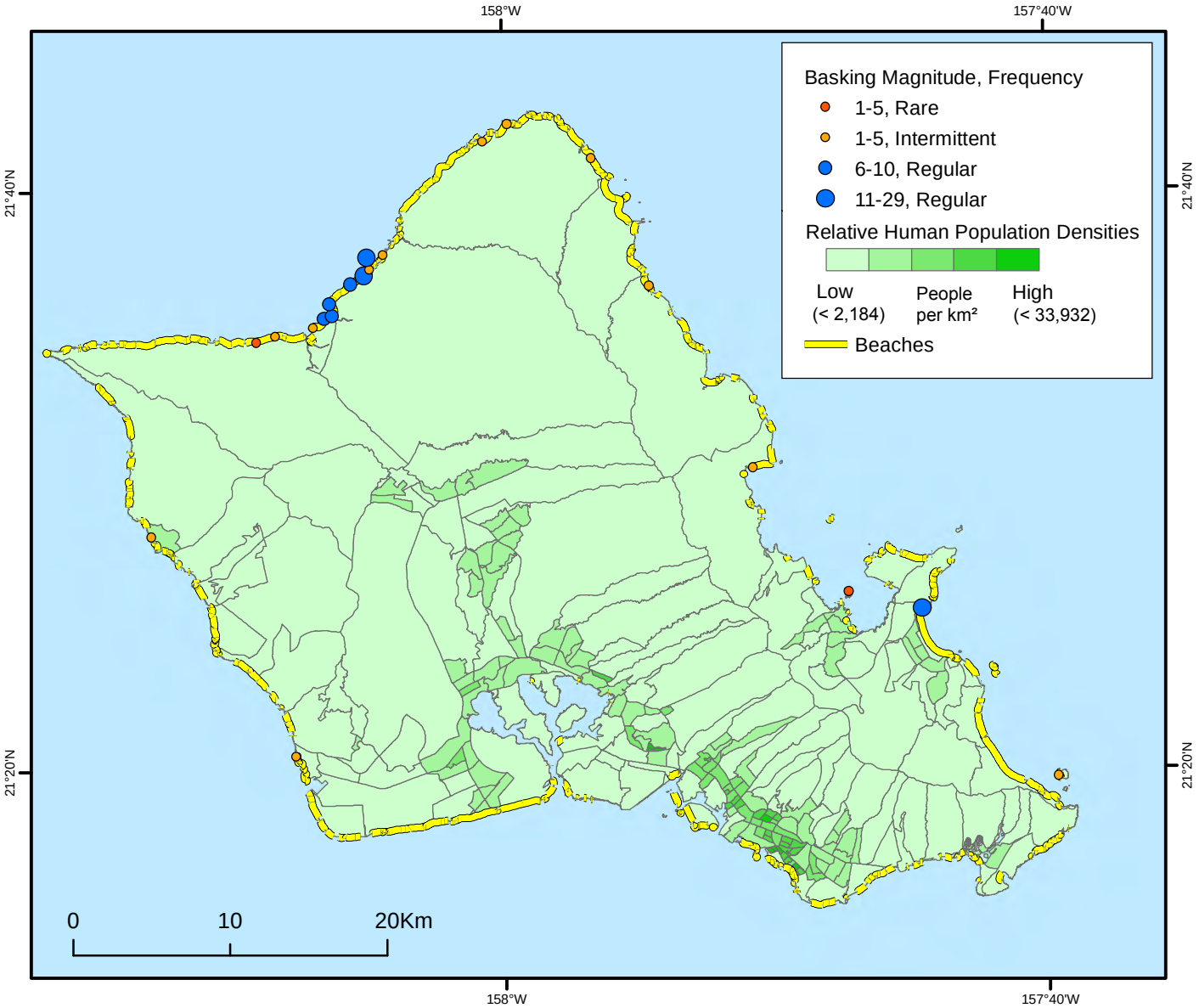

*Figure 5.2. Green turtle (*Chelonia mydas*) basking locations on Oʻahu. Data show magnitude and frequency of reported basking, 1990-2014. Frequency refers to how often an activity is reported at a particular location, and magnitude refers to the number of incidences or individuals involved. Data sources: basking (Parker et al., 2015), human population (State of Hawaiʻi, 2010), and beaches (NOAA ORR, 2001)*

Hawai'i

Hawai‘i Island’s basking activities were reported primarily along the west coast (Figure 5.3), along the Queen Ka`ahumanu Highway from Waikoloa Beach to Puako, with another concentration near Kailua-Kona. A third area of activity was reported along the east coast near Hilo. Again these areas correspond to good basking habitat that can be readily observed by humans.

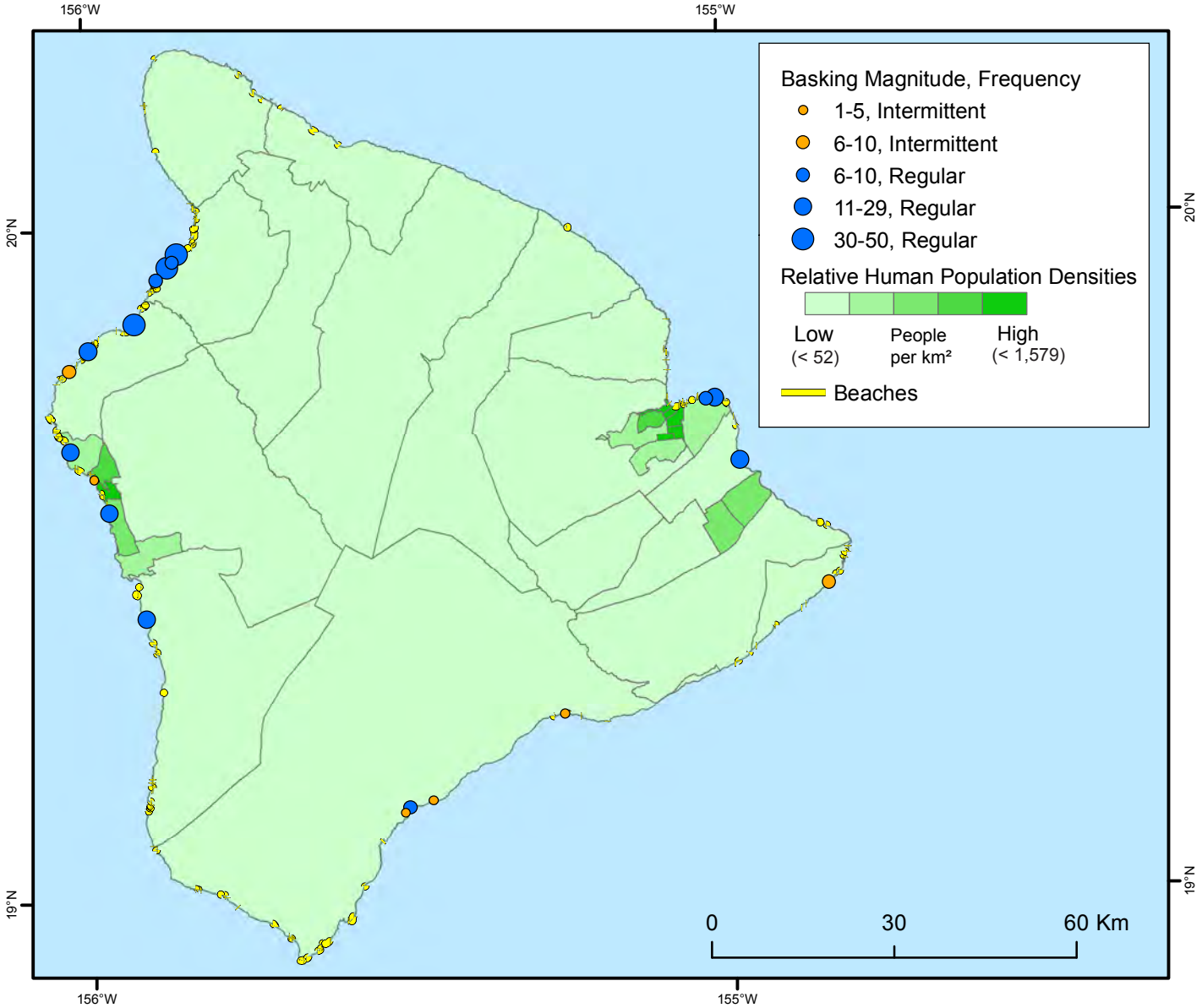

*Figure 5.3. Green turtle (*Chelonia mydas*) basking locations on the island of Hawai‘i. Data show magnitude and frequency of reported basking, 1990-2014. Frequency refers to how often an activity is reported at a particular location, and magnitude refers to the number of incidences or individuals involved. Data sources: basking (Parker et al., 2015), human population (State of Hawai‘i, 2010), and beaches (NOAA ORR, 2001)*

Sea Turtles

Maui

On Maui, most basking activity was reported in two areas: intermittent and regular basking in the northwest, south of Kapalua, near Napili Kai Beach Resort, and another concentration of regular basking in the north, near Ho`okipa Beach Park (Figure 5.4). Both areas have moderate relative human population densities and easy access to the coast, conditions that increase likelihood of reporting.

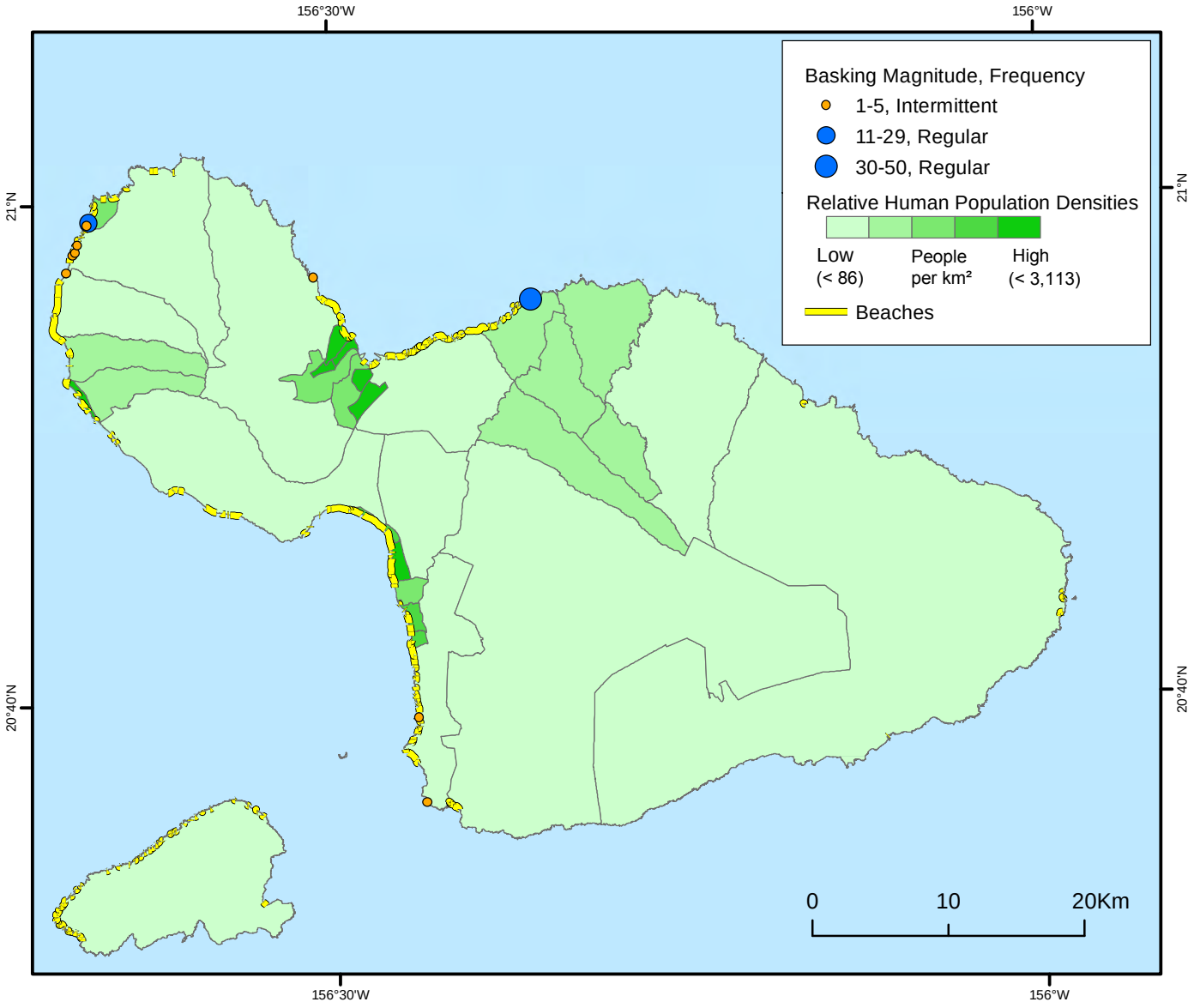

*Figure 5.4. Green turtle (*Chelonia mydas*) basking locations on Maui and Kaho'olawe. Data show magnitude and frequency of reported basking, 1990-2014. Frequency refers to how often an activity is reported at a particular location, and magnitude refers to the number of incidences or individuals involved. Data sources: basking (Parker et al., 2015), human population (State of Hawai'i, 2010), and beaches (NOAA ORR, 2001)*

Kaua'i

Interestingly, of Kaua'i's eight reported basking locations, the two regularly reported locations, with magnitudes of 30-50, are not near beaches, nor are they near highly populated area (Figure 5.5). The island of Hawai'i's three regularly reported locations with magnitudes of 30-50 are similarly not near highly populated areas.

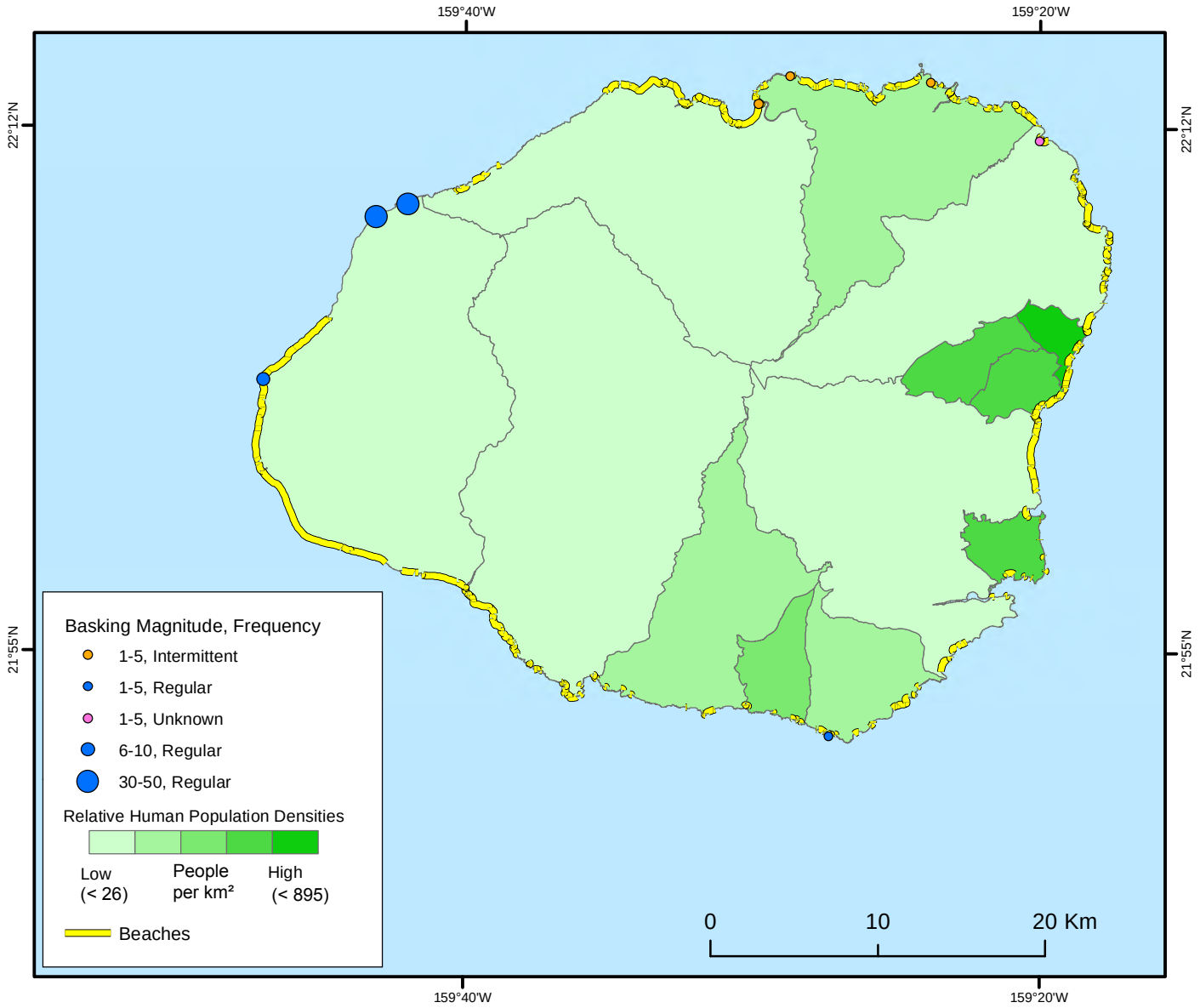

*Figure 5.5. Green turtle (*Chelonia mydas*) basking locations on Kaua'i. Data show magnitude and frequency of reported basking, 1990-2014. Frequency refers to how often an activity is reported at a particular location, and magnitude refers to the number of incidences or individuals involved. Data sources: basking (Parker et al., 2015), human population (State of Hawai'i, 2010), and beaches (NOAA ORR, 2001)*

Sea Turtles

Lāna‘i and Moloka‘i

There were very few reports of basking from Lāna‘i (Figure 5.6) and Moloka‘i (Figure 5.7). These islands both have relatively sparse human populations.

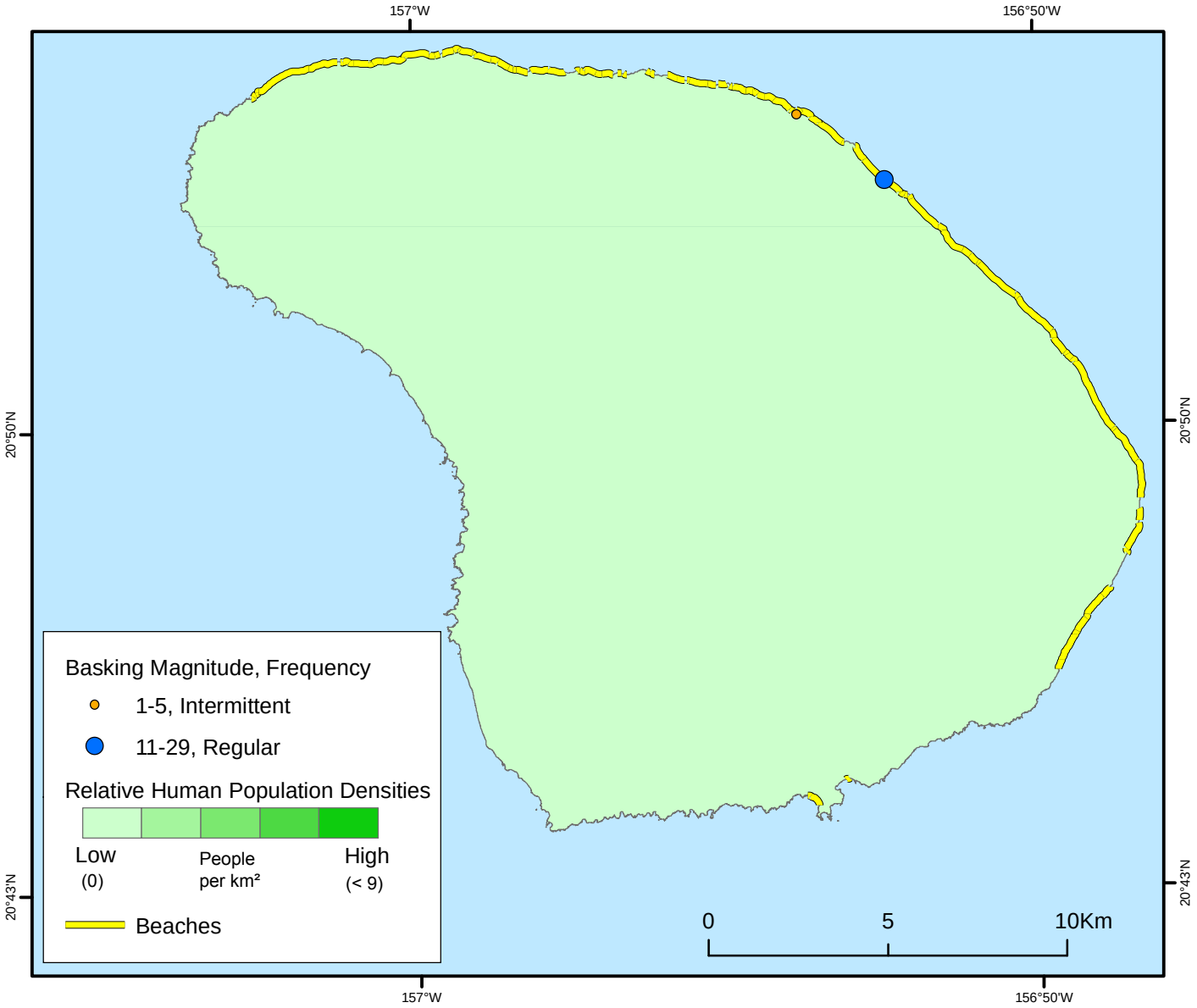

*Figure 5.6. Green turtle (*Chelonia mydas*) basking locations on Lāna‘i. Data show magnitude and frequency of reported basking, 1990-2014. Frequency refers to how often an activity is reported at a particular location, and magnitude refers to the number of incidences or individuals involved. Data sources: basking (Parker et al., 2015), human population (State of Hawai‘i, 2010), and beaches (NOAA ORR, 2001)*

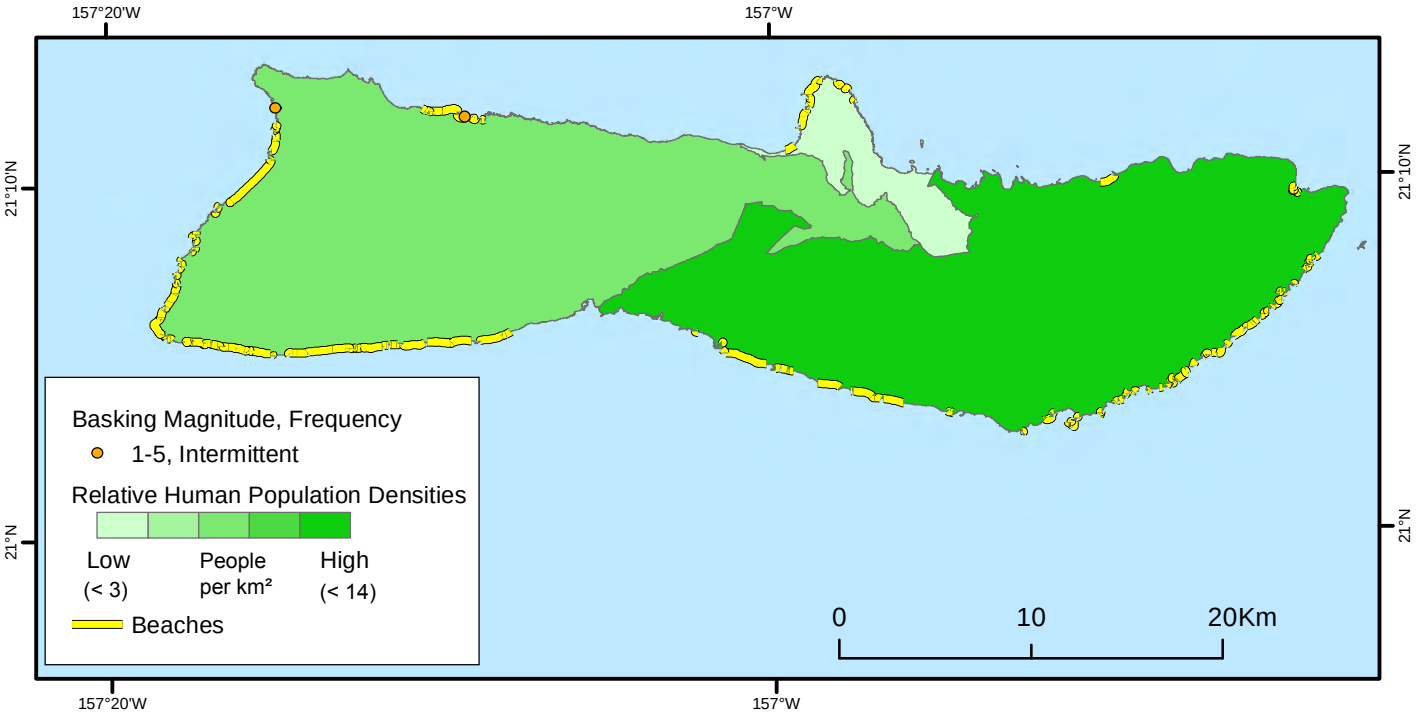

*Figure 5.7. Green turtle (*Chelonia mydas*) basking locations on Moloka'i. Data show magnitude and frequency of reported basking, 1990-2014. Frequency refers to how often an activity is reported at a particular location, and magnitude refers to the number of incidences or individuals involved. Data sources: basking (Parker et al., 2015), human population (State of Hawai'i, 2010), and beaches (NOAA ORR, 2001)*

5.3.2. Nesting

There were 79 locations with reported nesting activities for sea turtles around the Main Hawaiian Islands between 1900 to present. Of these 79 reports, 47 (60%) were green turtle nestings, 27 (34%) were hawksbill, 4 (5%) were olive ridley, and one (1%) was leatherback (Tables 5.5 and 5.6).

For green turtles, Kaua'i had the highest number of nesting locations reported (19 of 47 or 40%) despite having relatively low human population density, however, nearly 50 percent of these were rare sightings (Table 5.5). Maui and O'ahu each accounted for 23 percent (11 of 47) of reports. Most nesting reports consisted of intermittent or rare frequency and only 1-2 individuals for each event. In contrast, Moloka'i had the highest magnitude of regular nesting locations reported, with 3-4 individuals seen on a regular basis but only at one location. The islands of Hawai'i, Kaho'olawe and Lāna'i had few reports of nesting locations, always in the lowest frequency (rare) and smallest magnitude (<1). There were no reports from Ni'ihau. As stated previously, Ni'ihau and Kaho'olawe have limited scientific access. However, as access to both of these islands increases, reports of nesting turtles may also increase.

*Table 5.5. Frequency, magnitude, and number of nesting locations by green turtles (*Chelonia mydas*) in the MHI, 1900-2014. Frequency refers to how often an activity is reported at a particular location, and magnitude refers to the estimated number of individuals involved per year. Data source: Parker et al., 2015*

Species	Island	Frequency	Magnitude	# Locations
Green	Hawai'i	rare	<1	1
	Kaho'olawe	rare	<1	1
	Kaua'i	regular	1-2	2
		intermittent	<1	7
		unknown	<1	10
	Lāna'i	rare	<1	1
	Maui	intermittent	<1	11
	Moloka'i	regular	1-2	1
		regular	3-4	1
	O'ahu	regular	1-2	3
		intermittent	<1	8
		rare	<1	1
Total Green turtle nesting activities				**47**

Sea Turtles

Reports of green turtle nesting locations around Kauaʻi (Figure 5.8) are distributed around the island, with the fewest reports along the north Nāpali Coast to Princeville. This may be partly due to a lack of roads along the coastline in the area, and the relatively low human population density. This coastline has a few small pocket beaches where nesting activities may occur, but go unreported in this low-accessibility, sparsely-populated area. In contrast, to the east of Princeville, relative human population is denser, and more nesting activities are reported. Along the south coast, there are several beaches, accessibility is easy due to a shoreline highway, and human density increases. There are more nesting reports of regular frequency from this area of the island.

*Table 5.6. Magnitude and number of nesting locations by hawksbill (*Eretmochelys imbricata*), leatherback (*Dermochelys coriacea*) and olive ridley (*Lepidochelys olivacea*) sea turtles in MHI, 1900-2014. Magnitude refers to the number of incidences or individuals involved. Data source: Parker et al., 2015*

Species	Island	Magnitude	# Locations
Hawksbill	Hawaiʻi	<1	6
		1	10
		3	1
		5	1
	Maui	<1	5
	Molokaʻi	<1	2
	Oʻahu	<1	2
Leatherback	Lānaʻi	<1	1
Olive	Hawaiʻi	<1	1
	Maui	<1	1
	Oʻahu	<1	2
Total other species nesting activities			**32**

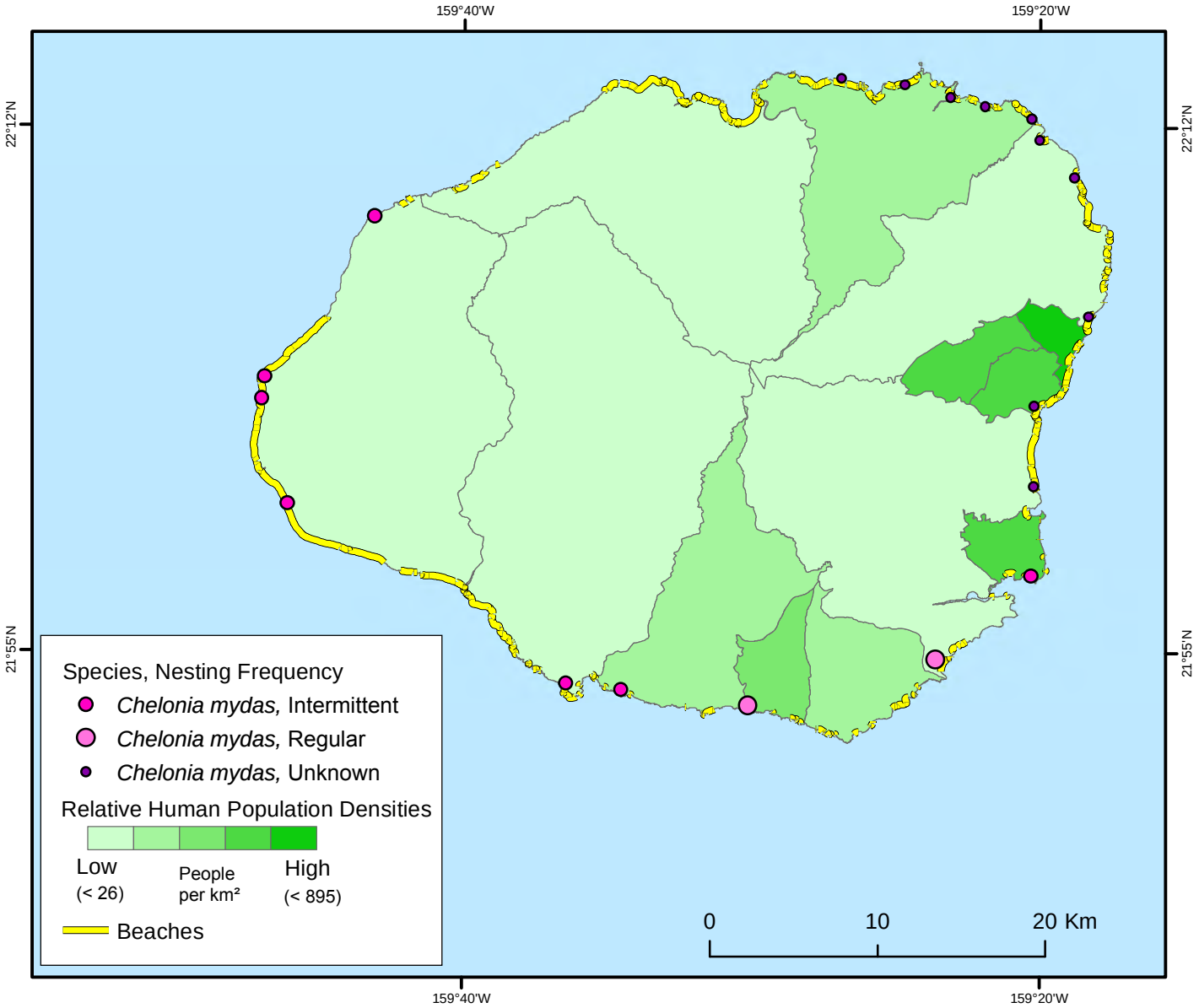

*Figure 5.8. Sea turtle nesting locations on Kauaʻi. Data show species and frequency (*Chelonia mydas *only) of reported nestings, 1900-2014. Data sources: nesting (NOAA MTBAP, 2014b), human population (State of Hawaiʻi, 2010), and beaches (NOAA ORR, 2001)*

Green turtle nesting reports were distributed somewhat evenly around O'ahu, with concentrations of regular nesting frequencies reported at Police Beach, near Kahuku in the north, and Sandy Beach Park in the southeast (Figure 5.9). These areas of regularly reported activities are, also, areas frequented by sight-seers, increasing the likelihood of reports.

Green sea turtle, Chelonia mydas. *Photo credit: Bryan M. Costa (NOAA NOS/NCCOS)*

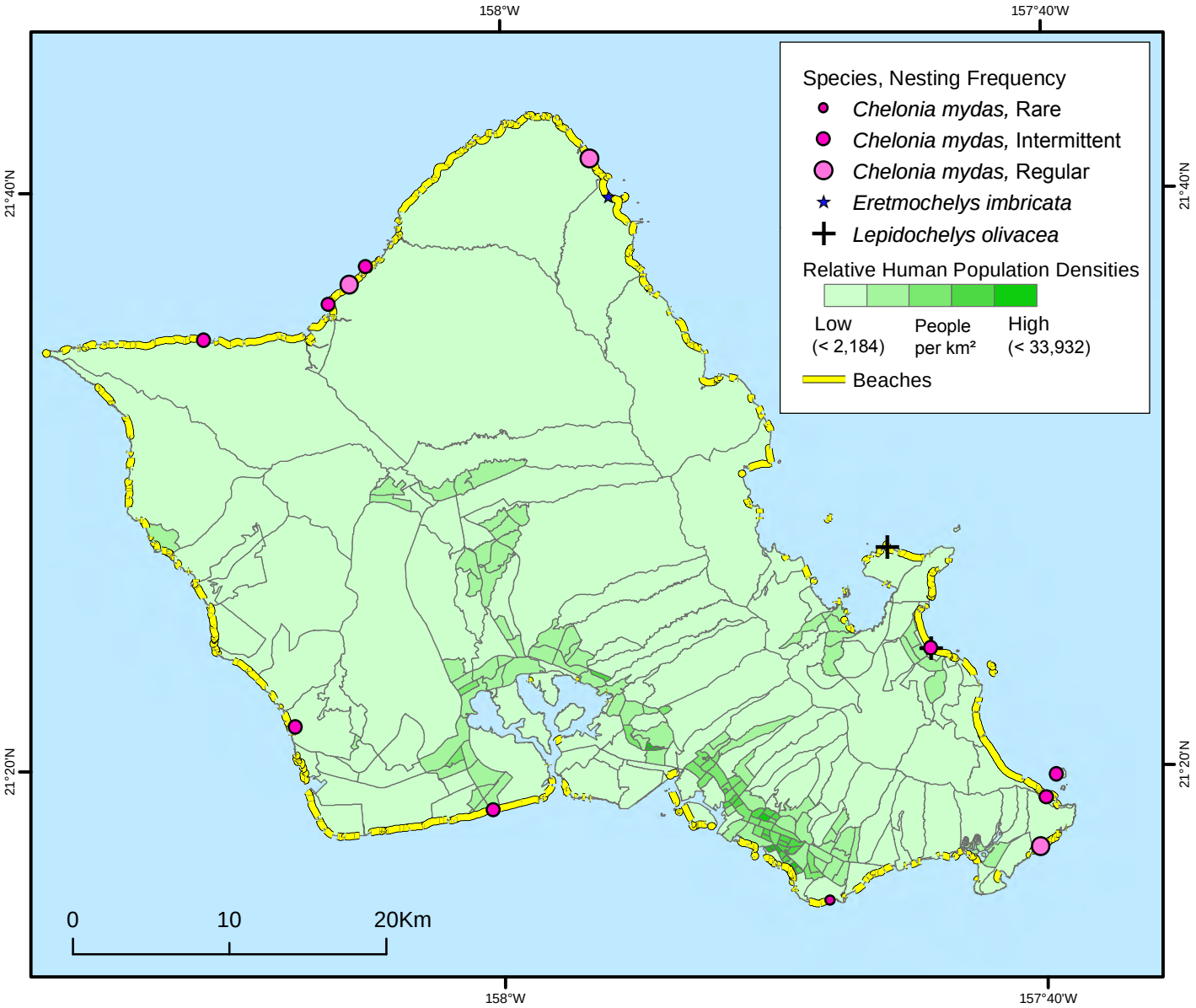

*Figure 5.9. Sea turtle nesting locations on O'ahu. Data show species and frequency (*Chelonia mydas *only) of reported nestings, 1900-2014. Data sources: nesting (NOAA MTBAP, 2014b), human population (State of Hawai'i, 2010), and beaches (NOAA ORR, 2001)*

Sea Turtles

Nesting activity around Maui (Figure 5.10), including green, hawksbill, and olive ridley turtles, is concentrated in three locations: Kahului to Ho`okipa Beach in the northeast, Mā`alaea Bay off Kīhei, and the northwest coast from near Lāhainā to Lipoa Point. Each of these sites is near human population centers, offers people easy access to beaches, and provides good nesting habitat for turtles.

Olive ridley turtle. Photo credit: Reuven Walder (Turtle Island Restoration Network)

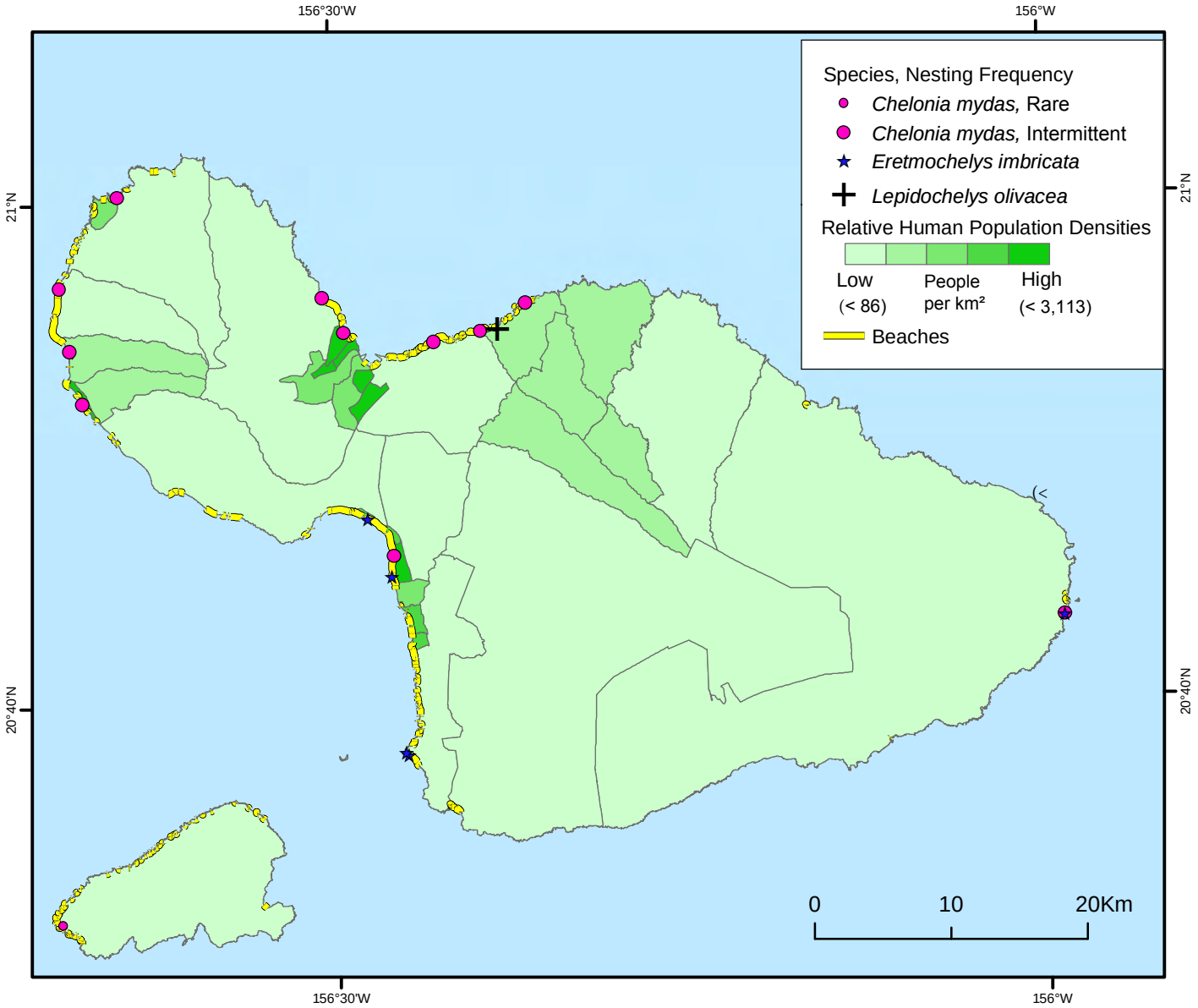

*Figure 5.10. Sea turtle nesting locations on Maui and Kaho'olawe. Data show species and frequency (*Chelonia mydas *only) of reported nestings, 1900-2014. Data sources: nesting (NOAA MTBAP, 2014b), human population (State of Hawai'i, 2010), and beaches (NOAA ORR, 2001)*

Of the other three species of sea turtles (hawksbill, olive ridley, and leatherback) for which nesting locations were reported (Table 5.6), hawksbill sea turtles were most commonly reported from the island of Hawai'i, with smaller numbers from Maui, Moloka'i, and O'ahu. Hawksbill nesting locations were reported around Hawai'i Island's southern coast (Figure 5.11), with concentrations near Keliuli Bay, near Punalu`u County Beach Park, and in the pocket beaches of Hawai'i Volcanoes National Park near Keauhoa Point. Of note, fewer than 20 hawksbills nest each year (Seitz et al., 2012; Snover et al., 2013). Given its 'endangered' status under the ESA (Table 5.1), there is great need to monitor the population closely and make strides toward conservation. The hawksbill telemetry study by Parker et al. (2009) indicates the nesters (n=3) from Hawai'i's Kamehame nesting area may forage around the Hamakua Coast, and that the hawksbills (n=3) nesting on beaches near Kīhei, Maui, also forage along Hawai'i's Hamakua Coast.

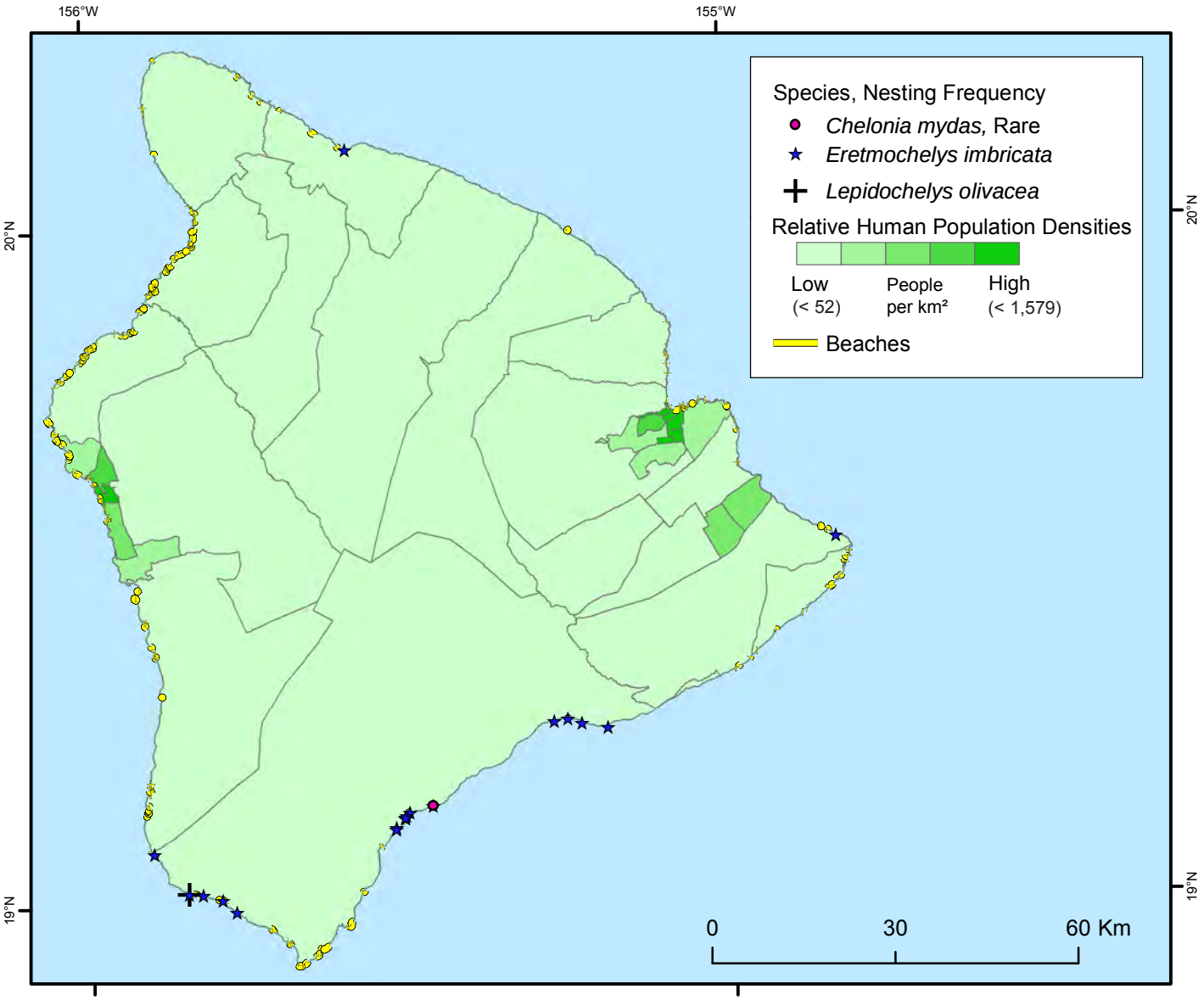

*Figure 5.11. Sea turtle nesting locations on the island of Hawai'i. Data show species and frequency (*Chelonia mydas *only) of reported nestings, 1900-2014. Data sources: nesting (NOAA MTBAP, 2014b), human population (State of Hawai'i, 2010), and beaches (NOAA ORR, 2001)*

Sea Turtles

On rare occasions, other species have been observed. Four olive ridley nests were reported on the islands of Hawai‘i (1), Maui (1), and O‘ahu (2). There has been only one leatherback nesting report in the MHI, which occurred on Lāna‘i (Figure 5.12). Few nesting reports are received around Moloka‘i despite the presence of good beach habitat (Figure 5.13). Placing all of these nesting magnitudes and frequencies for the MHI into context, it should be noted that green turtles regularly nest each year at French Frigate Shoals in the Northwestern Hawaiian Islands at magnitudes of greater than 200 individuals per year (Nurzia Humburg and Balazs, 2014).

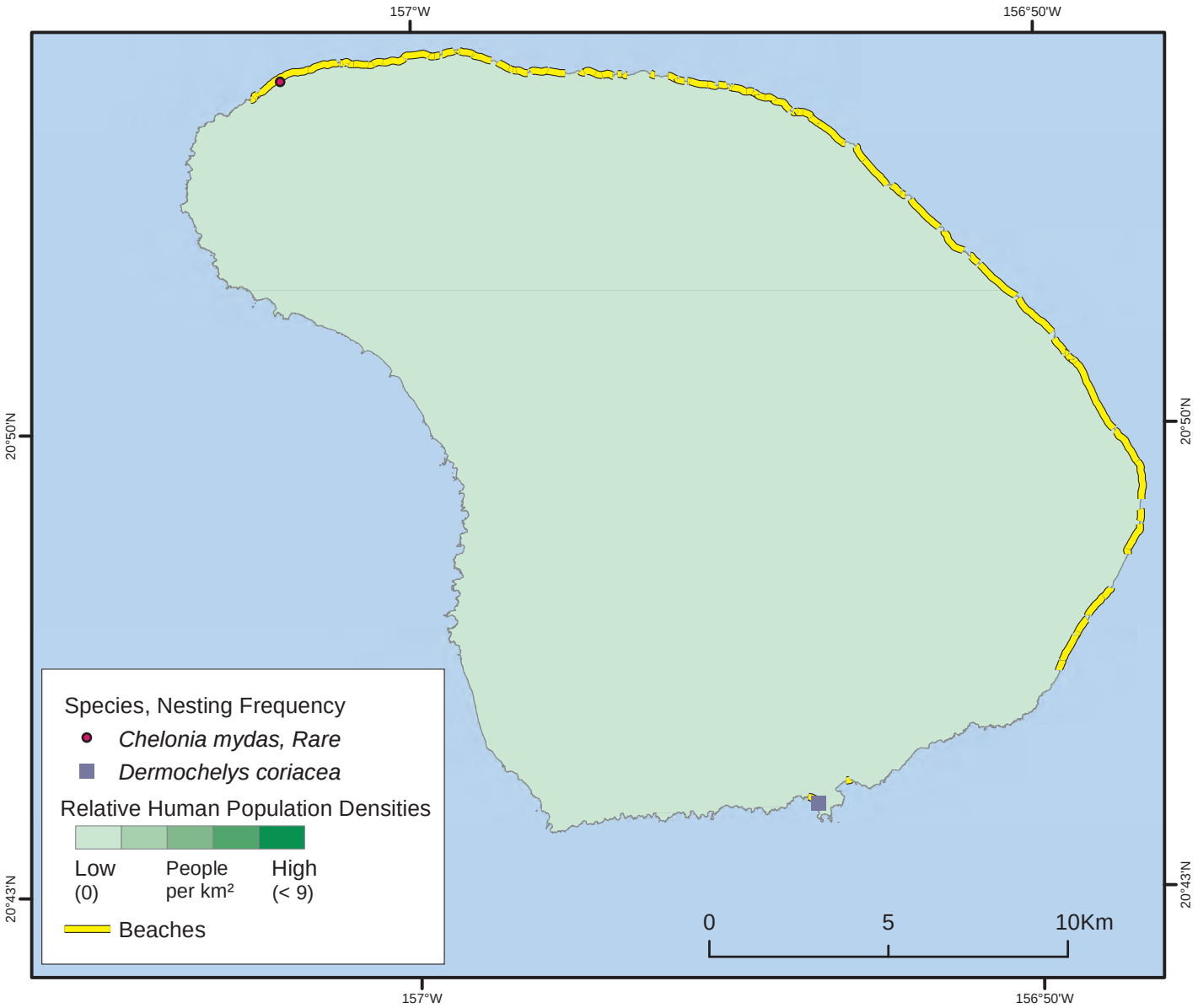

*Figure 5.12. Sea turtle nesting locations on Lāna‘i. Data show species and frequency (*Chelonia mydas *only) of reported nestings, 1900-2014. Data sources: nesting (NOAA MTBAP, 2014b), human population (State of Hawai‘i, 2010), and beaches (NOAA ORR, 2001)*

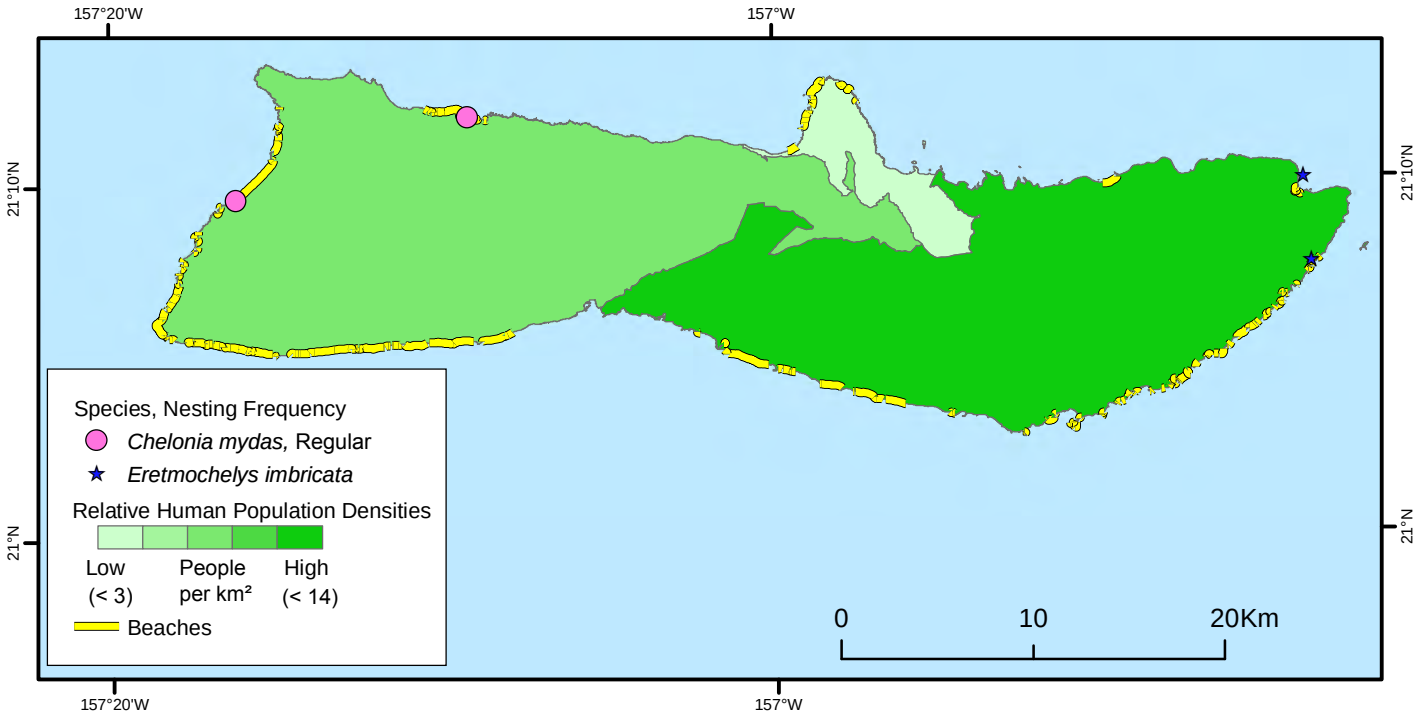

*Figure 5.13. Sea turtle nesting locations on Moloka'i. Data show species and frequency (*Chelonia mydas *only) of reported nestings, 1900-2014. Data sources: nesting (NOAA MTBAP, 2014b), human population (State of Hawai'i, 2010), and beaches (NOAA ORR, 2001)*

5.3.3. Stranding

There were 3,433 reports of sea turtle strandings throughout MHI from 1977 through July 2014, including 889 records with an unknown or pending cause of the stranding (includes 19 related to hatchling mortality; Table 5.7). Of the 3,433 stranding reports, 77 percent were from O'ahu, 10 percent from Maui, eight percent from the island of Hawai'i, and four percent from Kaua'i. Lāna'i and Moloka'i both had less than one percent; Kaho'olawe and Ni'ihau had no reports. The magnitude of these values corresponds closely to the magnitude of the human population of each island. Higher human populations result in more stressors and potential causes of strandings, as well as more people to observe and report stranding events when they occur.

Table 5.7. Number of sea turtle strandings by primary cause reported in MHI, 1975-July 2014 (Murakawa, 2014a, 2014b).

Cause of Stranding	Hawai'i	Kaua'i	Lāna'i	Maui	Moloka'i	O'ahu	Totals
Boat Impact	12	5	0	4	0	88	109
Entanglement	32	22	1	16	2	406	479
Fibropapillomatosis (FP)	54	35	2	218	2	1,120	1,431
Human-caused mortality	14	5	2	10	0	42	73
Ingestion	14	5	2	9	0	102	132
Natural predation	15	6	2	21	1	98	143
Other illnesses, etc.	38	9	0	7	0	55	109
Trauma	9	3	0	7	1	67	87
Unknown	96	57	10	60	7	640	870
Totals	284	147	19	352	13	2,618	3,433

Fibropapillomatosis, or FP, is a debilitating transmissible disease in sea turtles which causes growth of bulbous tumors on soft tissues (Balazs et al., 2000), and may be linked to nutrient-rich, polluted waters (Van Houtan et al., 2014; Herbst and Klein, 1995; Arthur et al., 2008; Work et al., 2014). FP accounted for 42 percent of all strandings reported (Table 5.8), and is the main cause of strandings of green turtles in the MHI (Chaloupka et al., 2008). Entanglement was the second highest stranding event, with 14 percent reported; natural predation

and ingestion accounted for four percent each. Human-caused mortality (apart from boat strikes) was the least reported reason for strandings, with two percent. Strandings attributed to boat impacts were only three percent of total strandings reported. Analyses in subsequent sections are segmented along island shorelines and include only those strandings with known cause (n=2,563).

Table 5.8. Percent of sea turtle strandings causes reported in MHI, July 6, 1977-July 26, 2014 (Murakawa, 2014a, 2014b).

Cause of Stranding	Percent
Boat impact	3
Entanglement	14
Fibropapillomatosis	42
Human-caused mortality	2
Ingestion	4
Natural predation	4
Other illnesses, etc.	3
Trauma	3
Unknown	25

Green turtle severely afflicted with fibropapillomatosis. Photo credit: Peter Bennett and Ursula Keuper-Bennett (Wikipedia)

O'ahu

O‘ahu stranding reports were from most shores around the island, with some strandings even being reported from areas with cliffs (Figure 5.14). FP accounted for 56 percent of O‘ahu strandings. FP far outnumbered any other reasons for strandings on all quadrants of O‘ahu except in the southwest, where entanglement (n=89) accounted for nearly one-third of reported strandings (n=277). Eighty-five percent of all entanglements reported were from O‘ahu. Across all islands, O‘ahu reports accounted for 58 percent of all human-caused mortality reports, however, this cause was O‘ahu’s lowest count category. On O‘ahu, four percent of all reported strandings were attributed to boat impacts, with southeast O‘ahu having the highest percentage at seven percent. Although FP accounted for the majority of strandings, a recent study focused on the larger Hawai‘i and insular Pacific region found that the majority of 230 turtles died from fishing-induced or boat strike trauma (Work et al., 2015).

Maui

On Maui, strandings were heavily reported along the north-central and south-central coasts, as well as the northwest coast (Figure 5.15). The majority of strandings were reported in areas without cliffs. Of all Maui strandings reported, 75 percent were attributed to FP. Maui reported the highest percentage of strandings due to FP and few differences among coastal regions.

Hawai‘i

On the island of Hawai‘i, strandings were reported heavily in three main clusters: on the west coast near Puako and near Kailua-Kona, and on the east coast near Hilo (Figure 5.16). The majority of strandings on the east coast were attributed to FP (57%, 49 of 86), whereas strandings on the west coast were caused primarily by other illnesses (29%, 30 of 102), but, also, many were attributed to other causes, including boat impacts, entanglements and natural predation. Presence of cliffs around the island of Hawai‘i did not seem to exclude stranding reports.

Kaua'i

On Kaua‘i, strandings were reported from around the island, except in areas with cliffs (Figure 5.17). Strandings were attributed primarily to entanglement in the northeast (41%, 20 of 49) and to FP in the southwest (63%, 26 of 41).

Lāna‘i and Moloka‘i

On Lāna‘i and Moloka‘i, only a few strandings were reported and those were from coasts without cliffs. Lāna‘i’s stranding reports were mostly from the beaches along the east coast (Figure 5.18), and Moloka‘i’s were from the south shore (Figure 5.19).

In conclusion, basking, nesting, and stranding data may be used to document current spatial patterns and avoid important habitats during wind-farm planning. Incidences of turtle activities are not expected to change following wind farm development; however, describing present patterns will provide an important biogeographic baseline to detect any changes.

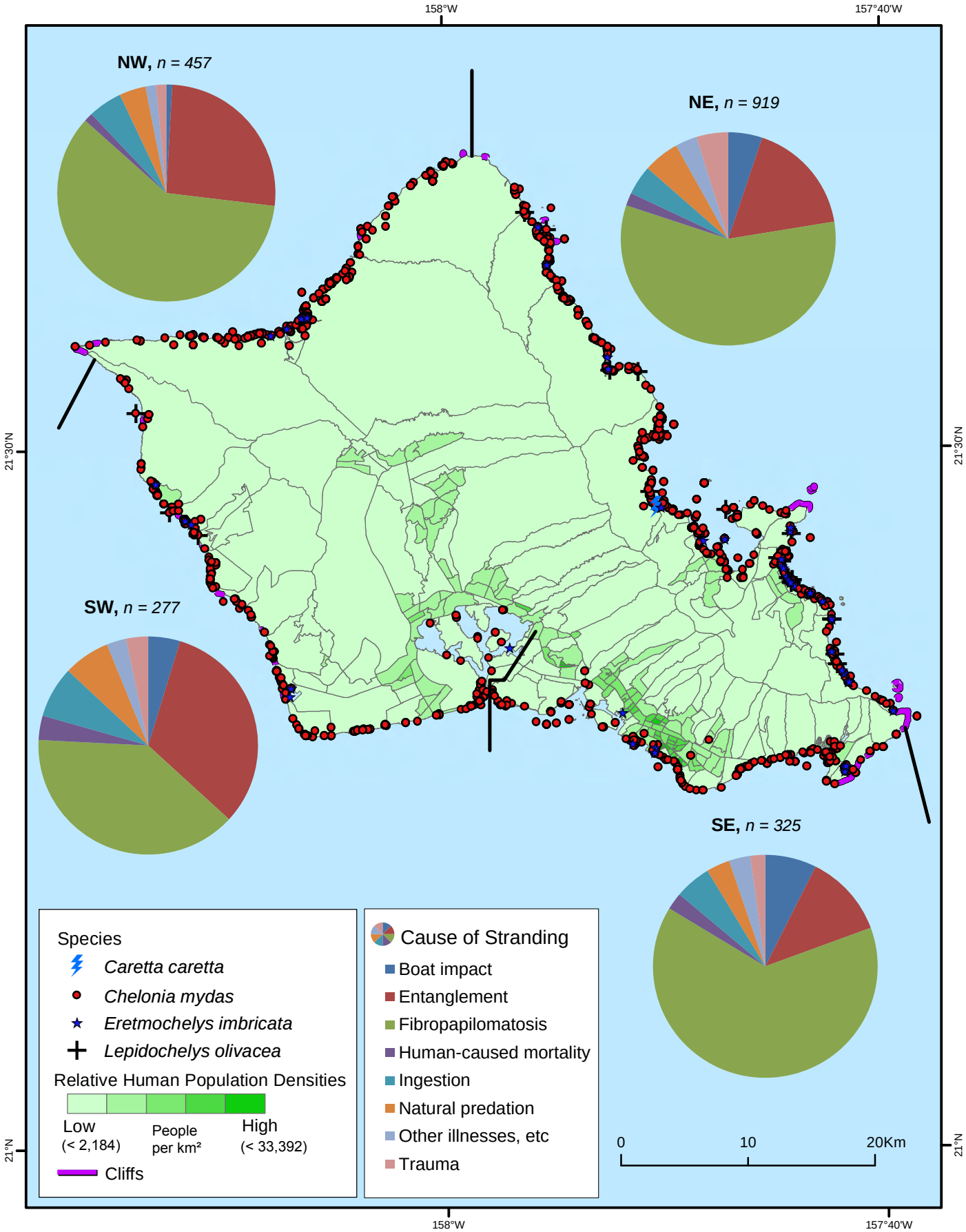

Figure 5.14. Sea turtle strandings on O'ahu. Data show species and location of reported strandings, 1978-2014. Data sources: strandings (Murakawa, 2014a, 2014b), human population (State of Hawai'i, 2010), and beaches (NOAA ORR, 2001)

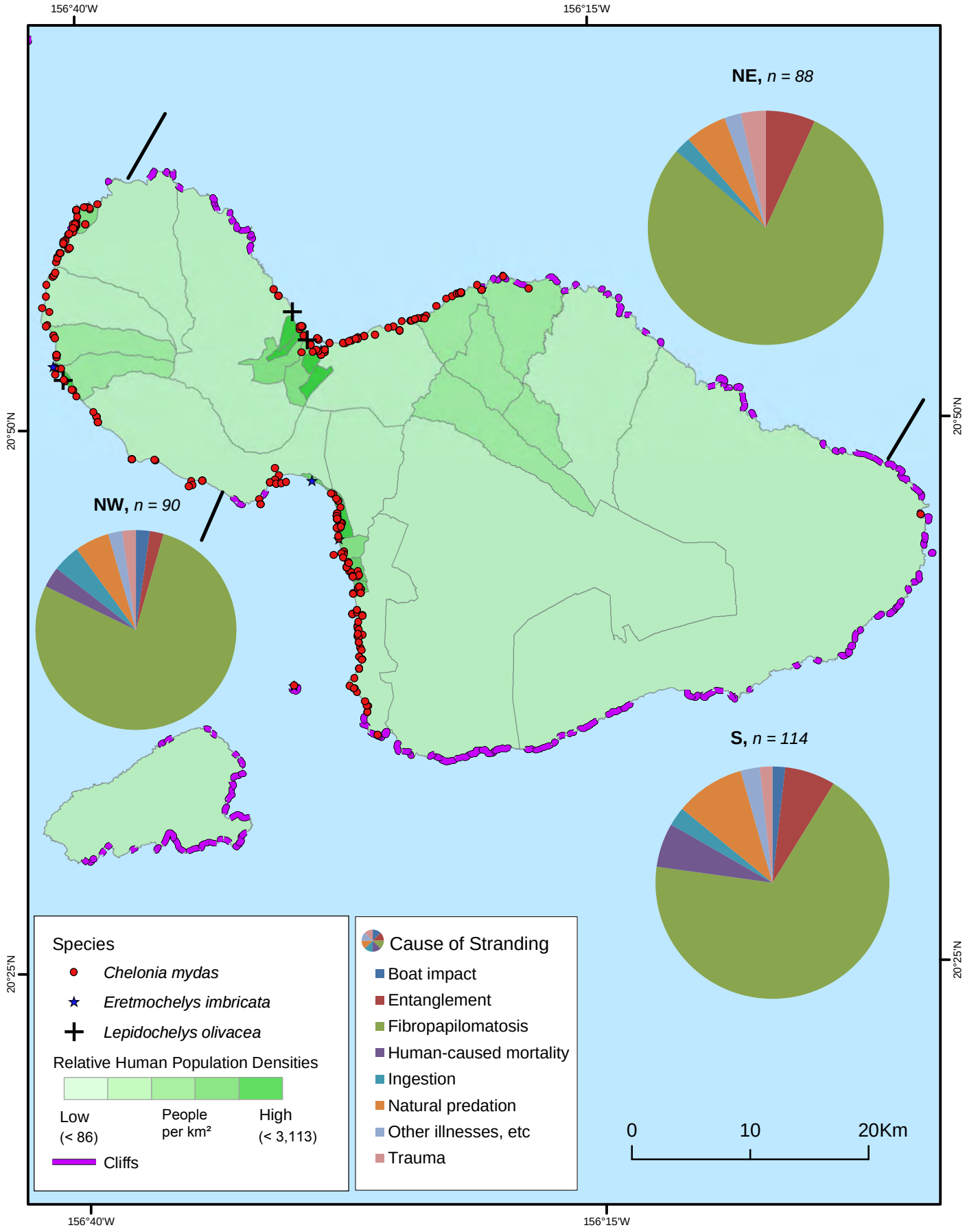

Figure 5.15. Sea turtle strandings on Maui and Kaho'olawe. Data show species and location of reported strandings, 1978-2014. Data sources: strandings (Murakawa, 2014a, 2014b), human population (State of Hawai'i, 2010), and beaches (NOAA ORR, 2001)

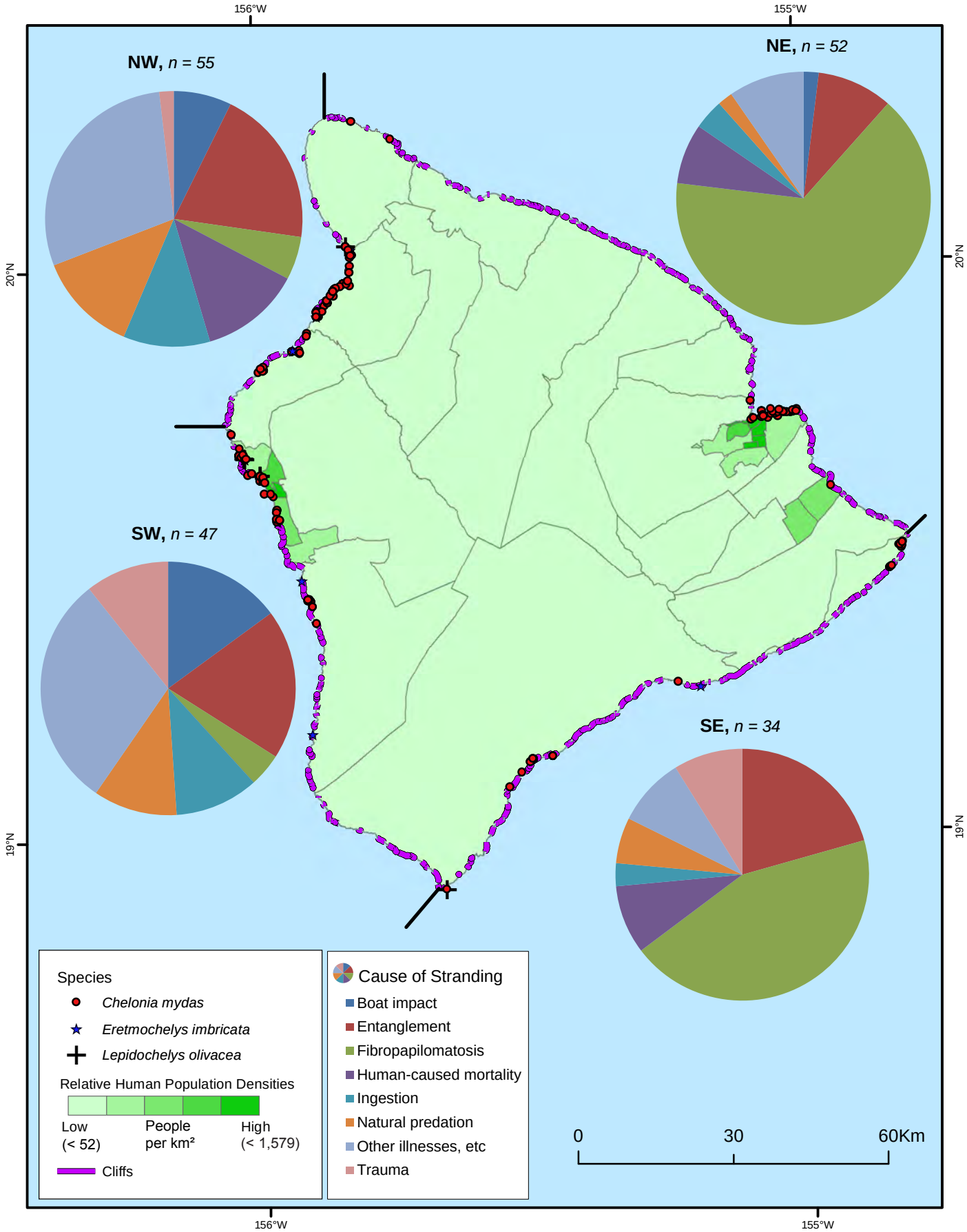

Figure 5.16. Sea turtle strandings on the island of Hawai'i. Data show species and location of reported strandings, 1978-2014. Data sources: strandings (Murakawa, 2014a, 2014b), human population (State of Hawai'i, 2010), and beaches (NOAA ORR, 2001)

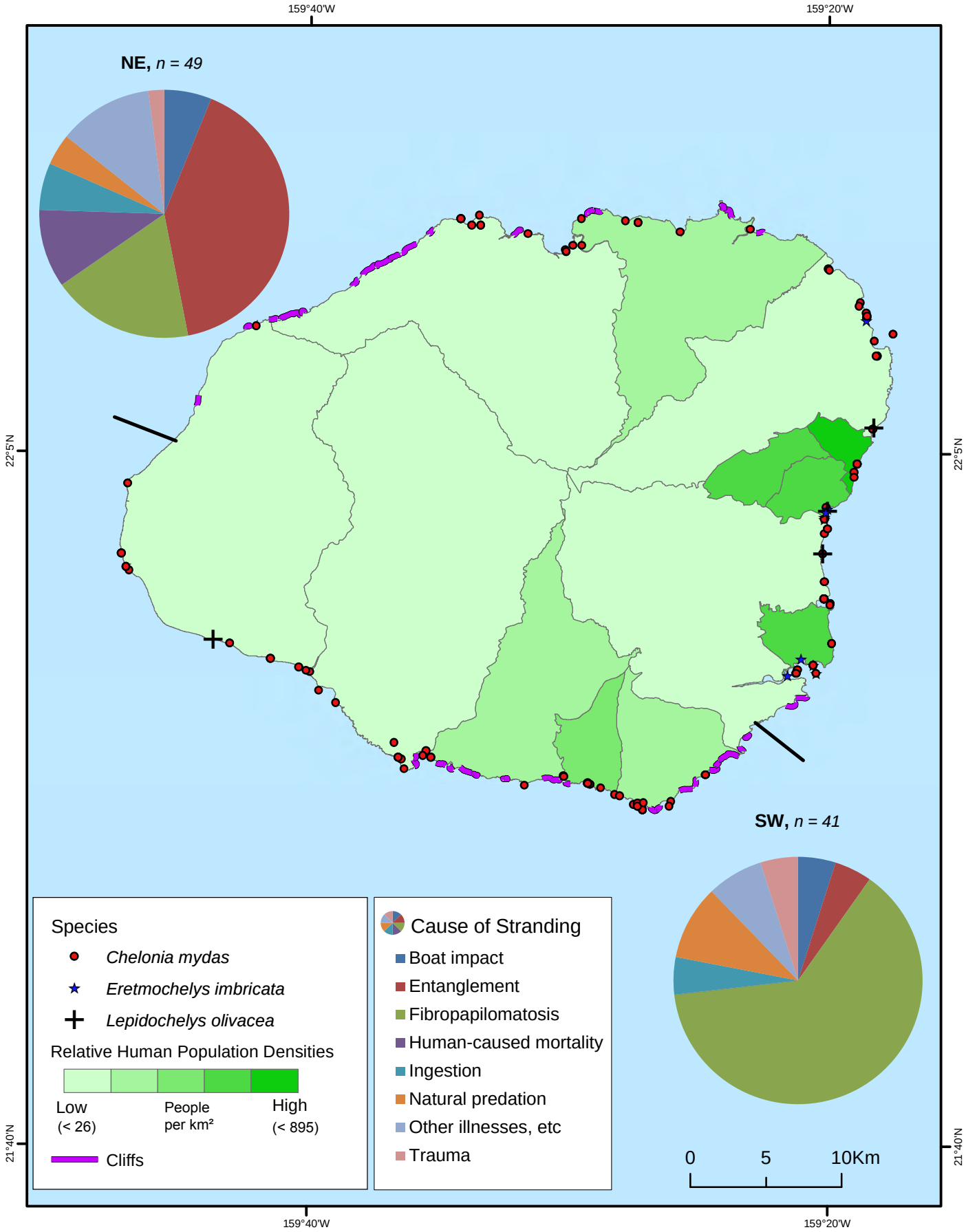

Figure 5.17. Sea turtle strandings on Kaua'i. Data show species and location of reported strandings, 1978-2014. Data sources: strandings (Murakawa, 2014a, 2014b), human population (State of Hawai'i, 2010), and beaches (NOAA ORR, 2001)

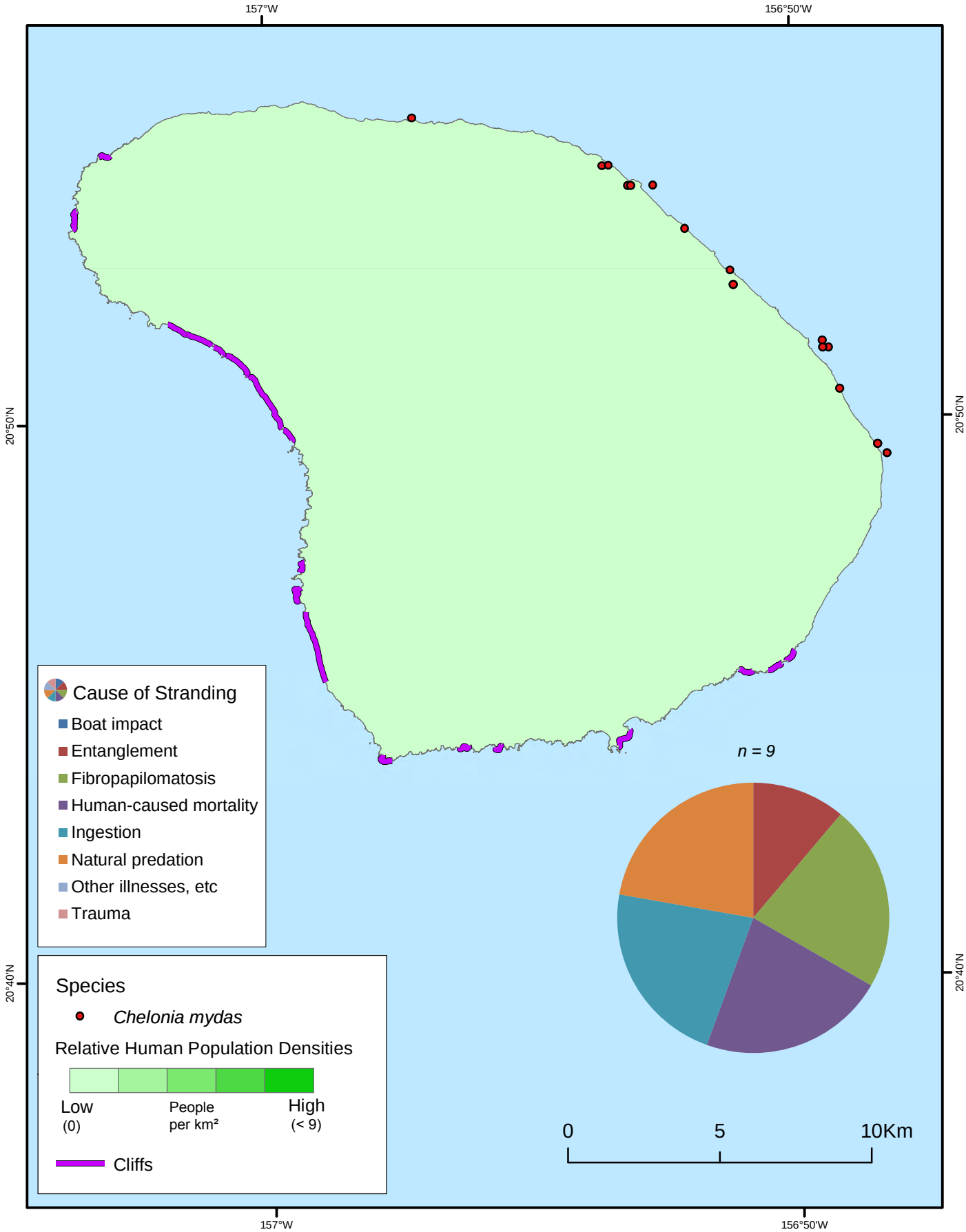

Figure 5.18. Sea turtle strandings on Lāna'i. Data show species and location of reported strandings, 1978-2014. Data sources: strandings (Murakawa, 2014a, 2014b), human population (State of Hawai'i, 2010), and beaches (NOAA ORR, 2001)

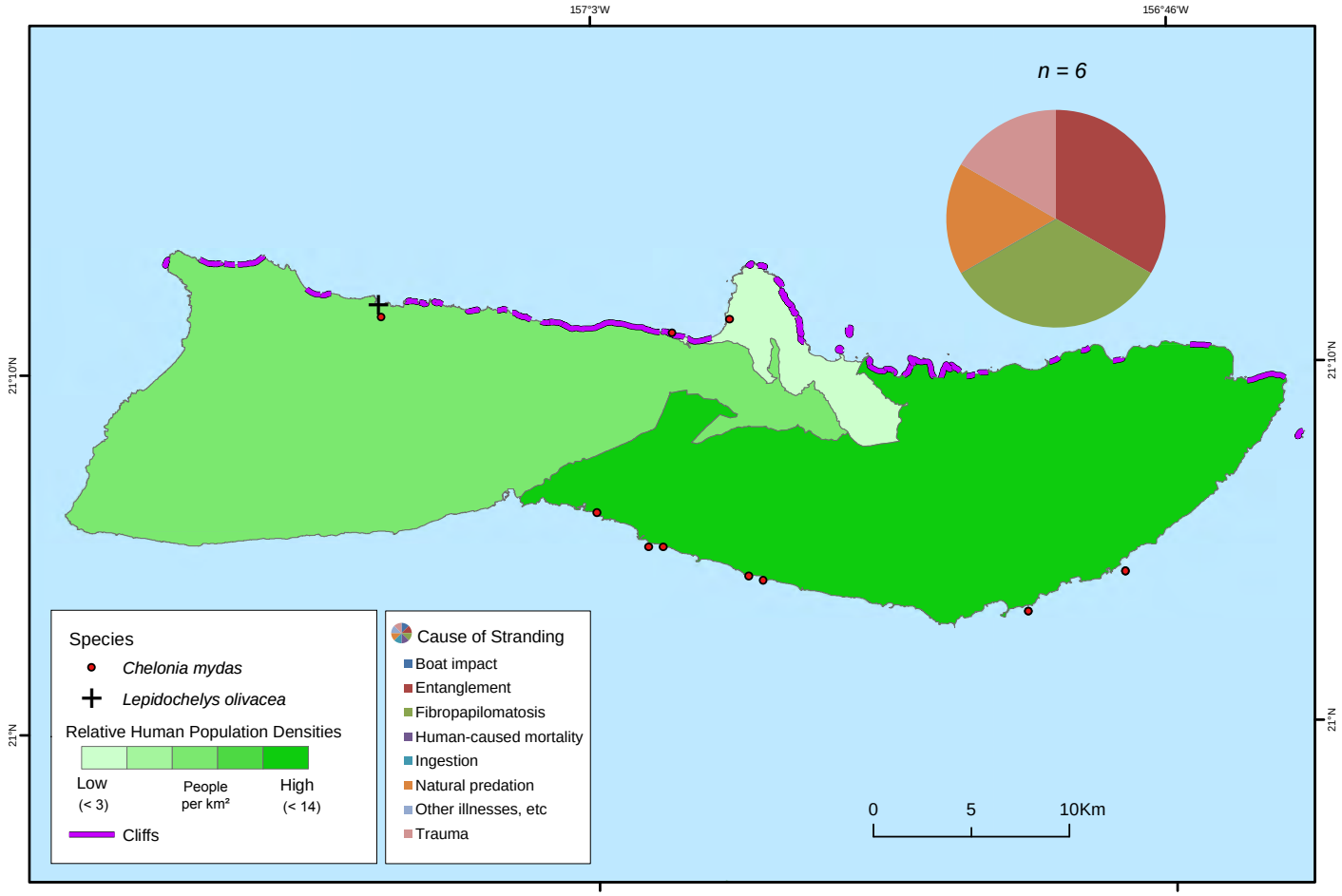

Figure 5.19. Sea turtle strandings on Moloka'i. Data show species and location of reported strandings, 1978-2014. Data sources: strandings (Murakawa, 2014a, 2014b), human population (State of Hawai'i, 2010), and beaches (NOAA ORR, 2001)

5.4. DATA LIMITATIONS AND INFORMATION GAPS

Data compiled by PIFSC for nesting, basking, and stranding turtles along coastlines of the MHI rely on a mixture of regular monitoring by trained professionals at some beaches, irregular assessments at others, and casual observations and reporting by community groups or the public for most areas. Although this maximizes the amount and extent of sea turtle information, it does not include a standardized measure of effort for calculating the density of sea turtle activities. As a result, rather than the amount of turtle activities actually taking place, values reported here are significantly influenced by the amount and spatial distribution of human effort to report them.

Literature review and consultation with local sea turtle researchers highlight additional data gaps limiting our present understanding of sea turtle distributions. Most notably, there are no comprehensive monitoring programs on either the distribution of sea turtles' inshore foraging areas or incidences farther out at-sea. Monitoring programs to identify broad scale distributions of turtle activities throughout the MHI are not funded at present, even for the critical life history phase of nesting. There have been localized investigations on the foraging behavior, habitats, and movement patterns of sea turtles using satellite tags and *in situ* observations (Parker et al., 2009), however, these have all been quite limited in sample size and geographic scope and cannot be used to provide a regional characterization for the MHI.

Loggerhead turtle bycatch. Credit: Mike Tork (NOAA)

At-sea survey data for birds and cetaceans (Chapter 6: Marine Mammals and Chapter 7: Seabirds) almost never include sea turtle sightings. Sightings that do occur are not controlled for effort, and species identifications are questionable. Bycatch data from longline fisheries were also considered but, due to the ESA status of sea turtles, fisheries bycatch thresholds are set extremely low and result in a shut-down of fisheries if even small numbers of turtles are taken. For example, prior to November 2012, Hawaiian shallow-set longline fishermen were allowed to catch only 16 leatherback or 17 North Pacific loggerhead sea turtles per year (Federal Register 50 CFR Part 665; Federal Register, 2012). This is a substantial disincentive to accidentally catch turtles or report them when interactions occur, resulting in very few catch records. Another recent analysis sought to reconstruct the offshore turtle fishery based on historical data (Kittinger et al., 2013; Van Houtan and Kittinger, 2014). Unfortunately, it, too, may not be applicable for estimating distributions today for several reasons: 1) it is questionable if today's distribution patterns would be consistent with historical observations; 2) the analysis was limited to Hawai'i's Division of Aquatic Resources (DAR) statistical reporting framework and, therefore, has limited spatial resolution (Chapter 4, Figure 4.3); and 3) catch patterns are partly confounded with the distribution of fishing effort rather than turtle abundance (e.g., higher catch observed near population centers with convenient access to fishable waters).

Only a few turtles have been tracked to evaluate broad scale navigation through the MHI. There is ongoing research of satellite-tagged green, loggerhead, leatherback (Benson et al., 2011) and olive ridley turtles that is focused on migration patterns, pelagic foraging and/or reduction of fishery-turtle interactions (NOAA PIFSC, 2016). However, due to limited sample size and the geographic scope needed for planning offshore wind farm developments, those few turtle tracks are not included in this report.

There have also been localized studies of foraging behavior (Balazs, 1994), but the spatial distribution of foraging sites is not monitored at the scale of the MHI. A small number of hawksbills have been tracked using satellite transmitters to evaluate foraging sites around Hawai'i Island and Maui Nui (Parker et al., 2009). Those data suggest that the Hamakua coast of northeast Hawai'i Island may be an important foraging area. However, further studies of their forage and habitat needs are necessary if their distribution and abundance are to be comprehensively addressed (D. Parker, pers. obs.).

ACKNOWLEDGEMENTS

We would like to thank Hawai'i Preparatory Academy (Marc Rice), HVNP Hawai'i Island Hawksbill Turtle Recovery Project (Will Seitz), the Kaho'olawe Island Reserve Commission, Malama na Honu (Joanne Pettigrew), Maui Coastal Land Trust, National Botanical Tropical Gardens, NOAA PIRO Protected Resources Division (Kimberly Maison, Irene Kelly), Pacific Missile Range Facility (John Burger), Sea Life Park Hawai'i (Jeff Pawloski), State of Hawai'i DLNR (Donald Heacock, Skippy Hau, Mike Coelho, Bill Puleloa), The Hawai'i Wildlife Fund (Cheryl King), The Nature Conservancy Moloka'i Turtle Trackers, Turtle Trax (Peter Bennett, Ursula Keuper-Bennett), U.S. Fish and Wildlife Service (Glynnis Nakai, John Klavitter, Joy Hiromasa), and the University of Hawai'i Maui College (Donna Brown). George Balazs provided contacts for tracking down data sets and key suggestions for presenting and interpreting the data.

LITERATURE CITED

Arthur, K., C. Limpus, G.H. Balazs, J.A. Capper, J. Udy, G. Shaw, U. Keuper-Bennett, and P. Bennett. 2008. The exposure of green turtles (*Chelonia mydas*) to tumour promoting compounds produced by the cyanobacterium *Lyngbya majuscula* and their potential role in the aetiology of Fibropapillomatosis. Harmful Algae 7 (1): 114–125.

Balazs, G. 1980. Synopsis of biological data on marine turtles in the Hawaiian Islands. NOAA Technical Memorandum NOAA-TM-NMFS-SWFC-7. 141 pp.

Balazs, G.H. 1994. Homeward bound: Satellite tracking of Hawaiian green turtles from nesting beaches to foraging pastures. pp. 205-208. In: B.A. Schroeder and B.E. Witherington (compilers), Proceedings of the 13th Annual Symposium on Sea Turtle Biology and Conservation. NOAA Technical Memorandum NMFS-SEFSC-341. 281 pp.

Balazs, G.H. and D.M. Ellis. 2000. Satellite telemetry of migrant male and female green turtles breeding in the Hawaiian Islands. pp. 281-283. In: F.A. Abreu-Grobois, R. Briseño-Dueñas, R. Márquez-Millán, and L. Sarti-Martínez (compilers), Proceedings of the 18th Annual Symposium on Sea Turtle Biology and Conservation. NOAA Technical Memorandum NMFS-SEFSC-436. 293 pp.

Balazs, G.H., S.K.K. Murakawa, D.M. Ellis, and A.A. Aguirre. 2000. Manifestation of Fibropapillomatosis and rates of growth of green turtles at Kaneohe Bay in the Hawaiian Islands. pp. 112-113. In: F.A. Abreu-Grobois, R. Briseño-Dueñas, R. Márquez-Millán, and L. Sarti-Martínez (compilers). Proceedings of the 18th Annual Symposium on Sea Turtle Biology and Conservation. NOAA Technical Memorandum NMFS-SEFSC-436. 293 pp.

Balazs, G.H., K.S. Van Houtan, S.A. Hargrove, S.M. Brunson, and S.K.K. Murakawa. 2015. A review of the demographic features of Hawaiian green turtles. Chelonian Conservation and Biology 14 (2): 119-129.

Battista, T.A., B.M. Costa, and S.M. Anderson. 2007. Benthic Habitats of the Main Hawaiian. NOAA Technical Memorandum NOS NCCOS CCMA 152. Silver Spring, MD. 48 pp. Data Downloaded 5 September 2014. Data Website: https://products.coastalscience.noaa.gov/collections/benthic/e97hawaii/data2007.aspx (Site Accessed 8 June 2016).

Benson, S.R., T. Eguchi, D.G. Foley, K.A. Forney, H. Bailey, C. Hitipeuw, B.P. Samber, R.F. Tapilatu, V. Rei, P. Ramohia, J. Pita, and P.H. Dutton. 2011. Large-scale movements and high-use areas of western Pacific leatherback turtles, *Dermochelys coriacea*. Ecosphere 2(7): 1-27.

Chaloupka, M., T.M. Work, G.H. Balazs, S.K.K. Murakawa, and R. Morris. 2008. Cause-specific temporal and spatial trends in green sea turtle strandings in the Hawaiian Archipelago (1982-2003). Marine Biology 154(5): 887-898.

Dodd, C.K., Jr. 1988. Synopsis of the biological data on the loggerhead sea turtle *Caretta caretta* (Linnaeus, 1758). U.S. Fish and Wildlife Service Biological Report 88(14). 110 pp.

Federal Register. 2012. Western Pacific Pelagic Fisheries; Revised Limits on Sea Turtle Interactions in the Hawai'i Shallow-Set Longline Fishery. 77 Fed. Reg. 60637 (October 4, 2012)(Final Rule 50 CFR 665). NOAA National Marine Fisheries Service. Online: http://www.fpir.noaa.gov/SFD/pdfs/77_FR_60637-Final_Rule-HI_SS_LL_sea_turtle_interaction_limits_2012-10-04.pdf (Site Accessed 8 June 2016).

Frazer, N.B. 1986. Survival from Egg to Adulthood in a Declining Population of Loggerhead Turtles, *Caretta caretta*. Herpetologica 42 (1): 47-55.

GEBCO. 2008. General Bathymetric Chart of the Oceans 08 Grid. GEBCO operates under the joint auspices of the International Hydrographic Organization and the Intergovernmental Oceanographic Commission of UNESCO. Data Downloaded 8 January 2014. Data Website: http://www.gebco.net/data_and_products/gridded_bathymetry_data/ (Site Accessed 8 June 2016).

Herbst, L. and P. Klein. 1995. Green turtle Fibropapillomatosis: challenges to assessing the role of environmental cofactors. Environmental Health Perspectives 103:27-30.

Hirth, H.F. 1997. Synopsis of the Biological Data on the Green Turtle, *Chelonia mydas* (Linnaeus, 1758). U.S. Fish and Wildlife Service Biological Report 97(1). 120 pp.

King, C.K, W. Gilmartin, S. Hau, H. Bernard, S. Canja, G. Nakai, M.J. Grady, S. Williams, and A.G. Hebard. 2007. Nesting hawksbill turtles (*Eretmochelys imbricata*) on the island of Maui, Hawai'i from 1996-2003. pp. 134-135. In: R.B. Mast, B.J. Hutchinson, and A.H. Hutchinson (compilers), Proceedings of the 24th Annual Symposium on Sea Turtle Biology and Conservation. NOAA Technical Memorandum NMFS-SEFSC-567. 205 pp.

Kittinger, J.N., K.S. Van Houtan, L.E. McClenachan, and A.L. Lawrence. 2013. Using historical data to assess the biogeography of population recovery. Ecography 36: 868-872.

Lohmann, K.J., C.M.F. Lohmann, and N.F. Putman. 2007. Magnetic maps in animals: nature's GPS. Journal of Experimental Biology 210: 3697-3705.

Lusci, P., S. Benhamou, C. Girard, S. Ciccione, D. Roos, J. Sundre, and S. Benvenuti. 2007. Marine turtles use geomagnetic cues during open-sea homing. Current Biology 17: 126-133.

Mangel, J.C, H. Bernard, S. Canja, S. Hau, K. Smith, and S. Williams. 2000. Summary of hawksbill turtles (*Eretmochelys imbricata*) nesting on Maui, Hawaii from 1991-1996. pp. 283-284. In: H.J. Kalb and T. Wibbels, (compilers), Proceedings of the 19th Annual Symposium on Sea Turtle Biology and Conservation. NOAA Technical Memorandum NMFS-SEFSC-443. 291 pp.

Miller, J.D. 1996. Reproduction in sea turtles. pp. 51-80. In: P.L. Lutz and J.A. Musick (eds.), The Biology of Sea Turtles, Vol. 1. CRC Press. 446 pp.

Murakawa, S.K.K. 2014a. Summary of sea turtle strandings in the Main Hawaiian Islands, 1975-July 2014. NOAA National Marine Fisheries Service, Pacific Islands Fisheries Science Center, Marine Turtle Biology and Assessment Program. Internal Report IR-14-029. Data Provided 20 October 2014. Provider Website: https://pifsc-www.irc.noaa.gov/marine_turtle/ (Site Accessed 8 June 2016).

Murakawa, S.K.K. 2014b. Data on sea turtle strandings in the Main Hawaiian Islands, 1975-July 2014. NOAA National Marine Fisheries Service, Pacific Islands Fisheries Science Center, Marine Turtle Biology and Assessment Program. Internal Report IR-14-032. Data Provided 20 October 2014. Provider Website: https://pifsc-www.irc.noaa.gov/marine_turtle/ (Site Accessed 8 June 2016).

NOAA NCEI. 2005. U.S. Coastal Relief Model - Hawai'i. NOAA National Environmental Satellite, Data, and Information Service, National Centers for Environmental Information. Data Downloaded 8 January 2014. Data Website: https://www.ngdc.noaa.gov/mgg/coastal/grddas10/grddas10.htm (Site Accessed 8 June 2016).

NOAA ORR. 2001. Environmental Sensitivity Index Shoreline Types – Polygons and Lines. NOAA National Ocean Service, Office of Response and Restoration. Data Downloaded 23 March 2016. Data Website: http://response.restoration.noaa.gov/maps-and-spatial-data/download-esi-maps-and-gis-data.html#Hawaii (Site Accessed 8 June 2016).

NOAA PIFSC. 2016. Marine Turtles: Life History and Ecology. NOAA National Marine Fisheries Service, Pacific Islands Fisheries Science Center. Online: http://www.pifsc.noaa.gov/marine_turtle/life_history_and_ecology.php (Site Accessed 8 June 2016).

NOAA PIRO. 2016. Sea Turtles, Species Information. About Protected Resources, Sea Turtles. NOAA National Marine Fisheries Service, Pacific Islands Regional Office, Protected Resources Division. Online: http://www.fpir.noaa.gov/DIR/dir_mammal_turtle_seabird.html#SeaTurtles (Site Accessed 8 June 2016).

Nurzia Humburg, I. and G.H. Balazs. 2014. Forty Years of Research: Recovery Records of Green Turtles Observed or Originally Tagged at French Frigate Shoals in the Northwestern Hawaiian Islands, 1973-2013. NOAA Technical Memorandum NOAA-TM-NMFS-PIFSC-40. Honoulu, HI. 14 pp.

Parker, D. NOAA Pacific Islands Fisheries Science Center, Protected Species Division, Marine Turtle Biology and Assessment Program. Newport, OR. Personal Observation.

Parker, D.M., G.H. Balazs, C.S. King, L. Katahria, and W. Gilmartin. 2009. Short-range movements of hawksbill turtles (*Eretmochelys imbricata*) from nesting to foraging areas within the Hawaiian Islands. Pacific Science 63 (3): 371-382.

Parker, D.M., G.H. Balazs, M. Rice, W. Seitz, Kaho'olawe Island Reserve Commission, J. Pettigrew, Maui Coastal Land Trust, National Botanical Tropical Gardens, K. Maison, I. Kelly, J. Burger, J. Pawloski, D. Heacock, S. Hau, M. Coelho, B. Puleloa, C. King, The Nature Conservancy Moloka'i Turtle Trackers, P. Bennett, U. Keuper-Bennett, G. Nakai, J. Klavitter, J. Hiromasa, and D. Brown. 2015. Map guide to marine turtle nesting and basking in the Hawaiian Islands. NOAA National Marine Fisheries Service, Pacific Islands Fisheries Science Center, Marine Turtle Biology and Assessment Program Internal Report. Honolulu, HI. Data Provided 20 October 2014. Provider Website: https://pifsc-www.irc.noaa.gov/marine_turtle/ (Site Accessed 8 June 2016).

Seitz, W.A., K.M. Kagimoto, B. Luehrs, and L. Katahira. 2012. Twenty years of conservation and research findings of the Hawai'i Island hawksbill turtle recovery project, 1989-2009. Technical Report No. 178. The Hawai'i-Pacific Islands Cooperative Ecosystem Studies Unit and Pacific Cooperative Studies Unit, University of Hawai'i. Honolulu, HI. 117 pp.

Snover, M.L, G.H. Balazs, S.K.K. Murakawa, S.K. Hargrove, M.R. Rice, and W.A. Seitz. 2013. Age and growth rates of Hawaiian hawksbill turtles (*Eretmochelys imbricata*) using skeletochronology. Marine Biology 160: 37-46.

Spotila, J.R., M.P. O'Connor, and F.V. Paladino. 1996. Thermal biology. pp. 297-314. In: P.L. Lutz and J.A. Musick (eds.), The Biology of Sea Turtles, Vol. 1. CRC Press. 446 pp.

State of Hawai'i. 2010. 2010 Census Data, Census Blocks – 2010, Cultural and Demographic, GIS Data. Data from U.S. Census Bureau. State of Hawai'i, Office of Planning, Hawaii Statewide GIS Program. Data Downloaded September 2015. Data Website: http://planning.hawaii.gov/gis/download-gis-data-expanded/ (Site Accessed 8 June 2016).

USFWS. 2015. General Sea Turtle Information. United States Fish and Wildlife Service, North Florida Ecological Services Office. Online: http://www.fws.gov/northflorida/SeaTurtles/seaturtle-info.htm (Site Accessed 8 June 2016).

USGS. 2015. The 3DEP National Map (1/3 arc-second DEMs for Hawai'i). The National Map. U.S. Geological Survey. Data Downloaded 15 September 2015. Data Website: http://viewer.nationalmap.gov/basic/?basemap=b1&category=ned,nedsrc&title=3DEP%20View#startUp (Site Accessed 8 June 2016).

Van Houtan, K.S. and N. Kittinger. 2014. Historical commercial exploitation and the recent recovery of Hawaiian green turtles. Biological Conservation 170: 20-27.

Van Houtan, K.S., C.M. Smith, M.L. Dailer, and M. Kawachi. 2014. Eutrophication and the dietary promotion of sea turtle tumors. PeerJ 2: e602.

Whittow, G.C. and G.H. Balazs. 1982. Basking behavior of the Hawaiian green turtle (*Chelonia mydas*). Pacific Science 36 (2): 129-139.

Witherington, B.E. and K.A. Bjorndal. 1991. Influences of artificial lighting on the seaward orientation of hatchling loggerhead turtles *Caretta caretta*. Biological Conservation 55 (2): 139-149.

Witzell, W.N. 1983. Synopsis of biological data on the hawksbill turtle, *Eretmochelys imbricata* (Linnaeus 1766). FAO Fisheries Synopsis 137: 1-78.

Work, T.M., M. Ackermann, J.W. Casey, M. Chaloupka, L. Herbst, J.M. Lynch, and B.A. Stacy. 2014. The story of invasive algae, arginine, and turtle tumors does not make sense. PeerJ PrePrints 2:e539v1.

Work, T.M., G.H. Balazs, T.M. Summers, J.R. Hapdei, and A.P. Tagarino. 2015. Causes of mortality in green turtles from Hawaii and the insular Pacific exclusive of fibropapillomatosis. Diseases of Aquatic Organisms 115: 103-110.

Chapter 6 Marine Mammals

CETACEANS
Simon J. Pittman[1,13], Arliss J. Winship[1,3], Matthew Poti[1,3], Brian P. Kinlan[1], Jeffery B. Leirness[1,3], Robin W. Baird[14], Jay Barlow[15], Elizabeth A. Becker[15], Karin A. Forney[15], Marie C. Hill[16], Peter I. Miller[4], Joseph Mobley[17], and Erin M. Oleson[18]

HAWAIIAN MONK SEAL
Simon J. Pittman[1,13], Arliss J. Winship[1,3], Kenady Wilson[19,20], and Charles L. Littnan[21]

False killer whale. Photo credit: Robin W. Baird (Cascadia Research Collective)

ABSTRACT

*Marine mammals are ecologically, economically and culturally important to Hawai'i. Reliable information on species space-use patterns is required to inform marine spatial planning, particularly for offshore renewable energy installations. This chapter provides distribution maps for marine mammals observed in the U.S. waters of the Main Hawaiian Islands from 1993 to 2014 using data integrated from multiple sources and spatial predictive modeling. At least 26 species of marine mammal (one seal and 25 cetaceans) have been recorded across the project area, of which eight species are listed as Endangered. This chapter has two sections: 6.1 Cetaceans, and 6.2 Hawaiian monk seal. For cetaceans, maps are provided for 22 species, including 15 showing locations of sightings and seven showing predicted spatial distributions. Sighting data from aircraft, ships and small research vessels were integrated and modeled using non-linear algorithms to map summer and winter distributions. These models were based on the statistical relationships between cetacean abundance and environmental variables at the locations of sightings. Model performance ranged from 17 to 59 percent PDE (percentage deviance explained). Highest performing models were achieved for common bottlenose dolphin (*Tursiops truncatus*; 59% summer), spinner dolphin (*Stenella longirostris; *56% winter) and humpback whale (*Megaptera novaeangliae; *37% winter). All categories of predictors (survey platform, temporal, climatic, atmospheric, geographic, physical and biological oceanographic, and topographic), contributed to models, with depth, slope, surface current direction and the strengths of temperature and chlorophyll fronts being relatively important environmental predictors across models. For Hawaiian monk seal (*Monachus schauinslandi*), we provide maps of sighting locations, individual space-use patterns and the newly released critical habitat maps, followed by discussion of priorities for future data collection to support marine spatial planning.*

Citation for Cetacean section
Pittman, S.J., A.J. Winship, M. Poti, B.P. Kinlan, J.B. Leirness, R.W. Baird, J. Barlow, E.A. Becker, K.A. Forney, M.C. Hill, P.I. Miller, J. Mobley, and E.M. Oleson. 2016. Chapter 6: Marine Mammals - Cetaceans. pp. 227-265. In: B.M. Costa and M.S. Kendall (eds.), Marine Biogeographic Assessment of the Main Hawaiian Islands. Bureau of Ocean Energy Management and National Oceanic and Atmospheric Administration. OCS Study BOEM 2016-035 and NOAA Technical Memorandum NOS NCCOS 214. 359 pp.

Citation for Hawaiian Monk Seal section
Pittman, S.J., A.J. Winship, K. Wilson, and C.L. Littnan. 2016. Chapter 6: Marine Mammals - Hawaiian Monk Seal. pp. 266-282. In: B.M. Costa and M.S. Kendall (eds.), Marine Biogeographic Assessment of the Main Hawaiian Islands. Bureau of Ocean Energy Management and National Oceanic and Atmospheric Administration. OCS Study BOEM 2016-035 and NOAA Technical Memorandum NOS NCCOS 214. 359 pp.

[1] *NOAA National Centers for Coastal Ocean Science, Biogeography Branch, Silver Spring, MD, U.S.A.* [3] *CSS-Dynamac, Fairfax, VA, U.S.A.*
[4] *Plymouth Marine Laboratory, Remote Sensing Group, Plymouth, United Kingdom*
[13] *Plymouth University, Centre for Marine and Coastal Policy Research, United Kingdom*
[14] *Cascadia Research Collective, WA, U.S.A.*
[15] *NOAA Southwest Fisheries Science Center, Marine Mammal and Turtle Division, CA, U.S.A.*
[16] *University of Hawai'i at Mānoa, Joint Institute for Marine and Atmospheric Research, HI, U.S.A.* [17] *University of Hawai'i at Mānoa, HI, U.S.A.*
[18] *NOAA Pacific Islands Fisheries Science Center, Protected Species Division, Cetacean Research Program, Honolulu, HI, U.S.A.*
[19] *Nicholas School of the Environment, Duke University, NC, U.S.A.*
[20] *NOAA Alaskan Fisheries Science Center, National Marine Mammal Laboratory, WA, U.S.A.*
[21] *NOAA Pacific Islands Fisheries Science Center, Protected Species Division, Hawaiian Monk Seal Research Program, Honolulu, HI, U.S.A.*

Marine Mammals

6.1. CETACEANS

6.1.1. Introduction

This section of the marine mammal chapter provides concise background information on the cultural significance, conservation status and distributions of cetacean species observed in the waters of the Main Hawaiian Islands (MHI). We then describe our synthesis of the best available sighting data across a 20 year period (1993 to 2013) in U.S. waters around the MHI. These data are used to build spatial predictive models for mapping suitable habitat as new representations of species distributions. This study is unique in its combination of broad geographical scale (project area = 860,250 km^2) and relatively fine spatial resolution distribution maps (1.2x1.2 km grid cells), and because of the integration of a large number (n=46) of diverse predictors including: survey characteristics, temporal variables including climate indices, geographic variables such as distance to features, seafloor topography variables, and physical and biological oceanographic variables. Our study is also unique in its integration of sighting data from multiple research groups using different survey platforms (i.e., ships, small vessels, and aircraft).

Cultural significance

Whales, called koholā in Hawaiian, hold a sacred place within native Hawaiian spirituality, as illustrated by their inclusion in the Kumulipo, the native Hawaiian chant of creation. Whales represent the largest ocean manifestation of Kanaloa, god of the ocean realm, ocean animals, and fresh water underground (Lebo, 2010). The cultural importance of the koholā is also prominent in Hawaiian oral and written history through legends, place names, artifacts and rock carvings (petroglyphs). The sperm whale (*Physeter macrocephalus*), palaoa, were highly prized for their ivory which were used as fishhooks and pendants. Whale ivory from animals that washed ashore was considered sacred and garlands made of whale tooth, lei niho palaoa, were symbols of status.

Sperm whale, Physeter macrocephalus. *Photo credit: Robin W. Baird (Cascadia Research Collective)*

Cetacean population status and spatial distributions

Twenty-five species of cetacean (seven baleen whales and 18 toothed whales and dolphins) have been sighted in Hawaiian waters, of which seven are listed as Endangered, eight recognized as depleted under the Marine Mammal Protection Act (MMPA) and six listed on Convention on International Trade in Endangered Species (CITES) Appendix I as threatened with extinction (Table 6.1).

The calving and breeding population of humpback whales (*Megaptera novaeangliae*) is the most seasonally abundant large whale in Hawaiian waters traveling from Alaska to overwinter in Hawai'i. Commercial whaling began in the Hawaiian Islands in 1819 when two New England ships became the first whaling ships to arrive, and by 1846 as many as 596 ships were actively whaling in the region. By the 20th century, the population of large whales, particularly humpback whales, was severely depleted with an estimated population of approximately 1,000 animals, compared with a pre-whaling population of 15,000 animals (Rice, 1978). In 1966, the International Whaling Commission gave legal protection to humpback whales from commercial whaling and in 1972 and 1973, the MMPA and the U.S. Endangered Species Act (ESA) recognized humpback whales as endangered, making it illegal to hunt, harm, or disturb them. In 1992, U.S. Congress established the Hawaiian Islands Humpback Whale National Marine Sanctuary, recognizing the important role that the Hawaiian Islands play in the

Humpback whale, Megaptera novaeangliae. *Photo credit: Robin W. Baird (Cascadia Research Collective).*

Table 6.1. Conservation status of twenty-five species of cetacean sighted around the Main Hawaiian Islands. ESA= Endangered Species Act, MMPA= Marine Mammal Protection Act, CITES= Convention on International Trade in Endangered Species. Refers to CITES appendices.*

Family	Scientific Name	Common Name	ESA Status	MMPA Status	CITES*
Delphinidae	*Stenella attenuata*	Pantropical spotted dolphin	None	Protected	Appendix II
	Stenella coeruleoalba	Striped dolphin	None	Protected	Appendix II
	Stenella longirostris	Spinner dolphin	None	Protected	Appendix II
	Steno bredanensis	Rough-toothed dolphin	None	Protected	Appendix II
	Tursiops truncatus	Common bottlenose dolphin	None	Protected	Appendix II
	Grampus griseus	Risso's dolphin	None	Protected	Appendix II
	Lagenodelphis hosei	Fraser's dolphin	None	Protected	Appendix II
	Peponocephala electra	Melon-headed whale	None	Protected	Appendix II
	Feresa attenuata	Pygmy killer whale	None	Protected	Appendix II
	Pseudorca crassidens	False killer whale	Endangered[1]	Depleted[1]	Appendix II
	Globicephala macrorhynchus	Short-finned pilot whale	None	Protected	Appendix II
	Orcinus orca	Killer whale	None	Protected	Appendix II
Physeteridae	*Physeter macrocephalus*	Sperm whale	Endangered	Depleted	Appendix II
Kogiidae	*Kogia breviceps*	Pygmy sperm whale	None	Protected	Appendix II
	Kogia sima	Dwarf sperm whale	None	Protected	Appendix II
Ziphiidae	*Mesoplodon densirostris*	Blainville's beaked whale	None	Protected	Appendix II
	Ziphius cavirostris	Cuvier's beaked whale	None	Protected	Appendix II
	Indopacetus pacificus	Longman's beaked whale	None	Protected	Appendix II
Balaenopteridae	*Balaenoptera acutorostrata*	Minke whale	None	Protected	Appendix I
	Balaenoptera edeni	Bryde's whale	None	Protected	Appendix I
	Megaptera novaeangliae	Humpback whale	Endangered[2]	Depleted	Appendix I
	Balaenoptera physalus	Fin whale	Endangered	Depleted	Appendix I
	Balaenoptera borealis	Sei whale	Endangered	Depleted	Appendix II
	Balaenoptera musculus	Blue whale	Endangered	Depleted	Appendix I
Balaenidae	*Eubalaena japonica*	North Pacific right whale	Endangered	Depleted	Appendix I

[1] Refers to insular population.
[2] There is a current proposal to divide North Pacific humpback whales into four distinct population segments (DPS), with the Hawai'i DPS no longer being listed as endangered or threatened under the ESA (Federal Register, 2015a).

preservation and long-term viability of the humpback whale. The size of the Central North Pacific population visiting Hawaiian waters has now been estimated at over 10,000 individuals and Hawai'i has been recognized as a distinct breeding area for whales that migrate to summer feeding grounds in Alaska, northern British Columbia and the Bering Sea (Barlow et al., 2011). There is a current proposal to divide North Pacific humpback whales into four distinct population segments (DPS), with the Hawai'i DPS no longer being listed as endangered or threatened under the ESA (81 FR 14820; Federal Register, 2015a).

Not all cetaceans are seasonal visitors. Several studies have identified island-associated populations within wide-ranging pelagic species, such as spinner dolphins (*Stenella longirostris*; Andrews et al., 2010), rough-toothed dolphins (*Steno bredanensis*; Baird et al., 2008a), and false killer whales (*Pseudorca crassidens*; Baird et al., 2008b). In fact, three discrete populations of false killer whales have been identified in Hawaiian waters: a main Hawaiian Islands insular population, a Northwestern Hawaiian Islands insular population, and a pelagic population (Baird et al., 2013b; Bradford et al., 2015; Carretta et al., 2015). Among these false killer whale populations a large proportion of individuals have been documented moving among islands at distances up to 283 km (Baird et al., 2008b). Melon-headed whales (*Peponocephala electra*) also have discrete sub-populations which appear to exist as a smaller, resident population over shallower nearshore waters and a larger population, seen throughout the MHI over deeper waters (Aschettino et al., 2012; Woodworth et al., 2012).

Marine Mammals

Striped dolphins, Stenella longirostris*. Photo credit: Greg Schorr (Cascadia Research Collective)*

In total, 11 species of odontocetes (toothed whales) are known to have, or there is some evidence to support the existence of, resident populations in the MHI on the basis of sighting data, genetic studies and satellite tagging including: dwarf sperm whale (*Kogia sima*), Blainville's beaked whale (*Mesoplodon densirostris*), Cuvier's beaked whale (*Ziphius cavirostris*), pygmy killer whale (*Feresa attenuata*), short-finned pilot whale (*Globicephala macrorhynchus*), melon-headed whale, false killer whale, pantropical spotted dolphin (*Stenella attenuata*), spinner dolphin, rough-toothed dolphin and common bottlenose dolphin (*Tursiops truncatus*; Baird et al., 2015). Three species (common bottlenose dolphin, spinner dolphin, and false killer whale) are regularly found in shallow (<50 m) nearshore waters, and four species (striped dolphins [*Stenella longirostris*], sperm whales, rough-toothed dolphins and pantropical spotted dolphins) are more commonly associated with deep (>3,000 m) offshore waters (Baird et al., 2013a).

Cuvier's beaked whale, Ziphius cavirostris*. Photo credit: Daniel Webster (Cascadia Research Collective)*

Several previous studies have focused on multi-species cetacean distributions to identify priority areas. Becker et al. (2012) and Forney et al. (2015) modeled cetacean distributions using National Oceanic and Atmospheric Administration (NOAA) sighting data associated with 10 km transect segments across the central Pacific Ocean. Using information from extensive studies of odontocete distributions and behavior in Hawaiian waters since 2000, Baird et al. (2015) designated 20 biologically important areas (BIAs) for resident populations of the 11 species of odontocetes, as well as a seasonal BIA representing important reproductive areas for humpback whales. All BIAs can be viewed via an online interactive map (http://cetsound.noaa.gov/important). Metadata tables detail the type and quantity of information used to define the BIAs (Van Parijs et al., 2015).

Environmental context

The MHI (Figure 6.1) exist in a subtropical biogeographic region (Insular Pacific-Hawaiian Large Marine Ecosystem) characterized by relatively stable ocean conditions, low oceanic productivity, seamounts and a diverse narrow insular shelf (Chapter 2). Little is known about the seascape patterns and processes that drive cetacean distributions in the MHI. In deeper offshore waters, oceanic frontal zones, eddies and seamounts are likely to be important features of biophysical convergence (Scales et al., 2014). Closer to shore, sheltered inshore habitats such as coral reefs, shallow banks, seagrass beds and nearshore hydrodynamic features that aggregate prey are likely to be important. For example, studies on movements of toothed whales suggest that eddies in the leeward side of islands are used by melon-headed whales (Woodworth et al., 2012), and offshore populations of false killer whales feed at seamounts where large prey fish are abundant (Baird et al., 2008c). The study presented here quantified a wide range of spatial predictors to represent offshore and nearshore oceanographic characteristics, as well as seafloor topography and shallow-water habitat types to examine correlations with locations of species sightings. Distance to land and distance to seamounts were also included as geographic predictor variables.

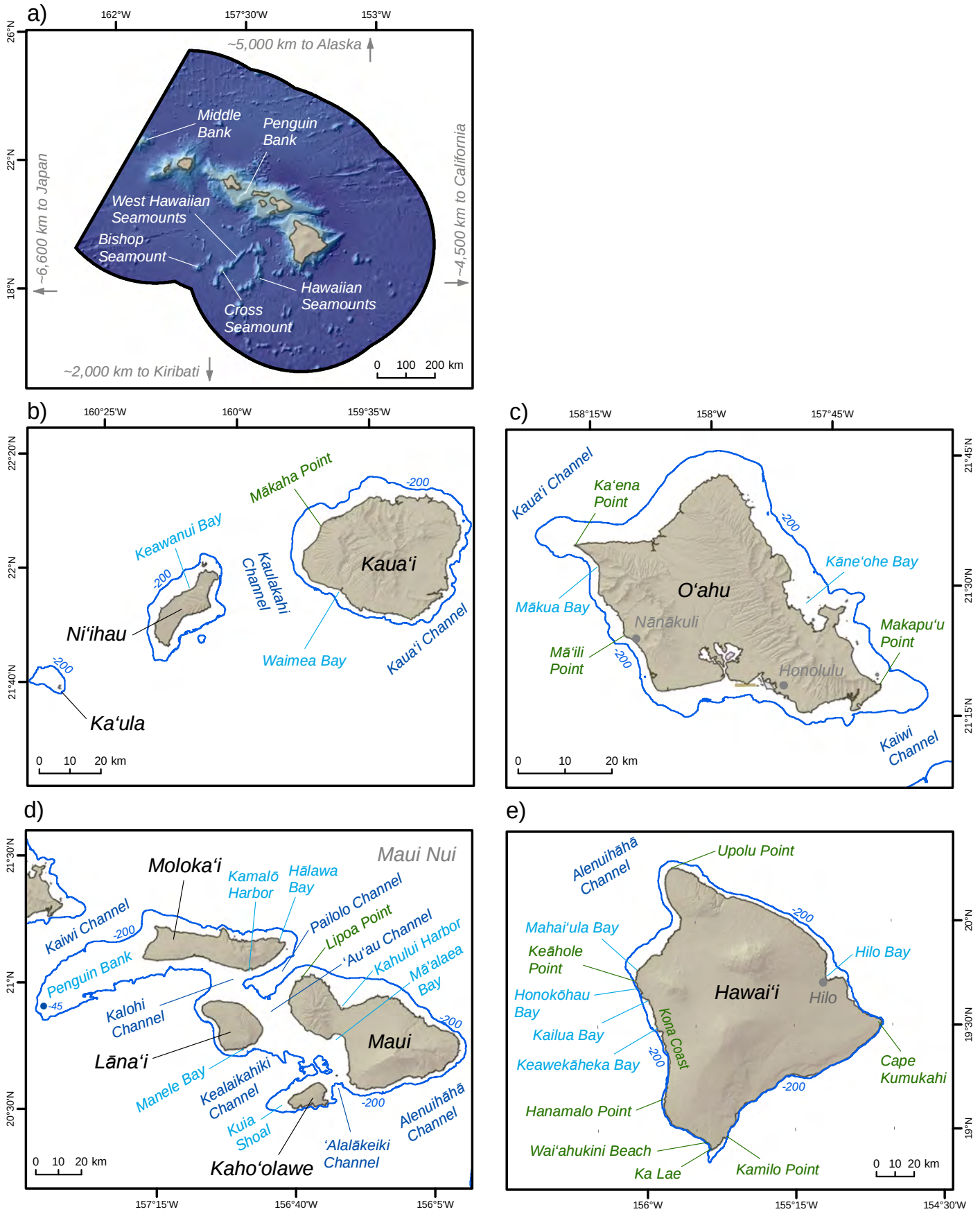

Figure 6.1. Key geographic features and place names around the MHI. These maps depict geographic features that are referenced in this chapter for: a) the project area; b) Ka'ula, Ni'ihau and Kaua'i; c) O'ahu; d) Maui Nui, which includes Moloka'i, Lāna'i, Maui and Kaho'olawe; and e) Hawai'i. All depths are in meters. Data sources: shoreline (Battista et al., 2007), elevation (USGS, 2015) and depths (NOAA NCEI, 2005; GEBCO, 2008)

6.1.2. Methods

Survey data

We analyzed visual at-sea cetacean sighting data from three sources: 1) NOAA National Marine Fisheries Service (NMFS) Pacific Islands Fisheries Science Center (PIFSC) and Southwest Fisheries Science Center (SWFSC), 2) Cascadia Research Collective, and 3) J. Mobley (University of Hawai'i at Mānoa). The combined dataset provided cetacean sightings across a 20 year period (1993 to 2013). Here we describe the data sets from each source, data processing to standardize data, and the spatial modeling techniques.

NOAA National Marine Fisheries Service data

NMFS survey data used here were collected between 2002 and 2013 (Figure 6.2a). The majority of these data were collected on two systematic ship surveys conducted in 2002 and 2010, the Hawaiian Islands Cetacean and Ecosystem Assessment Surveys (HICEAS; Barlow, 2006; Bradford et al., 2014), which covered the study area with widely spaced transects (Figure 6.2a). The NOAA vessel data were the only spatially extensive surveys for offshore U.S. managed waters. There were also data from other NOAA ship surveys that transited in and out of the study area en route to other survey locales, and from small boat surveys conducted between 2007 and 2013. The small boat surveys were conducted closer to shore with more limited geographic coverage. Most of the NMFS survey effort was from February, May, and September to November (Forney et al., 2015). Data from ship surveys were collected continuously using line transect distance-sampling protocols (Buckland et al., 2001; Barlow, 2006), while small boat surveys generally followed less structured transects recording continuous sighting data. Following NMFS analyses of their line transect data (e.g., Barlow, 2006), we excluded sightings of dolphins, small whales, and large whales whose perpendicular distance from the trackline exceeded 5.5, 4.0 and 5.5 km, respectively.

Cascadia Research Collective

Multi-species surveys of odontocetes were conducted from small boats (5.5 to 18 m length) between 2000 and 2012. These data are the most geographically intensive surveys for resident populations of odontocetes. Survey vessels operated from approximately 15 to 30 km h^{-1}, with two to six observers scanning 360° around the vessel. A global positioning system (GPS) logged locations every 5 minutes while on effort (Baird et al., 2013a). Survey effort was distributed throughout the year, with most effort in April, May, August, October, and December, and the least in January, February, March and September (Figure 6.2b). The surveys were mainly conducted on the leeward sides of all eight of the MHI islands in Beaufort sea states of 3 or less. Greatest effort was applied in three regions: southwest coast of the island of Hawai'i (Kona), west Maui and west Kaua'i (Figure 6.3). The survey transects did not follow a systematic design and often included periods of approaching or following animals for the purposes of species identification, group size estimation, photo-identification of individuals and tagging (Baird et al., 2008a, b). Sighting data were recorded continuously. Sighting cues were sometimes non-visual (e.g., reports from other vessels or acoustic detections; Baird et al., 2008b), so we excluded those sighting data from our analysis. The species focus was mainly odontocetes, but baleen whale sighting data were also collected. Humpback whales were not recorded consistently so this species was not included in this dataset. Cascadia Research Collective has also conducted tracking studies of multiple cetacean species (common bottlenose dolphin, Blainville's beaked whale, Cuvier's beaked whale, false killer whale, short-finned pilot whale, pygmy killer whale, melon-headed whale, rough-toothed dolphin and sperm whale) in Hawaiian waters (Baird et al., 2009b, 2010, 2012a, b, 2015; Schorr et al., 2009; Woodworth et al., 2012; Rone et al., 2015). For this project, only visual sighting data were included in the analyses.

Melon-headed whale, Peponocephala electra *(left) and pygmy killer whale,* Feresa attenuata *(right). Photo credit: Robin W. Baird (Cascadia Research Collective; left) and NOAA NMFS/SWFSC (right).*

Aerial surveys

Aerial surveys by light aircraft led by Professor J. Mobley of the University of Hawai'i at Mānoa were conducted in 1993, 1995, 1998, 2000 and 2003 during the peak season (February to April) for humpback whales (Figure 6.2c). Surveys were conducted relatively nearshore (<50 km from shore) around all eight main islands, with standardized effort collecting continuous sighting data (Mobley et al., 2001). The MHI were divided up into four main regions: 1) Hawai'i; 2) Moloka'i, Maui, Lāna'i and Kaho'olawe; 3) O'ahu and Penguin Bank; and 4) Kaua'i/Ni'ihau where surveys typically covered one region per day covering depths from less than 100 fathoms to more than 1,000 fathoms. Greatest effort due to overlapping flight paths across multiple years occurred in a region southeast of O'ahu (Figure 6.3). Surveys were flown at an average altitude of 816 feet (± 124 standard deviation [SD]) along north-south lines placed 26 km apart and extending from shore to

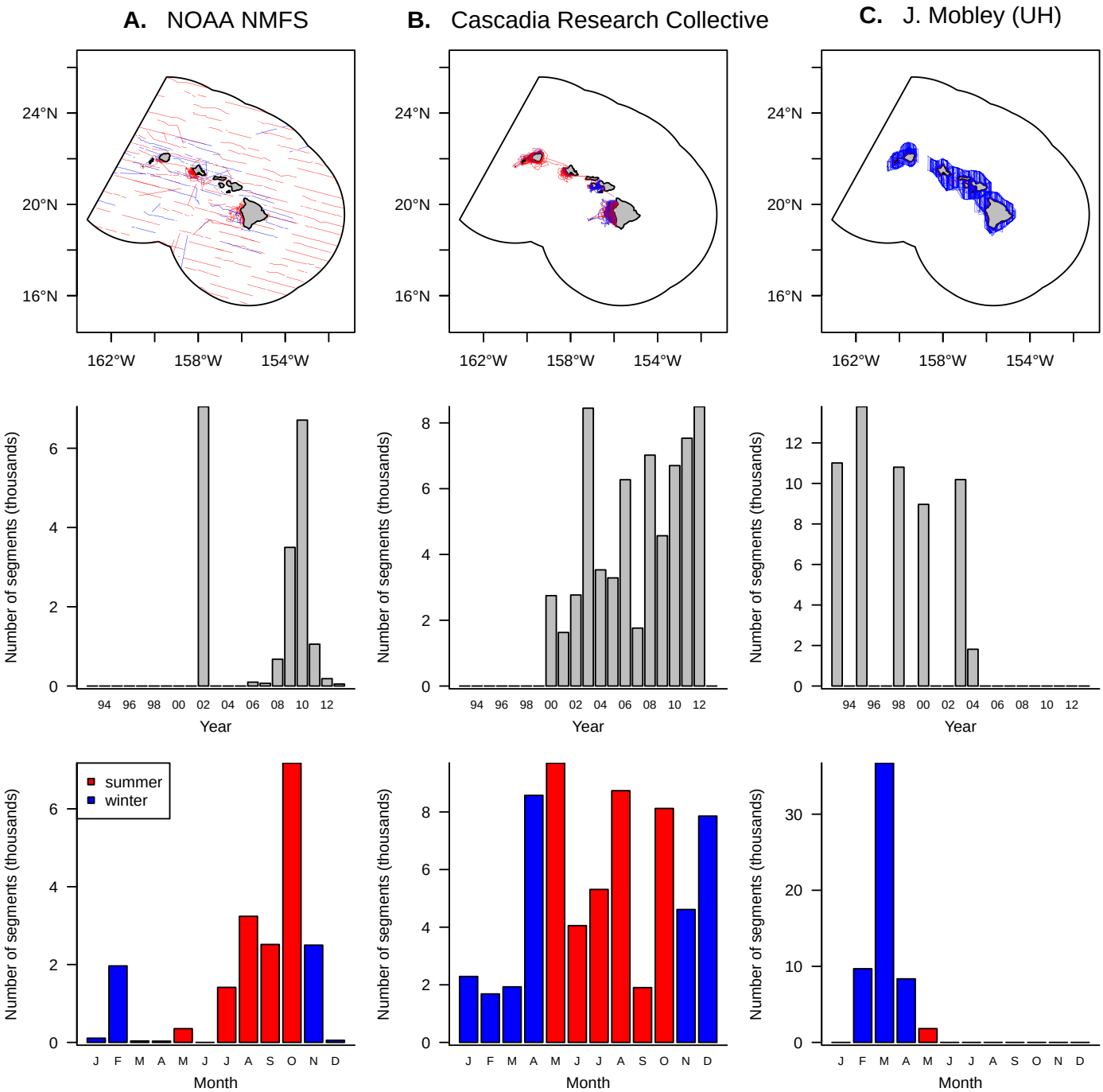

Figure 6.2. Cetacean survey effort showing transects and number of 1.2 km transect segments by season (summer and winter) for the Main Hawaiian Islands conducted by: a) NOAA NMFS ship and small boat surveys, b) Cascadia Research Collective small boat surveys, and c) aerial surveys led by J. Mobley, University of Hawai'i at Mānoa.

13 km past the 1,000 fathom limit (average of 46 km offshore). Location data from an onboard GPS receiver and altitude data from a radar altimeter were downloaded directly onto a laptop computer. One observer searched on each side of the aircraft and communicated verbally with a data recorder. Identification of species of a given sighting was made only when diagnostic features could be clearly identified. In cases where such features were not clearly visible, or when there was a dispute over species identity, the sighting was recorded as an unidentified dolphin, whale, or cetacean. In total, 16 cetacean species were identified. For more details see Mobley et al. (2001). In addition, a discrete spinner dolphin-focused survey was conducted during May 2004 on the northwest coast of Hawai'i, the Kealaikahiki Channel between Lāna'i and Kaho'olawe, 'Au'au Channel between Maui and Lāna'i, Kalohi Channel separating Lāna'i and Moloka'i, the entire coast of O'ahu, north Kaua'i, and nearshore Ni'ihau.

Figures 6.3 and 6.4 highlight the differences and overlap of sampling effort distributions by depth strata and distance to shore among survey platforms. The Cascadia Research Collective data and aerial surveys show a nearshore bias compared with NOAA ship-based surveys that covered a far greater geographical extent and sampled over deeper waters.

Data processing

To standardize across datasets, the data were discretized into 1.2 km transect 'segments' corresponding to the dimensions of a Bureau of Ocean Energy Management (BOEM) aliquot (Appendix B). Cetaceans were recorded on 138,813 transect segments (84,513 winter and 54,300 summer). The number of individuals of each species sighted was summed for each segment, and these 'counts' were the response variable for modeling. In the case of the NMFS survey data, our counts represented the sum of rounded mean group size estimates (average of observers' 'best' group size estimates). The mid-point of a segment was used as the location of the summed counts.

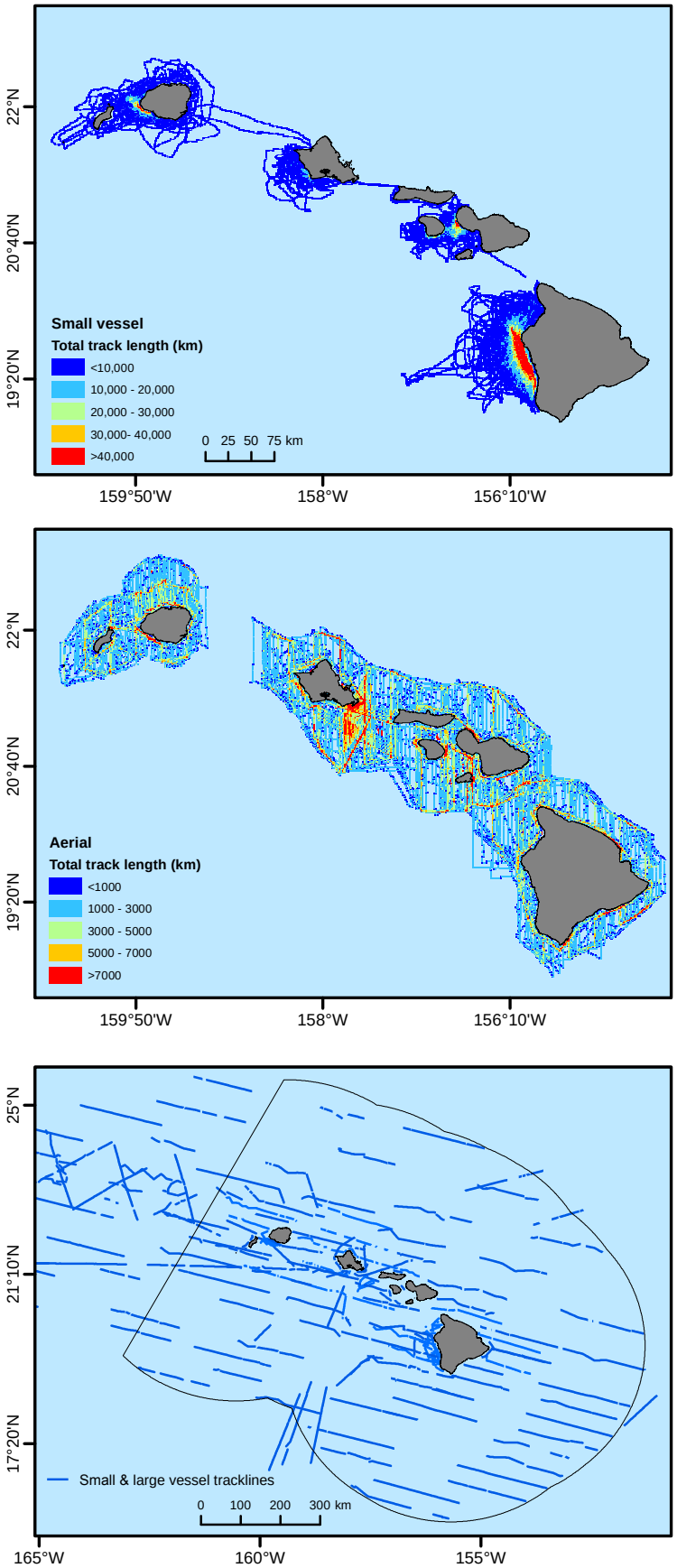

Figure 6.3. Survey effort as total track length per 1.2 km grid cell for: small vessels used by Cascadia Research Collective (top), aerial surveys led by J. Mobley, University of Hawai'i at Mānoa (middle), and individual tracklines for vessels used by NOAA NMFS (bottom).

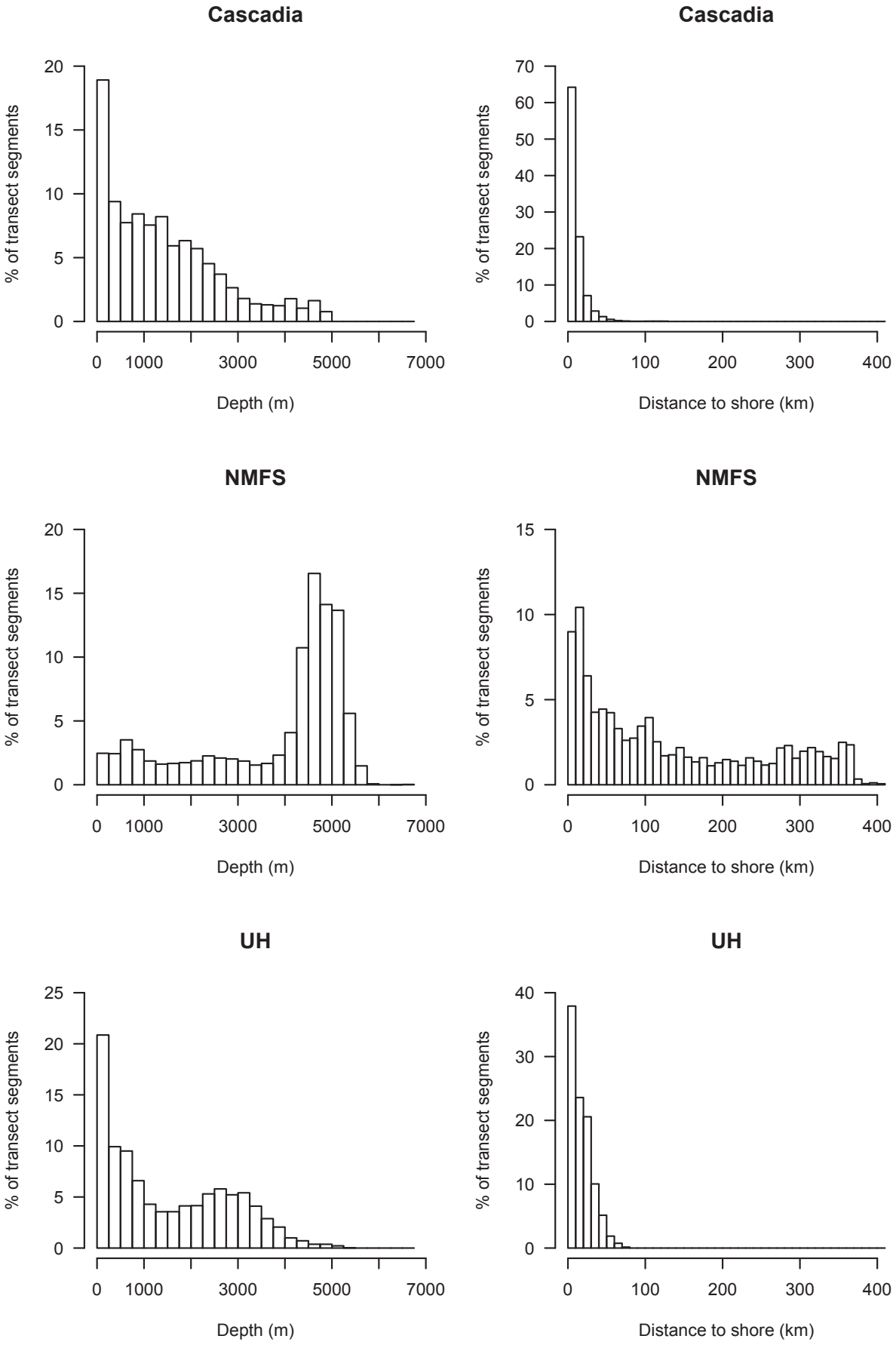

Figure 6.4. Distribution of sampling effort across depth strata and with distance to the nearest coastline for Cascadia Research Collective (top); NOAA NMFS (middle); and J. Mobley, University of Hawai'i at Mānoa (bottom).

Spatial predictive modeling and mapping

In Hawaiian waters, most species of cetaceans occur at low density with survey effort being patchy in time and space, resulting in a limited ability to reliably determine distribution patterns across the entire project area from sightings alone. To address this challenge, spatial predictive models were used to create maps of distributions based on habitat suitability. We created seasonal (summer or winter) models for species-season combinations that had ≥50 transect segments per season with sightings of ≥1 individual. By this criterion, seven species and 12 species-season combinations were considered (Table 6.2). Other species with fewer sightings were mapped as points showing where the sightings were located (Table 6.2). Several species that occur in the region were not recorded within the dataset used here, including blue whale (*Balaenoptera musculus*), North Pacific right whale (*Eubalaena japonica*), and minke whale (*Balaenoptera acutorostrata*).

Table 6.2. Number of transect segments with cetacean sightings used to identify species suitable for spatial predictive modeling of distributions around the MHI. Source: NOAA NMFS, Cascadia Research Collective and University of Hawai'i at Mānoa sighting data.

Common Name	No. of Transect Segments with Sightings		Assessment Technique
	Summer	Winter	
Humpback whale	7	2098	Winter model
Short-finned pilot whale	327	235	Summer & winter models
Pantropical spotted dolphin	212	226	Summer & winter models
Common bottlenose dolphin	144	142	Summer & winter models
Rough-toothed dolphin	166	74	Summer & winter models
Spinner dolphin	103	121	Summer & winter models
Sperm whale	18	54	Winter model
Cuvier's beaked whale	29	41	Point data map
Dwarf sperm whale	46	24	Point data map
False killer whale	24	40	Point data map
Melon-headed whale	33	25	Point data map
Striped dolphin	36	14	Point data map
Blainville's beaked whale	29	24	Point data map
Pygmy killer whale	24	15	Point data map
Risso's dolphin	13	4	Point data map
Pygmy sperm whale	4	3	Point data map
Bryde's whale	4	1	Point data map
Sei whale	1	3	Point data map
Killer whale	2	1	Point data map
Fraser's dolphin	1	1	Point data map
Longman's beaked whale	2	0	Point data map
Fin whale	0	2	Point data map
Minke whale	0	0	None
Blue whale	0	0	None
North Pacific right whale	0	0	None

Predictor variables

A wide range of predictor variables was used to model variation in the number of individuals sighted per transect segment, and to predict relative abundance throughout the study area. Categories of predictor variables included: survey, temporal, geographic, seafloor topography, physical and biological oceanographic, and atmospheric (Appendix B). Details of environmental variables are provided in Chapter 2.

Survey predictor variables were designed to account for variation in the type and characteristics of survey platform (e.g., observation height and method), observer identity and expertise, species focus, and sighting conditions. Temporal predictor variables were designed to account for variation in counts over time (i.e., day and year). Three climate indices (i.e., Pacific Decadal Oscillation, North Pacific Gyre Oscillation and Multivariate El Niño-Southern Oscillation) were also included as temporal predictor variables. Geographic predictor variables were designed to account for variation in counts arising from spatial location (i.e., longitude and latitude, distance to land, distance to seamounts). Seafloor topography variables (i.e., depth, slope, topographic complexity and curvature), physical and biological oceanographic variables, and atmospheric variables were developed from a range of data sources (see Chapter 2) to characterize the environmental conditions across the project area. The midpoint of a survey transect segment was used to spatially extract environmental predictor values from the corresponding project grid cell.

Modeling algorithm

A Boosted Zero-inflated Count (BZIC) Generalized Additive Modeling framework (Bühlmann and Hothorn, 2007; Hofner et al., 2014) was used to relate the survey count data to predictor variables (Appendix B, Figure B.1.). The estimated relationships between the number of individuals of each modeled species counted on each transect segment and the predictor variables were then used to predict the 'relative abundance' of these species across the entire study area. Relative abundance was defined as the expected number of individuals that would be counted per km travelled. Spatially explicit predicted values were calculated for each cell of the study grid from the values of the spatially explicit predictor variables for that cell. Thus, the predicted relative abundance in a given grid cell corresponded to predictions for a transect segment whose mid-point falls within that grid cell. For winter models, a 50 km buffer around a minimum convex hull of the survey effort locations was used to exclude predictions which were adversely effected by the absence of survey effort near the edges of the study area.

Our primary modeling objective was to provide the best estimates of at-sea distributions. The statistical modeling framework that we chose had several key features, that in combination provided advantages over alternative modeling approaches given this objective. First, the framework used appropriate statistical distributions to model counts of potentially aggregated animals. Second, the framework allowed for highly flexible relationships between expected counts and a large number (n = 46) of predictor variables, including complex multi-way interactions between predictor variables. Third, the framework accounted for differences in the data collection process between and within datasets.

It is important to recognize that modeled relative abundance does not equate to absolute abundance because individual animals may be missed during visual surveys, and animal movement can bias estimates of abundance. Our model predictions should only be interpreted as indices of abundance.

Model performance

The performance of each model was evaluated from a suite of performance metrics. The key performance metric was percent deviance explained (PDE) which indicates overall model fit and is analogous to the more familiar R^2 metric for a linear regression. The model with the highest PDE was chosen as the final model. Three additional performance metrics were calculated for each of the final models to provide a more complete assessment of model performance (Table 6.3). Model performance is displayed in the top right corner of each map figure (i.e., Figures 6.10-6.13, 6.15-6.22). The model performance metrics reflect the statistical fit of the models to the data. Performance categories were defined for each performance metric and assigned a numeric code (5 = highest to 1 = lowest). The performance of each final model was assigned an

Table 6.3. Model performance metrics. Metrics reflect the statistical fit of a model to the data; they do not necessarily reflect the accuracy of predictions away from the data.

Name	Description	Data	Stage	Performance categories
PDE	percent deviance explained[1]	all	final fit	5: ≥60% 4: 40-60% 3: 20-40% 2: 10-20% 1: <10%
AUC	area under the receiver operating characteristic curve	all, converted to presence/ absence	final fit	5: >0.9 4: 0.8-0.9 3: 0.7-0.8 2: 0.6-0.7 1: <0.6
Rank r	Gaussian rank correlation coefficient[2]	non-zero	final fit	5: >0.6 4: 0.4-0.6 3: 0.2-0.4 2: 0.1-0.2 1: <0.1
Percent error	median absolute residual error as percentage of data mean	non-zero, out-of-bag	during tuning of the number of boosting iterations[3]	5: <25% 4: 25-50% 3: 50-100% 2: 100-200% 1: >200%

[1] To calculate percent deviance explained, the saturated likelihood was assumed to be the maximum possible likelihood value, and the null likelihood was calculated from an intercepts-only zero-inflated model fit to the data (unpublished).
[2] Boudt et al. (2012) and Bodenhofer et al. (2013)
[3] Median value across cross-validation replicates

overall performance equal to the average performance across the four performance metrics. Precision of model predictions was determined using a bootstrap procedure (Appendix B). Specifically, the coefficient of variation (CV) for all spatial predictions was mapped to the analytical grid to allow examination of relative precision in the predicted relative abundance maps.

Predictor variable importance

While our primary objective was not to determine the ecological drivers and mechanisms behind the spatial distributions of cetaceans in the study area, our model results do provide measures of variable importance. The relative importance of each predictor variable in a given model essentially reflects the amount of variation in the data explained by each variable. Relative variable importance was re-scaled so that it summed to 1 across predictor variables.

6.1.3. Results and Discussion

First, we show mapped locations for cetacean species with occurrence observed on less than 50 transect segments within a season (*Non-modeled species distributions*). Next, we present the results of spatial predictive models (*Modeled species distributions*) using data on species sighted on more than 50 transect segments in a season.

Non-modeled species distributions

The data presented here for non-modeled species represent the midpoints of survey transect segments on which each species was sighted in each season. It is important to note that the distributions of these sightings partially reflects the amount and distribution of effort in each season. Differences in the distribution of sightings for a single species between seasons, or in the number of sightings between areas within a season, do not necessarily indicate differences in the distribution of relative abundance of that species. These sighting data were not effort-corrected, so comparison of sightings between seasons should not be attempted due to differences in winter and summer survey effort. Furthermore, there was less survey effort offshore (Figure 6.3), so even if the abundance of a species offshore was similar to the abundance nearshore, the expected number of sightings would be lower.

Several species of toothed whales exhibited year round (winter and summer) nearshore spatial occurrence around all island groups including: Cuvier's beaked whale (142 animals across 70 segments), Blainville's beaked whale (193 animals across 50 segments), dwarf sperm whale (184 across 69 segments), pygmy killer whale (411 across 37 segments), pygmy sperm whale (*Kogia breviceps;* 25 across 7 segments) and melon-headed whale (13,164 across 53 segments). The highest number of sightings was observed in an area with high survey effort off the west coast of the island of Hawai'i. All of the less frequently sighted cetacean species (n = 11) have been observed off the west coast of the island of Hawai'i, suggesting that this area has high importance for cetacean diversity regardless of the bias in survey effort. As such, waters off the west coast of Hawai'i have been identified as a year-round BIA for 11 odontocetes (Baird et al., 2015). Although most effort and sightings were leeward of the islands, several windward sightings were also recorded for Cuvier's and Blainville's beaked whales (Figure 6.5). In contrast, striped dolphin (1,590 across 47 segments) appeared to exhibit a wider distribution than other species, with more sightings offshore, including the southern and northern extremities of the project area (Figure 6.5). Similarly, Risso's dolphin (*Grampus griseus;* 243 across 17 segments) appeared to be more widely distributed offshore, at least in summer months, notably with sightings in the deeper waters and near seamounts to the south and southwest of the island of Hawai'i (Figure 6.6). It is difficult to interpret seasonal differences in the number of offshore sightings because there was less survey effort offshore in winter (Figure 6.2).

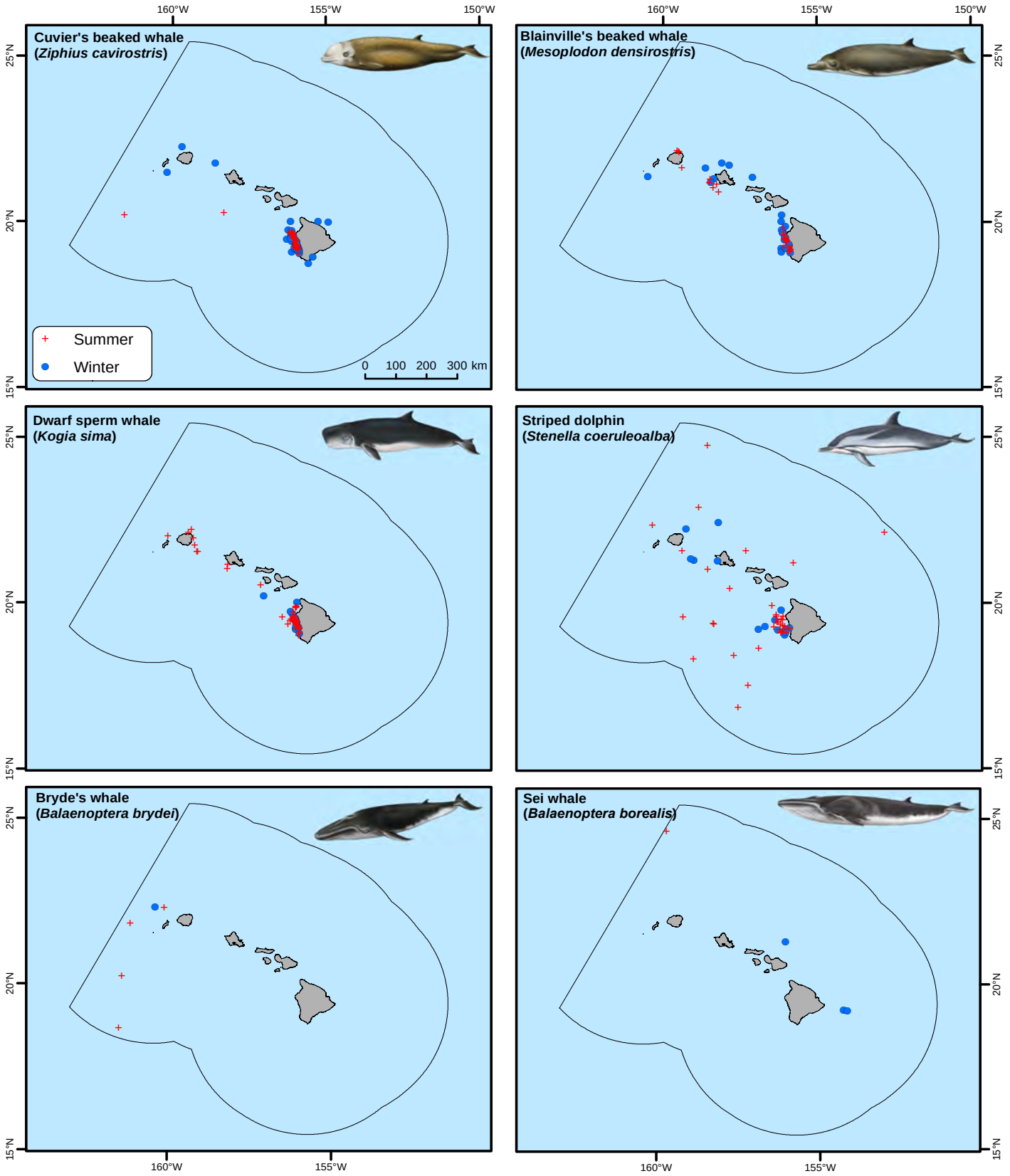

Figure 6.5. Cetacean sighting locations for non-modeled species for summer (May to October) and winter (November to April) seasons across the Main Hawaiian Islands project area (years 1993-2013). The amount and distribution of survey effort differed between seasons and between nearshore and offshore areas (Figures 6.2 and 6.3), so seasonal and spatial differences in the number of sightings do not necessarily reflect differences in relative abundance. Sighting data sources: Cascadia Research Collective, NOAA NMFS/SWFSC and PIFSC, and J. Mobley, University of Hawai'i at Mānoa. Artwork adapted from original by Justin Hart.

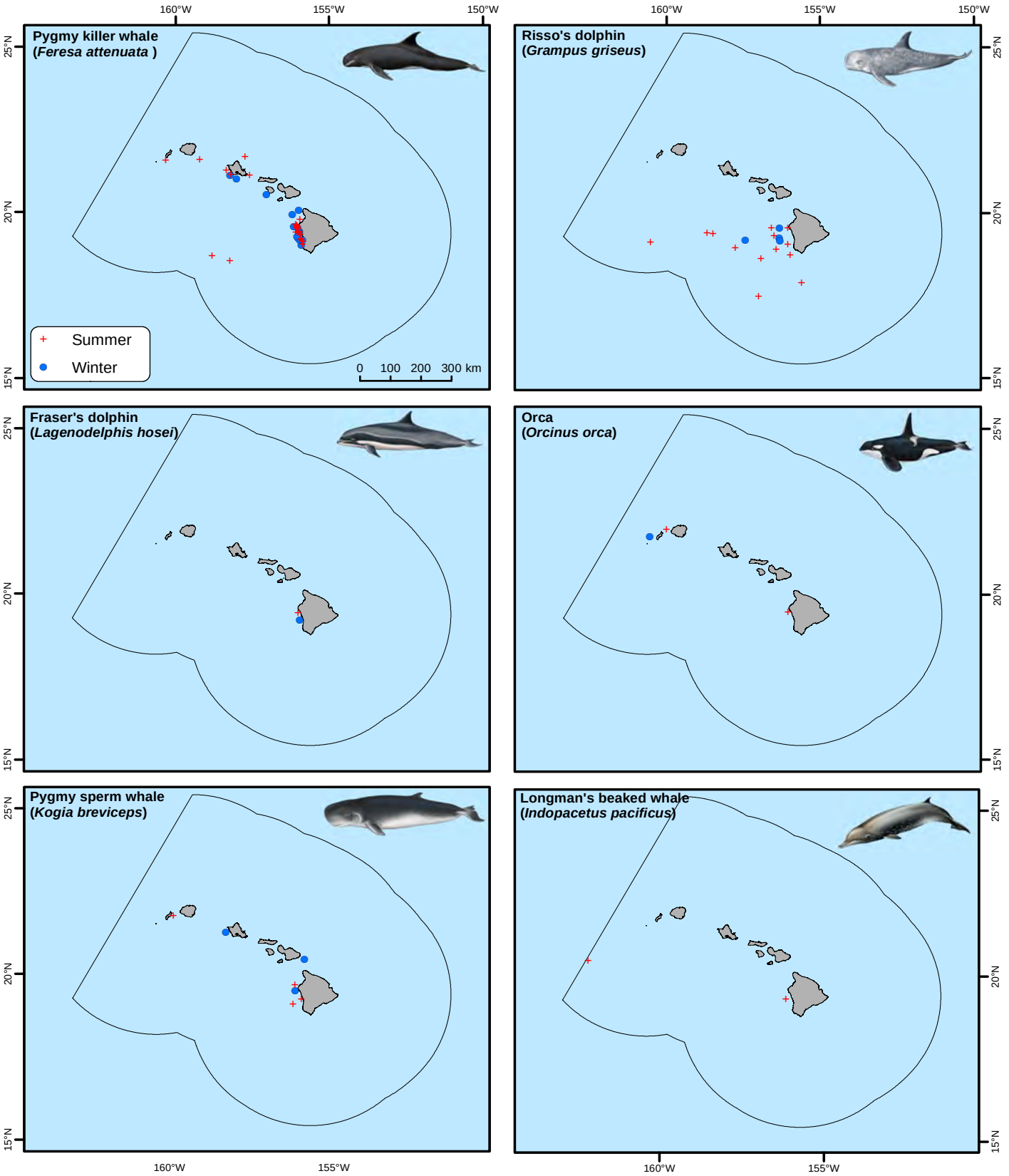

Figure 6.6. Cetacean sighting locations for non-modeled species for summer (May to October) and winter (November to April) seasons across the Main Hawaiian Islands project area (years 1993-2013). The amount and distribution of survey effort differed between seasons and between nearshore and offshore areas (Figures 6.2 and 6.3), so seasonal and spatial differences in the number of sightings do not necessarily reflect differences in relative abundance. Sighting data sources: Cascadia Research Collective, NOAA NMFS/SWFSC and PIFSC, and J. Mobley, University of Hawai'i at Mānoa. Artwork adapted from original by Justin Hart.

Two of the beaked whale species are thought to have distinct insular and offshore populations. The data presented here show two sightings of Cuvier's beaked whales located 100 and 200 km from land (Figure 6.5). Although this nearshore-offshore population distinction is not clearly articulated in the sighting data, previous photo-identification and tracking suggest high spatial association to individual islands for Cuvier's beaked whale (McSweeney et al., 2007; Baird, 2016). For Blainville's beaked whale, one tagged individual from the offshore population traveled from Hawai'i over 900 km to the edge of the Hawaiian Exclusive Economic Zone (EEZ; Baird et al., 2011a), while individuals from the resident population remained associated with the islands of Hawai'i, Maui and Moloka'i (Schorr et al., 2009; Baird, 2016).

There is some evidence to support the occurrence of a small resident population of pygmy killer whales in MHI (McSweeney et al., 2009) that primarily remains within 20 km of the shore (Baird et al., 2011b). Inter-island movements for the resident population are rare (Baird, 2016). Sightings for pygmy killer whales presented here show two sightings (31 and 19 individuals) in summer located more than 200 km from the nearest land (Figure 6.6). It is likely these represent individuals from an offshore (pelagic) population.

Three sightings in the summer season for false killer whale occurred offshore, while the majority of sightings were nearshore in both winter and summer seasons (Figure 6.7). Previous analyses using a combination of sightings, genetic studies and telemetry records indicate that these offshore sightings are individuals from a pelagic population which overlaps in places with the insular nearshore MHI population (Oleson et al., 2010). The discrete MHI insular false killer whale population is considered more vulnerable to extinction than the pelagic population due to statistically significant evidence of recent decline (Baird, 2009; Reeves et al., 2009; Oleson et al., 2010) and threats from human activity (e.g., fisheries and pollutants).

Pod of false killer whales, Pseudorca crassidens*. Photo credit: NOAA NMFS/SWFSC*

Sightings of melon-headed whales were mostly in nearshore waters in summer and winter (Figure 6.7). There were no sightings of individuals in offshore waters more than 50 km from shore, although satellite tracked individuals have been found to travel to more distant deeper offshore waters (Woodworth et al., 2012). Photo-identification, telemetry and genetic analyses suggest there are two demographically-independent populations of melon-headed whales: the Kohala resident stock with high fidelity to the waters (less than 2,500 m depth) off the northwest of the island of Hawai'i, and a broader Hawaiian Islands population with little or no interchange between populations (Aschettino et al., 2012; Oleson et al., 2013; Baird, 2016).

Dwarf sperm whales were only sighted in nearshore waters, with the largest number of sightings west of the island of Hawai'i (Figure 6.5). Studies by Baird et al. (2013a) and Baird (2016) highlight long-term site-fidelity in this region suggesting an island-resident population with all encounters less than 20 km from shore.

Several species were sighted very rarely (winter and summer) and only in offshore waters, such as the Bryde's whale (*Balaenoptera edeni*; far western region of the project area) and sei whale (*Balaenoptera borealis*; north of the island chain; Figure 6.5). Longman's beaked whale (*Indopacetus pacificus*) was sighted twice in summer at one nearshore (west of the island of Hawai'i) and one offshore location (Figure 6.6). Fin whales were only recorded twice during winter months (Figure 6.7).

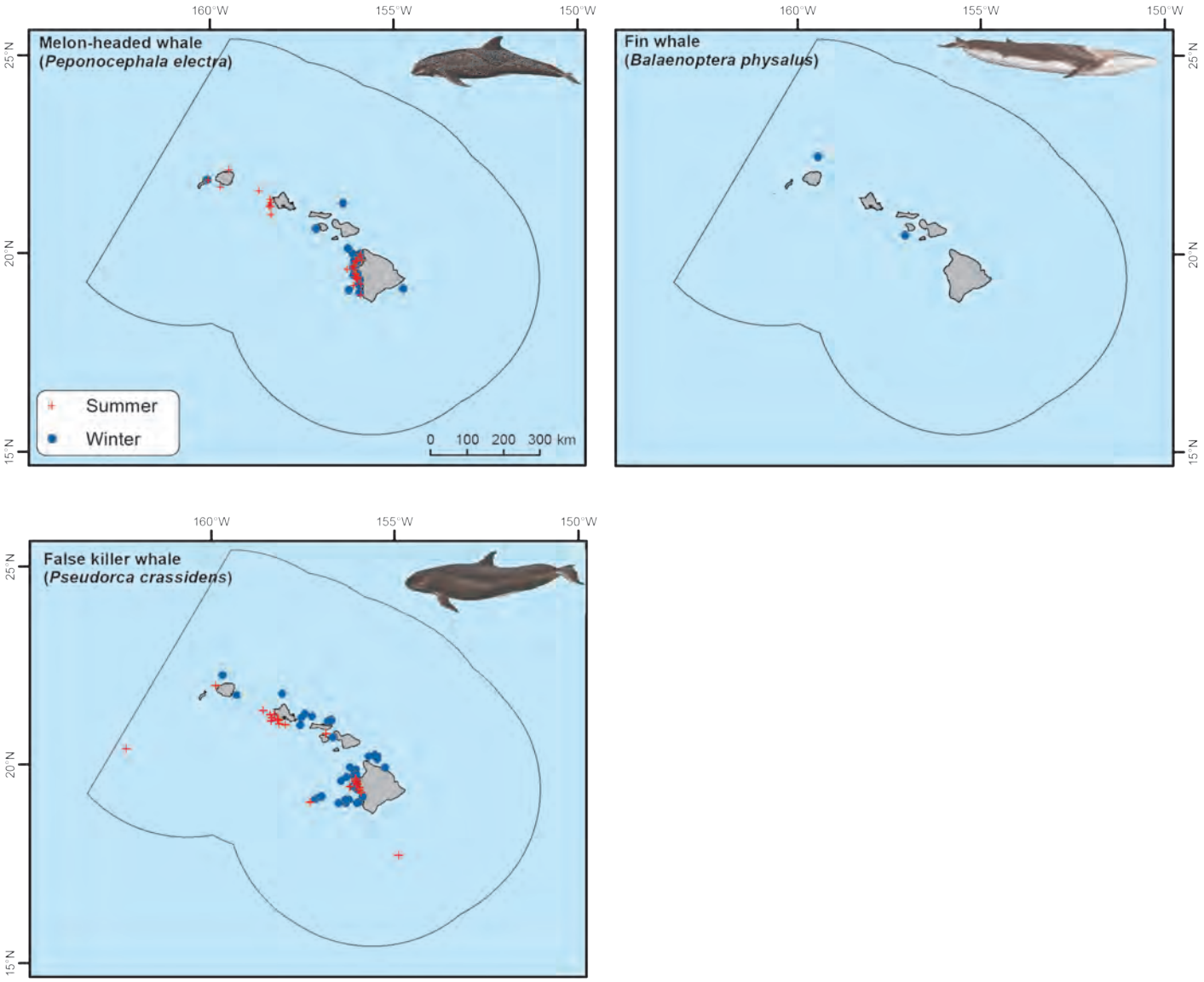

Figure 6.7. Cetacean sighting locations for non-modeled species for summer (May to October) and winter (November to April) seasons across the Main Hawaiian Islands project area (years 1993-2013). The amount and distribution of survey effort differed between seasons and between nearshore and offshore areas (Figures 6.2 and 6.3), so seasonal and spatial differences in the number of sightings do not necessarily reflect differences in relative abundance. Sighting data sources: Cascadia Research Collective, NOAA NMFS/SWFSC and PIFSC, and J. Mobley, University of Hawai'i at Mānoa. Artwork adapted from original by Justin Hart.

Modeled species distributions

A total of 12 spatial predictive models were computed and evaluated resulting in predicted distributions of relative abundance in winter and summer for five species (short-finned pilot whale, pantropical spotted dolphin, common bottlenose dolphin, rough-toothed dolphin and spinner dolphin) and in winter only for two species (humpback whale and sperm whale). Across all final models, the PDE ranged from 17 to 59 percent. Highest (37-59%) PDE was achieved for the summer model (59%) for common bottlenose dolphin, winter (56%) and summer (48%) models for spinner dolphin and the winter model (37%) for humpback whale, with the remaining models ranging from 17-35 percent PDE. Considering a second performance metric, the area under the receiver operating characteristic curve (AUC), most of the models with the highest AUC (=0.91-0.92) were also those with the highest PDE.

Pantropical spotted dolphin, Stenella attenuata*. Photo credit: NOAA NMFS/SWFSC*

Considering all four performance metrics, the statistical fit of seven models had a performance category of 4 (Appendix B), while the performance category of the remaining five models was 3. It is important to recognize that the model performance metrics and badge mainly reflect the statistical fit of the models to the data. They reflect only the data that were analyzed, and they do not reflect the quality of model predictions away from the data.

The modeling results revealed useful information about the contribution of predictor variables to each model (Figures 6.8 and 6.9). For example, sea state was a reasonably important predictor in most models. The probability of zero-inflation almost always showed a strong increase with sea state (i.e., a lower probability of sighting). It is important to note that this result was likely because the probability of detection is lower in higher sea states, not because true abundance is likely to be different. However, these two processes can be confounded and it is not possible to separate them in our analysis. Some of the more important environmental spatial predictor variables included: depth, slope (10 km), slope-of-slope (10 km), distance to shore, distance to seamounts, surface current direction (sine), chlorophyll-*a* concentration and front probability and strength, sea surface temperature front strength, and wind speed and divergence. Temporal predictor variables (year and day of year) were reasonably important in many models. Overall, climate indices played only a minor role and contributed most (Pacific Decadal Oscillation, one year lag) to the summer model for common bottlenose dolphin.

It is important to reiterate that the main objective of our modeling was to provide the best estimates of distributions. The models were not designed to determine which environmental predictors were most ecologically relevant in determining the distribution of cetaceans, nor to determine the functional relationships between environmental predictors and the distribution of cetaceans. Furthermore, many of the environmental predictor variables are likely to be proxies for unmeasured ecological processes linking cetaceans to their prey, rather than being variables that cetaceans respond to directly. Ecological inference from our model results should be cautious. Nevertheless, our results may suggest interesting hypotheses for future research.

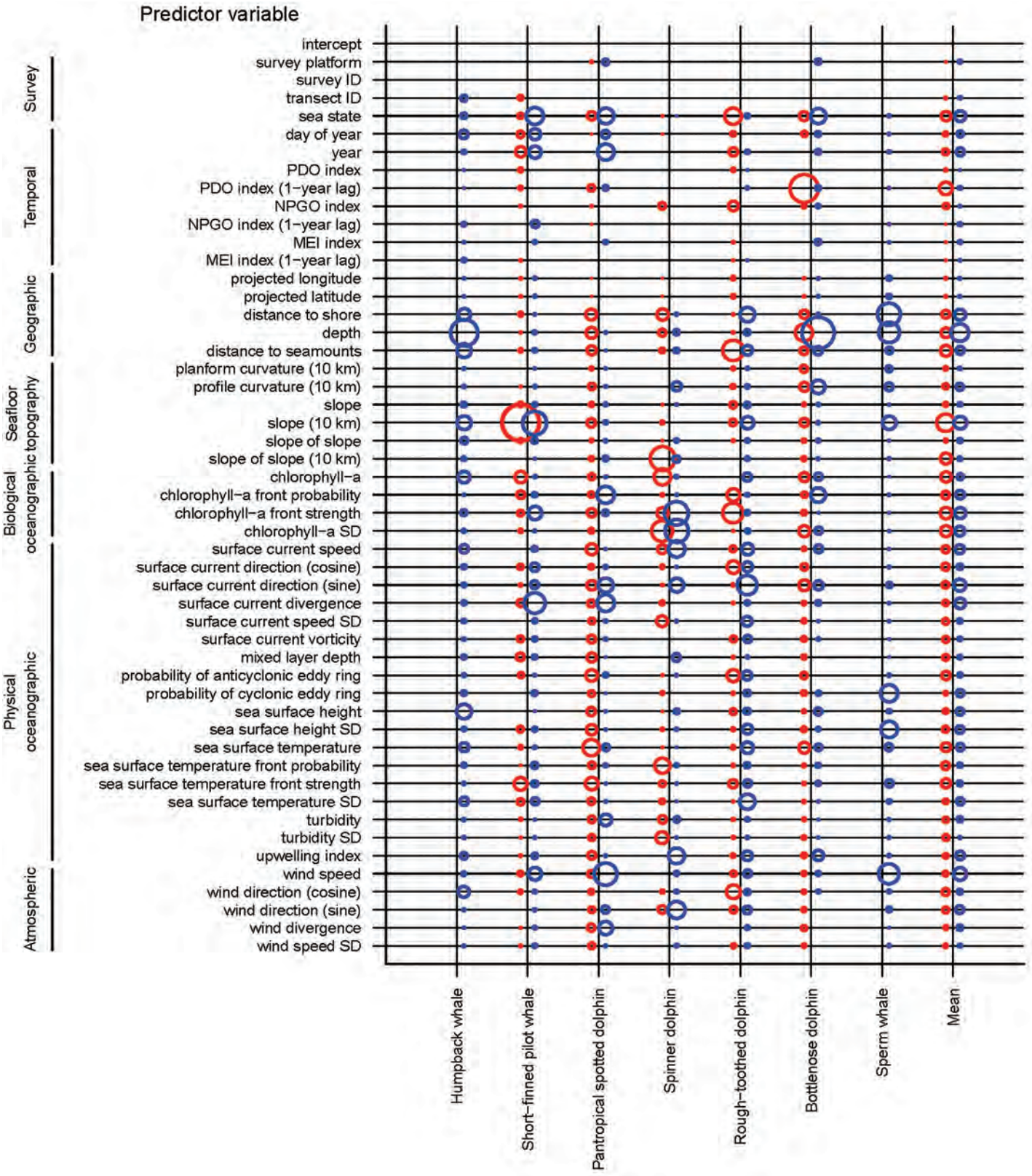

Figure 6.8. Predictor variable importance for the 'zero−inflation' component of each species' model. The area of a circle is proportional to relative variable importance, and the color indicates season (red = summer, blue = winter). Models had two components: a zero inflation and a count component (Appendix B). This figure displays the relative importance of each predictor variable for modeling the probability of zero inflation in the former component.

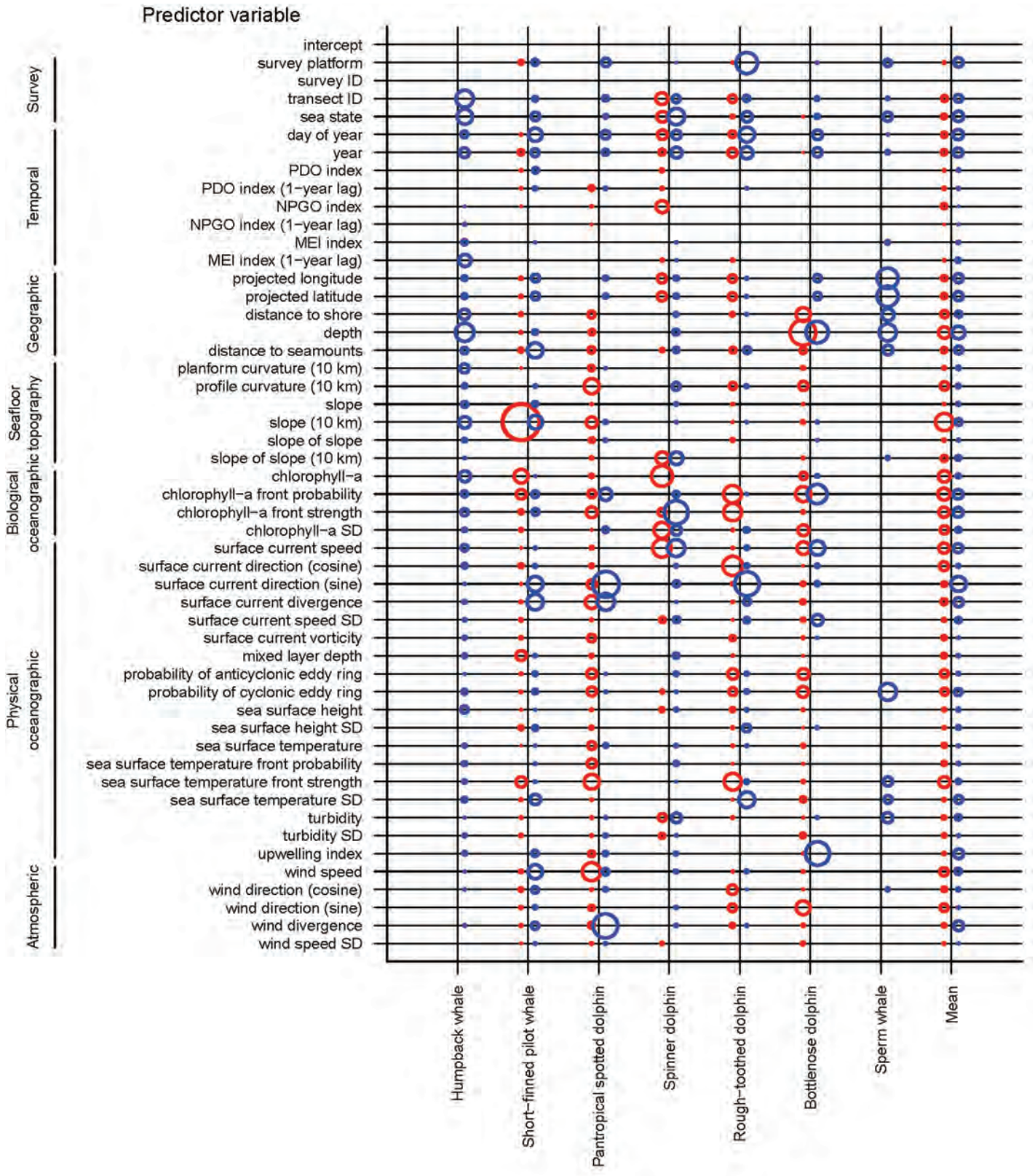

Figure 6.9. Predictor variable importance for the 'mean count' component of each species' model. The area of a circle is proportional to relative variable importance, and the color indicates season (red = summer, blue = winter). Models had two components: a zero inflation and a count component (Appendix B). This figure displays the relative importance of each predictor variable for modeling the mean count in the latter component.

Marine Mammals

Humpback whale (*Megaptera novaeangliae*) winter season

Humpback whale. Photo credit: NOAA NMFS/SWFSC.

The winter model (Figure 6.10) for humpback whale (PDE=37% and AUC=0.91) shows a nearshore distribution across all island groups of the MHI, with highest relative abundance predicted for sheltered, warmest waters primarily within the 200 m isobaths. This habitat preference has been documented in previous studies (e.g., Johnston et al., 2007). Important areas include Penguin Bank off Molokaʻi and the Kalohi, ʻAuʻau and Alalākeiki Channels between Maui, Molokaʻi and Lānaʻi. High relative abundance was also predicted for the island of Niʻihau, Kaʻula and the offshore Middle Bank region. For Oʻahu and Hawaiʻi, the north and northeast insular shelf waters were predicted to support higher abundance than the south coast. In general, these high relative abundance areas align with the areas selected for the Hawaiian Islands Humpback Whale National Marine Sanctuary. Depth contributed most to the predicted distribution maps with a steep increase in abundance at the shallowest depths. The day-of-year predictor indicated an increase then decrease in abundance during the winter period, with a peak in early March. Low coefficient of variation (CV) across the areas of predicted high abundance indicates high precision of model predictions.

Sperm whale (*Physeter macrocephalus*) winter season

Sperm whales. Photo credit: NOAA

The winter model for sperm whale (Figure 6.11; PDE=24% and AUC=0.91) shows an offshore distribution with higher predicted relative abundance over deeper waters far from shore. This pattern emerged despite a number of spatially clustered sightings in relatively deep waters off the southwest coast of Hawaiʻi, where high survey effort has taken place (Figure 6.3), suggesting that the model was not greatly biased by nearshore concentrations of survey effort. Clusters of sightings off the north coast of Kauaʻi and the northeast coast of Hawaiʻi were also in areas of predicted low relative abundance, but these areas had less survey effort (Figure 6.3), potentially indicating that modeled relative abundance in at least some nearshore areas was lower than expected. High relative abundance was predicted for the Middle Bank region and the regions surrounding the Hawaiian and West Hawaiian seamounts, and a region of high probability of cyclonic eddies west of the island of Hawaiʻi. Depth, distance to shore and probability of cyclonic eddy rings were the environmental predictors with the most influence on the predicted distribution of sperm whale relative abundance. Predicted relative abundance increased with depth and probability of cyclonic eddy rings. The predicted spatial distribution pattern is expected on the basis of analyses of sighting rates in relation to depth (Baird et al., 2013a), and satellite tag data available for sperm whales in Hawaiian waters (Rone et al., 2015). Acoustic monitoring of whale vocalizations indicates that sperm whales occur in the MHI throughout the year (Au et al., 2014), which is also indicated in the sighting data presented here.

Humpback whale
Megaptera novaeangliae
(winter)

Figure 6.10. Modeled long-term relative abundance of Humpback whale in winter. Spatial predictive modeling was applied to at-sea sighting data from 1993-2011 provided by J. Mobley (University of Hawai'i at Mānoa), NOAA NMFS/PIFSC and SWFSC.. A total of 59,442 transect segments were analyzed, on 2,098 of which this species was sighted for a total of 4,015 individuals sighted. Figure panels are: a) locations of sightings; b) model quality as a function of four performance metrics (Table 6.3); c,d) median bootstrapped estimates of relative abundance; and e,f) bootstrapped coefficients of variation. Predictions were circumscribed by a 50 km-buffered minimum convex polygon around survey effort locations; areas outside this polygon appear blank. Green lines indicate the boundaries of the Hawaiian Islands Humpback Whale National Marine Sanctuary. Artwork adapted from original by Justin Hart.

Sperm whale

Physeter macrocephalus

(winter)

Figure 6.11. Modeled long-term relative abundance of Sperm whale in winter. Spatial predictive modeling was applied to at-sea sighting data from 1993-2012 provided by Cascadia Research Collective, J. Mobley (University of Hawai'i at Mānoa), NOAA NMFS/PIFSC and SWFSC. A total of 84,513 transect segments were analyzed, on 54 of which this species was sighted for a total of 257 individuals sighted. Figure panels are: a) locations of sightings; b) model quality as a function of four performance metrics (Table 6.3); c,d) median bootstrapped estimates of relative abundance; and e,f) bootstrapped coefficients of variation. Predictions were circumscribed by a 50 km-buffered minimum convex polygon around survey effort locations; areas outside this polygon appear blank. Artwork adapted from original by Justin Hart.

Spinner dolphin (*Stenella longirostris*) summer and winter seasons

Spinner dolphin, Stenella longirostris. *Photo credit: Robin W. Baird (Cascadia Research Collective).*

Both winter (Figure 6.12; PDE=56% and AUC=0.86) and summer (Figure 6.13; PDE=48% and AUC=0.91) models predict a similar inshore distribution, but with a higher abundance for embayments and leeward island locations in the winter season. Given the predicted inshore distribution, areas of predicted high relative abundance are best visualized at a scale of tens of kilometers (e.g., Figure 6.14). The predicted higher relative abundance inshore is consistent with the known behavior of spinner dolphins in the MHI that rest in sheltered inshore waters during the day (Norris et al., 1994). NMFS recognizes a number of separate insular stocks of spinner dolphins in the MHI (Carretta et al., 2015), largely on the basis of genetic differentiation (Andrews et al., 2010). On Kaua'i, the Waimea Bay region on the southwest coast and the Makaha Point region emerged as important areas and have also been identified as resting areas by expert knowledge (TNC, 2009). Keawanui Bay on Ni'ihau is also highlighted by the model as a year round high potential use area. Around O'ahu, high relative abundance was predicted for Makua Bay and Nanakuli on the west coast (Figure 6.14). Kāne'ohe Bay on the east coast was predicted to be an area of high relative abundance in winter. Around the Maui Nui island group, the models predicted several suitable areas for spinner dolphins, including Kahului Harbor and Mā'alaea Bay and the Lipoa Point area on the north shore adjacent Pailolo Channel on Maui; Kamalō Harbor and the south shore of Moloka'i particularly in winter; and the south shore of Lāna'i, including Manele Bay and west Lāna'i in the Nanahoa area. Around the island of Hawai'i highest relative abundance was predicted for nearshore areas south of Upolu Point on the west coast, Mahaiula Bay, Keahole Point, Honokohau Bay in winter and Kailua Bay. Several of these predictions agree with expert knowledge on important resting areas (TNC, 2009). These west coast resting areas have also been identified through field surveys (Norris et al., 1994, Östman-Lind et al., 2004) and modeling (Thorne et al., 2012). The southeast shore from Wai'ahukini to Cape Kumukahi is an area of predicted high relative abundance, particularly in the summer months. In addition, Hilo Bay on the east coast of the island of Hawai'i has many high abundance cells in the summer months. Previous predictive models using presence only data showed that spinner dolphin resting habitat was associated with proximity to deep water foraging areas, water depth, the proportion of bays with shallow depths and seafloor rugosity (Thorne et al., 2012). Our models, which focused on a broader spatial scale, were influenced most by slope-of-slope (10 km); chlorophyll-*a* concentration, SD, and front strength; and surface current speed. These results suggest that spinner dolphins may be associated with high complexity seafloor (high slope of the slope values). The chlorophyll-*a* related predictors were likely important because of their ability to discriminate between nearshore and offshore conditions. For example, predicted relative abundance was negatively correlated with chlorophyll-*a* front strength.

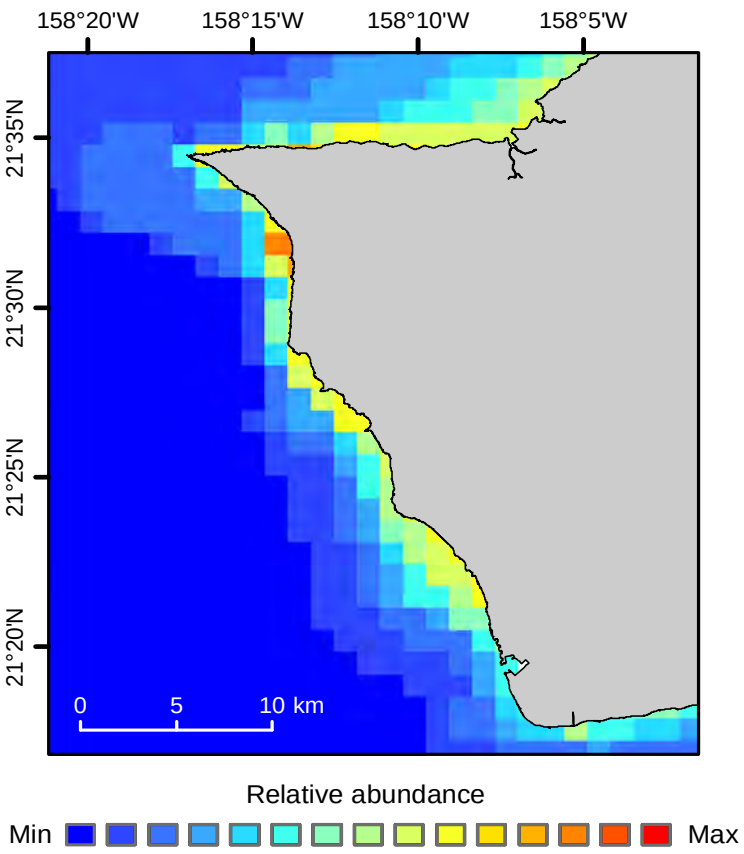

Figure 6.14. Modeled long-term relative abundance of Spinner dolphin in summer along west coast of O'ahu. Spatial predictive modelling was applied to at-sea sighting data from 2002-2013. Data provided by Cascadia Research Collective, J. Mobley (University of Hawai'i at Mānoa), and NOAA NMFS/PIFSC and SWFSC.

Spinner dolphin
Stenella longirostris
(winter)

Figure 6.12. Modeled long-term relative abundance of Spinner dolphin in winter. Spatial predictive modeling was applied to at-sea sighting data from 1993-2012 provided by Cascadia Research Collective, J. Mobley (University of Hawai'i at Mānoa) and NOAA NMFS/PIFSC and SWFSC. A total of 84,513 transect segments were analyzed, on 121 of which this species was sighted for a total of 4,943 individuals sighted. Figure panels are: a) locations of sightings; b) model quality as a function of four performance metrics (Table 6.3); c,d) median bootstrapped estimates of relative abundance; and e,f) bootstrapped coefficients of variation. Predictions were circumscribed by a 50 km-buffered minimum convex polygon around survey effort locations; areas outside this polygon appear blank. Artwork adapted from original by Justin Hart.

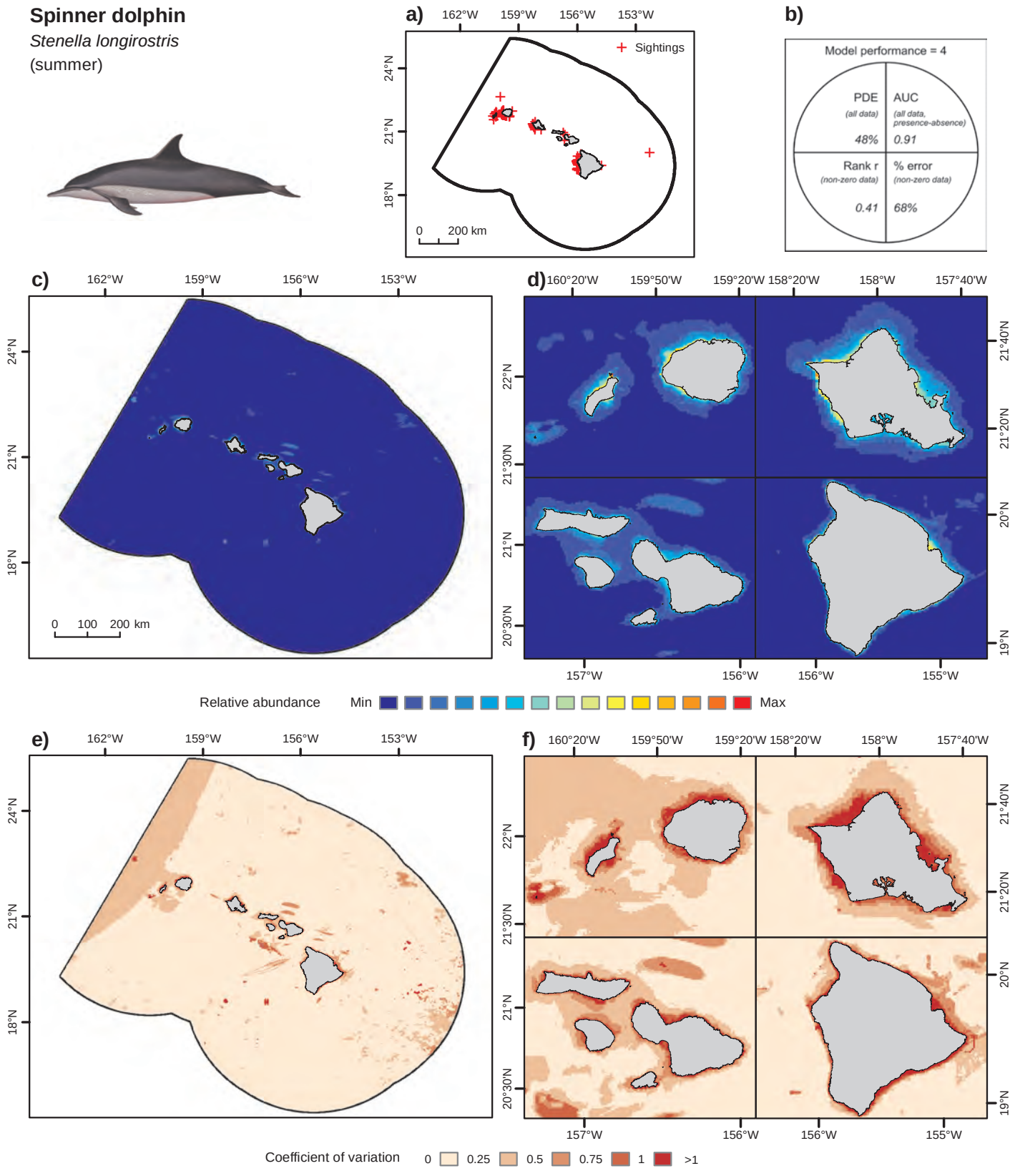

Figure 6.13. Modeled long-term relative abundance of Spinner dolphin in summer. Spatial predictive modeling was applied to at-sea sighting data from 2002-2013 provided by Cascadia Research Collective, J. Mobley (University of Hawai'i at Mānoa) and NOAA NMFS/PIFSC and SWFSC. A total of 54,300 transect segments were analyzed, on 103 of which this species was sighted for a total of 3,795 individuals sighted. Figure panels are: a) locations of sightings; b) model quality as a function of four performance metrics (Table 6.3); c,d) median bootstrapped estimates of relative abundance; and e,f) bootstrapped coefficients of variation. Artwork adapted from original by Justin Hart.

Common bottlenose dolphin (*Tursiops truncatus*) summer and winter season

Winter (Figure 6.15; PDE=17% and AUC=0.85) and summer (Figure 6.16; PDE=59% and AUC=0.92) models predicted similar nearshore distribution patterns, with additional high relative abundance at Middle Bank and seamounts. Depth was the most consistently important predictor across summer and winter models, possibly explaining the predictions at Middle Bank and seamounts. With the exception of tagged false killer whales (Baird et al., 2013b), very little is known about cetacean use of Middle Bank. The summer model also predicted relatively high abundance southwest of the island of Hawai'i. Previous studies using photo-identification, genetic analyses and satellite tagging suggest limited movement of common bottlenose dolphins between islands and between nearshore and offshore waters, indicating the existence of demographically distinct resident populations at each of the four main Hawaiian Island groups, and a distinct offshore pelagic population beyond the 1,000 m isobaths (Baird et al., 2009a; Martien et al., 2012; Baird, 2016). In summer, models showed highest nearshore abundance across the shallow (<200 m) insular shelf of Ka'ula, Keawanui Bay on Ni'ihau, the sloping shelf off Makaha Point on west Kaua'i and Waimea Bay on south Kaua'i. On O'ahu, highest relative abundance is predicted for the sloping shelf off Ka'ena Point, off Maili Point west O'ahu, Makapu'u Point, Kaiwi Channel and Penguin Bank. Relative abundance is moderate through the channels of the Maui Nui islands. Off the island of Hawai'i, two areas emerge with highest abundance: shelf waters straddling the 200 m isobath north of Upolu Point, and north of Keahole Point, which experiences high upwelling and persistent chlorophyll-*a* fronts (Chapter 2, Figures 2.23 and 2.20, respectively). Chlorophyll-*a* front probability was an important predictor, especially in the winter model, with abundance increasing with increasing front probability. Winter models show a similar all-island distribution, but with lower abundance and occurrence in the more exposed locations offshore, such as the Hawaiian Seamounts and areas such as Upolu Point (north island of Hawai'i), which experiences greater wind speeds in winter than summer (Chapter 2 Figure 2.7). The sheltered channels of Maui Nui are predicted to be relatively more suitable habitat for common bottlenose dolphins in winter than in summer, particularly the 'Au'au Channel between Maui and Lāna'i. Another discrete location highlighted as a higher abundance area only in the winter model was the Kuia Shoal (<200 m depth) off the western tip of Kaho'olawe.

Common bottlenose dolphin. Photo credit: Robin W. Baird (Cascadia Research Collective)

Common bottlenose dolphin

Tursiops truncatus

(winter)

Figure 6.15. Modeled long-term relative abundance of Common bottlenose dolphin in winter. Spatial predictive modeling was applied to at-sea sighting data from 1993-2012 provided by Cascadia Research Collective, J. Mobley (University of Hawai'i at Mānoa) and NOAA/NMFS PIFSC and SWFSC. A total of 84,513 transect segments were analyzed, on 142 of which this species was sighted for a total of 1,261 individuals sighted. Figure panels are: a) locations of sightings; b) model quality as a function of four performance metrics (Table 6.3); c,d) median bootstrapped estimates of relative abundance; and e,f) bootstrapped coefficients of variation. Predictions were circumscribed by a 50 km-buffered minimum convex polygon around survey effort locations; areas outside this polygon appear blank. Artwork adapted from original by Justin Hart.

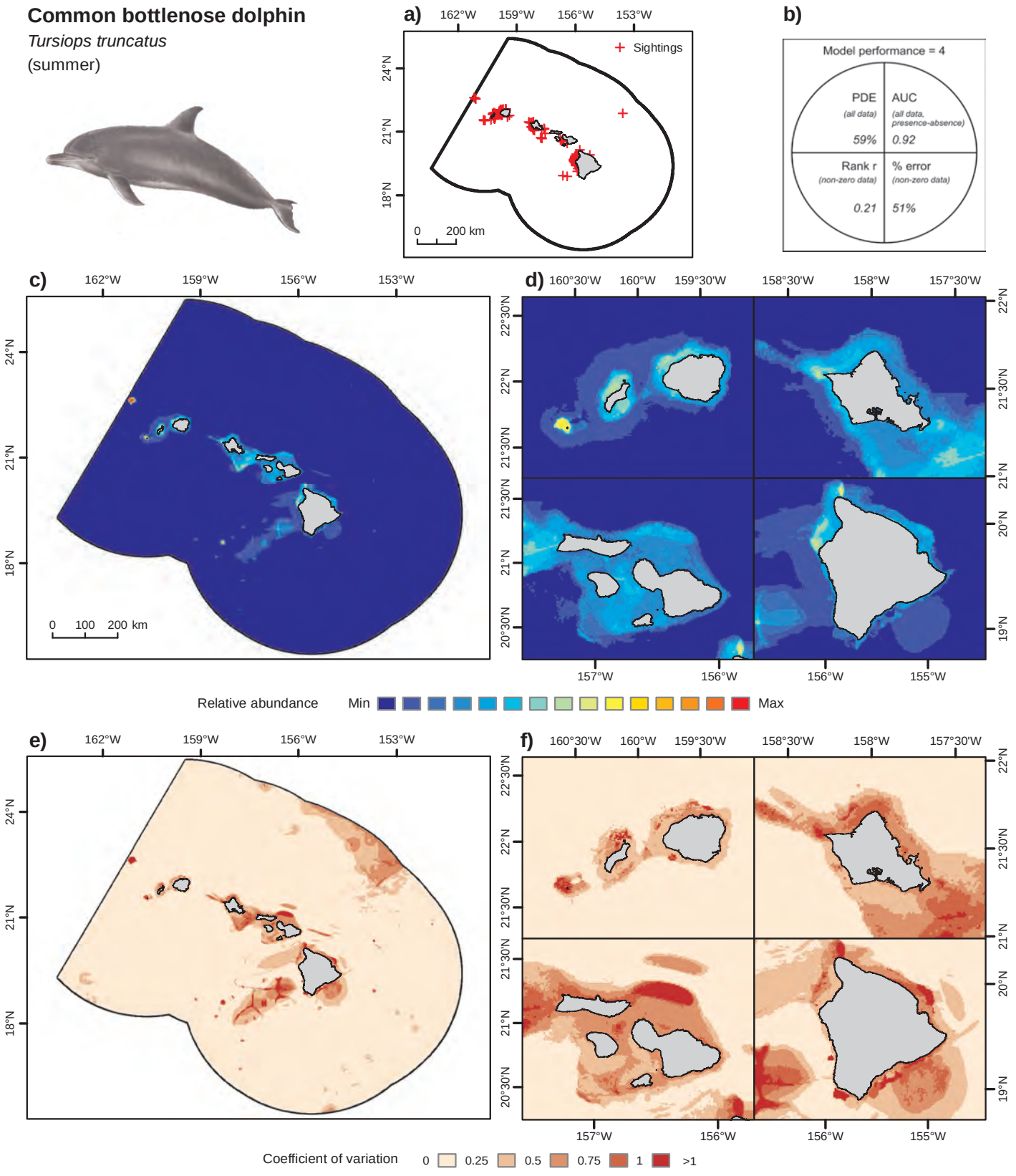

Figure 6.16. Modeled long-term relative abundance of Common bottlenose dolphin in summer. Spatial predictive modeling was applied to at-sea sighting data from 2002-2013 provided by Cascadia Research Collective, J. Mobley (University of Hawai'i at Mānoa) and NOAA/NMFS PIFSC and SWFSC. A total of 54,300 transect segments were analyzed, on 144 of which this species was sighted for a total of 1,395 individuals sighted. Figure panels are: a) locations of sightings; b) model quality as a function of four performance metrics (Table 6.3); c,d) median bootstrapped estimates of relative abundance; and e,f) bootstrapped coefficients of variation. Artwork adapted from original by Justin Hart.

Pantropical spotted dolphin (*Stenella attenuata*) summer and winter seasons

Winter (Figure 6.17; PDE=35% and AUC=0.86) and summer (Figure 6.18; PDE=26% and AUC=0.78) models predicted that spotted dolphin relative abundance was higher on the leeward side of the islands than on the windward side, with a considerably more restricted leeward distribution in winter. There were several distinct areas with predicted high relative abundance in summer. On O'ahu, the steeply sloping shelf waters beyond the 200 m isobath south of Ka'ena Point had high predicted relative abundance. This area has a high probability of anti-cyclonic eddies in the summer and winter months (Chapter 2 Figure 2.20). Around Maui Nui, highest abundance was predicted for Kuia Shoal west of Kaho'olawe, Alenuihāhā and 'Au'au Channels, and the sloping shelf waters leeward of Lāna'i. Around the island of Hawai'i, a large high relative abundance area exists for summer and winter along the west coast shelf with highest abundance in a band offshore from Keawekaheka Point. In the summer only, an additional high relative abundance area is predicted west of Upolu Point. These areas are characterized by a high persistence of chlorophyll-*a* fronts west and south of the island of Hawai'i, as well as low wave height and low mean current speed, with high variation and warmer seas than surrounding areas in both seasons. In winter, high relative abundance was also predicted for a windward area east of Kaua'i, but where no sightings occurred. It was not clear why this area would be suitable habitat, so that prediction requires future verification with field data. A range of predictors contributed to the models, with surface current direction and wind speed and divergence being most influential in winter, and wind speed, sea surface temperature and front strength, and profile curvature (10 km) being most influential in summer. Abundance was predicted to decrease with increasing wind speed, which could be a habitat preference for calmer areas or a result of decreased sightability or effort in windier areas. Circular patterns in predicted summer abundance at Middle Bank and seamounts southwest of the island of Hawai'i were likely a result of estimated relationships with bathymetry (e.g., profile curvature). The predicted higher relative abundance of spotted dolphin on the leeward side of the islands raises the question of whether this pattern was due, in part, to the larger amount of survey effort in those areas (Figure 6.3). While our modeling framework theoretically accounted for effort, it is still possible that geographic variation in effort contributed to the predicted spatial patterns, especially when offshore effort was relatively low (e.g., winter). Further, NMFS recognizes three insular stocks and a pelagic stock for this species in Hawaiian waters (Carretta et al., 2015) on the basis of genetics (Courbis et al., 2014). Our model results reflect the unspecified stock composition of the sighting data used. For example, if most of the sightings were of individuals belonging to insular stocks, then our results would mainly reflect the spatial distribution of the insular stocks.

Pantropical spotted dolphins. Photo credit: Robin W. Baird (Cascadia Research Collective)

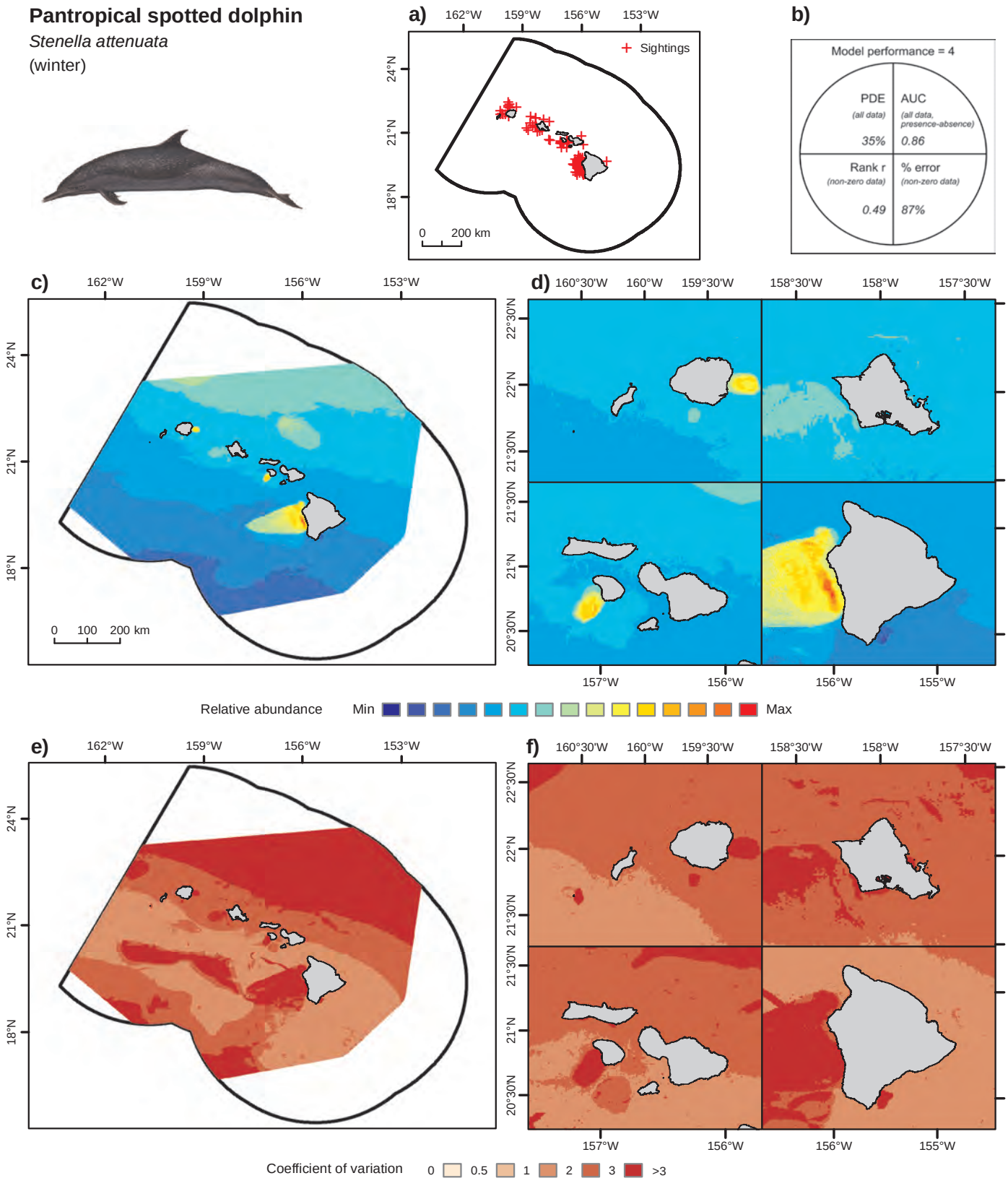

Figure 6.17. Modeled long-term relative abundance of Pantropical spotted dolphin in winter. Spatial predictive modeling was applied to at-sea sighting data from 1993-2012 provided by Cascadia Research Collective, J. Mobley (University of Hawai'i at Mānoa) and NOAA/NMFS PIFSC and SWFSC. A total of 84,513 transect segments were analyzed, on 226 of which this species was sighted for a total of 14,181 individuals sighted. Figure panels are: a) locations of sightings; b) model quality as a function of four performance metrics (Table 6.3); c,d) median bootstrapped estimates of relative abundance; and e,f) bootstrapped coefficients of variation. Predictions were circumscribed by a 50 km-buffered minimum convex polygon around survey effort locations; areas outside this polygon appear blank. Artwork adapted from original by Justin Hart.

Pantropical spotted dolphin

Stenella attenuata

(summer)

Figure 6.18. Modeled long-term relative abundance of Pantropical spotted dolphin in summer. Spatial predictive modeling was applied to at-sea sighting data from 2002-2013 provided by Cascadia Research Collective, J. Mobley (University of Hawai'i at Mānoa) and NOAA/NMFS PIFSC and SWFSC. A total of 54,300 transect segments were analyzed, on 212 of which this species was sighted for a total of 13,695 individuals sighted. Figure panels are: a) locations of sightings; b) model quality as a function of four performance metrics (Table 6.3); c,d) median bootstrapped estimates of relative abundance; and e,f) bootstrapped coefficients of variation. Artwork adapted from original by Justin Hart.

Rough-toothed dolphin (*Steno bredanensis*) summer and winter season

Winter (Figure 6.19; PDE=18% and AUC=0.81) and summer (Figure 6.20; PDE=33% and AUC=0.87) models both predicted highest relative abundance in offshore waters generally beyond the 200 m isobath, yet resulted in different spatial patterns in the predicted distributions. The winter model performed less well than the summer model, and the modeled winter distribution was more concentrated and did not correspond as well with the locations of sightings, suggesting that the modeled winter distribution for this species should be interpreted with caution. The winter model predicted that waters around the central MHI (O'ahu and Maui Nui) are less frequently used by rough-toothed dolphin, although there were quite a few sightings in these areas. The largest area with predicted high relative abundance in the winter was over the Hawaiian Seamounts in the lee of the island of Hawai'i, an area characterized by calmer, productive (persistent chlorophyll-*a* fronts), warmer water than surrounding areas. Two of the most important predictors in the winter model were current direction (sine) and sea surface temperature SD. The large area of predicted high relative abundance coincides with the Hawaiian Lee Counter Current (Chapter 2, Figures 2.9 and 2.10). A smaller area of predicted high relative abundance in winter was in the Kaulakahi Channel between Kaua'i and Ni'ihau. These two areas with higher density (Kaua'i and the island of Hawai'i) have been suggested as reflecting two different populations on the basis of genetic analyses and photo-identification (Baird et al., 2008a; Oleson et al., 2013; Albertson, 2014; Baird, 2016). Chlorophyll-a front strength and probability were among the most important predictors in the summer model resulting in a more dispersed but also speckled distribution. Summer relative abundance was predicted to be highest in the deep waters of the Kaulakahi Channel between Kaua'i and Ni'ihau; deep waters off Ka'ena Point off west O'ahu; Kaiwi Channel and offshore of Hālawa Bay, Moloka'i, 'Au'au Channel; Alalākeiki Channel southeast of Kaho'ulawe; and west of the island of Hawai'i offshore of Hanamalo Point and Keahole Point.

Rough-toothed dolphin, Steno bredanensis. *Photo credit: Robin W. Baird (Cascadia Research Collective)*

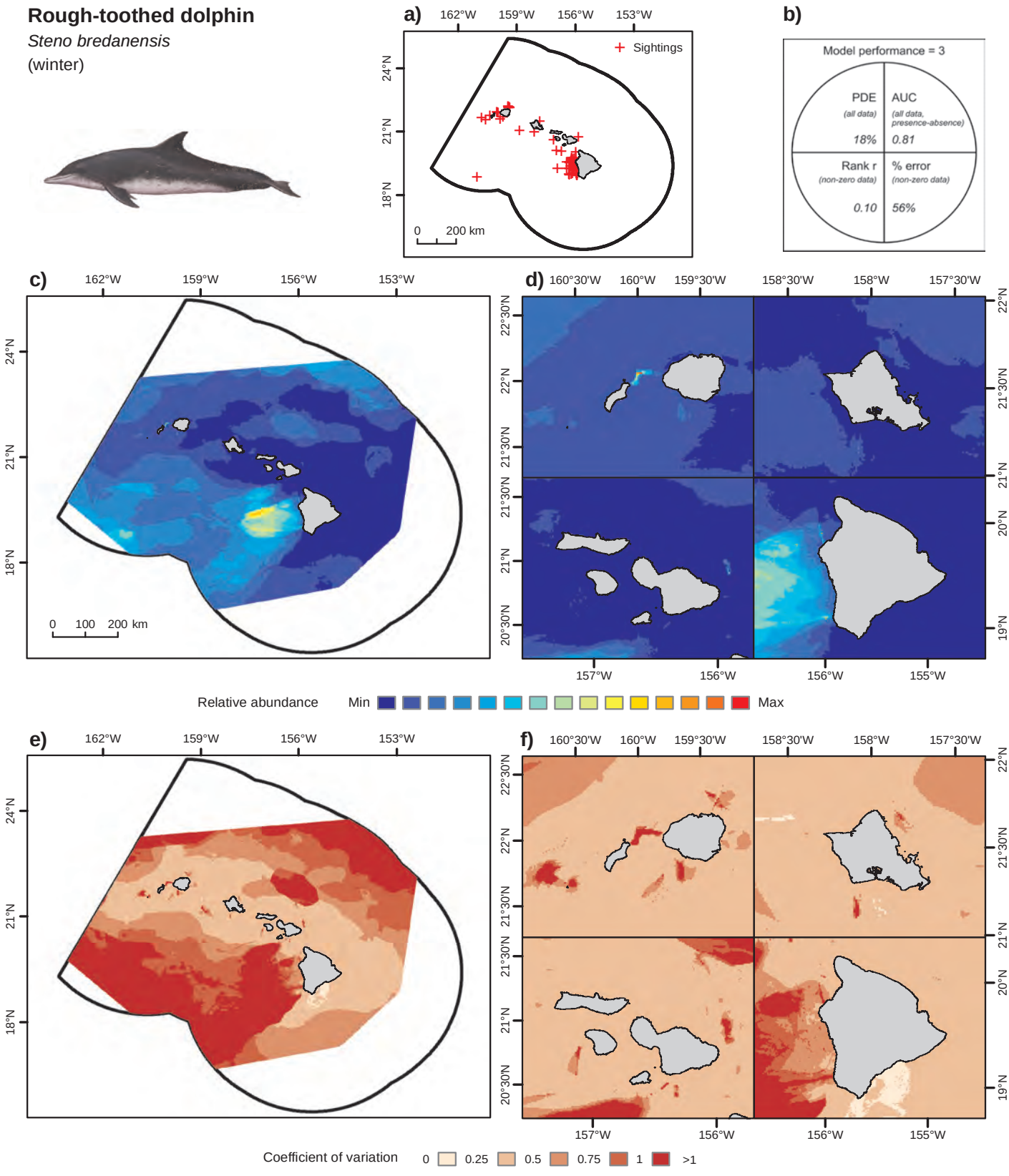

Figure 6.19. Modeled long-term relative abundance of Rough-toothed dolphin in winter. Spatial predictive modeling was applied to at-sea sighting data from 1993-2012 provided by Cascadia Research Collective, J. Mobley (University of Hawai'i at Mānoa) and NOAA NMFS/PIFSC and SWFSC. A total of 84,513 transect segments were analyzed, on 74 of which this species was sighted for a total of 919 individuals sighted. Figure panels are: a) locations of sightings; b) model quality as a function of four performance metrics (Table 6.3); c,d) median bootstrapped estimates of relative abundance; and e,f) bootstrapped coefficients of variation. Predictions were circumscribed by a 50 km-buffered minimum convex polygon around survey effort locations; areas outside this polygon appear blank. Artwork adapted from original by Justin Hart.

Rough-toothed dolphin

Steno bredanensis

(summer)

Figure 6.20. Modeled long-term relative abundance of Rough-toothed dolphin in summer. Spatial predictive modeling was applied to at-sea sighting data from 2002-2013 provided by Cascadia Research Collective, J. Mobley (University of Hawai'i at Mānoa) and NOAA NMFS/PIFSC and SWFSC. A total of 54,300 transect segments were analyzed, on 166 of which this species was sighted for a total of 2,009 individuals sighted. Figure panels are: a) locations of sightings; b) model quality as a function of four performance metrics (Table 6.3); c,d) median bootstrapped estimates of relative abundance; and e,f) bootstrapped coefficients of variation. Artwork adapted from original by Justin Hart.

Short-finned pilot whale (*Globicephala macrorhynchus*) summer and winter seasons

Winter (Figure 6.21; PDE=34% and AUC=0.83) and summer (Figure 6.22; PDE=22% and AUC=0.84) models showed fairly different spatial distribution patterns. High relative abundance in winter was predicted for a band of deep offshore water north of the MHI. A distinct gradient of southward declining abundance was predicted across the project area. Although low relative abundance was predicted for offshore waters north and south of all islands, several notable exceptions were predicted, including a patch of moderate relative abundance off the southern tip of Penguin Bank, the deep shelf at the lee of Lānaʻi and a small patch east of Kahoʻolawe. A striking band of high relative abundance was also predicted along the Kona coast of Hawaiʻi, well beyond the 200 m isobath, but including where the deep shelf waters exist near the coast off Keawekaheka Point. This area was also identified as a high-use area for tracked short-finned pilot whales (Abecassis et al., 2015). In addition, high relative abundance is shown over deep water off the southern tip of the island of Hawaiʻi, between Kalae and Kamilo Point. The summer model predicted distinct bands of higher abundance over deeper sloping shelf waters both north and south of the islands, as well as the Hawaiian Seamounts, including the slopes of Cross Seamount and Middle Bank. The summer model was strongly driven by slope at a 10 km resolution. Slope (10 km) was also a relatively important predictor in the winter model, and some of those same areas can be seen to have higher than average predicted relative abundance in winter. It is possible that the strong estimated relationship between slope and relative abundance was driven by data from certain areas (e.g., off the west coast of the island of Hawaiʻi) and that the predicted high relative abundance in other areas with similar slope are not realistic. For example, there were fewer data from the windward side of the islands to inform the models. Field observations and tracking studies suggest there may be inshore and pelagic populations of short-finned pilot whales in Hawaiian waters, and that island-associated populations exist with strong social cohesion and limited inter-island movements (Abecassis et al., 2015; Mahaffy et al., 2015; Baird, 2016). As with the other species, our model results reflect the unspecified stock composition of the sighting data used.

Short-finned pilot whale. Photo credit: Robin W. Baird (Cascadia Research Collective)

Becker et al. (2012) and Forney et al. (2015) developed habitat-based models of the distributions of our modeled species in the central North Pacific, including waters around the MHI. Their models were fit only to some of the data analyzed here (NOAA ship survey data), so their survey dataset was less concentrated in nearshore and leeward areas. Also, their models differed from ours in several ways. First, their models covered a wider geographic area and used a coarser spatial resolution. Second, their models considered a smaller set of environmental predictor variables but matched these dynamic variables to the sighting data in time ('contemporaneous' approach) allowing their models to capture inter-annual differences in species distributions. Third, their models employed a different statistical framework and incorporated species-specific detection rate parameters that allowed them to estimate absolute density, rather than relative abundance, which was estimated by our models. The predicted distributions presented by Becker et al. (2012) and Forney et al. (2015) reflect larger scale patterns than ours do, and it is difficult to make detailed comparisons. Nevertheless, there are perhaps some instances of broad correspondence between their predicted distributions and ours; for example, common bottlenose dolphin.

Short-finned pilot whale
Globicephala macrorhynchus
(winter)

Figure 6.21. Modeled long-term relative abundance of Short-finned pilot whale in winter. Spatial predictive modeling was applied to at-sea sighting data from 1993-2012 provided by Cascadia Research Collective, J. Mobley (University of Hawai'i at Mānoa) and NOAA NMFS/PIFSC and SWFSC. A total of 84,513 transect segments were analyzed, on 235 of which this species was sighted for a total of 4,397 individuals sighted. Figure panels are: a) locations of sightings; b) model quality as a function of four performance metrics (Table 6.3); c,d) median bootstrapped estimates of relative abundance; and e,f) bootstrapped coefficients of variation. Predictions were circumscribed by a 50 km-buffered minimum convex polygon around survey effort locations; areas outside this polygon appear blank. Photo credit: Robin W. Baird (Cascadia Research Collective)

Short-finned pilot whale
Globicephala macrorhynchus
(summer)

Figure 6.22. Modeled long-term relative abundance of Short-finned pilot whale in summer. Spatial predictive modeling was applied to at-sea sighting data from 2002-2013 provided by Cascadia Research Collective, J. Mobley (University of Hawai'i at Mānoa) and NOAA/NMFS PIFSC and SWFSC. A total of 54,300 transect segments were analyzed, on 327 of which this species was sighted for a total of 6,244 individuals sighted. Figure panels are: a) locations of sightings; b) model quality as a function of four performance metrics (Table 6.3); c,d) median bootstrapped estimates of relative abundance; and e,f) bootstrapped coefficients of variation. Photo credit: Robin W. Baird (Cascadia Research Collective)

6.1.4. Data Limitations and Information Gaps

Our assessment analyzed some of the best available at-sea visual survey data for cetaceans in the MHI from recent decades. Each dataset had particular strengths and limitations, many of which are discussed in publications by the data providers: NOAA (Barlow, 2006; Becker et al., 2012; Forney et al., 2015), Cascadia Research Collective (Baird et al., 2013a) and University of Hawai'i at Mānoa (Mobley, 2001). The data spanned 20 years with some survey effort in all months of the year. Nevertheless, given the size of the study area and the relatively low sighting rates for many species, additional years of survey effort especially in windward and offshore waters would help improve estimates of cetacean distributions around the MHI and could be used to validate our model predictions (Forney et al., 2015).

The combining of multiple survey datasets was a unique aspect of our assessment, and it posed special challenges. For example, the different datasets had different spatial coverages and densities. The Cascadia Research Collective data provided relatively intensive coverage of nearshore waters on the leeward sides of the islands using non-systematic transects. The aerial survey data were also from nearshore waters, but with more even coverage of the leeward and windward sides using systematic transects. The NOAA data had the most geographically extensive coverage with systematic transects, but effort was less dense. For species that we modeled, the predictive modeling framework theoretically accounted for these differences in survey effort, but it is still possible that the predicted distributions of relative abundance are biased because of imbalances in survey coverage among datasets.

Another important difference among datasets was the survey platform and protocol. The visual range of observers and the probability of sighting animals vary depending on a number of survey factors, including the height of the observation platform, use of binoculars and area of focus. These factors differed among the datasets, so species-specific sighting rates would also be expected to vary. For species that we modeled, the predictive modeling framework allowed for differences in mean sighting rates among survey platforms, but it is still possible that the predicted distributions of relative abundance are biased because of differences in survey platform and protocol among datasets.

It would be useful to further investigate apparent differences between the results of our habitat-based spatial models and those of Becker et al. (2012) and Forney et al. (2015) to determine the extent to which the additional datasets and the different modeling framework in our study contributed to those differences.

For many of the cetacean species in our assessment, population structure has been documented in the MHI with island-associated populations, and inshore and offshore pelagic populations with different levels of exchange (McSweeney et al., 2007, 2009; Aschettino et al., 2012; Martien et al., 2012; Courbis et al., 2014). Our assessment treated all sightings for a given species the same, so our results reflect the unspecified population composition of those sightings. For example, if most of the sightings were of individuals belonging to an insular population, then our results would mainly reflect the spatial distribution of the insular population.

Electronic tracking studies provide a complementary source of information about the at-sea distribution of cetaceans, and we would encourage current and future such efforts in the MHI. Tracking data provide detailed information about behavior, movements, and space use of individuals through time. It is also more feasible to assign tracked individuals to specific populations, and thereby obtain population-specific information about spatial distributions. Cascadia Research Collective has collected tracking data for 12 cetacean species (common bottlenose dolphin, Blainville's beaked whale, Cuvier's beaked whale, false killer whale, melon-headed whale, pygmy killer whale, killer whale, pantropical spotted dolphin, rough-toothed dolphin, short-finned pilot whale, Risso's dolphin and sperm whale) in Hawaiian waters, and has assessed spatial distributions and habitat

associations for some (Baird et al., 2009b, 2010, 2012a, b; Schorr et al., 2009; Woodworth et al., 2012; Baird, 2016). A comparison of our predicted spatial distributions with these tracking data would be a valuable contribution to the understanding and characterization of cetacean spatial distributions in the MHI (e.g., Figure 6.23).

Acoustic detections from surveys of cetacean vocalizations in Hawaiian waters are now available for many species, particularly odontocetes (e.g., Johnston et al., 2008; Baumann-Pickering et al., 2015), and those data could also be used to validate and improve our estimates of spatial distributions.

Risso's dolphin, Grampus griseus. *Photo credit: NOAA NMFS/ SWFSC*

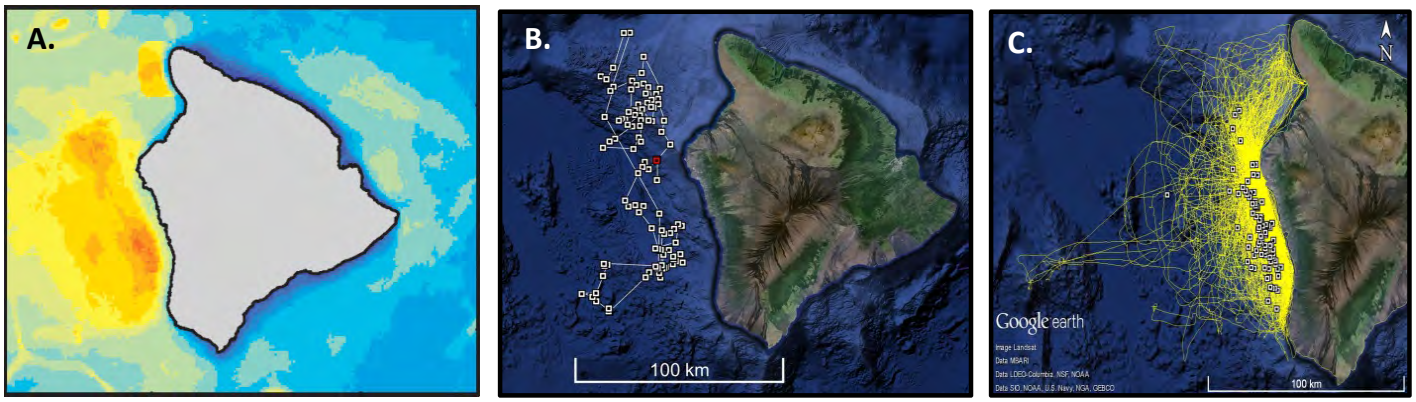

Figure 6.23. Pantropical spotted dolphin space use patterns off the island of Hawai'i. a) Predictive map of spotted dolphin relative abundance distribution in summer months; b) One individual spotted dolphin movement track from satellite telemetry over 11 days in April and May 2015 (from Baird, 2016); c) Survey tracks of Cascadia Research Collective (yellow lines) and spotted dolphin sightings (white squares). Data shown in panels B and C are from Cascadia Research Collective.

6.2. HAWAIIAN MONK SEAL (*Neomonachus schauinslandi*)

6.2.1. Introduction

This section of the marine mammal chapter provides background information on the cultural significance of Hawaiian monk seals (*Neomonachus schauinslandi*), and their biology, behavior, population ecology and conservation status. We then present data on the distribution of monk seals around the MHI and some examples of movement patterns of individual seals. The data and associated methods are described in detail followed by interpretation of spatial patterns. We map the locations of monk seals recorded in a NOAA sighting database, which includes public sightings and scientific survey data. We present maps of individual seal movements from tracking studies. Critical habitat maps developed to meet requirements of the Endangered Species Act identify important terrestrial and at-sea areas used by monk seals. The ESA critical habitat maps are based on a synthesis of the best-available information on the distribution of monk seals. Data gaps are highlighted and evaluated to inform future data collection strategies.

Hawaiian monk seal, Neomonachus schauinslandi*. Photo credit: NOAA*

The Hawaiian monk seal, Hawaiian language name ‘ilio holo i ka uaua (dog that runs in rough waters), is the only native pinniped in Hawaiian waters. Monk seals are mentioned in Hawaiian traditional literature and oral histories and have been associated with the god Lono and Kū, and referenced in many geographical place names (Pūkui et al., 1974; Kittinger et al., 2011).

The Hawaiian monk seal is one of the world’s most endangered mammals, designated as ‘depleted’ under the Marine Mammal Protection Act in 1972, and then listed as an Endangered Species under the U.S. Endangered Species Act (41 FR 51611; November 23, 1976). A high magnitude of threat, high recovery potential and rapid decline that has persisted for over 20 years resulted in the species receiving highest priority in the Recovery Priority Guidelines (55 FR 24296, June 15, 1990). The extinction of the Caribbean monk seal (*Neomonachus tropicalis*) in the 1950s, due to decades of unrestricted hunting, has resulted in the Hawaiian monk seal becoming the last remaining species of its genus (McClenachan and Cooper, 2008; Scheel et al., 2014).

Hawaiian monk seal. Photo credit: NOAA

The maximum age for the species is thought to be 25-30 years, with females reaching reproductive age at between 5 and 10 years of age. Adult monk seals reach lengths of 2.3 m and weigh up to 273 kg. Monk seals occur throughout the Hawaiian archipelago, with most residing in the NWHI and a smaller portion in the MHI (Baker and Johanos, 2004). Monk seal births have been documented in all months of the year (NOAA NMFS, unpublished data), but are most common between February and August, peaking in March and April (Johanos et al., 1994).

Hawaiian monk seals feed on a wide variety of prey, primarily benthic species (including eels and flatfish), crustaceans (lobster, crab, shrimp) and molluscs (octopus; Kenyon and Rice, 1959). Fecal and regurgitate samples collected across the NWHI and MHI revealed a diet that was little different between regions and comprised of fish (78-97%), followed by cephalopods (11-16%) and crustaceans (1-6%; Goodman-Lowe et al., 1998; Cahoon et al., 2013; NOAA NMFS, unpublished data). Telemetry tracking of seal foraging movements has shown that most foraging occurs in waters less than 100 m depth, with occasional excursions to deeper water foraging grounds beyond 300 meters depth (Parrish et al., 2002; Cahoon, 2011; NOAA NMFS, 2014).

Hawaiian monk seals are a wide-ranging species, with some individuals recorded to have travelled distances equivalent to the entire length of the Hawaiian archipelago, although this scale of movement is considered rare, with most seals foraging in shallow waters close to haul-out sites. Underwater observations have shown that seals rest in shallow tidal areas and sleep in underwater ledges close to shore (Wilson, 2015).

Monk seals commonly swim between neighboring islands. Analyses of re-sightings of tagged seals from 1981 to 2011 have shown that seals also travel between the NWHI and the MHI. Johanos et al. (2015) reported 10 seals from a total of 373 individuals making 14 trips between the NWHI, MHI and Johnston Atoll. Two percent of seals observed on Nihoa were also seen in the MHI at least 250 km away. The majority of movements are between locations less than 100 km apart, with comparatively very few movements between locations greater than 400 km apart.

The biogeographic range of the Hawaiian monk seal includes the entire Hawaiian Archipelago and Johnston Atoll. In 2000, the estimated minimum population of monk seal in the MHI was 45, increasing to 52 in 2001 (Baker and Johanos, 2004), 77 individuals in 2005 (NOAA NMFS, 2007) and an estimated minimum of 146 seals in 2011 (Carretta et al., 2013; Baker et al., 2011). Estimated survival from weaning to age 1 year is 77 percent in the MHI, compared with recent NWHI estimates ranging from 42-57 percent (Baker et al., 2011). Furthermore, females begin reproducing at a younger age and attain higher birth rates in the MHI than observed in the NWHI (Baker et al., 2011). As such, the establishment of reproductively sustainable seal subpopulations in the MHI is thought to provide an important role in the recovery of species and reduction of extinction risk (Ragen, 2003). Recovery strategies have focused on protection of vulnerable young female seals to increase the proportion of females surviving to reproductive maturity (NOAA NMFS, 2007). Low genetic variability across the population is an additional risk factor for the long term viability of the species (Kretzmann et al., 1997; Shultz et al., 2009).

Across its range, Hawaiian monk seal abundance has declined 60 percent in the last 40 years and continues to decline at an estimated rate of 3.4 percent per year for the NWHI population (Caretta, 2013), with the current population size at approximately 1,100 individuals. In the MHI, however, the species has been described as recolonizing, and the population growth rate was estimated to be about 7 percent per year in 2008 (Baker et al., 2011), yet it is this segment of the population that is most threatened by direct anthropogenic impacts (Watson et al., 2011).

Female monk seal with pup. Photo credit: NOAA

Female monk seals are also increasingly pupping on popular recreational beaches. These “pupping events” entail mother-pup pairs remaining on the beach to nurse for up to 7 weeks, during which time they are particularly vulnerable to human disturbance. The species is threatened by multiple human stressors, including intentional killing, entanglement in fishing gear, competition with fisheries for food, loss and disturbance of coastal habitats, ocean pollution, collision with vessels, and emerging diseases (NOAA NMFS, 2007; Lowry and Aguilar, 2008). Predicted sea level rise is expected to gradually reduce the availability of breeding locations at the lowest elevation atolls during the next 100 years (Baker et al., 2006). One of the greatest recent constraints to population growth is thought to be food limitation due to its negative impact on the survival of juvenile seals, age of sexual maturity, and fecundity. At one location, French Frigate Shoals in the NWHI, predation of pups by sharks has reduced the sub-population dramatically (Gobush and Farry, 2012).

Marine Mammals

Under the Endangered Species Act (ESA), federal agencies have a legal mandate to promote the recovery of endangered species. Specific agencies with marine and wildlife management duties support implementation of the ESA as specified in the Monk Seal Recovery Plan, including U.S. Fish and Wildlife Service (USFWS), NOAA National Ocean Service (NOS), Hawai'i Department of Land and Natural Resources (DLNR), U.S. Coast Guard and the U.S. Navy. NOAA NMFS Pacific Islands Regional Office (PIRO) is responsible for coordination of the implementation of the Main Hawaiian Islands Monk Seal Recovery Plan (released January 2016) through the Marine Mammal Branch of the Protected Resources Division. NOAA NMFS's Office of Law Enforcement-Pacific Division (OLE-PD) investigates illegal acts against seals and pursues legitimate cases in partnership with the State Division of Conservation and Resources Enforcement (DOCARE) within DLNR. State agencies have responsibilities under state law, specifically the Hawai'i Endangered Species Act to protect monk seals (Chapter 195 D-4 Endangered species and threatened species). For the State, jurisdiction over monk seal protection is with the Marine Wildlife Program (MWP) of the Division of Aquatic Resources in the DLNR. Research and monitoring, as well as rescue and rehabilitation of injured seals, is led by the Protected Species Division of NOAA NMFS Pacific Island Fisheries Science Center (PIFSC).

Hawaiian monk seal. Photo credit: Mark Sullivan (NOAA NMFS/ PIFSC/PRD)

Studies on the behavioral response of seals to marine infrastructure, such as renewable energy installations, are rare. A recent tracking study of harbor and grey seals in the North Sea, in Europe, however, showed that infrastructure, including wind turbines and pipelines, influenced the foraging patterns of individual seals (Russell et al., 2014). Some seals concentrated their activity at individual turbines and individuals were found to move along pipelines. Based on very few studies, the impact of wind farms on seals is thought to be a positive influence on abundance due to an increase in food and reduced risk of mortality from bycatch (Hammar et al., 2016).

6.2.2. Methods

Individual monk seal tracking data

Global positioning system (GPS) location points for 19 individual monk seals were provided by PIFSC and Duke University from cell phone telemetry studies conducted between 2007 and 2014 (Littnan and Wilson, 2015). These data included data logger information on time spent at the surface and out of water, as well as dive depths and duration. Data on animal behavior are stored for up to six months and transmitted via the cell phone network (Wilson, 2015). When at the surface, the tags were programmed to record a GPS position (< 30 m accuracy) every 20 minutes. Fifteen male and four female monk seals were tracked. Monk seal tracks were mapped by creating lines between the location points. In addition, location point density was mapped as a simple way of representing the intensity of space use across a grid of cells (1.2x1.2 km) for all tracked seals combined.

Monk seal location data (NOAA PIFSC)

PIFSC provided our Biogeographic Assessment with a dataset composed of monk seal location data from various sources, including opportunistic sightings, tagged seal locations and sightings from aerial surveys (Littnan and Maison, 2015). These data were gridded as the sum of seal locations in 5 km cells surrounding all major land masses of the MHI (2007-2011). This dataset includes many opportunistic sightings collected through the public sightings hotline and observer programs (http://www.pifsc.noaa.gov/hawaiian_monk_seal/sightings.php). These data have some inherent bias due to some sites having greater access to the public than others, yet offer

benefit by providing seal locations across a broad geographical area. For instance, absence of sightings could be related to poor accessibility or low reporting. The bias is difficult to correct and therefore spatial uncertainty is not easily mapped when visualizing the spatial distribution of seal abundance. In some cases, it is likely that the data also include multiple sightings for the same seal at the same time and place. However, due to their broad geographical coverage and richness of observations, the data are a valuable and important source of information and contributed to the delineation of critical habitat. NMFS researchers carefully evaluated the data to identify significant haul-out areas to inform the critical habitat mapping process. Comparisons among the individual sources of data demonstrated that the voluntary sighting data successfully identified areas used by monk seals, and provide a reliable dataset for identifying significant haul-out areas. Since point locations provided insufficient spatial resolution to encompass space use for highly mobile animals, a pragmatic solution was to group sightings into 5 km grid cells over each island to create a standardized grid. Seal location data were binned into grid cells along the coast of each island, and counts within coastal grids were then evaluated to determine frequency of monk seal use within these squares. Areas of significance were defined as those coastal grid cells where the count equaled 10 percent or more of the grid cell with the highest count value for each island. This description of significant haul-out areas allows stretches of coastline used contiguously by monk seals to be included in the description of essential features, accommodates for data that may be underrepresented in frequency due to a lower likelihood of reporting, and in areas with lower seal numbers provides adequate habitat for monk seals to use as the population expands (NOAA NMFS, 2014).

In addition to the 5 km grid of seal locations, here we have provided the same spatial grid, but with the data reduced to presence only data. Where the 5 km cell contains one or more seal sightings, or has been visited by a tracked seal, then it receives a value of 1 to indicate that the site has been used by the species. If no location data were available then the cell received a value of zero to indicate absence of use. This simplification of the data presents a rapid visualization of confirmed seal habitat use patterns around the coastline and nearshore waters of MHI.

Monk seal critical habitat maps

Hawaiian monk seal scratching nose. Photo credit: NOAA NMFS/PIFSC/PRD

Critical habitat is defined in Section 3 of the ESA, and refers to areas that contain habitat features that are essential for the survival and recovery of a listed species, and which may require special management considerations or protections. Critical habitat areas may include: areas occupied by the species; an area that the species is not currently using, but will need to use for its population to grow and recover; and special management, like protection from development. To map critical habitat, NMFS experts used the best scientific data and knowledge available to identify habitat features essential to the conservation of the species, delineate specific areas within the geographical area occupied which contain at least one essential habitat feature, including those features that support resting, reproduction, molting, predator avoidance, and foraging. Areas of proposed terrestrial critical habitat within the MHI were delineated by including all significant haul-out areas and preferred pupping and nursing sites within the designation (Figure 6.24; NOAA NMFS, 2015). The end points for the stretches of coastline were identified by using haul-out data, pupping and nursing data, natural geographic features, and/or hardened shorelines which lack the features of monk seal critical habitat (80 FR 50925; Federal Register, 2015b).

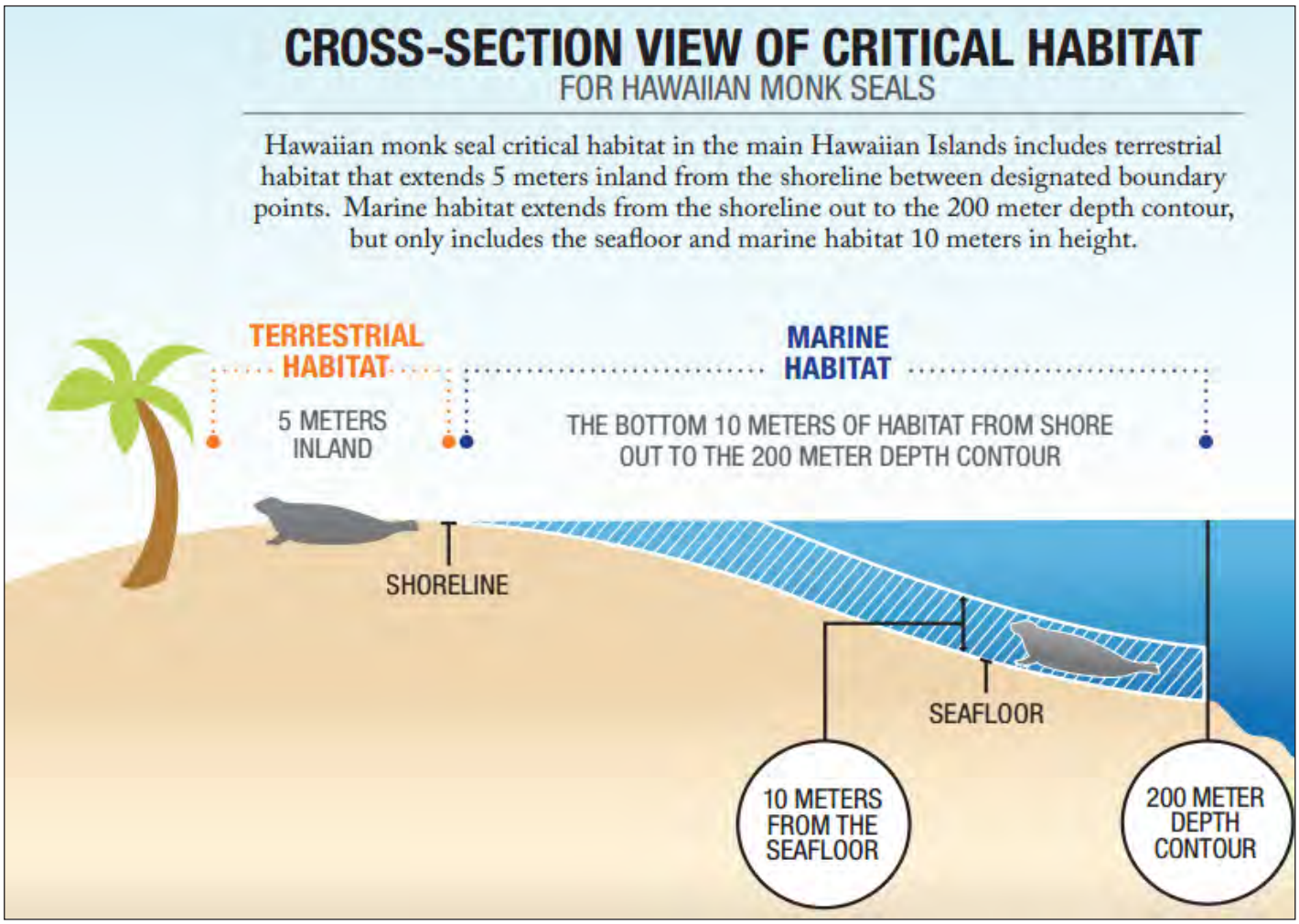

Figure 6.24. Infographic explaining the marine and terrestrial critical habitat dimensions (NMFS, 2014).

6.2.3. Results and Discussion

Key space use patterns

Monk seals have been sighted around all major islands of the MHI (leeward and windward sides; Figure 6.28). Haul-out sites are located on all MHI, but more sites were identified on the westernmost islands that are closest to the NWHI, where most monk seals reside. For example, eight haul out and pupping sites were known to experts on Kaua'i, but only three on Hawai'i. Examination of geographical patterns in the movement data revealed a high frequency of alongshore movements within a single island, but also high connectivity between neighboring islands (Figure 6.25). For instance, the telemetry data highlight the importance of Penguin Bank to monk seals which are known to forage over the shallow sandy banks (Figure 6.26). Although most seal movements are confined to State waters, one individual travelled across the EEZ into international waters and then returned to the MHI.

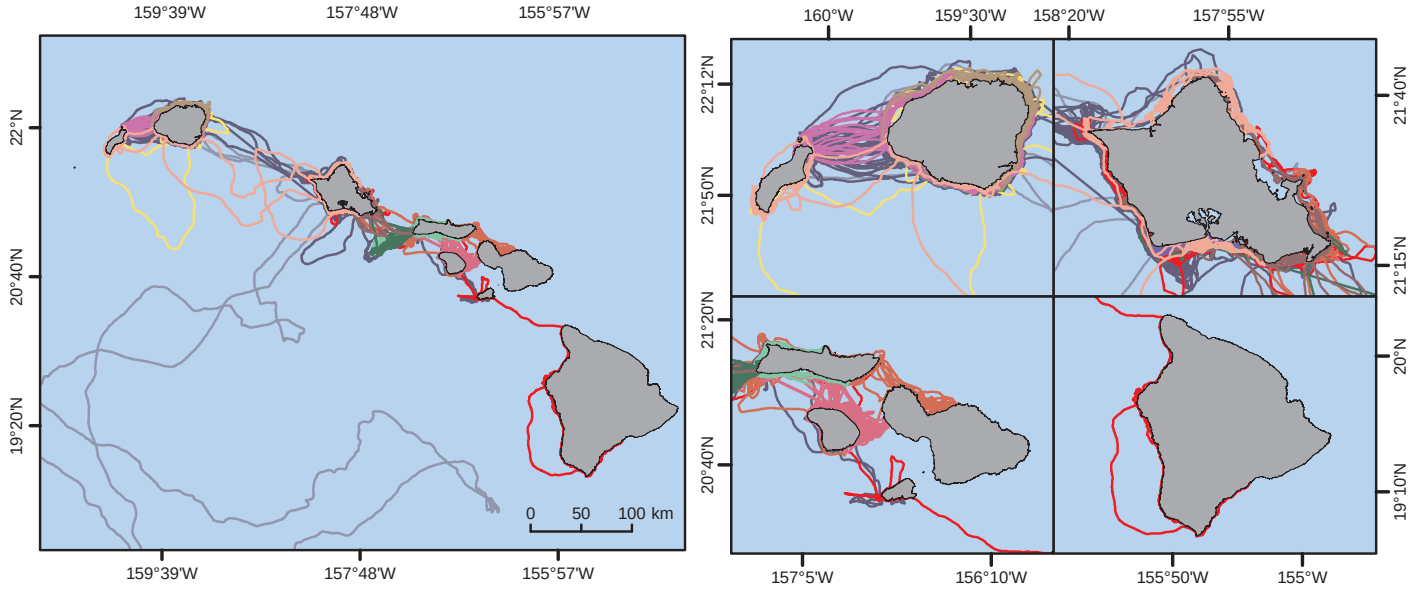

*Figure 6.25. Track lines for individual Hawaiian monk seal (*Monachus schauinslandi*) during the period 2007 to 2014. Movement pathways for individual monk seals tagged with GPS/cell phone transmitters across MHI between 2007 and 2014 (left) and by island group from western islands to eastern islands (right; top - Niʻihau and Kauaʻi, and Oʻahu; bottom - Molokaʻi, Lānaʻi, Maui and Kahoʻolawe, and Hawaiʻi). Data source: NOAA NMFS/PIFSC*

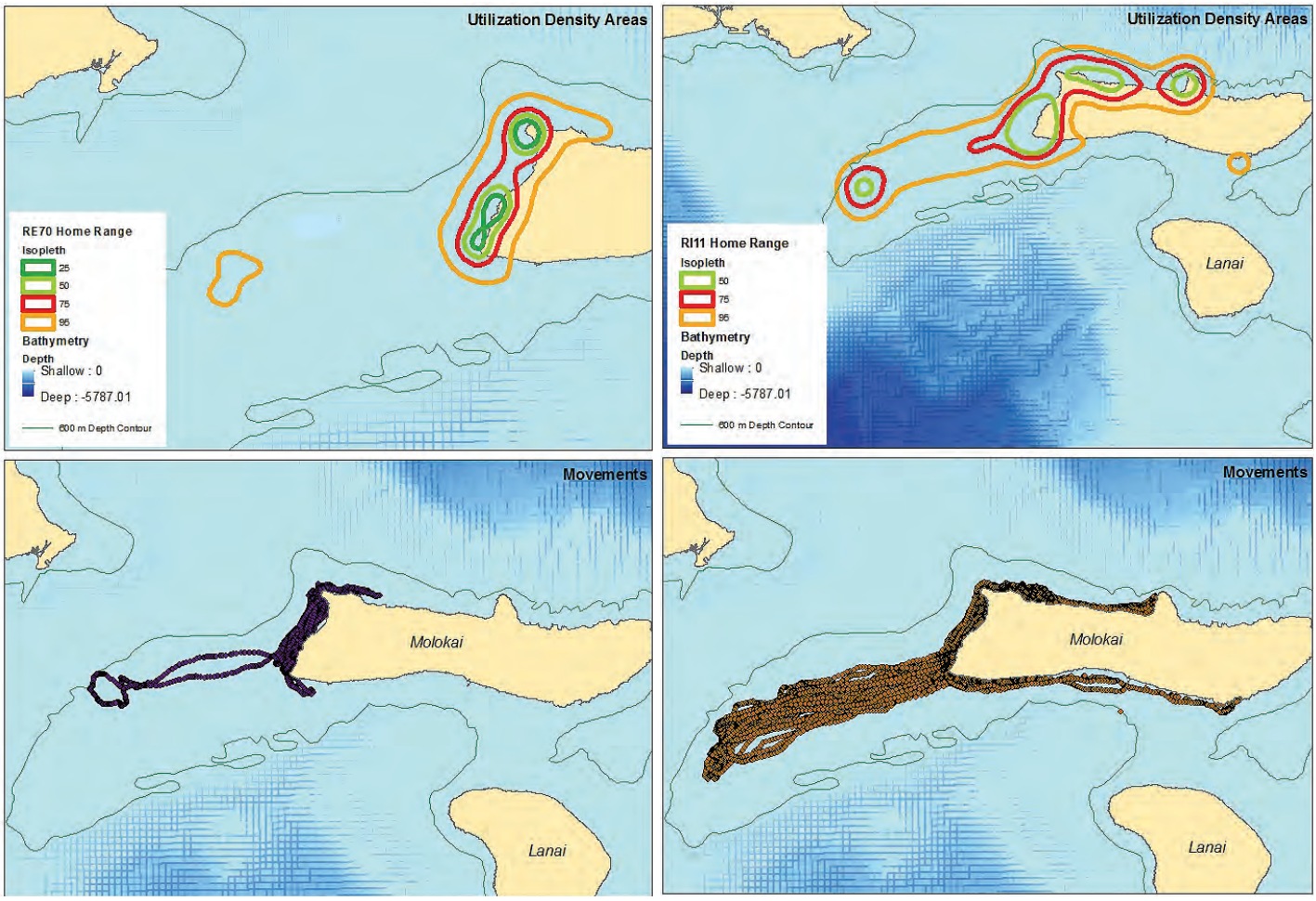

Figure 6.26. Movement tracks and space-use patterns of individual monk seals (id: RE70 and RI11) from Molokaʻi, and the high use area of Penguin Bank, an important foraging area for Hawaiian monk seals. Data source: Wilson, 2014

Marine Mammals

Individual monk seal tracking data

On average, monk seals spent 51.1 percent of their day diving, 19.6 percent at the surface, and 29.3 percent of the day hauled-out on land (Wilson, 2015). Analyses of these data by Wilson (2015) revealed two distinct movement modes: near shore and offshore/inter-island movements (Wilson, 2015). Wilson (2015) provides the following description: "There was a high level of individual variation in the movements of monk seals, but general descriptions of their behavior were accurate at the population level. On average, foraging trips lasted 0.81 ± 1.38 days and seals traveled 28.5 ± 82.0 km per trip. Most seals began benthic dives shortly after entering the water, with most dives occurring between 20 to 40 m. The median home range and core area size for seals in the MHI was 265.6 km² and 1,564.6 km², respectively". Maps of the density of location points for multiple individual seals indicate that some high-use areas exist and are shown in warmest colors (i.e., red cells were the highest use areas and blue the lowest; Figure 6.27). This simple snapshot of space use includes inherent bias, for example, seals were tracked for different durations and location data were not necessarily regular in time.

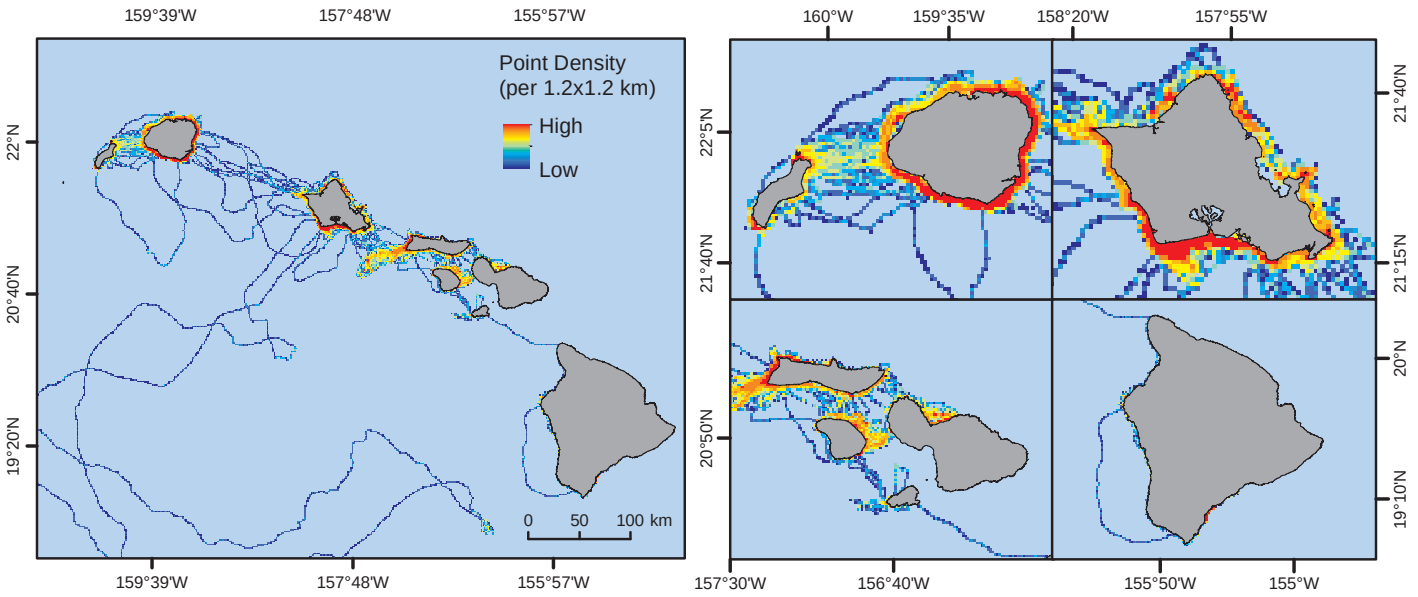

Figure 6.27. Density of location points for individual Hawaiian monk seal tracked between 2007 and 2014. Maps showing the total density of location points recorded from all tagged seals within each 1.2x1.2 km grid cells across the project area (left) and by island group from western islands to eastern islands (right; top - Niʻihau and Kauaʻi, and Oʻahu; bottom - Molokaʻi, Lānaʻi, Maui and Kahoʻolaw, and Hawaiʻi). Data source: NOAA NMFS/PIFSC

Distribution of monk seal sighting locations

The proportion of coastline with at least one seal located decreases from west to southeast across the MHI (Figure 6.28). Around Niʻihau, the most western of the MHI, 15 (of 17) of the 5 km cells had seal presence recorded between 2007 and 2009. Only two cells that intersect the coastline have no seals recorded, resulting in an almost entire coastline with seal presence. Kauaʻi had 37 (of 40) 5 km cells with seal presence recorded between 2007 and 2010 covering almost all of the cells that intersect the coastline. The continuous coastal use patterns displayed at Kauaʻi were only separated by three coastal cells where no seals have been recorded. Given that monk seals are highly mobile, it is highly unlikely that the cells with no sightings represent true absence. The coasts of Niʻihau and Kauaʻi are dominated by sand and rocky beaches providing suitable haul-out sites for seals. Oʻahu showed 46 (of 57) 5 km cells with seal presence recorded between 2007 and 2010, with 11 cells that intersect the coastline having no presence recorded. Regardless, seal presence cells form an almost continuous area surrounding the entire island. No sightings were recorded for cells covering the inner Pearl Harbor, Oʻahu-Keehi Lagoon and the lagoon adjacent Kahaluʻu – embayment areas with a high proportion of wetlands and artificial structure (NOAA ORR, 2001) unsuitable or providing low quality as haul-out sites.

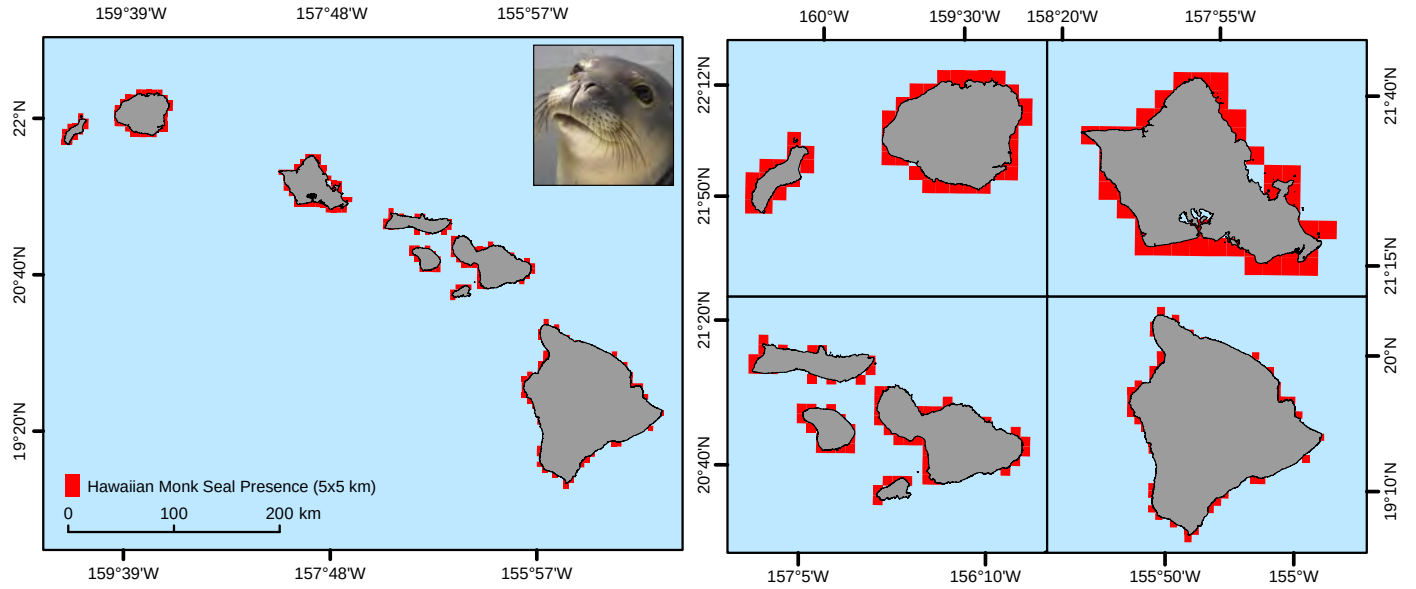

Figure 6.28. Areas used by Hawaiian monk seal. Presence of seals within 5 km cells across MHI (left) and by island group from western islands to eastern islands (right; top - Niʻihau and Kauaʻi, and Oʻahu; bottom - Molokaʻi, Lānaʻi, Maui and Kahoʻolawe, and Hawaiʻi). Data source: NOAA NMFS/PIFSC

Molokaʻi had 15 (of 35) 5 km cells with seal presence recorded between 2007 and 2009, and 20 cells having no recorded presence. Presence was generally associated with the areas where sand and rocky shorelines dominated the coast, particularly on exposed rocky shores at the east and west ends of the island. However, with a gradual eastward expansion of the growing MHI Hawaiian monk seal population, it is likely that more sightings have been recorded there since 2009. It is also important to note that data were not adjusted for sightability relative to coastal relief. That is, cells were not excluded from the mapped data where monk seals were unlikely to be seen because of hardened shoreline, sheer cliffs or other factors that would prevent hauling out, and where shorelines are inaccessible to people resulting in no sightings.

Lanaʻi had 13 (of 18) 5 km cells with seal presence recorded between 2007 and 2011, with five cells intersecting the coastline which showed no recorded seal presence. Kahoʻolawe had only half of its coastal cells with seal presence recorded between 2007 and 2010, with five coastal cells having no recorded seal presence. Location data for Maui showed that 25 (of 45) 5 km cells have seal presence recorded between 2007 and 2010, with 20 cells intersecting the coastline that showed no seal presence. Cells without sightings co-occurred with exposed rocky shores on the south and east coast of Maui. For the island of Hawaiʻi, the farthest east in the archipelago, 55 (of 118) 5 km cells had seal presence recorded between 2007 and 2010, with more than half of the coastal cells (63 cells) with no recorded seal presence. A gap in presence was noted on the exposed rocky shores on the northeast coast.

Critical habitat maps

Marine areas of critical habitat include a 10 m deep band along the seafloor from shore out to 200 m from shore (Figure 6.24), where the majority of monk seal foraging is known to occur. Specific areas designated include 16 areas within the range of the Hawaiian monk seal, six of which are in the MHI. These areas contain one or a combination of the features essential to seal conservation, including: preferred pupping and nursing areas, significant haul-out areas, and marine foraging areas out to 200 m in depth. In the MHI, monk seal critical habitat includes the seafloor and marine habitat to 10 m above the seafloor from the 200 m depth contour through the shoreline and extending into terrestrial habitat 5 m inland from the shoreline between identified boundary points around the following islands: Kaʻula Island (includes marine habitat only); Niʻihau (includes marine habitat from 10-200 m in depth; Kauaʻi; Oʻahu; Maui Nui (including Kahoʻolawe, Lānaʻi, Maui, and Molokaʻi); Hawaiʻi (Figure 6.29). Boundary coordinates for designated areas are provided here.

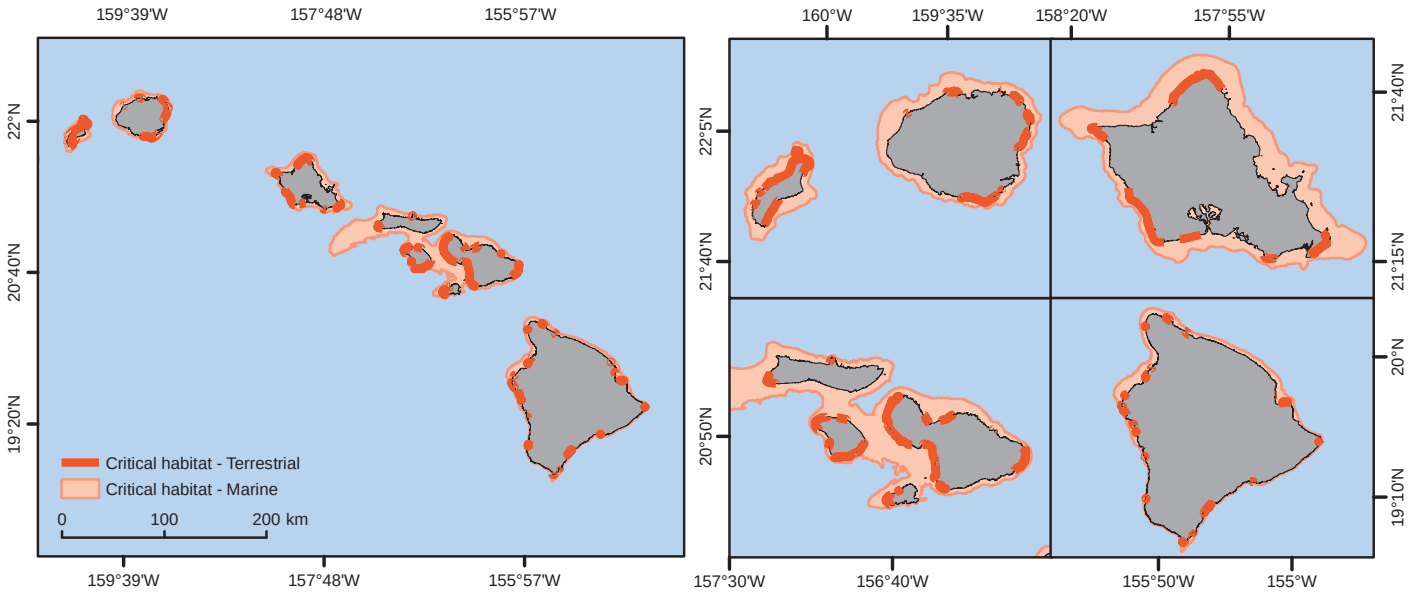

Figure 6.29. Areas used by Hawaiian monk seal. Maps showing terrestrial and marine critical habitat designations for Hawaiian monk seal across MHI (left) and by island group from western islands to eastern islands (right; top - Niʻihau and Kauaʻi, and Oʻahu; bottom - Molokaʻi, Lānaʻi, Maui and Kahoʻolawe, and Hawaiʻi). Data source: NOAA NMFS/PIFSC

Section 4(b)(2) of the ESA requires consideration of economic impacts, impacts to national security, and any other relevant impacts of designation prior to designating any area as critical habitat. As such, several military facilities are excluded from designation as critical habitat (NOAA NMFS, 2015b). In addition, cliffs and manmade shorelines and structures in existence are not included in the designation because these areas do not meet the definition of critical habitat. Examples of manmade shorelines include docks, seawalls, piers, fishponds, roads, pipelines, boat ramps, platforms, buildings, ramparts and pilings. More details on the designations can be found in 'Revision of Critical Habitat for Hawaiian Monk Seals' (NOAA NMFS, 2015b).

6.2.4. Data Limitations and Information Gaps

Expansion of the distribution of Hawaiian monk seals across the MHI is a dynamic process which will require continual monitoring to determine the need for expansion of the critical habitat beyond those mapped areas presented here. Some features are known as foraging grounds (i.e., Penguin Bank), but a more complete geographical knowledge of areas important for foraging is needed across the entire MHI region. Telemetry combined with devices that record pressure, temperature, heart rate and video observations of prey will provide the necessary data to better understand foraging and resting activities. Where detailed data on seal behavior are available, in most cases, geographic/habitat/prey availability data are missing or have been sampled at a scale that is not compatible with the fine scale movements of monk seals. Detailed prey and habitat surveys throughout the MHI would be useful for modeling foraging with telemetry and biologging instruments. Furthermore, the telemetry dataset is biased towards males and juvenile animals. Due to a conservative sampling regime, potentially pregnant females are not handled for these studies. The ecology and habitat use of females may be different from other age-sex classes and should be a focus of study in the future. Tracking data also demonstrate that some individuals will undertake extensive excursions into deep waters considerable distance from the islands. Very little is known about the importance of deeper water areas to the recovering seal population. The absence of information about the potential response of monk seals to artificial structure and coastal development is another major knowledge gap. Continued reporting of sightings and telemetry will provide the necessary data to understand seal responses through mapping of space use patterns.

Shifts in foraging habitat use may occur in more densely populated areas. For instance, as the population of seals continues to grow on Kauaʻi and Oʻahu, resident seals may forage further afield or use deeper areas to search for prey resources. This could change diet, foraging success, and habitat use and should be a focus of future research. With particular relevance to the present project is a need for more information to understand the potential impacts of wind turbine construction (i.e., noise) and operation (i.e., introduction of subsurface structure) on monk seal behavior, foraging and distributions. A review of noise impacts from construction and operation of wind farms in Europe concluded that the disturbance to marine mammals is more severe during the construction of wind farms than during their operation (Madsen et al., 2006). More research is needed to assess the potential impacts to Hawaiian monk seals of noise from wind farm construction and operation.

ACKNOWLEDGEMENTS

The NOAA NMFS cetacean sighting surveys were funded by the NOAA's Southwest Fisheries Science Center and Pacific Islands Fisheries Science Center. We thank the many observers, cruise leaders, cruise coordinators, officers, and crew, who dedicated many months of hard work collecting the data. NOAA surveys were conducted under NMFS Permit Nos. 774-1437 and 14097 and State of Hawaiʻi Permit SH2002-11. We thank Amanda Bradford for assistance interpreting the NOAA survey data. Aerial surveys conducted by Joseph Mobley of University of Hawaiʻi at Mānoa were funded as follows: 1993-98 funded as part of the Acoustic Thermometry of Ocean Climate, Marine Mammal Research Program (ATOC, MMRP) funded by the Strategic Environmental Research and Development Program through the Advanced Research Projects Agency (ARPA; Grant MDA972- 93-1-003); 2000-03 funded by the Office of Naval Research (ONR) (Award #N000140210841). We thank Jason Baker for helpful comments that improved the monk seal section. James Bowcott (PML) and NEODAAS assisted with the processing of ocean front metrics. Peter Miller was funded by PML Core Research Programme. Government contract labor (SJP, AJW, MP, and JBL) was provided by CSS-Dynamac, Inc. under NOAA contract EA-133C-14-NC-1384.

LITERATURE CITED

Abecassis, M., J. Polovina, R.W. Baird, A. Copeland, J.C. Drazen, R. Domokos, Oleson E., Y. Jia, G.S. Schorr, D.L. Webster, and R.D. Andrews. 2015. Characterizing a foraging hotspot for short-finned pilot whales and Blainville's beaked whales located off the west side of Hawai'i Island by using tagging and oceanographic data. PLoS ONE 10: 1-22.

Albertson, G.R. 2014. Worldwide phylogeography and local population structure of the rough-toothed dolphin (*Steno bredanensis*). PhD dissertation. Oregon State University. Corvallis, OR. 160 pp.

Andrews, K.R., L. Karczmarski, W.W.L. Au, S.H. Rickards, C.A. Vanderlip, B.W. Bowen, E.G. Grau, and R.J. Toonen. 2010. Rolling stones and stable homes: social structure, habitat diversity and population genetics of the Hawaiian spinner dolphin (*Stenella longirostris*). Molecular Ecology 19:732-748.

Aschettino, J.M., R.W. Baird, D.J. McSweeney, D.L. Webster, G.S. Schorr, J.L. Huggins, K.K. Martien, S.D. Mahaffy, and K.L. West. 2012. Population structure of melon-headed whales (*Peponocephala electra*) in the Hawaiian Archipelago: Evidence of multiple populations based on photo identification. Marine Mammal Science 28(4): 666-689.

Au, W.W.L., G. Giorli, J. Chen, A. Copeland, M.O. Lammers, M. Richlen, S. Jarvis, R. Morrissey, and D. Moretti, 2014. Presence and seasonal variation of deep diving foraging odontocetes around Kaua'i, Hawai'i using remote autonomous acoustic recorders. The Journal of the Acoustical Society of America 135(1): 521-530.

Baird, R.W., D.L. Webster, S.D. Mahaffy, D.J. McSweeney, G.S. Schorr, and A.D. Ligon. 2008a. Site fidelity and association patterns in a deep-water dolphin: Rough-toothed dolphins (*Steno bredanensis*) in the Hawaiian Archipelago. Marine Mammal Science 24: 535-553.

Baird, R.W., A.M. Gorgone, D.J. McSweeney, D.L. Webster, D.R. Salden, M.H. Deakos, A.D. Ligon, G.S. Schorr, J. Barlow, and S.D. Mahaffy. 2008b. False killer whales (*Pseudorca crassidens*) around the main Hawaiian Islands: Long-term site fidelity, inter-island movements, and association patterns. Marine Mammal Science 24: 591–612.

Baird, R.W., G.S. Schorr, D.L. Webster, D.J. McSweeney, A.M. Gorgone, and S.J. Chivers. 2008c. A survey to assess overlap of insular and offshore false killer whales (*Pseudorca crassidens*) off the island of Hawai'i. Report prepared under Order No. AB133F07SE4484 for the Pacific Islands Fisheries Science Center, National Marine Fisheries Service. Honolulu, HI. Cascadia Research Collective. Olympia, WA.

Baird, R.W. 2009. A review of false killer whales in Hawaiian waters: biology, status, and risk factors. Report prepared for the U.S. Marine Mammal Commission under Order No. E40475499. Cascadia Research Collective. Olympia, WA. 40 pp.

Baird. R.W., A.M. Gorgone, D.J. McSweeney, A.D. Ligon, M.H. Deakos, D.L. Webster, G.S. Schorr, K.K. Martien, D.R. Salden, and S.D. Mahaffy. 2009a. Population structure of island-associated dolphins: Evidence from photo-identification of common bottlenose dolphins (*Tursiops truncatus*) in the main Hawaiian Islands. Marine Mammal Science 25: 251-274.

Baird, R.W., G.S. Schorr, D.L. Webster, S.D. Mahaffy, D.J. McSweeney, M.B. Hanson, and R.D. Andrews. 2009b. Movements of satellite-tagged Cuvier's and Blainville's beaked whales in Hawai'i: Evidence for an offshore population of Blainville's beaked whales. Report prepared under contract no. AB133F-08-SE-4534 to Cascadia Research Collective, Olympia, WA from the Southwest Fisheries Science Center, National Marine Fisheries Service. La Jolla, CA.

Baird, R.W., G.S. Schorr, D.L. Webster, D.J. McSweeney, M.B. Hanson, and R.D. Andrews. 2010. Movements and habitat use of satellite-tagged false killer whales around the main Hawaiian Islands. Endangered Species Research 10: 107-121.

Baird, R.W., G.S. Schorr, D.L. Webster, S.D. Mahaffy, D.J. McSweeney, M.B. Hanson, and R.D. Andrews. 2011a. Open-ocean movements of a satellite-tagged Blainville's beaked whale (*Mesoplodon densirostris*): Evidence for an offshore population in Hawai'i. Aquatic Mammals 37(4): 506-511.

Baird, R.W., G.S. Schorr, D.L. Webster, D.J. McSweeney, M.B. Hanson, and R.D. Andrews. 2011b. Movements of two satellite-tagged pygmy killer whales (*Feresa attenuata*) off the island of Hawai'i. Marine Mammal Science 27(4): E332-E337.

Baird, R.W., M.B. Hanson, G.S. Schorr, D.L. Webster, D.J. McSweeney, A.M. Gorgone, S.D. Mahaffy, D.M. Holzer, E.M. Oleson, and R.D. Andrews. 2012a. Range and primary habitats of Hawaiian insular false killer whales: informing determination of critical habitat. Endangered Species Research 18: 47-61.

Baird, R.W., D.L. Webster, G.S. Schorr, J.M. Aschettino, A.M. Gorgone, and S.D. Mahaffy. 2012b. Movements and spatial use of odontocetes in the western main Hawaiian Islands: results from satellite-tagging and photo-identification off Kaua'i and Ni'ihau in July/August 2011. Annual progress report under Grand No. N00244-10-1-0048. Cascadia Research Collective and NOAA National Marine Fisheries Service, Southeast Fisheries Science Center. 20 pp.

Baird, R.W., D.L. Webster, J.M. Aschettino, G.S. Schorr, and D.J. McSweeney. 2013a. Odontocete cetaceans around the main Hawaiian Islands: Habitat use and relative abundance from small-boat sighting surveys. Aquatic Mammals 39:253-269.

Baird, R.W., E.M. Oleson, J. Barlow, A.D. Ligon, A.M. Gorgone, and S.D. Mahaffy. 2013b. Evidence of an island-associated population of false killer whales (*Pseudorca crassidens*) in the Northwestern Hawaiian Islands. Pacific Science 67(4): 513-521.

Baird, R.W., D. Cholewiak, D.L. Webster, G.S. Schorr, S.D. Mahaffy, C. Curtice, J. Harrison, and S.M. Van Parijs. 2015. Biologically important areas for cetaceans within U.S. waters - Hawai'i region. Aquatic Mammals 41: 54-64.

Baird, R.W. 2016. The lives of Hawai'i's dolphins and whales: natural history and conservation. University of Hawai'i Press. 304 pp.

Baker, J.D. and T.C. Johanos. 2004. Abundance of the Hawaiian monk seal in the main Hawaiian Islands. Biological Conservation 116: 103-110.

Baker, J.D., C.L. Littnan, and D.W. Johnston. 2006. Potential effects of sea level rise on terrestrial habitats of endangered and endemic megafauna of the Northwestern Hawaiian Islands. Endangered Species Research 4: 1-10.

Baker, J.D., A.L. Harting, T.A. Wurth, and T.C. Johanos. 2011. Dramatic shifts in Hawaiian monk seal distribution predicted from divergent regional trends. Marine Mammal Science 27(1): 78-93.

Barlow, J. 2006. Cetacean abundance in Hawaiian waters estimated from a summer/fall survey in 2002. Marine Mammal Science 22: 446-464.

Barlow, J., J. Calambokidis, E.A. Falcone, C.S. Baker, A.M. Burdin, P.J. Clapham, J.K.B. Ford, C.M. Gabriele, R. LeDuc, D.K. Mattila, T.J. Quinn II, L. Rojas-Bracho, J.M. Straley, B.L. Taylor, , R. Urbán, P. Wade, D. Weller, B.H. Witteveen, and M. Yamaguchi. 2011. Humpback whale abundance in the North Pacific estimated by photographic capture-recapture with bias correction from simulation studies. Marine Mammal Science 27: 793-818.

Battista, T.A., B.M. Costa, and S.M. Anderson. 2007. Benthic Habitats of the Main Hawaiian. NOAA Technical Memorandum NOS NCCOS CCMA 152. Silver Spring, MD. 48 pp. Data Downloaded 5 September 2014. Data Website: https://products.coastalscience.noaa.gov/collections/benthic/e97hawaii/data2007.aspx (Site Accessed 8 June 2016).

Baumann-Pickering, S., A.E. Simonis, E.M. Oleson, R.W. Baird, M.A. Roch, and S.W. Wiggins. 2015. False killer whale and short-finned pilot whale acoustic identification. Endangered Species Research 28: 97-108.

Becker, E.A., K.A. Forney, D.G. Foley, and J. Barlow. 2012. Density and spatial distribution patterns of cetaceans in the central North Pacific based on habitat models. NOAA Technical Memorandum NOAA-TM-NMFS-SWFSC-490. 34 pp.

Bodenhofer, U., M. Krone, and F. Klawonn. 2013. Testing noisy numerical data for monotonic association. Information Sciences 245: 21-37.

Boudt, K., J. Cornelissen, and C. Croux. 2012. The Gaussian rank correlation estimator: robustness properties. Statistics and Computing 22: 471-483.

Bradford, A.L., K.A. Forney, E.M. Oleson, and J. Barlow. 2014. Accounting for subgroup structure in line-transect abundance estimates of false killer whales (*Pseudorca crassidens*) in Hawaiian waters. PLoS One 9: e90464.

Bradford, A.L., E.M. Oleson, R.W. Baird, C.H. Boggs, K.A Forney, and N.C Young. 2015. Revised stock boundaries for false killer whales (*Pseudorca crassidens*) in Hawaiian waters. NOAA Technical Memorandum NOAA-TM-NMFS-PIFSC-47. 29 pp.

Buckland, S.T., D.R. Anderson, K.P. Burnham, J.L. Laake, D.L. Borchers, and L. Thomas. 2001. Introduction to distance sampling: Estimating abundance of biological populations. Oxford University Press. Oxford, UK. 432 pp.

Bühlmann, P. and T. Hothorn. 2007. Boosting algorithms: Regularization, prediction and model fitting. Statistical Science 22(4): 477-505.

Cahoon, M. 2011. The foraging ecology of monk seals in the main Hawaiian Islands. Master of Science, University of Hawai'i. Honolulu, HI.

Cahoon, M.K., C.L. Littnan, K. Longenecker, and J.R. Carpenter. 2013. Dietary comparison of two Hawaiian monk seal populations: the role of diet as a driver of divergent population trends. Endangered Species Research 20: 137-146.

Carretta, J.V., E. Oleson, D.W. Weller, A.R. Lang, K.A. Forney, J. Baker, and M.C. Hill. 2013. US Pacific marine mammal stock assessments: 2012. NOAA Technical Memorandum NOAA-TM-NMFS-SWFSC-504. La Jolla, CA. 378 pp.

Carretta, J.V., E.M. Oleson, J. Baker, D.W. Weller, A.R. Lang, K.A. Forney, M.M. Muto, B. Hanson, A.J. Orr, H. Huber, M.S. Lowry, J. Barlow, J.E. Moore, D. Lynch, L. Carswell, and R.L. Brownell, Jr. 2015. U.S. Pacific draft marine mammal stock assessments: 2015. NOAA Technical Memorandum NOAA-TM-NMFS-SWFSC-XXX. La Jolla, CA. 53 pp.

Courbis, S., R.W. Baird, F. Cipriano, and D. Duffield. 2014. Multiple populations of pantropical spotted dolphins in Hawaiian waters. Journal of Heredity 105: 627-641.

Federal Register. 2015a. Proposed Rule: Endangered and Threatened Species; Identification of 14 Distinct Population Segments of the Humpback Whale (*Megaptera novaeangliae*). 81 Fed. Reg. 14820, p22304-22356 (50 CFR 223/224)(April 18, 2016). NOAA National Marine Fisheries Service. Online: https://www.federalregister.gov/articles/2016/03/18/2016-06116/endangered-and-threatened-species-identification-of-14-distinct-population-segments-of-the-humpback (Site Accessed 8 June 2016).

Federal Register. 2015b. Endangered and threatened species: Final rulemaking to revise Critical Habitat for Hawaiian monk seals. 80 Fed. Reg. 50925 (50926-50988)(50 CFR 226) September 21, 2015. NOAA National Marine Fisheries Service. Online: https://www.federalregister.gov/articles/2015/08/21/2015-20617/endangered-and-threatened-species-final-rulemaking-to-revise-critical-habitat-for-hawaiian-monk (Site Accessed 8 June 2016).

Forney, K.A., E.A. Becker, D.G. Foley, J. Barlow, and E.M. Oleson. 2015. Habitat-based models of cetacean density and distribution in the central North Pacific. Endangered Species Research 27: 1-20.

GEBCO. 2008. General Bathymetric Chart of the Oceans 08 Grid. GEBCO operates under the joint auspices of the International Hydrographic Organization and the Intergovernmental Oceanographic Commission of UNESCO. Data Downloaded 8 January 2014. Data Website: http://www.gebco.net/data_and_products/gridded_bathymetry_data/ (Site Accessed 8 June 2016).

Gobush, K.S. and S.C. Farry. 2012. Non-lethal efforts to deter shark predation of Hawaiian monk seal pups. Aquatic Conservation: Marine and Freshwater Ecosystems 22(6): 751-761.

Goodman-Lowe, G.D. 1998. Diet of the Hawaiian monk seal (*Monachus schauinslandi*) from the Northwestern Hawaiian Islands during 1991 to 1994. Marine Biology 132(3): 535-546.

Hammar, L., D. Perry, and M. Gullstrom. 2016. Offshore wind power for marine conservation. Open Journal of Marine Science 6: 66-78.

Hofner, B., A. Mayr, A. Robinzonov, and M. Schmid. 2014. Model-based boosting in R: A hands-on tutorial using the R package m-boost. Computational Statistics 29: 3-35.

Johanos, T.C., B.L. Becker, and T.J. Ragen. 1994. Annual reproductive cycle of the female Hawaiian monk seal (*Monachus schauinslandi*). Marine Mammal Science 10:13-30.

Johanos, T.C., A.L. Harting, T.L. Wurth, and J.D. Baker. 2015. Range-wide patterns in Hawaiian monk seal movements among islands and atolls. NOAA Technical Memorandum NOAA-TM-NMFS-PIFSC-44. 26 pp.

Johnston, D.W., M.E. Chapla, L.E. Williams, and D.K. Mattila. 2007. Identification of humpback whale *Megaptera novaeangliae* wintering habitat in the Northwestern Hawaiian Islands using spatial habitat modeling. Endangered Species Research 3: 249-257.

Johnston, D.W., M. McDonald, J. Polovina, R. Domokos, S. Wiggins, and J. Hildebrand. 2008. Temporal patterns in the acoustic signals of beaked whales at Cross Seamount. Biology Letters 4(2): 208-211.

Kenyon, K.W. and D.W. Rice. 1959. Life history of the Hawaiian monk seal. Pacific Science 13: 215-252.

Kittinger, J.N., T.M. Bambico, T.K. Watson, and E.W. Glazier. 2011. Historical and contemporary significance of the endangered Hawaiian monk seal in Native Hawaiian culture. A report prepared for the NOAA National Marine Fisheries Service, Pacific Islands Regional Office, Protected Species Division. Impact Assessment, Inc. Honolulu, HI. 46 pp.

Kretzmann, M.B., W.G. Gilmartin, A. Meyer, G.P. Zegers, S.R. Fain, B.F. Taylor, and D.P. Costa. 1997. Low genetic variability in the Hawaiian monk seal: Conservation implications. Conservation Biology 11: 482-490.

Lebo, S.A. 2010. A local perspective of Hawaii 's whaling economy: whale traditions and government regulation of the kingdoms native seamen and whale fishery. Coriolis 1: 3-37.

Littnan, C. and K. Maison. 2015. Hawaiian Monk Seal Presence (Location) Data. National Oceanic and Atmospheric Administration, National Marine Fisheries Service. Data Provided 16 January 2015. Provider Website: http://www.nmfs.noaa.gov/ (Site Accessed 8 June 2016).

Littnan, C. and K. Wilson. 2015. Hawaiian Monk Seal Telemetry (Tracking) Data. National Oceanic and Atmospheric Administration, Pacific Island Fisheries Science Center, Protected Species Division, Hawaiian Monk Seal Research Program, and Duke University. Data Provided 2 November 2015. Provider Website: https://pifsc-www.irc.noaa.gov/hawaiian_monk_seal/ (Site Accessed 8 June 2016).

Lowry, L. and A. Aguilar. 2008. *Monachus schauinslandi*. IUCN Red List of Threatened Species. Version 2013.2. Online: http://www.iucnredlist.org/details/13654/0 (Site Accessed 8 June 2016).

Madsen, P.T., M. Wahlberg, J. Tougaard, K. Lucke, and P. Tyack. 2006. Wind turbine underwater noise and marine mammals: implications of current knowledge and data needs. Marine Ecology Progress Series 309: 279-295.

Mahaffy, S.D., R.W. Baird, D.J. McSweeney, D.L. Webster, and G.S. Schorr. 2015. High site fidelity, strong associations, and long-term bonds: Short-finned pilot whales off the island of Hawai'i. Marine Mammal Science 31: 1427–1451.

Martien, K.K., R.W. Baird, N.M. Hedrick, A.M. Gorgone, J.L. Thieleking, D.J. McSweeney, K.M. Robertson, and D.L. Webster. 2012. Population structure of island-associated dolphins: Evidence from mitochondrial and microsatellite markers for common bottlenose dolphins (*Tursiops truncatus*) around the main Hawaiian Islands. Marine Mammal Science 28: E208-E232.

McClenachan, L. and A.B. Cooper. 2008. Extinction rate, historical population structure and ecological role of the Caribbean monk seal. Proceedings of the Royal Society of London B: Biological Sciences 275(1641): 1351-1358.

McSweeney, D.J., R.W. Baird, and S.D. Mahaffy. 2007. Site fidelity, associations, and movements of Cuvier's (*Ziphius cavirostris*) and Blainville's beaked (*Mesoplodon densirostris*) whales off the island of Hawai'i. Marine Mammal Science 23: 666-687.

McSweeney, D.J., R.W. Baird, S.D. Mahaffy, D.L. Webster, and G.S. Schorr. 2009. Site fidelity and association patterns of a rare species: Pygmy killer whales (*Feresa attenuata*) in the main Hawaiian Islands. Marine Mammal Science 25: 557-572.

Mobley, J.M., S. Spitz, R. Grotefendt, P. Forestell, A. Frankel, and G. Bauer. 2001. Abundance of humpback whales in Hawaiian waters: Results of 1993-2000 aerial surveys. Report to NOAA Office of National Marine Sanctuaries Hawaiian Islands Humpback Whale National Marine Sanctuary and State of Hawai'i Department of Land and national Resources. 16 pp.

NOAA NCEI. 2005. U.S. Coastal Relief Model - Hawai'i. NOAA National Environmental Satellite, Data, and Information Service, National Centers for Environmental Information. Data Downloaded 8 January 2014. Data Website: https://www.ngdc.noaa.gov/mgg/coastal/grddas10/grddas10.htm (Site Accessed 8 June 2016).

NOAA NMFS. 2007. Recovery plan for the Hawaiian monk seal (*Monachus schauinslandi*), 2nd revision. NOAA National Marine Fisheries Service. 160 pp. Online: www.nmfs.noaa.gov/pr/pdfs/recovery/hawaiianmonkseal.pdf (Site Accessed 8 June 2016).

NOAA NMFS. 2014. Revision of critical habitat for Hawaiian Monk Seals: Final Biological Report. NOAA National Marine Fisheries Service, Pacific Islands Regional Office, Protected Resources Division. 105 pp. Online: http://www.fpir.noaa.gov/Library/PRD/Hawaiian%20monk%20seal/Hawaiian_monk_seal_Biological_Report_for_Critical_Habitat.pdf (Site Accessed 8 June 2016).

NOAA NMFS. 2015. Critical Habitat Maps: Marine Mammals: Hawaiian Monk Seal. National Oceanic and Atmospheric Administration, National Marine Fisheries Service. Data Downloaded 10 September 2015. Data Website: http://www.nmfs.noaa.gov/pr/species/criticalhabitat.htm (Site Accessed 8 June 2016).

NOAA ORR. 2001. Environmental Sensitivity Index Shoreline Types – Polygons and Lines. NOAA National Ocean Service, Office of Response and Restoration. Data Downloaded 23 March 2016. Data Website: http://response.restoration.noaa.gov/maps-and-spatial-data/download-esi-maps-and-gis-data.html#Hawaii (Site Accessed 8 June 2016).

Norris, K.S., B. Würsig, R.S. Wells, and M. Würsig. 1994. The Hawaiian spinner dolphin. University of California Press, Berkeley, CA. 408 pp.

Oleson, E.M., C.H. Boggs, K.A. Forney, M.B. Hanson, D.R. Kobayashi, B.L. Taylor, P.R. Wade, and G.M. Ylitalo. 2010. Status Review of Hawaiian Insular False Killer Whales (*Pseudorca crassidens*) under the Endangered Species Act. NOAA Technical Memorandum NOAA-TM-NMFS-PIFSC-22. 140 pp.

Oleson, E.M., R.W. Baird, K.K. Martien, and B.L. Taylor. 2013. Island-associated stocks of odontocetes in the main Hawaiian Islands: A synthesis of available information to facilitate evaluation of stock structure. PIFSC Working Paper WP-13-003.

Östman-Lind, J., A.D. Driscoll-Lind, and S.H. Rickards. 2004. Delphinid abundance, distribution and habitat use off the western coast of the island of Hawaii. NOAA National Marine Fisheries Service, Southwest Fisheries Science Center Administrative Report LJ-04-02C. La Jolla, CA. 28 pp.

Parrish, F.A., K. Abernathy, G.J. Marshall, and B.M. Buhleier. 2002. Hawaiian monk seals (*Monachus schauinslandi*) foraging in deep-water coral beds. Marine Mammal Science 18: 244-258.

Pūkui, M.K., S.H. Elbert, and E.T. Mo'okini. 1974. Place names of Hawaii. University of Hawai'i Press. Honolulu, HI. 289 pp.

Ragen, T.J. 2003. The role of the main Hawaiian Islands in the recovery of the Hawaiian monk seal. pp. 3. In: Workshop on the Management of Hawaiian Monk Seals on Beaches in the Main Hawaiian Islands. 51 pp.

Reeves, R.R., S. Leatherwood, and R.W. Baird. 2009. Evidence of a possible decline since 1989 in false killer whales (*Pseudorca crassidens*) around the Main Hawaiian Islands. Pacific Science 63: 253-261.

Rice, D.W. 1978. The humpback whale in the North Pacific: Distribution, exploration and numbers. pp. 29-44. In: K.S. Norris and R.S. Reeves (eds.), Report on a workshop on Annual progress report under Grant No. N00244-10-1-0048 from the Naval Postgraduate School. Cascadia Research Collective, Olympia, WA.

Rone, B.K., R.W. Baird, D.L. Webster, and D.B. Anderson. 2015. Satellite telemetry results indicate an open-ocean population of sperm whales (*Physeter macrocephalus*) in Hawaiian waters. Poster presented at the 21st Biennial Conference on the Biology of Marine Mammals. San Francisco, CA.

Russell, D.J., S.M. Brasseur, D. Thompson, G.D. Hastie, V.M. Janik, G. Aarts, B.T. McClintock, J. Matthiopoulos, S.E. Moss, and B. McConnell. 2014. Marine mammals trace anthropogenic structures at sea. Current Biology 24(14): R638-R639.

Scales, K.L., P.I. Miller, L.A. Hawkes, S.N. Ingram, D.W. Sims, and S.C. Votier. 2014. On the front line: frontal zones as priority at-sea conservation areas for mobile marine vertebrates. Journal of Applied Ecology 51: 1575-1583.

Scheel, D.M., G.J. Slater, S.O. Kolokotronis, C.W. Potter, D.S. Rotstein, K. Tsangaras, A.D. Greenwood, and K.M. Helgen. 2014. Biogeography and taxonomy of extinct and endangered monk seals illuminated by ancient DNA and skull morphology. ZooKeys 409: 1.

Schorr, G.S., R.W. Baird, M.B. Hanson, D.L. Webster, D.J. McSweeney, and R.D. Andrews. 2009. Movements of satellite-tagged Blainville's beaked whales off the island of Hawai'i. Endangered Species Research 10: 203-213.

Schultz, J.K., J. Baker, R. Toonen, and B. Bowen. 2009. Extremely low genetic diversity in the endangered Hawaiian monk seal (*Monachus schauinslandi*). Journal of Heredity 1 100 (1): 25-33.

TNC. 2009. Hawaiian Islands Marine Ecoregional Assessment (Draft). The Nature Conservancy of Hawai'i Marine Program. Honolulu, HI.

Thorne, L.H., D.W. Johnston, D.L. Urban, J. Tyne, L. Bejder, R.W. Baird, S. Yin, S.H. Rickards, M.H. Deakos, J.R. Mobley, Jr, A.A. Pack, and M. Chapla Hill. 2012. Predictive modeling of spinner dolphin (*Stenella longirostris*) resting habitat in the Main Hawaiian Islands. PLoS ONE 7(8): e43167.

USGS. 2015. The 3DEP National Map (1/3 arc-second DEMs for Hawai'i). The National Map. U.S. Geological Survey. Data Downloaded 15 September 2015. Data Website: http://viewer.nationalmap.gov/basic/?basemap=b1&category=ned,nedsrc&title=3DEP%20View#startUp (Site Accessed 8 June 2016).

Marine Mammals

Van Parijs, S.M., C. Curtice, and M.C. Ferguson (eds.). 2015. Biologically Important Areas for cetaceans within U.S. waters. Aquatic Mammals (Special Issue) 41(1). 128 pp.

Watson, T.K., J.N. Kittinger, J.S. Walters, and T.D. Schofield. 2011. Culture, conservation, and conflict: assessing the human dimensions of Hawaiian monk seal recovery. Aquatic Mammals 37(3): 386.

Wilson, K.C. 2015. Integrating multiple technologies to understand the foraging behavior and habitat use of monk seals in the Main Hawaiian Islands. Ph.D. Thesis. Nicholas School of the Environment, Duke University, NC.

Woodworth, P.A., G.S. Schorr, R.W. Baird, D.J. McSweeney, M.B. Hanson, R.D. Andrews, and J.J. Polovina. 2012. Eddies as offshore foraging grounds for melon-headed whales (*Peponocephala electra*). Marine Mammal Science 28(3): 638-647.

Chapter 7 Seabirds

Arliss J. Winship[1,3], Brian P. Kinlan[1], Lisa T. Ballance[15,22], Trevor Joyce[22], Jeffery B. Leirness[1,3], Bryan M. Costa[1], Matthew Poti[1,3], and Peter I. Miller[4]

Laysan Albatross at Kaena Point,O'ahu. Photo credit: Arliss Winship (NOAA NOS/NCCOS)

ABSTRACT

This chapter describes an assessment of the at-sea distribution of seabirds around the Main Hawaiian Islands (MHI). We analyzed at-sea visual sighting data collected by the National Oceanic and Atmospheric Administration's (NOAA) National Marine Fisheries Service (NMFS) Southwest Fisheries Science Center (SWFSC) on shipboard surveys conducted during May and August-December between 1989 and 2012. We present the locations of sightings of 24 species, and for 14 of these species we develop spatial predictive models of relative density throughout the study area. Model predictions are presented with associated measures of precision and statistical fit in terms of a suite of performance metrics. Spatial distributions varied across species, with the majority of sightings occurring relatively close to land, occurring in particular parts of the study area, or occurring more evenly throughout the study area. Predicted spatial distributions for species that were modeled broadly aligned with the distributions of sightings. Some of the most important model predictor variables across species were day of the year, distance to shore or nearest terrestrial site, depth, sea surface height and projected longitude/latitude. Our assessment provides broad-scale spatial information that can aid marine spatial planning around the MHI. Importantly, our assessment also highlights gaps and limitations in the available data, which can guide future data collection efforts. In addition to our assessment, we discuss other studies and available datasets on the at-sea distribution of seabirds around the MHI.

Citation for chapter
Winship, A.J., B.P. Kinlan, L.T. Ballance, T. Joyce, J.B. Leirness, B.M. Costa, M. Poti and P.I. Miller. 2016. Chapter 7: Seabirds. pp. 283-319. In: B.M. Costa and M.S. Kendall (eds.), Marine Biogeographic Assessment of the Main Hawaiian Islands. Bureau of Ocean Energy Management and National Oceanic and Atmospheric Administration. OCS Study BOEM 2016-035 and NOAA Technical Memorandum NOS NCCOS 214. 359 pp.

[1] *NOAA National Centers for Coastal Ocean Science, Biogeography Branch, Silver Spring, MD, U.S.A.*
[3] *CSS-Dynamac, Fairfax, VA, U.S.A.*
[4] *Plymouth Marine Laboratory, Remote Sensing Group, Plymouth, United Kingdom*
[15] *NOAA Southwest Fisheries Science Center, Marine Mammal and Turtle Division, CA, U.S.A.*
[22] *Scripps Institution of Oceanography, U.C. San Diego, CA, U.S.A.*

Seabirds

7.1. INTRODUCTION

Seabirds are a group of species that have a large potential for being negatively affected by offshore wind energy development (Garthe and Hüppop, 2004). Seabirds may avoid areas with temporary or permanent structures, possibly being displaced from areas they would normally use for foraging, migrating, etc. (May 2015). There is also a potential mortality risk from collisions with man-made structures, such as wind turbines. Collisions of birds with wind turbines have been well documented in North America and Europe and can result in non-negligible mortality at the population level (Drewitt and Langston, 2006; Erickson et al., 2014). The probability of collision will likely vary with a species' typical flight height (Robinson Willmott, 2013; Cleasby et al., 2015). Seabird mortality from collisions with other man-made structures has been documented in the Hawaiian Islands (Cooper and Day, 1998).

At least 22 species of seabirds breed in the Hawaiian Archipelago, 20 of which are documented as or suspected of breeding in the Main Hawaiian Islands (MHI; Table 7.1). Two endemic species that are federally listed under the U.S. Endangered Species Act, Hawaiian Petrel (*Pterodroma sandwichensis*; Federal Register, 1967) and Newell's Shearwater (*Puffinus newelli*; Federal Register, 1975), breed only in the MHI. Many species of non-breeding, migratory seabirds can also be found in waters around the MHI.

Seasonal timing of presence of each species in the MHI (Table 7.1, Figure 7.1) is dictated by the timing of life history events, like breeding, juvenile dispersal, and migration. The spatial distributions of birds at sea are a result of interactions between behavior (e.g., foraging) and the environment. Important environmental variables that may affect habitat use include distance to breeding colonies, wind speed and direction, thermocline depth and gradient, primary productivity, water temperature, salinity, fronts, and meso- and large-scale ocean features (King, 1970; Ballance et al., 1997; Ribic and Ainley, 1997; Spear et al., 2001; Ballance et al., 2006; Kappes et al., 2010). The relative importance of these variables may differ among species (e.g., planktivores versus piscivores; Spear et al., 2001). Behaviors like multi-species flocking and inter-specific competition, foraging in association with tunas and dolphins, and following fishing vessels (e.g., Black-footed Albatross [*Phoebastria nigripes*]) may also influence spatial distributions (King, 1970; Ballance et al., 1997; Ballance and Pitman, 1999; Hebshi et al., 2008). Inter-annual environmental variability and extreme events (e.g., El Niño) may influence both habitat use and the timing and success of breeding (USFWS, 1983; Vandenbosch, 2000; Ballance et al., 2006; Devney et al., 2009; Thorne et al., 2015).

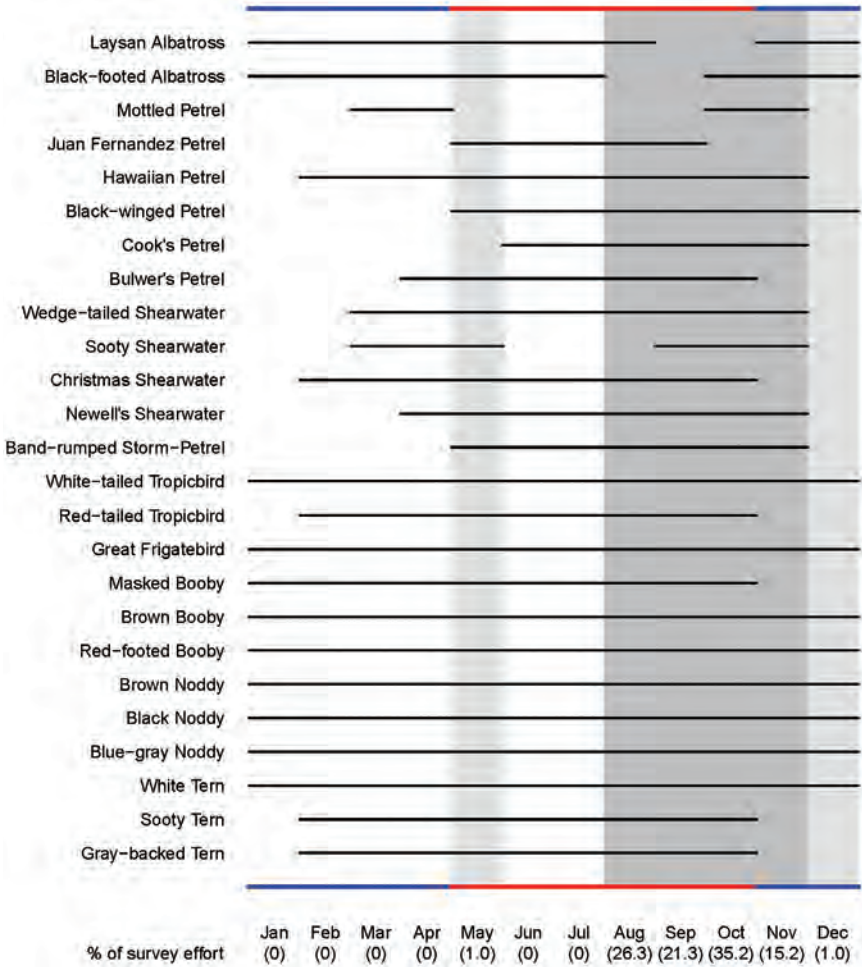

Figure 7.1. Monthly presence of seabird species in the Main Hawaiian Islands. Black lines indicate months present, based on a literature review. Blue and red lines indicate winter and summer (as defined in Chapter 2), respectively. Dark grey shading indicates months with 98 percent of the survey effort, light grey shading indicates months with the remaining 2 percent of the survey effort, and no shading indicates no survey effort.

Table 7.1. Seabird species considered in assessment. Birds are mainly present in the Main Hawaiian Islands (MHI) during the indicated month ranges but can occur at other times. Conservation statuses are BCC (bird of conservation concern), V (vulnerable), NT (near threatened), T (threatened), E (endangered), C (candidate for listing) , Y (yellow Watch List) and R (red Watch List) according to the U.S. Endangered Species Act (ESA), State of Hawai'i endangered species legislation (HI), U.S. Fish and Wildlife Service (USFWS), International Union for Conservation of Nature (IUCN) and State of the Birds U.S.A. (SB; Rosenberg et al., 2014). Estimates of maximum breeding foraging range, if they were available, are only presented for breeding species that were not modeled.

Family	Common Name	Scientific Name	Breeds In MHI	Months Present[1,2,3]	Conservation Status	Model	Maximum Breeding Foraging Range (km)
Diomedeidae	Laysan Albatross	*Phoebastria immutabilis*	yes	Nov – Aug	BCC (USFWS), NT (IUCN), Y (SB)	no	3,929[4]
	Black-footed Albatross	*Phoebastria nigripes*	yes	Oct – Jul	T (HI), BCC (USFWS), NT (IUCN), Y (SB)	no	3,779[4]
Procellariidae	Mottled Petrel	*Pterodroma inexpectata*	no	Mar – Apr, Oct – Nov	NT (IUCN)	yes	N/A
	Juan Fernandez Petrel	*Pterodroma externa*	no	May – Sep	V (IUCN)	yes	N/A
	Hawaiian Petrel	*Pterodroma sandwichensis*	yes	Feb – Nov	E (ESA, HI), V (IUCN), R (SB)	yes	model
	Black-winged Petrel	*Pterodroma nigripennis*	no	May – Dec		yes	N/A
	Cook's Petrel	*Pterodroma cookii*	no	Jun – Nov	V (IUCN)	yes	N/A
	Bulwer's Petrel	*Bulweria bulwerii*	yes	Apr – Oct	Y (SB)	yes	model
	Wedge-tailed Shearwater	*Puffinus pacificus*	yes	Mar – Nov		yes	model
	Sooty Shearwater	*Puffinus griseus*	no	Mar – May, Sep – Nov	NT (IUCN)	yes	N/A
	Christmas Shearwater	*Puffinus nativitatis*	yes	Feb – Oct	BCC (USFWS), Y (SB)	no	unknown
	Newell's Shearwater	*Puffinus newelli*	yes	Apr – Nov	T (ESA, HI), E (IUCN), R (SB)	yes	model
Hydrobatidae	Band-rumped Storm-Petrel	*Oceanodroma castro*	yes	May – Nov	C (ESA), E (HI), BCC (USFWS), Y (SB)	no	unknown
Phaethontidae	White-tailed Tropicbird	*Phaethon lepturus*	yes	year round	Y (SB)	yes	model
	Red-tailed Tropicbird	*Phaethon rubricauda*	yes	Feb – Oct	Y (SB)	no	1,034[5]
Fregatidae	Great Frigatebird	*Fregata minor*	suspected	year round	Y (SB)	no	612[5]
Sulidae	Masked Booby	*Sula dactylatra*	yes	Jan – Oct	Y (SB)	no	158[3]
	Brown Booby	*Sula leucogaster*	yes	year round	Y (SB)	yes	model
	Red-footed Booby	*Sula sula*	yes	year round		yes	model
Laridae	Brown Noddy	*Anous stolidus*	yes	year round		no	163[3]
	Black Noddy	*Anous minutus*	yes	year round	Y (SB)	no	80[6]
	Blue-gray Noddy	*Procelsterna cerulea*	suspected	year round	Y (SB)	no	9[5]
	White Tern	*Gygis alba*	yes	year round	T (HI)	yes	model
	Sooty Tern	*Onychoprion fuscatus*	yes	Feb – Oct		yes	model
	Gray-backed Tern	*Onychoprion lunatus*	yes	Feb – Oct	Y (SB)	no	unknown

[1]USFWS, 1983; [2]Pyle and Pyle, 2009; [3]Keller et al., 2009; [4]Fernandez et al., 2001; [5]Maxwell and Morgan, 2013; [6]USFWS, 2005

Seabirds

This chapter describes an assessment of the at-sea distributions of seabirds around the Main Hawaiian Islands (MHI; Figure 7.2). Data on the at-sea distributions of seabirds around the MHI have mainly been collected two ways, vessel-based sighting surveys (Table 7.2) and electronic tracking (Table 7.3). For our assessment we focused on sighting data, specifically the most comprehensive, scientific at-sea survey dataset for seabirds in the MHI in recent decades, which was collected by the National Oceanic and Atmospheric Administration (NOAA) National Marine Fisheries Service (NMFS) Southwest Fisheries Science Center (SWFSC). We present the locations of sightings of 24 species: all 19 breeding species with sightings in the dataset and five non-breeding visitors with the greatest numbers of sightings in the survey data. For nine of the breeding species and all five non-breeding visitors, we develop spatial predictive models of relative density throughout the study area.

Our assessment was designed to provide broad-scale spatial information that can be used to guide future data collection efforts and aid marine spatial planning around the MHI. The results of our assessment represent spatial distributions of seabird sightings and relative density around the MHI averaged over time. Our assessment was not designed to provide precise predictions of the absolute number of individuals of a given species that would be expected in a specific location at a specific time. Our assessment was also not designed to determine the ecological drivers of seabird spatial distributions around the MHI, although our modeling results provide related hypotheses for future research.

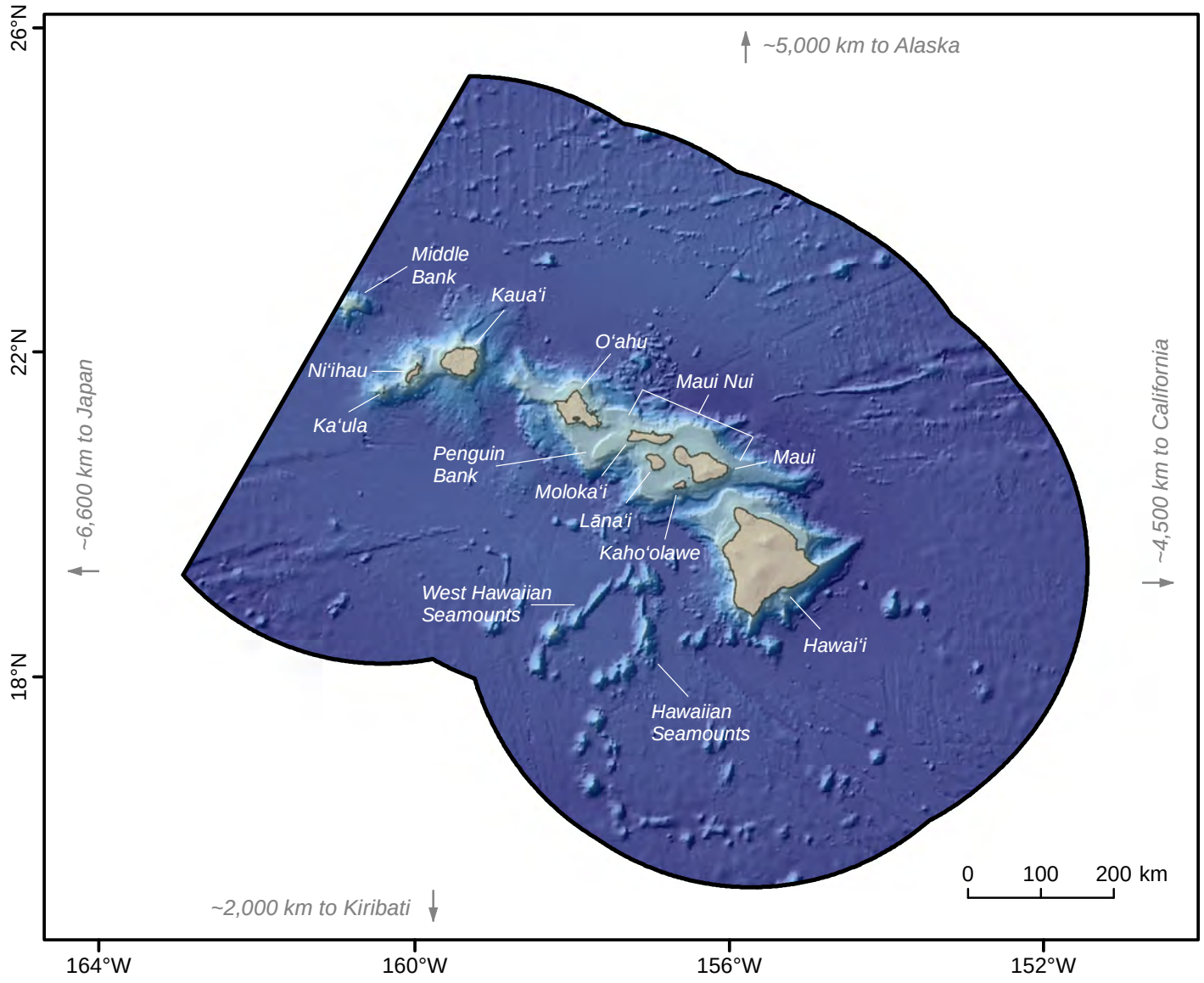

Figure 7.2. Map of the study area with place names referred to in the text.

Table 7.2. Seabird sighting surveys and datasets with survey effort in the MHI not analyzed in our assessment. We did not analyze data from these surveys for several reasons, including data availability, limited spatial coverage, limited spatial resolution, or lack of associated effort data.

Survey/Dataset	At Sea/Terrestrial	Source
Western Pacific	at sea	Dixon and Starrett, 1952
Smithsonian Institution Pacific Ocean Biological Survey Program	at sea	King, 1970; King, 1974
Southeastern Hawaiian Waters	at sea	Spear et al., 1999
South Of O'ahu	at sea	VanderWerf et al., 2005
Cascadia Research Collective	at sea	Robin Baird (Cascadia Research Collective, Olympia, WA) http://www.cascadiaresearch.org
NOAA NMFS/PIRO Observer Program	at sea	NOAA National Marine Fisheries Service Pacific Islands Regional Office, Honolulu, HI (e.g, NOAA NMFS, 2014)
eBird	both	http://ebird.org
Audubon Christmas Bird Count	terrestrial	http://www.audubon.org/conservation/science/christmas-bird-count

Table 7.3. Electronic tracking studies of seabirds in the Hawaiian Islands.

Species	Source
Laysan Albatross	Fernandez et al., 2001; Hyrenbach et al., 2002; Kappes et al., 2010; Conners et al., 2015; Kappes et al., 2015; Josh Adams (USGS, Santa Cruz, CA)[1]
Black-footed Albatross	Fernandez et al., 2001; Hyrenbach et al., 2002; Kappes et al., 2010; Conners et al., 2015; Kappes et al., 2015
Hawaiian Petrel	Josh Adams (USGS, Santa Cruz, CA)[1]
Wedge-tailed Shearwater	Josh Adams (USGS, Santa Cruz, CA)[1]
Newell's Shearwater	Josh Adams (USGS, Santa Cruz, CA)[1] ; Andre Raine (Kaua'i Endangered Seabird Recovery Project, HI)
Red-tailed Tropicbird	Josh Adams (USGS, Santa Cruz, CA)[1]
Masked Booby	Young et al., 2015
Brown Booby	Josh Adams (USGS, Santa Cruz, CA)[1]
Red-footed Booby	Young et al., 2015; Josh Adams (USGS, Santa Cruz, CA)[1]
Brown Noddy	Harrison and Stone-Burner, 1981

[1] BOEM-funded project PC-13-03

Red-footed Booby, Sula sula *(left; Robin W. Baird, Cascadia Research Collective); and Black-footed Albatross,* Phoebastria nigripes *(right; David Pereksta, BOEM).*

7.2. METHODS

7.2.1. At-sea survey data

Our assessment focused on at-sea survey data collected by SWFSC. These data were visual sightings on shipboard surveys conducted between 1989 and 2012 (Figure 7.3). The majority of these data were collected on two ship surveys in 2002 and 2010 (Figure 7.4), the Hawaiian Islands Cetacean and Ecosystem Assessment Surveys (HICEAS), that covered the study area with widely spaced transects. There were also data from other shipboard surveys that transited in and out of the study area en route to other survey locales. Most of the survey effort was from August-November, with smaller amounts of effort in May and December (Figure 7.5). The monthly timing of surveys was chosen for historical reasons and consistency over time. Sighting data were collected continuously using strip transect sampling methodology (Ballance et al., 2002). Strip transects were generally 300 m wide, but were sometimes narrower depending on the sighting conditions and species. For analysis, survey transects were divided into 1.2 km 'segments' (Appendix B), and species-specific counts were summed for each segment. The mid-point of a segment was used as the location of the summed counts.

Other surveys have been conducted partially or entirely in waters around the MHI (Table 7.2). We did not analyze sighting data from those surveys for several reasons, including data availability, limited spatial coverage, limited spatial resolution, or lack of associated effort data. Nevertheless, those surveys provide a supplementary source of information about the at-sea distributions of seabirds in the MHI.

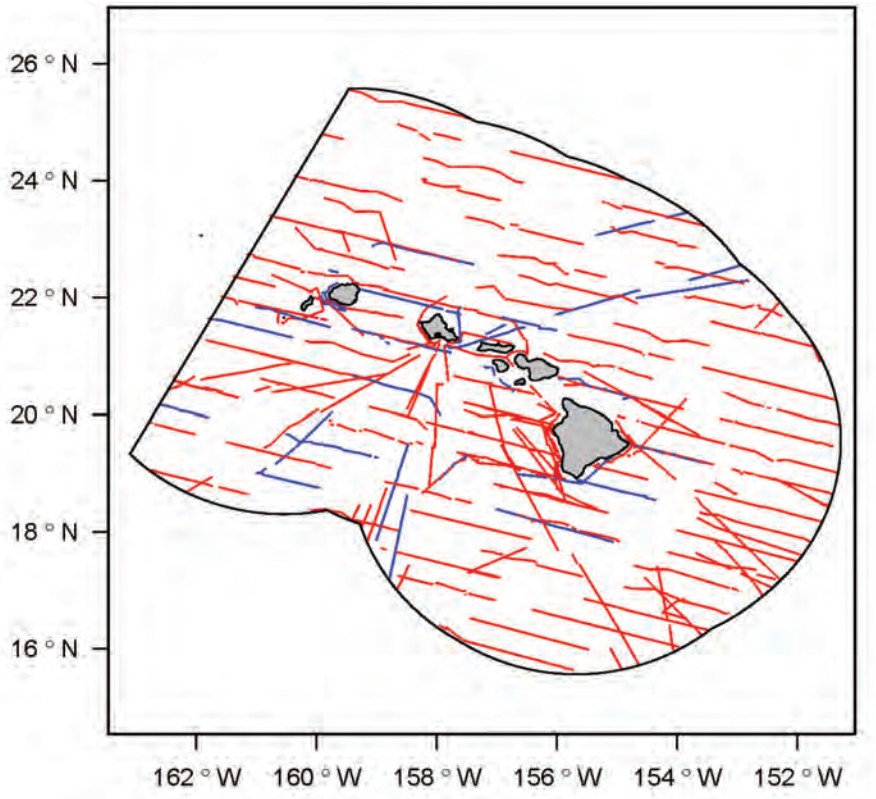

Figure 7.3. Seabird survey transects by NOAA NMFS/SWFSC from 1989–2012. Survey effort was 16,377 1.2–km transect segments during May and August–October (summer; shown in red) and 3,168 during November–December (winter; shown in blue).

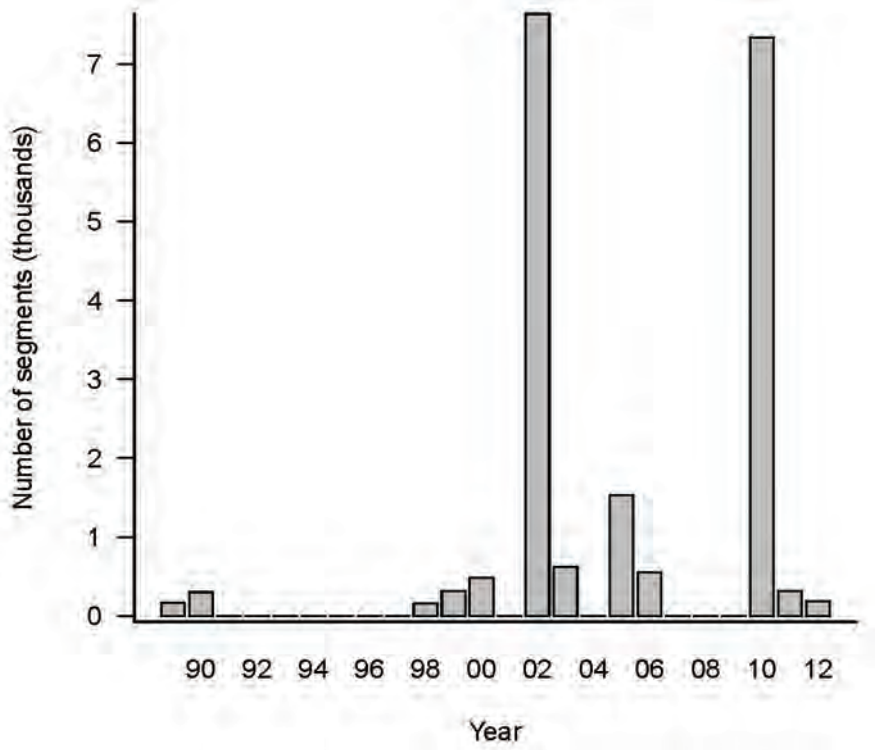

Figure 7.4. Number of survey transect segments by year. Data were collected by NOAA NMFS/SWFSC. Most segments were 1.2 km.

7.2.2. Terrestrial site data

While our assessment was focused on the at-sea distribution of seabirds, we also compiled data on the locations of terrestrial sites used by seabirds in the MHI (e.g., breeding colonies, roosting sites) for two purposes. First, we used the terrestrial site data to develop distance-to-nearest-terrestrial-site predictor variables for use in modeling of relevant species (Section 7.2.3). Second, we used the terrestrial site data to develop potential maximum foraging areas for breeding species that were not modeled (Section 7.2.4).

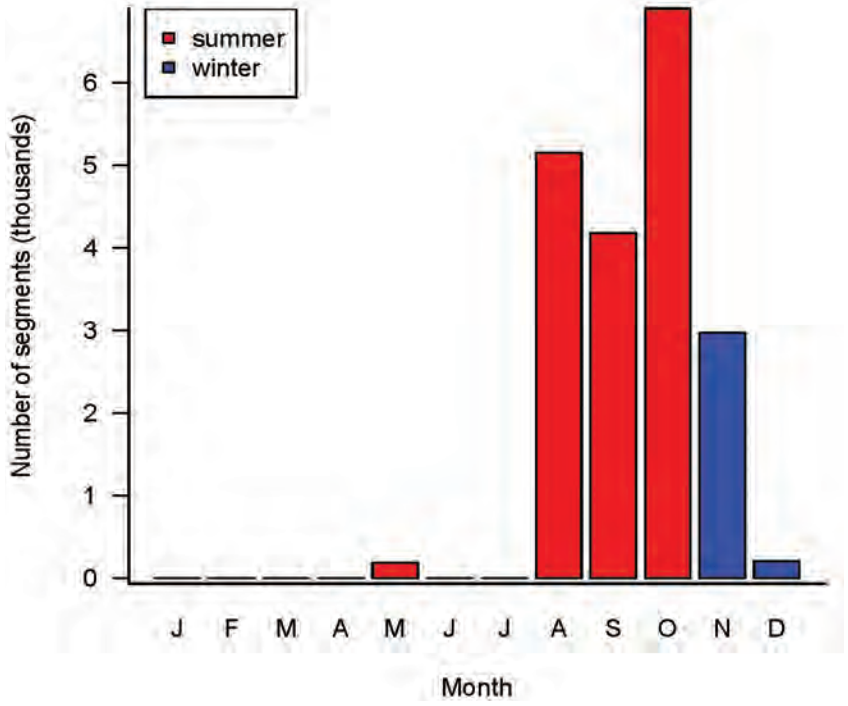

Figure 7.5. Number of survey transect segments by month. Data were collected by NOAA NMFS/SWFSC. Most segments were 1.2 km.

Many terrestrial and coastal surveys and other studies have provided information about the locations of seabird breeding colonies and roosting sites in the MHI (e.g., Hirai, 1978; USFWS, 1983; Day and Cooper, 1995; Reynolds and Ritchotte, 1997; Cooper and Day, 2003; Day et al., 2003; VanderWerf, 2003; Wood et al., 2003; Kozar et al., 2007; VanderWerf et al., 2007; Wood and Bily, 2008; Pepi et al., 2009; Anders et al., 2011; Fujimoto, 2011; Fujimoto and Juola, 2012; Welch et al., 2012; Wiley et al., 2013; VanderWerf and Young, 2014). Harrison (1990), USFWS (2005) and Pyle and Pyle (2009) provide overviews of terrestrial sites used by seabirds throughout the Hawaiian Islands. There is also at least one publicly available dataset on terrestrial sites and nearshore areas used by seabirds in the Hawaiian Islands (Environmental Sensitivity Index [ESI] database produced by NOAA National Ocean Service Office of Response and Restoration, http://response.restoration.noaa.gov/maps-and-spatial-data/environmental-sensitivity-index-esi-maps.html). We consulted all of these sources, as well as multiple local experts (A. Dibben-Young, T. Joyce, S. Judge, S. Plentovich, A. Raine, and E. VanderWerf), and developed a compilation of terrestrial site location data for seabirds in the MHI. It is important to note that this dataset is almost certainly incomplete, and the nature of what was considered an individual terrestrial site varied considerably (e.g., isolated occurrence of breeding, large breeding colony, roosting site), as did the precision of the location information. Nevertheless, the dataset provided a useful and reasonably comprehensive representation of terrestrial sites used by seabirds in the MHI that could be used as a predictor for at-sea distributions.

In addition to the sources that we consulted, at least two other terrestrial survey datasets exist for the MHI: eBird and the Audubon Christmas Bird Count (Table 7.2). These datasets are a result of citizen science. We did not incorporate those data in our terrestrial site compilation because they do not specifically identify terrestrial sites used by seabirds. Nevertheless, those datasets provide a supplementary source of information about terrestrial and nearshore areas in the MHI where seabirds have been observed.

Current estimates of the number of birds using each terrestrial site were not available for every species and site. As a result, we developed the distance-to-nearest-terrestrial-site predictor variables by treating every site equally. However, to the extent that locations of terrestrial sites influence at-sea distributions, it is likely that areas near terrestrial sites with larger numbers of birds will exhibit higher relative densities at sea. This effect was not captured by our distance-to-nearest-terrestrial-site predictor variables. Had the requisite data been available, it may have been more useful to weight proximity to terrestrial sites by the numbers of birds using each site.

7.2.3. Spatial predictive modeling

For species with sufficient numbers of sightings in the at-sea survey dataset, we conducted spatial predictive modeling (Figure 1.5). For our Biogeographic Assessment, environmental predictor variables were characterized as summer (May-October) and winter (November-April) climatologies (Chapter 2), but the sighting data were from May and August-December. To maintain consistency between the environmental predictors and the sighting data, we limited the models to the summer time frame and used the sighting data from May and August-October, along with the summer environmental predictors. Fourteen species had sufficient numbers of sightings to model during these months (≥48 transect segments with sightings of ≥1 individual; Table 7.1). Nine of these species breed in the MHI and the remaining five species were non-breeding migratory visitors. It is important to recognize that the models apply to specific months of the year and may not be applicable to other months.

A Boosted Zero-inflated Count (BZIC) statistical modeling framework was used to relate the survey count data to a range of temporal and spatial environmental predictor variables (Appendix B). The estimated relationships between the counts of the modeled species and the predictor variables were then used to predict the relative density of these species across the entire study area. Relative density was defined as the expected number of individuals that would be counted per km^2 observed. It is important to recognize that the model predictions do not represent absolute density because during visual surveys, individual birds may be missed, and animal movement can bias estimates of density. Our model predictions should only be interpreted as indices of density.

7.2.4. Species that were not modeled

For breeding species with insufficient numbers of sightings in the at-sea survey dataset, we characterized their spatial distributions by mapping the locations of survey transect segments with sightings of ≥1 individual. Of these 11 species (Table 7.1), only Gray-backed Tern (*Onychoprion lunatus*) had no sightings in the at-sea survey dataset, which is perhaps not surprising given this species' limited breeding range and population size in the MHI.

To indicate potential foraging areas for breeding individuals of these non-modeled species on maps of the MHI, we reviewed the literature for estimates of the maximum foraging ranges of individuals of each species, and overlaid circular areas centered on the species' terrestrial sites with radii equal to these estimates (Soanes et al., 2016). This methodology was also applied to seabirds in a previous Biogeographic Assessment of the Northwestern Hawaiian Islands (Keller et al., 2009). Maximum foraging range estimates were available for eight of the 11 non-modeled breeding species (Table 7.1).

Gray-backed Tern, Onychoprion lunatus*. Photo credit: Cascadia Research Collective.*

There are several important caveats associated with these potential foraging areas. First, the foraging areas are only applicable to individuals that are coming and going from terrestrial sites (e.g., breeding individuals); they are not necessarily applicable to non-breeding individuals of breeding species (e.g., immatures). Second, the foraging range estimates reflect the maximum foraging ranges of individuals and do not necessarily reflect the average or typical foraging range. Third, there can be directional bias in foraging trips so that a circular area around terrestrial sites encapsulates much more area than the actual foraging area. The two albatross species are a good example of this directional bias, where individuals usually forage northward of the Hawaiian Islands (King, 1970; Kappes et al., 2010; Conners et al., 2015). In general, many seabirds (e.g., procellariids) make directed movements influenced by wind direction (Adams and Flora, 2010).

7.3. RESULTS AND DISCUSSION

7.3.1. Spatial distributions

The spatial distributions of sightings varied across species (Figures 7.6-7.21). The majority of sightings for some species were relatively close to land, for example Black Noddy (*Anous minutus*), Brown Noddy (*Anous stolidus*) and Brown Booby (*Sula leucogaster*). The majority of sightings for some other species occurred in particular parts of the study area, for example most Juan Fernandez Petrel (*Pterodroma externa*) and Mottled Petrel (*Pterodroma inexpectata*) sightings were in the southeast. Sightings of other species were more evenly distributed throughout the study area, for example Great Frigatebird (*Fregata minor*), Sooty Tern (*Onychoprion fuscatus*) and Wedge-tailed Shearwater (*Puffinus pacificus*). It is important to note that the distributions of sightings partially reflect the amount and distribution of effort in each season. Differences in the distribution of sightings for a single species between seasons, or in the number of sightings between areas within a season, do not necessarily indicate differences in the distribution of relative abundance of that species.

Masked Booby, Sula dactylatra. *Photo credit: David Pereksta (BOEM).*

When available, potential maximum foraging areas for breeding species that were not modeled captured most, but not necessarily all, of the sightings (Figures 7.6-7.7). There were many Masked Booby (*Sula dactylatra*) sightings outside of the potential maximum foraging area suggesting that the estimated foraging range for this species may have been too small for the MHI. The estimated maximum foraging area for four species (Black-footed Albatross, Laysan Albatross [*Phoebastria immutabilis*], Great Frigatebird and Red-tailed Tropicbird [*Phaethon rubricauda*]) exceeded the study area.

Predicted spatial distributions for species that were modeled broadly aligned with the distributions of sightings (Figures 7.8-7.21). When most sightings were relatively close to land (e.g., Brown Booby), or when most sightings were in a particular part of the study area (e.g., Juan Fernandez Petrel), the pattern of predicted relative density matched. Predicted areas of high relative density for breeding species tended to be more centered near land than for non-breeding, migratory species. Some offshore areas of high predicted relative density for multiple species included west and southwest of the island of Hawai'i (Bulwer's Petrel [*Bulweria bulwerii*], Black-winged Petrel [*Pterodroma nigripennis*], Hawaiian Petrel, Juan Fernandez Petrel, Sooty Tern, and Wedge-tailed Shearwater), north of Kaua'i (Cook's Petrel [*Pterodroma cookii*], Hawaiian Petrel, Newell's Shearwater, Sooty Shearwater [*Puffinus griseus*], and White-tailed Tropicbird [*Phaethon lepturus*]), and the southwest corner of the study area (Black-winged Petrel, Red-footed Booby [*Sula sula*], Sooty Tern, and White-tailed Tropicbird).

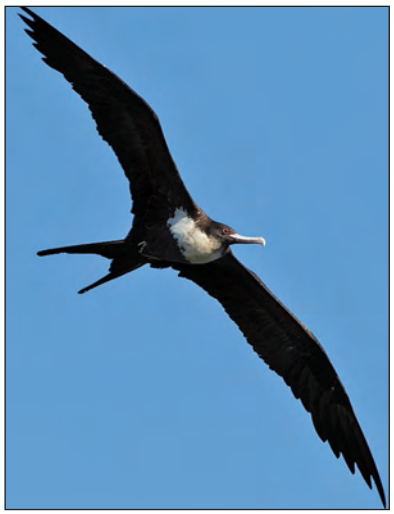

Great Frigatebird, Fregata minor. *Photo credit: David Pereksta (BOEM)*

For modeled species, predictions of relative density are accompanied by estimates of the statistical uncertainty in those predictions, specifically the coefficient of variation (CV; Figures 7.8-7.21). CVs were highly variable across species and across the study area for individual species. In many cases, the CV of predictions was higher when predicted relative density was higher, but not always. Some of the predictions had very high CVs (>1), indicating substantial statistical uncertainty and variability associated with the corresponding predictions of relative density, so these predictions should be interpreted cautiously.

Seabirds

Certain model predictions of high relative density are particularly questionable. In some cases, estimated relationships between relative density and environmental predictor variables may apply in certain areas, but extrapolations to other areas are questionable. For example, the Brown Booby model suggests high relative density near the Hawaiian and West Hawaiian seamounts, but there were few if any sightings in those areas. It is possible that these predictions are an artifact of a relatively nearshore distribution and a resulting estimated negative relationship between relative density and depth.

Cook's Petrel, Pterodroma cookii. *Photo credit: David Pereksta (BOEM).*

Other questionable predictions of high relative density may partially reflect large temporal and spatial aggregations of birds coinciding with survey effort rather than average spatial patterns per se. For example, Sooty Shearwaters migrate through the study area in large numbers during short periods of time (March-May and September-November). The predicted area of high relative density for this species north of Kaua'i corresponds to a large number of sightings on a single survey cruise. Similarly, the predicted area of high relative density of Black-winged Petrel southwest of the island of Hawai'i arose from a few transects on which a large number of sightings occurred. In the case of Cook's Petrel, the predicted area of high relative density in the northwest corner of the study area may have been driven by a limited number of transects combined with a less constrained model near the edge of the data extent. In general, predictions near the edges of the data extent should be interpreted more cautiously, as with most models. While our spatial predictive modeling framework theoretically accounts for effort and attempts to account for the aggregated nature of animal distributions and sightings, limited sample size combined with extreme aggregations can unduly influence model predictions.

For some modeled species there were many sightings in areas where the predicted relative density was low; e.g., Black-winged Petrel and Wedge-tailed Shearwater. However, low relative density does not imply low absolute density. In other words, the minimum predicted relative density (Figures 7.8-7.21) may still correspond to a substantial number of birds and therefore a substantial number of sightings.

The potential foraging areas (unmodeled species) and predicted areas of high relative density (modeled species) identified in this assessment can help inform marine spatial planning around the MHI by indicating areas where human activities could affect relatively larger numbers of seabirds. That being said, there is also the potential to affect birds in other areas, particularly during months not covered by the data analyzed here. At a finer temporal scale, there are large short-term aggregations of birds that might not have been reflected in the survey data. For example, large numbers of birds staging nearshore prior to returning to breeding colonies each day may have been missed depending on the specific timing of surveys in those areas. Similarly, regular movements of large numbers of birds through specific areas could have been missed. Model predictions of relative density in particular will not necessarily reflect areas that are used by birds regularly but for only short periods of time (e.g., movement corridors).

Interpretation of our model predictions of relative density to inform spatial planning should be at the regional scale (i.e., 10-100 km). Large variations in model predictions of relative density at a finer spatial scale may not be realistic. Several models exhibited narrow strips or features of predicted high relative density; e.g., Brown Booby around the islands and Juan Fernandez Petrel and Sooty Tern west and southwest of the island of Hawai'i. Other times modeled patterns of relative density were patchy; e.g., Mottled Petrel in southeast part of study area. Such large variation in average long-term relative density at such fine spatial scales is likely unrealistic in many cases. These patterns in modeled relative density arose because of strong estimated correlations between counts and environmental predictor variables that exhibited fine scale variation (e.g., bathymetry) or patchiness (e.g., chlorophyll-*a*). Management applications should not assume that fine-scale variation in model predictions of relative density (i.e., 1-10 km) is realistic.

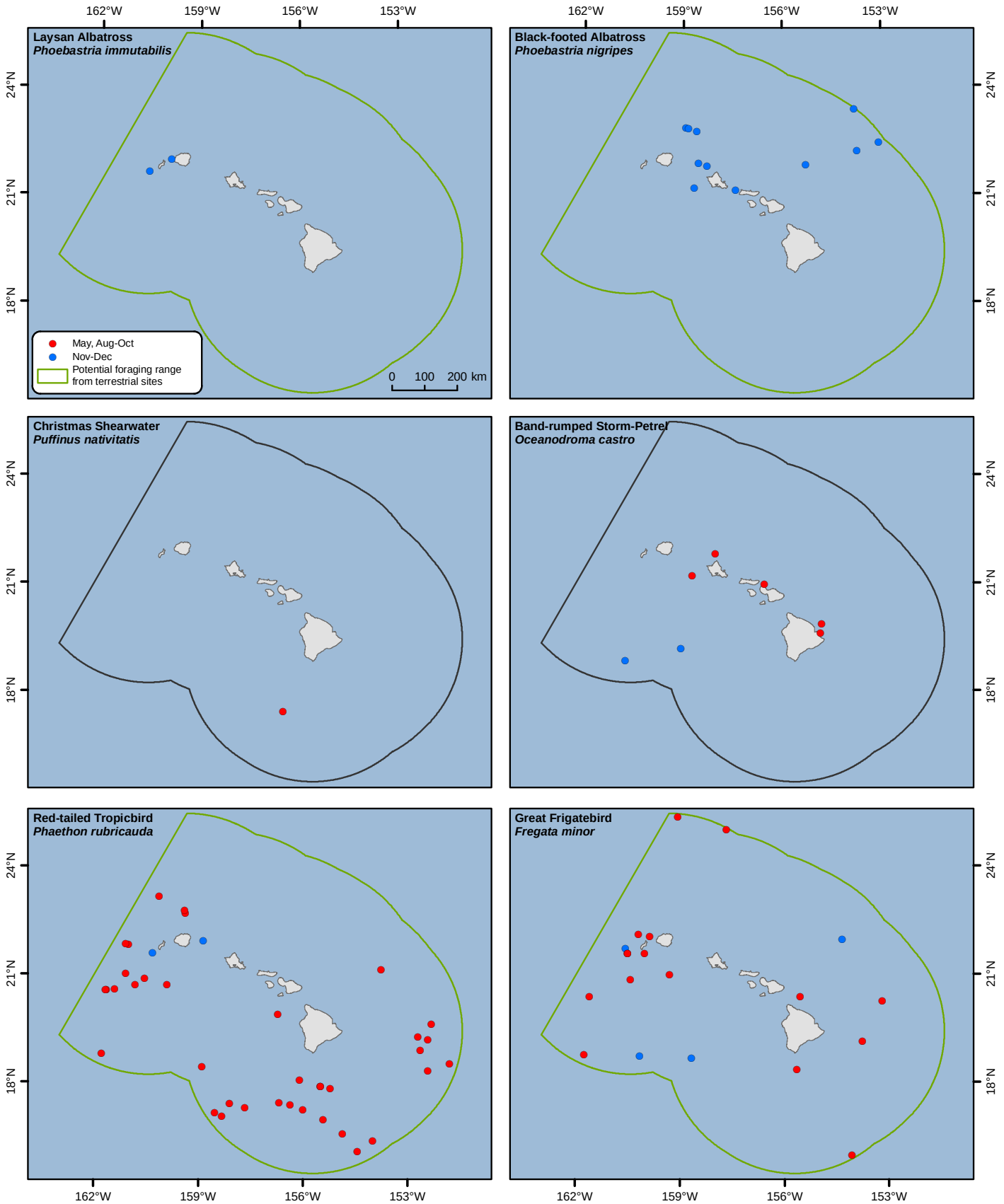

Figure 7.6. Locations of sightings of unmodeled seabird species. Survey data span 1989-2012 (most from 2002 and 2010) and were provided by NOAA NMFS/SWFSC. Survey effort was 16,377 transect segments during May and August-October (summer) and 3,168 during November-December (winter), and the distribution of survey effort differed between seasons (Figure 7.3), so seasonal differences in the number and distribution of sightings do not necessarily reflect differences in relative abundance. Potential foraging ranges only apply to breeding individuals. Foraging ranges were clipped to the study area, and are not displayed if foraging range estimates were not available.

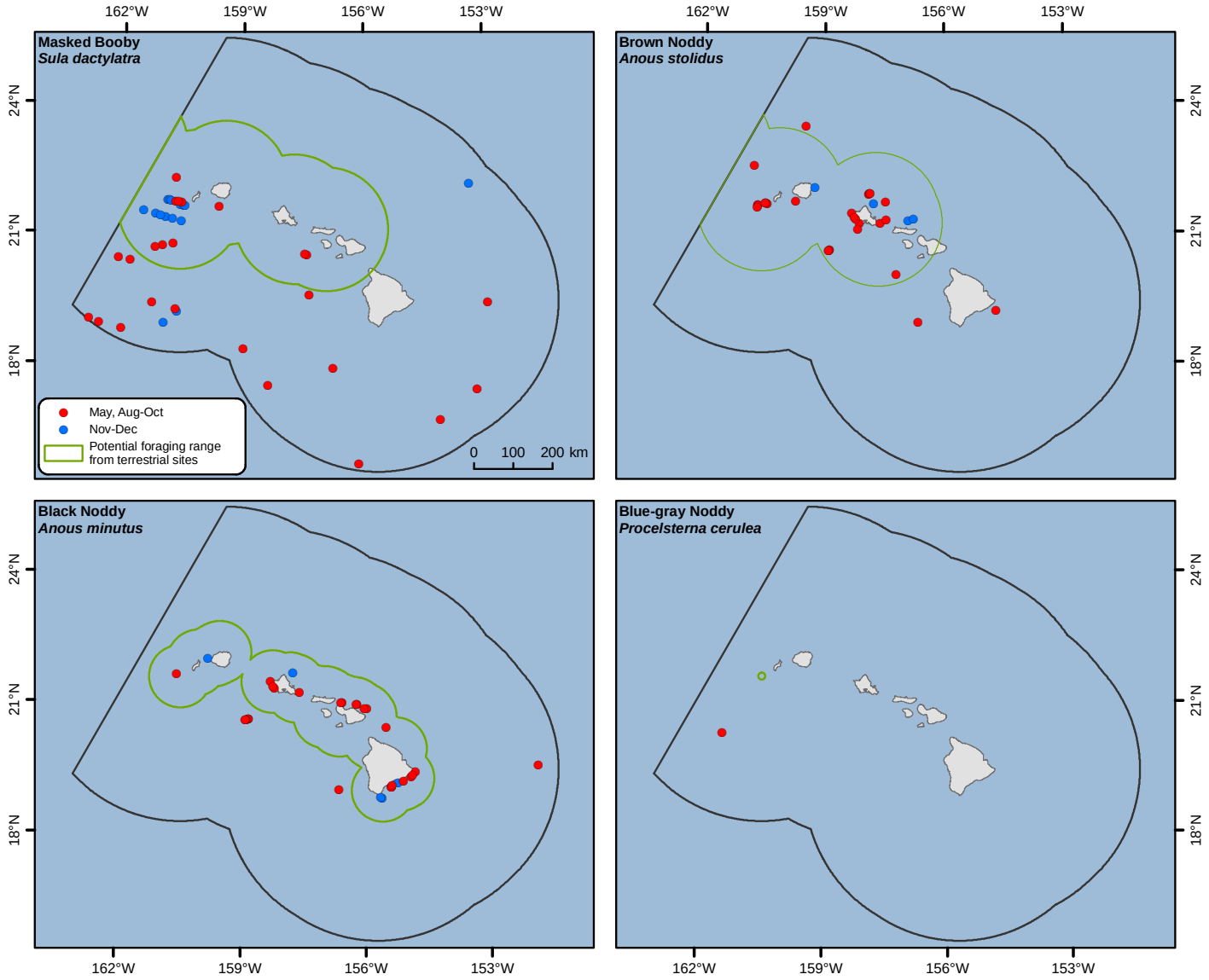

Figure 7.7. Locations of sightings of unmodeled seabird species. Survey data span 1989-2012 (most from 2002 and 2010) and were provided by NOAA NMFS/SWFSC. Survey effort was 16,377 transect segments during May and August-October (summer) and 3,168 during November-December (winter), and the distribution of survey effort differed between seasons (Figure 7.3), so seasonal differences in the number and distribution of sightings do not necessarily reflect differences in relative abundance. Potential foraging ranges only apply to breeding individuals. Foraging ranges were clipped to the study area, and are not displayed if foraging range estimates were not available.

Juan Fernandez Petrel, Pterodroma externa, *and Red-tailed Tropicbird,* Phaethon rubricauda *(left and middle; Daniel Webster, Cascadia Research Collective) and Brown Booby,* Sula leucogaster *(right; David Pereksta, BOEM).*

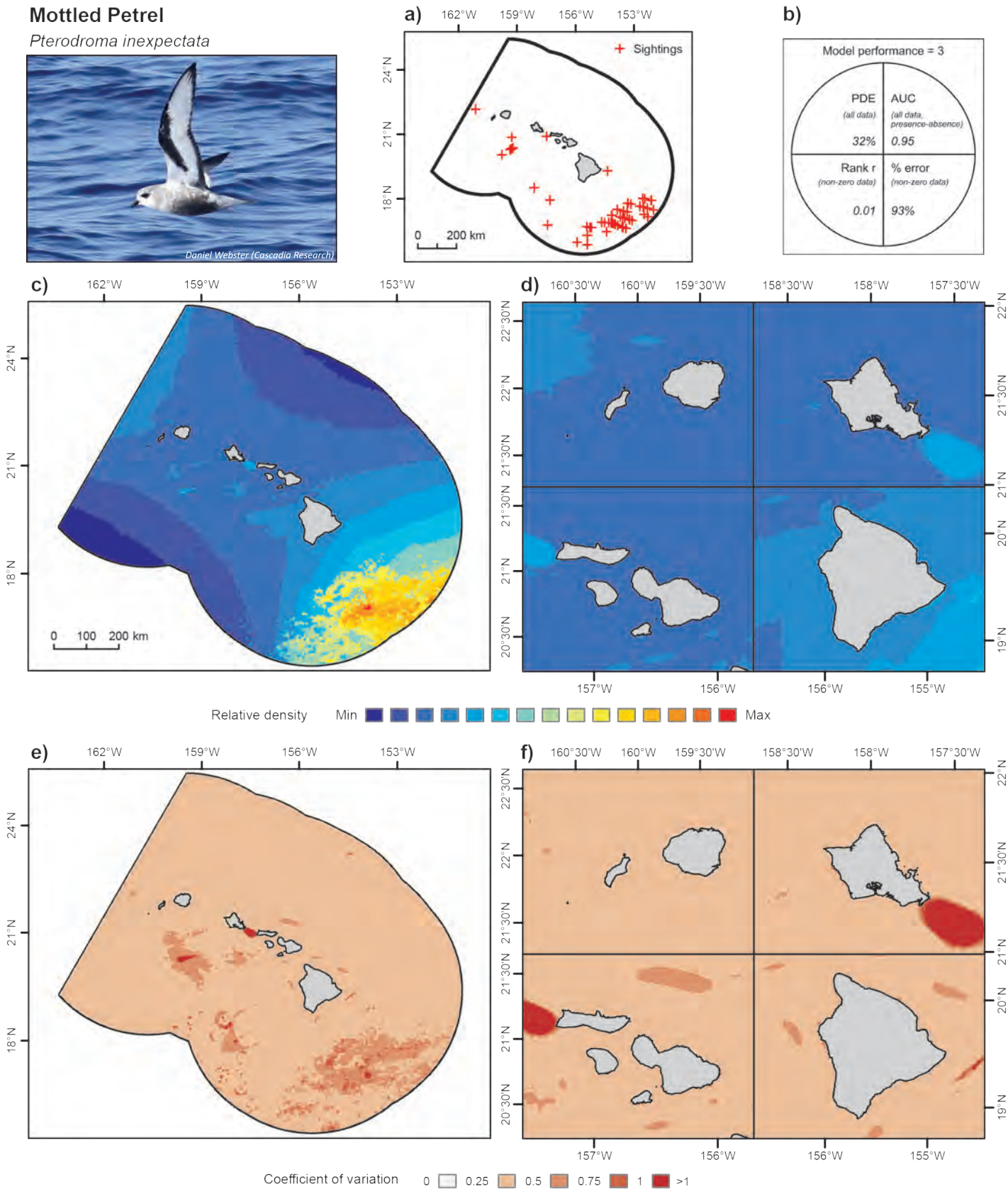

*Figure 7.8. Modeled relative density of Mottled Petrel (*Pterodroma inexpectata*). Predictive modelling was applied to at-sea sightings data spanning 1989-2012 (most data from 2002 and 2010) provided by NOAA NMFS/SWFSC. Modeled data were mainly from August-October with some additional data from May. A total of 16,377 transect segments were analyzed, on 55 of which this species was sighted for a total of 56 individuals sighted. Figure panels are: a) locations of sightings; b) model quality as a function of four performance metrics (Table B.4); c,d) median bootstrapped estimates of relative density; and e,f) bootstrapped coefficients of variation. Photo credit: Daniel Webster (Cascadia Research Collective)*

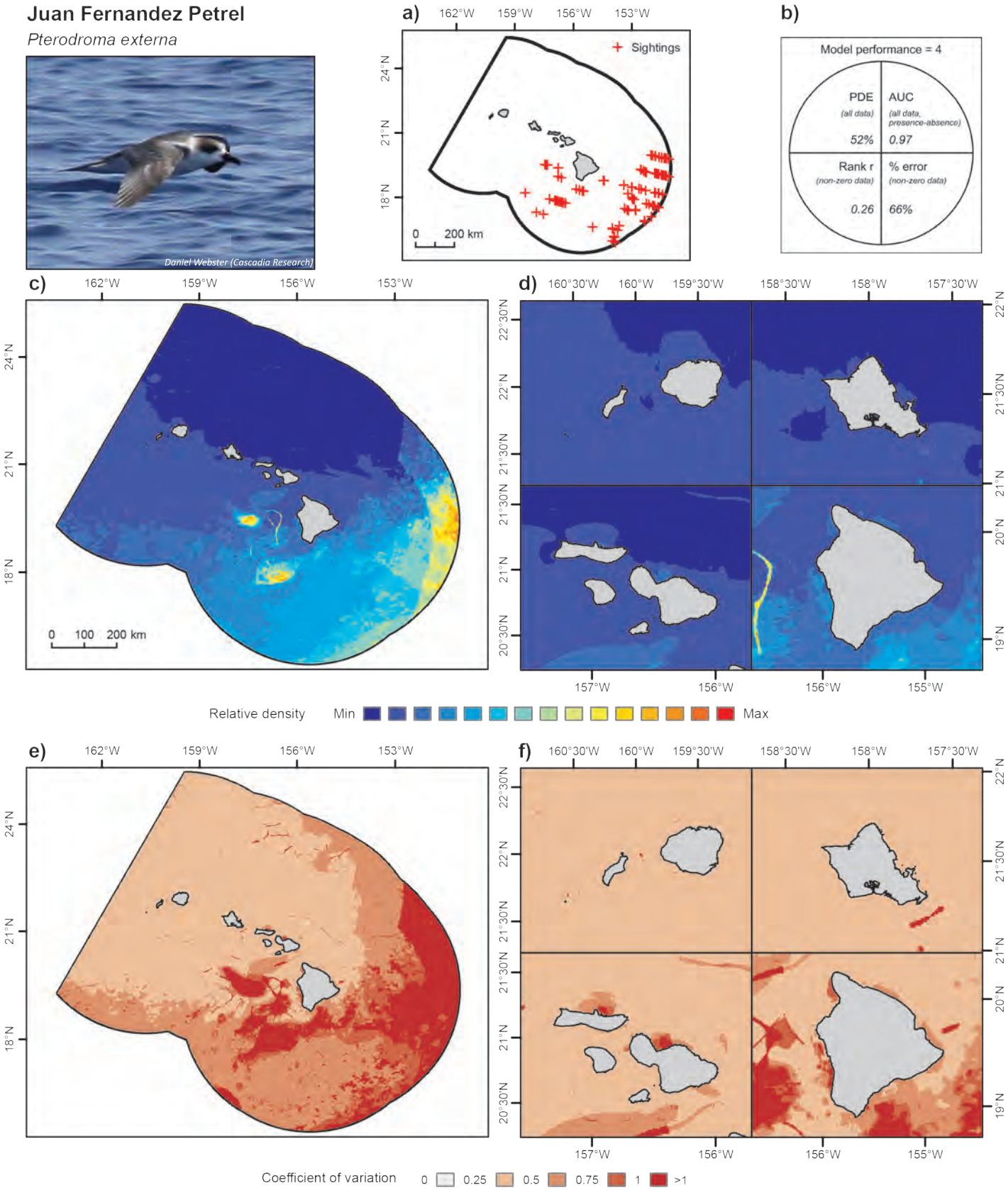

*Figure 7.9. Modeled relative density of Juan Fernandez Petrel (*Pterodroma externa*). Predictive modelling was applied to at-sea sightings data spanning 1989-2012 (most data from 2002 and 2010) provided by NOAA NMFS/SWFSC. Modeled data were mainly from August-October with some additional data from May. A total of 16,377 transect segments were analyzed, on 108 of which this species was sighted for a total of 157 individuals sighted. Figure panels are: a) locations of sightings; b) model quality as a function of four performance metrics (Table B.4); c,d) median bootstrapped estimates of relative density; and e,f) bootstrapped coefficients of variation. Photo credit: Daniel Webster (Cascadia Research Collective)*

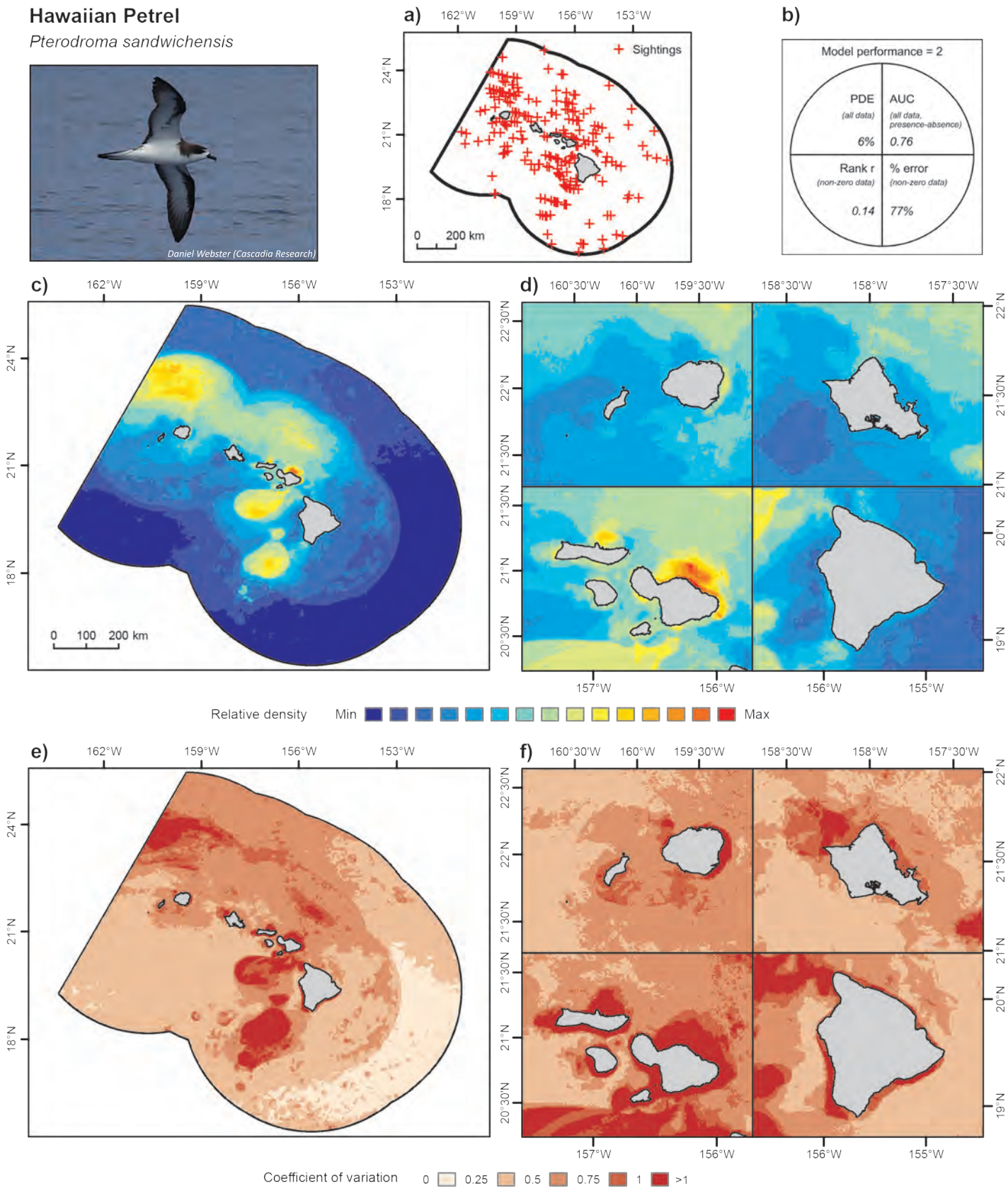

*Figure 7.10. Modeled relative density of Hawaiian Petrel (*Pterodroma sandwichensis*). Predictive modelling was applied to at-sea sightings data spanning 1989-2012 (most data from 2002 and 2010) provided by NOAA NMFS/SWFSC. Modeled data were mainly from August-October with some additional data from May. A total of 16,377 transect segments were analyzed, on 230 of which this species was sighted for a total of 292 individuals sighted. Figure panels are: a) locations of sightings; b) model quality as a function of four performance metrics (Table B.4); c,d) median bootstrapped estimates of relative density; and e,f) bootstrapped coefficients of variation. Photo credit: Daniel Webster (Cascadia Research Collective)*

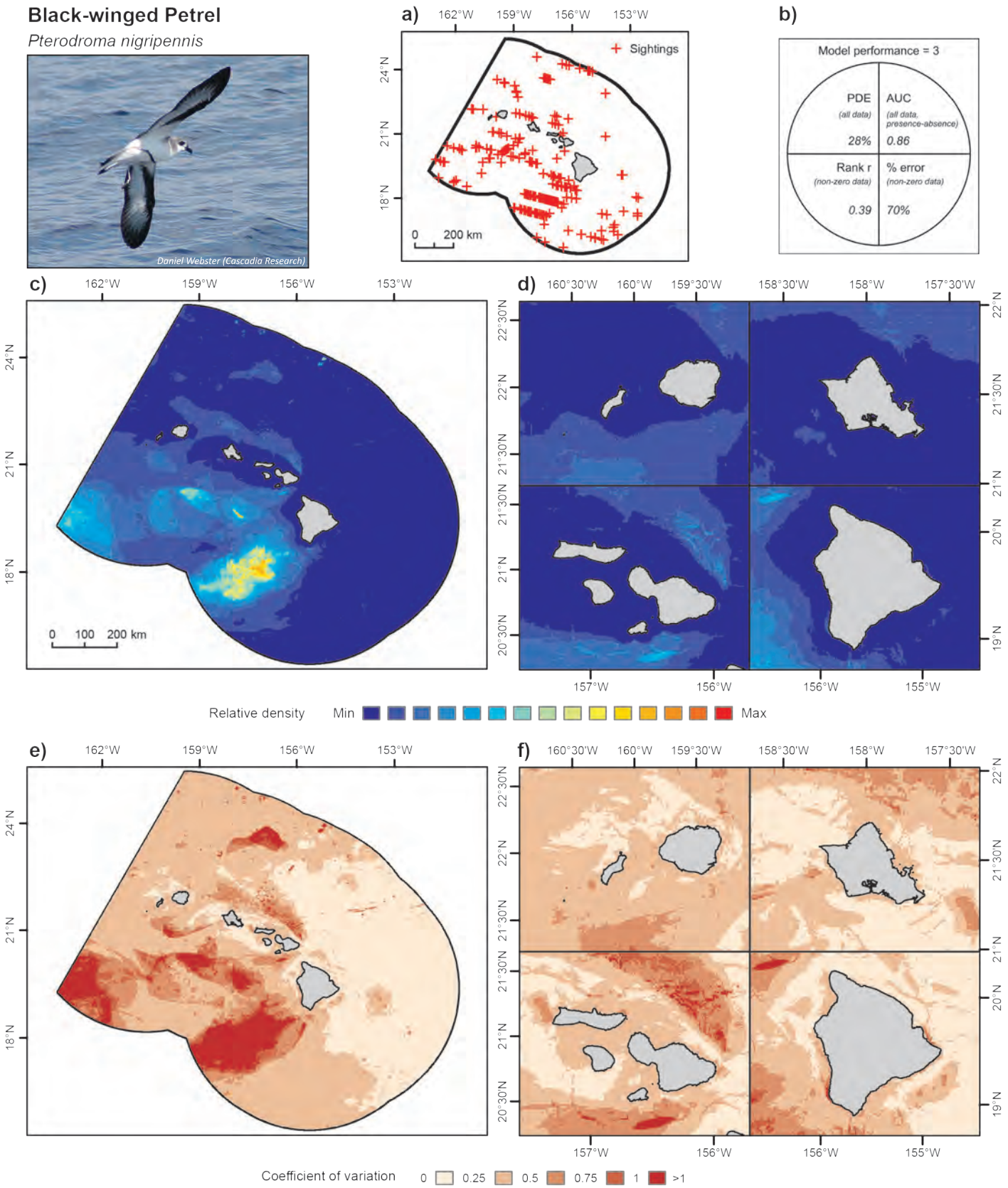

*Figure 7.11. Modeled relative density of Black-winged Petrel (*Pterodroma nigripennis*). Predictive modelling was applied to at-sea sightings data spanning 1989-2012 (most data from 2002 and 2010) provided by NOAA NMFS/SWFSC. Modeled data were mainly from August-October with some additional data from May. A total of 16,377 transect segments were analyzed, on 243 of which this species was sighted for a total of 337 individuals sighted. Figure panels are: a) locations of sightings; b) model quality as a function of four performance metrics (Table B.4); c,d) median bootstrapped estimates of relative density; and e,f) bootstrapped coefficients of variation. Photo credit: Daniel Webster (Cascadia Research Collective)*

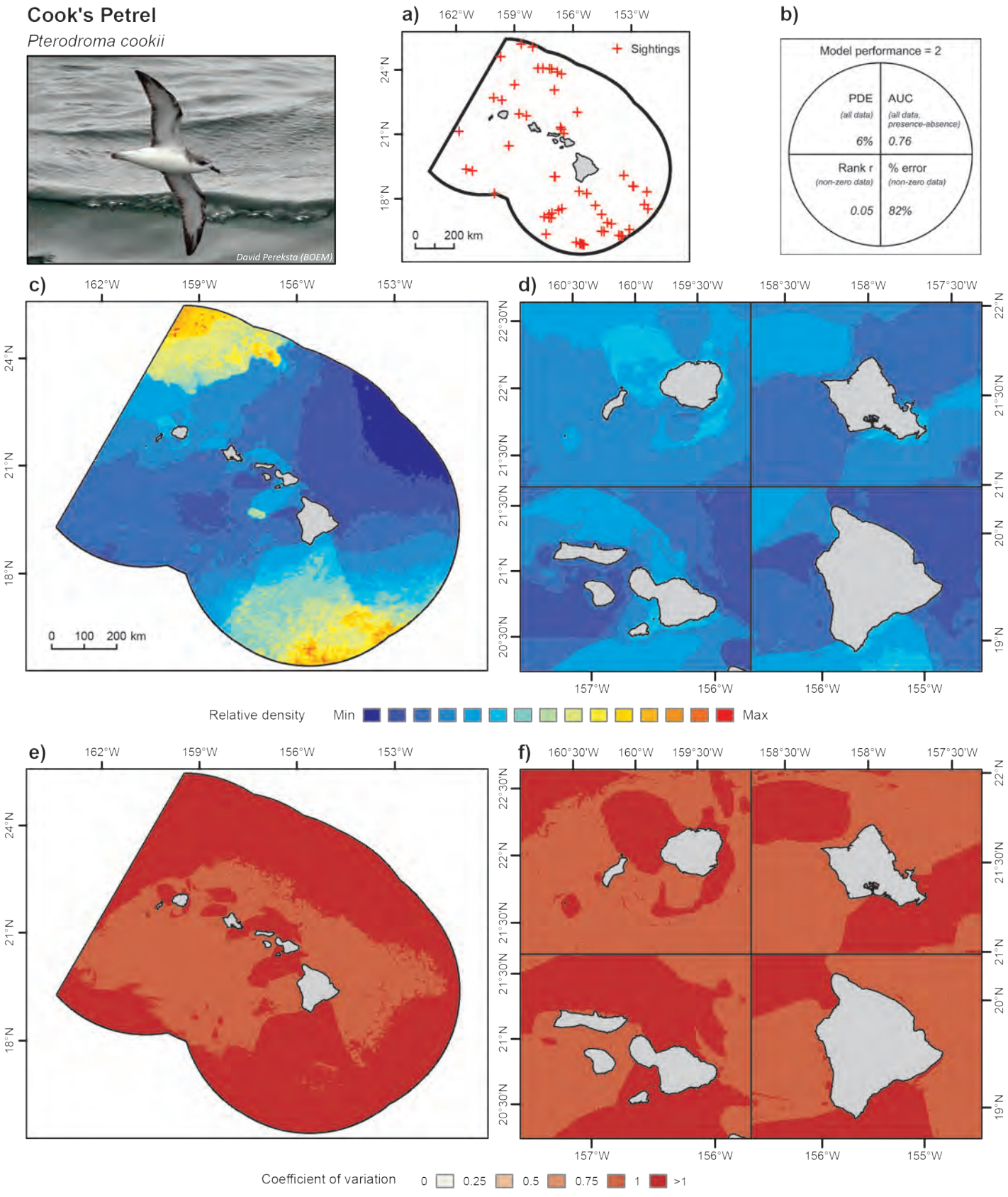

*Figure 7.12. Modeled relative density of Cook's Petrel (*Pterodroma cookii*). Predictive modelling was applied to at-sea sightings data spanning 1989-2012 (most data from 2002 and 2010) provided by NOAA NMFS/SWFSC. Modeled data were mainly from August-October with some additional data from May. A total of 16,377 transect segments were analyzed, on 62 of which this species was sighted for a total of 75 individuals sighted. Figure panels are: a) locations of sightings; b) model quality as a function of four performance metrics (Table B.4); c,d) median bootstrapped estimates of relative density; and e,f) bootstrapped coefficients of variation. Photo credit: David Pereksta (BOEM)*

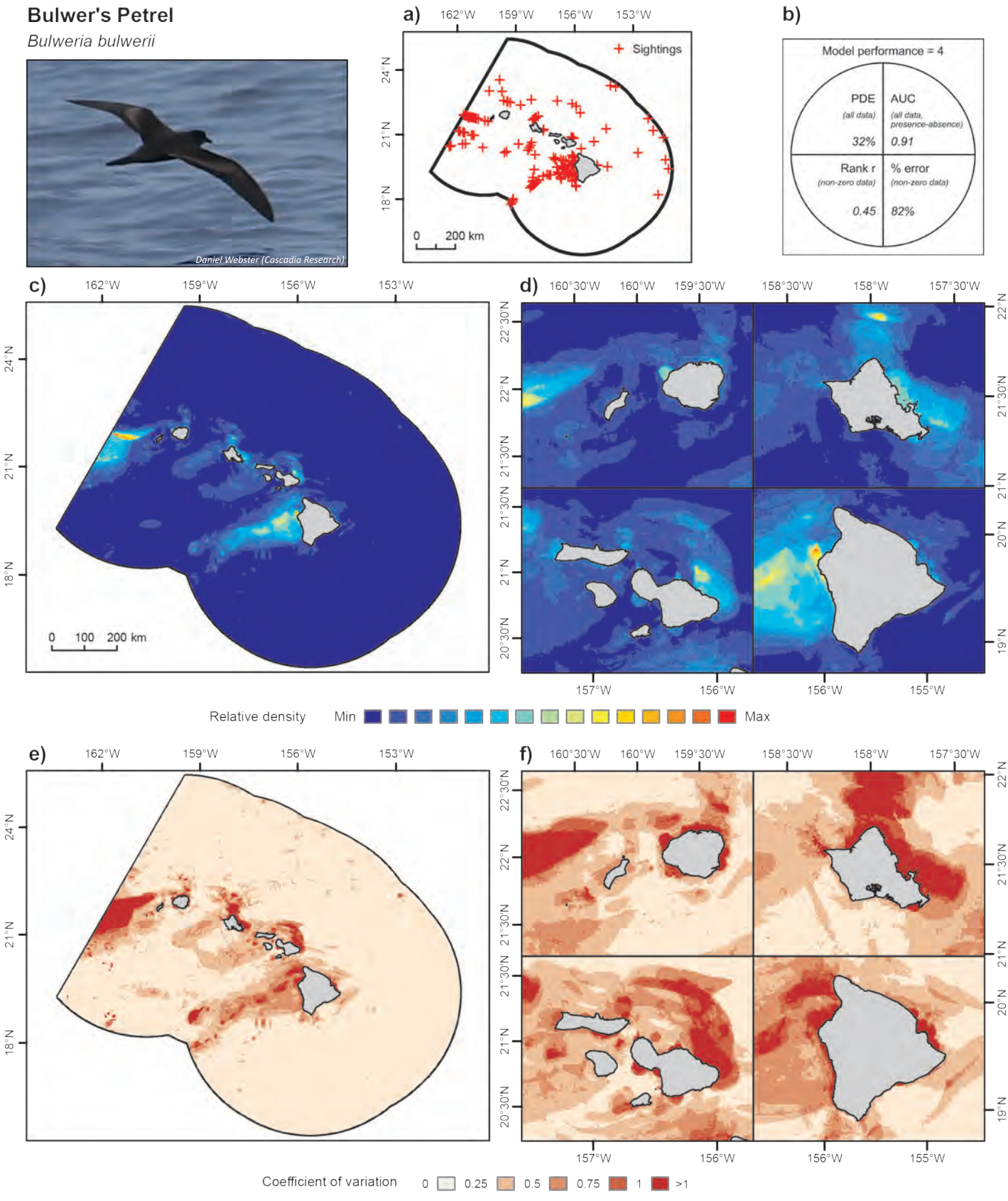

*Figure 7.13. Modeled relative density of Bulwer's Petrel (*Bulweria bulwerii*). Predictive modelling was applied to at-sea sightings data spanning 1989-2012 (most data from 2002 and 2010) provided by NOAA NMFS/SWFSC. Modeled data were mainly from August-October with some additional data from May. A total of 16,377 transect segments were analyzed, on 194 of which this species was sighted for a total of 230 individuals sighted. Figure panels are: a) locations of sightings; b) model quality as a function of four performance metrics (Table B.4); c,d) median bootstrapped estimates of relative density; and e,f) bootstrapped coefficients of variation. Photo credit: Daniel Webster (Cascadia Research Collective)*

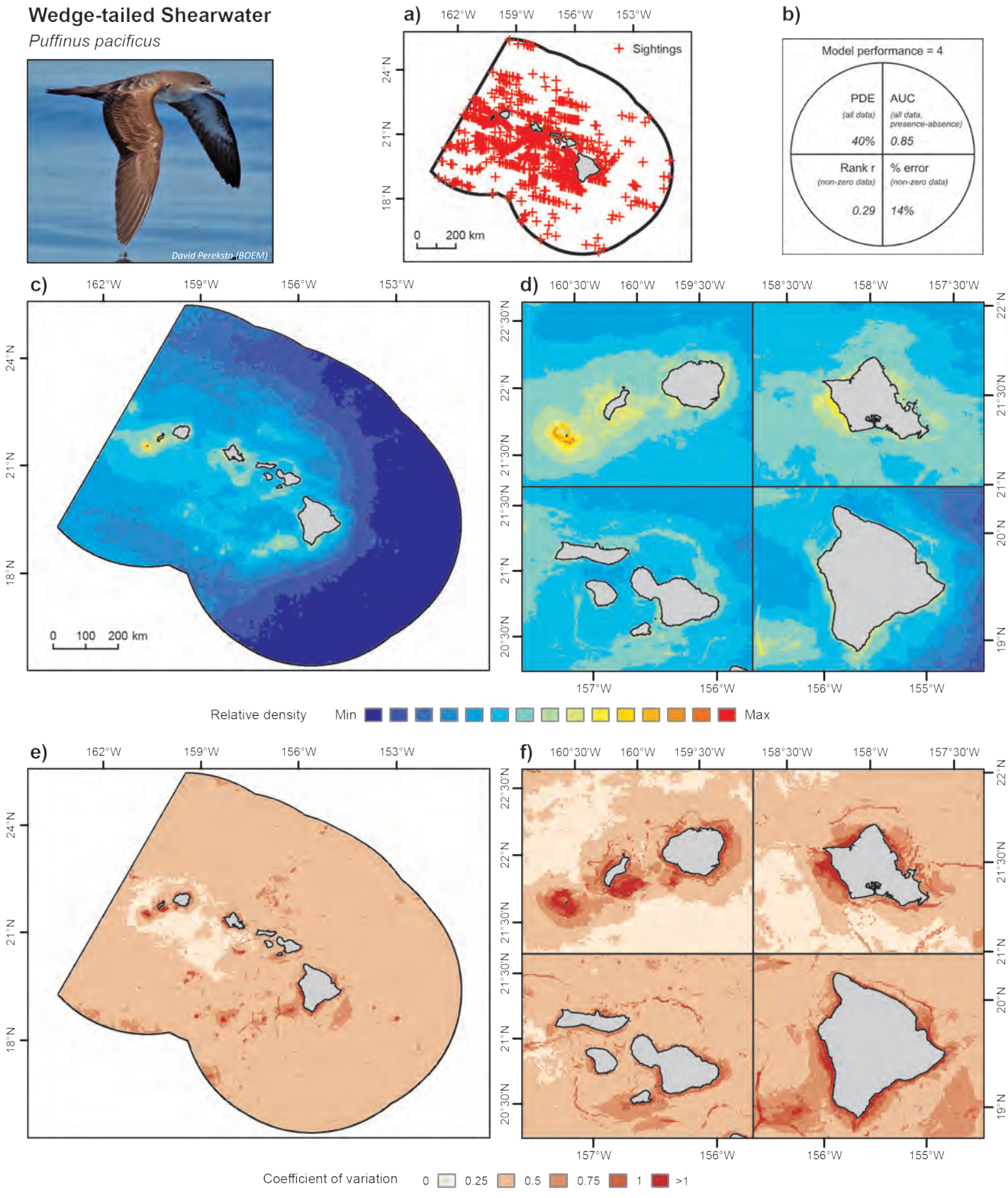

*Figure 7.14. Modeled relative density of Wedge-tailed Shearwater (*Puffinus pacificus*). Predictive modelling was applied to at-sea sightings data spanning 1989-2012 (most data from 2002 and 2010) provided by NOAA NMFS/SWFSC. Modeled data were mainly from August-October with some additional data from May. A total of 16,377 transect segments were analyzed, on 1375 of which this species was sighted for a total of 6442 individuals sighted. Figure panels are: a) locations of sightings; b) model quality as a function of four performance metrics (Table B.4); c,d) median bootstrapped estimates of relative density; and e,f) bootstrapped coefficients of variation. Photo credit: David Pereksta (BOEM)*

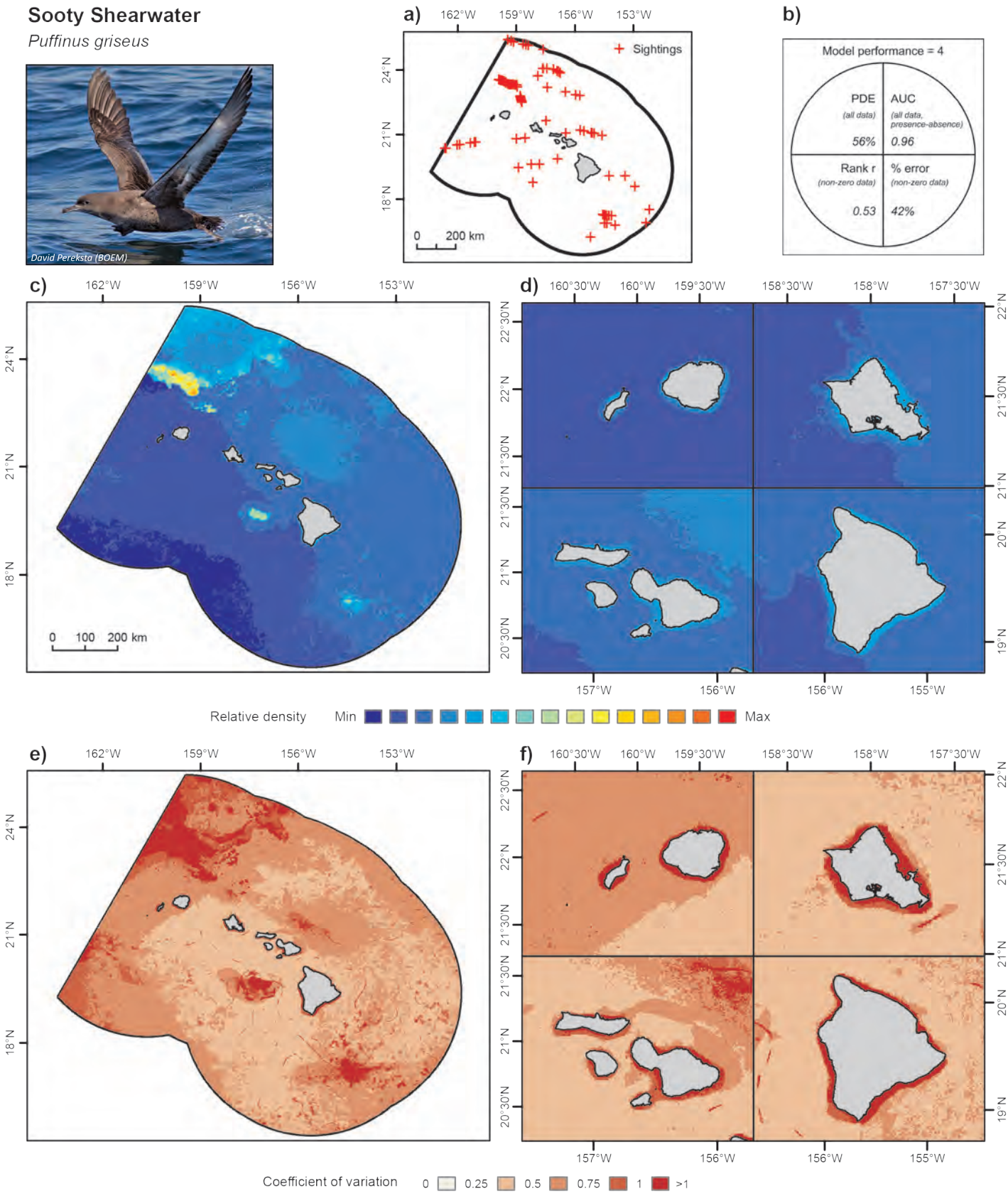

*Figure 7.15. Modeled relative density of Sooty Shearwater (*Puffinus griseus*). Predictive modelling was applied to at-sea sightings data spanning 1989-2012 (most data from 2002 and 2010) provided by NOAA NMFS/SWFSC. Modeled data were mainly from August-October with some additional data from May. A total of 16,377 transect segments were analyzed, on 115 of which this species was sighted for a total of 268 individuals sighted. Figure panels are: a) locations of sightings; b) model quality as a function of four performance metrics (Table B.4); c,d) median bootstrapped estimates of relative density; and e,f) bootstrapped coefficients of variation. Photo credit: David Pereksta (BOEM)*

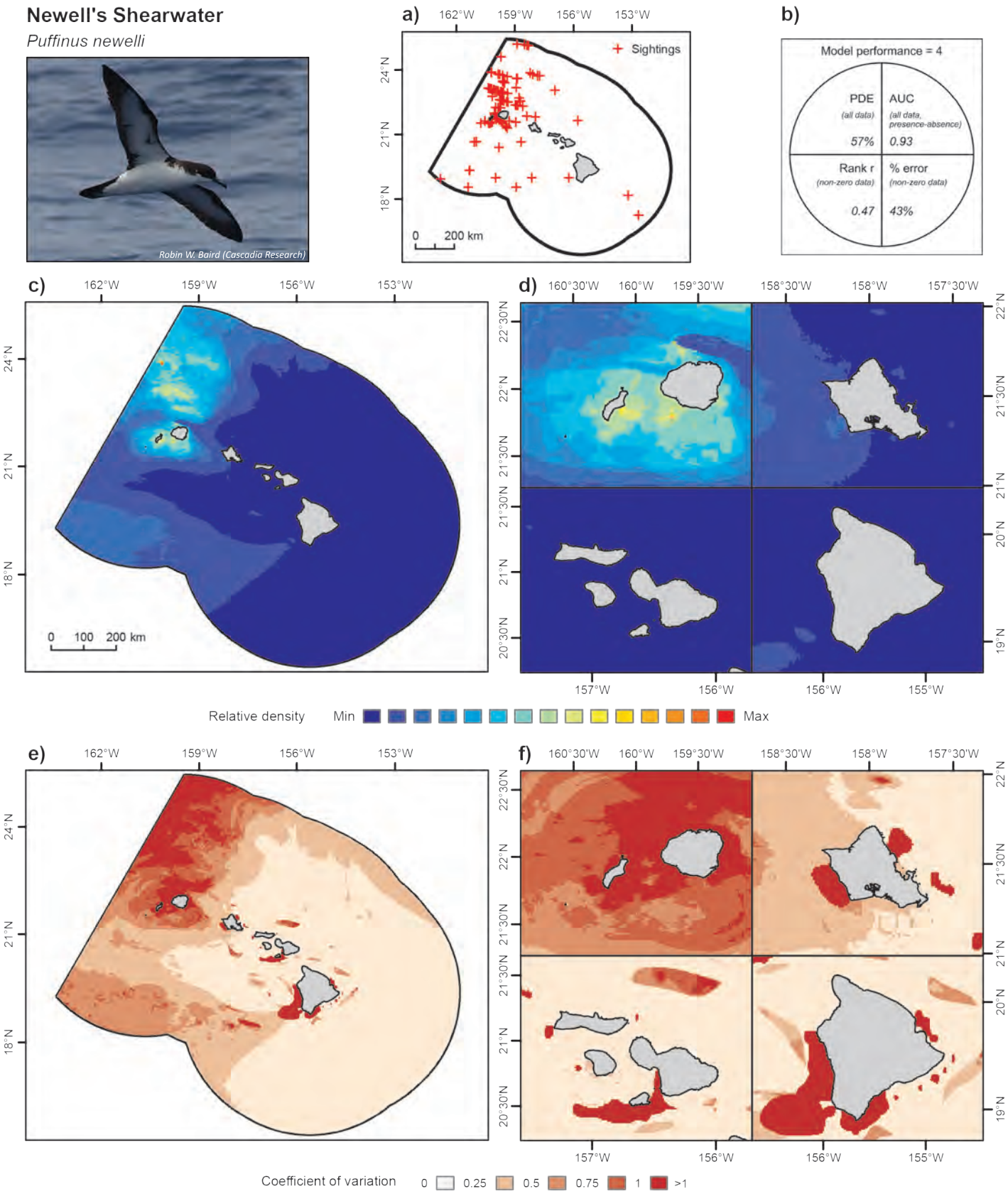

*Figure 7.16. Modeled relative density of Newell's Shearwater (*Puffinus newelli*). Predictive modelling was applied to at-sea sightings data spanning 1989-2012 (most data from 2002 and 2010) provided by NOAA NMFS/SWFSC. Modeled data were mainly from August-October with some additional data from May. A total of 16,377 transect segments were analyzed, on 105 of which this species was sighted for a total of 235 individuals sighted. Figure panels are: a) locations of sightings; b) model quality as a function of four performance metrics (Table B.4); c,d) median bootstrapped estimates of relative density; and e,f) bootstrapped coefficients of variation. Photo credit: Robin W. Baird (Cascadia Research Collective)*

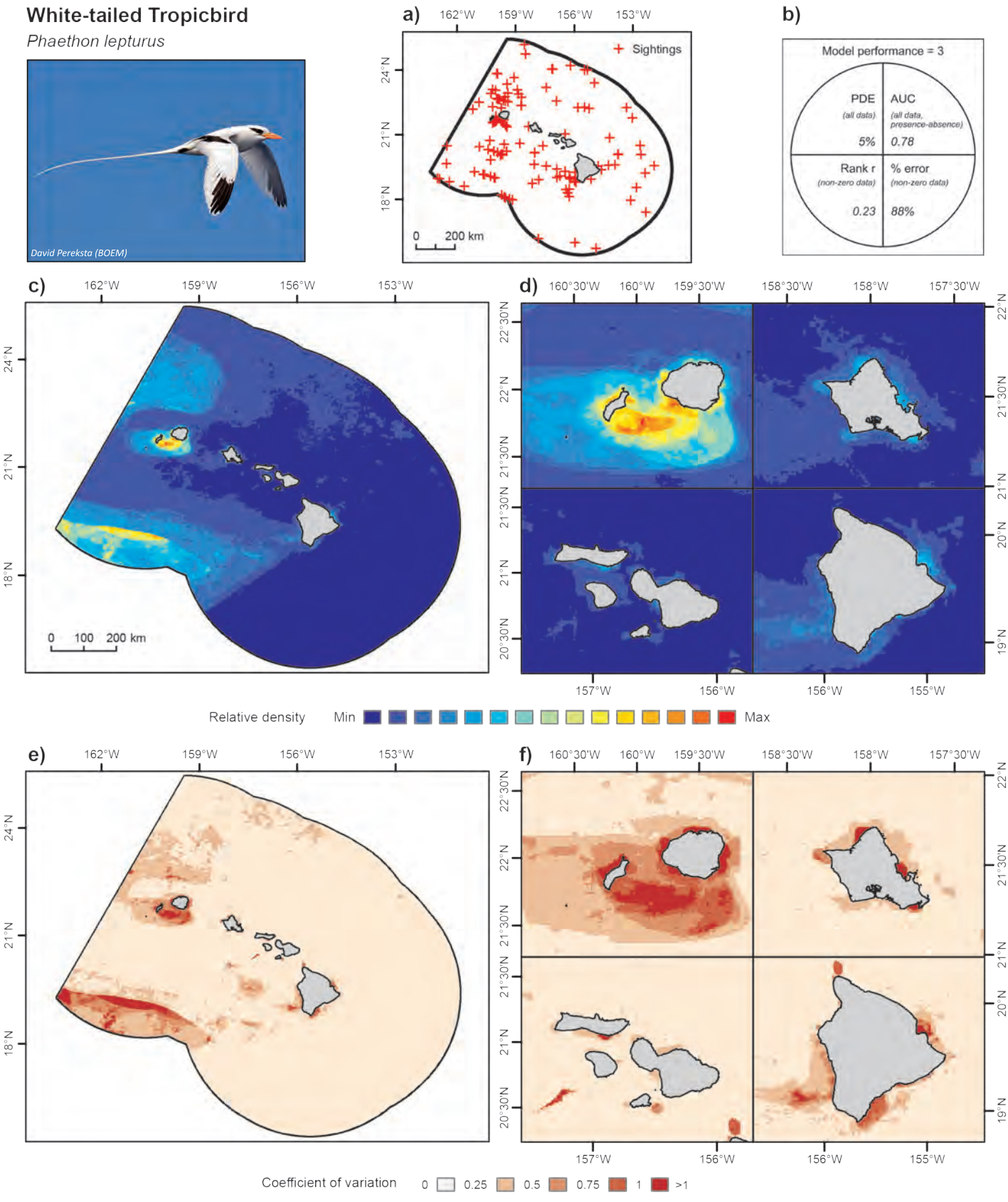

*Figure 7.17. Modeled relative density of White-tailed Tropicbird (*Phaethon lepturus*). Predictive modelling was applied to at-sea sightings data spanning 1989-2012 (most data from 2002 and 2010) provided by NOAA NMFS/SWFSC. Modeled data were mainly from August-October with some additional data from May. A total of 16,377 transect segments were analyzed, on 128 of which this species was sighted for a total of 144 individuals sighted. Figure panels are: a) locations of sightings; b) model quality as a function of four performance metrics (Table B.4); c,d) median bootstrapped estimates of relative density; and e,f) bootstrapped coefficients of variation. Photo credit: David Pereksta (BOEM)*

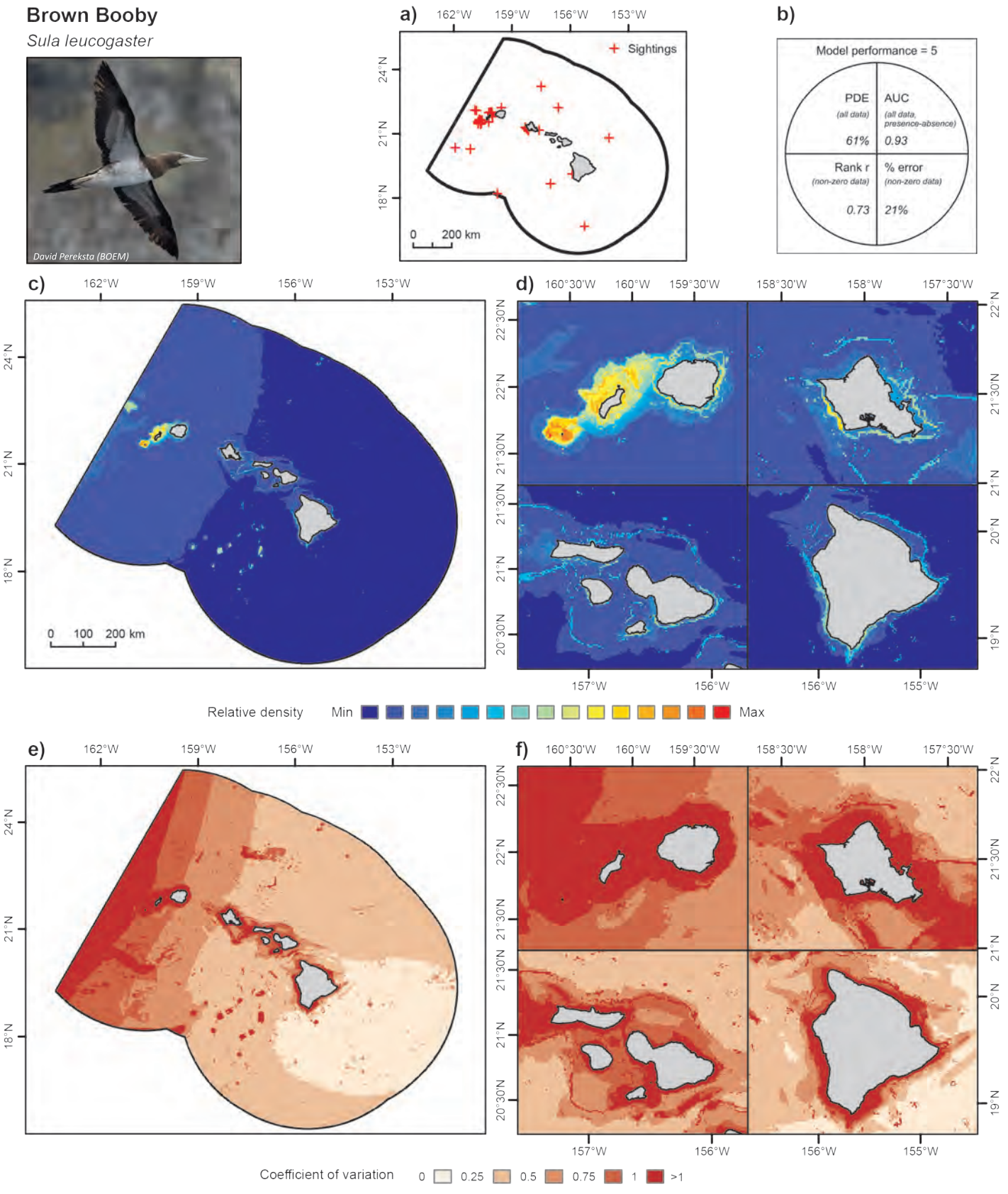

*Figure 7.18. Modeled relative density of Brown Booby (*Sula leucogaster*). Predictive modelling was applied to at-sea sightings data spanning 1989-2012 (most data from 2002 and 2010) provided by NOAA NMFS/SWFSC. Modeled data were mainly from August-October with some additional data from May. A total of 16,377 transect segments were analyzed, on 48 of which this species was sighted for a total of 232 individuals sighted. Figure panels are: a) locations of sightings; b) model quality as a function of four performance metrics (Table B.4); c,d) median bootstrapped estimates of relative density; and e,f) bootstrapped coefficients of variation. Photo credit: David Pereksta (BOEM)*

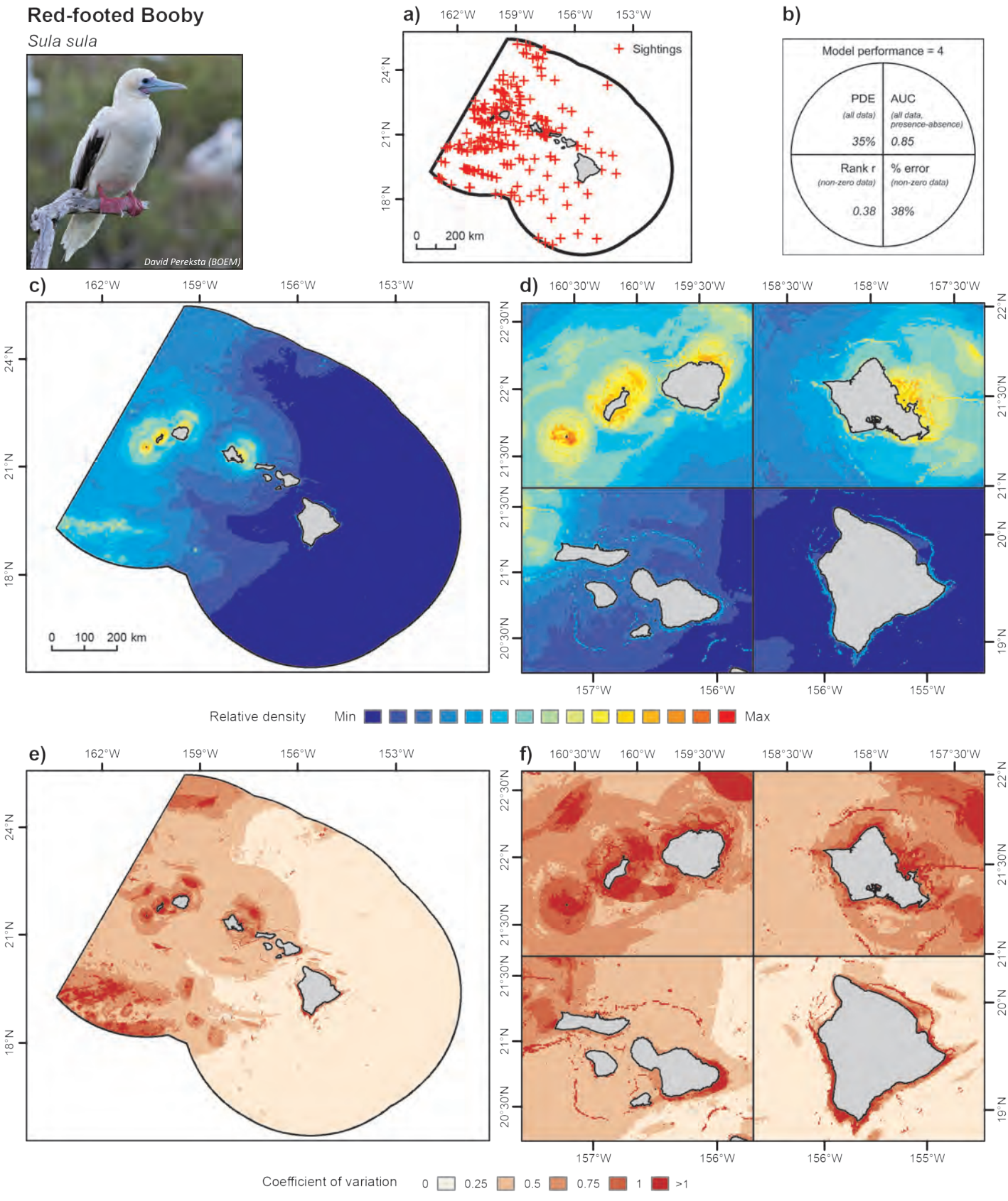

*Figure 7.19. Modeled relative density of Red-footed Booby (*Sula sula*). Predictive modelling was applied to at-sea sightings data spanning 1989-2012 (most data from 2002 and 2010) provided by NOAA NMFS/SWFSC. Modeled data were mainly from August-October with some additional data from May. A total of 16,377 transect segments were analyzed, on 271 of which this species was sighted for a total of 669 individuals sighted. Figure panels are: a) locations of sightings; b) model quality as a function of four performance metrics (Table B.4); c,d) median bootstrapped estimates of relative density; and e,f) bootstrapped coefficients of variation. Photo credit: David Pereksta (BOEM)*

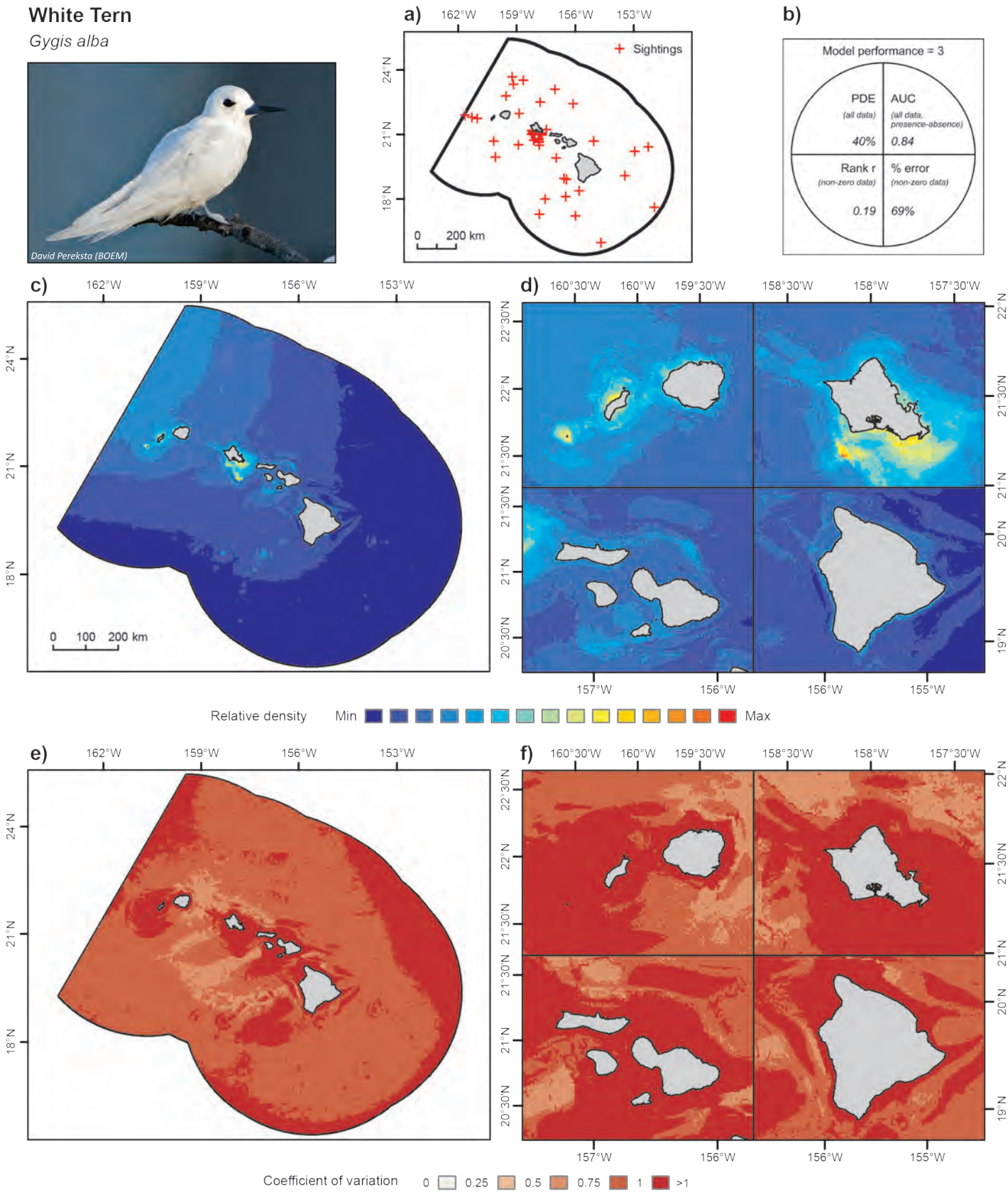

*Figure 7.20. Modeled relative density of White Tern (*Gygis alba*). Predictive modelling was applied to at-sea sightings data spanning 1989-2012 (most data from 2002 and 2010) provided by NOAA NMFS/SWFSC. Modeled data were mainly from August-October with some additional data from May. A total of 16,377 transect segments were analyzed, on 60 of which this species was sighted for a total of 86 individuals sighted. Figure panels are: a) locations of sightings; b) model quality as a function of four performance metrics (Table B.4); c,d) median bootstrapped estimates of relative density; and e,f) bootstrapped coefficients of variation. Photo credit: David Pereksta (BOEM)*

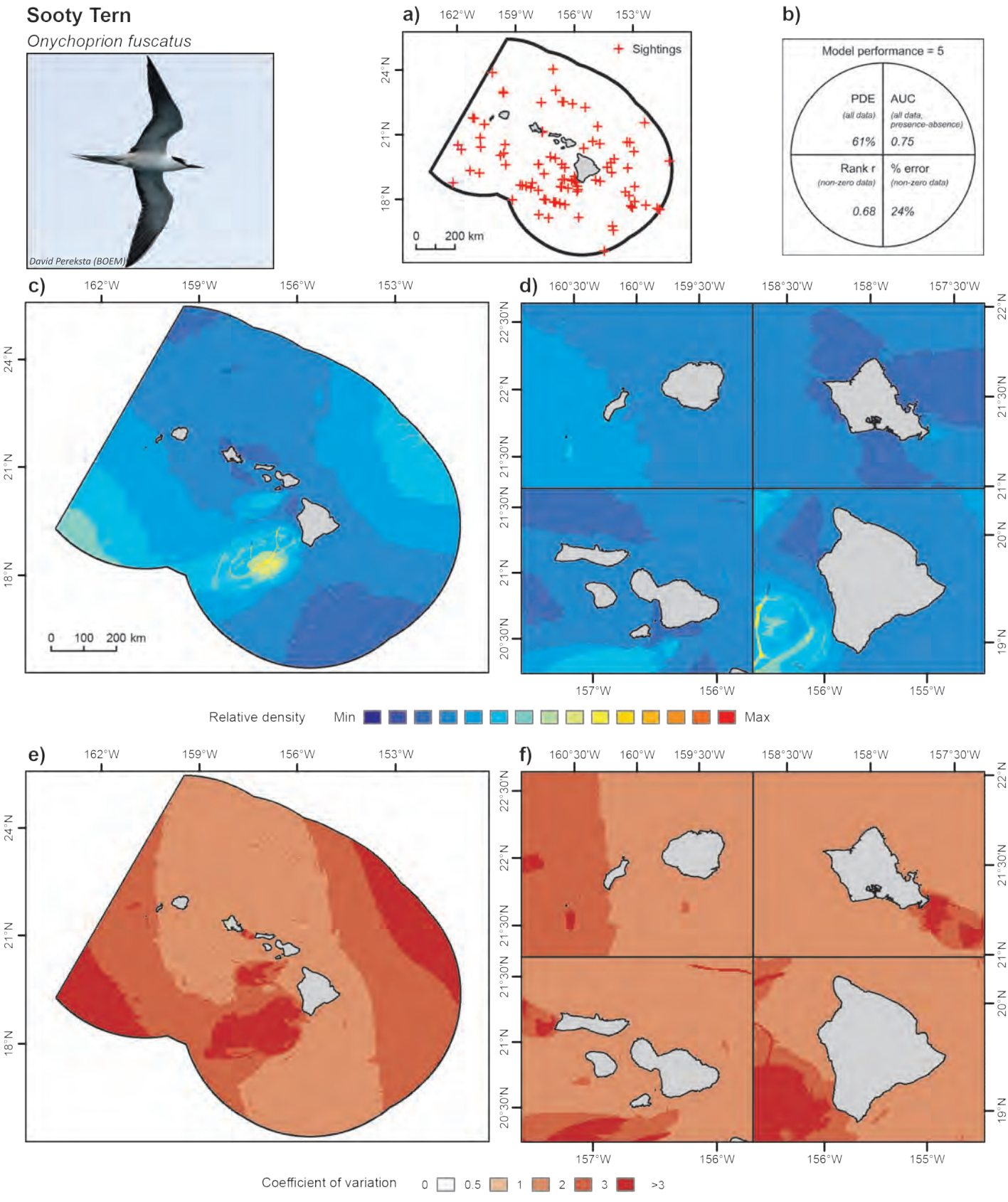

*Figure 7.21. Modeled relative density of Sooty Tern (*Onychoprion fuscatus*). Predictive modelling was applied to at-sea sightings data spanning 1989-2012 (most data from 2002 and 2010) provided by NOAA NMFS/SWFSC. Modeled data were mainly from August-October with some additional data from May. A total of 16,377 transect segments were analyzed, on 94 of which this species was sighted for a total of 734 individuals sighted. Figure panels are: a) locations of sightings; b) model quality as a function of four performance metrics (Table B.4); c,d) median bootstrapped estimates of relative density; and e,f) bootstrapped coefficients of variation. Photo credit: David Pereksta (BOEM)*

7.3.2. Model statistical performance

Of the eight candidate models for each of the 14 species (Appendix B), no one model was consistently selected as the best model. Over half of the selected final models converged well before the allowed maximum number of boosting iterations, but four models reached near the maximum number of iterations before converging.

Final model statistical performance was highly variable across species and performance metrics. Percent deviance explained (PDE) ranged from 5-61 percent. The Brown Booby and Sooty Tern models had the highest PDE (60-61%), indicating that those models explained substantially more of the variation in the survey count data than did a simpler model with no predictor variables. The models for Cook's Petrel, Hawaiian Petrel and White-tailed Tropicbird had the lowest PDE (5-6%). Area under the receiver operating characteristic curve (AUC) ranged from 0.75-0.97, indicating that all models predicted presence/absence better than random. The models for Juan Fernandez Petrel, Mottled Petrel and Sooty Shearwater had the highest AUC (0.95-0.97), while the models for Cook's Petrel, Hawaiian Petrel, Sooty Tern and White-tailed Tropicbird had AUC between 0.7 and 0.8. The Gaussian rank correlation coefficient (*r*) ranged from 0.01-0.73. The models for Brown Booby and Sooty Tern had *r* between 0.68 and 0.73, indicating that the observed and predicted non-zero counts of these species were fairly correlated. The models for Cook's Petrel, Hawaiian Petrel and White Tern (*Gygis alba*) had $r < 0.2$, and the model for Mottled Petrel had the lowest *r*. Percent error ranged from 0.14-0.93, indicating that the median absolute difference between predicted and observed non-zero counts ranged from 14-93 percent of the average non-zero count. Brown Booby, Sooty Tern and Wedge-tailed Shearwater had the lowest percent error (0.14-0.24), while Mottled Petrel and White-tailed Tropicbird had the highest percent error (0.88-0.93).

Sooty Tern, Onychoprion fuscatus. *Photo credit: Daniel Webster (Cascadia Research Collective)*

White Tern, Gygis alba. *Photo credit: David Pereksta (BOEM)*

Considering all four performance metrics, the final models for Brown Booby and Sooty Tern had the best overall performance (Class 5), while the models for Hawaiian Petrel and Cook's Petrel had the worst performance (Class 2). The performance of all other models was intermediate (Classes 3 and 4).

It is important to recognize that the model performance metrics and badge mainly reflect *the statistical fit of the models to the data*. They reflect only the data that were analyzed, and they do not reflect the quality of model predictions away from the data. For example, the survey data were primarily from two years and three months. The performance metrics do not necessarily indicate how accurate the model predictions may be for other years and months. Similarly, survey data did not cover everywhere within the study area, so some model predictions are essentially interpolations/extrapolations from data in other parts of the study area. The accuracy of those predictions is not necessarily reflected by the model performance metrics. Data from additional years, months, and areas would be required to fully evaluate the accuracy of model predictions outside of the observed data coverage. Nevertheless, the performance metrics and overall performance class give a relative indication of how accurately a model was able to predict the observed data, and better performance provides a measure of confidence in the model predictions, especially within the temporal and spatial coverage of the observed survey data.

7.3.3. Potentially important ecological predictors for modeled species

Our spatial predictive modeling framework was designed to provide the best estimates of at-sea distributions. It was not designed to determine which environmental predictors were most ecologically relevant in determining the distributions of birds, nor was it designed to determine the functional relationships between environmental predictors and the distributions of birds. Correlations between at-sea distributions and environmental variables do not necessarily indicate direct or even indirect connections between behavior and those variables. For example, Sooty Shearwaters pass through the study area during their trans-equatorial migrations (Shaffer et al., 2006), and the degree to which their distribution in waters surrounding the MHI reflects local environmental conditions may be small. Ecological inference from our model results should be cautious. Nevertheless, our correlative results may suggest interesting hypotheses for future research.

Some of the most important predictor variables across modeled species and model components were day of the year, distance to shore/nearest terrestrial site, depth, sea surface height, and projected longitude/latitude (Figures 7.22-7.23). Day of the year effects accounted for changes in the overall number of individuals of a given species in the study area during the modeled time frame. The effect was especially important for many of the non-breeding migratory species (Black-winged Petrel, Cook's Petrel, Mottled Petrel and Sooty Shearwater), some of whom pass through the study area during relatively short periods of time (Mottled Petrel and Sooty Shearwater). Distance to the nearest terrestrial site was frequently an important variable for breeding species (e.g., Hawaiian Petrel, Newell's Shearwater, Red-footed Booby, White Tern and Wedge-tailed Shearwater), with predicted relative density generally decreasing with increasing distance from terrestrial sites. Depth was also an important variable in the models for a few species (Brown Booby, White Tern and Wedge-tailed Shearwater), with predicted relative density generally decreasing with increasing depth. Given the high correlation between depth and distance to land it is difficult to say how important of a driving factor depth is. Sea surface height was a relatively important predictor in the models for several species, especially Newell's Shearwater, Red-footed Booby and White-tailed Tropicbird, with predicted relative density generally increasing with sea surface height. This relationship is most evident in the southwest part of the study area where sea surface height was high and the predicted density of these species was also relatively high. The relative importance of projected longitude/latitude in many of the models indicated that there was additional spatial variability in the distributions of these species that was not explained by the other environmental predictor variables.

Hawaiian Petrel, Pterodroma sandwichensis*. Photo credit: Daniel Webster (Cascadia Research Collective)*

Sooty Shearwater, Puffinus griseus*. Photo credit: David Pereksta (BOEM)*

Some other environmental predictor variables that were important in some models were sea surface temperature (SST), standard deviation (SD), surface chlorophyll-*a* concentration, and the probability of an anticyclonic eddy ring (Figures 7.22-7.23). SST SD was important in the models for Hawaiian Petrel, Newell's Shearwater and Sooty Shearwater with predicted relative density generally increasing with increasing SST SD.

The predicted spatial distributions of these species reflected this relationship with higher relative density in areas where SST was more variable, like the northwest part of the study area (Newell's Shearwater and Sooty Shearwater) and west of the island of Hawai'i/south of Maui Nui (Hawaiian Petrel). Surface chlorophyll-*a* was an important predictor in the Juan Fernandez Petrel and Mottled Petrel models, with predicted relative density decreasing with increasing chlorophyll-*a*. This apparent negative correlation may be more a result of geographic correspondence than a negative relationship between chlorophyll-*a* and the relative density of these species per se. Chlorophyll-*a* tended to increase from south to north within the study area, while the predicted relative density of these species tended to decrease from south to north. Probability of an anticyclonic eddy ring was an important predictor variable in the Sooty Tern model, and was somewhat important in the models for other species (e.g., Black-winged Petrel, Juan Fernandez Petrel and Wedge-tailed Shearwater). Predicted relative density of these species generally increased with increasing probability of an anticyclonic eddy ring. These species had areas of relatively high predicted density overlapping with the area of frequent anticyclonic eddy activity extending southwest from the island of Hawai'i.

Other predictor variables were relatively less important across models (Figures 7.22-7.23). Climate index variables were not very important predictors for any modeled species. Chlorophyll-*a* and SST front strength and probability also did not stand out as especially important predictors. Chlorophyll-*a* front strength in the Wedge-tailed Shearwater model, and SST front strength in the Bulwer's Petrel model, were two of the largest effects, relatively speaking. In both cases, predicted relative density increased with increasing front strength.

Brown Booby, Sula leucogaster. *Photo credit: Daniel Webster (Cascadia Research Collective)*

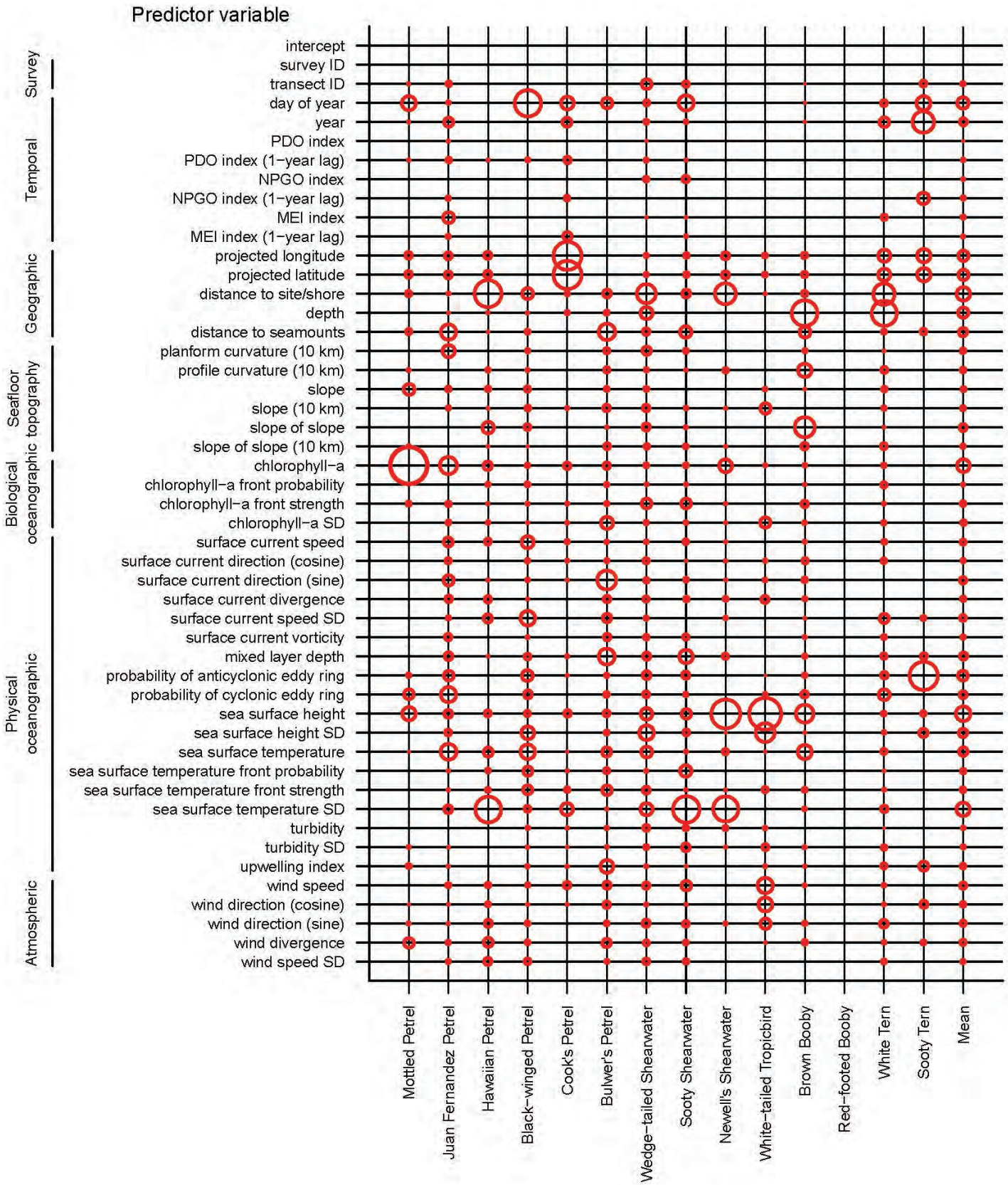

Figure 7.22. Predictor variable importance for the 'zero−inflation' component of each species' model. The area of a circle is proportional to relative variable importance. Models had two components: a zero inflation and a count component (Appendix B). This figure displays the relative importance of each predictor variable for modeling the probability of zero inflation in the former component. The probability of zero inflation in the Red−footed Booby model converged to a single value, so there were no predictor effects for this component.

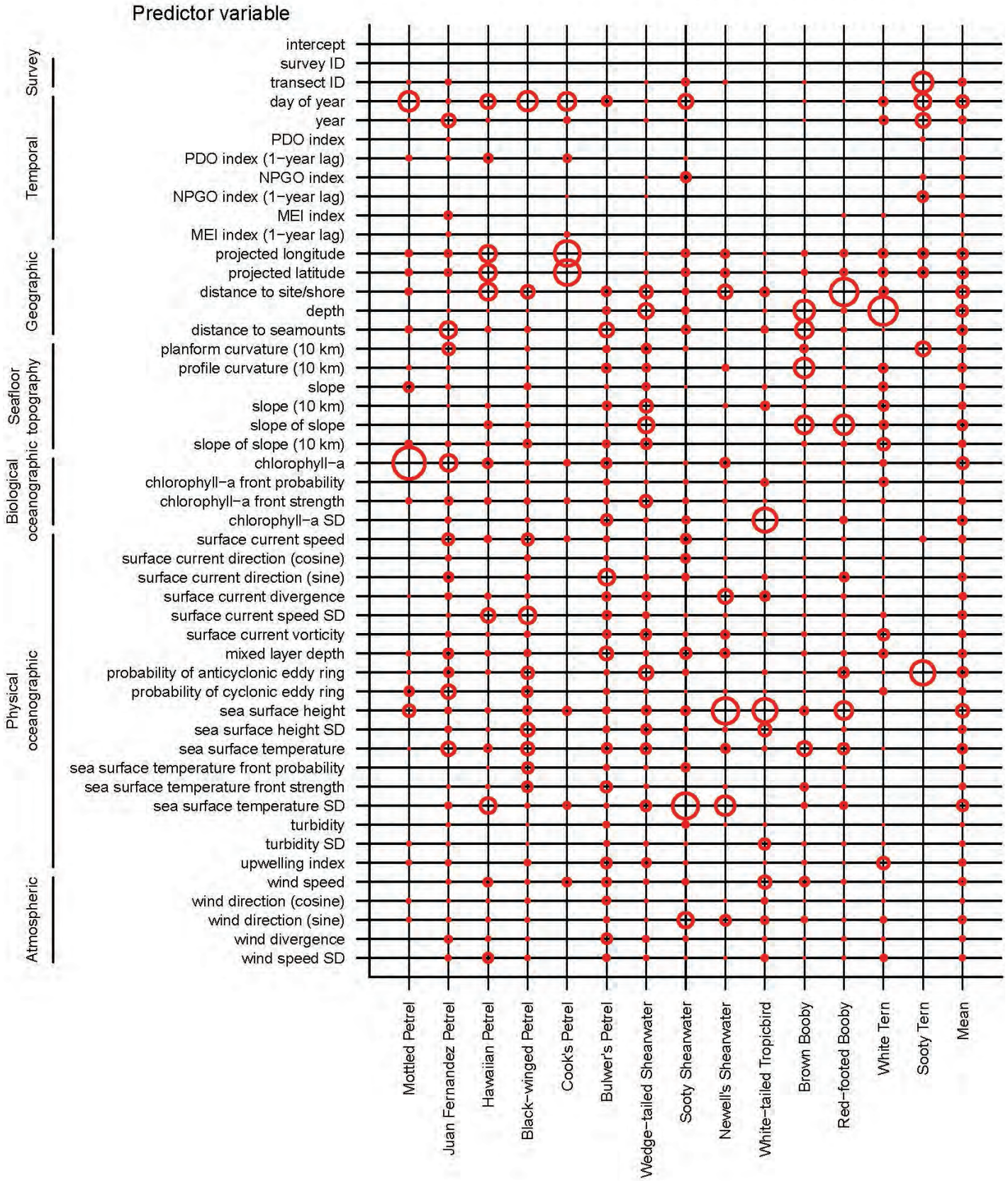

Figure 7.23. Predictor variable importance for the 'mean count' component of each species' model. The area of a circle is proportional to relative variable importance. Models had two components: a zero inflation and a count component (Appendix B). This figure displays the relative importance of each predictor variable for modeling the mean count in the latter component.

7.4. DATA LIMITATIONS AND INFORMATION GAPS

Our assessment of the at-sea distribution of seabirds in the MHI focused on the best available, most recent sighting dataset. The data covered the entire study area and spanned more than two decades. However, due to the expense and logistics required to conduct ship surveys, there were some limitations to the data.

The majority of the sighting data were collected during two years, 2002 and 2010. Seabird distributions can vary substantially from year to year, in part because of environmental variation over time (Ballance et al., 2006), so our results may not be representative of long-term average distributions. For instance, to the extent that seabird distributions in the MHI are influenced by the El Niño Southern Oscillation (ENSO; Ribic et al., 1992), the sighting data that contributed to our assessment mainly reflect ENSO conditions during the latter half of 2002 and 2010. The last seven months of 2002 were characterized as a warm period with respect to the Oceanic Niño Index (3.4 region), while the last half of 2010 was characterized as a cool period (Chapter 2, Figure 2.12). Additional survey effort from more years covering a range of environmental conditions would improve the ability to assess the long-term distributions of seabirds in the MHI.

The sighting data were collected in May and August-December, with the majority from August-November. Our spatial predictive modeling was further limited to only data from May and August-October. For species that are present in the MHI during other months (Figure 7.1), our results may not be representative of their average distribution around the MHI. Additional survey effort from December-July would improve the ability to assess the average annual distributions of seabirds in the MHI.

At-sea sighting surveys are an effective means for collecting data on all species simultaneously across a wide geographic area. Future survey effort during all months of the year would improve the ability to assess the average long-term distributions of seabirds in the MHI. That being said, at-sea surveys can be expensive and logistically challenging, and traditional strip transect methodology may not be especially well-suited for estimating the density and distribution of flocking species associated with sub-surface predators (Ballance and Pitman, 1999).

There is a large, growing online database of global bird sightings contributed by the public, eBird (Sullivan et al., 2014; http://ebird.org), that provides some information about at-sea sightings of seabirds in the MHI. Data from eBird were excluded from our analysis given their limited offshore coverage, often opportunistic nature, and lack of documentation of effort. Nevertheless, eBird now has a Pelagic Protocol, and as this database grows and appropriate analytical techniques develop (e.g., Fink et al., 2010) we would encourage the exploration of the usefulness of these data for providing additional information about the at-sea distribution of seabirds in the MHI.

Electronic tracking studies (Table 7.3) provide a complementary source of information about the at-sea distribution of seabirds, and we would encourage current and future efforts in the MHI, especially those with large sample sizes and wide species coverage. Tracking data provide detailed information about behavior and space use of individuals through time, although it can be difficult to track some species (e.g., small birds), and the number of individuals tracked is sometimes small so results may not be representative of the population.

A supplementary type of information that our assessment relied on was data on the locations of terrestrial sites used by seabirds in the MHI (e.g., breeding colonies and roosting sites). We did not find a comprehensive, up-to-date dataset on terrestrial sites, so we compiled information from several sources and consulted local seabird biologists. The information that we compiled is almost certainly incomplete, and the nature of what was considered an individual terrestrial site varied considerably, as did the precision of the location information. We would encourage any efforts to compile the locations of terrestrial sites used by seabirds in the MHI into a single, publicly available atlas or database. Furthermore, estimates of the number of birds of each species using each site would be a valuable addition to such a database.

For many species that were not modeled, estimates of potential foraging areas for breeding individuals were based on limited data or data from other geographic locations. Continued electronic tracking of breeding seabirds in the MHI would help improve estimates of their foraging areas.

ACKNOWLEDGEMENTS

The NOAA surveys were funded by NOAA NMFS/SWFSC and PIFSC. We thank the many observers, cruise leaders, cruise coordinators, officers and crew, who dedicated many months of hard work collecting the data. In particular, we thank Michael Force, Jay Barlow, Erin Oleson and Annette Henry. We are grateful to Arleone Dibben-Young, William Haase, Seth Judge, Sheldon Plentovich, Andre Raine and Eric VanderWerf for providing information about the locations of terrestrial sites used by seabirds in the MHI. We thank Mary Donovan and Hillary Holt for providing Audubon Christmas Bird Count data. Beth Flint, Amarisa Marie, David Pereksta and Lindsay Young provided helpful comments and feedback. Chris Clement, Dan Dorfman and Timothy White assisted with components of the work presented here. James Bowcott (PML) and NEODAAS assisted with the processing of ocean front metrics. We thank Robert Rankin for initial development of the BZIC modeling framework and computer code. Peter Miller was funded by PML Core Research Programme. David Pereksta, Daniel Webster and Robin Baird generously provided photographs of seabirds. Government contract labor (AJW, JBL, and MP) was provided by CSS-Dynamac, Inc. under NOAA contract EA-133C-14-NC-1384.

LITERATURE CITED

Seabirds

Adams, J. and S. Flora. 2010. Correlating seabird movements with ocean winds: linking satellite telemetry with ocean scatterometry. Marine Biology 157: 915-929.

Anders, A.D., R.K. Uyeyama, and S.F. Hanser. 2011. Kaula Island ship-based seabird and marine mammal surveys, 26-28 June 2010. Prepared by Naval Facilities Engineering Command Pacific for Commander, Pacific Fleet. Department of the Navy.

Ballance, L.T. and R.L. Pitman. 1999. Foraging ecology of tropical seabirds. pp. 2057-2071. In: N.J. Adams and R.H. Slotow (eds.), Proceedings of the 22nd International Ornithological Congress, Durban. Johannesburg, South Africa.

Ballance, L.T., R.L. Pitman, and S.B. Reilly. 1997. Seabird community structure along a productivity gradient: importance of competition and energetic constraint. Ecology 78(5): 1502- 1518.

Ballance, L.T., R.L. Pitman, L.B. Spear, and P.C. Fiedler. 2002. Investigations into temporal patterns in distribution, abundance and habitat relationships within seabird communities of the Eastern Tropical Pacific. NOAA NMFS Southwest Fisheries Science Center, Administrative Report LJ-02-17. 79 pp.

Ballance, L.T., R.L. Pitman, and P.C. Fiedler. 2006. Oceanographic influences on seabirds and cetaceans of the eastern tropical Pacific: A review. Progress in Oceanography 69: 360-390.

Cleasby, I.R., E.D. Wakefield, S. Bearhop, T.W. Bodey, S.C. Votier, and K.C. Hamer. 2015. Three-dimensional tracking of a wide-ranging marine predator: flight heights and vulnerability to offshore wind farms. Journal of Applied Ecology 52: 1474-1482.

Conners, M.G., E.L. Hazen, D.P. Costa, and S.A. Shaffer. 2015. Shadowed by scale: subtle behavioral niche partitioning in two sympatric, tropical breeding albatross species. Movement Ecology 3: 28.

Cooper, B.A. and R.H Day. 1998. Summer behavior and mortality of Dark-rumped Petrels and Newell's Shearwaters at Power Lines on Kauai. Colonial Waterbirds 21: 11-19.

Cooper, B.A. and R.H. Day. 2003. Movement of the Hawaiian Petrel to inland breeding sites on Maui Island, Hawai'i. Waterbirds 26: 62-71.

Day, R.H. and B.A. Cooper. 1995. Patterns of movement of Dark-rumped Petrels and Newell's Shearwaters on Kauai. Condor 97: 1011-1027.

Day, R.H., B.A. Cooper, and R.J. Blaha. 2003. Movement patterns of Hawaiian Petrels and Newell's Shearwaters on the Island of Hawai'i. Pacific Science 57: 147-159.

Devney, C.A., M. Short, and B.C. Congdon. 2009. Sensitivity of tropical seabirds to El Niño precursors. Ecology 90(5): 1175-1183.

Dixon, K.L. and C. Starrett. 1952. Offshore observations of tropical sea birds in the Western Pacific. Auk 69: 266-272.

Drewitt, A.L. and R.H.W. Langston. 2006. Assessing the impacts of wind farms on birds. Ibis 148: 29-42.

Erickson, W.P., M.M. Wolfe, K.J. Bay, D.H. Johnson, and J.L. Gehring. 2014. A comprehensive analysis of small-passerine fatalities from collision with turbines at wind energy facilities. PLoS ONE 9: e107491.

Federal Register. 1967. Native fish and wildlife: Endangered species. 32 Fed. Reg. 4001 (February 24, 1967). U.S. Fish and Wildlife Service. Online: http://www.nmfs.noaa.gov/pr/pdfs/fr/fr32-4001.pdf (Accessed 14 June 2016).

Federal Register. 1975. Endangered and threatened wildlife: Listing of endangered and threatened fauna. 40 Fed. Reg. 44149 (September 25, 1975). U.S. Fish and Wildlife Service.

Fernández, P., D.J. Anderson, P.R. Sievert, and K.P. Huyvaert. 2001. Foraging destinations of three low-latitude albatross (*Phoebastria*) species. Journal of Zoology 254: 391-404.

Fink, D., W.M. Hochachka, B. Zuckerberg, D.W. Winkler, B. Shaby, M.A. Munson, G. Hooker, M. Riedewald, D. Sheldon, and S. Kelling. 2010. Spatiotemporal exploratory models for broad-scale survey data. Ecological Applications 20: 2131-2147.

Fujimoto, J. 2011. Kaula ship-based surveys, 30 June 2011. Prepared by Naval Facilities Engineering Command Pacific for Commander, Pacific Fleet. Department of the Navy.

Fujimoto, J. and F. Juola. 2012. Kaula Island ship-based seabird survey, July 6, 2012. Prepared by Naval Facilities Engineering Command Pacific for Commander, Pacific Fleet. Department of the Navy.

Garthe, S. and O. Hüppop. 2004. Scaling possible adverse effects of marine wind farms on seabirds: developing and applying a vulnerability index. Journal of Applied Ecology 41: 724-734.

Harrison, C. S. and D.L. Stone-Burner. 1981. Radiotelemetry of the Brown Noddy in Hawaii. Journal of Wildlife Management 45: 1021-1025.

Harrison, C.S. 1990. Seabirds of Hawaii: Natural history and conservation. Cornell University Press. Ithaca, NY. 249 pp.

Hebshi, A.J., D.C. Duffy, and K.D. Hyrenbach. 2008. Associations between seabirds and subsurface predators around Oahu, Hawaii. Aquatic Biology 4: 89-98.

Hirai, L.T. 1978. Native birds of Lanai, Hawaii. Western Birds 9: 71-77.

Hyrenbach, K.D., P. Fernández, and D.J. Anderson. 2002. Oceanographic habitats of two sympatric North Pacific albatrosses during the breeding season. Marine Ecological Progress Series 233: 283-301.

Kappes, M.A., S.A. Shaffer, Y. Tremblay, D.G. Foley, D.M. Palacios, P.W. Robinson, S.J. Bograd, and D.P. Costa. 2010. Hawaiian albatrosses track interannual variability of marine habitats in the North Pacific. Progress in Oceanography 86: 246-260.

Kappes, M.A., S.A. Shaffer, Y. Tremblay, D.G. Foley, D.M. Palacios, S.J. Bograd, and D.P. Costa. 2015. Reproductive constraints influence habitat accessibility, segregation, and preference of sympatric albatross species. Movement Ecology 3: 34.

Keller, K.E., A.D. Anders, S.A. Shaffer, M.A. Kappes, B. Flint, and A. Friedlander. 2009. Seabirds. pp. 235-274. In: A. Friedlander, K. Keller, L. Wedding, A. Clarke, and M. Monaco (eds.). 2009. A marine biogeographic assessment of the Northwestern Hawaiian Islands. NOAA Technical Memorandum NOS NCCOS 84. Silver Spring, MD. Online: https://coastalscience.noaa.gov/datasets/e98/docs/nwhi-2009.pdf (Site Accessed 8 June 2016).

King, W.B. 1970. The Trade Wind Zone Oceanography Pilot Study Part VII: Observations of Sea Birds March 1964 to June 1965. U.S. Fish and Wildlife Service Special Scientific Report – Fisheries No. 586. Washington, DC.

King, W.B. (ed.) 1974. Pelagic studies of seabirds in the central and eastern Pacific Ocean. Number 158 in Smithsonian contributions to zoology. Smithsonian Institution Press, Washington, DC.

Kozar, K., R. Swift, and S. Marshall. 2007. Shoreline bird inventories in three National Parks in Hawai'i : Kalaupapa National Historical Park, Haleakala National Park and Hawaii Volcanoes National Park. Pacific Cooperative Studies Unit, University of Hawai'i at Manoa and National Park Service, Inventory and Monitoring Program. Technical Report 149. 34 pp.

Maxwell, S.M. and L.E. Morgan. 2013. Foraging of seabirds on pelagic fishes: implications for management of pelagic marine protected areas. Marine Ecology Progress Series 481: 289-303.

May, R.F. 2015. A unifying framework for the underlying mechanisms of avian avoidance of wind turbines. Biological Conservation 190: 179-187.

NOAA NMFS. 2014. Seabird interactions and mitigation efforts in Hawaii longline fisheries: 2013 Annual Report. NOAA National Marine Fisheries Service, Pacific Islands Regional Office. Honolulu, HI. 12 pp.

Pepi, V.E., A. Kumar, M.E. Laut, J. Hallman, J. Kim, and A.D. Anders. 2009. Kaula Island ship-based seabird and marine mammal surveys, 21-22 July 2009. Prepared for Commander, Pacific Fleet. NAVFAC Pacific. Department of the Navy.

Pyle, R.L. and P. Pyle. 2009. The Birds of the Hawaiian Islands: Occurrence, history, distribution, and status. B.P. Bishop Museum. Honolulu, HI. Version 1. Online: http://hbs.bishopmuseum.org/birds/rlp-monograph/ (Site Accessed 8 June 2016).

Reynolds, M.H. and G.L. Ritchotte. 1997. Evidence of Newell's Shearwater breeding in Puna District, Hawaii. Journal of Field Ornithology 68: 26-32.

Ribic, C.A., D.G. Ainley, and L.B. Spear. 1992. Effects of El Niño and La Niña on seabird assemblages in the Equatorial Pacific. Marine Ecology Progress Series 80: 109-124.

Ribic, C.A. and D.G. Ainley. 1997. The relationships of seabird assemblages to physical habitat features in Pacific equatorial waters during spring 1984-1991. ICES Journal of Marine Science 54: 593-599.

Robinson Willmott, J.C., G. Forcey, and A. Kent. 2013. The relative vulnerability of migratory bird species to offshore wind energy projects on the Atlantic Outer Continental Shelf: An assessment method and database. Final Report to the U.S. Department of the Interior, Bureau of Ocean Energy Management, Office of Renewable Energy Programs. OCS Study BOEM 2013-207. Herndon, VA.

Rosenberg, K.V., D. Pashley, B. Andres, P.J. Blancher, G.S. Butcher, W.C. Hunter, D. Mehlman, A.O. Panjabi, M. Parr, G. Wallace, and D. Wiedenfeld. 2014. The State of the Birds 2014 Watch List. North American Bird Conservation Initiative, U.S. Committee. Washington, DC. Online: http://www.stateofthebirds.org/2014/extinctions/watchlist.pdf (Site Accessed 8 June 2016).

Shaffer, S.A., Y. Tremblay, H. Weimerskirch, D. Scott, D.R. Thompson, P.M. Sagar, H. Moller, G.A. Taylor, D.G. Foley, B.A. Block, and D.P. Costa. 2006. Migratory shearwaters integrate oceanic resources across the Pacific Ocean in an endless summer. Proceedings of the National Academy of Sciences 103: 12799-12802.

Soanes, L.M., J.A. Bright, L.P. Angel, J.P.Y. Arnould, M. Bolton, M. Berlincourt, B. Lascelles, E. Owen, B. Simon-Bouhet, and J.A. Green. 2016. Defining marine important bird areas: Testing the foraging radius approach. Biological Conservation 196: 69-79.

Spear, L.B., D.G. Ainley, and P. Pyle. 1999. Seabirds in southeastern Hawaiian waters. Western Birds 30:1-32.

Spear, L.B., L.T. Ballance, and D.G. Ainley. 2001. Response of seabirds to thermal boundaries in the tropical Pacific: the thermocline versus the Equatorial Front. Marine Ecology Progress Series 219: 275-289.

Sullivan, B.L., J.L. Aycrigg, J.H. Barry, R.E. Bonney, N. Bruns, C.B. Cooper, T. Damoulas, A.A. Dhondt, T. Dietterich, A. Farnsworth, D. Fink, J.W. Fitzpatrick, T. Fredericks, J. Gerbracht, C. Gomes, W.M. Hochachka, M.J. Iliff, C. Lagoze, F.A. La Sorte, M. Merrifield, W. Morris, T.B. Phillips, M. Reynolds, A.D. Rodewald, K.V. Rosenberg, N.M. Trautmann, A. Wiggins, D.W. Winkler, W.K. Wong, C.L. Wood, J. Yu, and S. Kelling. 2014. The eBird enterprise: An integrated approach to development and application of citizen science. Biological Conservation 169: 31-40.

Thorne, L.H., E.L. Hazen, S.J. Bograd, D.G. Foley, M.G. Conners, M.A. Kappes, H.M. Kim, D.P. Costa, Y. Tremblay, and S.A. Shaffer. 2015. Foraging behavior links climate variability and reproduction in North Pacific albatrosses. Movement Ecology 3: 27.

USFWS. 1983. Atlas of Hawaiian seabird colonies. U.S. Fish and Wildlife Service. Honolulu, HI.

USFWS. 2005. Regional seabird conservation plan, Pacific Region. U.S. Fish and Wildlife Service, Migratory Birds and Habitat Programs, Pacific Region. Portland, OR.

Vandenbosch, R. 2000. Effects of ENSO and PDO events on seabird populations as revealed by Christmas Bird Count data. Waterbirds 23: 416-422.

VanderWerf, E.A. 2003. Distribution, abundance, and breeding biology of White Terns on Oahu, Hawaii. Wilson Bulletin 115: 258-262.

VanderWerf, E.A., L. Elliott, and J.S. Fretz. 2005. Observations on the abundance and behavior of seabirds south of O‘ahu during the F/V *Ehime Maru* relocation and fuel spill. ‘Elepaio 65: 25-29.

VanderWerf, E.A., K.R. Wood, C. Swenson, M. LeGrande, H. Eijzenga, and R.L. Walker. 2007. Avifauna of Lehua Islet, Hawai‘i: Conservation value and management needs. Pacific Science 61: 39-52.

VanderWerf, E.A. and L.C. Young. 2014. Breeding biology of Red-tailed Tropicbirds *Phaethon rubricauda* and response to predator control on O‘ahu, Hawai‘i. Marine Ornithology 42: 73-76.

Welch, A.J., R.C. Fleischer, H.F. James, A.E. Wiley, P.H. Ostrom, J. Adams, F. Duvall, N. Holmes, D. Hu, J. Penniman, and K.A. Swindle. 2012. Population divergence and gene flow in an endangered and highly mobile seabird. Heredity 109: 19-28.

Wiley, A.E., P.H. Ostrom, A.J. Welch, R.C. Fleischer, H. Gandhi, J.R. Southon, T.W. Stafford Jr., J.F. Penniman, D. Hu, F.P. Duvall, and H.F. James. 2013. Millenial-scale isotope records from a wide-ranging predator show evidence of recent human impact to oceanic food webs. Proceedings of the National Academy of Sciences 110: 8972-8977.

Wood, K.R., D. Boynton, E. VanderWerf, L. Arnold, M. LeGrande, J.W. Slotterback, and D. Kuhn. 2003. The distribution and abundance of the Band-rumped Storm-Petrel (*Oceanodroma castro*): A preliminary survey of Kaua‘i, Hawai‘i 2002. Report to the U.S. Fish and Wildlife Service, Pacific Islands Office. Honolulu, HI.

Wood, K.R. and P. Bily. 2008. Vegetation description of a nesting site for Newell’s Shearwater (*Puffinus auricularis newelli*), Pi‘ina‘au Stream, East Maui, Hawai‘i. ‘Elepaio 68: 63-66.

Young, H.S., S.M. Maxwell, M.G. Conners, and S.A. Shaffer. 2015. Pelagic marine protected areas protect foraging habitat for multiple breeding seabirds in the central Pacific. Biological Conservation 181:226-235.

APPENDIX A: Chapter 2: Environmental Setting Supplementary Maps

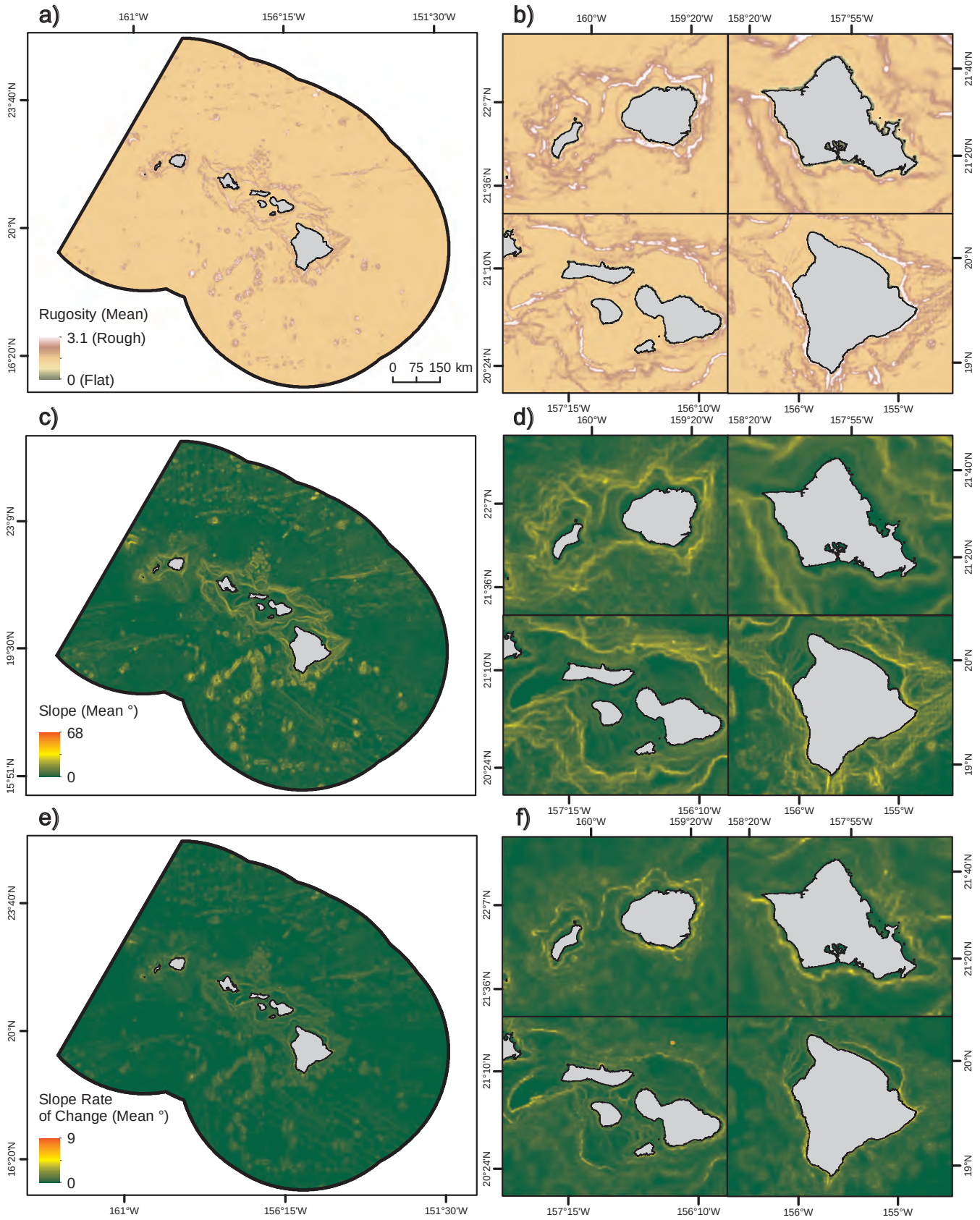

Figure A.1. Seafloor topography around the MHI. These maps depict the: a,b) mean rugosity (unitless); c,d) mean slope (°); and e,f) mean rate of change for slope (°) within the study area. These surfaces were created at a 90x90 m spatial resolution, and then averaged spatially within 1.2x1.2 km bins. Dates: N/A. Data source: Table 2.8 #58, 59, 60

Appendices

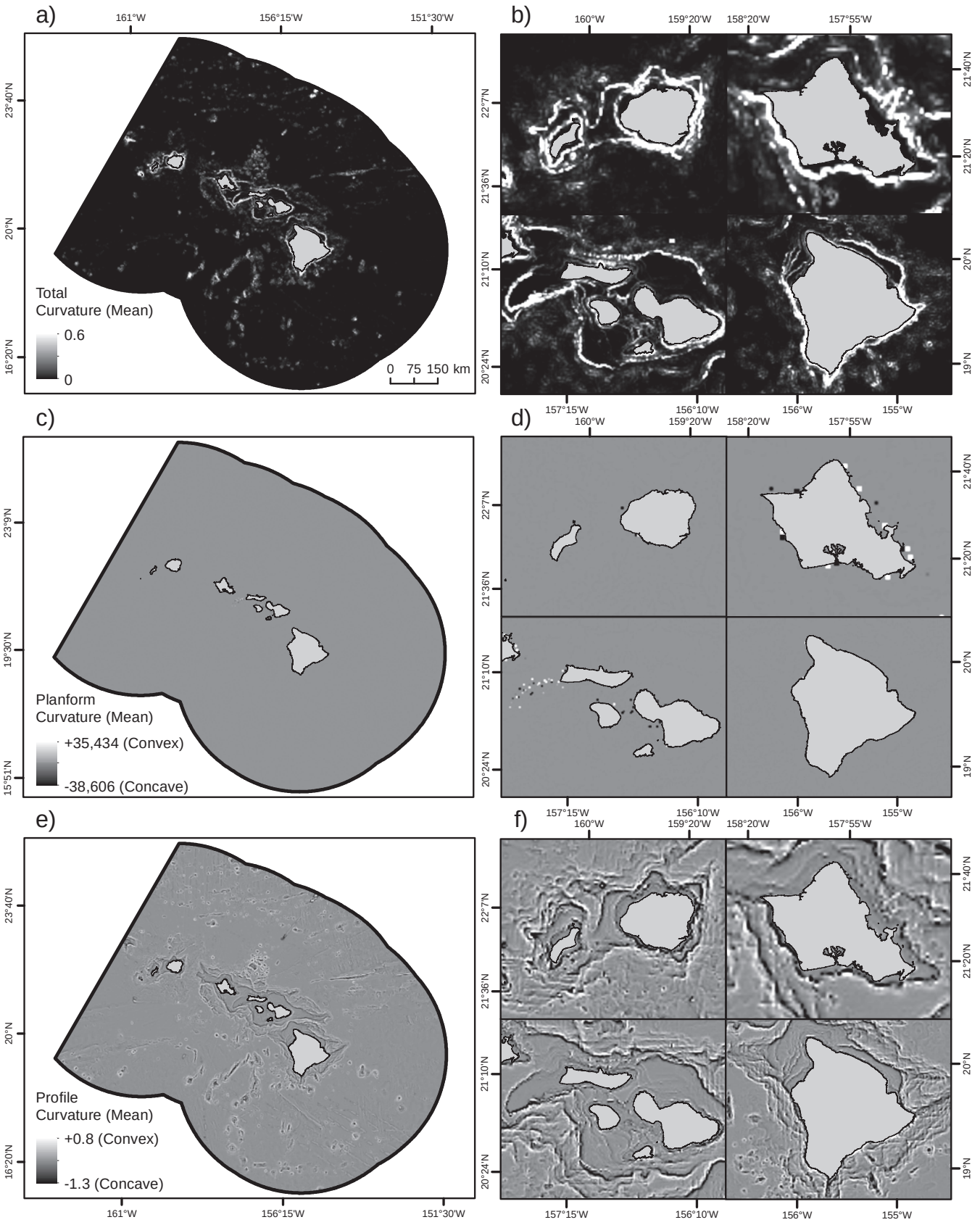

Figure A.2. Seafloor topography around the MHI (continued). These maps depict the: a,b) mean total curvature (radians per m^2); c,d) mean planform curvature (radians per meter); and e,f) mean profile curvature (radians per meter) within the study area. These surfaces were created at a 90x90 m spatial resolution, and then averaged spatially within 1.2x1.2 km bins. Dates: N/A. Data source: Table 2.8 #55, 56, 57

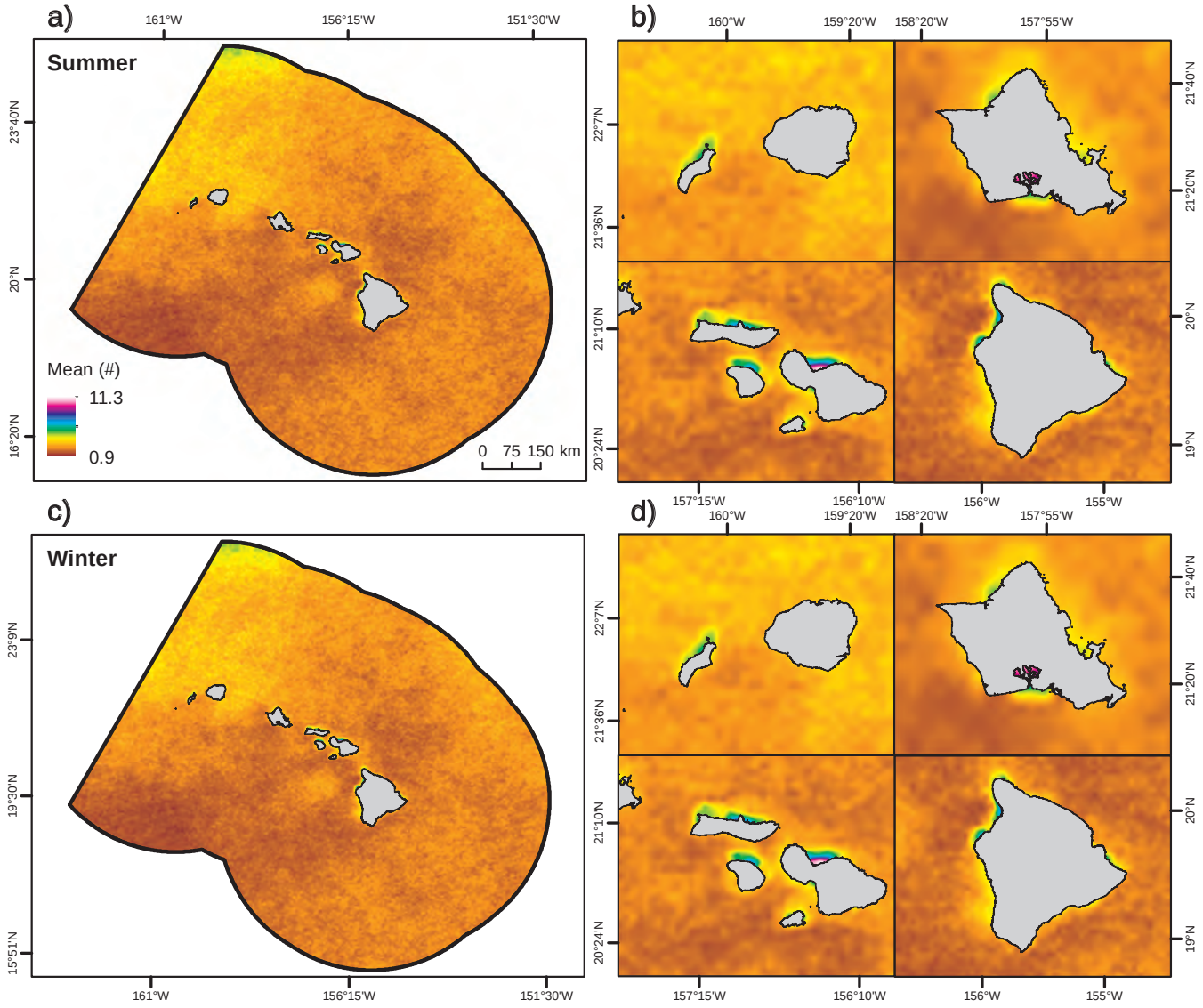

Figure A.3. Frequency of sea surface temperature anomalies (SSTA) around the MHI. These maps depict the average frequency of sea surface temperature anomalies in the summer a,b) and winter c,d) within the study area. Temperature anomalies are defined as the number of times (over previous 52 weeks) that SST changed by 1°C or more. Dates: 1982-2009. Data source: Table 2.6 #37

Appendices

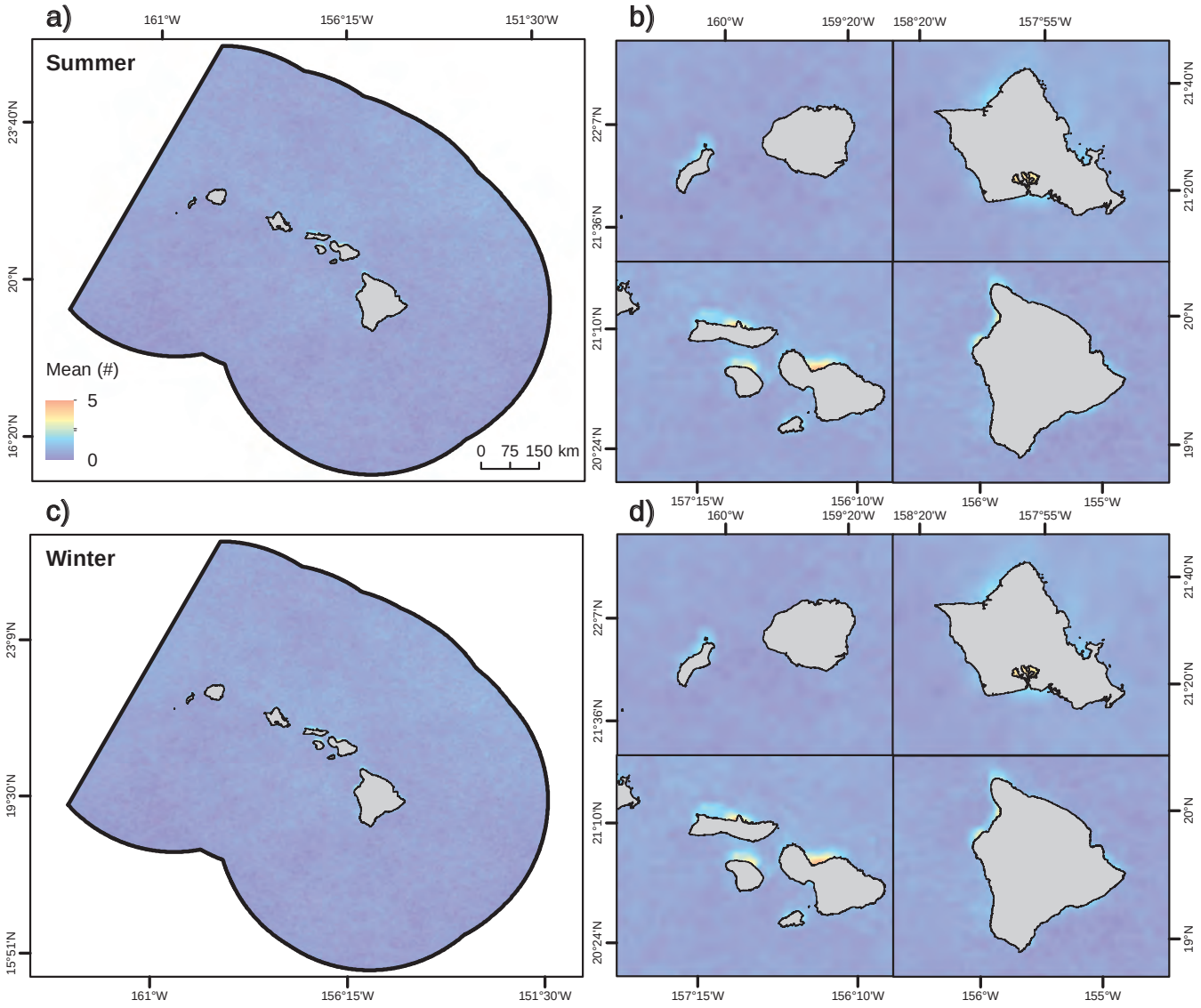

Figure A.4. Frequency of thermal stress anomalies (TSA) around the MHI. These maps depict the average frequency of thermal stress anomalies in the summer a,b) and winter c,d) within the study area. Thermal stress anomalies are calculated by subtracting weekly SST values from the maximum weekly climatological SST. Dates: 1982-2009. Data source: Table 2.6 #41

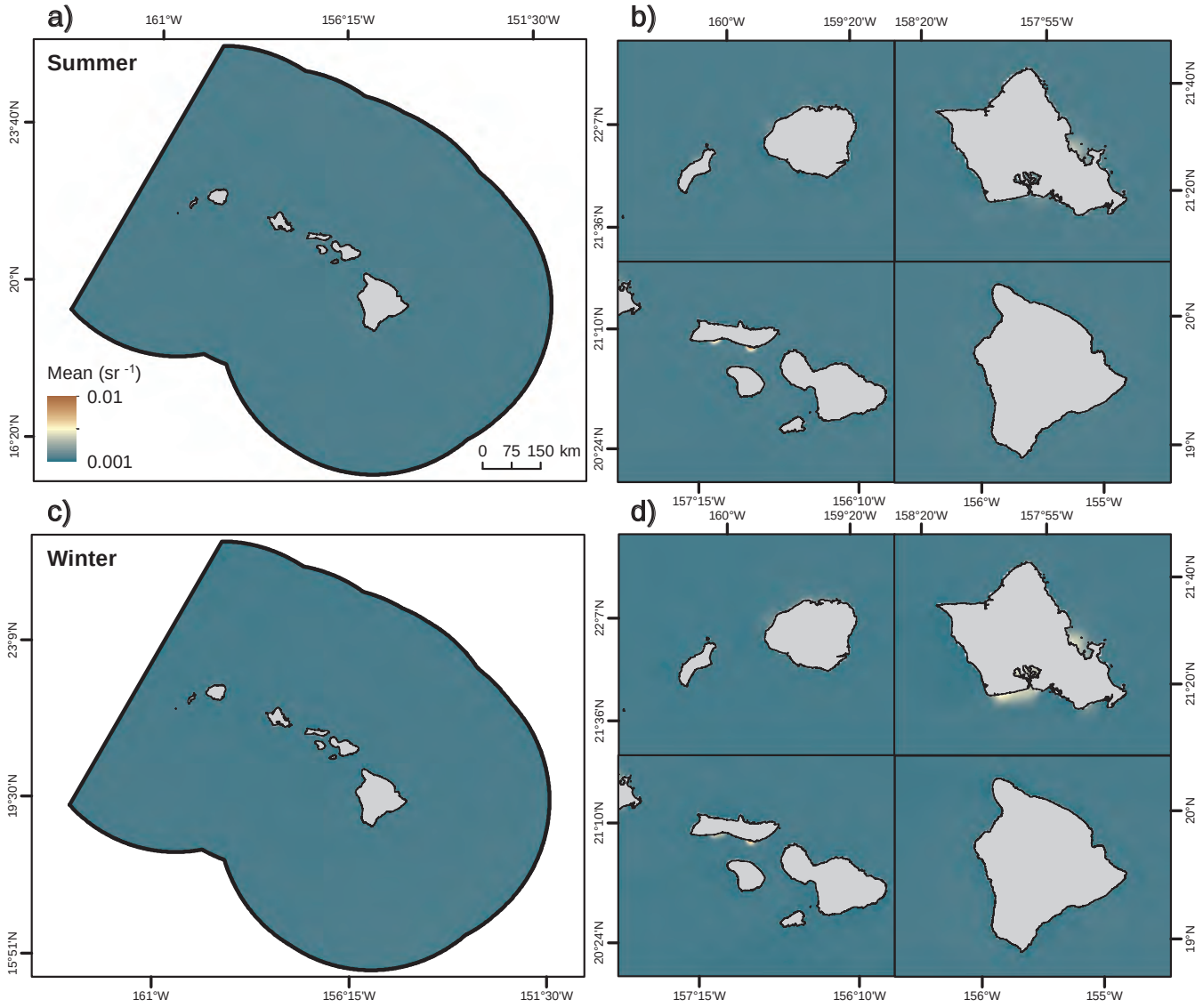

Figure A.5. Turbidity around the MHI. These maps depict the average surface turbidity (sr^{-1}) in the summer a,b) and winter c,d) within the study area. Turbidity is measured in sr^{-1} (steridians), and is derived by quantifying the amount of light reflected in the 547 nm wavelength. This wavelength includes light reflected by both organic and inorganic matter. Dates: July 2002-March 2015. Data source: Table 2.4 #18

Appendices

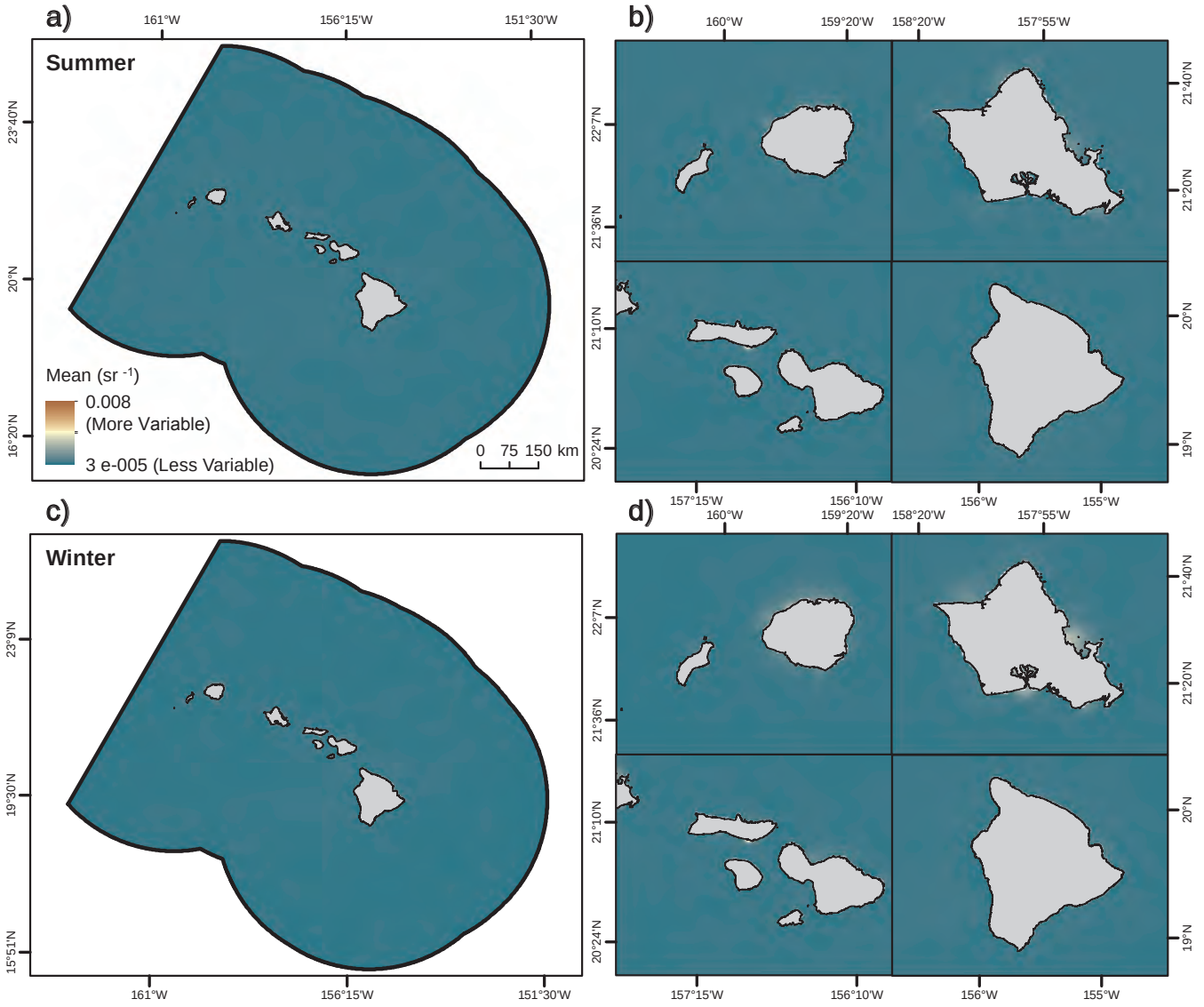

Figure A.6. Variation in turbidity around the MHI. These maps depict the standard deviation of surface turbidity (sr^{-1}) in the summer a,b) and winter c,d) within the study area. Turbidity is measured in sr^{-1} (steridians), and is derived by quantifying the amount of light reflected by organic and inorganic matter in the 547 nm wavelength. Dates: July 2002-March 2015. Data source: Table 2.4 #18

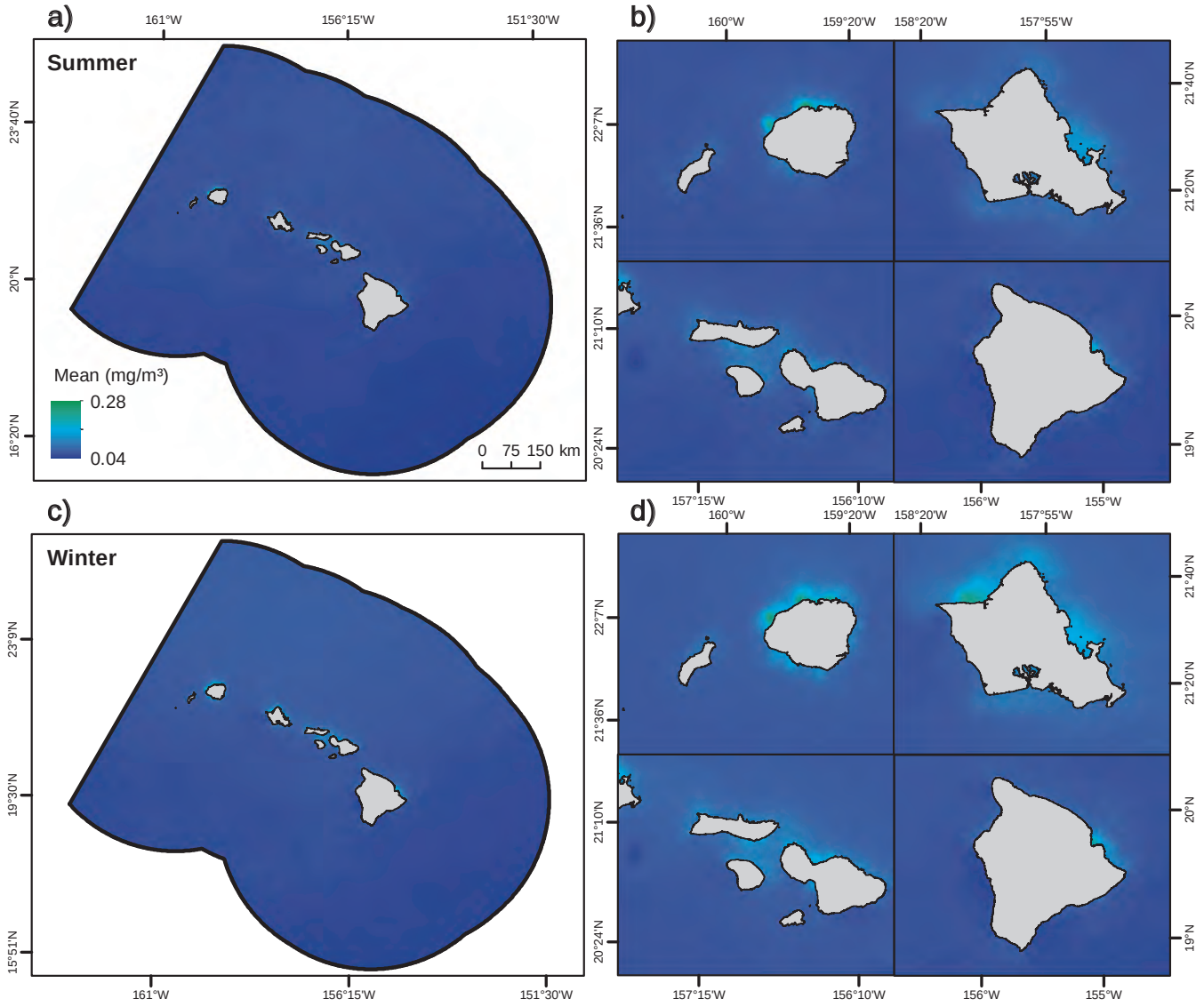

Figure A.7. Surface chlorophyll-a concentrations around the MHI. These maps depict the average surface chlorophyll-a concentrations (mg/m³) in the summer a,b) and winter c,d) within the study area. Dates: July 2002-October 2013. Data source: Table 2.2 #6

Appendices

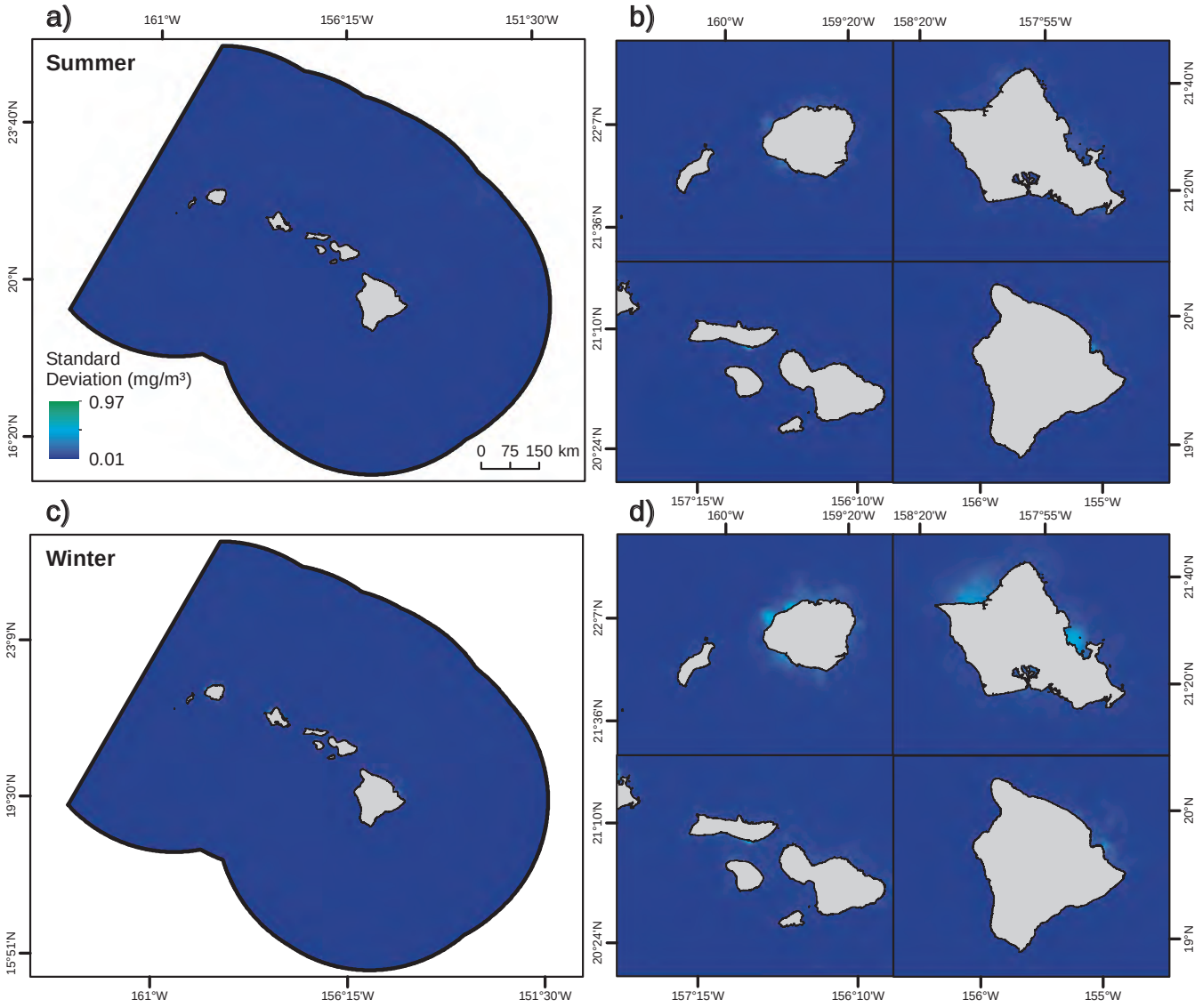

Figure A.8. Variation of surface chlorophyll-a concentrations around the MHI. These maps depict the standard deviation of chlorophyll-a concentrations (mg/m³) over the summer a,b) and winter c,d) within the study area. Dates: July 2002-October 2013. Data source: Table 2.2 #6

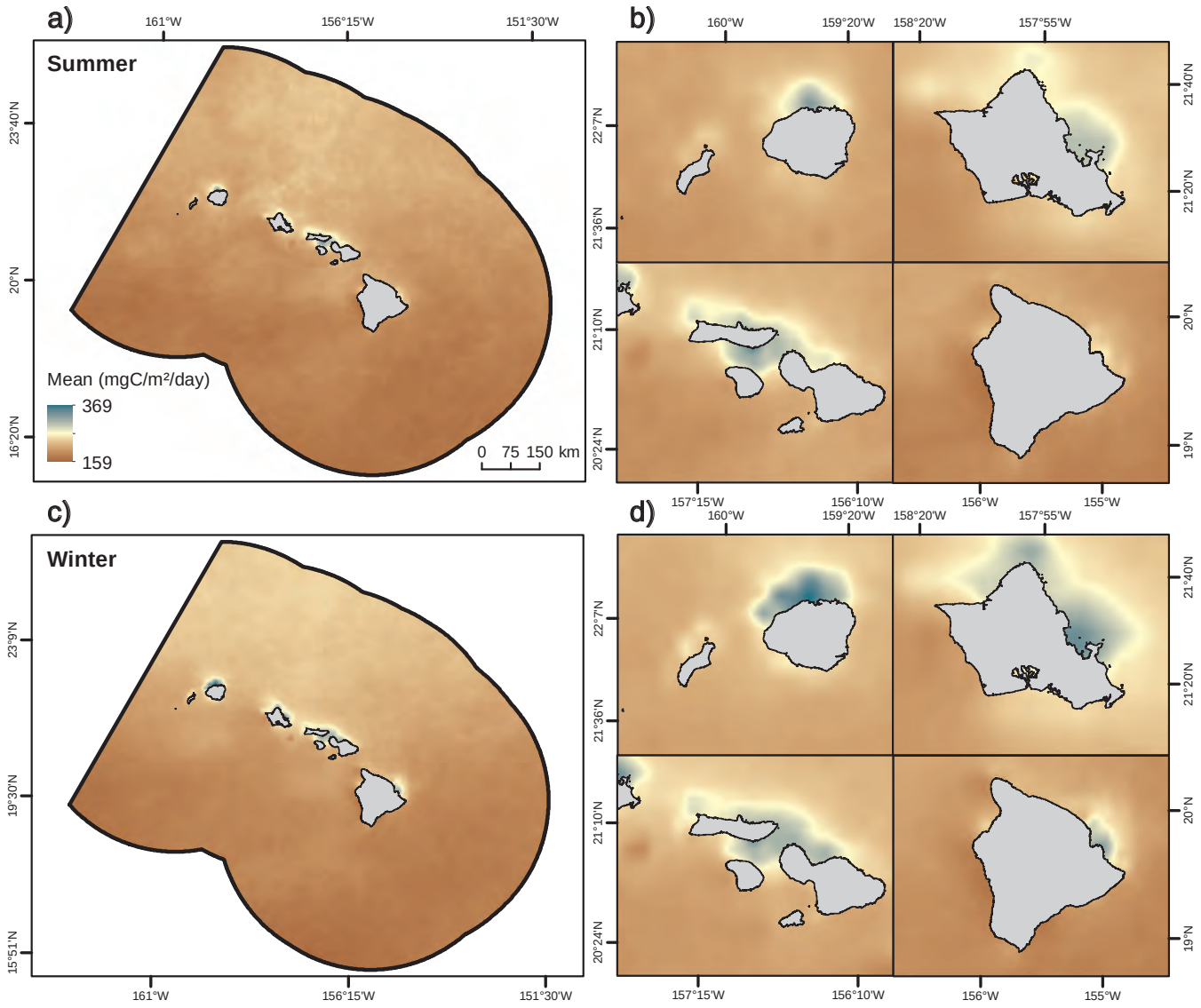

Figure A.9. Net surface primary productivity (NPP) around the MHI. These maps depict the average net surface primary productivity (mg Carbon/ m²/day) in the summer a,b) and winter c,d) within the study area. Dates: July 2002-October 2013. Data source: Table 2.2 #10

Appendices

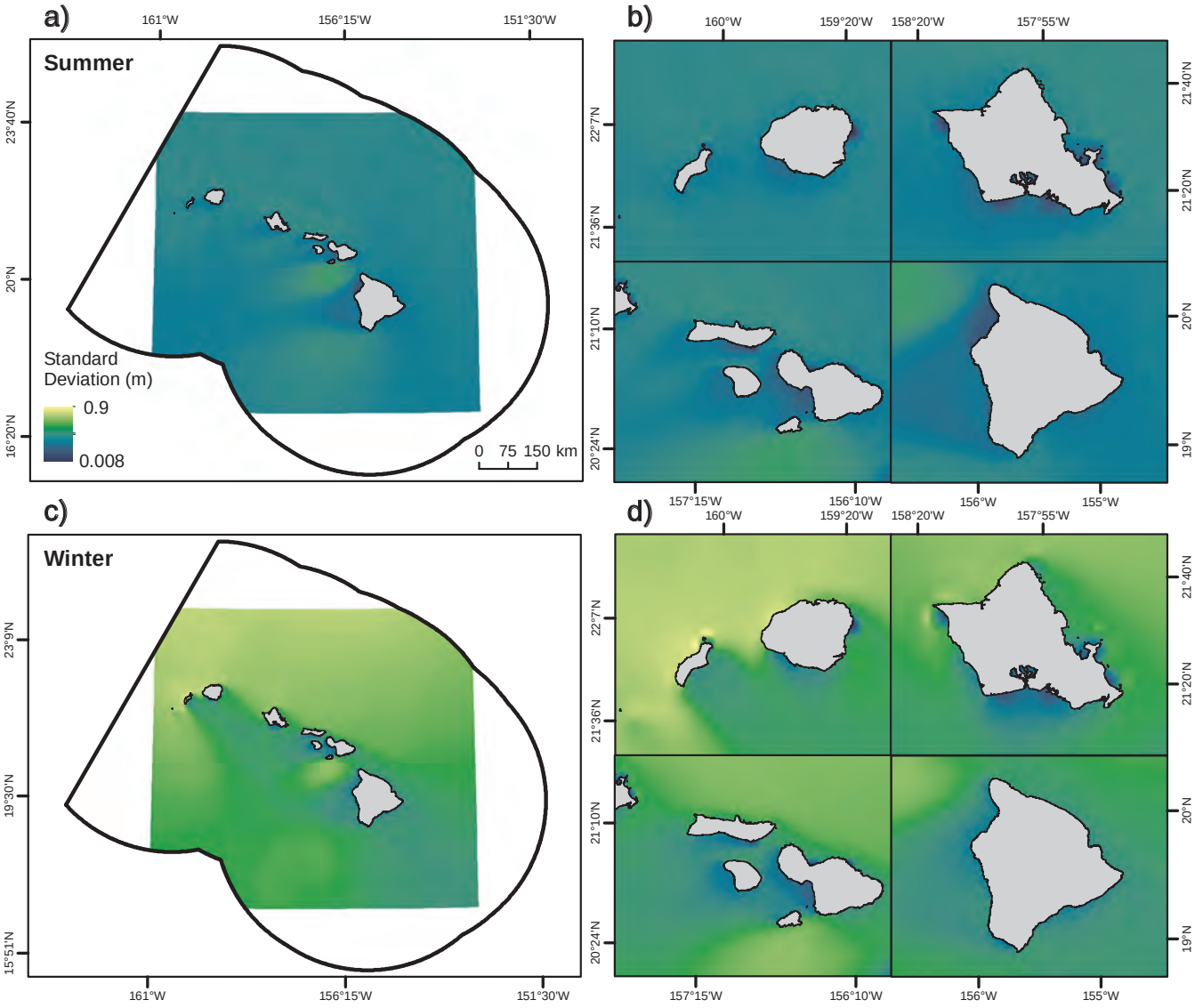

Figure A.10. Variation in wave heights around the MHI. These maps depict the standard deviation of significant wave heights (m) in the summer a,b) and winter c,d) within the study area. Wave data is missing for portions of the project area (a,c). Dates: January 2000-December 2009. Data source: Table 2.6 #43

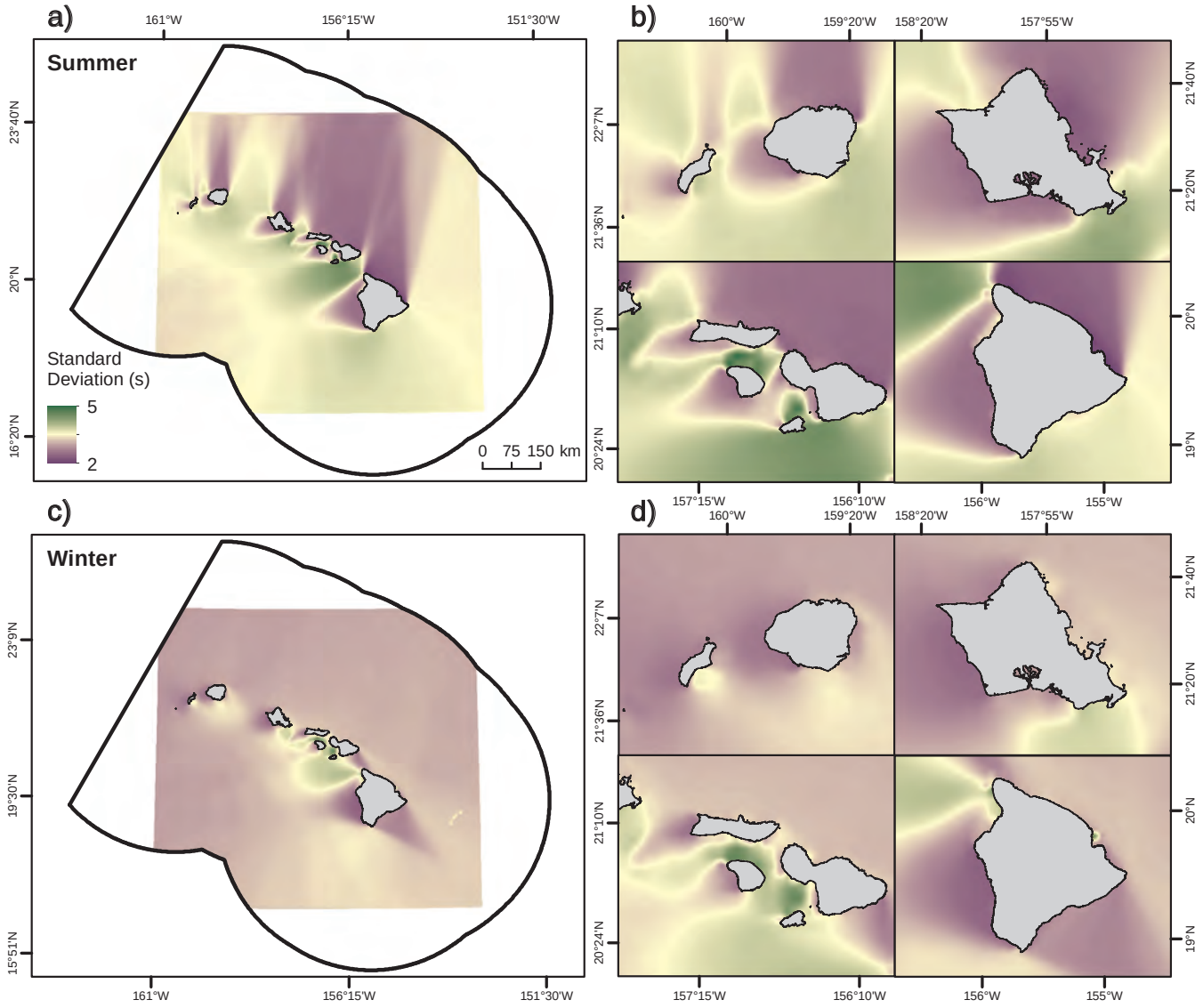

Figure A.11. Variation in wave periods around the MHI. These maps depict the standard deviation of wave periods(s) in the summer a,b) and winter c,d) within the study area. Wave data is missing for portions of the project area (a,c). Dates: January 2000-December 2009. Data source: Table 2.6 #42

Appendices

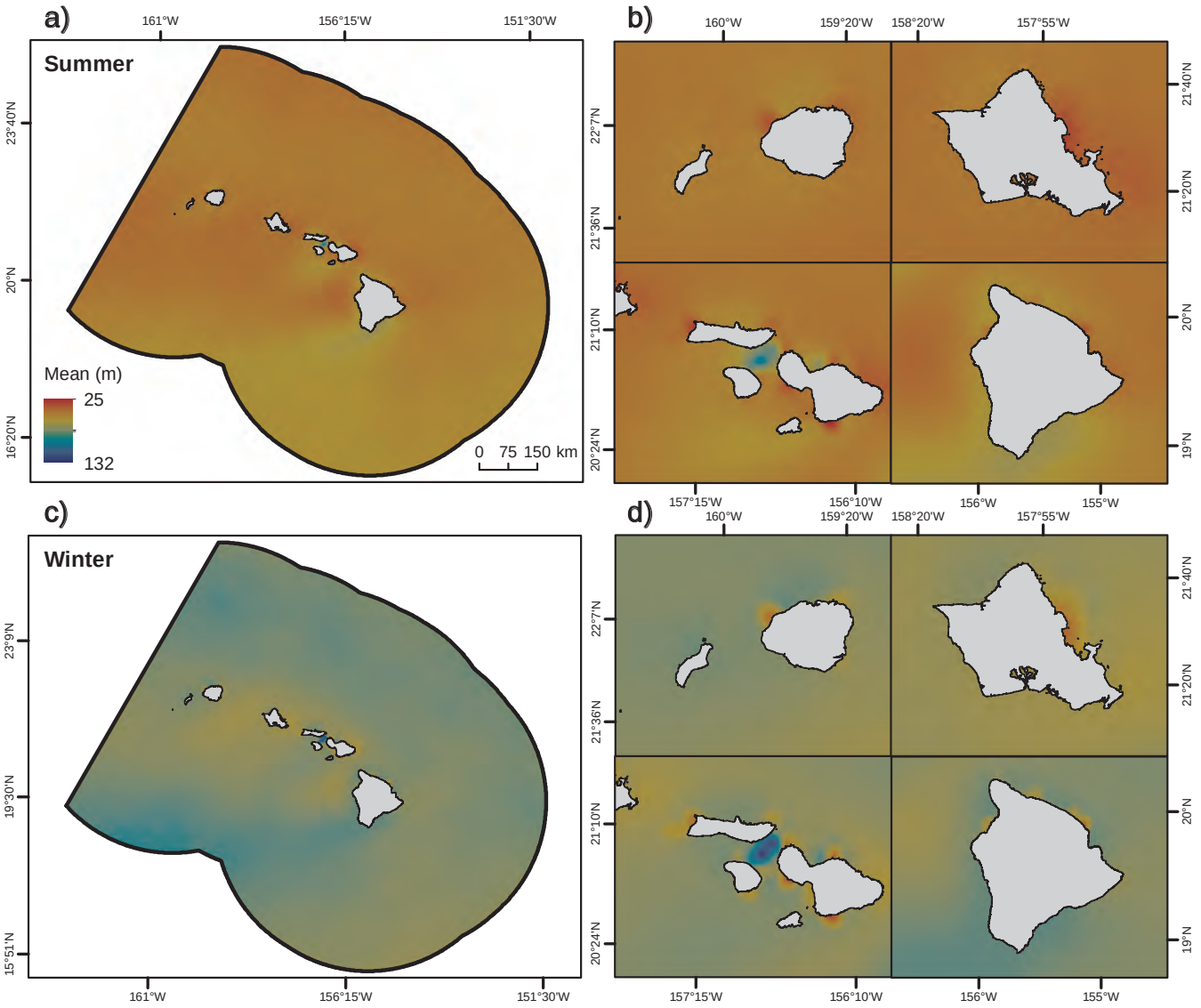

Figure A.12. Mixed layer depth (MLD) around the MHI. These maps depict the average depth (m) to which water is mixed by various oceanographic processes in the summer a,b) and winter c,d) within the study area. Dates: 1992-2005. Data source: Table 2.4 #24

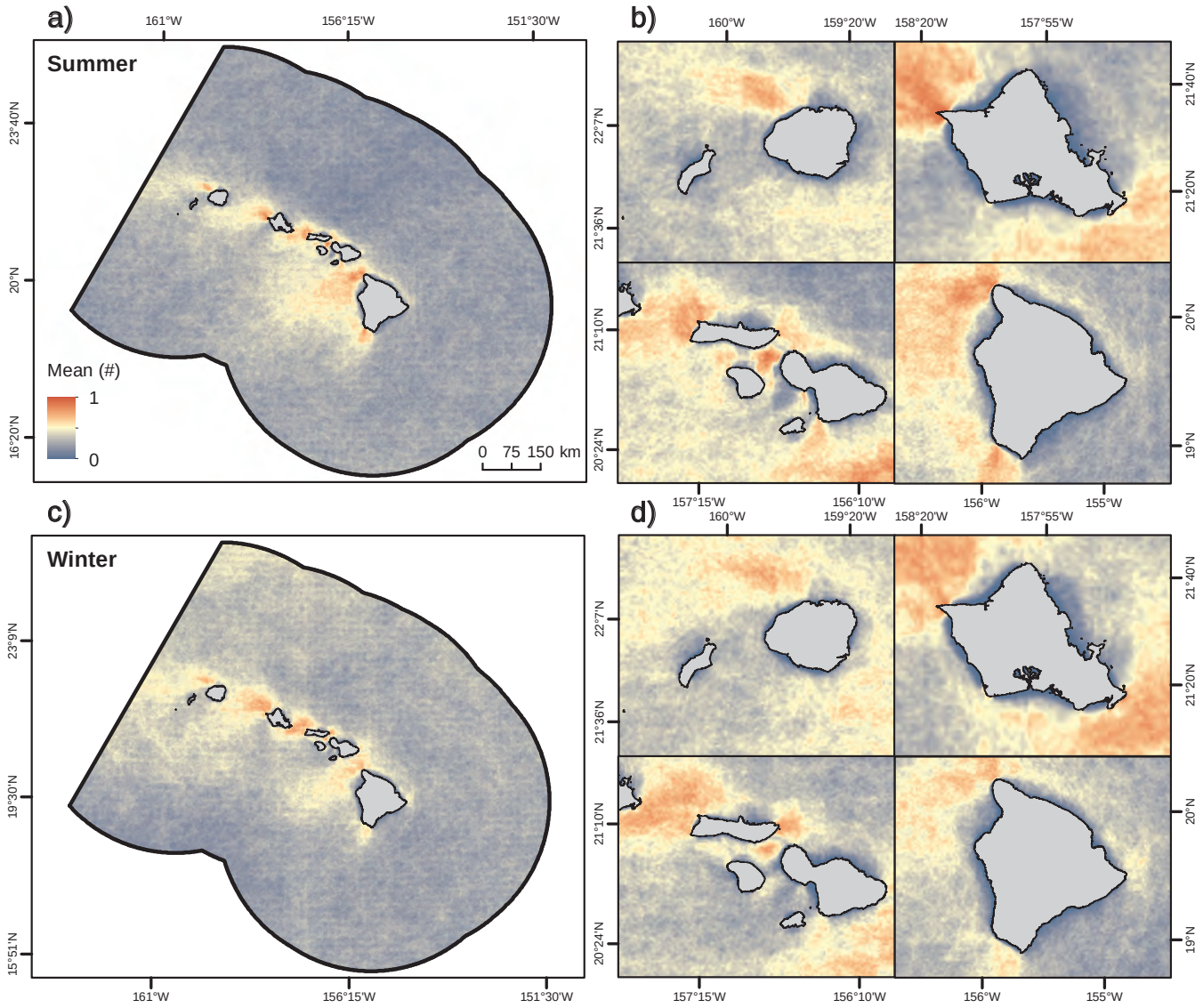

Figure A.13. Frequency of SST fronts around the MHI. These maps denote the average frequency of SST fronts in the summer a,b) and winter c,d) within the study area. Frontal frequency is defined as the number of months for which a front was observed at a particular pixel, divided by the total number of months. A front was detected if there was a ≥0.4 °C between two water masses within a 32x32 pixel moving window. Dates: June 2002-December 2013. Data source: Table 2.6 #38. Data provided courtesy of the Plymouth Marine Laboratory, Dr. Peter Miller.

Appendices

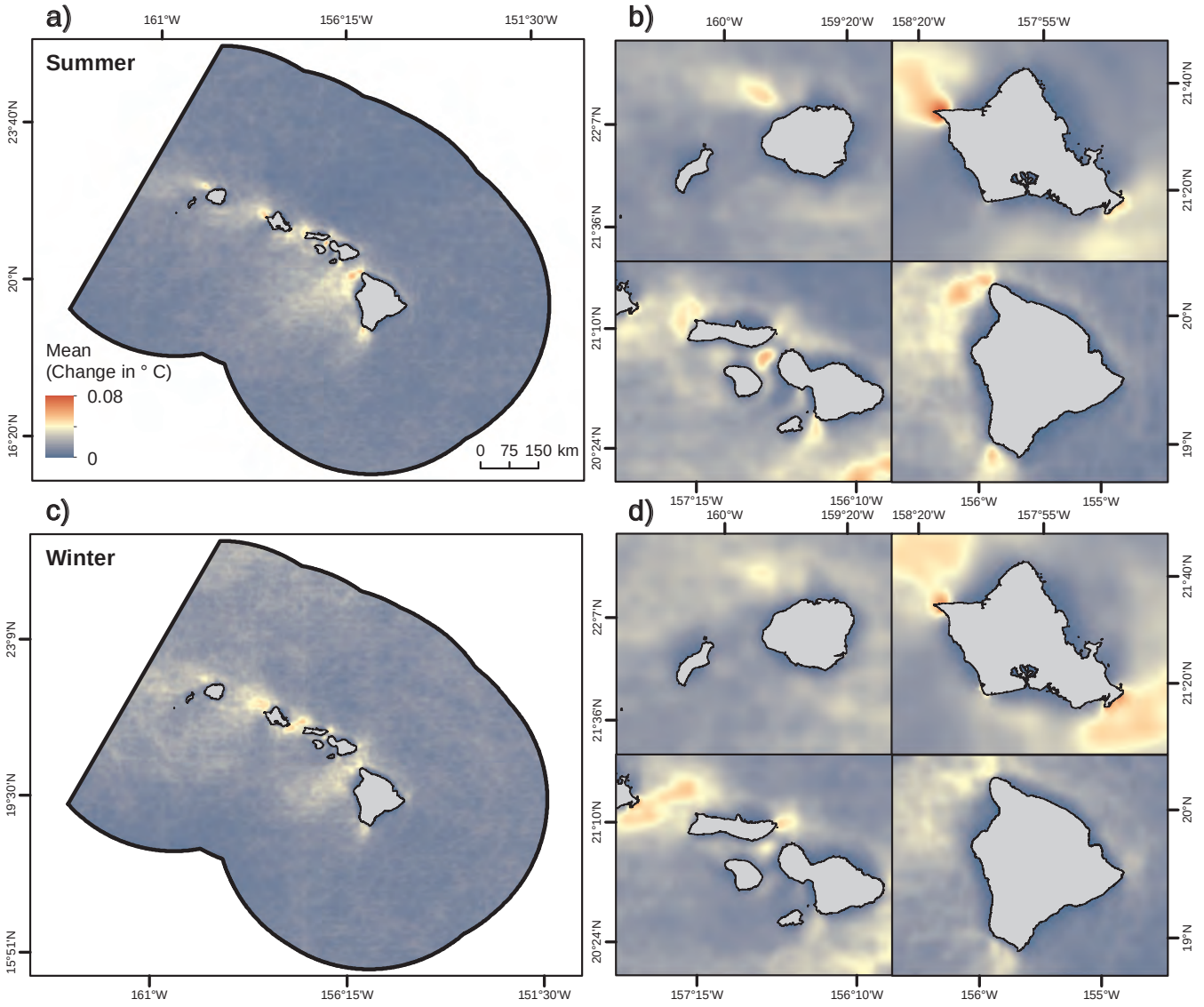

Figure A.14. Strength of SST fronts around the MHI. These maps denote the average strength of SST fronts in the summer a,b) and winter c,d) within the study area. Frontal strength is defined as the magnitude of change (°C) in surface water temperatures. Dates: June 2002-December 2013. Data source: Table 2.6 #40. Data provided courtesy of the Plymouth Marine Laboratory, Dr. Peter Miller.

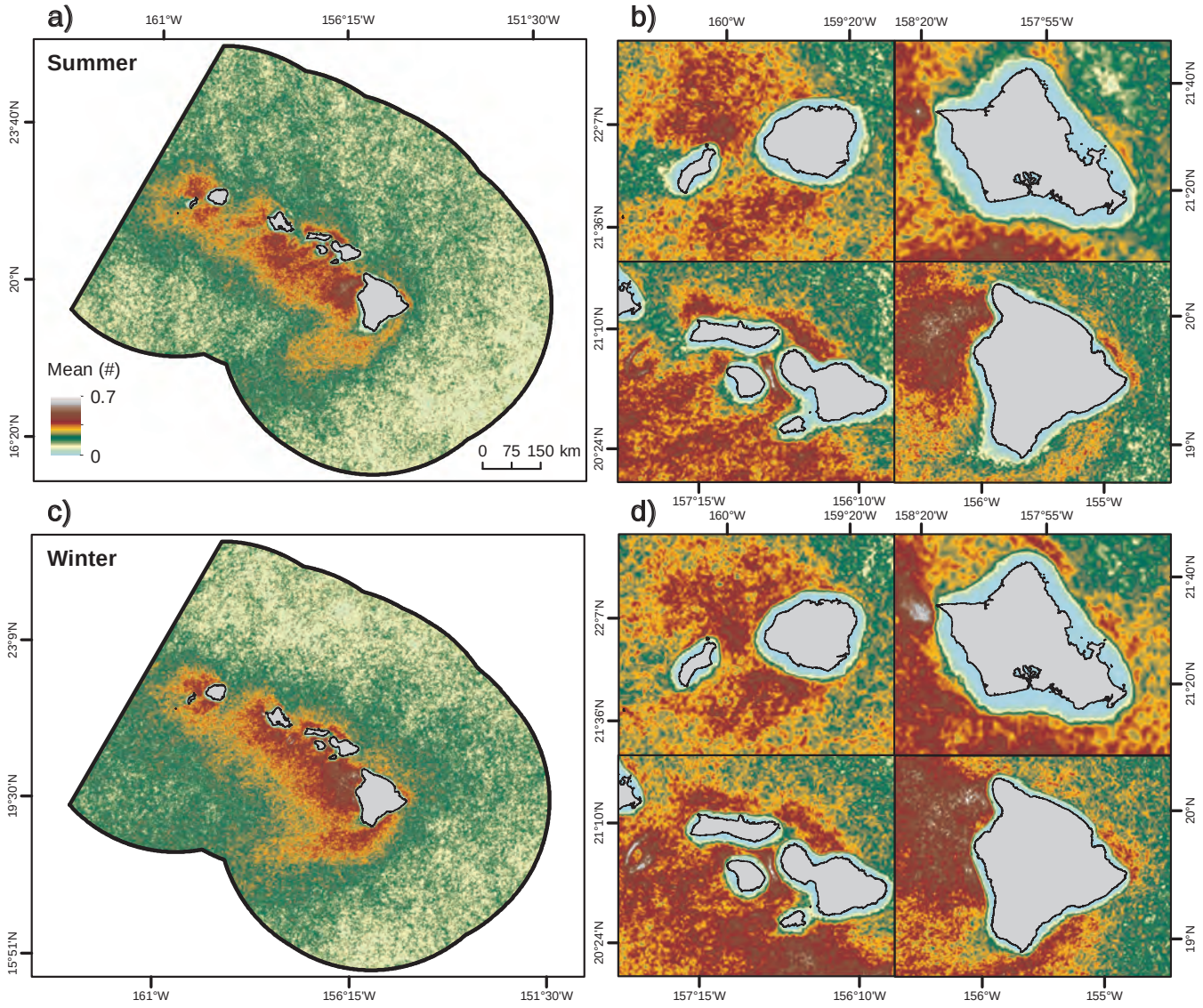

Figure A.15. Frequency of surface chlorophyll-a fronts around the MHI. These maps denote the average frequency of surface chlorophyll-a fronts in the summer a,b) and winter c,d) within the study area. Frontal frequency is defined as the number of months for which a front was observed at a particular pixel, divided by the total number of months. A front was detected if there was a ≥0.06 log mg/m³ between two water masses within a 32x32 pixel moving window. Dates: June 2002-December 2013. Data source: Table 2.2 #7. Data provided courtesy of the Plymouth Marine Laboratory, Dr. Peter Miller.

Appendices

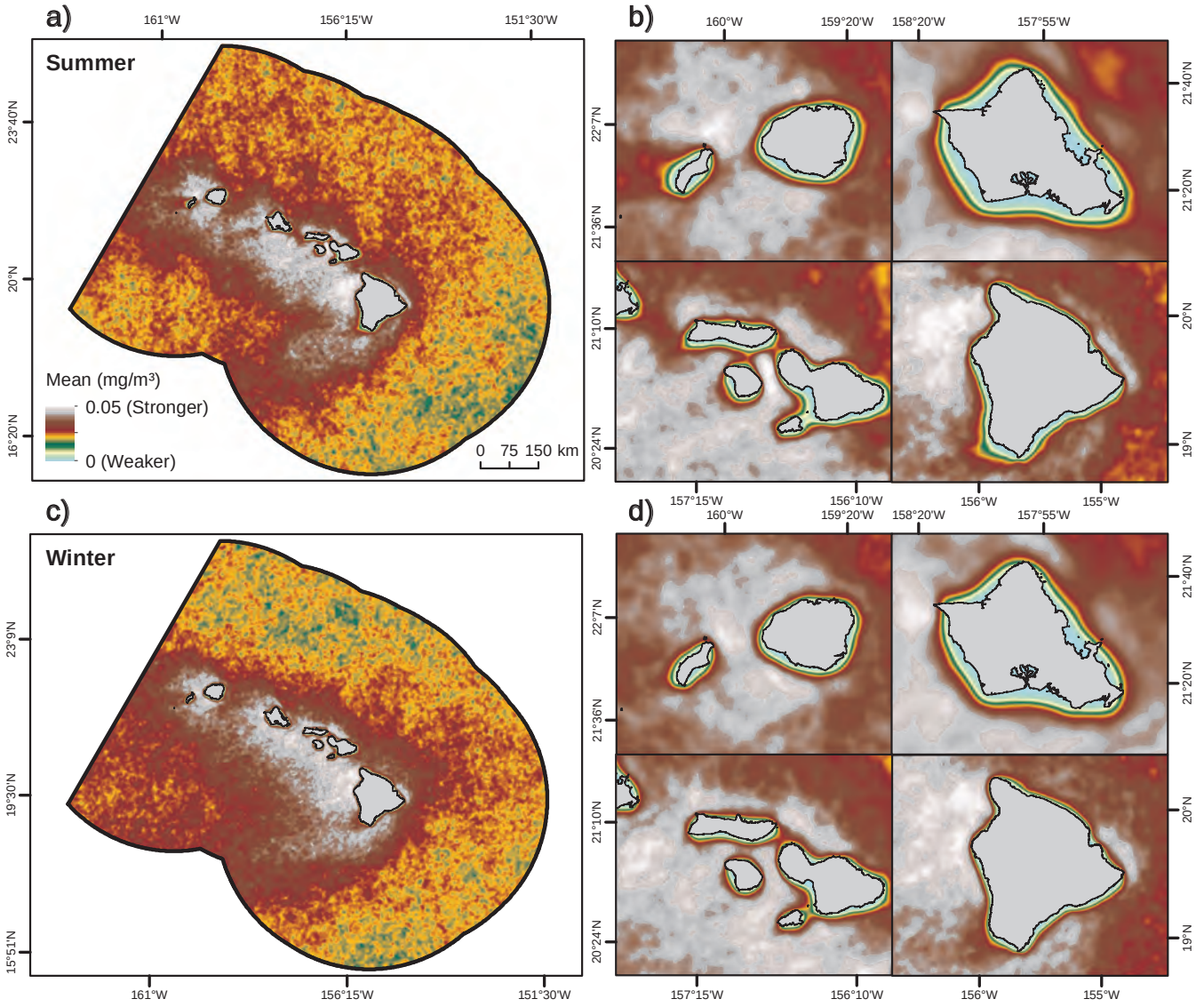

Figure A.16. Strength of surface chlorophyll-a fronts around the MHI. These maps denote the average strength of surface chlorophyll-a fronts in the summer a,b) and winter c,d) within the study area. Strength is defined as the magnitude of change (mg/m³) in surface chlorophyll-a concentrations. Dates: June 2002-December 2013. Data source: Table 2.2 #9. Data provided courtesy of the Plymouth Marine Laboratory, Dr. Peter Miller.

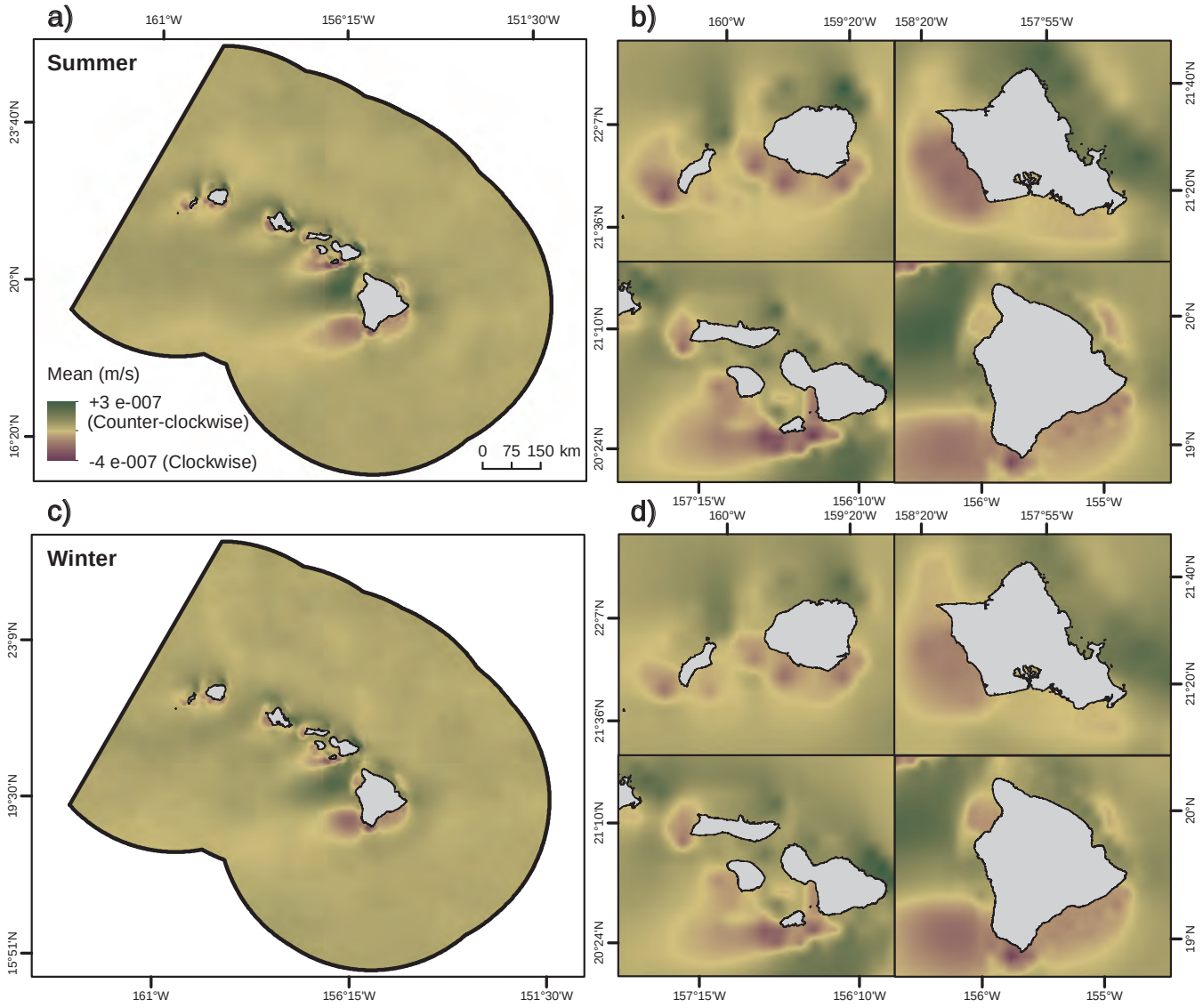

Figure A.17. Vorticity (i.e., rotation) of surface currents around the MHI. These maps depict the average counter-clockwise (+m/s) and clockwise (-m/s) rotation of surface waters in the summer a,b) and winter c,d) within the study area. Dates: 1992-2005. Data source: Table 2.5, #33

Appendices

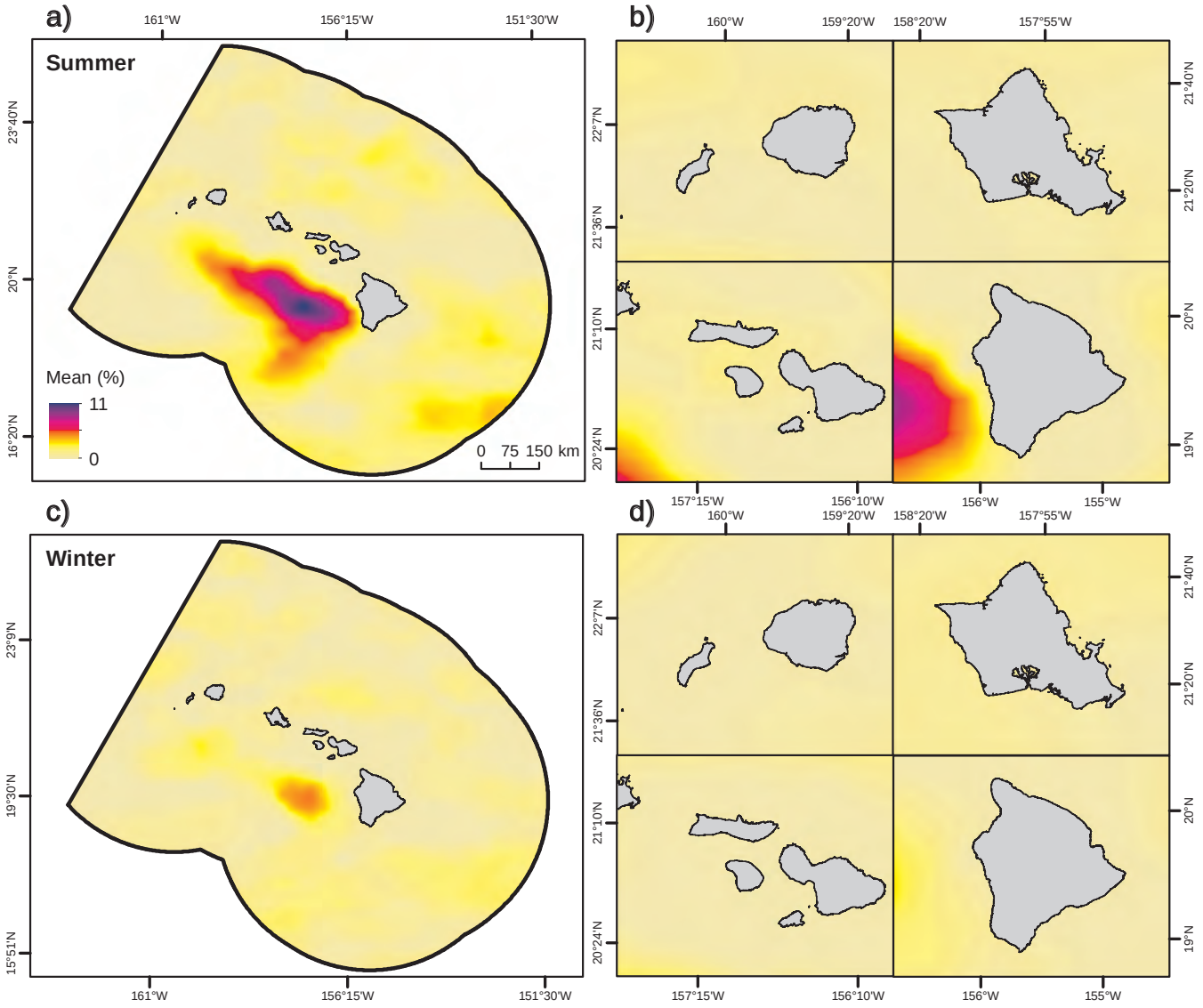

Figure A.18. Probability of eddy rings around the MHI. These maps depict the average probability (%) that eddy rings will form in the summer a,b) and winter c,d) within the study area. These maps combine both anti-cyclonic (clockwise rotating) and cyclonic (counter-clockwise rotating) eddies. Dates: 1992-2014. Data source: Table 2.5 #27

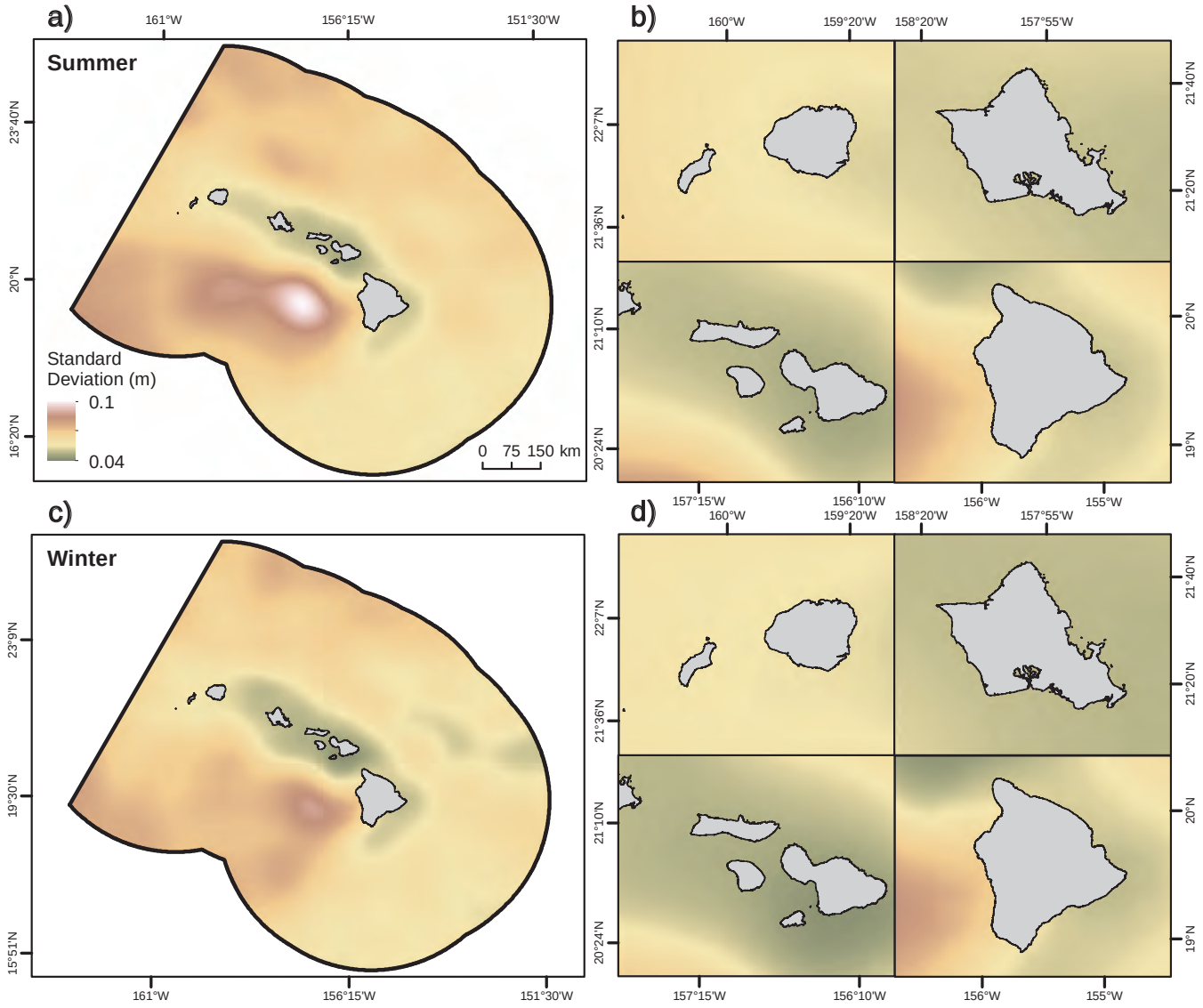

Figure A.19. Variation in sea surface height (SSH) around the MHI. These maps depict the standard deviation in sea level heights (m) in the summer a,b) and winter c,d) within the study area. Height is measured relative to the geoid. Dates: October 1992-July 2012. Data source: Table 2.4 #19

Appendices

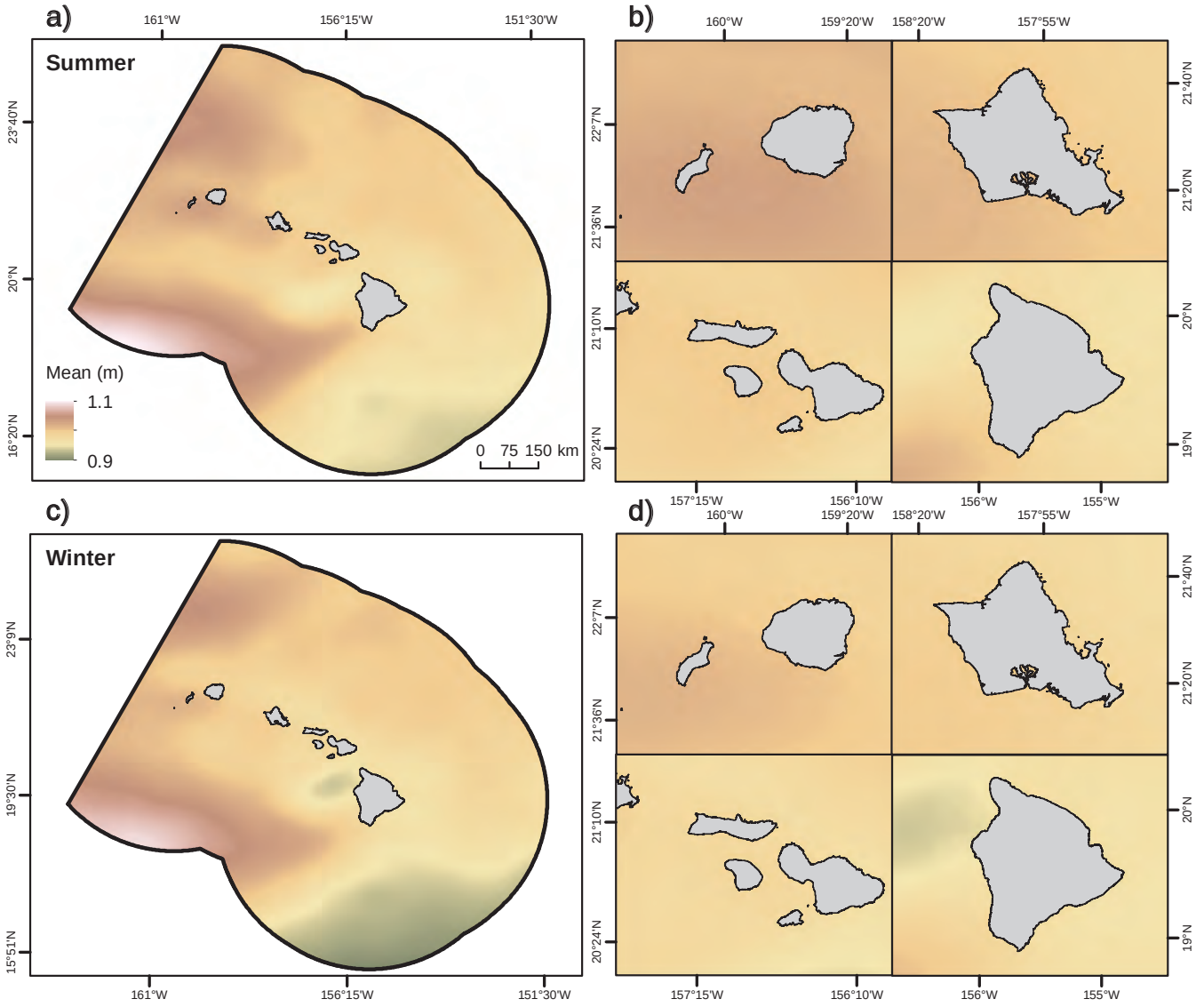

Figure A.20. Sea surface height (SSH) around the MHI. These maps depict the average height (m) of the sea level in the summer a,b) and winter c,d) within the study area. Height is measured relative to the geoid. Dates: October 1992-July 2012. Data source: Table 2.4 #19

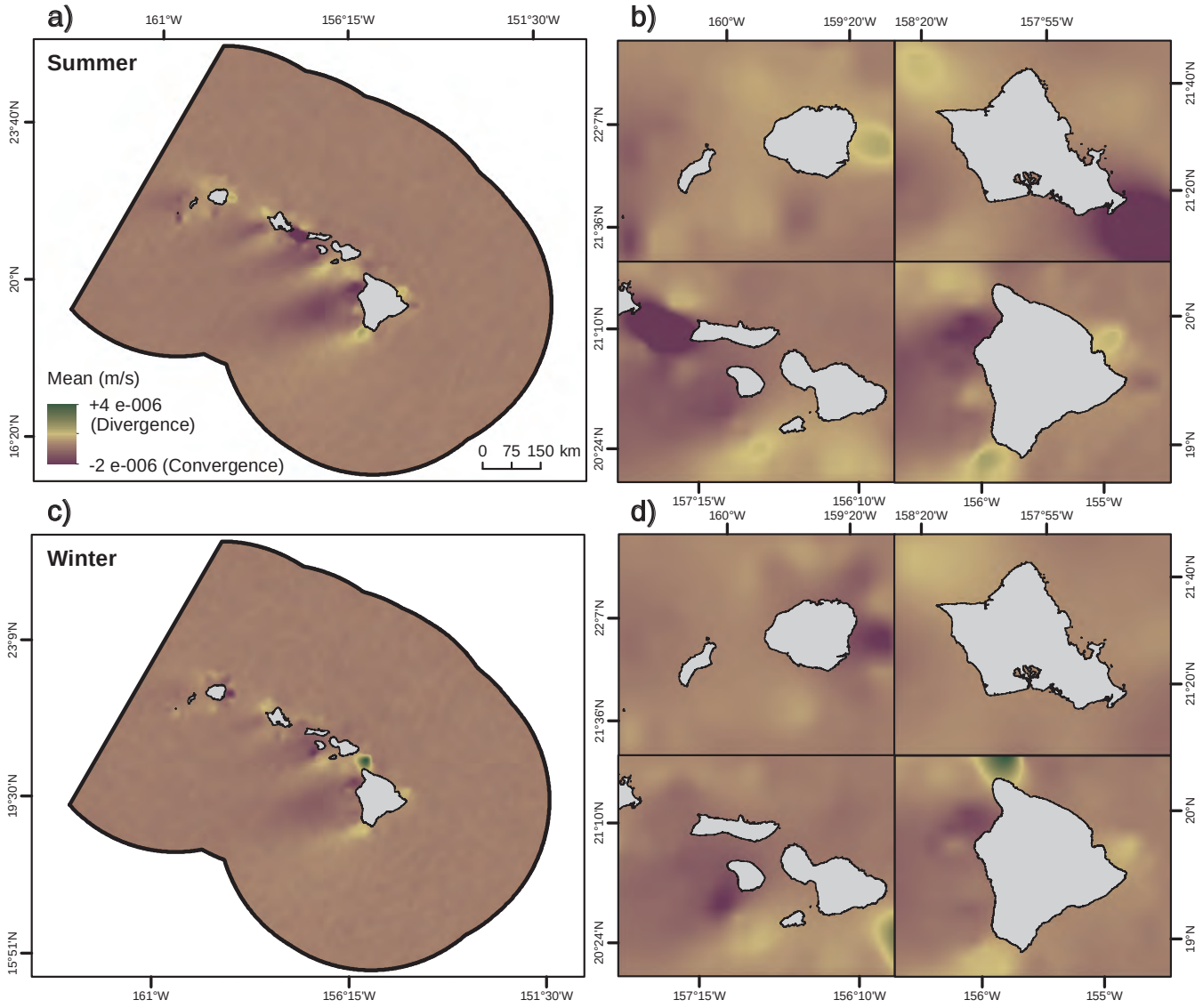

Figure A.21. Divergence and convergence of wind around the MHI. These maps depict the divergence (+m/s) and convergence (-m/s) of winds in the summer; a,b) and winter; c,d) within the study area. Wind movements were measured at an altitude of 30 m. Dates: July 1999-November 2009. Data source: Table 2.1 #2

Appendices

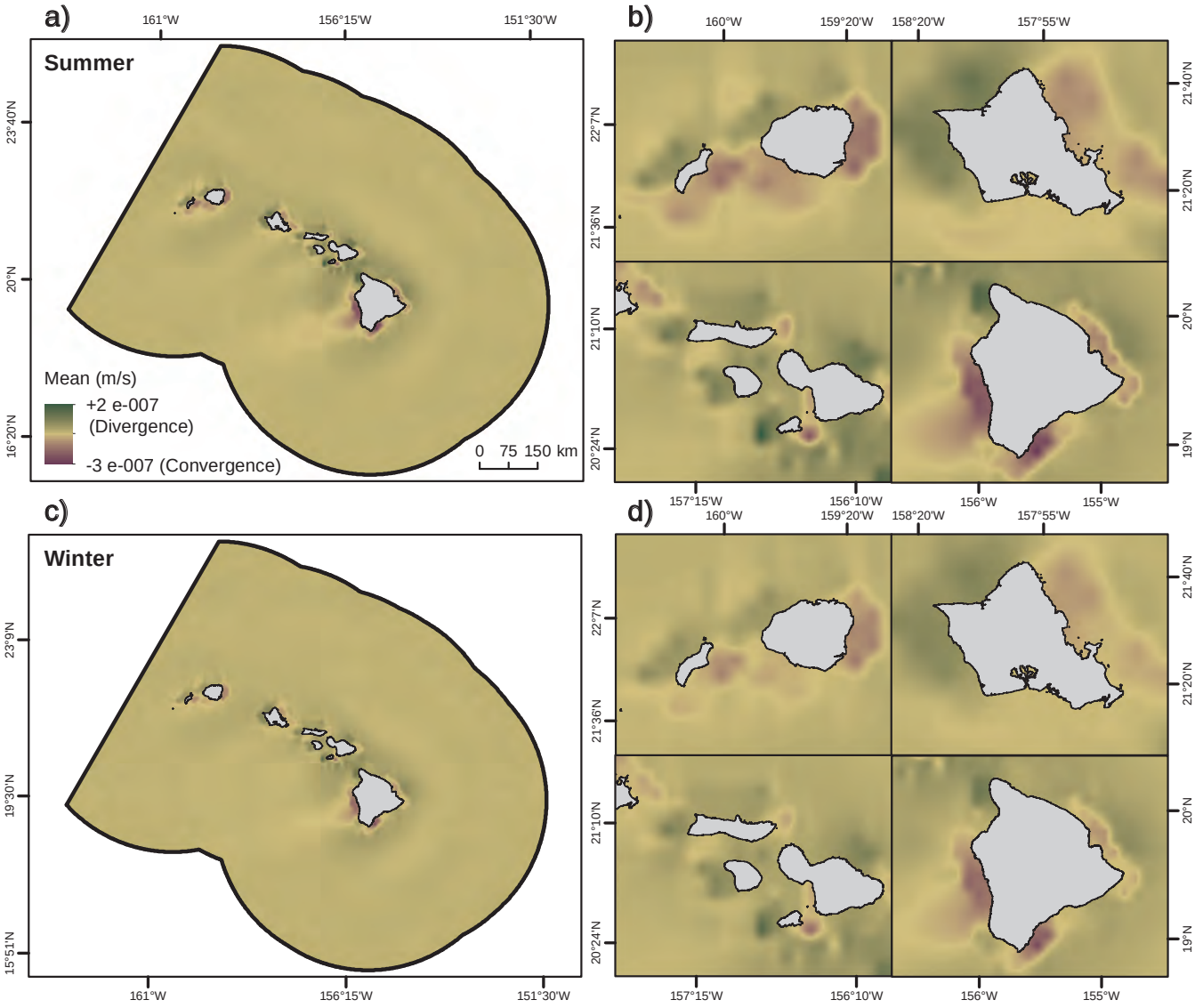

Figure A.22. Divergence and convergence of surface currents around the MHI. These maps depict the divergence (+m/s) and convergence (-m/s) of surface currents in the summer a,b) and winter c,d) within the study area. Dates: 1992-2005. Data source: Table 2.5 #29

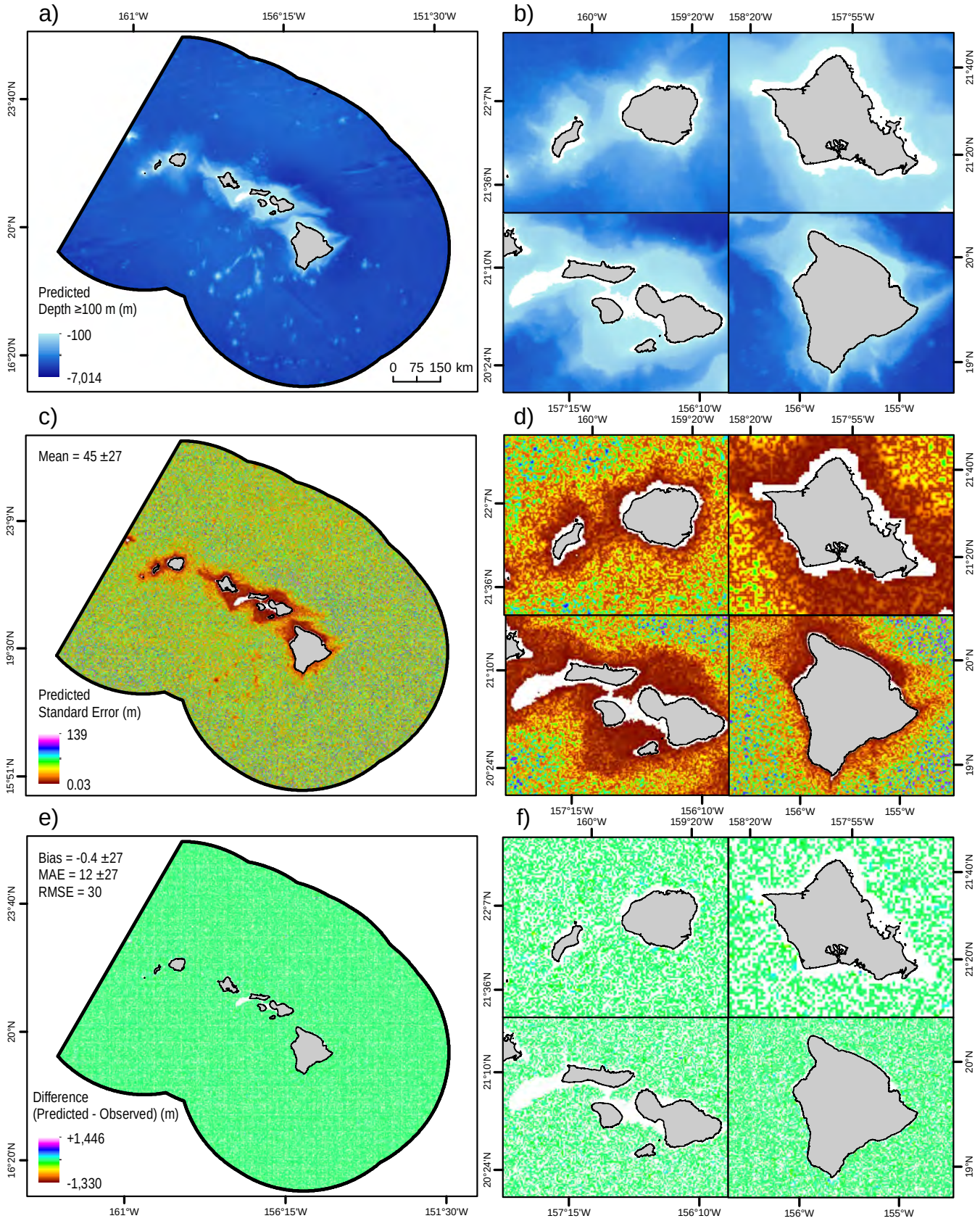

Figure A.23. Precision and error associated with predicted seafloor depths (deeper than 100 m) around the MHI. These maps depict: a,b) the predicted seafloor depths (m); c,d) the standard error (m) associated with those predicted depths; and e,f) the difference (m) between predicted and observed depths within the study area. Dates: N/A. Data source: Table 2.7 #47, 48, 49

Appendices

APPENDIX B: Boosted Zero-inflated Count (BZIC) Predictive Modeling

A boosted generalized additive modeling framework (Bühlmann and Hothorn, 2007; Hofner et al., 2012) was used to relate cetacean and seabird count data to a range of predictor variables (Figure B.1). The estimated relationships were then used to predict the distributions of relative abundance or relative density of modeled species across the entire study area.

Our primary modeling objective was to provide the best estimates of at-sea distributions of cetaceans and seabirds. Given this objective, the statistical modeling framework that we chose had several key features that, in combination, provided advantages over alternative modeling approaches. First, this framework used appropriate statistical distributions to model counts of potentially aggregated animals. Second, this framework allowed for highly flexible relationships between expected counts and a large number of predictor variables, including complex multi-way interactions between predictor variables. Third, this framework accounted for differences in the data collection process between and within datasets.

B.1. Model variables

B.1.1. Response variable

The raw survey data were continuously recorded counts of individual cetaceans and seabirds (Chapters 6 and 7). To standardize across datasets, the data were discretized into transect segments 1.2 km long, corresponding to the spatial resolution of our study grid and the dimensions of a BOEM aliquot. Counts of the number of individuals of each species were summed within each transect segment. Because the length of any given transect was not necessarily divisible by 1.2 km, the remainder distance was treated as its own segment (if it was >0.6 km), or was added to another segment (if it was <0.6 km). The placement of the resulting short or long segment was randomized to avoid it always occurring at the end of a transect (K. Forney, pers. comm.). Thus, the response variable in the BZIC modeling framework was the number of individuals of each species counted on each 1.2 km transect segment.

B.1.2. Predictor variables

A wide range of predictor variables were used to model variation in the number of individuals sighted per transect segment and to predict relative abundance or relative density throughout the study area (Table B.1, Chapter 2). Predictor variables fell into one of six categories: survey, temporal, geographic, seafloor topography, physical and biological oceanographic, and atmospheric.

Survey predictor variables were designed to account for variation in counts arising from heterogeneity in the type and characteristics of survey platform (e.g., observation height and method), observer identity and expertise, species focus, and sightings conditions. These factors influence the probability that individual animals will be detected and correctly identified to the species level. Type of survey platform (ship, small boat, or plane) was directly incorporated as a predictor variable. To account for variation in sighting conditions, sea state was incorporated as a predictor variable in cetacean models, and 'observation condition' data were used to adjust the effort offset in seabird models (Section B.3).

We attempted to account for the effects of the remaining factors through two random-effect predictor variables representing survey identity (ID) and transect ID, respectively. The exact definition of transect ID differed somewhat between datasets, but unique transect identities generally represented pre-defined survey transects or individual days of effort.

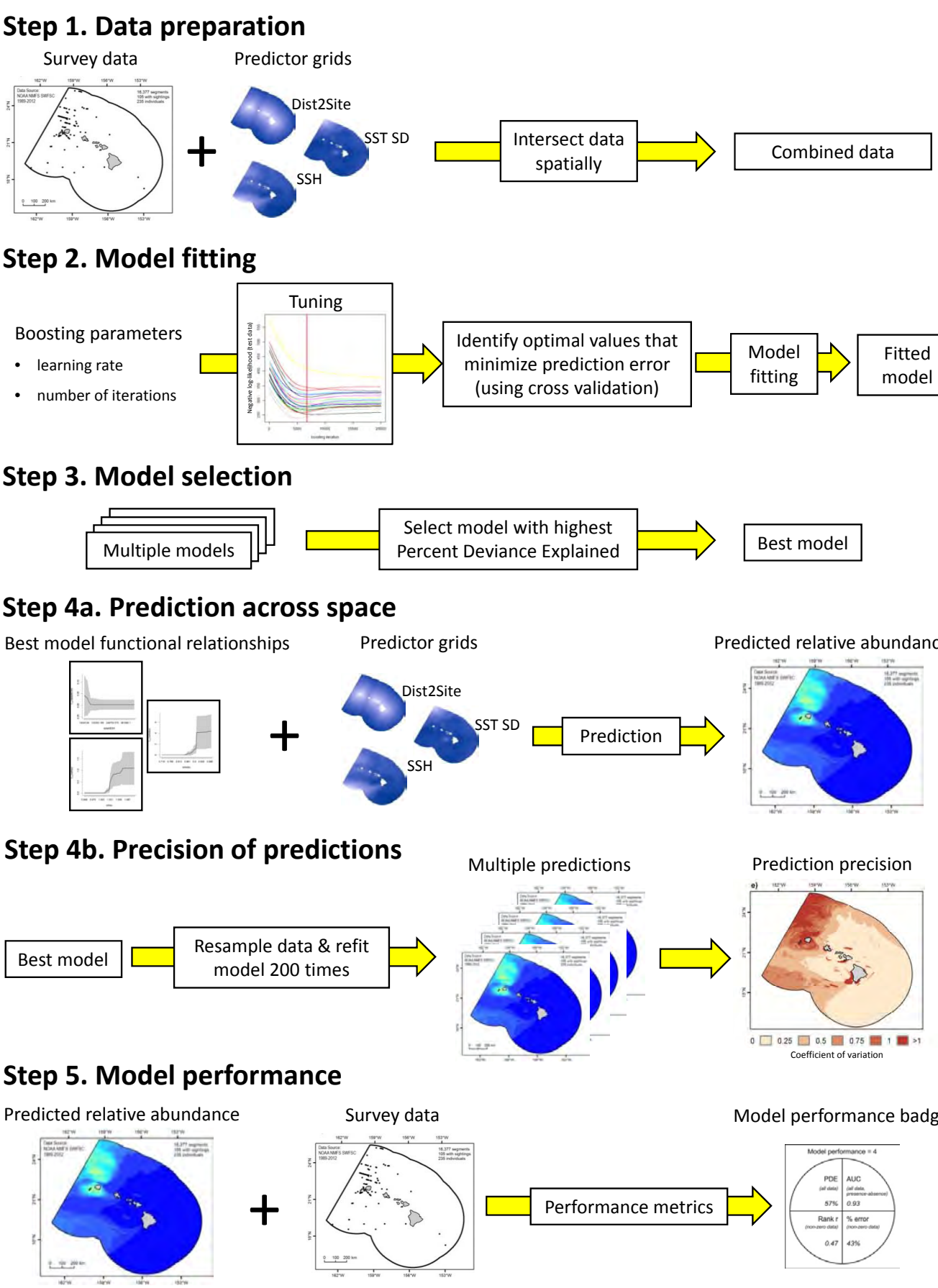

Figure B.1. BZIC modeling framework, including data preparation, model fitting, model selection, prediction across space, and evaluation of model performance.

Appendices

Table B.1. Predictor variables used in BIZC modeling.

Predictor variable	Source
Survey variables	
Survey platform[1]	survey data[2] (see Chapters 6 and 7)
Sea state[1]	survey data[2] (see Chapters 6 and 7)
Survey ID	survey data[2] (see Chapters 6 and 7)
Transect ID	survey data[2] (see Chapters 6 and 7)
Temporal variables	
Year	survey data[2] (see Chapters 6 and 7)
Day of year	survey data[2] (see Chapters 6 and 7)
Pacific Decadal Oscillation (PDO) index (current and 1 year lag)	Mantua, 2015
North Pacific Gyre Oscillation (NPGO) index (current and 1 year lag)	Di Lorenzo, 2015
Multivariate El Niño-Southern Oscillation Index (MEI) (current and 1 year lag)	NOAA ESRL, 2015
Geographic variables	
Longitude projected (oblique Mercator)	n/a
Latitude projected (oblique Mercator)	n/a
Distance to land/nearest terrestrial site[3]	see Chapter 2 (Table 2.3) and Chapter 7
Distance to seamounts	see Chapter 2 (Table 2.3)
Seafloor topography variables	
Depth	see Chapter 2 (Table 2.8)
Slope	see Chapter 2 (Table 2.8)
Slope (derived at 10 km scale)[4]	see Chapter 2 (Table 2.8)
Slope of slope	see Chapter 2 (Table 2.8)
Slope of slope (derived at 10 km scale)[4]	see Chapter 2 (Table 2.8)
Planform curvature (derived at 10 km scale)[4]	see Chapter 2 (Table 2.8)
Profile curvature (derived at 10 km scale)[4]	see Chapter 2 (Table 2.8)
Physical oceanographic and atmospheric variables (seasonal climatologies)	
Sea surface height	see Chapter 2 (Table 2.4)
Sea surface height standard deviation	see Chapter 2 (Table 2.4)
Probability of anticyclonic eddy ring	see Chapter 2 (Table 2.4)
Probability of cyclonic eddy ring	see Chapter 2 (Table 2.5)
Sea surface temperature	see Chapter 2 (Table 2.6)
Sea surface temperature standard deviation	see Chapter 2 (Table 2.6)
Sea surface temperature front probability	see Chapter 2 (Table 2.6)
Sea surface temperature front strength	see Chapter 2 (Table 2.6)
Surface current speed	see Chapter 2 (Table 2.5)
Surface current speed standard deviation	see Chapter 2 (Table 2.5)
Surface current direction (sine)	see Chapter 2 (Table 2.5)
Surface current direction (cosine)	see Chapter 2 (Table 2.5)
Surface current divergence	see Chapter 2 (Table 2.5)
Surface current vorticity	see Chapter 2 (Table 2.5)

[1] Cetacean models only.

[2] Seabird survey data provided by NOAA NMFS/SWFSC; and cetacean survey data provided by Cascadia Research Collective, J. Mobley (University of Hawai'i), and NOAA NMFS/SWFSC and PIFSC.

[3] For breeding seabirds, distance to the nearest terrestrial site, otherwise shortest distance to land.

[4] Calculated from depth grids that were smoothed using a Gaussian low-pass filter at a 10 km spatial scale.

Table B.1. cont. Predictor variables used in BIZC modeling.

Predictor variable	Source
Physical variables (seasonal climatologies) cont.	
Mixed layer depth	see Chapter 2 (Table 2.4)
Wind speed	see Chapter 2 (Table 2.1)
Wind speed standard deviation	see Chapter 2 (Table 2.1)
Wind direction (sine)	see Chapter 2 (Table 2.1)
Wind direction (cosine)	see Chapter 2 (Table 2.1)
Wind divergence	see Chapter 2 (Table 2.1)
Upwelling index	see Chapter 2 (Table 2.5)
Turbidity	see Chapter 2 (Table 2.4)
Turbidity standard deviation	see Chapter 2 (Table 2.4)
Biological oceanographic variables (seasonal climatologies)	
Surface chlorophyll-*a*	see Chapter 2 (Table 2.2)
Surface chlorophyll-*a* standard deviation	see Chapter 2 (Table 2.2)
Surface chlorophyll-*a* front probability	see Chapter 2 (Table 2.2)
Surface chlorophyll-*a* front strength	see Chapter 2 (Table 2.2)

[1] Cetacean models only.

[2] Seabird survey data provided by NOAA NMFS/SWFSC; and cetacean survey data provided by Cascadia Research Collective, J. Mobley (University of Hawai'i), and NOAA NMFS/SWFSC and PIFSC.

[3] For breeding seabirds, distance to the nearest terrestrial site, otherwise shortest distance to land.

[4] Calculated from depth grids that were smoothed using a Gaussian low-pass filter at a 10 km spatial scale.

Temporal predictor variables were designed to account for variation in counts over time. Day of the year was used to account for changes in the numbers of individuals in the study area over time within a season, for example, arising from migratory movements in and out of the study area. Year was used to account for changes in the number of individuals in the study area across years, for example, arising from changes in population abundance or distributional shifts. Effects of day of the year and year were modeled as smooth continuous changes over time. Three climate indices (Pacific Decadal Oscillation, North Pacific Gyre Oscillation, and Multivariate El Niño-Southern Oscillation) were also included as temporal predictor variables to account for variation in counts across years arising from linkages between the environment and population abundance and distribution. For each climate index, two values were included as predictor variables: the value for the month and year of a given transect segment, and the value for the same month one year previous. The latter was included to allow for possible lagged effects.

Geographic predictor variables were designed to account for variation in counts arising from spatial location per se. Projected longitude and latitude were included as predictor variables and their effects were modeled two ways. The first longitude-latitude predictor term allowed for smooth changes in numbers across the study area arising from spatial factors not captured by the other predictor variables. The second longitude-latitude predictor term was formulated using radial basis functions with the intent of capturing some of the spatial autocorrelation in the data after accounting for the effects of other predictor variables. Distance to land, distance to seamounts, and distance to terrestrial sites (breeding seabird species only) were also included as geographic predictor variables.

Seafloor topography variables were designed to account for variation in counts arising from the direct and indirect effects of bathymetry on animal distributions. Depth was the fundamental topographic variable, and other topographic variables were derived from depth, including slope, slope of slope, and planform and profile curvature.

Appendices

Physical oceanographic and atmospheric predictor variables were designed to account for variation in counts arising from the direct and indirect effects of the physical state and dynamics of the ocean and air above the ocean. Twenty three physical oceanographic and atmospheric predictor variables were developed from a range of data sources (Chapter 2). Remote sensing data were used to characterize sea surface height, temperature, turbidity, and wind speed and direction. Other variables were derived from the remotely sensed variables including sea surface height and temperature variability, probabilities of cyclonic and anticyclonic eddy rings, probability and strength of sea surface temperature fronts, wind speed variability and divergence, and an index of upwelling. Estimates from a data-assimilating ocean dynamics model were used to characterize water currents and stratification, with divergence and vorticity derived from current velocities and mixed layer depth derived from temperature and salinity.

Sea surface chlorophyll-*a* related variables were included as biological oceanographic predictor variables to account for variation in counts arising from the direct and indirect effects of ocean productivity. Remote sensing data were used to characterize sea surface chlorophyll-*a* concentration. Chlorophyll-a variability and the probability and strength of chlorophyll-*a* fronts were derived from concentration.

Geographic, seafloor topography, physical and biological oceanographic, and atmospheric predictor variables were spatially explicit. Each survey transect segment was matched to the environmental predictor variable values from the study grid cell that contained the midpoint of that segment.

All of the physical and biological oceanographic and atmospheric variables that we considered are dynamic. We formulated these predictor variables to characterize long-term spatial patterns in average values and variability. To characterize average values, monthly mean climatologies across years were developed and then integrated to create seasonal climatologies. To characterize variability, standard deviations or probabilities (frequencies) were calculated from the native temporal resolution of the corresponding predictor variables.

Because the physical and biological oceanographic and atmospheric predictor variables represented average long-term spatial patterns, our modeling framework only allowed the predicted distribution of animals to respond to these average long-term spatial patterns. Any responses of animals' spatial distributions to changes in the spatial patterns of these dynamic environmental variables over time are not captured by our 'climatological' modeling framework, and would contribute to residual model error. An alternative approach would have been to match the survey data to contemporaneous data for dynamic environmental predictor variables, thereby allowing predicted animal distributions to respond to this temporal variability. This alternative approach would require complete temporal datasets for every dynamic environmental predictor variable for the entire time frame of the survey data. The performance of climatological versus contemporaneous approaches to habitat-based species distribution modeling is an active area of research (e.g., Mannocci et al., 2014; Scales et al., 2014).

B.2. Statistical framework

The response variable, the number of individuals of a given species counted per transect segment, was modeled using one of two statistical distributions: a zero-inflated Poisson distribution or a zero-inflated negative binomial distribution. The standard Poisson and negative binomial distributions are appropriate for modeling count data. The negative binomial distribution in particular can account for aggregated animal distributions. The zero-inflated versions of these distributions can further account for highly aggregated distributions. The parameters of the count and zero-inflation components of these distributions were modeled as separate functions of the predictor variables (Schmid et al., 2008; Mayr et al., 2012).

B.3. Effort offset

To account for variation in the lengths of survey transect segments (and effective widths of seabird strip transects) an effort 'offset' was included in the models. For cetacean models the effort offset was the length of a given transect segment, which enforced a proportional relationship between distance travelled and the number of individuals of each species counted. Thus, for cetacean models the predictions represent the expected number of individuals sighted per unit distance travelled. This quantity represents an index of abundance, so we refer to this quantity as 'relative abundance'. For seabird models the effort offset was the area of a given strip transect segment, which enforced a proportional relationship between area surveyed and the number of individuals of each species counted. Thus, for seabird models the predictions represent the expected number of individuals sighted per unit area surveyed. We refer to this quantity as 'relative density'. The widths of seabird strip transect segments were set for each species on the basis of 'observation conditions' data, and the corresponding effective strip widths from the survey observer instruction manual (L. Ballance, pers. comm.).

B.4. Base-learners

Within the boosted generalized additive modeling framework, the estimated overall relationships between the response and predictor variables are essentially the sum of multiple relationships between the response variable and each individual predictor variable or small subsets of predictor variables. Each individual relationship is referred to as a 'base-learner' and is of a specific type, for example, a linear relationship. We utilized a suite of base-learners each associated with specific predictor variables, and different sets of base-learners were employed for different model components (Table B.2).

All spatially explicit predictor variables, except geographic coordinates, were included together in a single tree base-learner. The trees for that learner had a maximum depth of either 4 or 5, which allowed for interacting effects among the spatially explicit predictor variables. Projected longitude and latitude appeared in two base learners, and those variables always entered the model as a pair. The remaining survey and temporal predictor variables entered the model individually, either through their own base-learners or, in the case of climate indices, one at a time through a tree base-learner with a maximum depth of 1. Thus, our model structure did not allow for interactions between temporal and spatial predictor variables.

Table B.2. Base-learners employed in the boosted generalized additive modeling framework. Base- learner names are from the 'mboost' package for R (Hothorn et al., 2014; R Core Team, 2015), and predictor variable names are defined in Table B.1. Model components were: p *(probability of zero inflation),* μ *(mean of standard count distribution), and* θ *(dispersion parameter of negative binomial distribution).*

Name	Description	Predictor variables	Model component
bols	linear	model intercept	p, μ, θ
bols	linear (fixed effect)	survey platform	p, μ, θ
brandom	random effect	survey ID	θ
brandom	random effect	transect ID	p, μ
bbs	penalized regression spline[1]	sea state	p, μ
bbs	penalized regression spline[1]	year	p, μ
bbs	penalized regression spline[1]	day of year	p, μ
btree	tree[2]	all climate indices (current and lagged)	p, μ
bspatial	penalized tensor product[1]	projected longitude, projected latitude	p, μ
brad	penalized radial basis[3]	projected longitude, projected latitude	p, μ
btree	tree[4]	distance to shore, distance to seamounts, all seafloor topography, physical and biological oceanographic and atmospheric variables	p, μ

[1] P-spline basis; [2] Maximum depth = 1; [3] Matern correlation function; [4] Maximum depth = 4 or 5

Appendices

B.5. Stochastic gradient boosting

Model fitting through boosting is an iterative process. In each step each base-learner is fit to determine which base-learner essentially explains the most of the remaining variation in the data, and that base-learner is selected for that step. We employed a version of this technique, referred to as 'stochastic gradient boosting', whereby the base-learners are fitted only to a sub-sample of the data in each iteration (Friedman, 2002). A set of 25 or 50 random sub-samples was created before the model fitting process began, and one randomly selected sub-sample was used in each boosting iteration.

B.6. Boosting 'offsets'

Prior to model fitting through boosting, each model component must be set to some initial value, or 'offset' in boosting terminology (Hofner et al., 2012). We used two methods to derive these initial values. The first employed simple estimates ignoring the predictor data, and the second considered the predictor data along with a somewhat simplified model.

B.7. Tuning of learning rate and number of iterations

There are two key parameters that control the iterative model fitting process during boosting. The first is the learning rate or 'shrinkage rate', and the second is the number of boosting iterations. As discussed in Section B.5, a single base-learner is selected in each iteration, and the learning rate essentially controls how much each selected base-learner contributes to the overall model fit. Ideally, the iterative process is continued until the prediction error of the fitted model is minimized.

Cross-validation is a technique that is commonly used to measure the prediction error of models. The data are divided into two subsets, the model is fit to one of the subsets, and then the fitted model's ability to predict the other subset is measured. We employed a cross-validation approach to determine the learning rate and number of boosting iterations that minimized prediction error. We refer to this process as 'tuning'. The learning rate was tuned first by fixing the number of boosting iterations, and then the number of boosting iterations was tuned by fixing the learning rate at its previously determined optimal value. Cross-validation was conducted multiple times for each tuning step. We allowed for a maximum of 20,000 boosting iterations, so models that reached that number of iterations should be interpreted with caution as their performance may have improved with additional iterations.

B.8. Model selection and performance

For each modeled species (and season) eight different models were fitted (Table B.3). The performance of each model was evaluated from a suite of performance metrics (Table B.4). The key performance metric was percent deviance explained (PDE), which is essentially the percentage of variation in the data explained by the fitted model beyond the amount of variation explained by a simpler model without predictor variables. PDE indicates overall model fit. PDE is somewhat analogous to the more familiar R^2 metric for a linear regression. The model with the highest PDE was chosen as the 'final' model.

Table B.3. Candidate models considered for each modeled species and season.

Model Number	Zero-Inflated Likelihood	Maximum Tree Depth	Boosting Offset Method[1]
1	Poisson	4	1
2	negative binomial	4	1
3	Poisson	5	1
4	negative binomial	5	1
5	Poisson	4	2
6	negative binomial	4	2
7	Poisson	5	2
8	negative binomial	5	2

[1] Described in Section B.6

Three additional performance metrics were calculated for each of the final models to provide a more complete assessment of model performance (Table B.4). The first of these metrics was the area under the receiver operating characteristic curve (AUC), which indicates how well a model predicts binary data. We calculated AUC by converting the count data to presence/absence data. The AUC metric indicates how well the models predicted the observed presence of a species, but not necessarily how well the models predicted the relative abundance or relative density of a species. The second of these metrics was the Gaussian rank correlation coefficient (*r*) between the observed and predicted non-zero data. The *r* metric indicates how well the models predicted the number of individuals observed when a species was observed. The third of these metrics was the median absolute residual error for non-zero data as a percentage of the mean non-zero value (percent error). As with *r*, this metric indicates how well the models predicted the number of individuals observed when a species was observed. The percent error metric was calculated during the cross-validation tuning of the number of boosting iterations, so it better reflects prediction error.

Table B.4. Model performance metrics.

Name	Description	Data	Stage	Performance categories
PDE	percent deviance explained[1]	all	final fit	5: ≥60% 4: 40-60% 3: 20-40% 2: 10-20% 1: <10%
AUC	area under the receiver operating characteristic curve	all, converted to presence/absence	final fit	5: >0.9 4: 0.8-0.9 3: 0.7-0.8 2: 0.6-0.7 1: <0.6
Rank r	Gaussian rank correlation coefficient[2]	non-zero	final fit	5: >0.6 4: 0.4-0.6 3: 0.2-0.4 2: 0.1-0.2 1: <0.1
Percent error	median absolute residual error as percentage of data mean	non-zero, out-of-bag	during tuning of the number of boosting iterations[3]	5: <25% 4: 25-50% 3: 50-100% 2: 100-200% 1: >200%

[1] To calculate percent deviance explained, the saturated likelihood was assumed to be the maximum possible likelihood value, and the null likelihood was calculated from an intercepts-only zero-inflated model fit to the data (unpublished).

[2] Boudt et al., 2012; Bodenhofer et al., 2013

[3] Median value across cross-validation replicates

Performance categories were defined for each performance metric and assigned a numeric code (5=highest to 1=lowest; Table B.4). The performance of each final model was assigned an overall performance equal to the average performance across the four performance metrics. Model performance is displayed on each map figure using a 'badge' (e.g., Figures 6.10-6.13; 6.15-6.22; and 7.8-7.21).

It is important to recognize that the model performance metrics and badge mainly reflect *the statistical fit of the models to the data*. They reflect only the data that were analyzed, and they do not reflect the quality of model predictions away from the data. For example, the seabird survey data were primarily from two years and three months. The performance metrics do not necessarily indicate how applicable the seabird models may be for other years and months. Similarly, survey data did not cover everywhere within the study area, so some model predictions are essentially interpolations/extrapolations from data in other parts of the study area. The accuracy of those predictions is not necessarily reflected by the model performance metrics. Data from additional years, months, and areas would be required to fully evaluate the accuracy of model predictions outside of the observed data coverage. Nevertheless, the performance metrics and badge give an indication of how accurately a model was able to predict the observed data, and good performance provides a measure of confidence in the modeled distributions, especially within the temporal and spatial coverage of the observed survey data.

Appendices

B.9. Spatial prediction

The final models were used to predict 'relative abundance' or 'relative density' across the study area. Relative abundance was defined as the expected number of individuals that would be counted per km travelled (cetaceans), while relative density was defined as the expected number of individuals that would be counted per km^2 observed (seabirds). Relative abundance and density integrated the zero- inflated and count components of the statistical model.

It is important to recognize that the model predictions do not represent actual absolute abundance or density. During visual surveys, individual birds and cetaceans may be missed either because they are below the surface of the water (availability bias) or simply because observers failed to notice them (perception bias) (Barlow, 2015). The failure to count some individuals biases estimates of abundance and density downward relative to actual abundance or density. Animal movement can also bias estimates of abundance or density. Cetaceans and birds may be attracted or repelled by ships, small boats, and planes biasing estimates upward or downward, respectively. Flying birds or fast moving cetaceans can also bias estimates, with the direction of the bias depending on the speed and direction of the animals' movement relative to those of the survey platform (Spear et al., 1999). Our model predictions should only be interpreted as indexes of abundance or density.

Spatially explicit predicted values were calculated for each cell of the study grid from the values of the spatially explicit predictor variables for that cell. Thus, the predicted relative abundance or density in a given grid cell corresponded to predictions for a transect segment whose mid-point falls within that grid cell. All non-spatial predictor variables were set to their mean values.

B.10. Variable importance

While our primary objective was not to determine the ecological drivers and mechanisms behind the spatial distributions of cetaceans and seabirds in the study area, our model results do provide some indication of which variables were most useful for predicting those distributions. Those variables may provide useful starting points for future studies aimed more at ecological inference.

We calculated the relative importance of a given predictor variable in a given model by essentially summing the amount of variation in the data explained by that predictor variable. Relative variable importance was a function of the frequency with which a given predictor variable was selected during boosting and that variable's ability to explain variation in the data when it was selected. Relative variable importance was re-scaled so that it summed to 1 across predictor variables.

B.11. Precision of model predictions

The precision of model predictions was estimated using a non-parametric bootstrapping framework. Non-parametric bootstrapping is a technique in which the data are randomly re-sampled and the model is refit multiple times. The precision of the model predictions can then be assessed from the variability in predictions across the bootstrap replicates.

For each bootstrap iteration, the set of unique transect IDs was resampled with replacement, and the data for each transect ID were assigned weights proportional to the frequency of that ID in the sample. These data weights were then applied when fitting the model during that bootstrap replicate. Predictor variables that were not included in the final model were excluded from the bootstrap analysis. Two hundred bootstrap replicates were conducted producing a sample of predictions from which we calculated the coefficient of variation (CV) to characterize uncertainty in the predictions.

Appendices

As with the model performance metrics, the CVs of the model predictions are conditional on the model and the data. They do not capture all of the uncertainty associated with our model predictions, for example, uncertainty about predictions outside of the data coverage. Nevertheless, the CVs are an important indication of the precision of the model predictions, and they should be an integral consideration when using the model predictions.

B.12. Implementation

The analysis was coded in R version 3.2.1 (R Core Team, 2015) and relied on multiple existing contributed packages, including 'boot' version 1.3-17 (Canty and Ripley, 2016), 'fastcluster' version 1.1.16 (Müllner, 2013), 'fields' versions 8.2-1 and 8.3-5 (Nychka et al., 2015), 'maptools' versions 0.8-36 and 0.8-37 (Bivand and Lewin-Koh, 2015), 'MASS' versions 7.3-43 and 7.3-44 (Venables and Ripley, 2002), 'Matrix' version 1.2-2 (Bates and Maechler, 2015), 'mboost' versions 2.4-2 and 2.5-0 (Hothorn et al., 2015), 'modeltools' version 0.2-21 (Hothorn et al., 2013), 'party' versions 1.0-22 and 1.0-23 (Hothorn et al., 2006), 'pROC' version 1.8 (Robin et al., 2011), 'pscl' version 1.4.9 (Jackman, 2015), 'raster' versions 2.4-15 and 2.4-20 (Hijmans, 2014), 'reshape' version 0.8.5 (Wickham, 2007), 'rgdal' versions 1.0-4 and 1.0-7 (Bivand et al., 2015), 'rgeos' versions 0.3-11 and 0.3-14 (Bivand and Rundel, 2015), 'rococo' version 1.1.2 (Bodenhofer et al., 2013), 'sqldf' version 0.4-10 (Grothendieck, 2014), 'sp' versions 1.1-1 and 1.2-1 (Pebesma and Bivand, 2005), and 'VGAM' version 0.9-8 (Yee, 2015).

Appendices

LITERATURE CITED

Ballance, L. NOAA Southwest Fisheries Science Center, Marine Mammal and Turtle Division. La Jolla, CA. Personal Communication.

Barlow, J. 2015. Inferring trackline detection probabilities, g(0), for cetaceans from apparent densities in different survey conditions. Marine Mammal Science 31:923-943.

Bates, D. and M. Maechler. 2015. R package, Matrix: Sparse and dense matrix classes and methods. Software Downloaded October 2014. Software Website: https://CRAN.R-project.org/package=Matrix (Site Accessed 8 June 2016).

Bivand, R. and N. Lewin-Koh. 2015. R package, maptools: Tools for reading and handling spatial objects. Software Downloaded October 2014. Software Website: https://cran.r-project.org/web/packages/maptools/index.html (Site Accessed 8 June 2016).

Bivand, R. and C. Rundel. 2015. R package, rgeos: Interface to Geometry Engine - Open Source (GEOS). Software Downloaded October 2014. Software Website: https://cran.r-project.org/web/packages/rgeos/index.html (Site Accessed 8 June 2016).

Bivand, R., T. Keitt, and B. Rowlingson. 2015. R package, rgdal: Bindings for the Geospatial Data Abstraction Library. Software Downloaded October 2014. Software Website: https://cran.r-project.org/web/packages/rgdal/index.html (Site Accessed 8 June 2016).

Bodenhofer, U., M. Krone, and F. Klawonn. 2013. Testing noisy numerical data for monotonic association. Information Sciences 245:21-37.

Boudt, K., J. Cornelissen, and C. Croux. 2012. The Gaussian rank correlation estimator: robustness properties. Statistics and Computing 22:471-483.

Bühlmann, P. and T. Hothorn. 2007. Boosting algorithms: Regularization, prediction and model fitting. Statistical Science 22(4):477-505.

Canty, A. and B. Ripley. 2015. R package, boot: Bootstrap R (S-Plus) functions. Software Downloaded October 2014. Software Website: https://cran.r-project.org/web/packages/boot/index.html (Site Accessed 8 June 2016).

Di Lorenzo, E. 2015. NPGO index monthly averages from Jan-1950 to Apr-2015. Data Downloaded 22 May 2015. Data Website: http://www.o3d.org/npgo/npgo.php (Site Accessed 8 June 2016).

Forney, K. NOAA National Marine Fisheries Service, Southwest Fisheries Science Center, Marine Mammal and Turtle Division. Santa Cruz, CA. Personal Communication.

Friedman, J.H. 2002. Stochastic gradient boosting. Computational Statistics & Data Analysis 38:367-378.

Grothendieck, G. 2014. R package, sqldf: Perform SQL Selects on R Data Frames. Software Downloaded October 2014. Software Website: https://cran.r-project.org/web/packages/sqldf/index.html (Site Accessed 8 June 2016).

Hijmans, R.J. 2014. R package, Raster: Geographic data analysis and modeling. Software Downloaded October 2014. Software Website: http://CRAN.R-project.org/package=raster (Site Accessed 8 June 2016).

Hofner, B., A. Mayr, N. Robinzonov, and M. Schmid. 2012. Model-based boosting in R: A hands-on tutorial using the R package mboost. Technical Report 120. Department of Statistics, University of Munich, Germany.

Appendices

Hothorn, T., K. Hornik, and A. Zeileis. 2006. Unbiased recursive partitioning: A conditional inference framework. Journal of Computational and Graphical Statistics 15:651-674.

Hothorn, T., F. Leisch, and A. Zeileis. 2013. R package, modeltools: Tools and classes for statistical models. Software Downloaded October 2014. Software Website: https://cran.r-project.org/web/packages/modeltools/index.html (Site Accessed 8 June 2016).

Hothorn, T., P. Buehlmann, T. Kneib, M. Schmid, and B. Hofner. 2015. R package, mboost: Model-based boosting. Software Downloaded October 2014. Software Website: https://cran.r-project.org/web/packages/mboost/index.html (Site Accessed 8 June 2016).

Jackman, S. 2015. R package, pscl: Classes and methods for R developed in the Political Science Computational Laboratory, Stanford University. Software Downloaded October 2014. Software Website: https://cran.r-project.org/web/packages/pscl/index.html (Site Accessed 8 June 2016).

Mannocci, L., M. Catalogna, G. Dorémus, S. Laran, P. Lehodey, W. Massart, P. Monestiez, O. Van Canneyt, P. Watremez, and V. Ridoux. 2014. Predicting cetacean and seabird habitats across a productivity gradient in the South Pacific gyre. Progress in Oceanography 120:383-398.

Mantua, N.J. 2015. The Pacific Decadal Oscillation. Joint Institute for the Study of the Atmosphere and Ocean, University of Washington. Data Downloaded 30 December 2015. Data Website: http://research.jisao.washington.edu/pdo/PDO.latest (Site Accessed 8 June 2016).

Mayr, A., N. Fenske, B. Hofner, T. Kneib, and M. Schmid. 2012. Generalized additive models for location, scale and shape for high dimensional data - a flexible approach based on boosting. Applied Statistics 61(3):403-427.

Müllner, D. 2013. R package, fastcluster: Fast hierarchical, agglomerative clustering routines for R and Python. Journal of Statistical Software 53:1-18. Software Downloaded October 2014. Software Website: https://cran.r-project.org/web/packages/fastcluster/index.html (Site Accessed 8 June 2016).

NOAA ESRL. 2015. Climate Indices, Monthly Atmospheric and Ocean Time Series: MEI (Multivariate ENSO Index). NOAA Earth Systems Research Laboratory, Physical Sciences Division. Data Downloaded 22 May 2015. Data Website: http://www.esrl.noaa.gov/psd/data/climateindices/list/ (Site Accessed 8 June 2016).

Nychka, D., R. Furrer, and S. Sain. 2015. R package, fields: Tools for spatial data. Software Downloaded October 2014. Software Website: https://cran.r-project.org/web/packages/fields/index.html (Site Accessed 8 June 2016).

Pebesma, E.J. and R.S. Bivand. 2005. Classes and methods for spatial data in R. R News 5(2). Online: https://www.r-project.org/doc/Rnews/Rnews_2005-2.pdf (Site Accessed 8 June 2016).

R Core Team. 2015. R: A language and environment for statistical computing (Versions 3.1.1 to 3.1.3). R Foundation for Statistical Computing, Vienna, Austria. Software Online: http://www.r-project.org (Site Accessed 8 June 2016).

Robin, X., N. Turck, A. Hainard, N. Tiberti, F. Lisacek, J.C. Sanchez, and M. Müller. 2011. R package, pROC: an open-source package for R and S+ to analyze and compare ROC curves. BMC Bioinformatics 12:77. Software Downloaded October 2014. Software Website: https://cran.r-project.org/web/packages/pROC/index.html (Site Accessed 8 June 2016).

Scales, K.L., P.I. Miller, C.B. Embling, S.N. Ingram, E. Pirotta, and S.C. Votier. 2014. Mesoscale fronts as foraging habitats: composite front mapping reveals oceanographic drivers of habitat use for a pelagic seabird. Journal of The Royal Society Interface 11:20140679.

Appendices

Schmid, M., S. Potapov, A. Pfahlberg, and T. Hothorn. 2008. Estimation and regularization techniques for regression models with multidimensional prediction functions. Technical Report 42, Department of Statistics, University of Munich, Germany.

Spear, L.B., D.G. Ainley, and P. Pyle. 1999. Seabirds in southeastern Hawaiian waters. Western Birds 30:1-32.

Venables, W.N. and Ripley, B. D. 2002. Modern applied statistics with S. Fourth Edition. Springer, New York, NY, USA.

Wickham, H. 2007. Reshaping data with the reshape package. Journal of Statistical Software 21(12).

Yee, T.W. 2015. R package, VGAM: Vector Generalized Linear and Additive Models. Software Downloaded October 2014). Software Website: https://cran.r-project.org/web/packages/VGAM/index.html (Site Accessed 8 June 2016).

Note: many of these definitions are specific to the context of this project.

Aliquot – Smallest designated subdivision of a BOEM lease block; 1.2×1.2 km (= 1/16th of a 4.8×4.8 km standard lease block).

Area under the receiver operating characteristic (ROC) curve (AUC) – An ROC curve is a graphical representation of how well a model can discriminate between (or predict) two categories of data (e.g., presence/absence), and the AUC is the integral of this curve. AUC values range between 0 and 1 where a value of 0.5 indicates model performance equivalent to random; a value >0.5 indicates performance better than random; and a value <0.5 indicates performance worse than random. Thus, higher AUC values indicate better model performance.

Autocorrelation – Correlation between data points or residual errors that are close in space and/or time. Spatial data often exhibit autocorrelation, and not accounting for it in predictive models can bias model predictions and artificially inflate statistical precision and significance.

Bag fraction – In a boosting context, a parameter that defines the fraction of the data drawn at random, without replacement, from the full training dataset at each iteration.

Base-learner – In a boosted generalized additive modeling framework, a relatively simple model relating the response variable to a predictor variable(s). One base-learner is selected in each boosting iteration, and the final model is essentially the sum of modeled relationships across the selected base-learners.

Boosted regression tree model – A modeling approach that combines a machine learning technique, boosting, with traditional tree-based statistical modeling. In this approach, a large number of regression trees are fit stagewise (i.e., after each tree is fit, the remaining variation in the data is used to fit the next tree) and then combined to generate a final, ensemble model.

Boosted zero-inflated count (BZIC) model – A boosted generalized additive modeling framework designed for count data with a large proportion of zeroes. Employs a zero-inflated Poisson or a zero-inflated negative binomial statistical distribution to model the count data. The zero-inflation and count components of the distribution are modeled as separate functions of the predictor variables.

Boosting – Iterative model fitting technique. In each iteration a single base-learner is selected. Each selected base learner's contribution to the final model is controlled by the learning rate.

Bootstrap (non-parametric) – A data re-sampling technique for estimating the statistical uncertainty in model predictions. A dataset of size n is re-sampled with replacement x times to derive x new datasets of size n. The model is fit to each new dataset to derive x predictions. The variability across these x predictions can then be used to evaluate their precision (e.g., confidence interval, coefficient of variation, etc.).

Climatology – Long-term spatial pattern in an environmental variable. For example, average values across years at different locations in space during a given annual time period (e.g., monthly, seasonal).

Coefficient of variation (CV) – Measure of dispersion for a distribution, representing the standard deviation as a proportion of the mean. In the context of a model prediction, a larger CV indicates more variation (uncertainty) in the prediction relative to the mean prediction.

Cross-validation – A technique for evaluating the predictive ability of a fitted model. The data are divided into training data and test data, the model is fit to the training data, and then the fitted model's ability to predict the test data is measured.

Cross-validation percent deviance explained (PDE) – Percent deviance explained calculated from test data and model predictions of the test data.

Technical Glossary

Ensemble model – A model created by combining multiple models into a single model. In the context of boosting, models are fit stagewise (i.e., after a model is fit, the remaining variation is used to fit the next model) and then combined.

Gaussian rank correlation coefficient (rank r) – Measure of the correspondence between observed and predicted values. Values range between -1 and 1 where a value of 0 indicates no correspondence between observed and predicted values; a value >0 indicates positive correspondence between observed and predicted values; and a value <0 indicates negative correspondence between observed and predicted values. Thus, positive values closer to 1 indicate better model performance.

Generalized additive model – A model whose response variable is the sum of multiple, potentially non-linear (e.g., smooth) functional relationships with predictor variables. A statistical distribution from the exponential family and a corresponding link function are employed for the response variable.

Learning rate – In a boosting context, the degree to which each base learner contributes to the final model. The optimal learning rate is one that results in well-defined model convergence sooner than later.

Maximum Entropy (MaxEnt) – A modeling algorithm that estimates the functional relationships between habitat suitability and a set of environmental predictor variables, with the relationships constrained by the mean value of the predictors at observed presence locations. It then uses these relationships to estimate the relative likelihood of suitable habitat at each model grid cell.

Offset (boosting) – In a boosting context, the initial values of each model component that are used to initialize the boosting algorithm.

Offset (effort) – In count models, a model term that accounts for survey effort by enforcing a proportional relationship between the expected count and effort (e.g., area surveyed).

Overfit – When a model does a very good job of explaining variation in training data but does a poor job of explaining variation in test data. A model that is overfit has very low bias but very high variance, and thus it is not generalizable.

Percent deviance explained (PDE) – Measure of the percentage of variation in the data explained by a model beyond that explained by the simplest model without predictor variables. Values normally range between 0 and 100 percent, although negative values are possible. Higher values indicate better model performance. PDE is a generalized model analogue of the coefficient of determination (R^2).

Permutation Importance – A measure of relative predictor variable importance output from a MaxEnt model that indicates how heavily the model depends on each variable. To measure permutation importance, for each predictor variable the values at the model training data locations and background locations are randomly scrambled, and model performance is re-evaluated. A greater decline in model performance results in a higher permutation importance value.

Predictor – An independent variable in a model that is used to explain variation in the response.

Pseudo-absences – In presence-only predictive models, randomly chosen locations used to contrast the environmental conditions of presence locations with environmental conditions where there are not presences. In MaxEnt, the "background" locations are treated as pseudo-absences for model evaluation, but, importantly, are not used in model fitting.

Re-sampling – A method of using randomly drawn subsets of data to estimate statistical precision (e.g., variation in model predictions), to perform a significance test (e.g., permutation test of predictor importance), or to perform model validation (e.g., cross-validation).

Residual error (percent error) – Difference between observed data and corresponding model predictions. In this report, residual error is expressed as a percentage of the mean of the data and referred to as 'percent error'.

Response – The dependent variable in a model representing the quantity of interest for which predictions are to be made.

Sensitivity – Also known as the true positive rate, a measure of model performance for binary classification models (e.g., suitable versus unsuitable habitat) that measures the proportion of positives that are correctly identified as positives. In the context of a MaxEnt model of habitat suitability, this is calculated as the fraction of presences correctly classified as suitable habitat.

Spatial predictive modeling – Modeling technique whereby relationships between environmental predictors and a response variable are estimated for areas with survey data, and then these relationships are used to predict the response as a function of the same environmental predictors in areas without survey data.

Specificity – Also known as the true negative rate, a measure of model performance for binary classification models (e.g., suitable versus unsuitable habitat) that measures the proportion of negatives that are correctly identified as negatives. In the context of a MaxEnt model of habitat suitability, this is calculated as the fraction of background locations correctly classified as unsuitable habitat. The false positive rate can be calculated by taking 1 - Specificity.

Stochastic gradient boosting – A type of boosting whereby the data are sub-sampled in each iteration before the base-learner(s) is fit to the gradient.

Test data – Data that are excluded during model fitting and later used to test the predictive performance of the fitted model (e.g., during cross-validation).

Test percent deviance explained (PDE) – PDE calculated for a fitted model in terms of test data.

Training data – Data to which a model is fitted in order to estimate model parameter values.

Tree complexity – In a boosted regression tree model, a parameter that controls the number of allowable nodes in a tree. This limits the number of possible interactions between predictor variables In general, greater tree complexity results in fewer iterations needed for model convergence.

Tuning – Procedure by which model fitting parameters are adjusted to minimize the predictive error of a model. For example, in boosting the learning rate and number of boosting iterations are adjusted during tuning.

Variable importance – Measure of the importance of a predictor variable usually in terms of how much of the variation in the response variable it explains.

Zero-inflated negative binomial distribution – A statistical distribution used to model count data that accounts for a large number of zeroes and an overdispersed count distribution (e.g., because of aggregative behavior of animals).

Zero-inflated Poisson distribution – A statistical distribution used to model count data that accounts for a large number of zeroes.

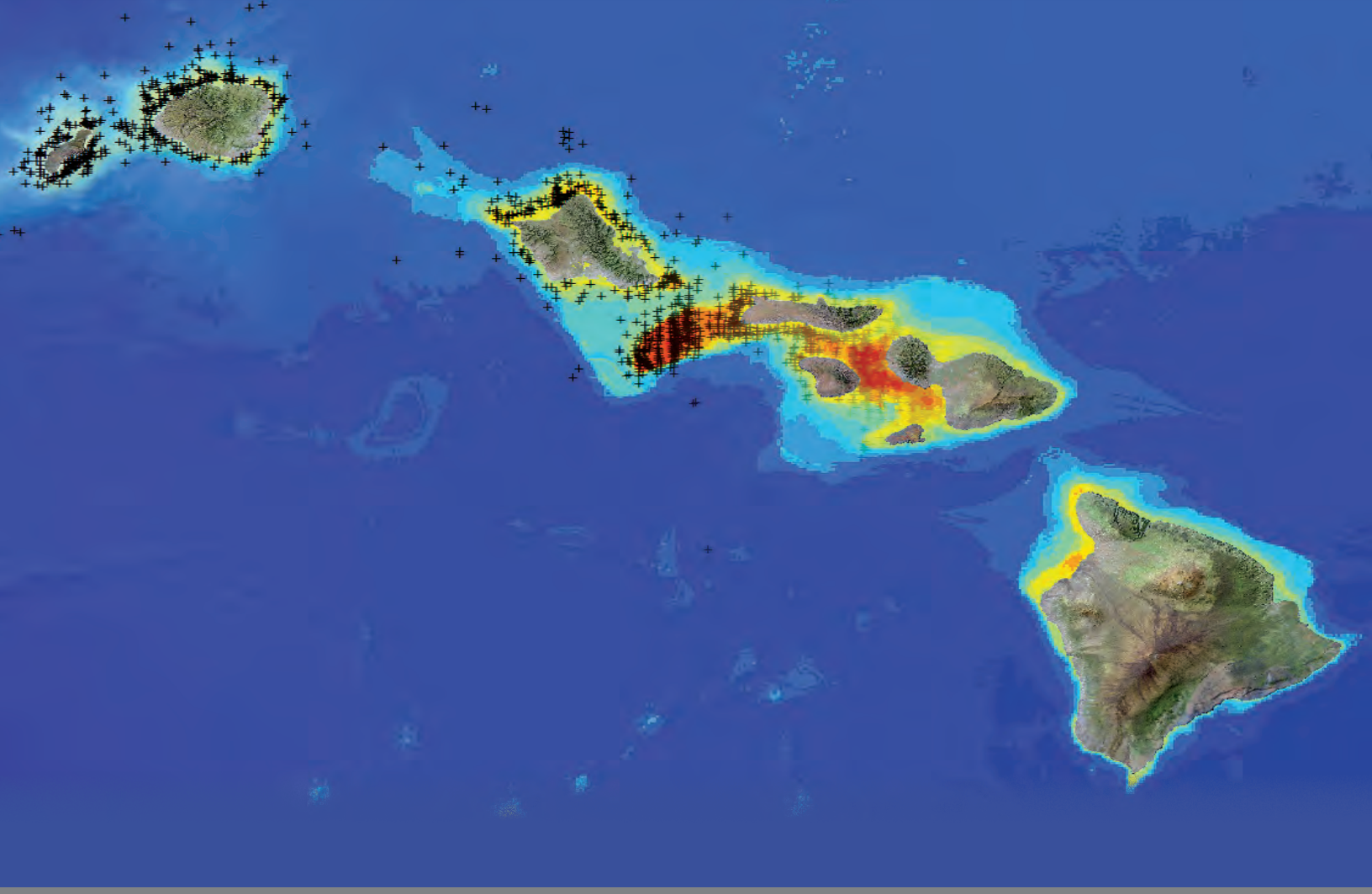

U.S. Department of Commerce

Penny Pritzker, *Secretary of Commerce*

National Oceanic and Atmospheric Administration

Kathryn Sullivan, *Acting Under Secretary for Oceans and Atmosphere*

National Ocean Service

Holly Bamford, *Assistant Administrator for National Ocean Service*

The mission of the National Centers for Coastal Ocean Science is to provide managers with scientific information and tools needed to balance society's environmental, social and economic goals. For more information, visit: http://www.coastalscience.noaa.gov/.

BOEM
Bureau of Ocean Energy Management

Marine Biogeographic Assessment of the Main Hawaiian Islands

OCS Study BOEM 2016-035 and
NOAA Technical Memorandum
NOS NCCOS 214